# Atlas of Earth System Hazards for Tasmania

—

## Future Projections of Regional Heatwave and Bushfire Danger

**The Climate Futures Research Group**

**University of Tasmania**

**August 2022**

**V 1.0**

UNIVERSITY *of* TASMANIA

## Disclaimer

*The material in this atlas is based on computer modelling projections for climate change scenarios and, as such, there are inherent uncertainties in the data. While every effort has been made to ensure the material in this atlas is accurate, the University of Tasmania provides no warranty, guarantee or representation that the material will prove to be accurate, complete, up-to-date, non-infringing or fit for purpose. The use of the material is entirely at the risk of the user. The user must independently verify the suitability of the material for their own use.*

*To the maximum extent permitted by law, the University of Tasmania, any other participating organisation and their officers, employees, contractors and agents exclude liability for any loss, damage, costs or expenses whether direct, indirect, consequential including loss of profits, opportunity and third party claims that may be caused through the use of, reliance upon, or interpretation of the material in this atlas.*

## Citation

Remenyi, T.A., Rollins, D.A., Love, P.T., Earl, N.O., Harris, R.M.B., & Beyer, K. (2022) *Atlas of Earth System Hazards for Tasmania*, University of Tasmania, Hobart, Tasmania. [add DOI]

DOI: NUMBERS

## Requests and enquiries

Requests and enquiries concerning reproduction rights should be addressed to:

Communications and Media Office
University of Tasmania
+61 3 6226 2124
Media.Office@utas.edu.au



## Acknowledgements

This project was funded under the Natural Disaster Risk Reduction Grants Program (NDRRGP), provided by the Australian Commonwealth Government's Attorny-General's Department, coordinated by the Tasmanian Government's State Emergency Service. This research was supported by use of the Nectar Research Cloud, a collaborative Australian research platform within the the Australian Research Data Commons (ARDC), supported by funding from the National Collaborative Research Infrastructure Strategy (NCRIS). This project used the R programming language and would therefore like to recognise the efforts of the *R-core team* and those of *RStudio* in providing the tools and interfaces that made data analysis and visualisation possible and innovative. This project also used the LaTeX typesetting system, and we would like to recognise the contributors to this system.

## Dedication to Dr Rebecca Harris

Co-author of this report, Dr Rebecca (Bec) Harris lost a brave battle with cancer at the end of 2021. She contributed to this chapter until shortly before her death. This work stands as testimony to her career-long focus on the parallel tasks of both climate science and science translation, for the betterment of humanity and the planet. Her strength, sharp intellect, kindness and sense of fun are sorely missed by her colleagues at Climate Futures, UTAS and the IPCC. Vale Bec.

# Contents

Atlas of
Earth System Hazards
for Tasmania
–
# Introduction

## Purpose of this document

A growing interest in future climate information across society has become clear since 2019. This interest is particularly evident from those working in government departments, local councils, engineers, property managers and investors. People want to understand the natural hazard risks they need to manage across the Tasmanian landscape, including how these may change into the future. They also want this information at the highest resolution possible. The *Earth System Hazards Climate Atlas for Tasmania*, allows Tasmanians to better understand the scale and magnitude of natural hazards Tasmania must manage together. This document is designed to assist operational staff with responsibilities in strategic planning and emergency management across both public and private sectors.

This document is the outcome of the initial Phase-1, that creates the first pages within the atlas, but is designed such that additional sections/hazards can be added in future phases.

This atlas is in alignment with the *National Disaster Risk Reduction Programme's* (the funding body) Goal 1 (Understanding disaster risk) and Goal 2 (Working together), as it provides a visual communication device for engaging the community, industry and department personnel, while also providing data layers (where appropriate) for technical users, (through TheList). Both tools will aid to improve the understanding of disaster risk (at varying levels of sophistication) while also providing the capacity to identify areas (conceptual and physical) of shared responsibility across our communities. This project also supports the *National Disaster Risk Reduction Programme's* Goals 3 and 4 indirectly, by providing the underpinning data that can be used to select the most appropriate treatment options to achieve these goals.

## Background context

This project has built on the previously released work by the Climate Futures team—*Australia's Wine Future – A Climate Atlas*—which developed new approaches to provide tailored climate information for particular regions and industries. The *Earth System Hazards Atlas for Tasmania* both extends the spatial coverage across all of Tasmania, while also identifying current and emerging climate risks across the State. In version 1.0 it provides extensive technical information on the extreme events of heatwave and bushfire. The fine-scaled climate information that underpins this document is accessible within the Tasmanian Government TheList, making it usable in hard-copy and digital forms to support the prioritisation of future strategic investments to help build resilience to current and emerging natural hazards.

Previous experience with the Australian Wine Industry demonstrated that a climate atlas, focused on the variables of interest to a particular stakeholder group, can be an excellent engagement tool that rapidly allows individuals, organisations, and communities to understand what their climate is like today, the hazards they are exposed to, and how these are likely to change into the future. It has also demonstrated that it mobilises these people into action and enhances their capacity to manage current and future risks.

Tasmania has some of the highest quality climate data available—both historical products (BARRA-TA) and future projections (CFAP2019)—which have been supported and funded by various federal and state government funding schemes. These data are managed by the Climate Futures Programme at the University of Tasmania and made available to emergency managers on request (e.g., Tasmanian Fire Service, State Emergency Service, Parks and Wildlife Service, Department of Health and Human Services, Tasmania Health Service). However, the skills required to access and use these archives require significant training, with few individuals within government, industry, or the community capable of leveraging this information. An atlas for the public (and non-technical users) along with associate data layers uploaded to the TheList (for engineers and technical users) will increase the utility of these existing data archives, unlocking the value held within these previous investments.

## The approach

The climate indices of highest priority to emergency management within Tasmania were taken from the *Tasmanian Disaster Risk Assessment 2021* process. Each of these Earth system hazard indices were considered with regards to the ease of inclusion. This separated indices into two groups: 1) those able to be produced in the current funding round (this document, Phase 1); and 2) those that will need to be completed in future funding rounds (Phase 2, possibly Phase 3 depending on stakeholder needs). Earth system hazards were prioritised drawing on our knowledge in the emergency services sector, and our understanding of what is immediately possible from a *science/understanding* perspective. Insights from both TSNDRA 2016 and the more recent TASDRA 2021 were also considered. The assessment criteria that guided the prioritisation of each hazard is described in Table 1.

| Earth system hazard | Collaboration required | Expediency (in Feb 2021) | Assessment |
|---|---|---|---|
| Bushfire | No | High | The desired metrics are known based on previous decade of engagement with Tasmania's fire managers; data is at hand; data-visualisation techniques are known; spatial scales for visualisation are understood. |
| Heatwave | No | High | The desired metrics are known based on previous 5 years of engagement with Tasmania's heatwave managers; data is at hand; data-visualisation techniques are known; spatial scales for visualisation are understood. |
| Drought | Yes (many stakeholders) | Moderate | The desired metrics need consultation/confirmation from different users (farmers vs emergency management vs water managers); data is at hand; spatial scales for visualisation are understood. It is possible to include some metrics without consultation if desired. |
| Tsunami | Yes (MRT) | Moderate | The current metrics/maps are known/completed (by Mineral Resources Tasmania, MRT); and maps could be included with assistance from MRT; however, mapping with consideration of future sea-level rise has not been completed—given the changing volume of water as sea level rises in embayment's, climate change could have significant effects; modelling of future impacts to Tsunami risk would be achievable given the hydrodynamic models have been developed, but would require dedicated scoping, resources and collaboration with MRT. |
| Earthquake | Yes (GA; MRT) | Moderate | Mapping of earthquake risk is currently (February 2022) being done by Geosciences Australia (GA). Outputs could be included in the atlas (with GA's assistance). Although relevant spatial scales required could prove challenging (possibly very fine-scale resolution is needed). Climate change does not affect Earthquake hazard. |
| Landslide | Yes (MRT) | Low | The current risk can be done (by/with Mineral Resources Tasmania, MRT), although relevant spatial scales required could prove challenging to visualise in a meaningful way in a static product. Further, this still requires the consideration of future high-intensity rainfall to develop future landslide hazard metrics. This would require dedicated scoping, resources, and collaboration with MRT. |
| Flood | Yes (SES) | Low | To be informed by the Tasmanian State Emergency Services (SES) flood management team. This requires the completion of the current SES flood mapping projects; once completed, using their workflow to develop future climate flood layers may be straight forward (for that team), but requires dedicated resourcing and collaboration with the SES flood mapping team. |
| Severe Storm / Wind | Yes (BoM) | Low | Significant effort is required to develop useful storm/wind metrics that meet user needs, as there are different needs for different sectors over historical, current, and future time periods; further, mapping and visualisation techniques need to be investigated. Collaboration with the Bureau of Meteorology (BoM) would be very useful, if not essential. |
| Biosecurity | Yes (many stakeholders) | Low | Biosecurity hazards are complicated and complex, requiring specific attention for each species/hazard and thus is a very large collection of projects. However, the maps and trends could be included in the atlas. Dedicated effort would be required to determine the prioritised scope of hazards to include and the best visualisation techniques. Note these may change depending on the target hazard. This would be a significant, multi-year piece of work. |

Table 1: The assessment criteria applied to prioritise which hazards to include in the first phase of this project.

Atlas of
Earth System Hazards
for Tasmania

–

# Part 1: Heatwave

# FURNEAUX ISLANDS

## Heatwaves — Number of Heatwave Days

Figure 1: Observed
mean annual number of heatwave days

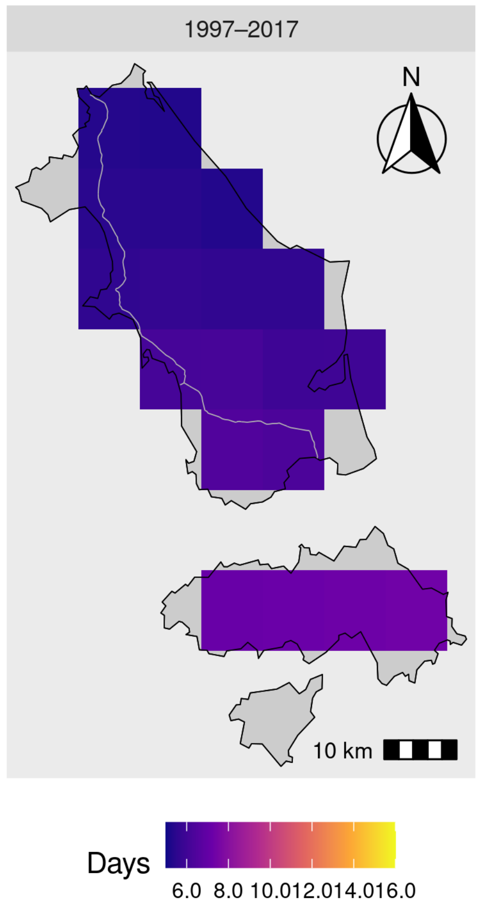


Figure 2: Observed change in
mean annual number of heatwave days

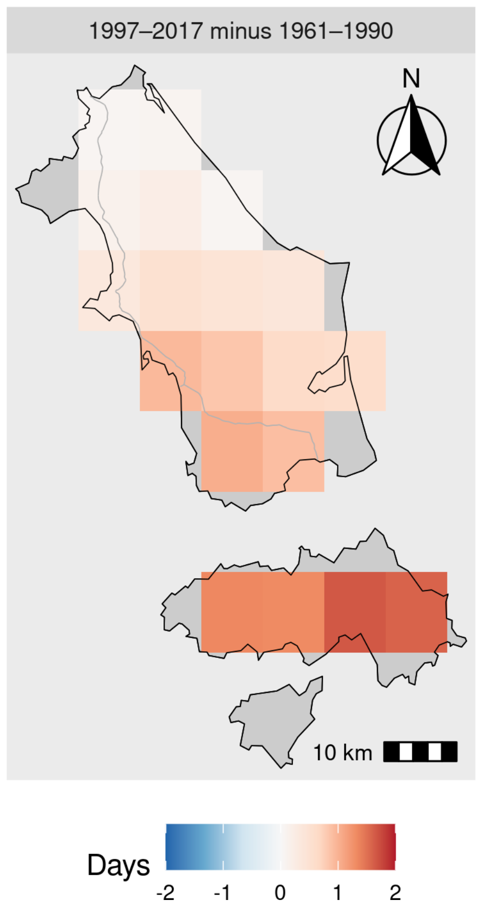


Figure 3: Projected mean
annual number of heatwave day

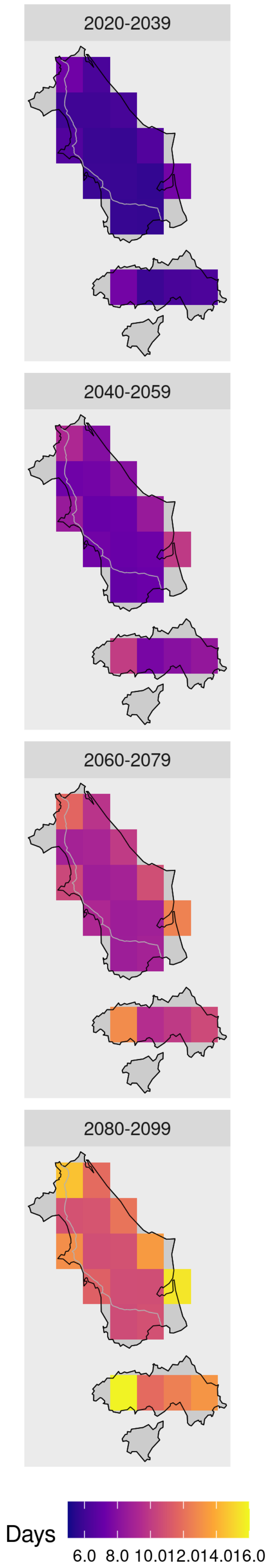


Figure 1: Observed mean *annual number of heatwave days* across all years from 1997–2017.

Figure 2: The change in the mean *annual number of heatwave days* between the current (1997–2017) and historical (1961–1990) periods. Mean *annual number of heatwave days* has increased across the region over recent decades.

Figure 3: Projected mean *annual number of heatwave days* for 20-year time periods from 2001 to 2100. Mean *annual number of heatwave days* is expected to increase steadily into the future. Each grid cell is the mean of the 6 ensemble members.

Figure 4: Projected annual number of heatwave days from 1961 to 2100

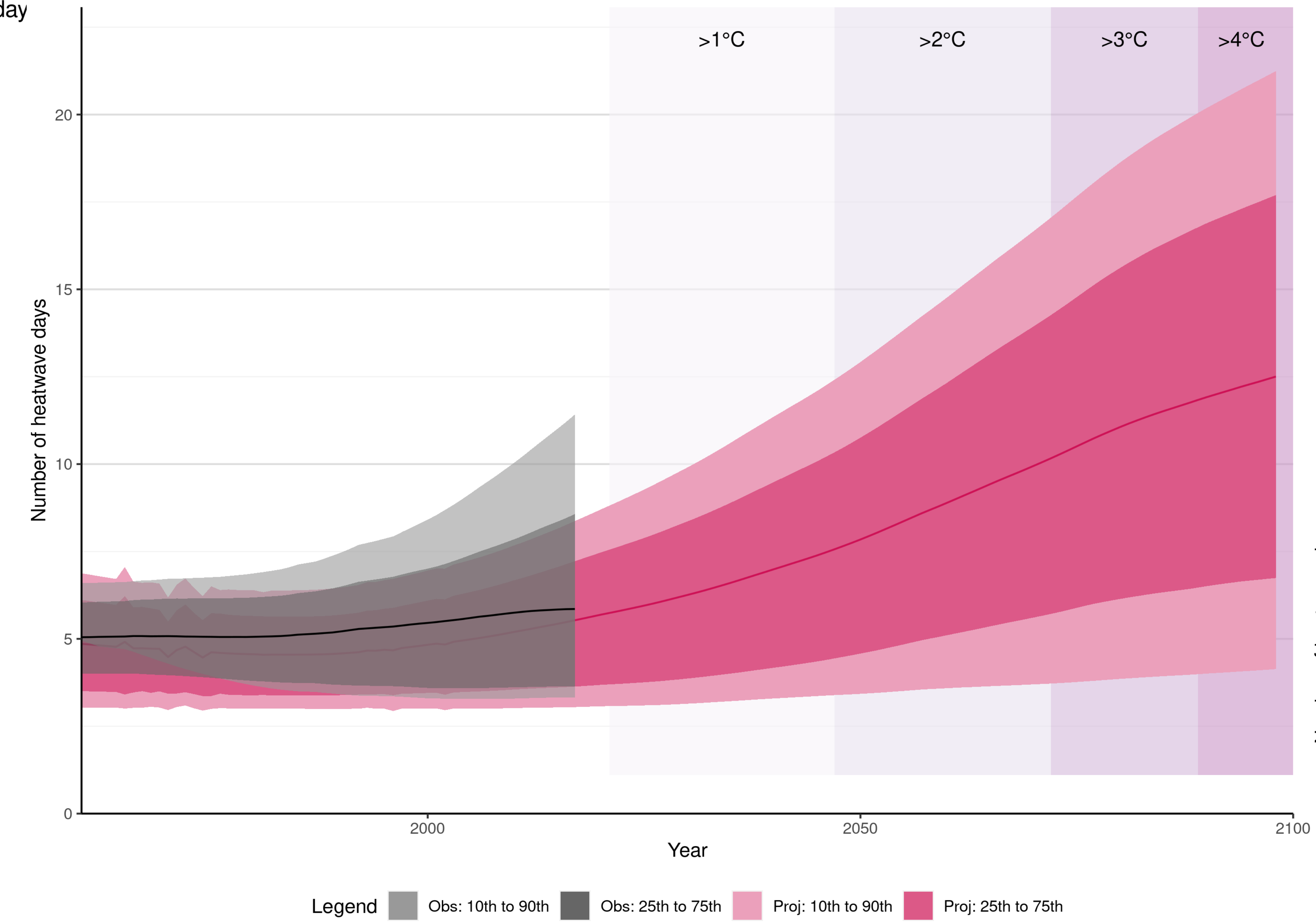


Figure 4: Projected change in mean *annual number of heatwave days* from 1990 to 2100. Historical values (*grey*) are the 30-year rolling means of AGCD. Projected values (*peach*) are the ensemble mean of the 30-year rolling mean of each CCAM ensemble member. *Lighter ribbons* represent the 10th to 90th percentiles of mean *annual number of heatwave days*. *Darker ribbons* represent the 25th to 75th percentiles of mean *annual number of heatwave days*. *Solid lines* represent the mean *annual number of heatwave days*.

Figure 5: Projected range in the annual number of heatwave days

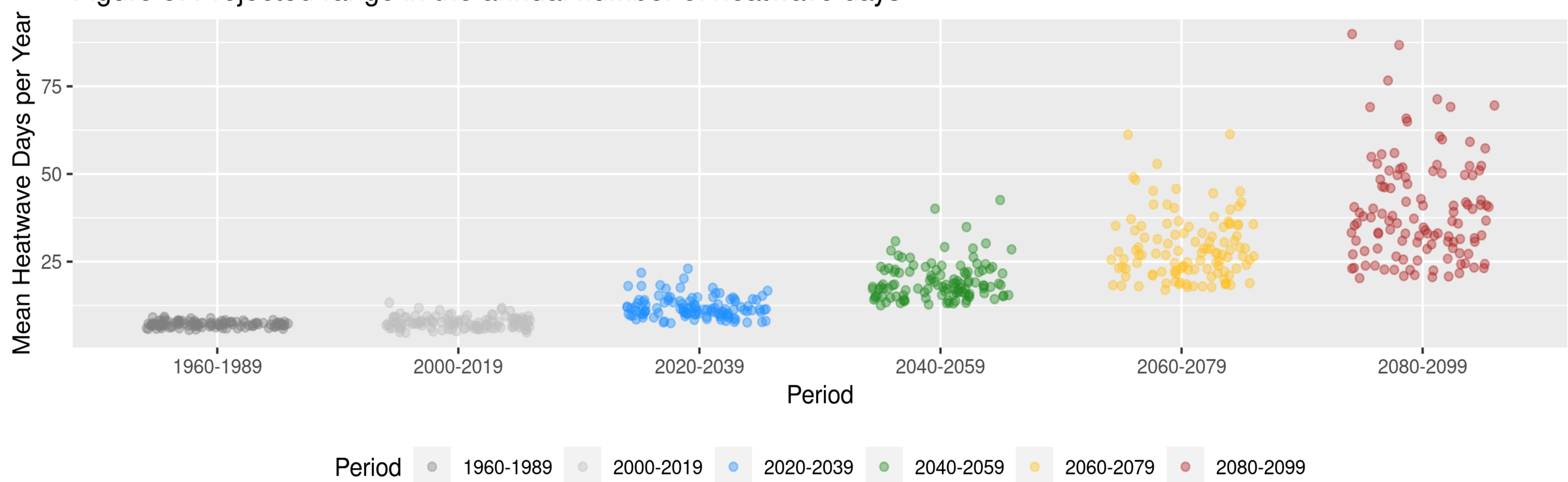


Figure 5: Comparison of the distribution of the *annual number of heatwave days* over the historical period for both model outputs (*¡colour¿* and observations (*black*).

Figure 6: Projected mean annual number of hea

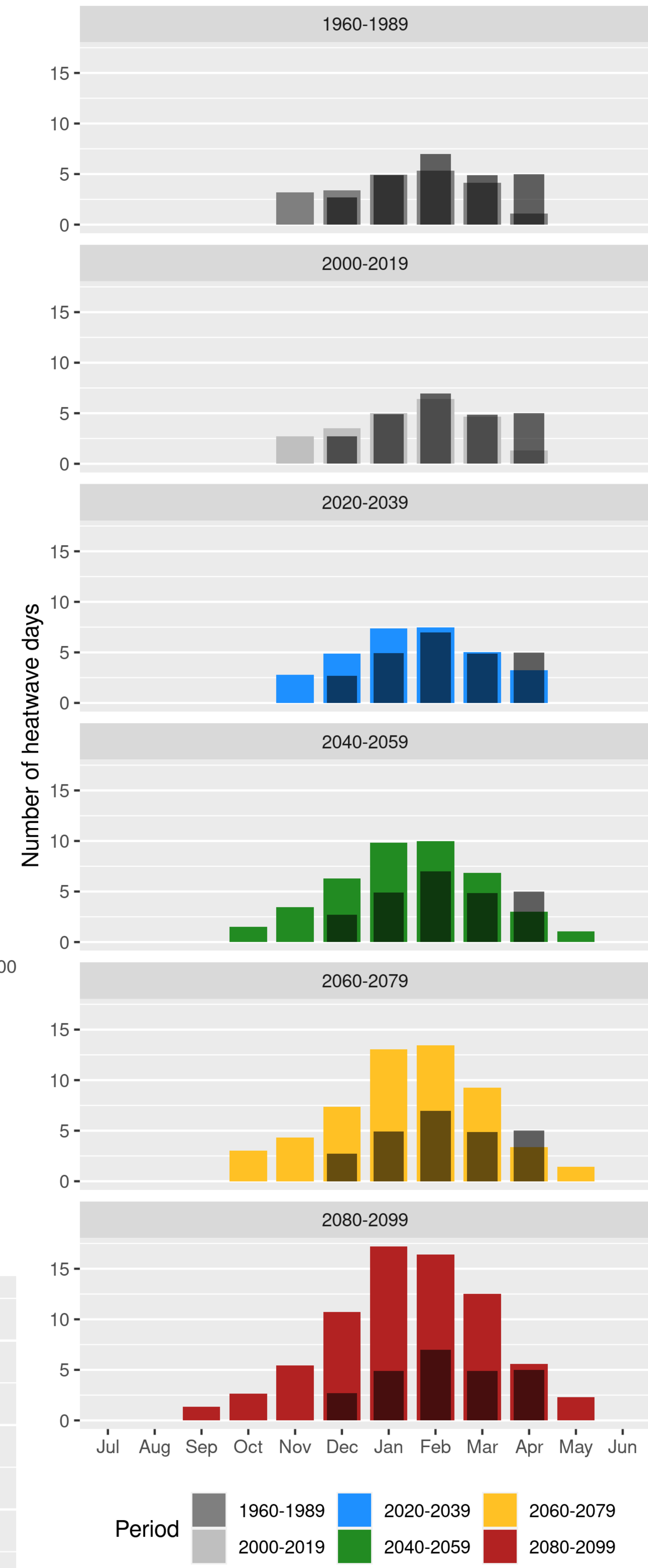


Figure 6: *Bar plots of typical number of heatwave days in each month* for 20-year time periods from 1961 to 2100. Each bar represents the 20-year *typical number of heatwave days in each month*, average across space and time. The observations for the baseline period (1961–1990) are shadowed on top of the future time periods to highlight any differences expected into the future. Higher (lower) bars indicate more (less) heatwave days.

# FURNEAUX ISLANDS

## Heatwaves — Cumulative Intensity

Figure 1: Observed mean cumulative intensity

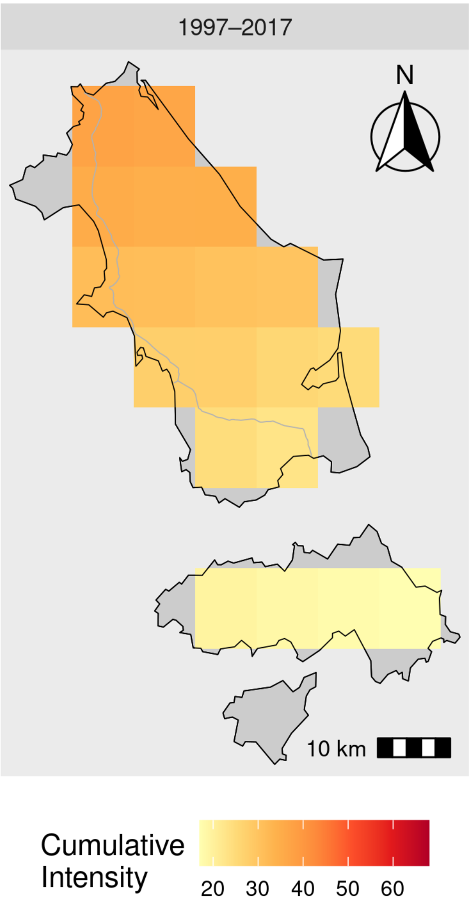


Figure 2: Observed change in mean cumulative intensity

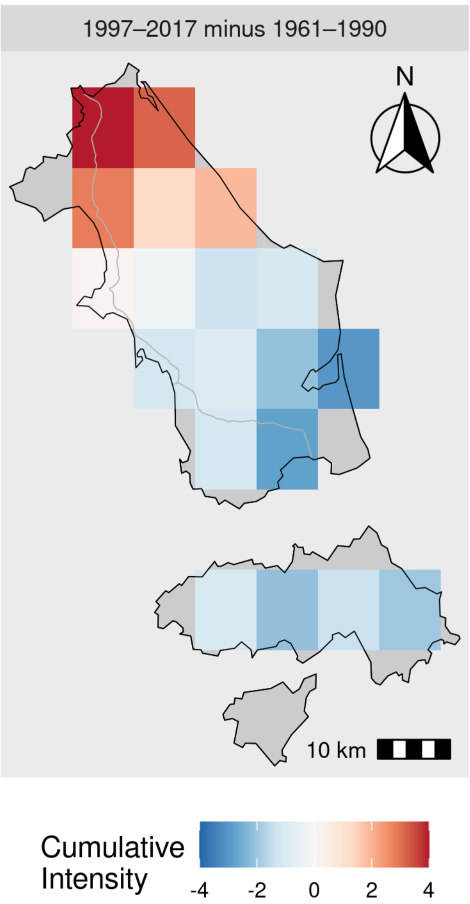


Figure 3: Projected mean cumulative intensity

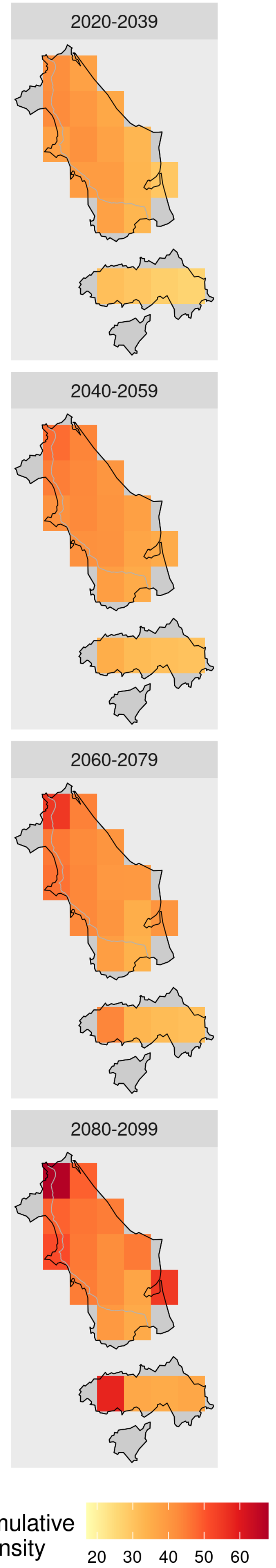


Figure 7: Observed mean *cumulative intensity during a heatwave* across all years from 1997–2017.

Figure 8: The change in mean *cumulative intensity during a heatwave* between the current (1997–2017) and historical (1961–1990) periods. Mean *cumulative intensity during a heatwave* has increased across the region over recent decades.

Figure 9: Projected mean *cumulative intensity during a heatwave* for 20-year time periods from 2001 to 2100. Mean *cumulative intensity during a heatwave* is expected to increase steadily into the future. Each grid cell is the mean of the 6 ensemble members.

Figure 10: Projected cumulative intensity

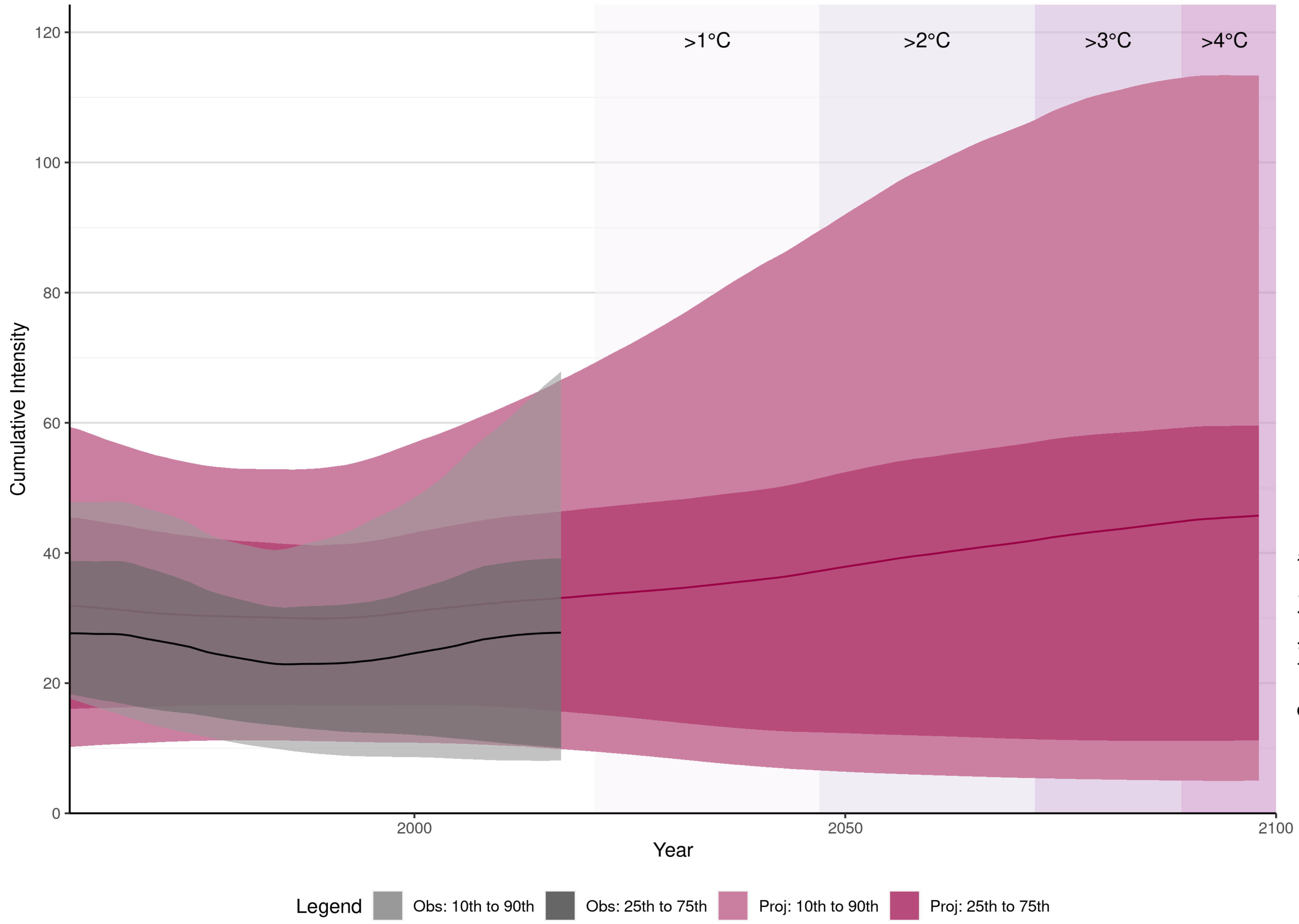


Figure 10: Projected change in *cumulative intensity during a heatwave* from 1990 to 2100. Historical values are the 30-year rolling means from AGCD (*grey*). Projected values (*peach*) are the ensemble mean of the 30-year rolling mean of each ensemble member. *Lighter ribbons* represent the 10th to 90th percentiles of *cumulative intensity during a heatwave. Darker ribbons* represent the 25th to 75th percentiles of *cumulative intensity during a heatwave. Solid lines* represent the mean of *cumulative intensity during a heatwave.*

Figure 11: Distribution of cumulative intensity

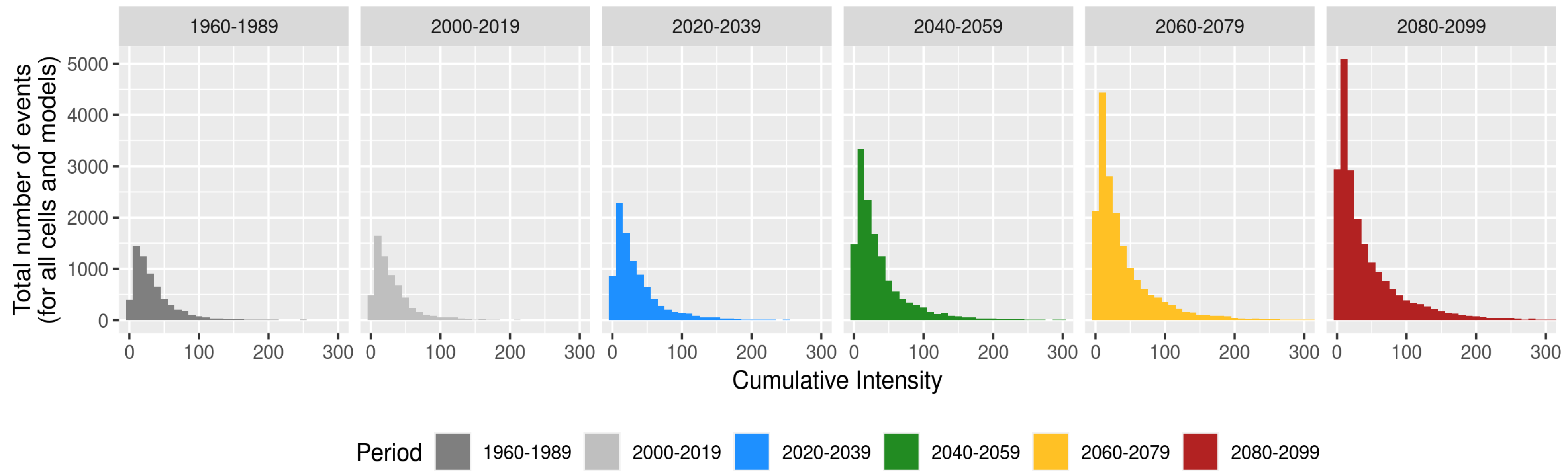


Figure 11: Comparison of the distribution of *cumulative intensity during a heatwave* for different time periods.

Figure 12: Projected mean cumulative intensity

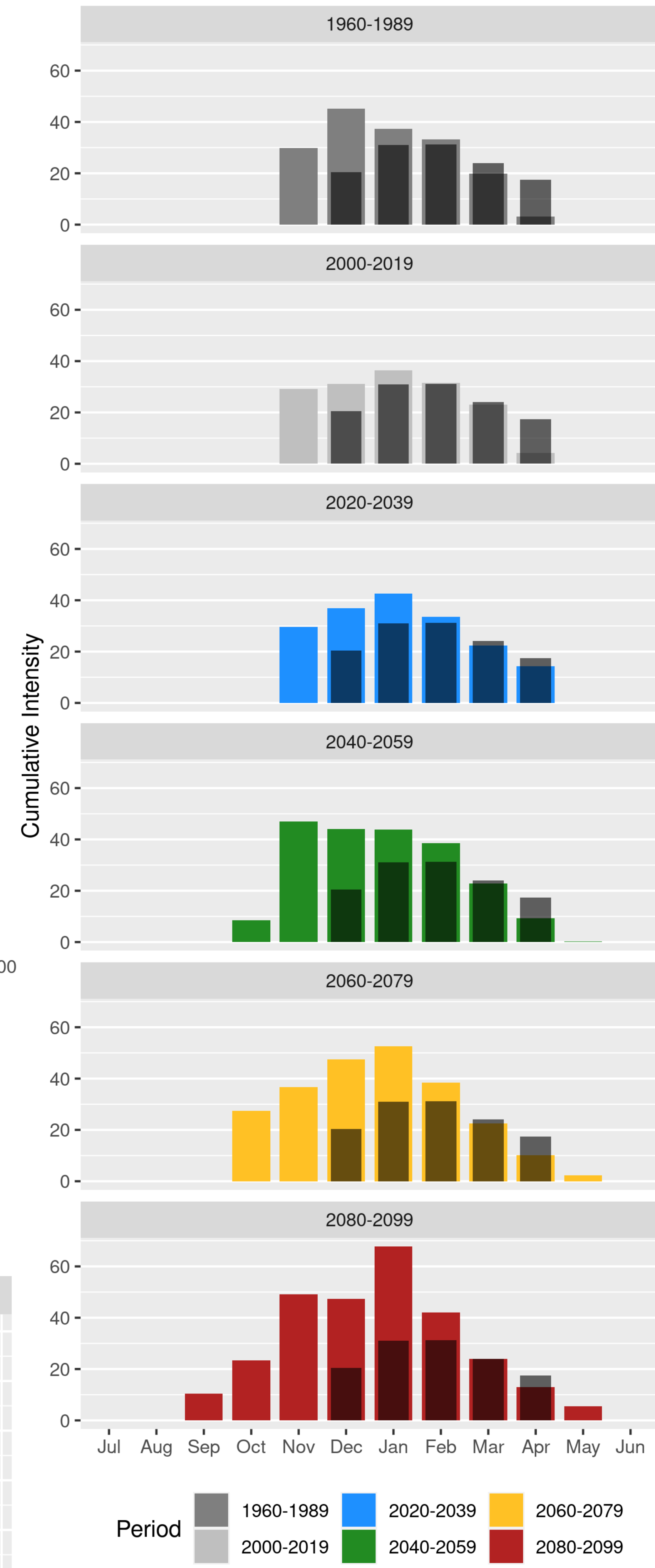


Figure 12: *Bar plots of cumulative intensity during heatwaves* in each month for 20-year time periods from 1961 to 2100. Each bar represents the 20-year mean of *cumulative intensity during a heatwave*, average across space and time. The observations for the baseline period (1961–1990) are shadowed on top of the future time periods to highlight any differences expected into the future. Higher (lower) bars indicate hotter (cooler) heatwave intensities.

# FURNEAUX ISLANDS

## Heatwaves — Duration

Figure 1: Observed mean duration

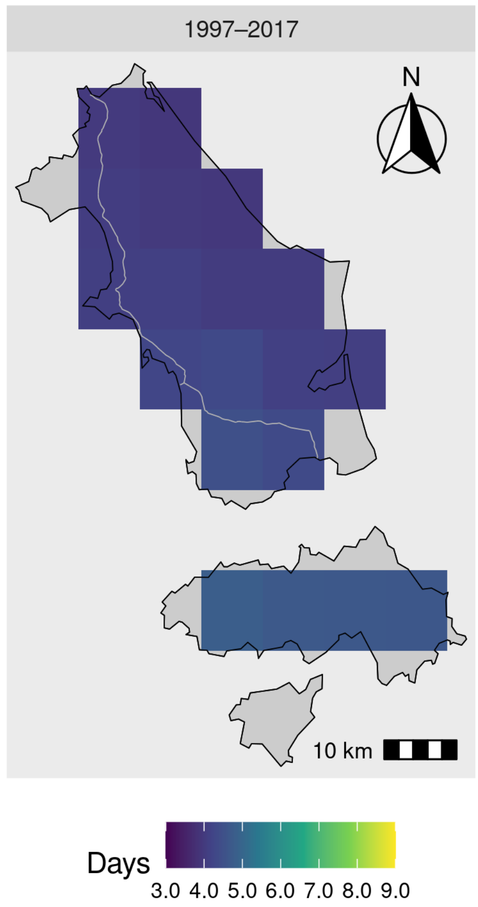


Figure 2: Observed change in mean duration

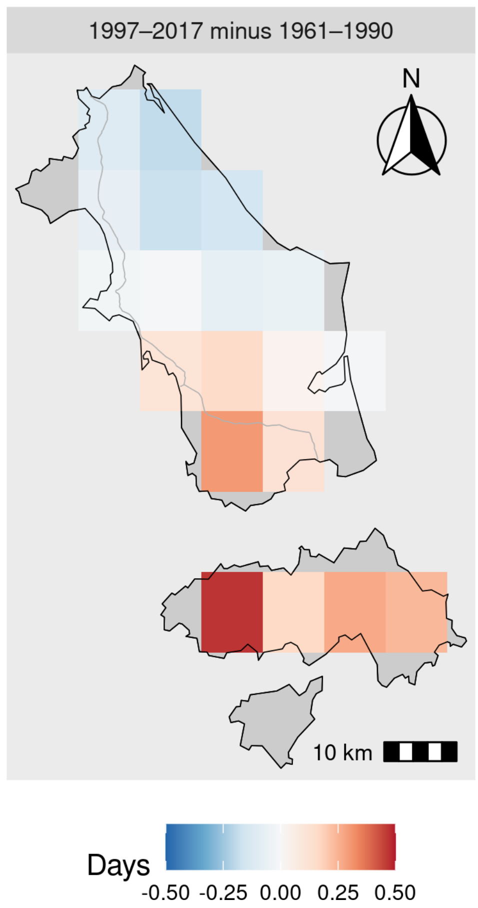


Figure 3: Projected mean duration

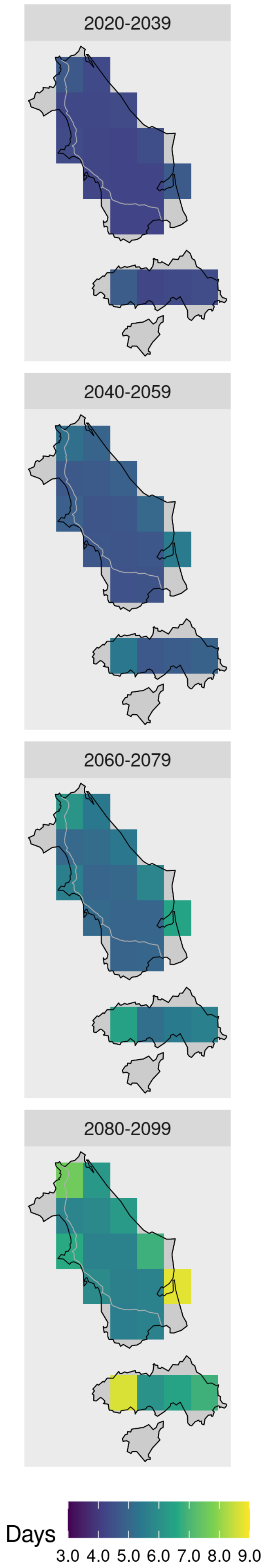


Figure 13: Observed mean *heatwave durations* across all years from 1997–2017.

Figure 14: The change in mean *heatwave duration* between the current (1997–2017) and historical (1961–1990) periods. Mean *heatwave durations* have increased across the region over recent decades.

Figure 15: Projected mean *heatwave durations* for 20-year time periods from 2001 to 2100. Mean *heatwave duration* is expected to increase steadily into the future. Each grid cell is the mean of the 6 ensemble members.

Figure 16: Projected heatwave duration

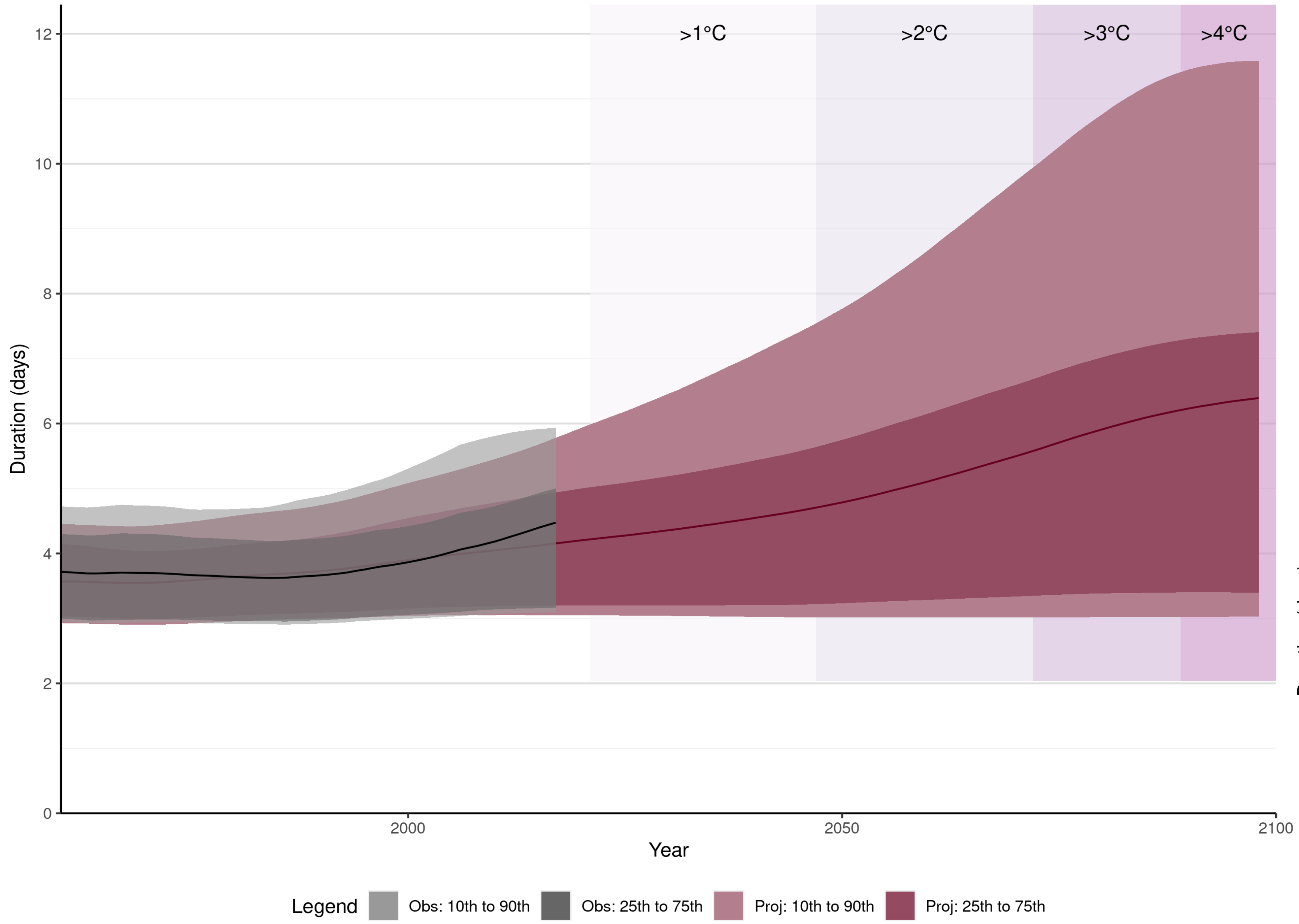


Figure 16: Projected change in *heatwave duration* from 1990 to 2100. Historical values (*grey*) are the 30-year rolling means of AGCD. Projected values (*orange*) are the ensemble mean of the 30-year rolling mean of each CCAM ensemble member. *Lighter ribbons* represent the 10th to 90th percentiles of *heatwave duration*. *Darker ribbons* represent the 25th to 75th percentiles of *heatwave duration*. *Solid lines* represent the mean of *heatwave duration*.

Figure 17: Projected count of heatwave duration

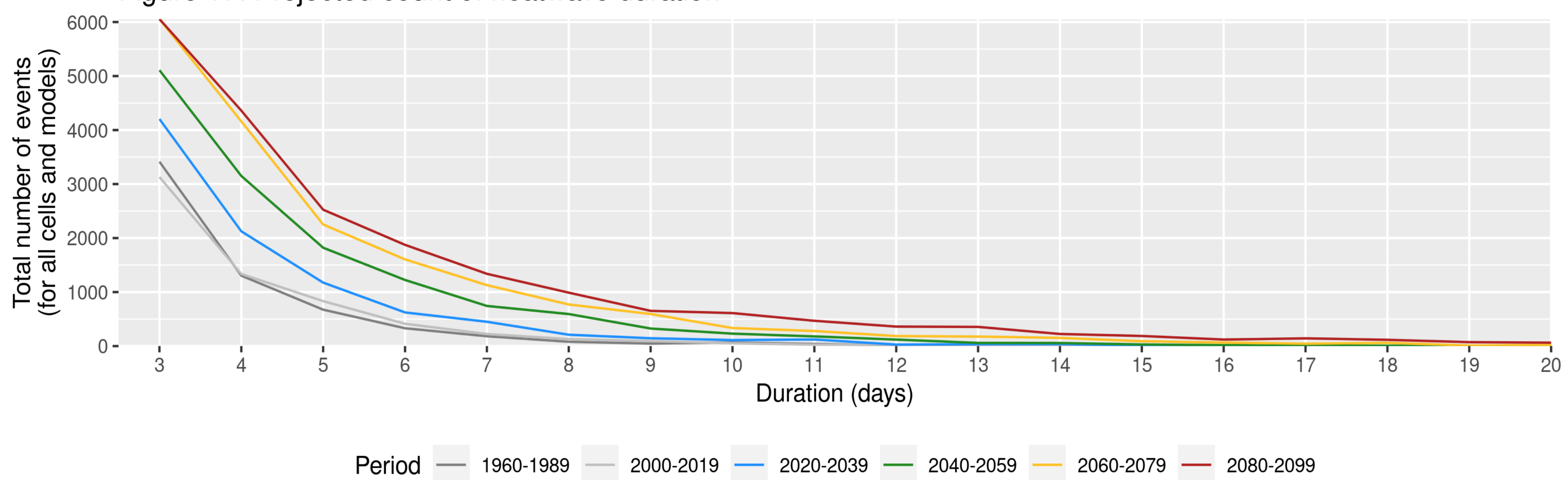


Figure 17: Comparison of the distribution of *heatwave durations* for different time periods.

Figure 18: Projected mean heatwave duration by

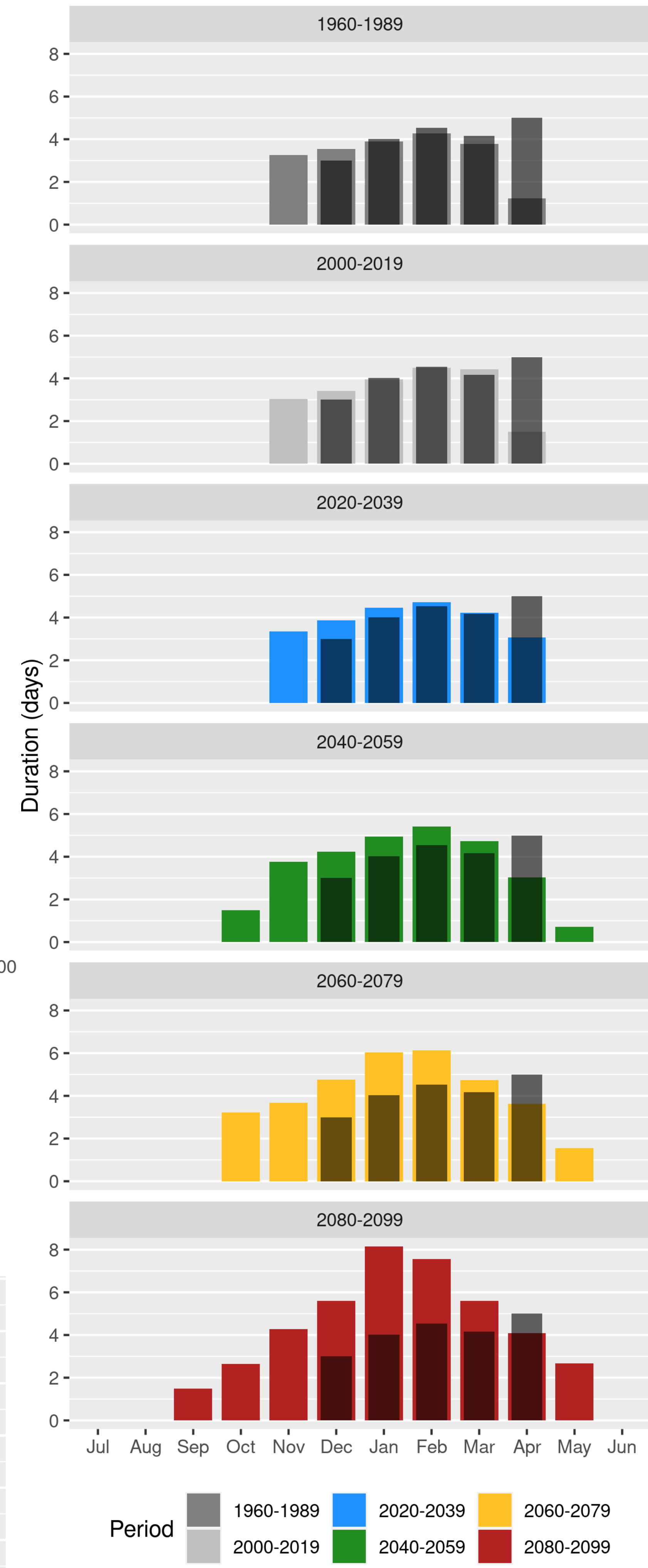


Figure 18: *Bar plots* of mean *heatwave durations* in each month for 20-year time periods from 1961 to 2100. Each bar represents the 20-year mean of *heatwave durations*, average across space and time. The observations for the baseline period (1961–1990) are shadowed on top of the future time periods to highlight any differences expected into the future. Higher (lower) bars indicate longer (shorter) *heatwave durations*.

# NORTH EAST

## Heatwaves — Number of Heatwave Days

Figure 1: Observed mean annual number of heatwave days

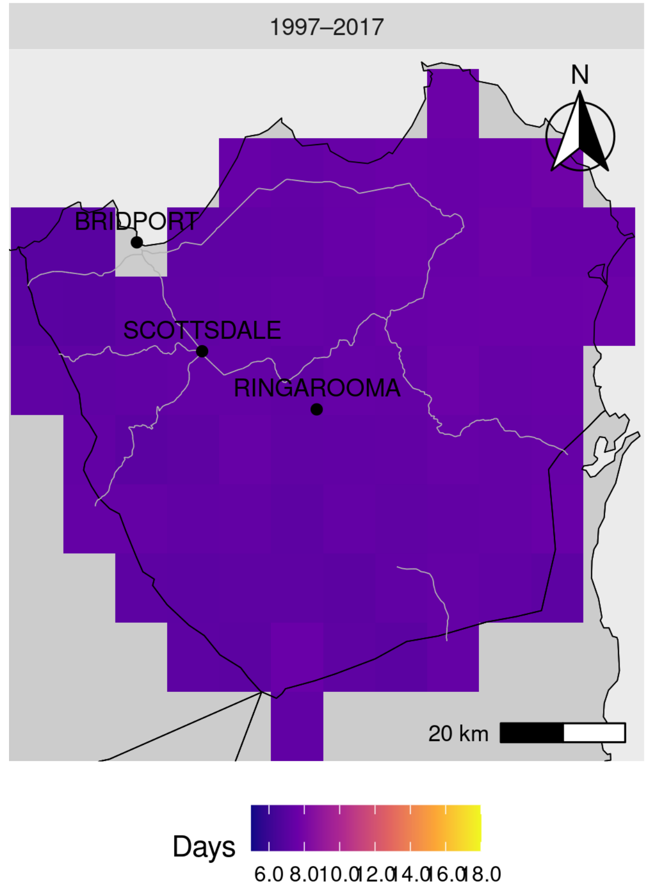


Figure 2: Observed change in mean annual number of heatwave days

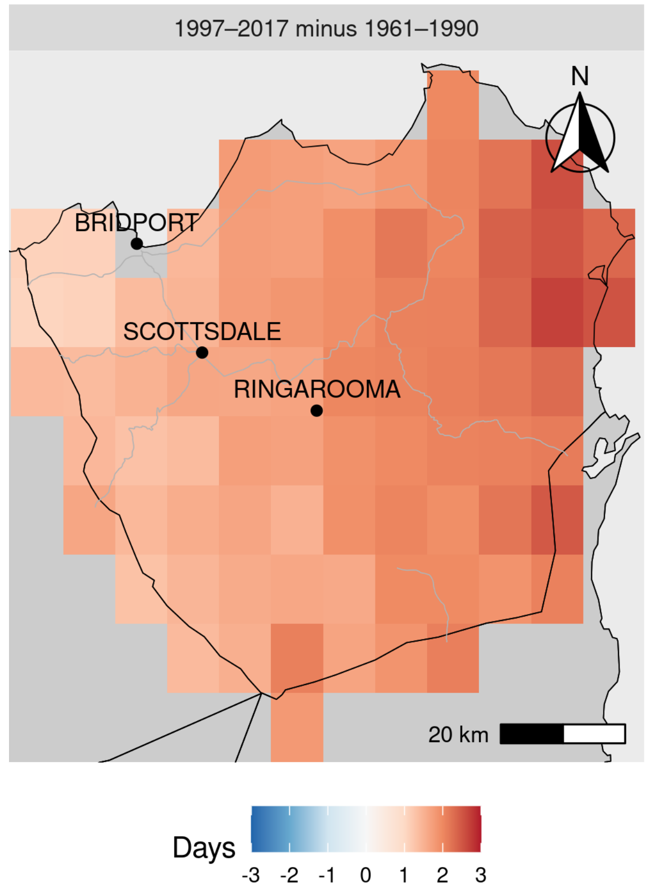


Figure 3: Projected mean annual number of heatwave day

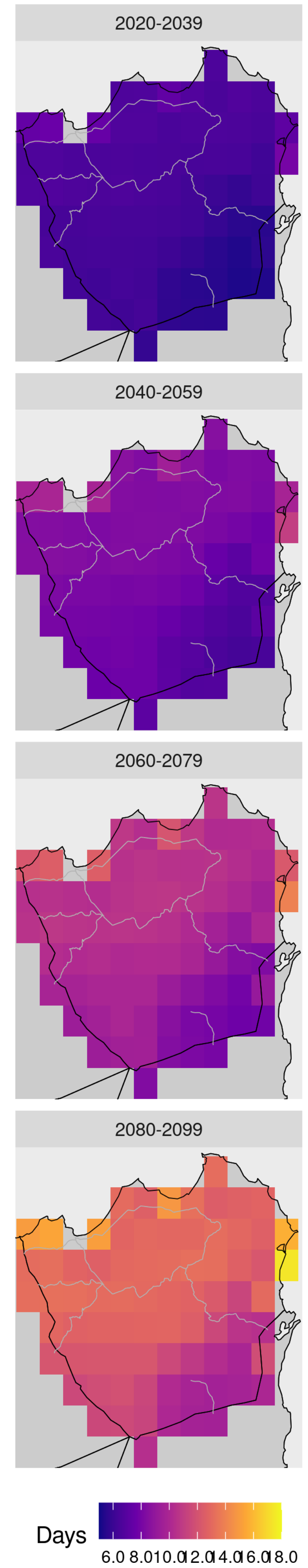


Figure 4: Projected annual number of heatwave days from 1961 to 2100

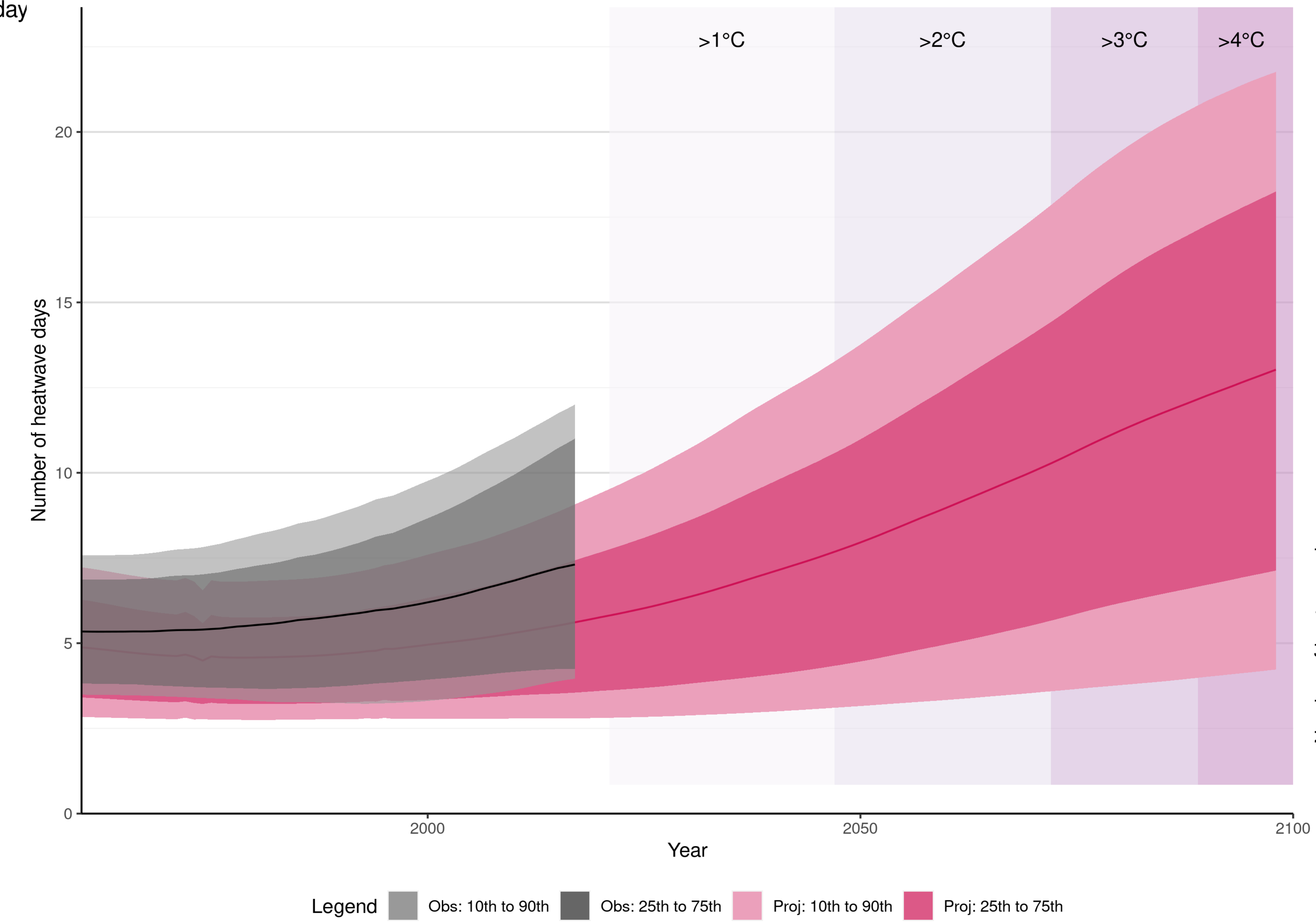


Figure 4: Projected change in mean *annual number of heatwave days* from 1990 to 2100. Historical values (*grey*) are the 30-year rolling means of AGCD. Projected values (*peach*) are the ensemble mean of the 30-year rolling mean of each CCAM ensemble member. *Lighter ribbons* represent the 10th to 90th percentiles of mean *annual number of heatwave days*. *Darker ribbons* represent the 25th to 75th percentiles of mean *annual number of heatwave days*. *Solid lines* represent the mean *annual number of heatwave days*.

Figure 5: Projected range in the annual number of heatwave days

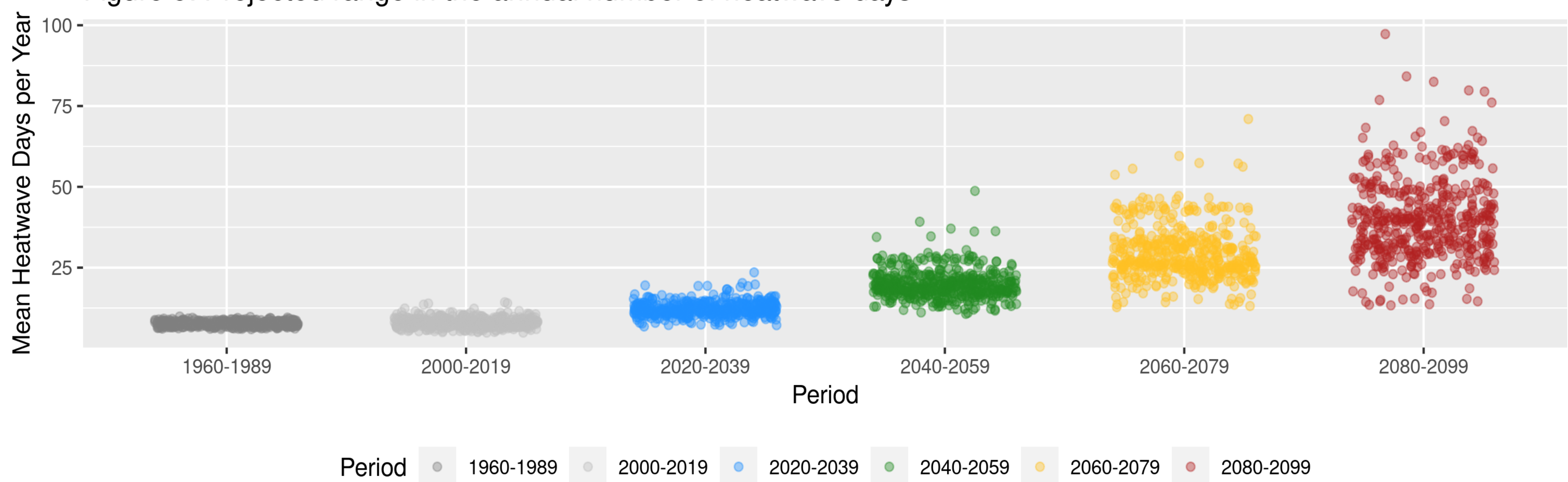


Figure 5: Comparison of the distribution of the *annual number of heatwave days* over the historical period for both model outputs (¡colour¿ and observations (*black*).

Figure 6: Projected mean annual number of hea

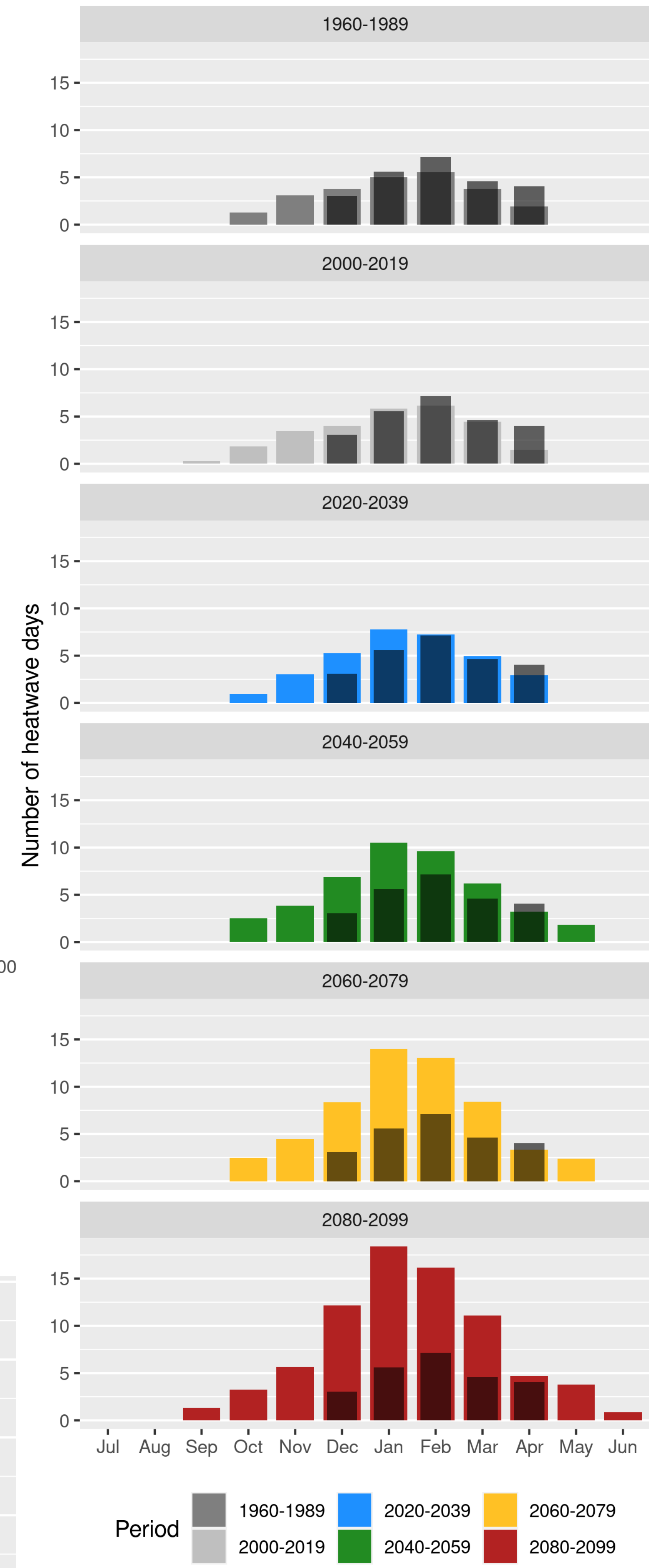


Figure 6: *Bar plots of typical number of heatwave days in each month* for 20-year time periods from 1961 to 2100. Each bar represents the 20-year *typical number of heatwave days in each month*, average across space and time. The observations for the baseline period (1961–1990) are shadowed on top of the future time periods to highlight any differences expected into the future. Higher (lower) bars indicate more (less) heatwave days.

Figure 1: Observed mean *annual number of heatwave days* across all years from 1997–2017.

Figure 2: The change in the mean *annual number of heatwave days* between the current (1997–2017) and historical (1961–1990) periods. Mean *annual number of heatwave days* has increased across the region over recent decades.

Figure 3: Projected mean *annual number of heatwave days* for 20-year time periods from 2001 to 2100. Mean *annual number of heatwave days* is expected to increase steadily into the future. Each grid cell is the mean of the 6 ensemble members.

# NORTH EAST

## Heatwaves — Cumulative Intensity

Figure 1: Observed mean cumulative intensity

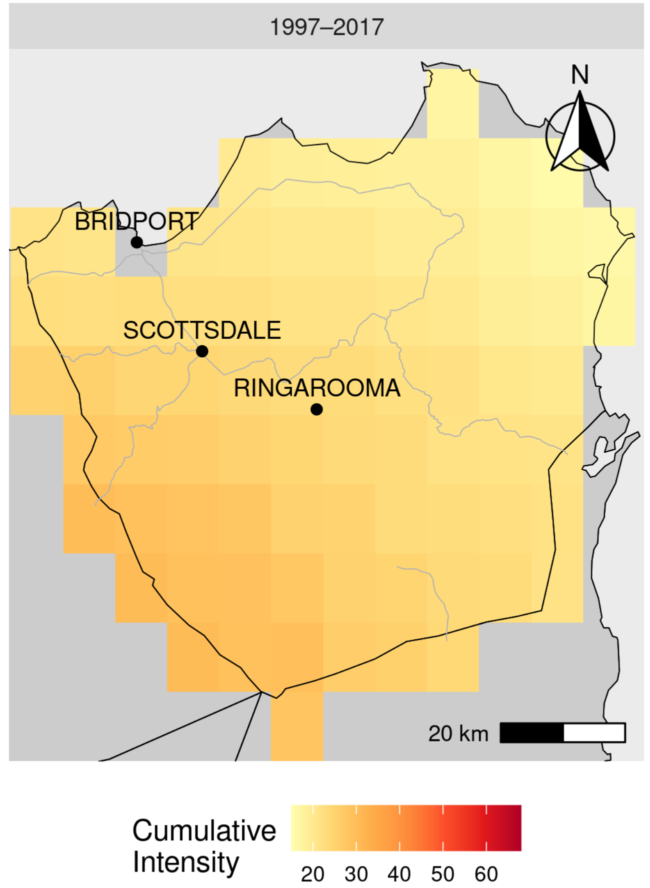


Figure 2: Observed change in mean cumulative intensity

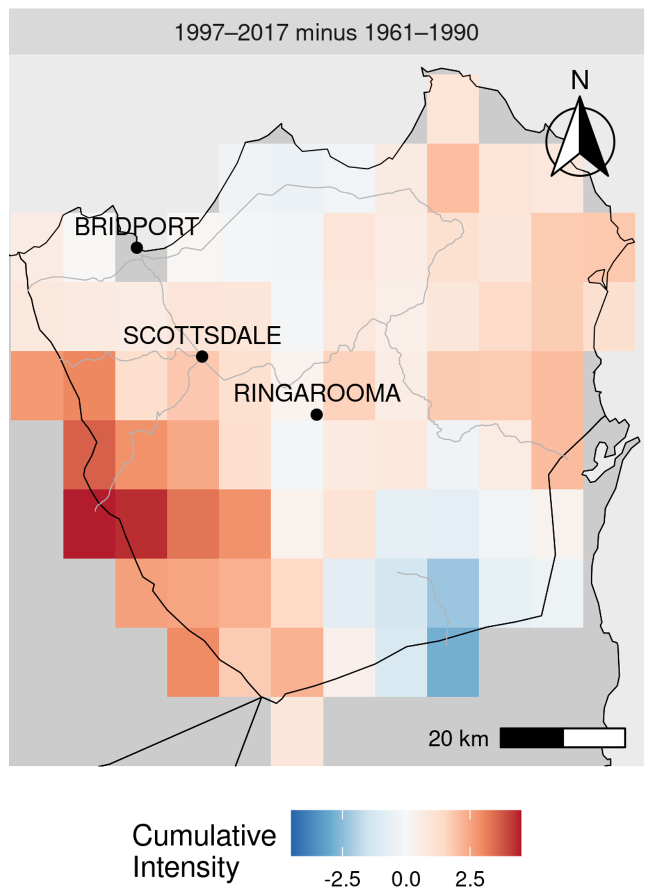


Figure 3: Projected mean cumulative intensity

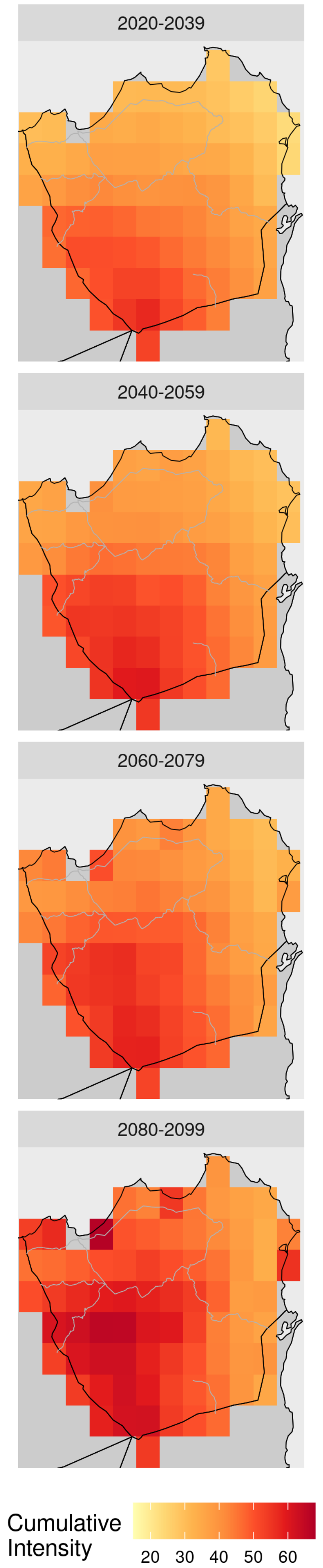


Figure 7: Observed mean *cumulative intensity during a heatwave* across all years from 1997–2017.

Figure 8: The change in mean *cumulative intensity during a heatwave* between the current (1997–2017) and historical (1961–1990) periods. Mean *cumulative intensity during a heatwave* has increased across the region over recent decades.

Figure 9: Projected mean *cumulative intensity during a heatwave* for 20-year time periods from 2001 to 2100. Mean *cumulative intensity during a heatwave* is expected to increase steadily into the future. Each grid cell is the mean of the 6 ensemble members.

Figure 10: Projected cumulative intensity

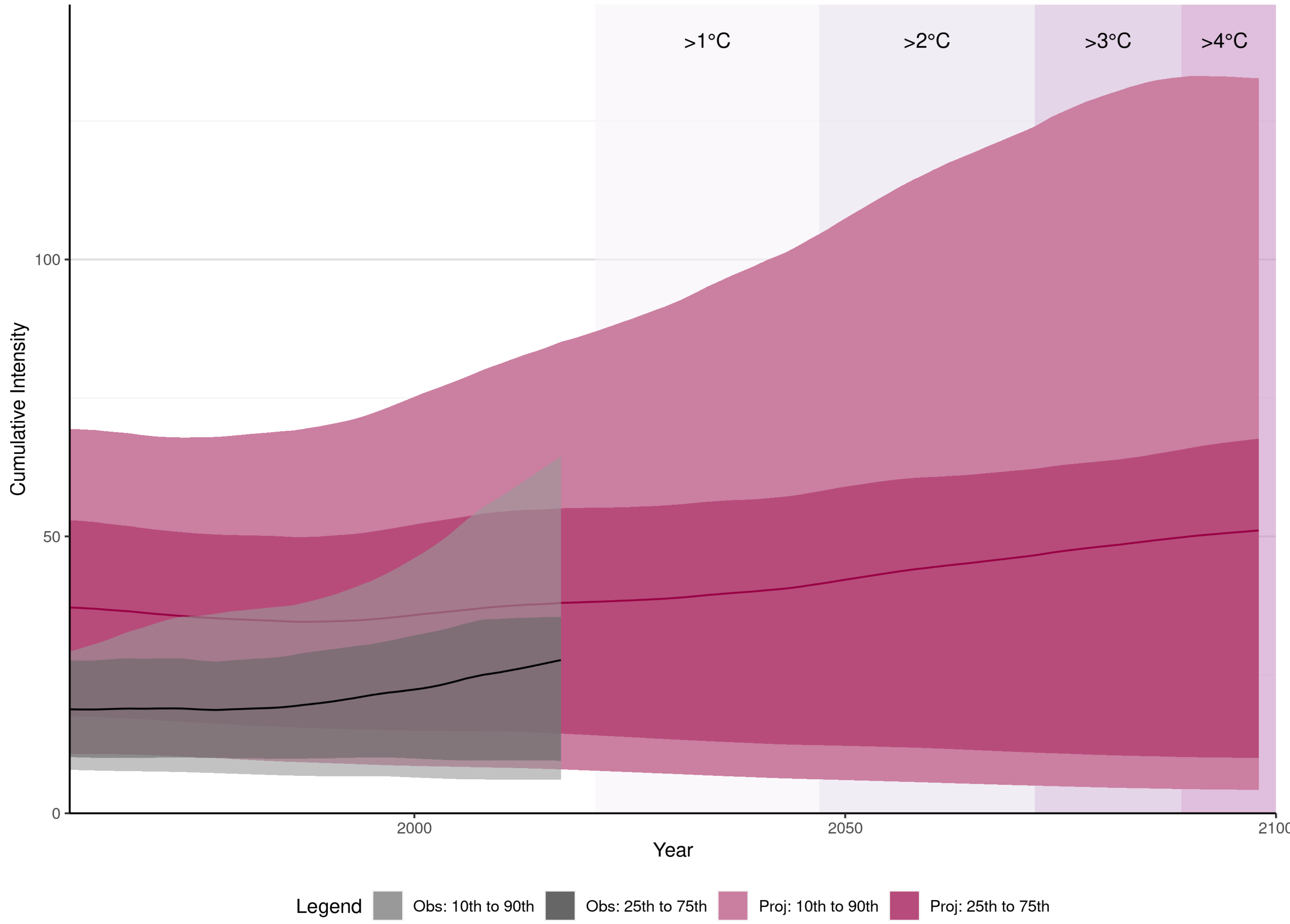


Figure 10: Projected change in *cumulative intensity during a heatwave* from 1990 to 2100. Historical values are the 30-year rolling means from AGCD (*grey*). Projected values (*peach*) are the ensemble mean of the 30-year rolling mean of each ensemble member. *Lighter ribbons* represent the 10th to 90th percentiles of *cumulative intensity during a heatwave. Darker ribbons* represent the 25th to 75th percentiles of *cumulative intensity during a heatwave. Solid lines* represent the mean of *cumulative intensity during a heatwave.*

Figure 11: Distribution of cumulative intensity

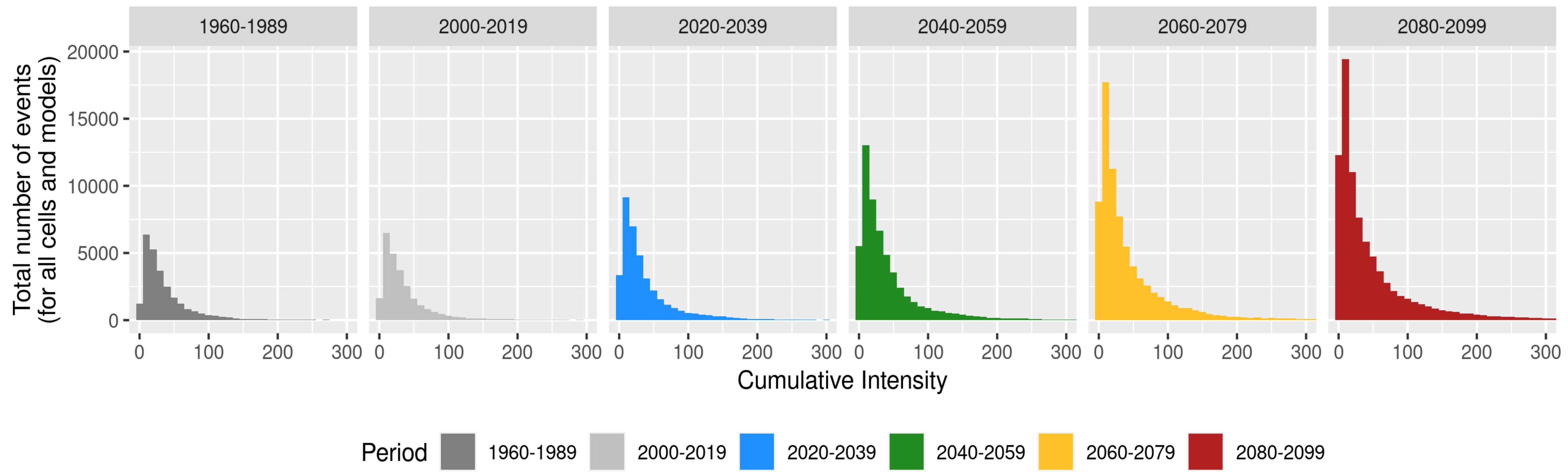


Figure 11: Comparison of the distribution of *cumulative intensity during a heatwave* for different time periods.

Figure 12: Projected mean cumulative intensity

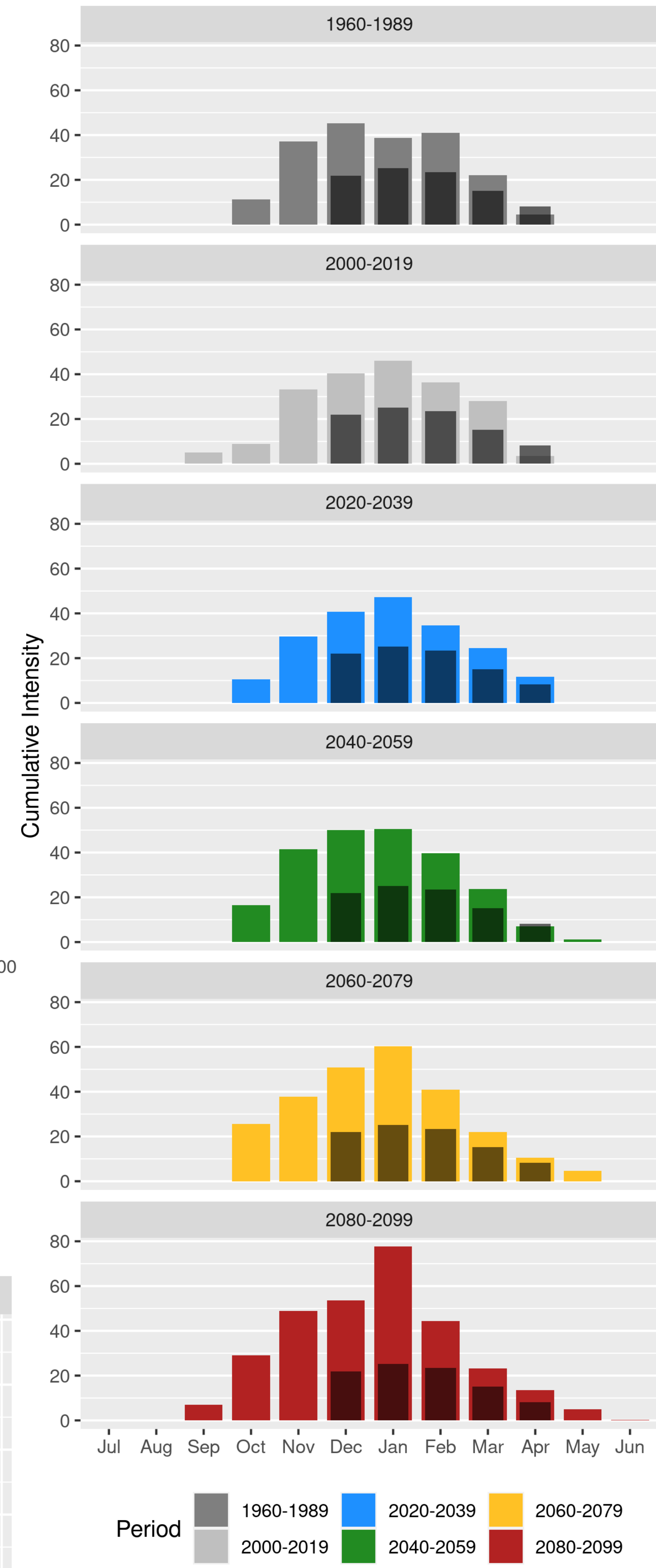


Figure 12: *Bar plots of cumulative intensity during heatwaves* in each month for 20-year time periods from 1961 to 2100. Each bar represents the 20-year mean of *cumulative intensity during a heatwave*, average across space and time. The observations for the baseline period (1961–1990) are shadowed on top of the future time periods to highlight any differences expected into the future. Higher (lower) bars indicate hotter (cooler) heatwave intensities.

# NORTH EAST

## Heatwaves — Duration

Figure 1: Observed mean duration

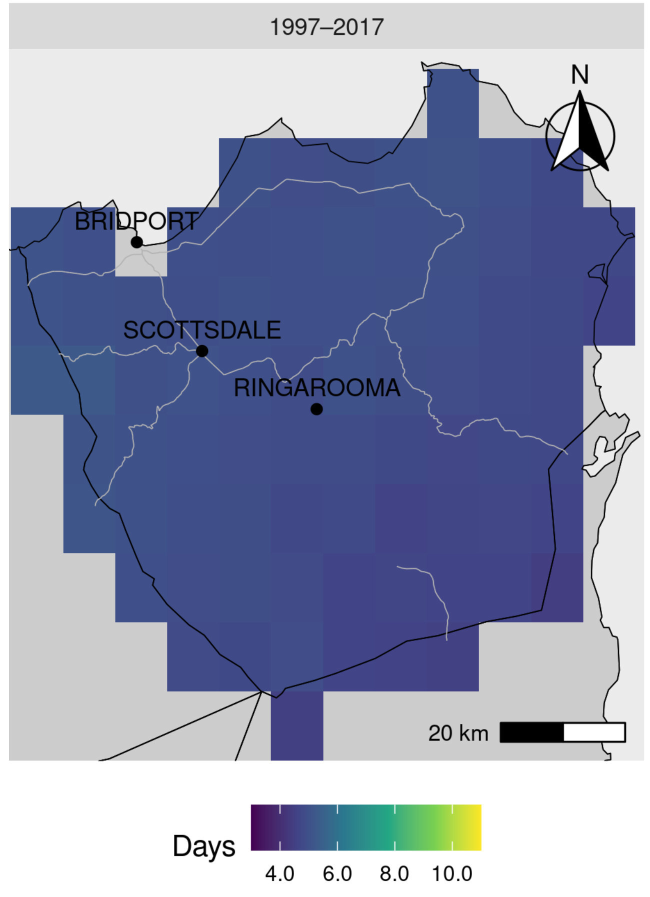


Figure 2: Observed change in mean duration

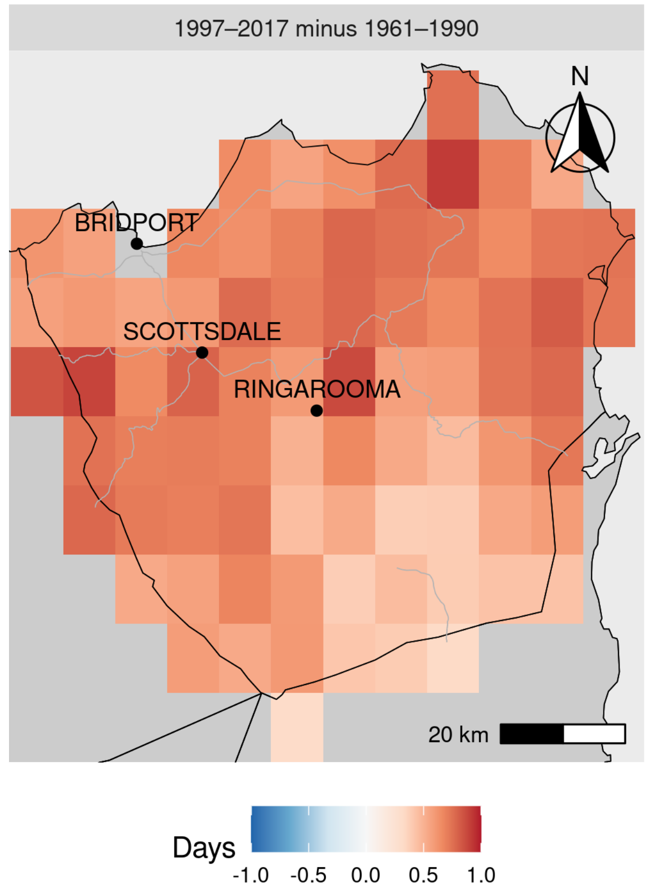


Figure 13: Observed mean *heatwave durations* across all years from 1997–2017.

Figure 14: The change in mean *heatwave duration* between the current (1997–2017) and historical (1961–1990) periods. Mean *heatwave durations* have increased across the region over recent decades.

Figure 15: Projected mean *heatwave durations* for 20-year time periods from 2001 to 2100. Mean *heatwave duration* is expected to increase steadily into the future. Each grid cell is the mean of the 6 ensemble members.

Figure 3: Projected mean duration

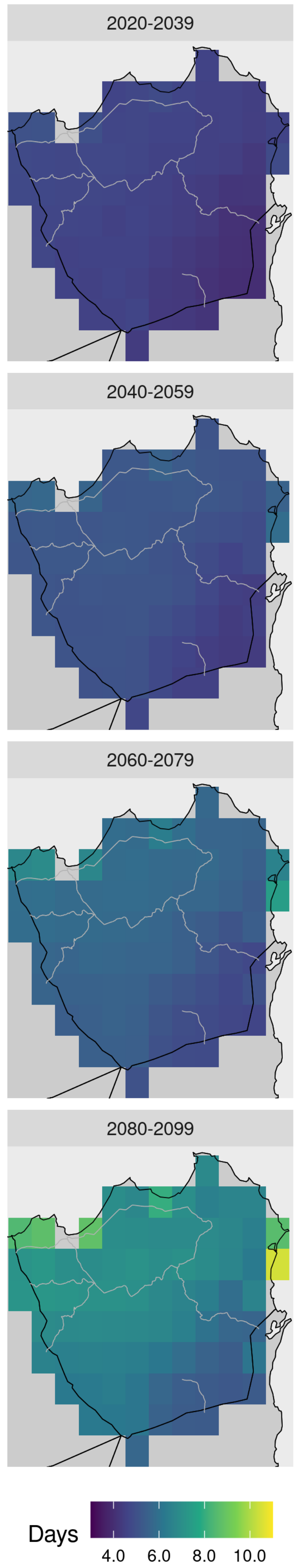


Figure 16: Projected heatwave duration

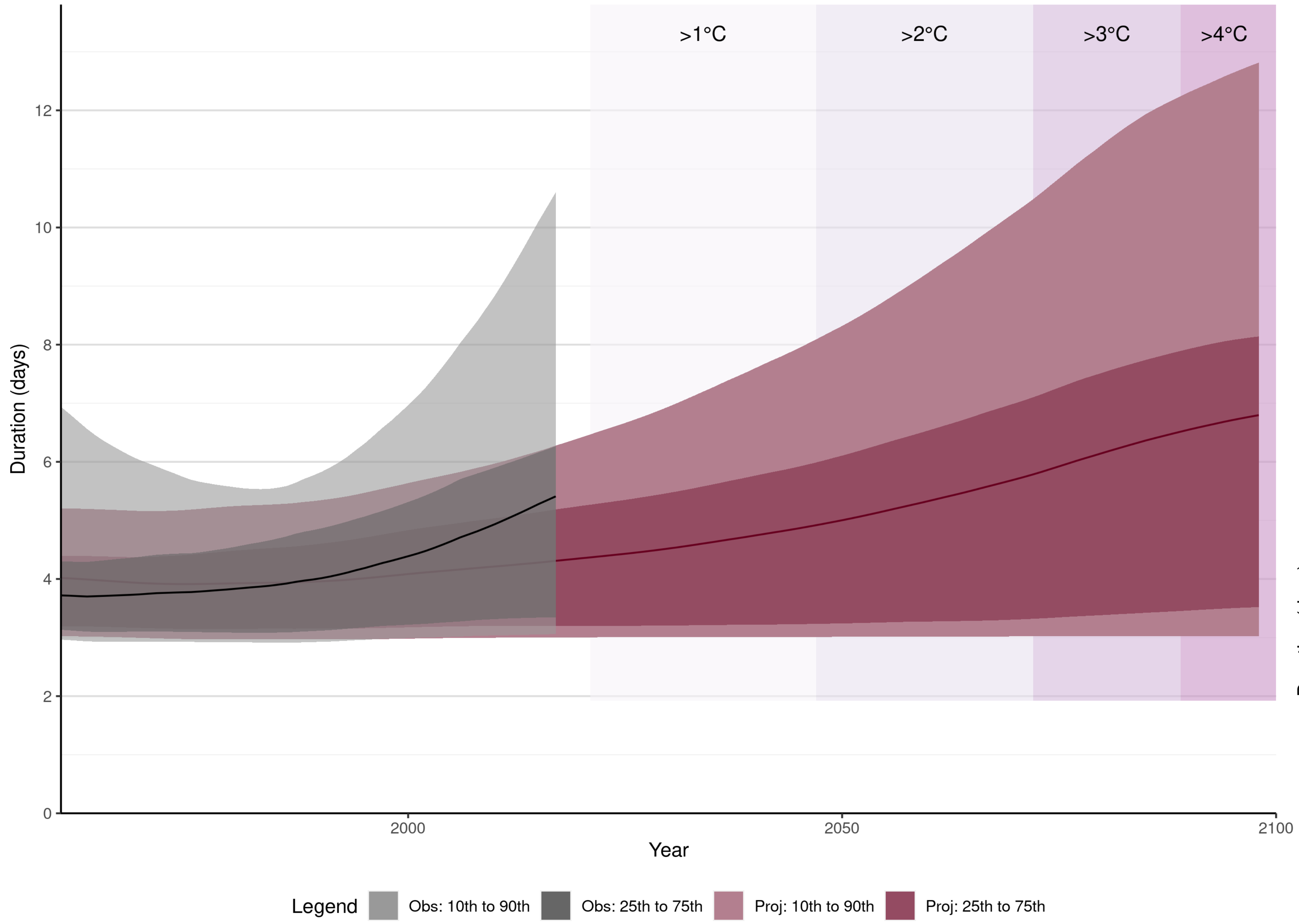


Figure 16: Projected change in *heatwave duration* from 1990 to 2100. Historical values (*grey*) are the 30-year rolling means of AGCD. Projected values (*orange*) are the ensemble mean of the 30-year rolling mean of each CCAM ensemble member. *Lighter ribbons* represent the 10th to 90th percentiles of *heatwave duration*. *Darker ribbons* represent the 25th to 75th percentiles of *heatwave duration*. *Solid lines* represent the mean of *heatwave duration*.

Figure 17: Projected count of heatwave duration

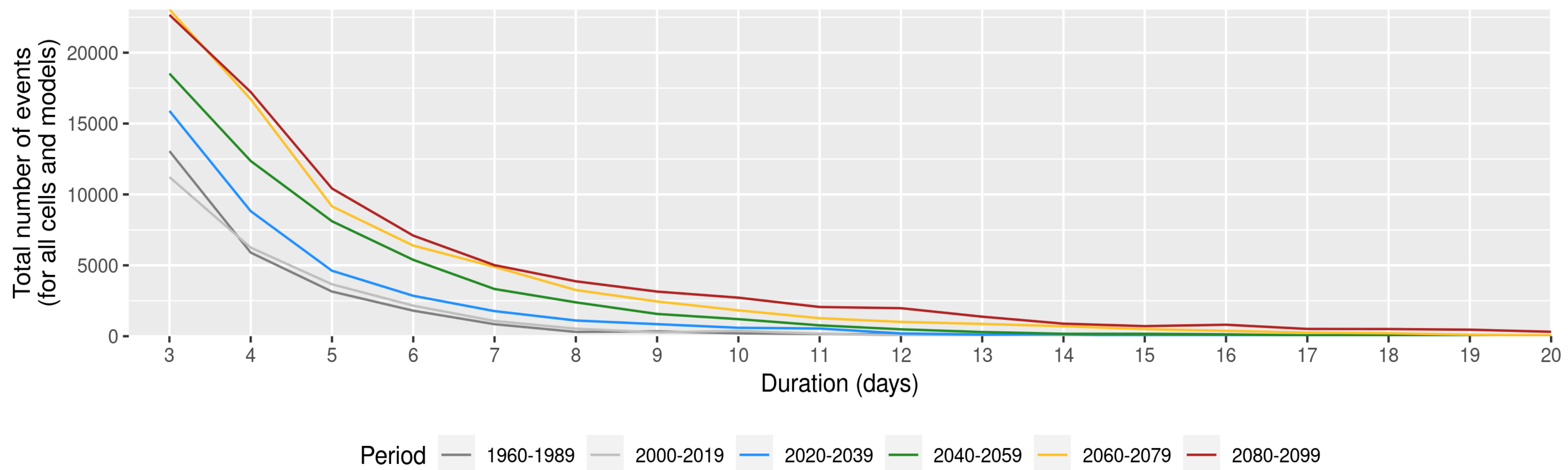


Figure 17: Comparison of the distribution of *heatwave durations* for different time periods.

Figure 18: Projected mean heatwave duration by

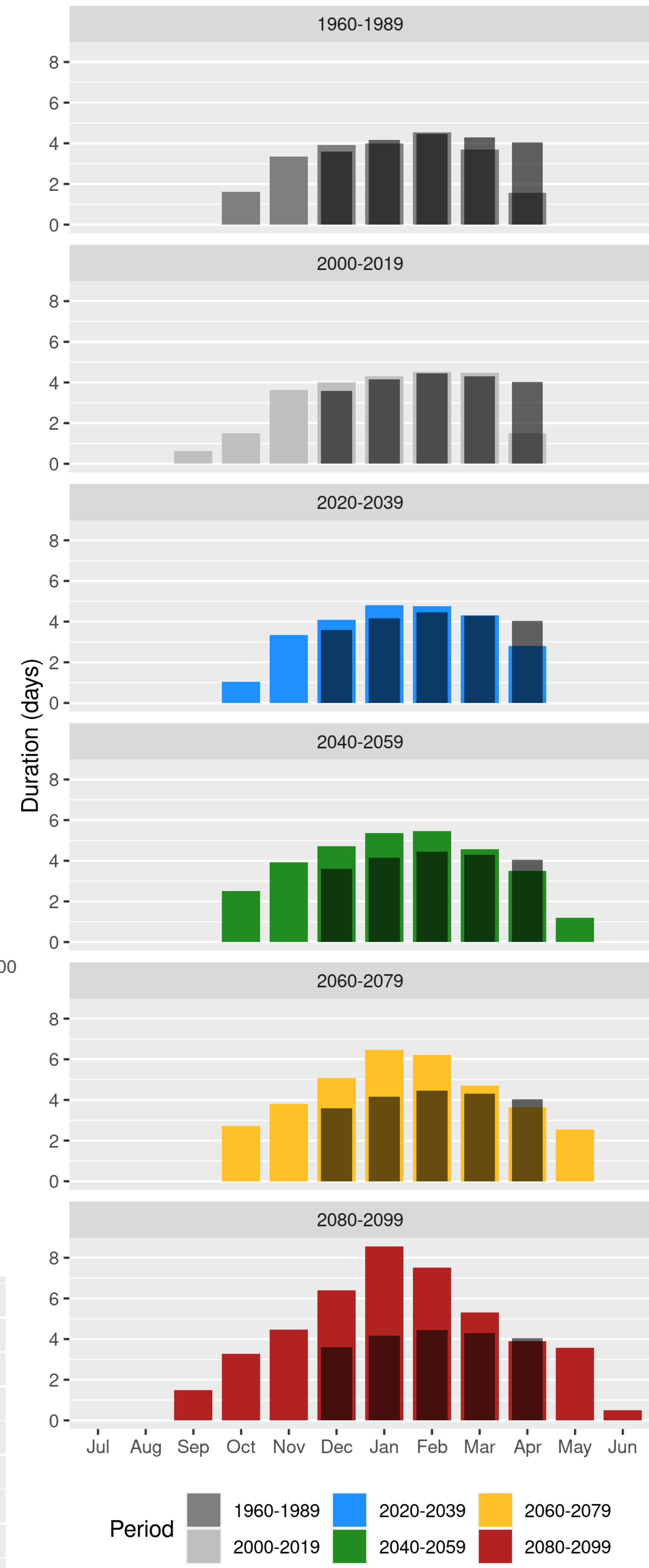


Figure 18: *Bar plots* of mean *heatwave durations* in each month for 20-year time periods from 1961 to 2100. Each bar represents the 20-year mean of *heatwave durations*, average across space and time. The observations for the baseline period (1961–1990) are shadowed on top of the future time periods to highlight any differences expected into the future. Higher (lower) bars indicate longer (shorter) *heatwave durations*.

Figure 1: Observed nean annual number of heatwave days

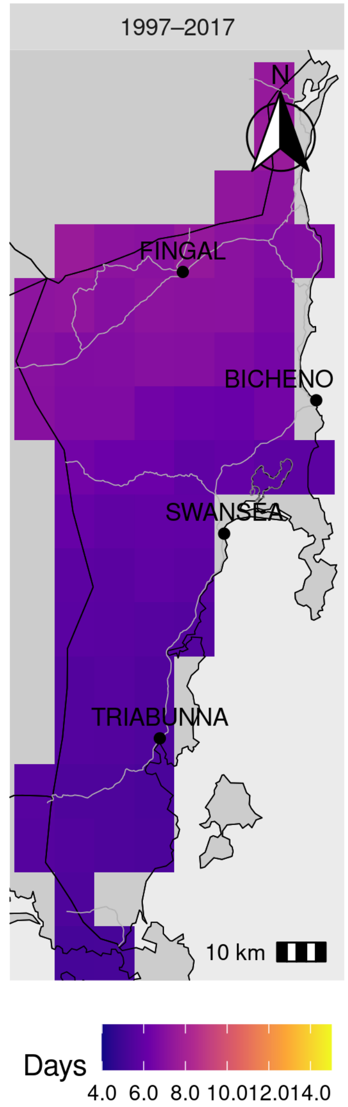


Figure 2: Observed change in mean annual number of heatwave day

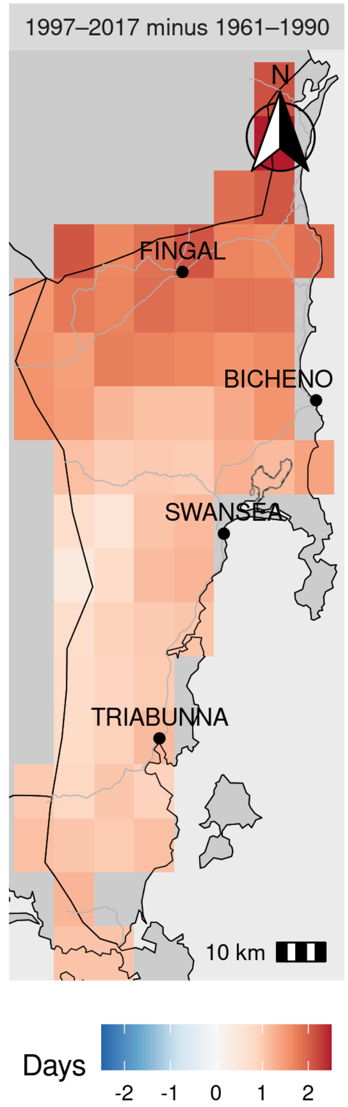


Figure 3: Projected mean annual number of heatwave days

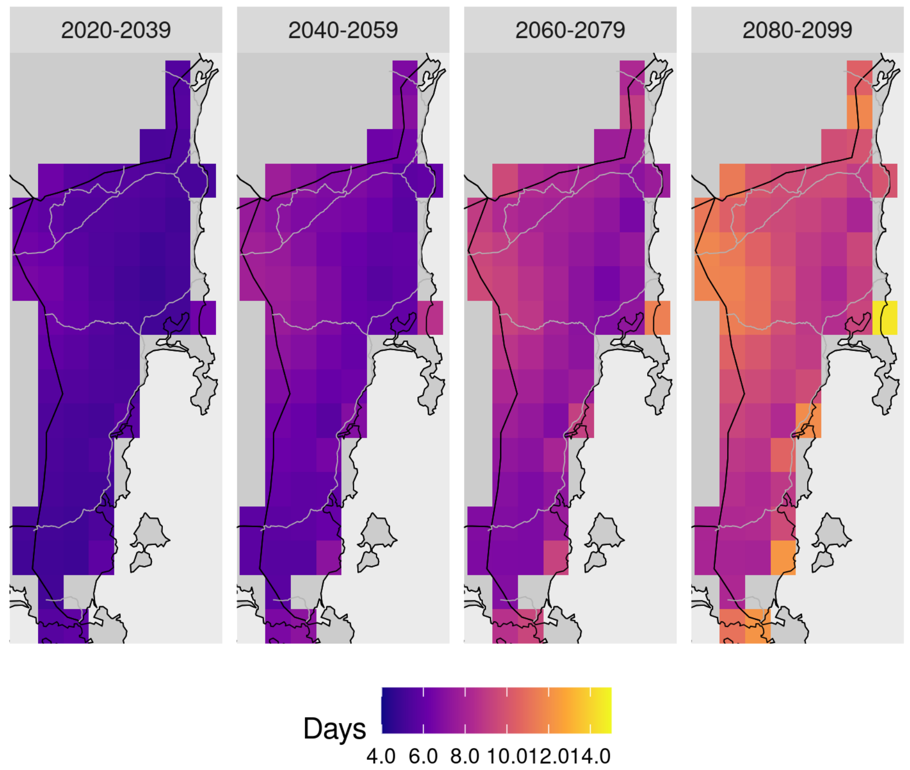


Figure 1: Observed mean *annual number of heatwave days* across all years from 1997–2017.

Figure 2: The change in the mean *annual number of heatwave days* between the current (1997–2017) and historical (1961–1990) periods. Mean *annual number of heatwave days* has increased across the region over recent decades.

Figure 3: Projected mean *annual number of heatwave days* for 20-year time periods from 2001 to 2100. Mean *annual number of heatwave days* is expected to increase steadily into the future. Each grid cell is the mean of the 6 ensemble members.

Figure 4: Projected annual number of heatwave days from 1961 to 2100

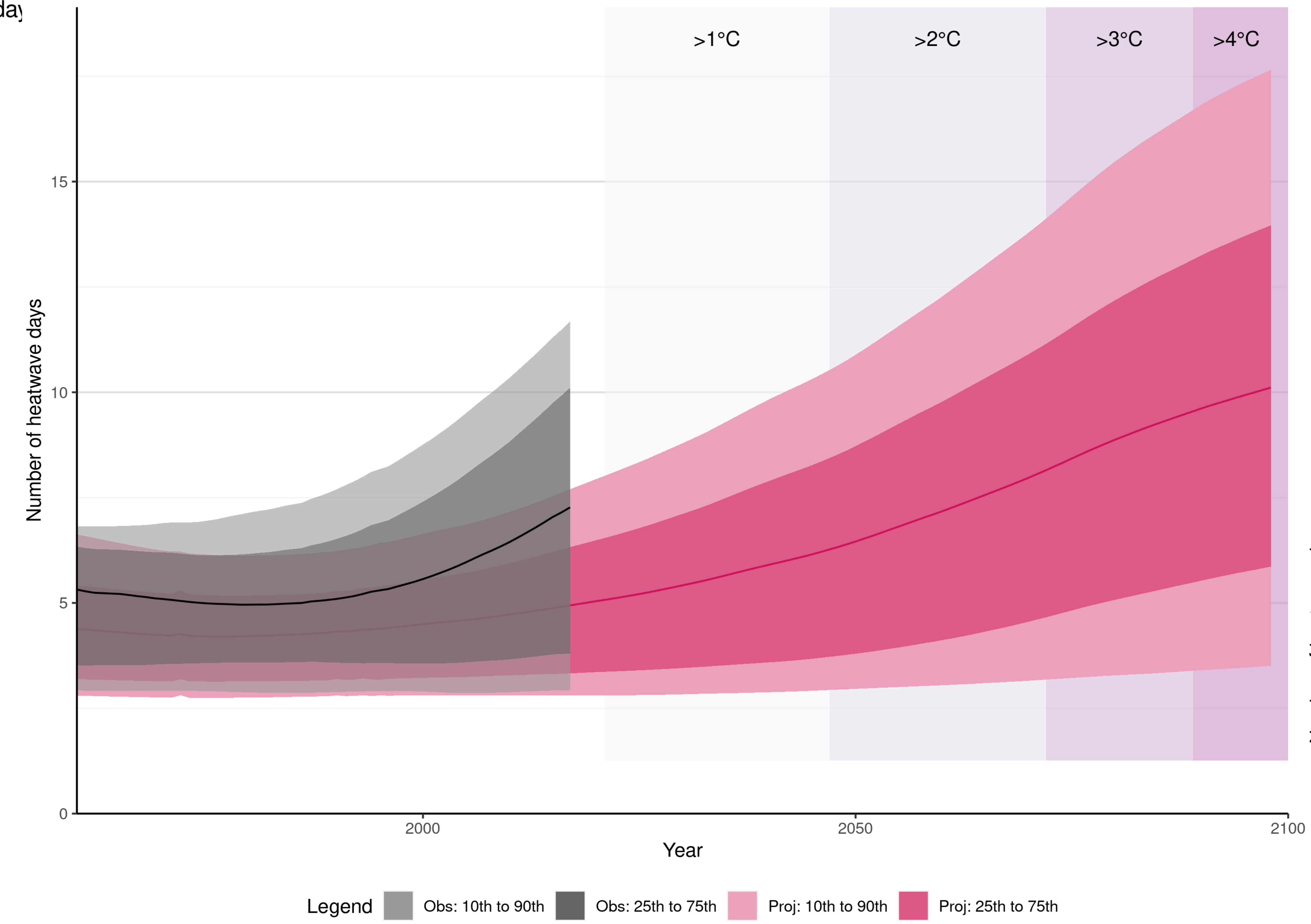


Figure 4: Projected change in mean *annual number of heatwave days* from 1990 to 2100. Historical values (*grey*) are the 30-year rolling means of AGCD. Projected values (*peach*) are the ensemble mean of the 30-year rolling mean of each CCAM ensemble member. *Lighter ribbons* represent the 10th to 90th percentiles of mean *annual number of heatwave days*. *Darker ribbons* represent the 25th to 75th percentiles of mean *annual number of heatwave days*. *Solid lines* represent the mean *annual number of heatwave days*.

Figure 5: Projected range in the annual number of heatwave days

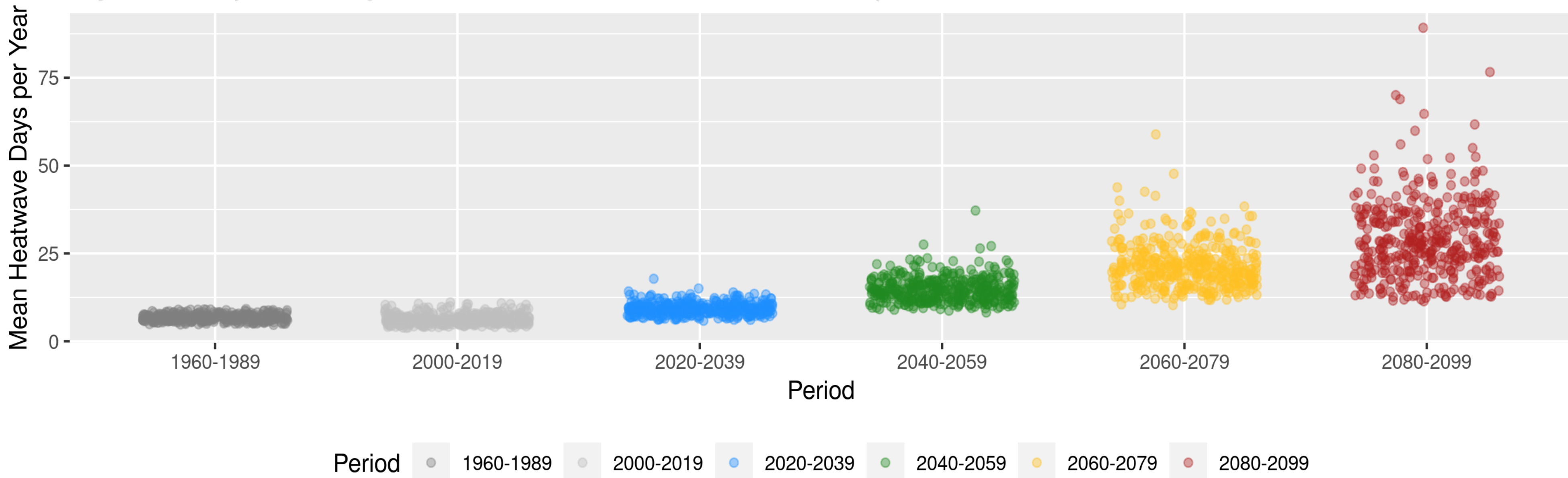


Figure 5: Comparison of the distribution of the *annual number of heatwave days* over the historical period for both model outputs (¡colour¿ and observations (*black*).

Figure 6: Projected mean annual number of hea

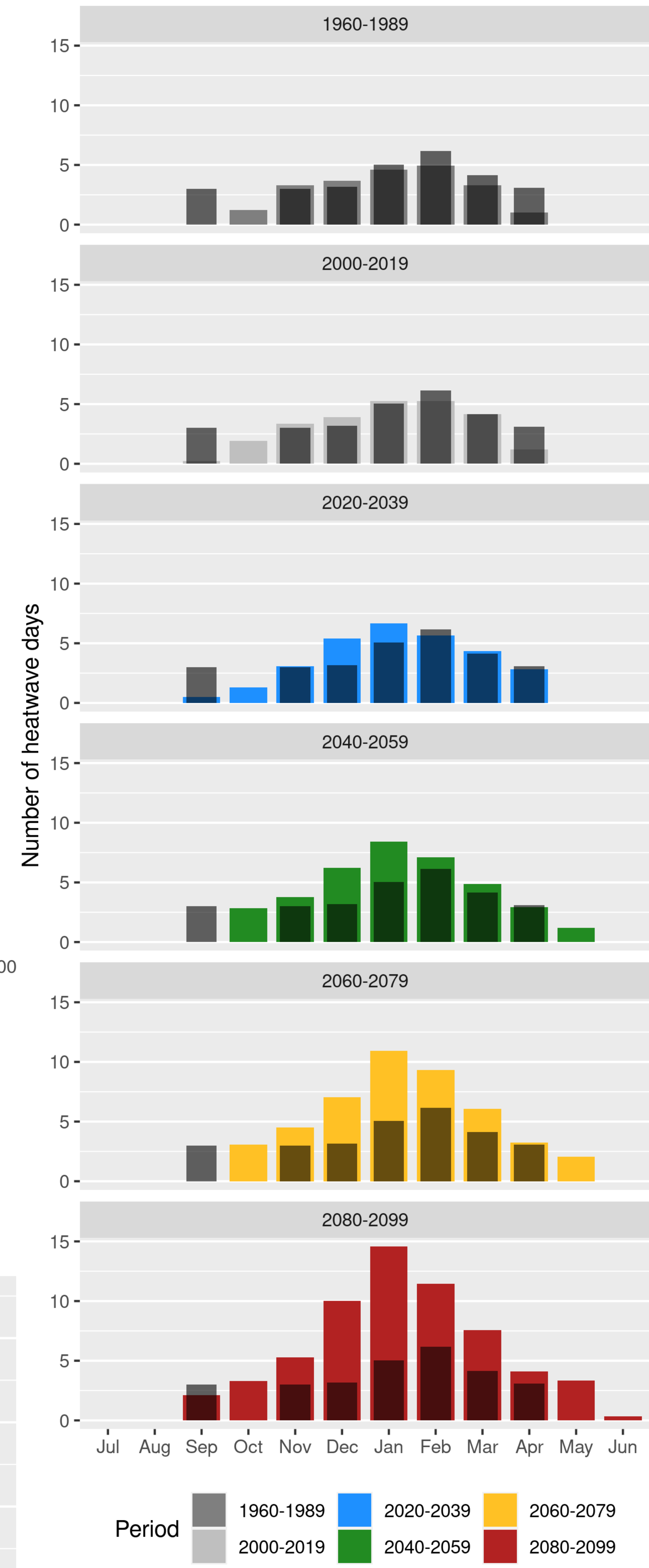


Figure 6: *Bar plots of typical number of heatwave days in each month* for 20-year time periods from 1961 to 2100. Each bar represents the 20-year *typical number of heatwave days in each month*, average across space and time. The observations for the baseline period (1961–1990) are shadowed on top of the future time periods to highlight any differences expected into the future. Higher (lower) bars indicate more (less) heatwave days.

# EAST COAST

## Heatwaves — Cumulative Intensity

Figure 1: Observed mean cumulative intensity

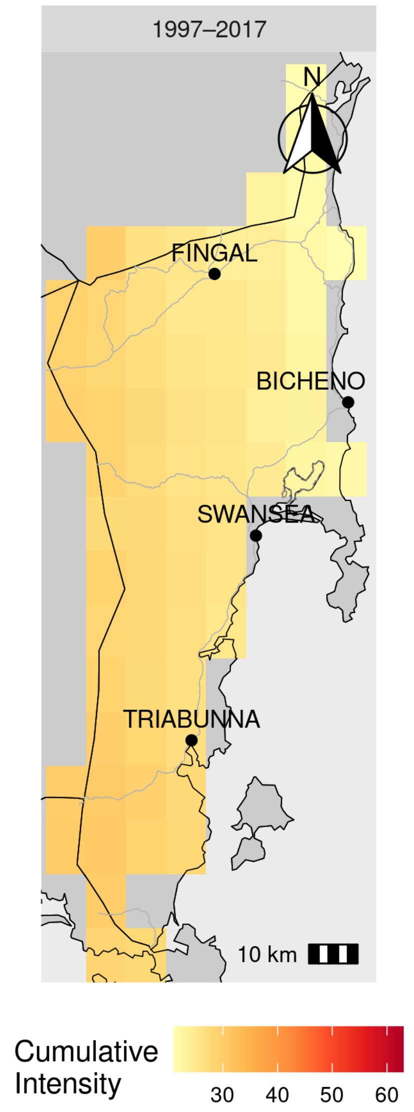


Figure 2: Observed change in mean cumulative intensity

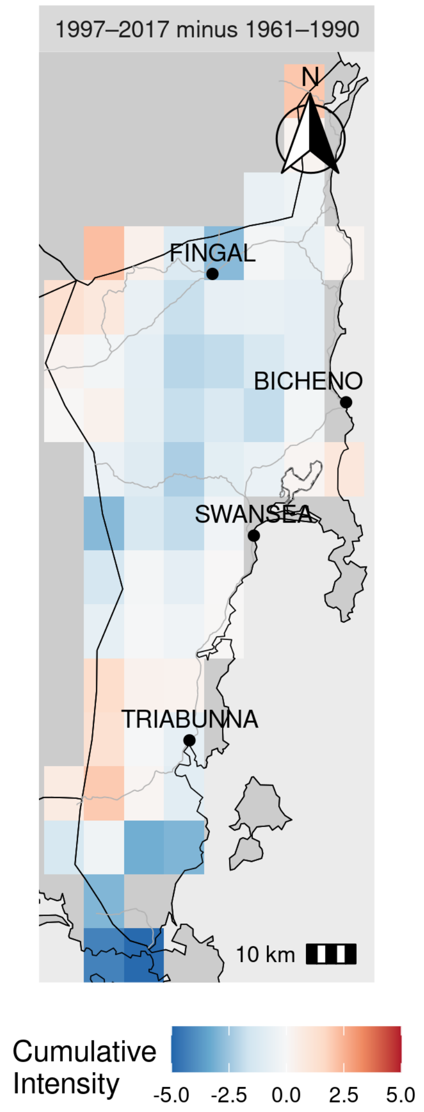


Figure 3: Projected mean cumulative intensity

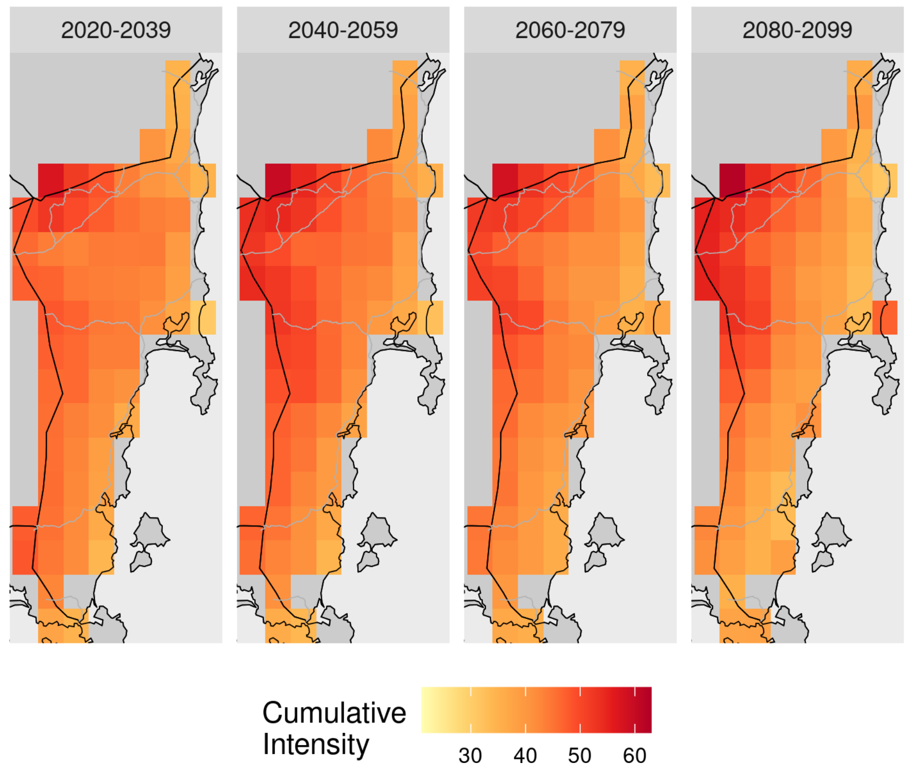


Figure 7: Observed mean *cumulative intensity during a heatwave* across all years from 1997–2017.

Figure 8: The change in mean *cumulative intensity during a heatwave* between the current (1997–2017) and historical (1961–1990) periods. Mean *cumulative intensity during a heatwave* has increased across the region over recent decades.

Figure 9: Projected mean *cumulative intensity during a heatwave* for 20-year time periods from 2001 to 2100. Mean *cumulative intensity during a heatwave* is expected to increase steadily into the future. Each grid cell is the mean of the 6 ensemble members.

Figure 10: Projected cumulative intensity

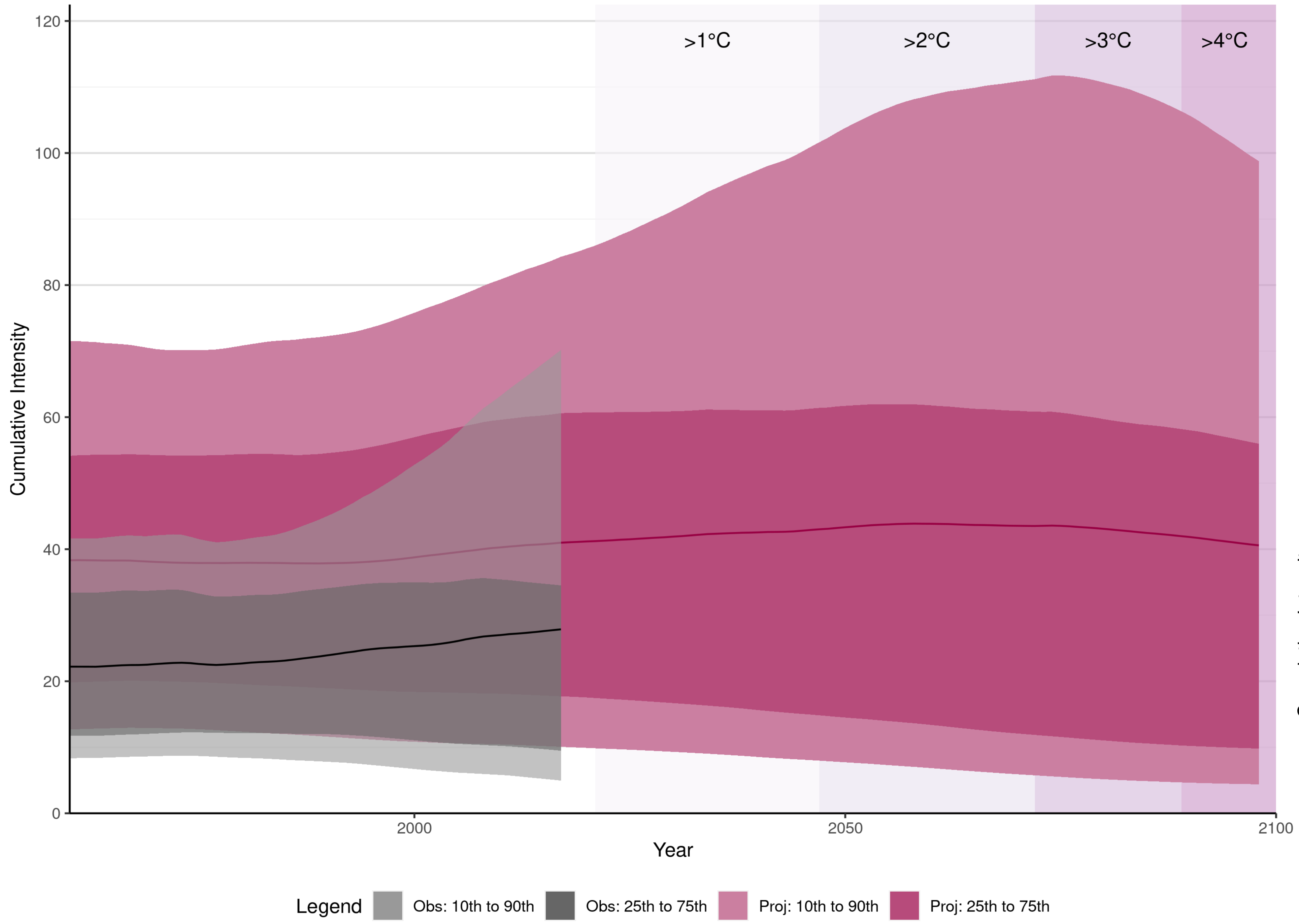


Figure 10: Projected change in *cumulative intensity during a heatwave* from 1990 to 2100. Historical values are the 30-year rolling means from AGCD (*grey*). Projected values (*peach*) are the ensemble mean of the 30-year rolling mean of each ensemble member. *Lighter ribbons* represent the 10th to 90th percentiles of *cumulative intensity during a heatwave*. *Darker ribbons* represent the 25th to 75th percentiles of *cumulative intensity during a heatwave*. *Solid lines* represent the mean of *cumulative intensity during a heatwave*.

Figure 11: Distribution of cumulative intensity

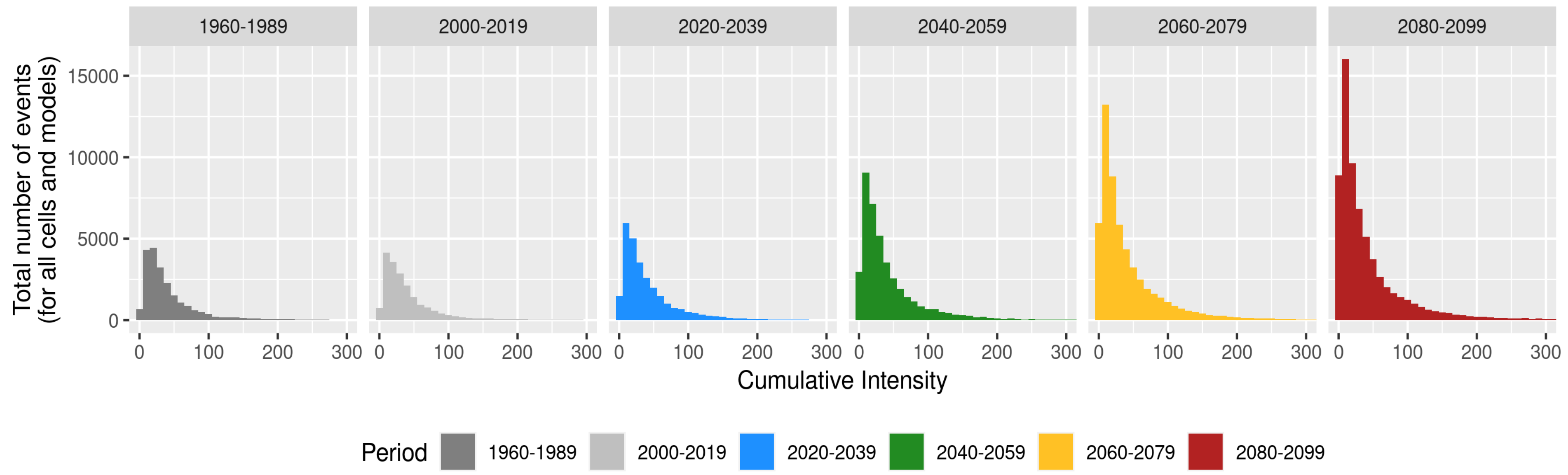


Figure 11: Comparison of the distribution of *cumulative intensity during a heatwave* for different time periods.

Figure 12: Projected mean cumulative intensity

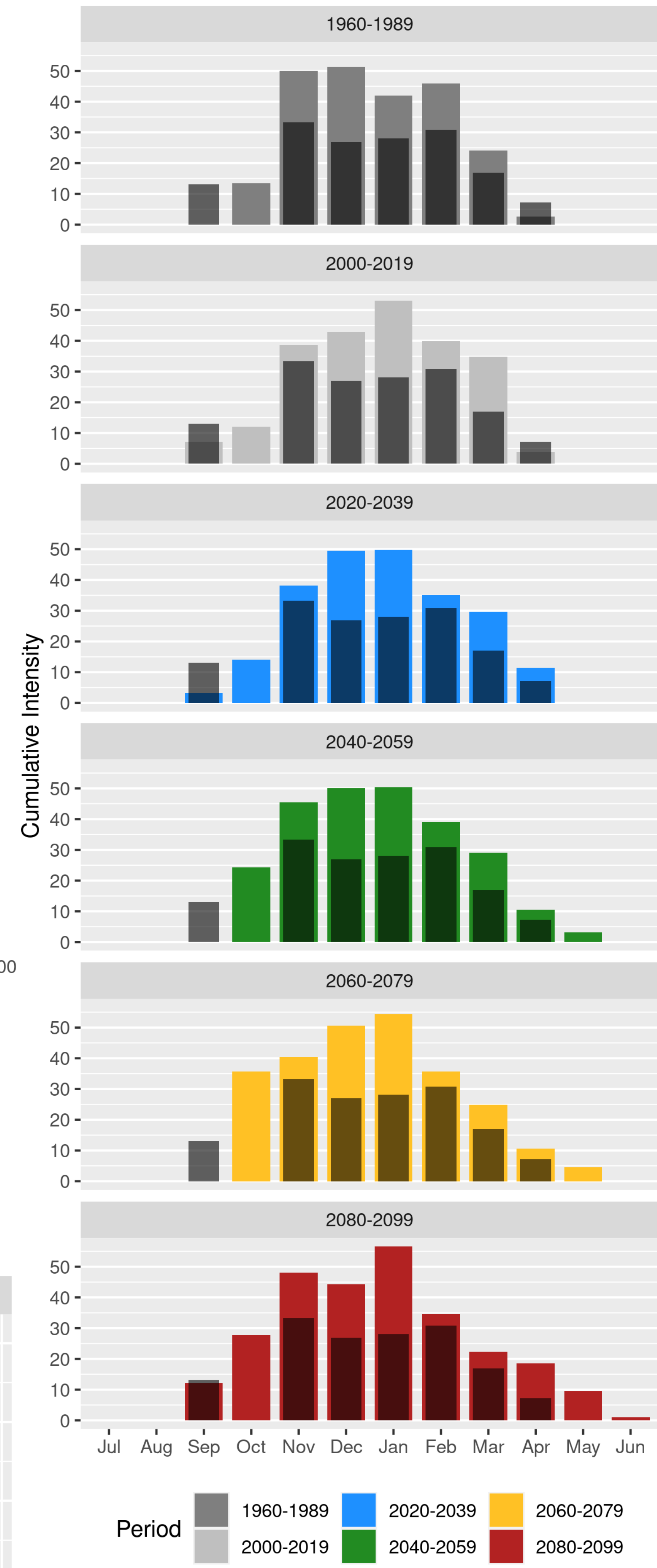


Figure 12: *Bar plots of cumulative intensity during heatwaves* in each month for 20-year time periods from 1961 to 2100. Each bar represents the 20-year mean of *cumulative intensity during a heatwave*, average across space and time. The observations for the baseline period (1961–1990) are shadowed on top of the future time periods to highlight any differences expected into the future. Higher (lower) bars indicate hotter (cooler) heatwave intensities.

# EAST COAST

## Heatwaves — Duration

Figure 1: Observed mean duration

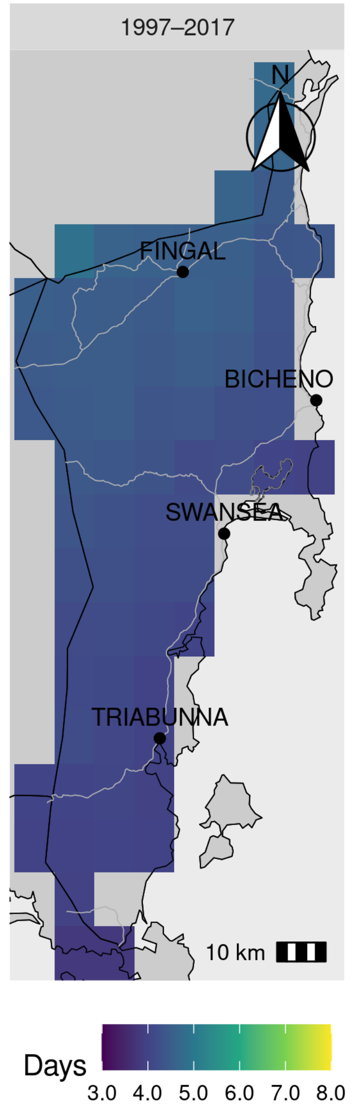


Figure 2: Observed change in mean duration

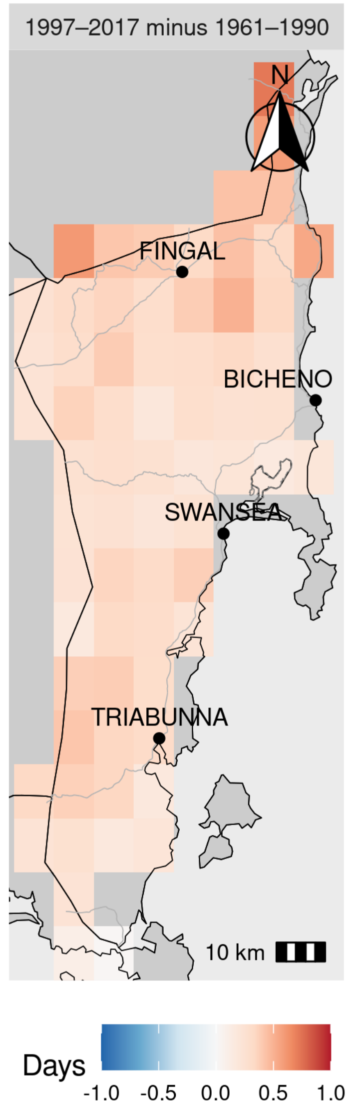


Figure 16: Projected heatwave duration

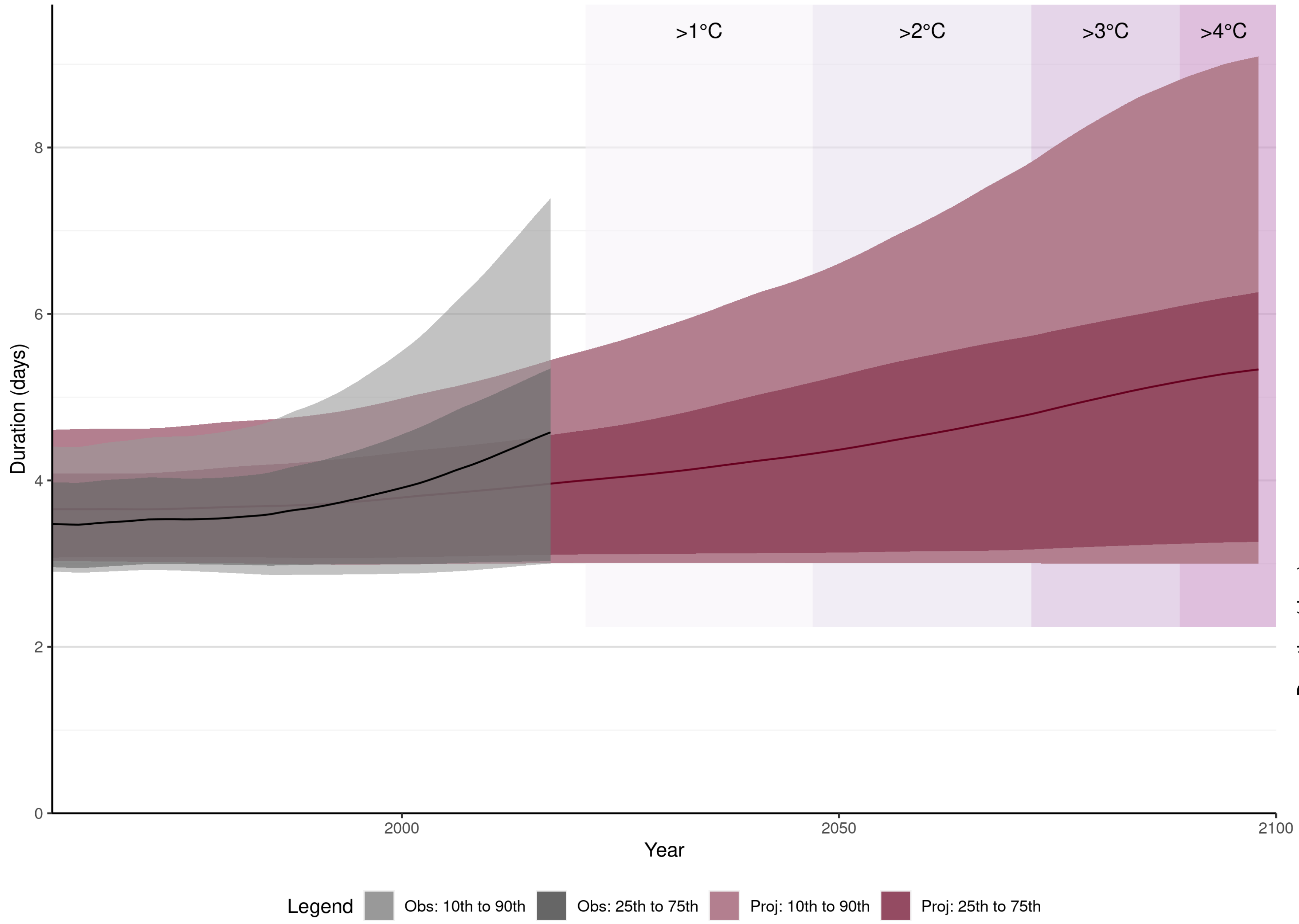


Figure 16: Projected change in *heatwave duration* from 1990 to 2100. Historical values (*grey*) are the 30-year rolling means of AGCD. Projected values (*orange*) are the ensemble mean of the 30-year rolling mean of each CCAM ensemble member. *Lighter ribbons* represent the 10th to 90th percentiles of *heatwave duration*. *Darker ribbons* represent the 25th to 75th percentiles of *heatwave duration*. *Solid lines* represent the mean of *heatwave duration*.

Figure 18: Projected mean heatwave duration by

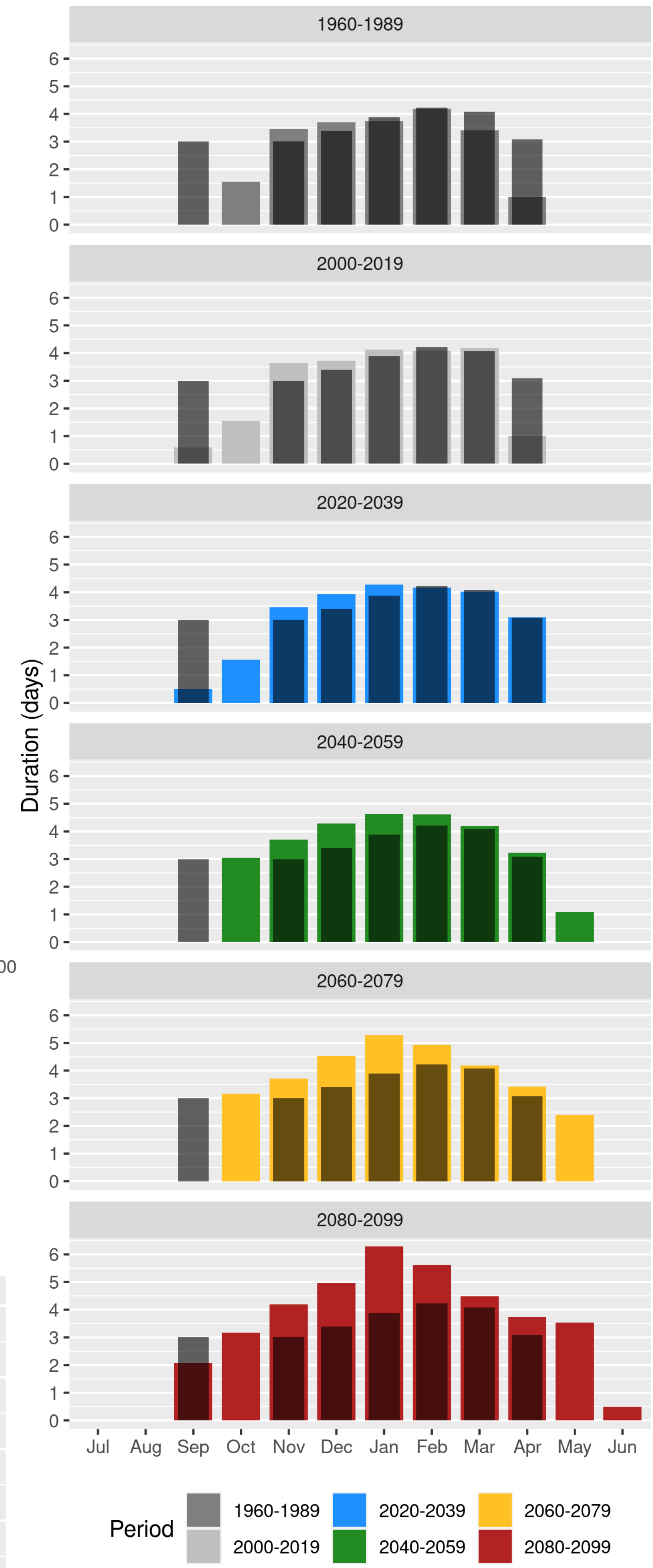


Figure 18: *Bar plots* of mean *heatwave durations* in each month for 20-year time periods from 1961 to 2100. Each bar represents the 20-year mean of *heatwave durations*, average across space and time. The observations for the baseline period (1961–1990) are shadowed on top of the future time periods to highlight any differences expected into the future. Higher (lower) bars indicate longer (shorter) *heatwave durations*.

Figure 3: Projected mean duration

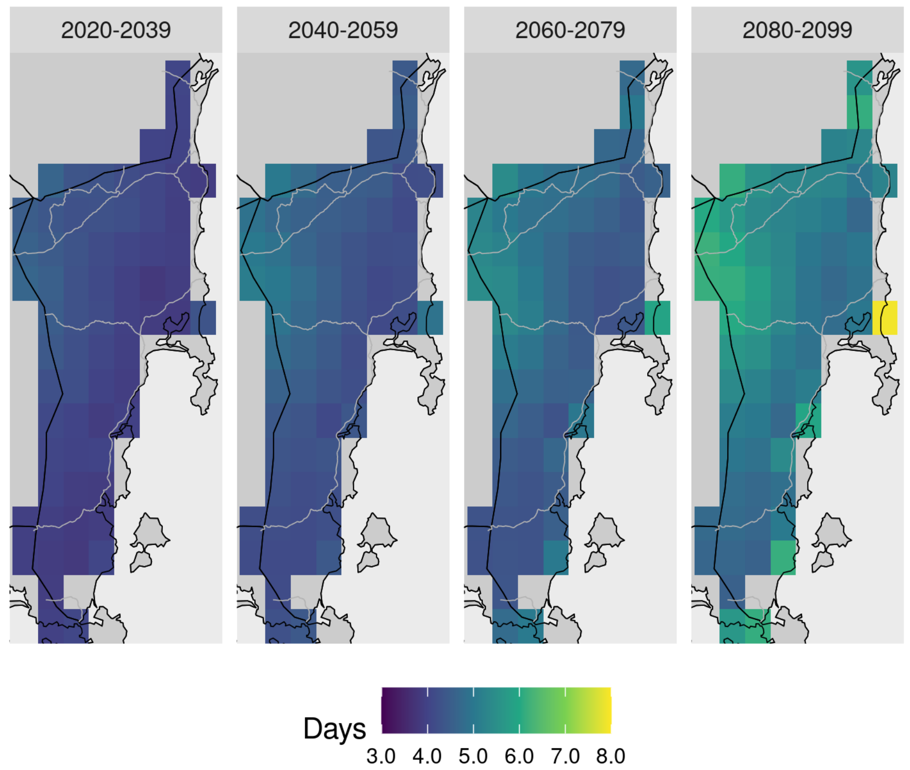


Figure 17: Projected count of heatwave duration

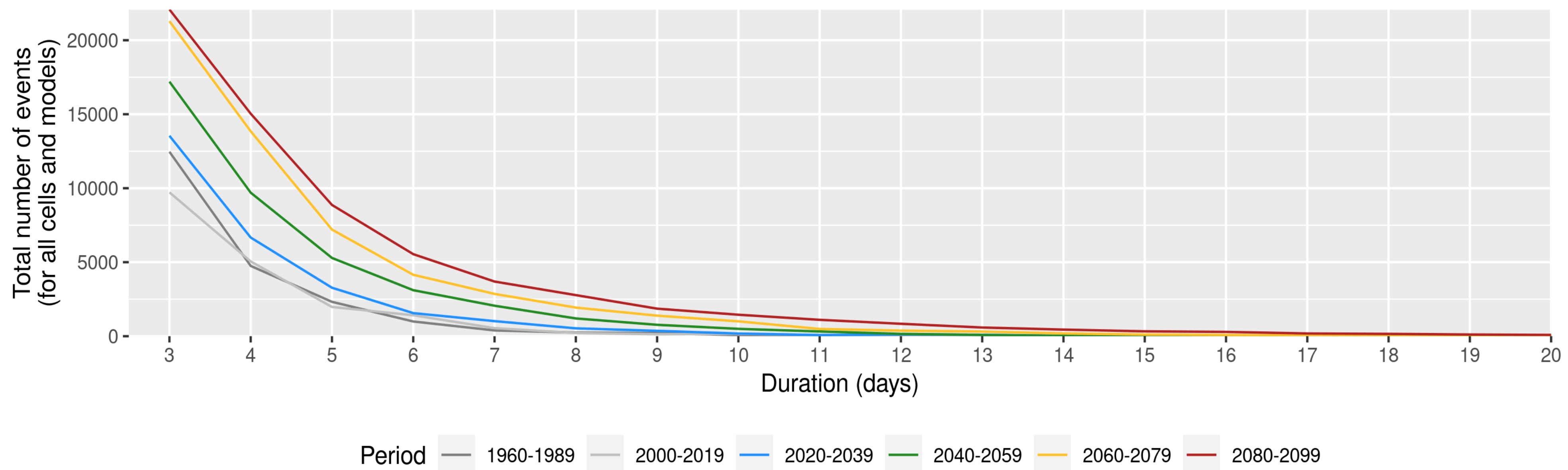


Figure 17: Comparison of the distribution of *heatwave durations* for different time periods.

Figure 13: Observed mean *heatwave durations* across all years from 1997–2017.

Figure 14: The change in mean *heatwave duration* between the current (1997–2017) and historical (1961–1990) periods. Mean *heatwave durations* have increased across the region over recent decades.

Figure 15: Projected mean *heatwave durations* for 20-year time periods from 2001 to 2100. Mean *heatwave duration* is expected to increase steadily into the future. Each grid cell is the mean of the 6 ensemble members.

# CENTRAL NORTH

## Heatwaves — Number of Heatwave Days

### Figure 1: Observed mean annual number of heatwave days

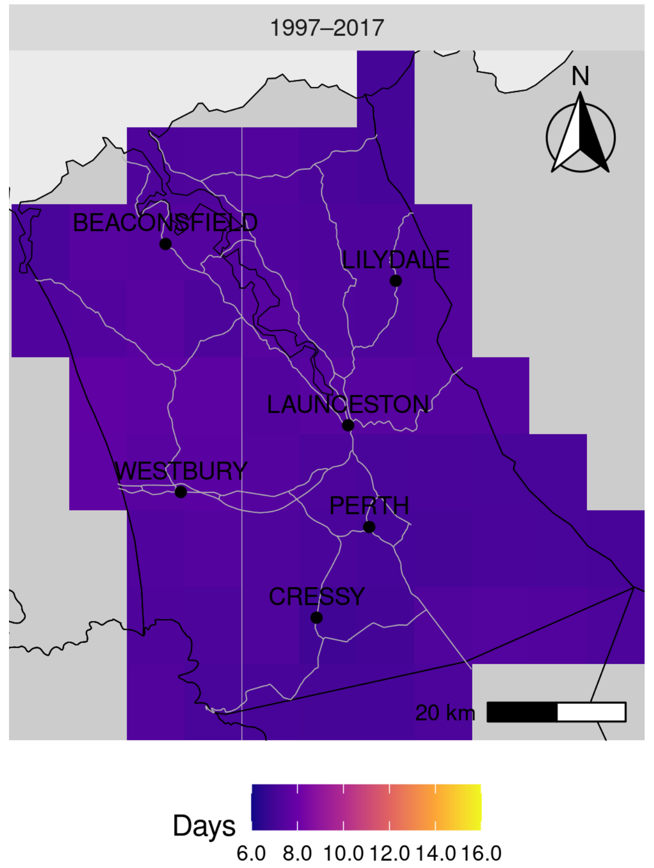


### Figure 2: Observed change in mean annual number of heatwave days

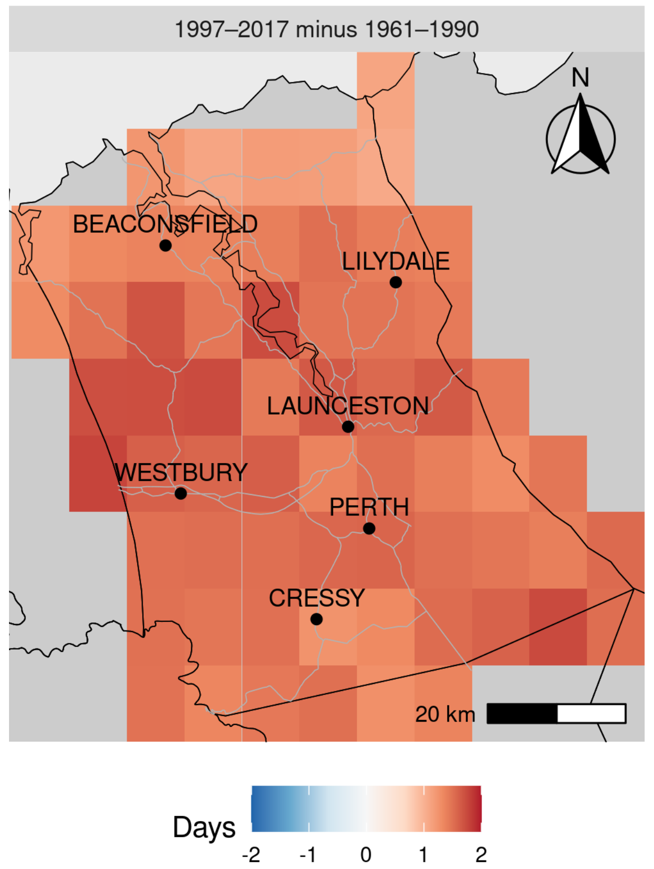


### Figure 3: Projected mean annual number of heatwave day

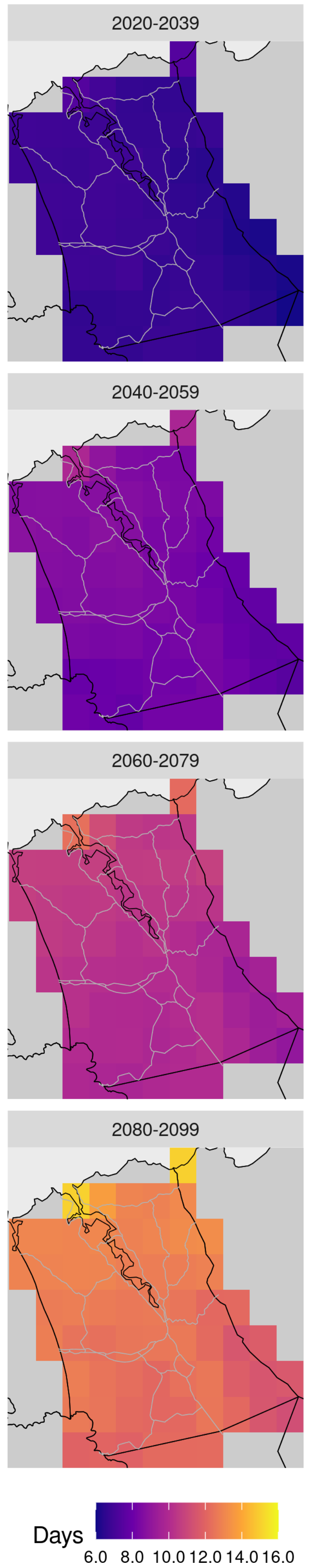


### Figure 4: Projected annual number of heatwave days from 1961 to 2100

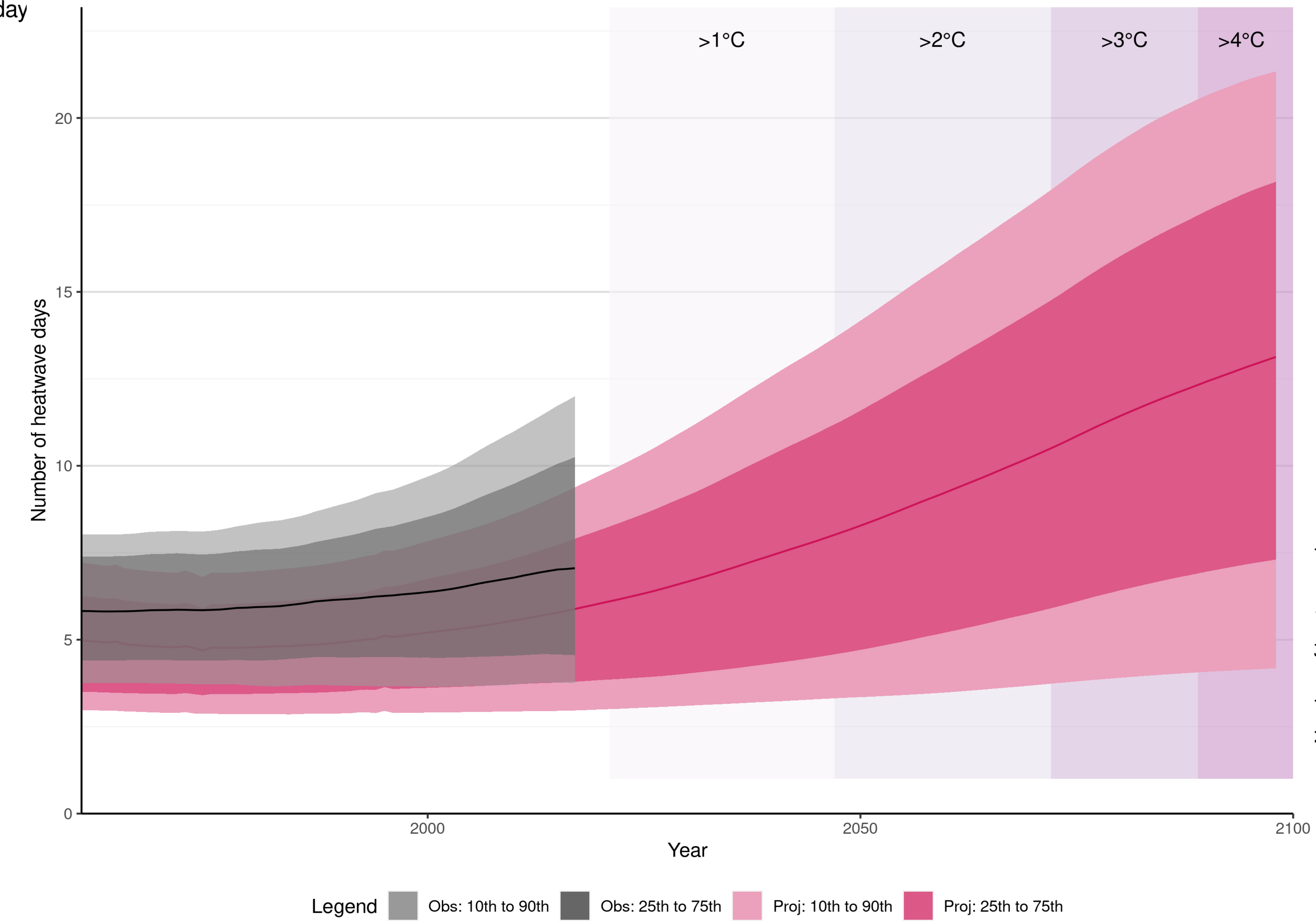


Figure 4: Projected change in mean *annual number of heatwave days* from 1990 to 2100. Historical values (*grey*) are the 30-year rolling means of AGCD. Projected values (*peach*) are the ensemble mean of the 30-year rolling mean of each CCAM ensemble member. *Lighter ribbons* represent the 10th to 90th percentiles of mean *annual number of heatwave days*. *Darker ribbons* represent the 25th to 75th percentiles of mean *annual number of heatwave days*. *Solid lines* represent the mean *annual number of heatwave days*.

### Figure 5: Projected range in the annual number of heatwave days

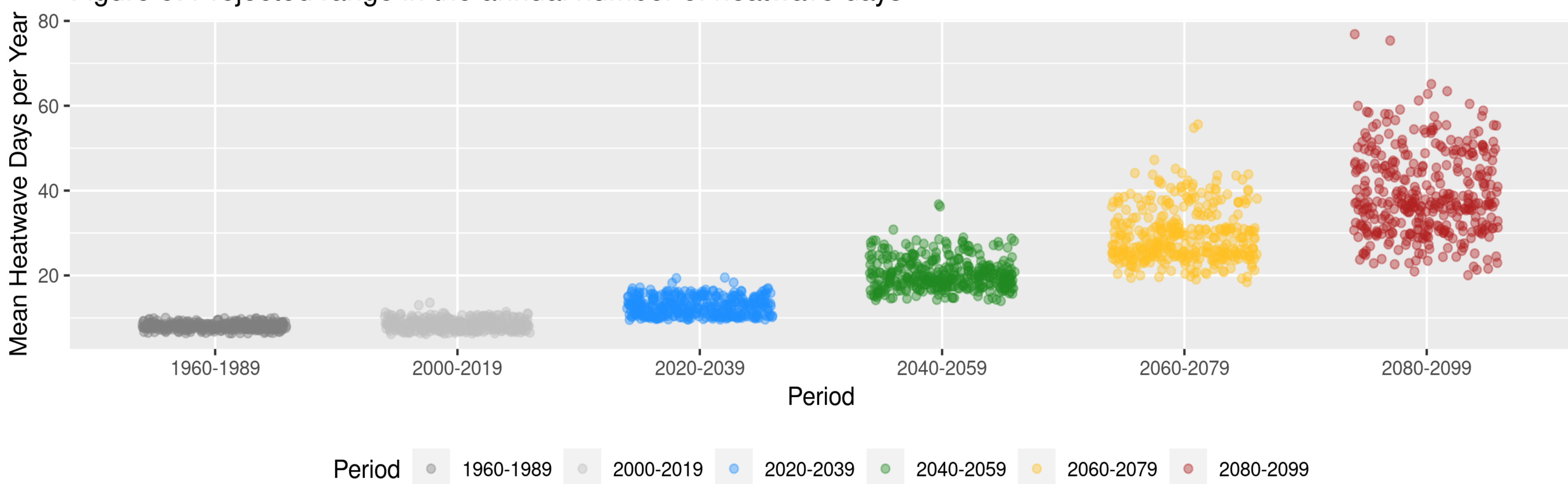


Figure 5: Comparison of the distribution of the *annual number of heatwave days* over the historical period for both model outputs (¡colour¿ and observations (*black*).

### Figure 6: Projected mean annual number of hea

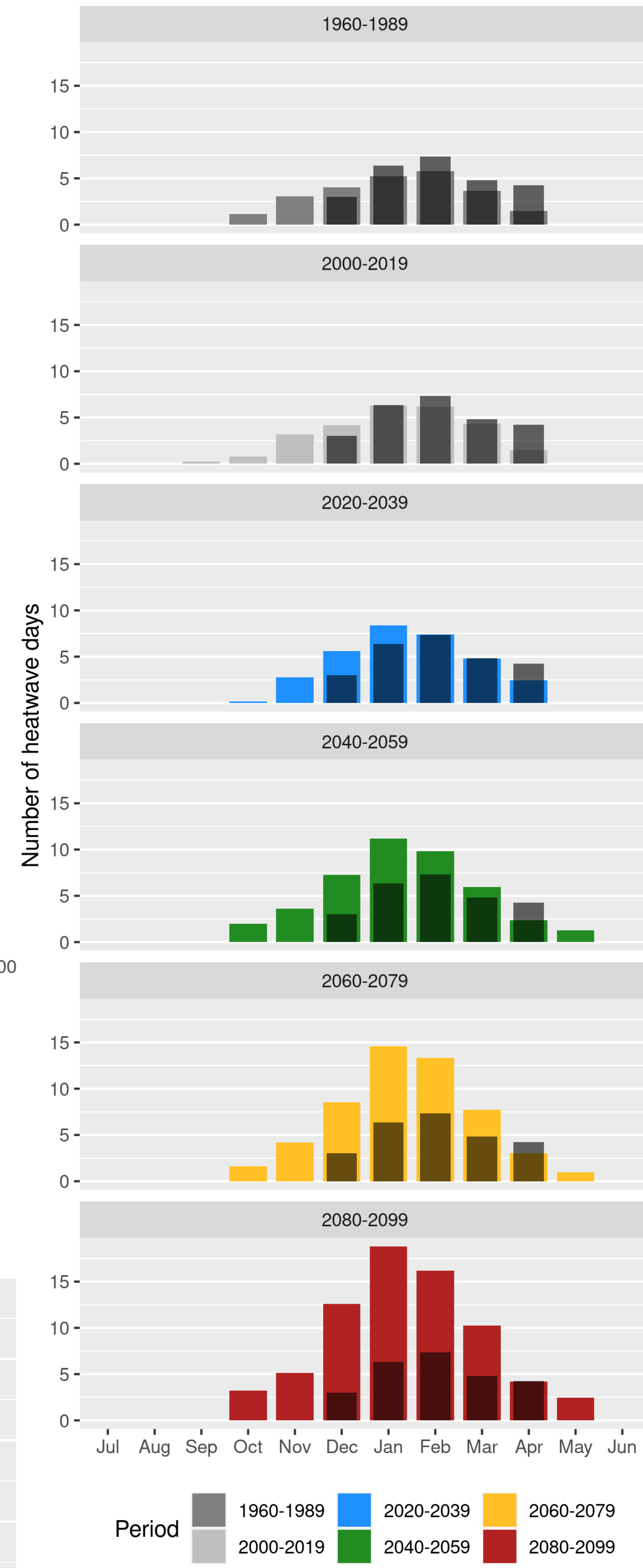


Figure 6: *Bar plots of typical number of heatwave days in each month* for 20-year time periods from 1961 to 2100. Each bar represents the 20-year *typical number of heatwave days in each month*, average across space and time. The observations for the baseline period (1961–1990) are shadowed on top of the future time periods to highlight any differences expected into the future. Higher (lower) bars indicate more (less) heatwave days.

Figure 1: Observed mean *annual number of heatwave days* across all years from 1997–2017.

Figure 2: The change in the mean *annual number of heatwave days* between the current (1997–2017) and historical (1961–1990) periods. Mean *annual number of heatwave days* has increased across the region over recent decades.

Figure 3: Projected mean *annual number of heatwave days* for 20-year time periods from 2001 to 2100. Mean *annual number of heatwave days* is expected to increase steadily into the future. Each grid cell is the mean of the 6 ensemble members.

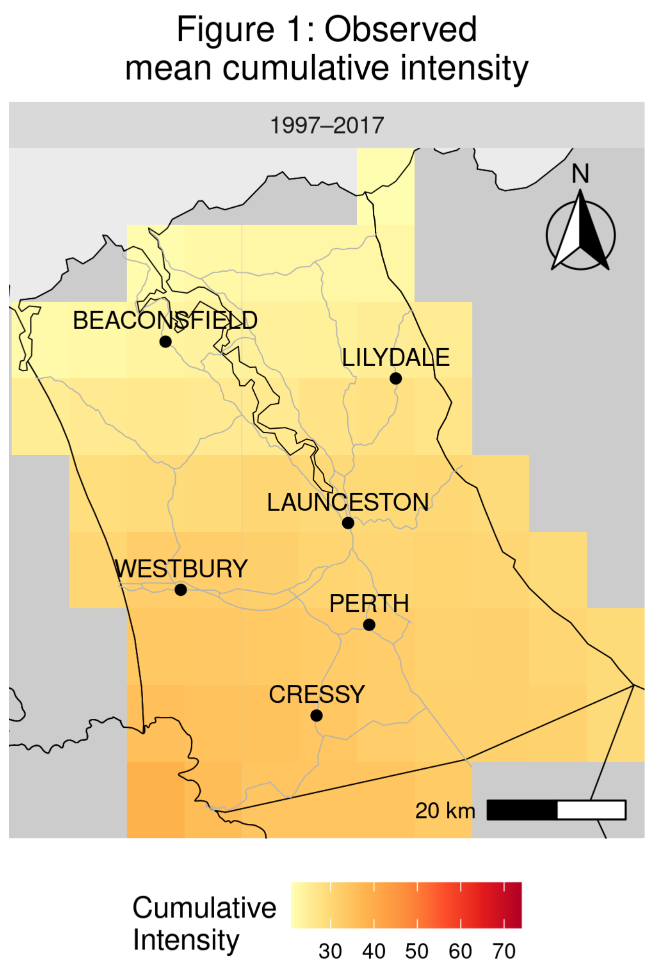


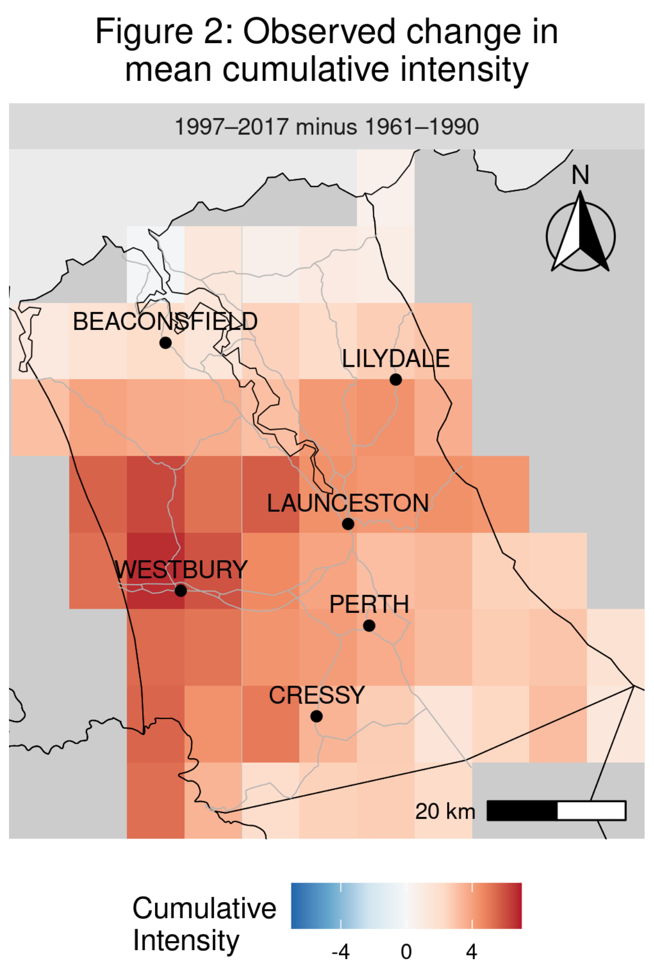


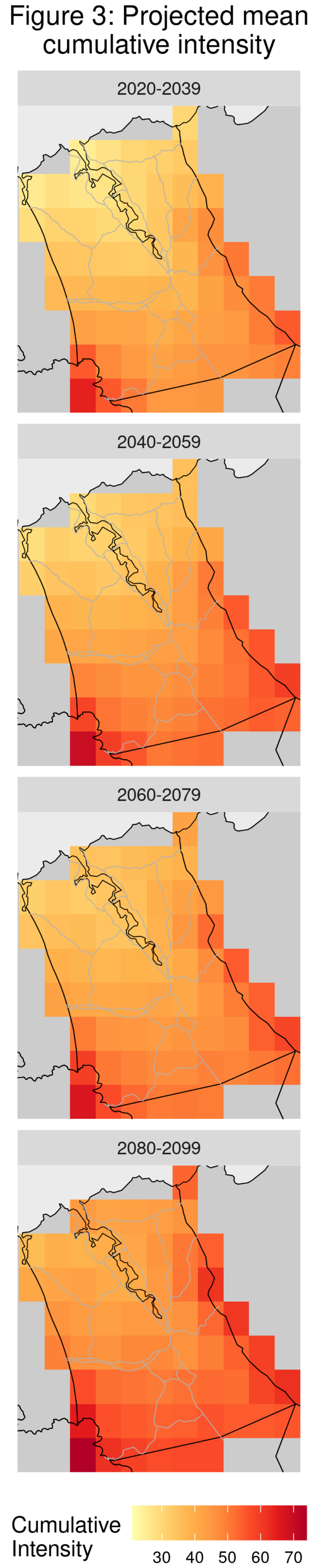


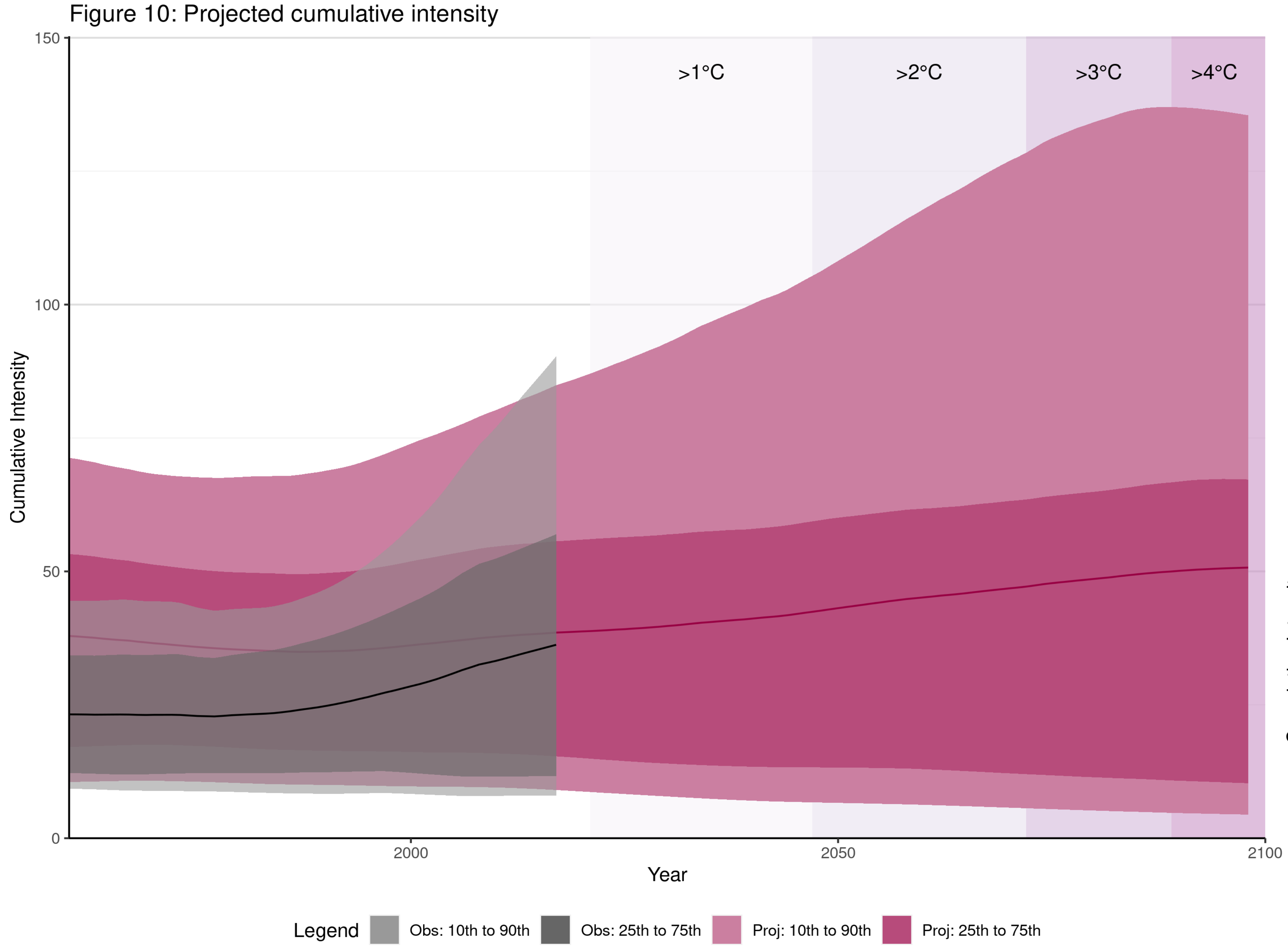


Figure 10: Projected change in *cumulative intensity during a heatwave* from 1990 to 2100. Historical values are the 30-year rolling means from AGCD (*grey*). Projected values (*peach*) are the ensemble mean of the 30-year rolling mean of each ensemble member. *Lighter ribbons* represent the 10th to 90th percentiles of *cumulative intensity during a heatwave*. *Darker ribbons* represent the 25th to 75th percentiles of *cumulative intensity during a heatwave*. *Solid lines* represent the mean of *cumulative intensity during a heatwave*.

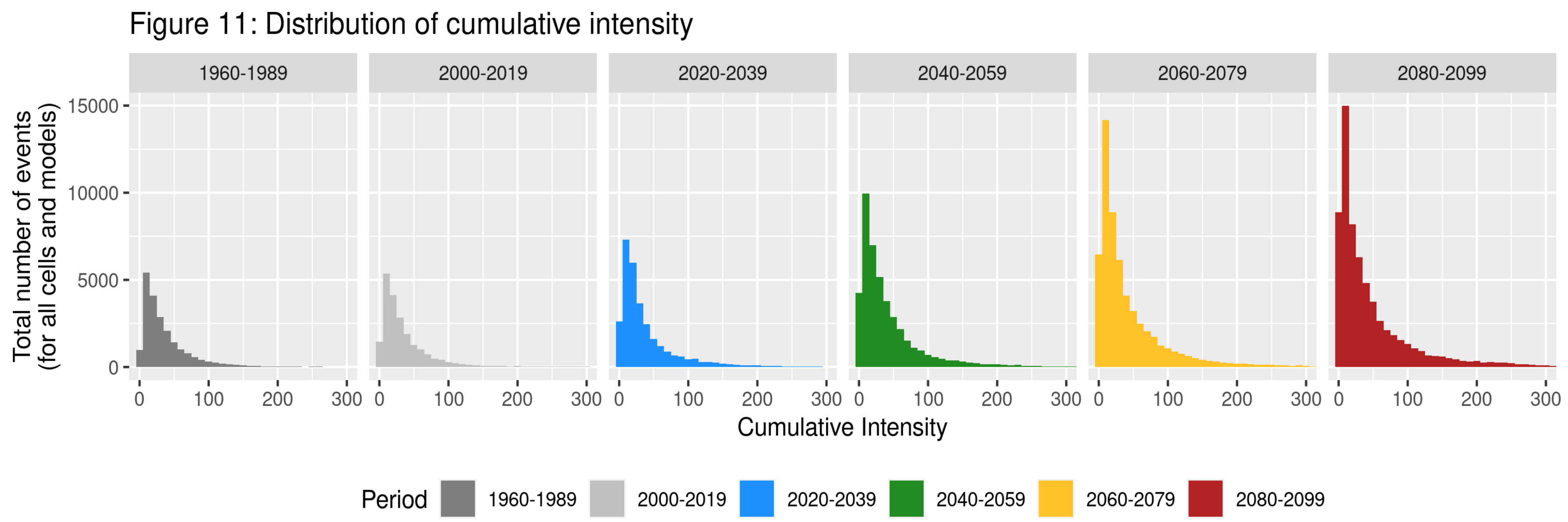


Figure 11: Comparison of the distribution of *cumulative intensity during a heatwave* for different time periods.

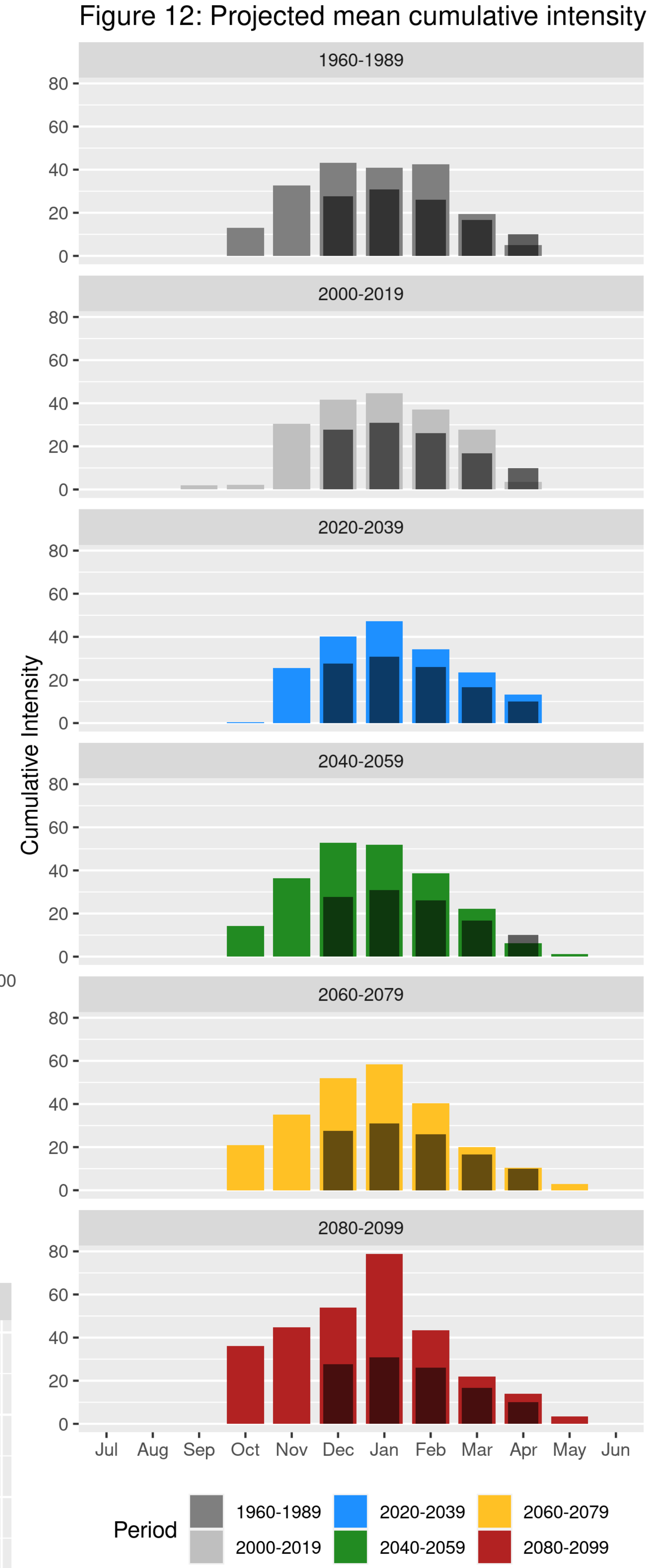


Figure 12: *Bar plots of cumulative intensity during heatwaves* in each month for 20-year time periods from 1961 to 2100. Each bar represents the 20-year mean of *cumulative intensity during a heatwave*, average across space and time. The observations for the baseline period (1961–1990) are shadowed on top of the future time periods to highlight any differences expected into the future. Higher (lower) bars indicate hotter (cooler) heatwave intensities.

Figure 7: Observed mean *cumulative intensity during a heatwave* across all years from 1997–2017.

Figure 8: The change in mean *cumulative intensity during a heatwave* between the current (1997–2017) and historical (1961–1990) periods. Mean *cumulative intensity during a heatwave* has increased across the region over recent decades.

Figure 9: Projected mean *cumulative intensity during a heatwave* for 20-year time periods from 2001 to 2100. Mean *cumulative intensity during a heatwave* is expected to increase steadily into the future. Each grid cell is the mean of the 6 ensemble members.

Figure 1: Observed mean duration

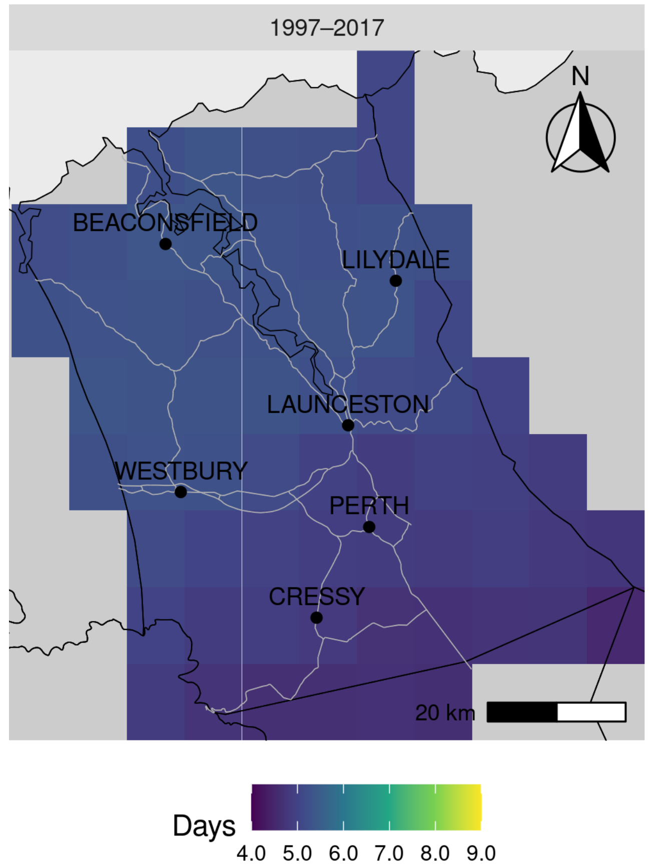


Figure 2: Observed change in mean duration

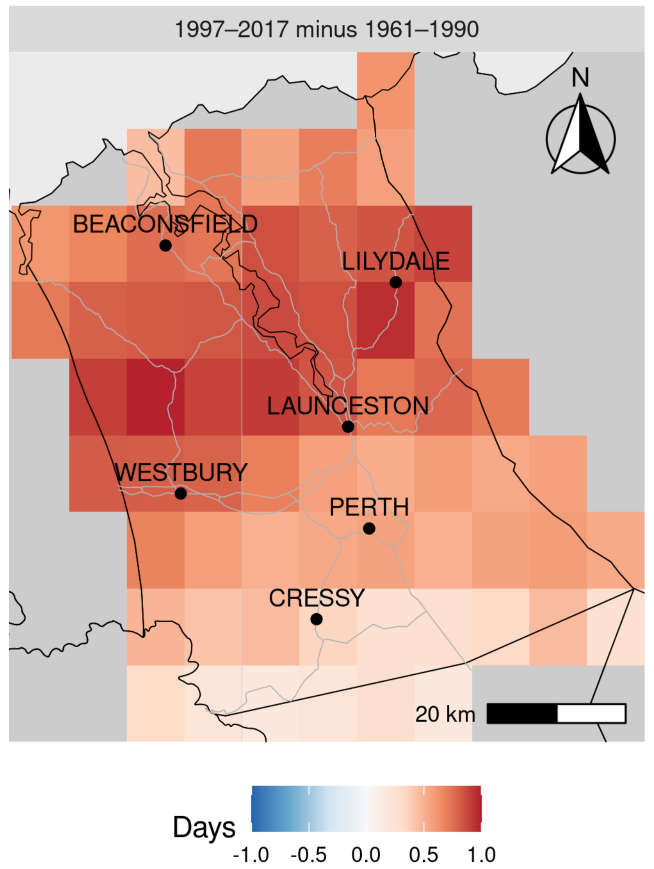


Figure 3: Projected mean duration

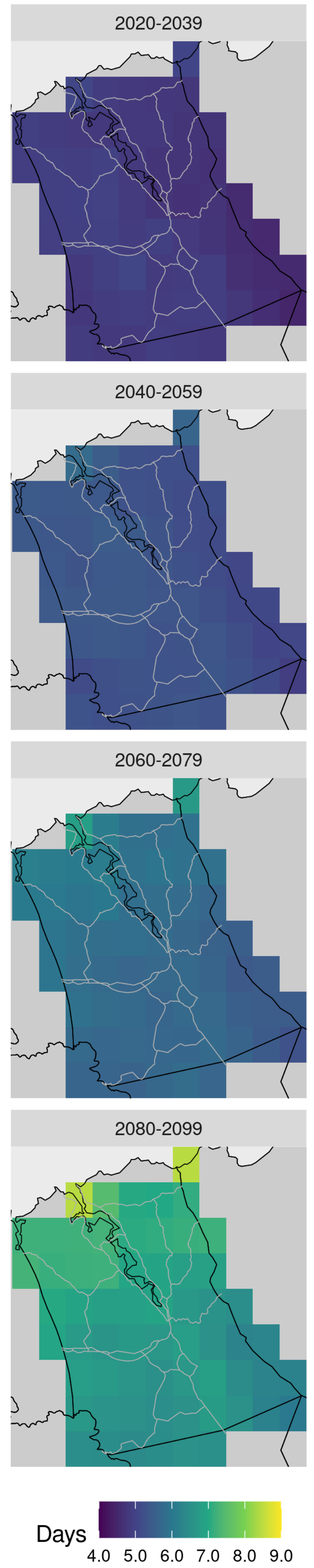


Figure 13: Observed mean *heatwave durations* across all years from 1997–2017.

Figure 14: The change in mean *heatwave duration* between the current (1997–2017) and historical (1961–1990) periods. Mean *heatwave durations* have increased across the region over recent decades.

Figure 15: Projected mean *heatwave durations* for 20-year time periods from 2001 to 2100. Mean *heatwave duration* is expected to increase steadily into the future. Each grid cell is the mean of the 6 ensemble members.

Figure 16: Projected heatwave duration

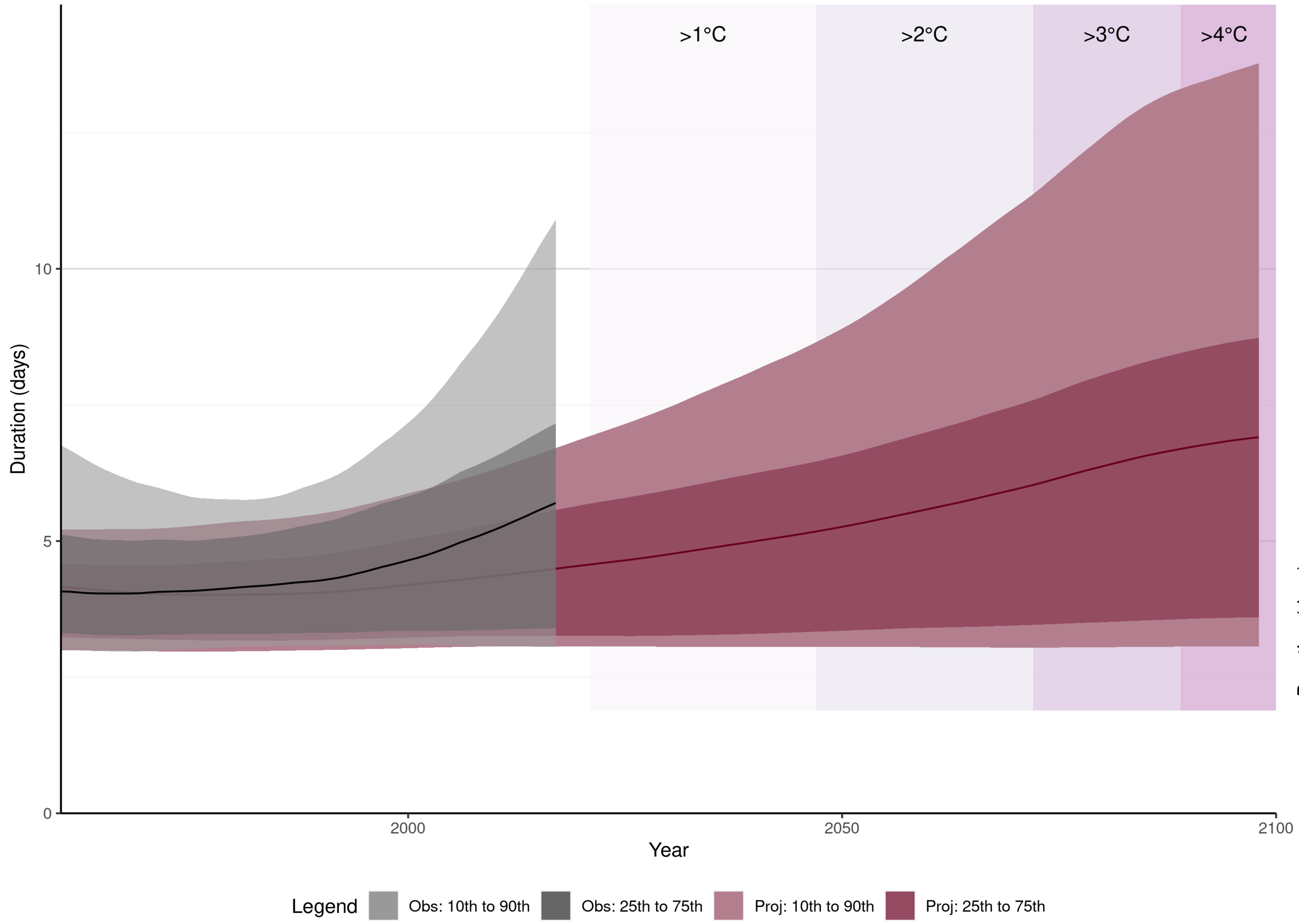


Figure 16: Projected change in *heatwave duration* from 1990 to 2100. Historical values (*grey*) are the 30-year rolling means of AGCD. Projected values (*orange*) are the ensemble mean of the 30-year rolling mean of each CCAM ensemble member. *Lighter ribbons* represent the 10th to 90th percentiles of *heatwave duration*. *Darker ribbons* represent the 25th to 75th percentiles of *heatwave duration*. *Solid lines* represent the mean of *heatwave duration*.

Figure 17: Projected count of heatwave duration

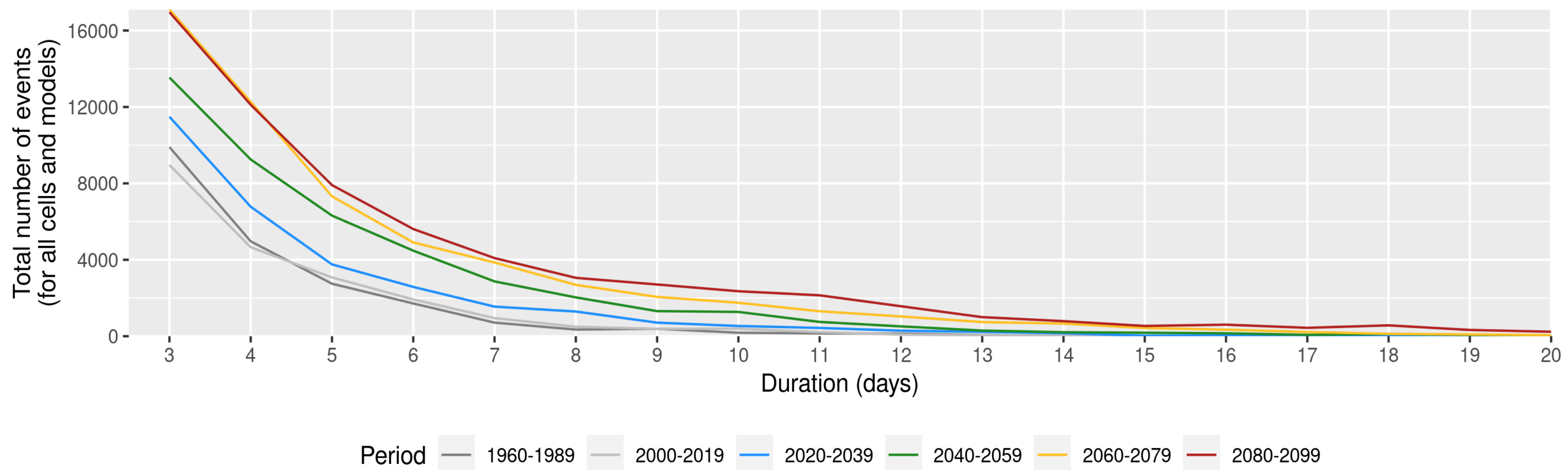


Figure 17: Comparison of the distribution of *heatwave durations* for different time periods.

Figure 18: Projected mean heatwave duration by

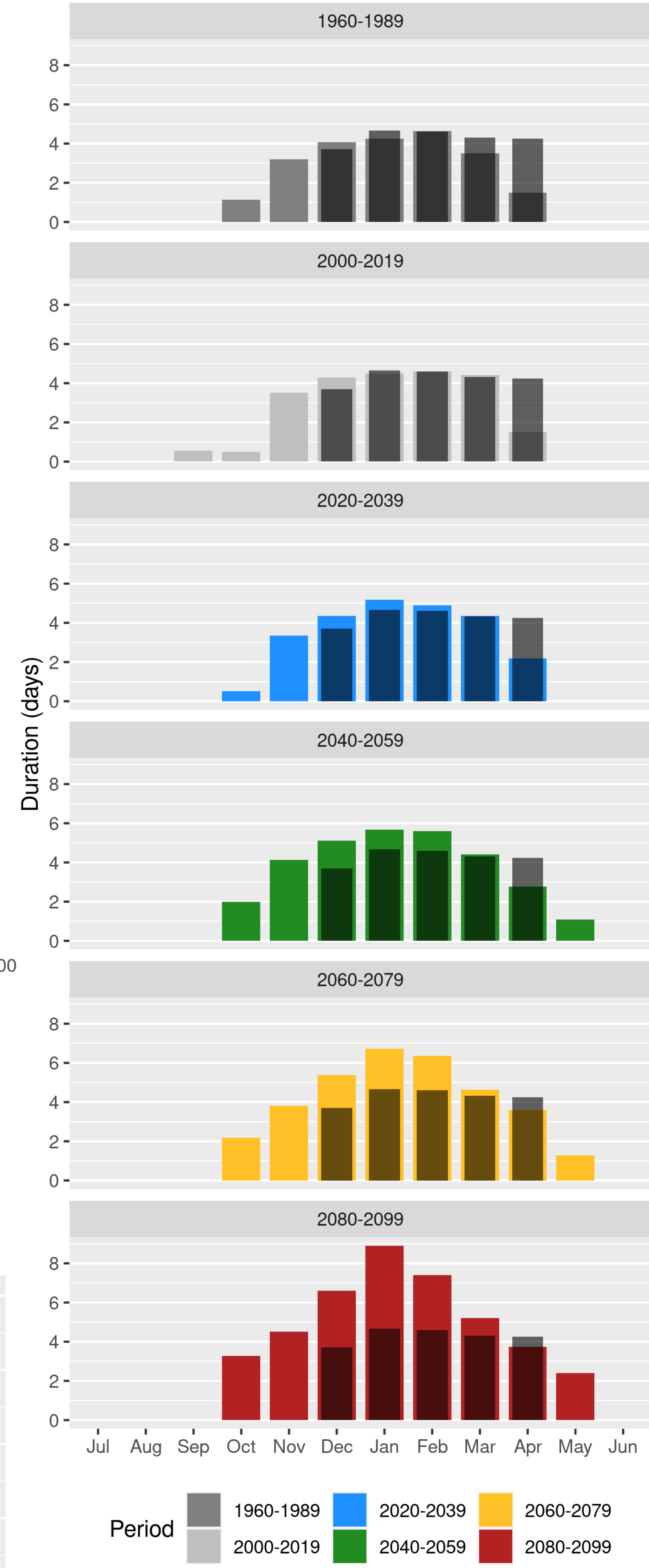


Figure 18: *Bar plots* of mean *heatwave durations* in each month for 20-year time periods from 1961 to 2100. Each bar represents the 20-year mean of *heatwave durations*, average across space and time. The observations for the baseline period (1961–1990) are shadowed on top of the future time periods to highlight any differences expected into the future. Higher (lower) bars indicate longer (shorter) *heatwave durations*.

Figure 1: Observed
mean annual number of heatwave days

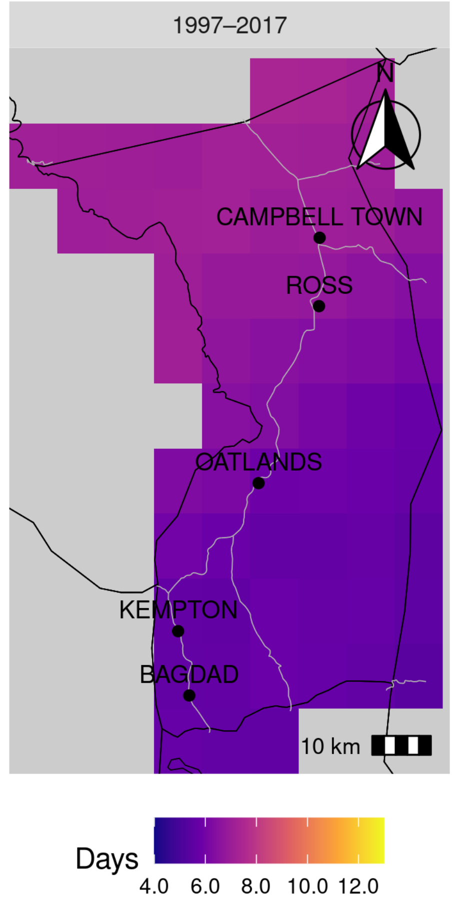


Figure 2: Observed change in
mean annual number of heatwave days

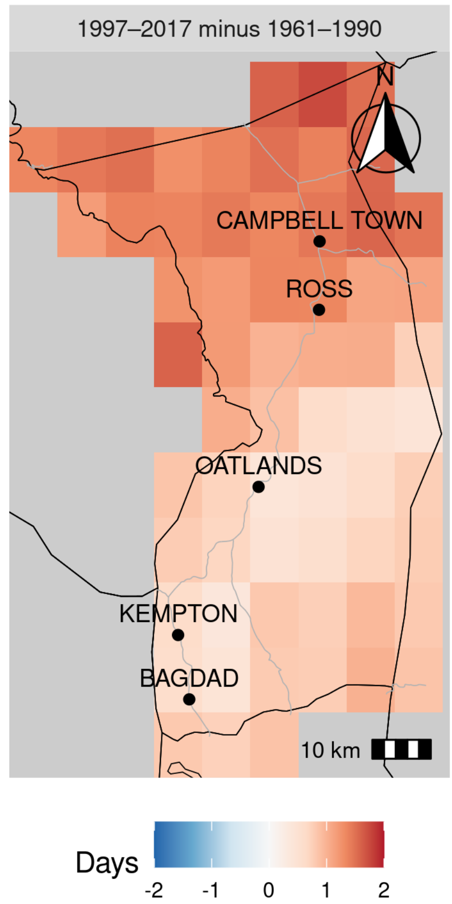


Figure 3: Projected mean
annual number of heatwave day

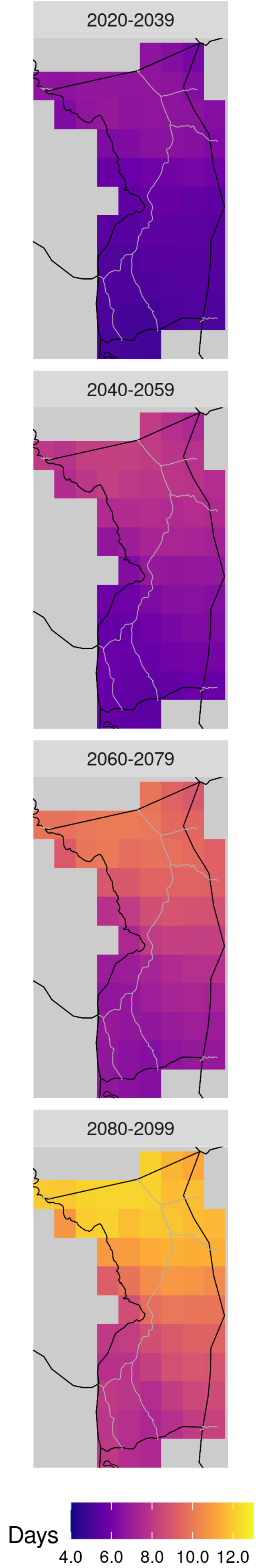


Figure 4: Projected annual number of heatwave days from 1961 to 2100

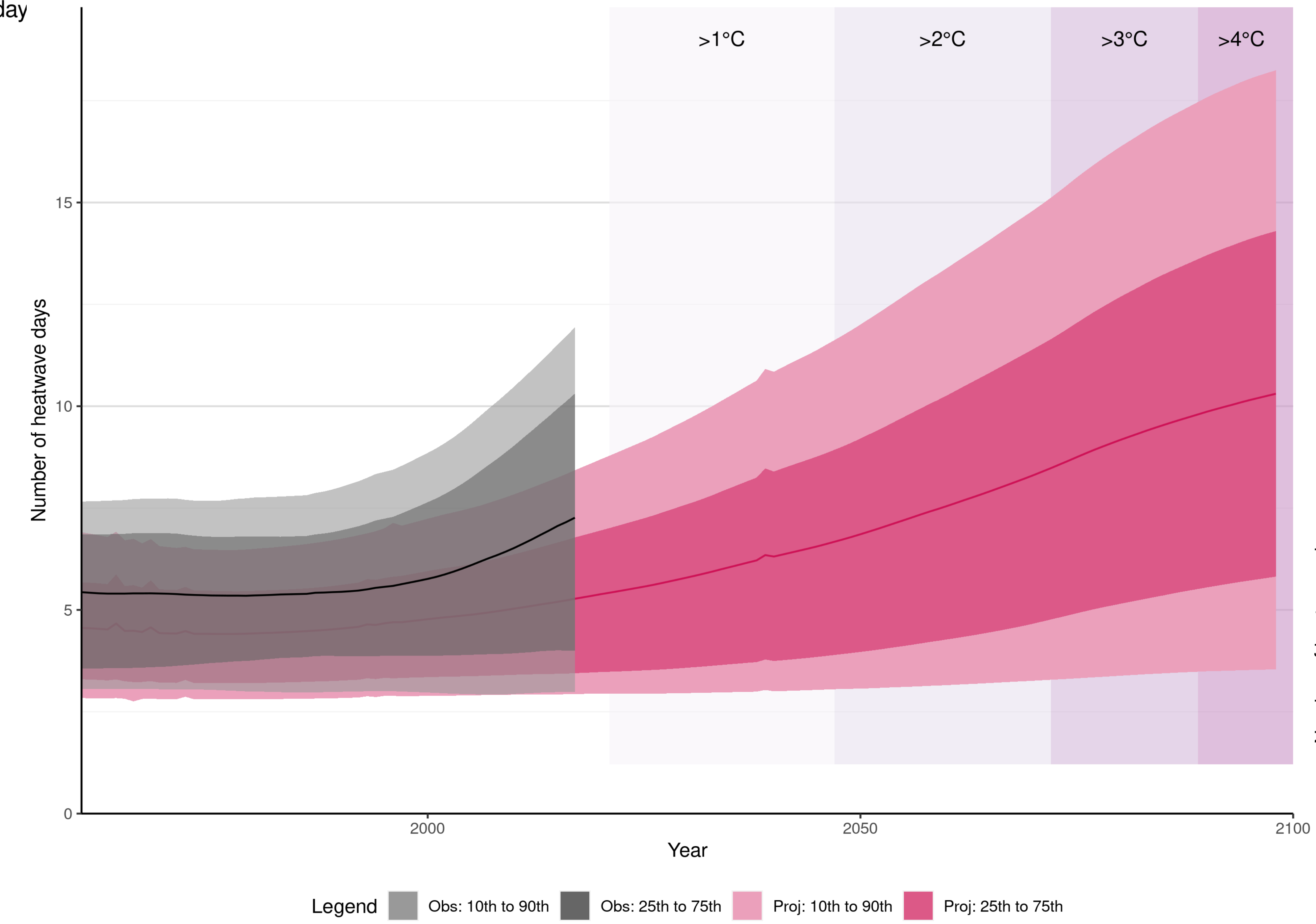


Figure 4: Projected change in mean *annual number of heatwave days* from 1990 to 2100. Historical values (*grey*) are the 30-year rolling means of AGCD. Projected values (*peach*) are the ensemble mean of the 30-year rolling mean of each CCAM ensemble member. *Lighter ribbons* represent the 10th to 90th percentiles of mean *annual number of heatwave days*. *Darker ribbons* represent the 25th to 75th percentiles of mean *annual number of heatwave days*. *Solid lines* represent the mean *annual number of heatwave days*.

Figure 5: Projected range in the annual number of heatwave days

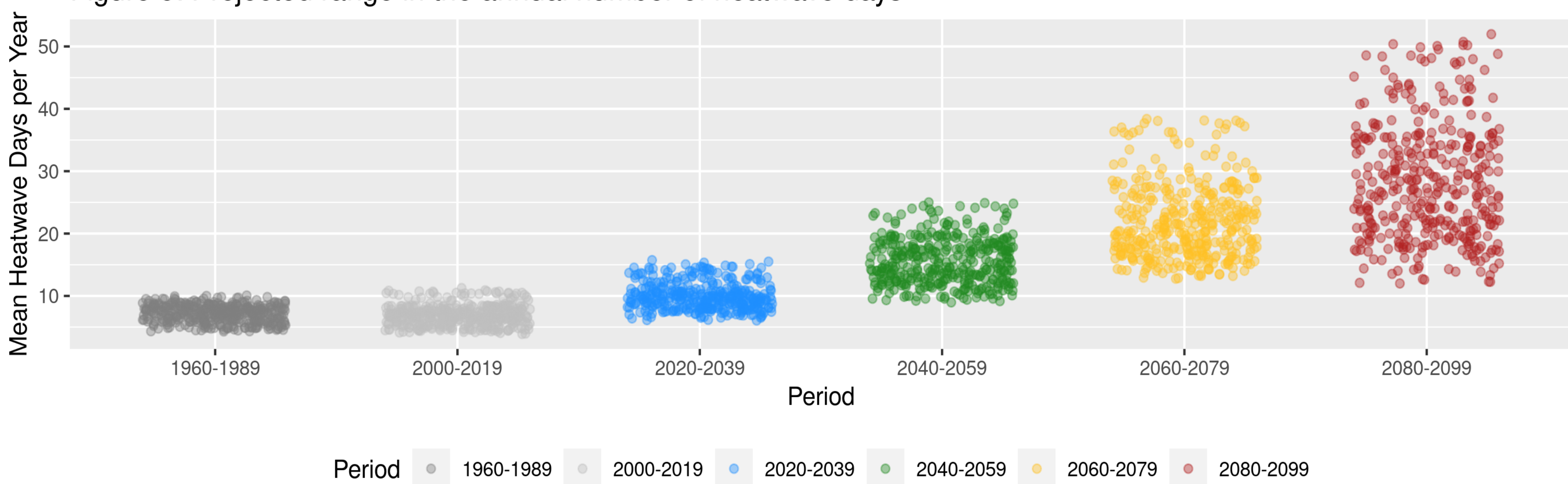


Figure 5: Comparison of the distribution of the *annual number of heatwave days* over the historical period for both model outputs (¡colour¿ and observations (*black*).

Figure 6: Projected mean annual number of hea

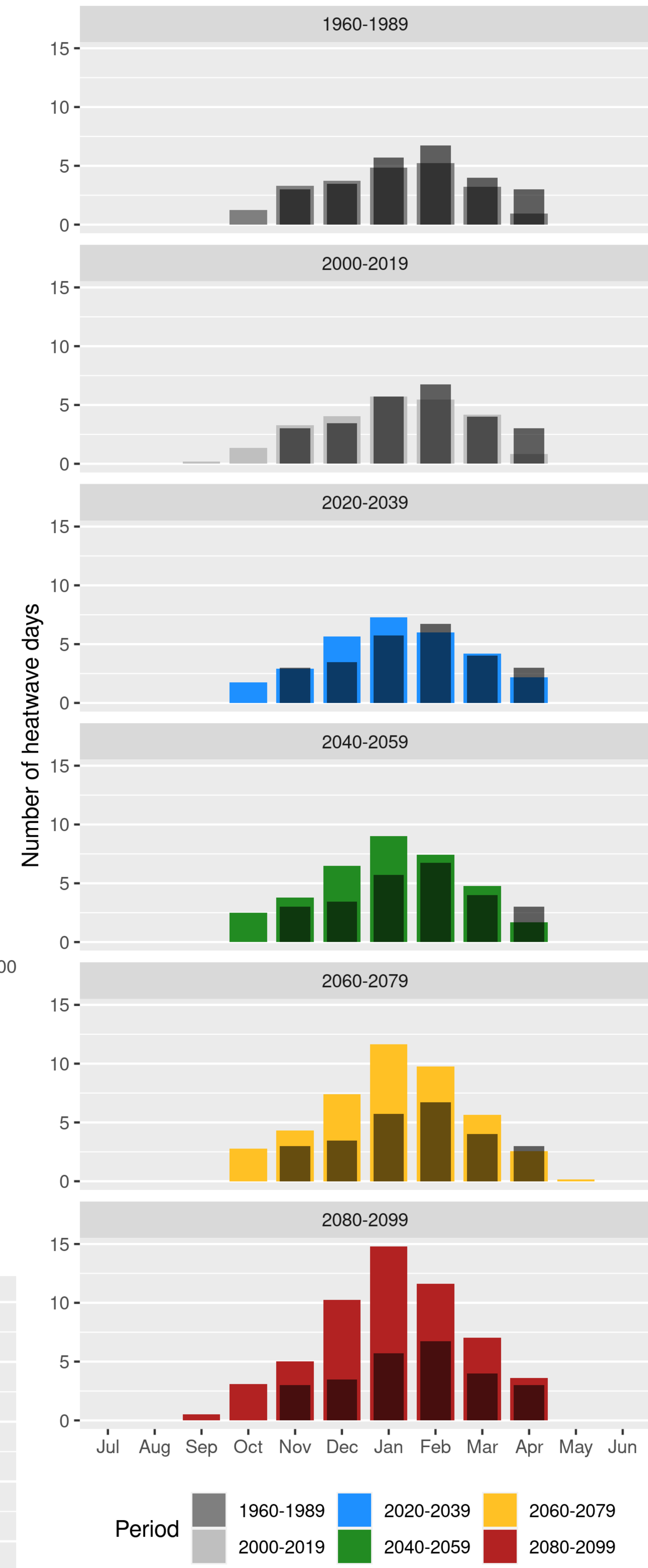


Figure 6: *Bar plots of typical number of heatwave days in each month* for 20-year time periods from 1961 to 2100. Each bar represents the 20-year *typical number of heatwave days in each month*, average across space and time. The observations for the baseline period (1961–1990) are shadowed on top of the future time periods to highlight any differences expected into the future. Higher (lower) bars indicate more (less) heatwave days.

Figure 1: Observed mean *annual number of heatwave days* across all years from 1997–2017.

Figure 2: The change in the mean *annual number of heatwave days* between the current (1997–2017) and historical (1961–1990) periods. Mean *annual number of heatwave days* has increased across the region over recent decades.

Figure 3: Projected mean *annual number of heatwave days* for 20-year time periods from 2001 to 2100. Mean *annual number of heatwave days* is expected to increase steadily into the future. Each grid cell is the mean of the 6 ensemble members.

# MIDLANDS

## Heatwaves — Cumulative Intensity

Figure 1: Observed mean cumulative intensity

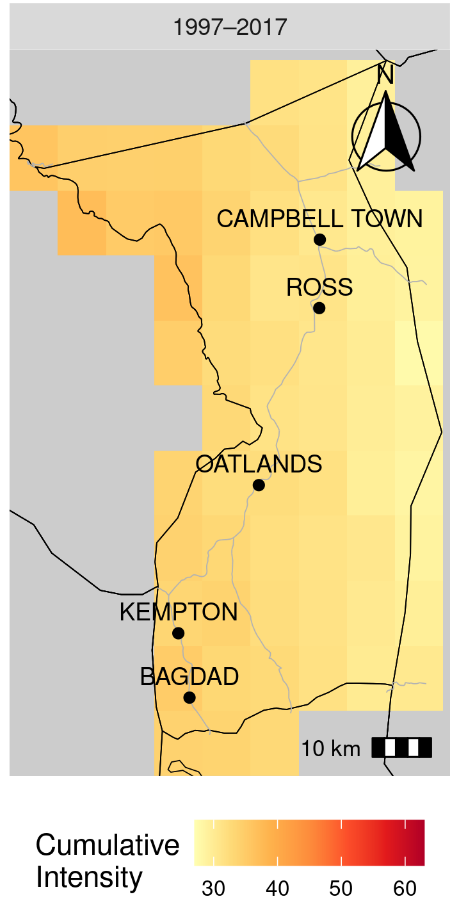


Figure 2: Observed change in mean cumulative intensity

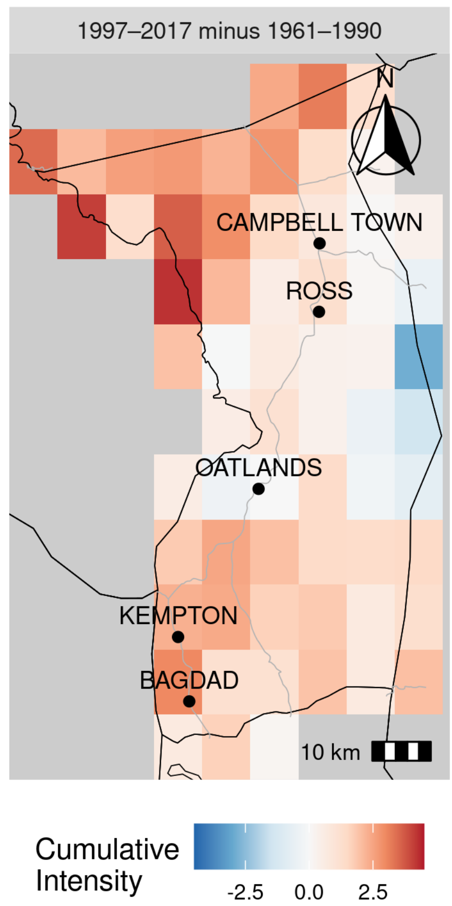


Figure 3: Projected mean cumulative intensity

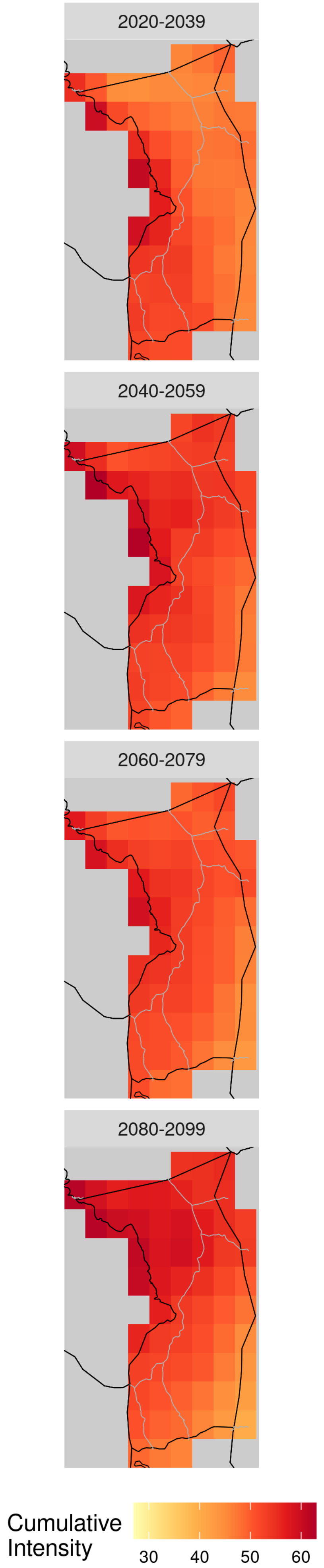


Figure 7: Observed mean *cumulative intensity during a heatwave* across all years from 1997–2017.

Figure 8: The change in mean *cumulative intensity during a heatwave* between the current (1997–2017) and historical (1961–1990) periods. Mean *cumulative intensity during a heatwave* has increased across the region over recent decades.

Figure 9: Projected mean *cumulative intensity during a heatwave* for 20-year time periods from 2001 to 2100. Mean *cumulative intensity during a heatwave* is expected to increase steadily into the future. Each grid cell is the mean of the 6 ensemble members.

Figure 10: Projected cumulative intensity

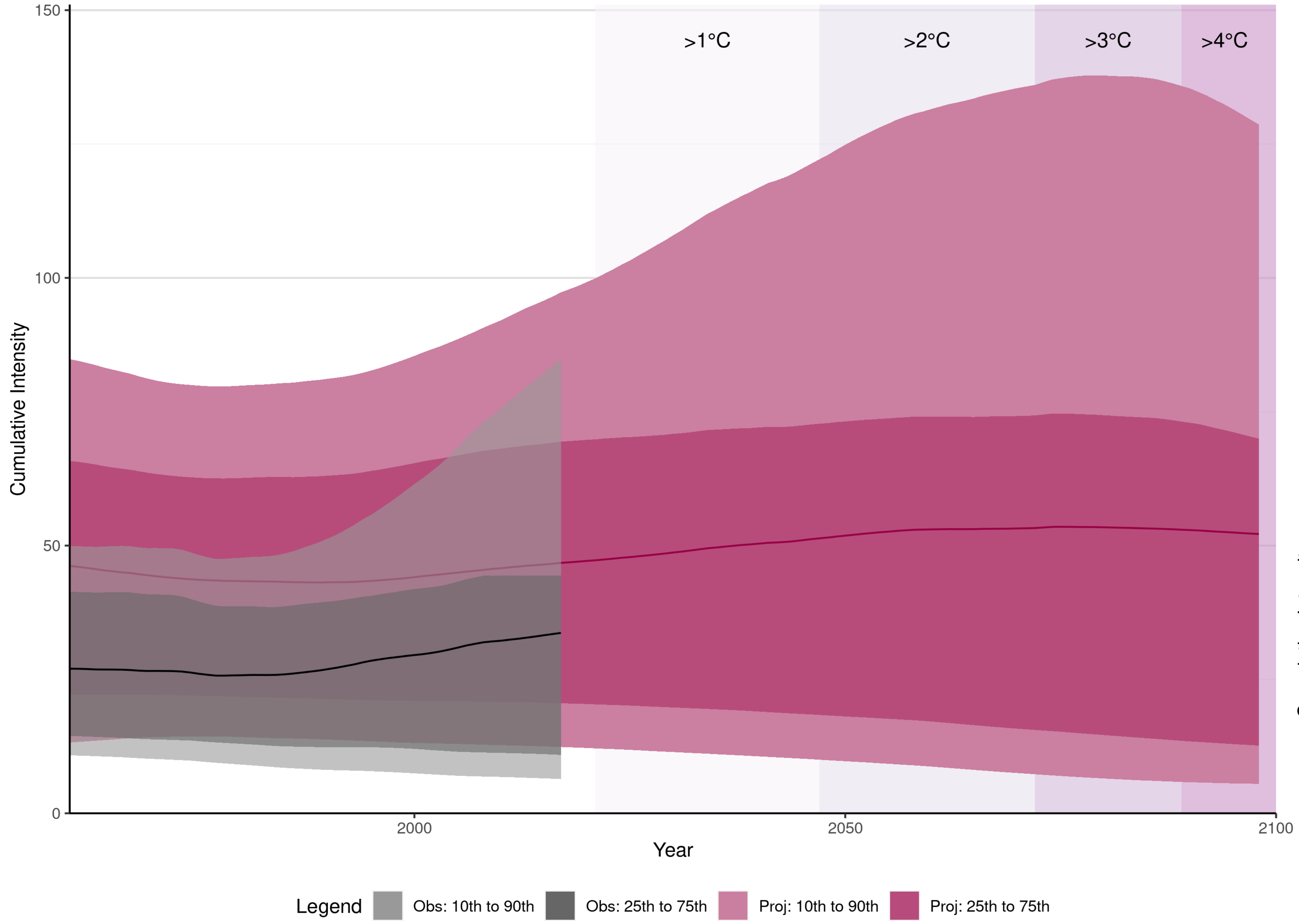


Figure 10: Projected change in *cumulative intensity during a heatwave* from 1990 to 2100. Historical values are the 30-year rolling means from AGCD (*grey*). Projected values (*peach*) are the ensemble mean of the 30-year rolling mean of each ensemble member. *Lighter ribbons* represent the 10th to 90th percentiles of *cumulative intensity during a heatwave*. *Darker ribbons* represent the 25th to 75th percentiles of *cumulative intensity during a heatwave*. *Solid lines* represent the mean of *cumulative intensity during a heatwave*.

Figure 11: Distribution of cumulative intensity

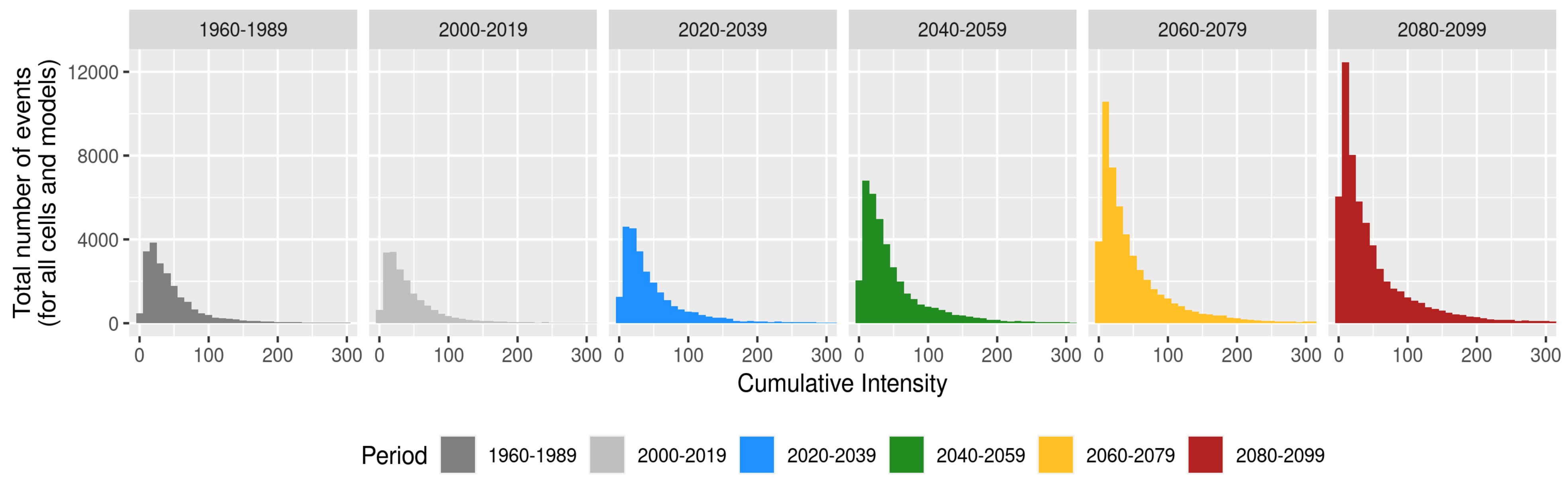


Figure 11: Comparison of the distribution of *cumulative intensity during a heatwave* for different time periods.

Figure 12: Projected mean cumulative intensity

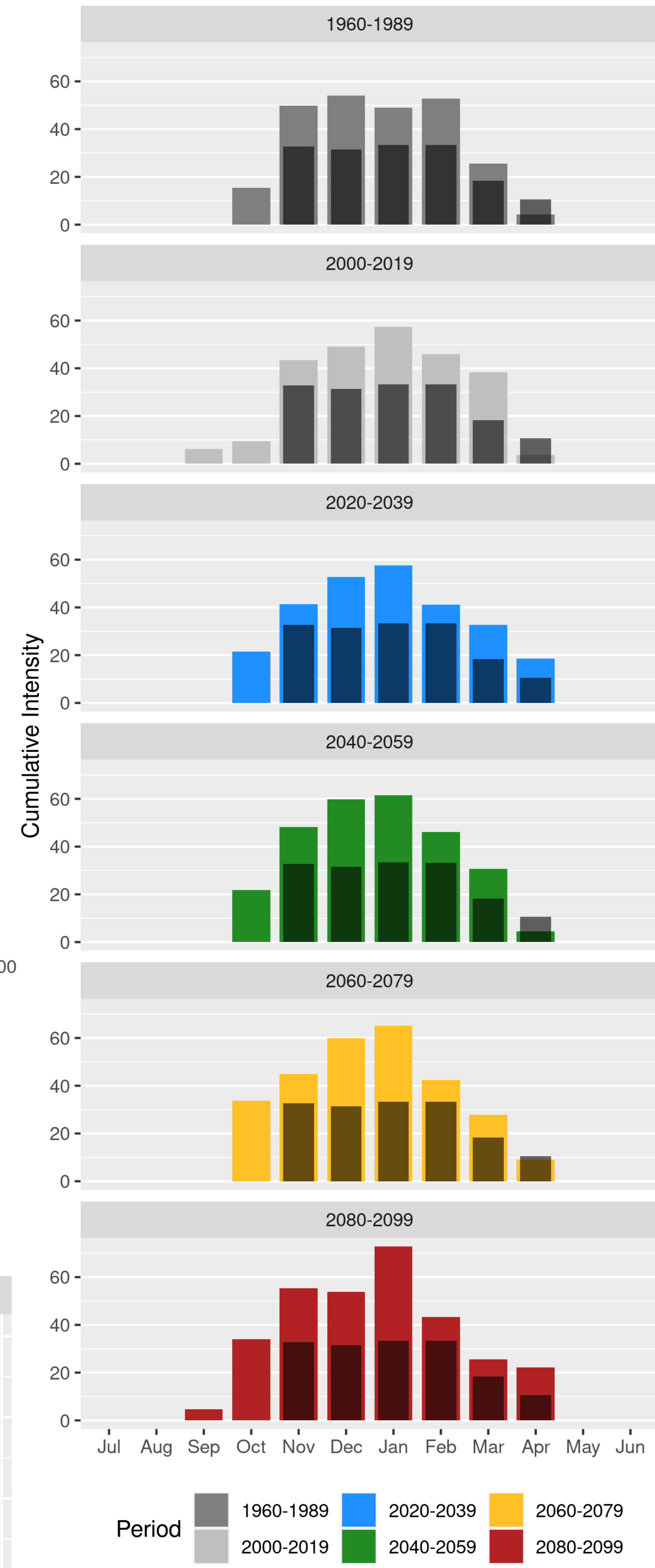


Figure 12: *Bar plots of cumulative intensity during heatwaves* in each month for 20-year time periods from 1961 to 2100. Each bar represents the 20-year mean of *cumulative intensity during a heatwave*, average across space and time. The observations for the baseline period (1961–1990) are shadowed on top of the future time periods to highlight any differences expected into the future. Higher (lower) bars indicate hotter (cooler) heatwave intensities.

Figure 1: Observed mean duration

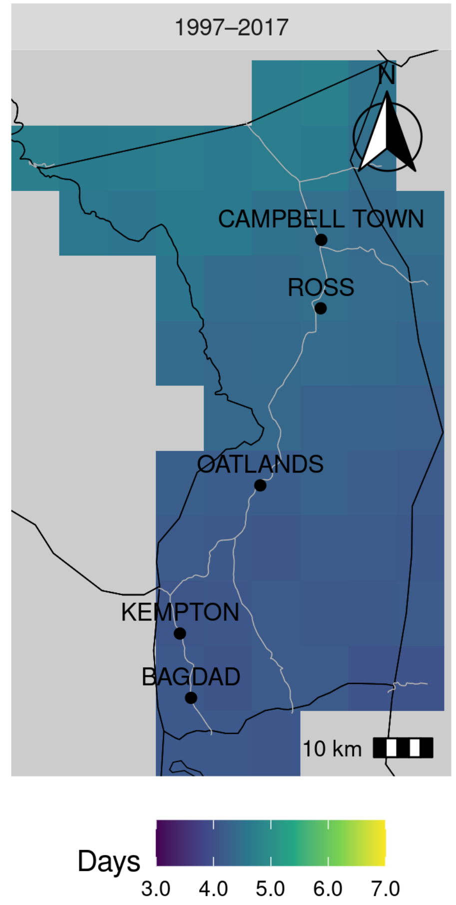


Figure 2: Observed change in mean duration

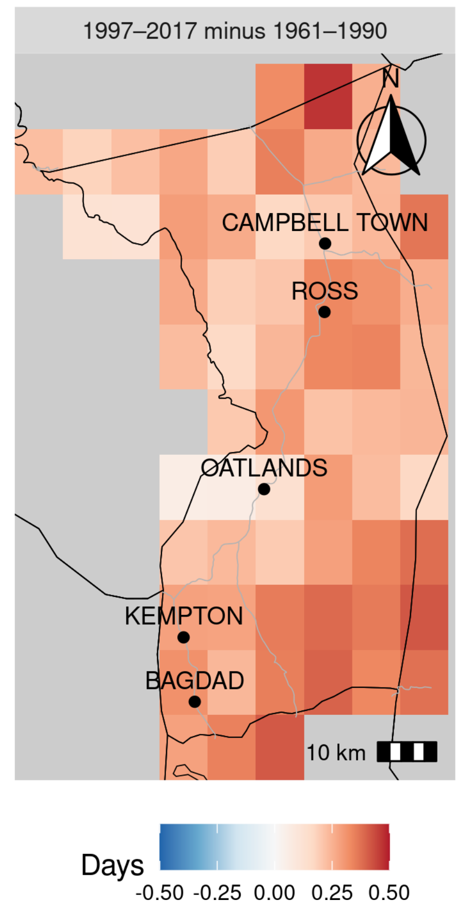


Figure 3: Projected mean duration

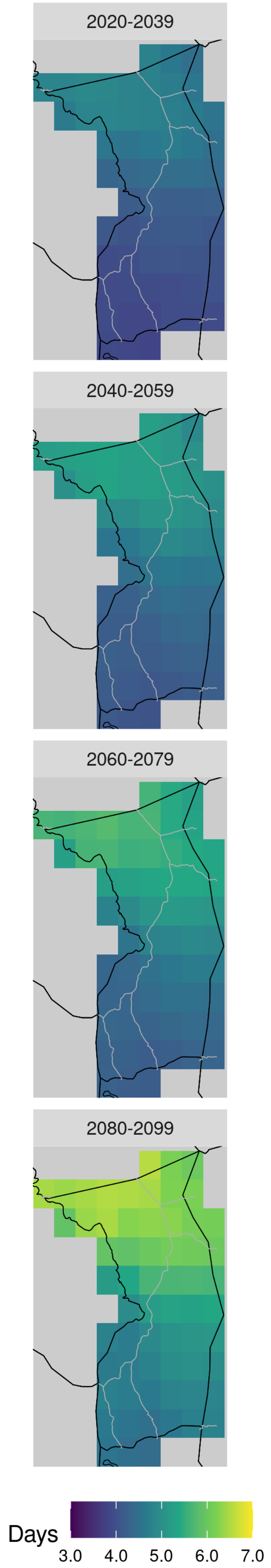


Figure 16: Projected heatwave duration

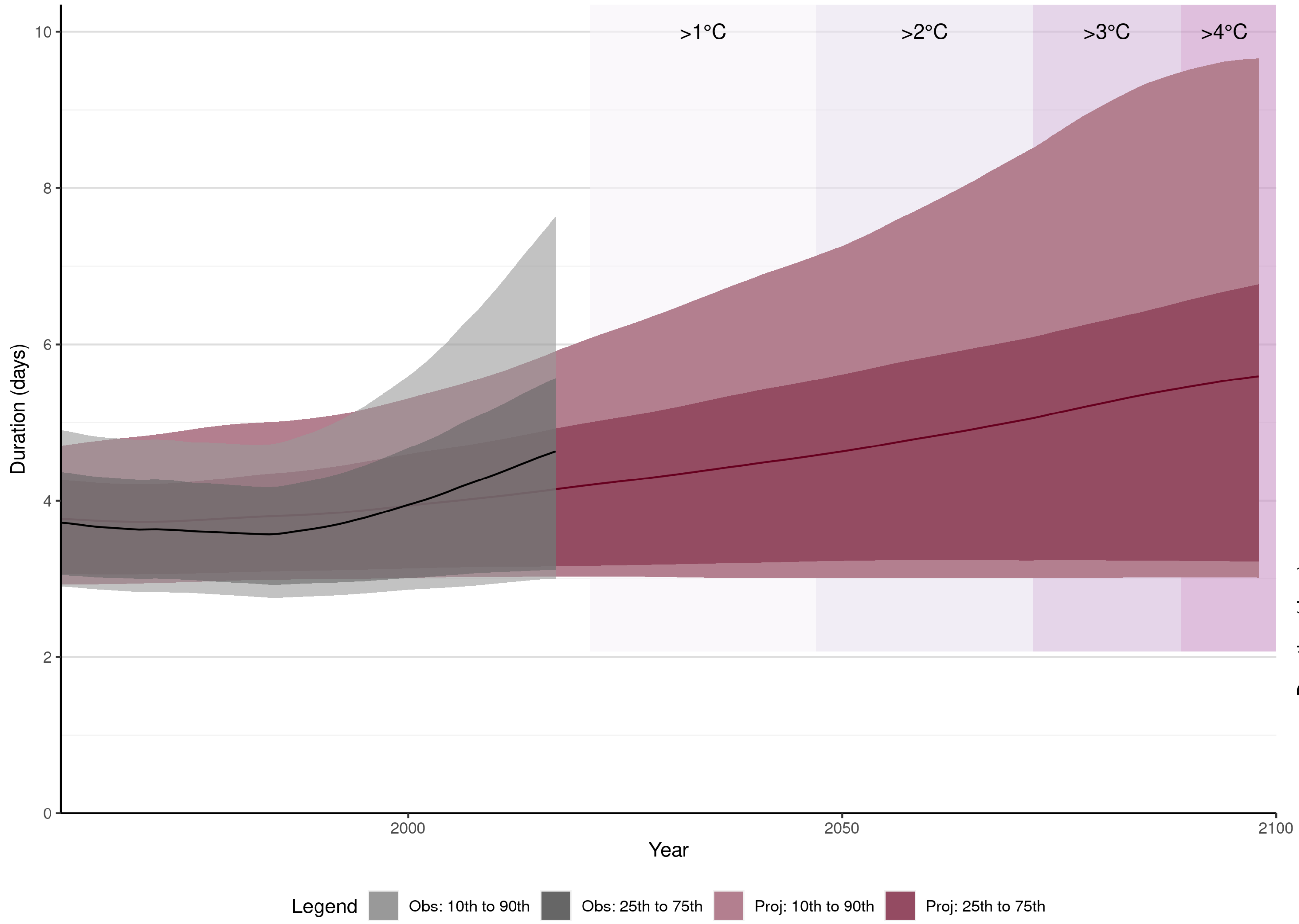


Figure 16: Projected change in *heatwave duration* from 1990 to 2100. Historical values (*grey*) are the 30-year rolling means of AGCD. Projected values (*orange*) are the ensemble mean of the 30-year rolling mean of each CCAM ensemble member. *Lighter ribbons* represent the 10th to 90th percentiles of *heatwave duration*. *Darker ribbons* represent the 25th to 75th percentiles of *heatwave duration*. *Solid lines* represent the mean of *heatwave duration*.

Figure 17: Projected count of heatwave duration

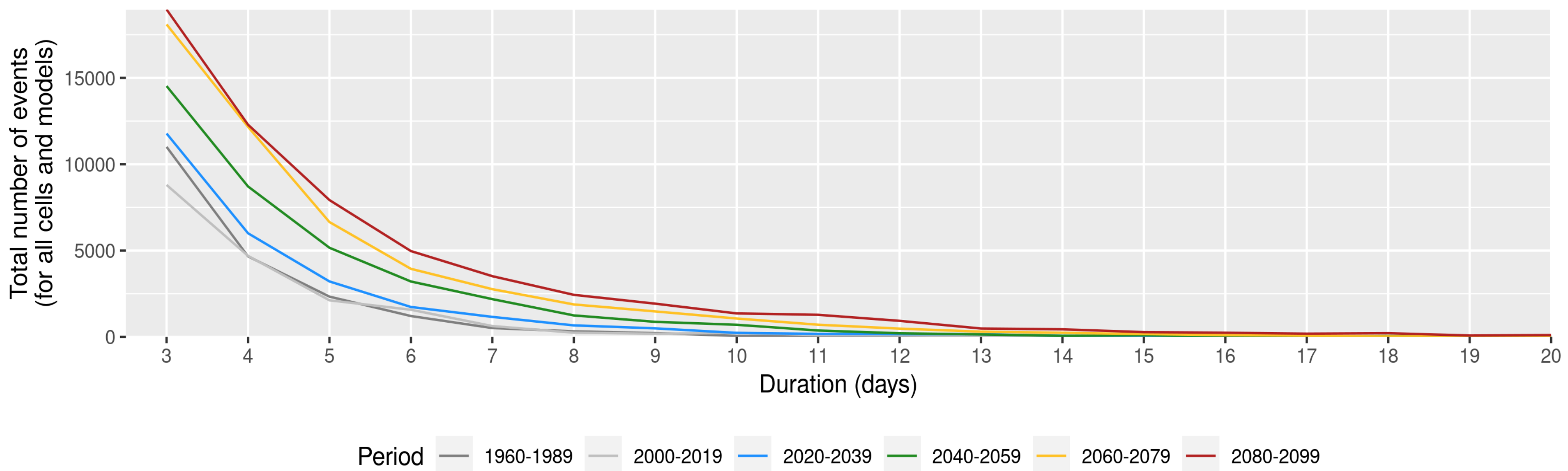


Figure 17: Comparison of the distribution of *heatwave durations* for different time periods.

Figure 18: Projected mean heatwave duration by

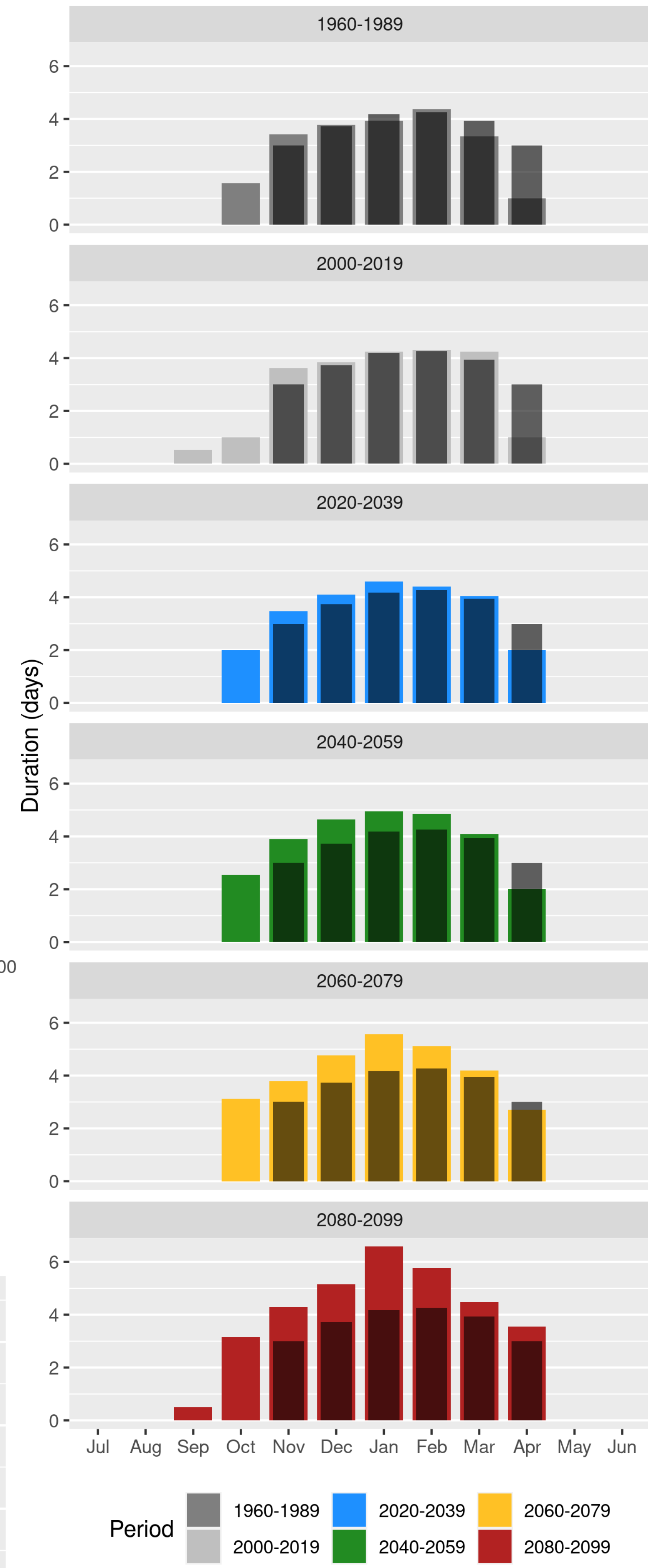


Figure 18: *Bar plots* of mean *heatwave durations* in each month for 20-year time periods from 1961 to 2100. Each bar represents the 20-year mean of *heatwave durations*, average across space and time. The observations for the baseline period (1961–1990) are shadowed on top of the future time periods to highlight any differences expected into the future. Higher (lower) bars indicate longer (shorter) *heatwave durations*.

Figure 13: Observed mean *heatwave durations* across all years from 1997–2017.

Figure 14: The change in mean *heatwave duration* between the current (1997–2017) and historical (1961–1990) periods. Mean *heatwave durations* have increased across the region over recent decades.

Figure 15: Projected mean *heatwave durations* for 20-year time periods from 2001 to 2100. Mean *heatwave duration* is expected to increase steadily into the future. Each grid cell is the mean of the 6 ensemble members.

Figure 1: Observed
mean annual number of heatwave days

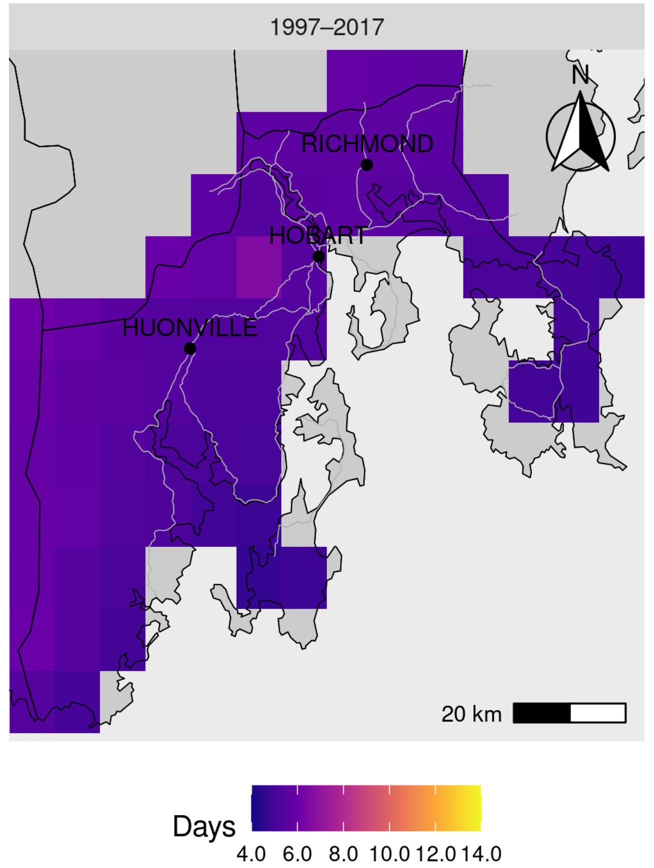


Figure 2: Observed change in
mean annual number of heatwave days

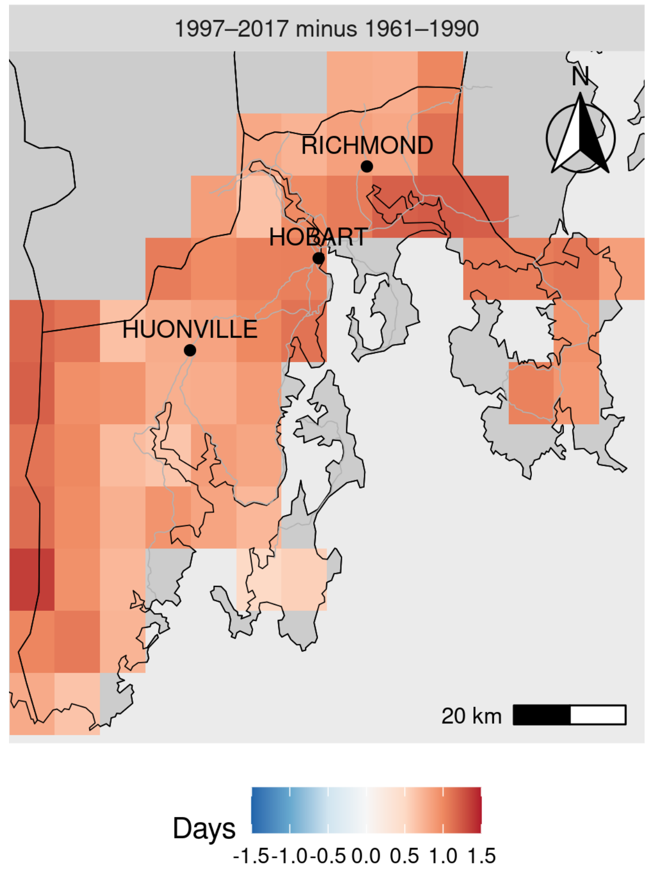


Figure 3: Projected mean
annual number of heatwave day

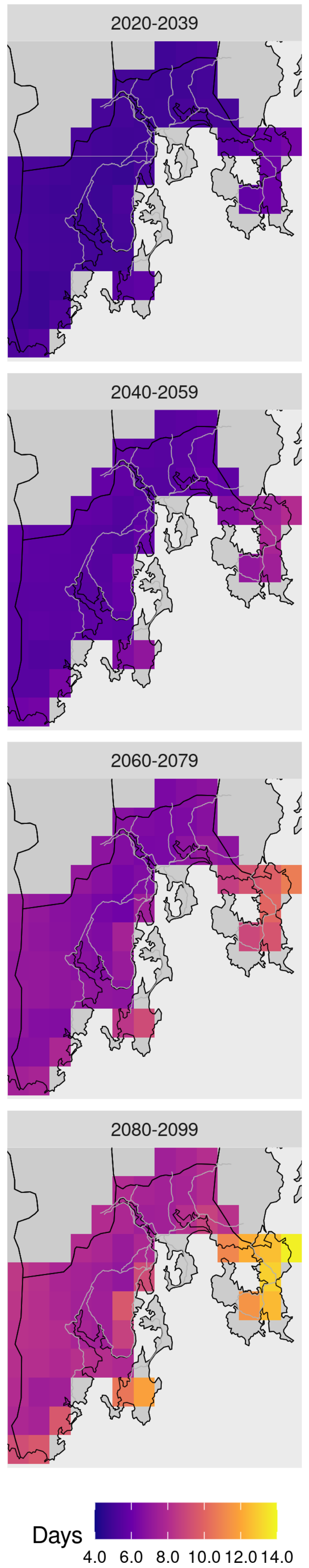


Figure 4: Projected annual number of heatwave days from 1961 to 2100

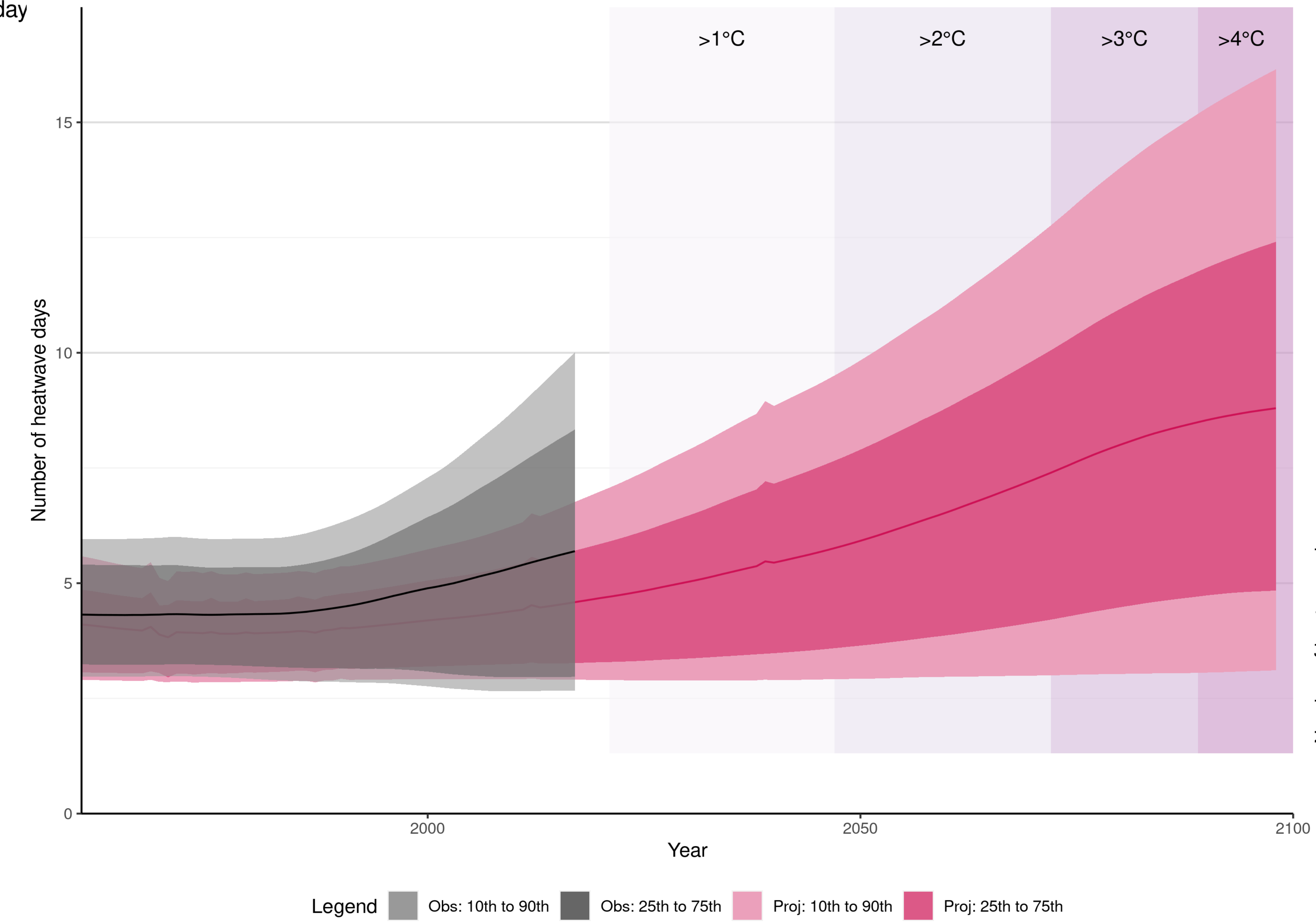


Figure 4: Projected change in mean *annual number of heatwave days* from 1990 to 2100. Historical values (*grey*) are the 30-year rolling means of AGCD. Projected values (*peach*) are the ensemble mean of the 30-year rolling mean of each CCAM ensemble member. *Lighter ribbons* represent the 10th to 90th percentiles of mean *annual number of heatwave days. Darker ribbons* represent the 25th to 75th percentiles of mean *annual number of heatwave days. Solid lines* represent the mean *annual number of heatwave days.*

Figure 5: Projected range in the annual number of heatwave days

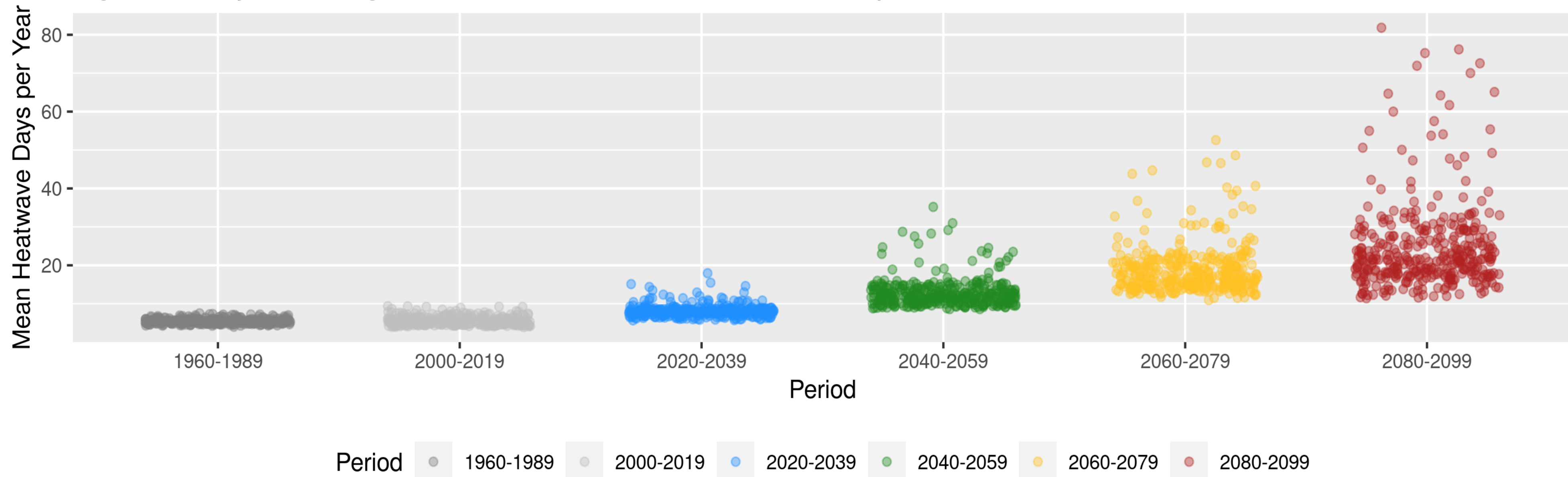


Figure 5: Comparison of the distribution of the *annual number of heatwave days* over the historical period for both model outputs (¡colour¿ and observations (*black*).

Figure 6: Projected mean annual number of hea

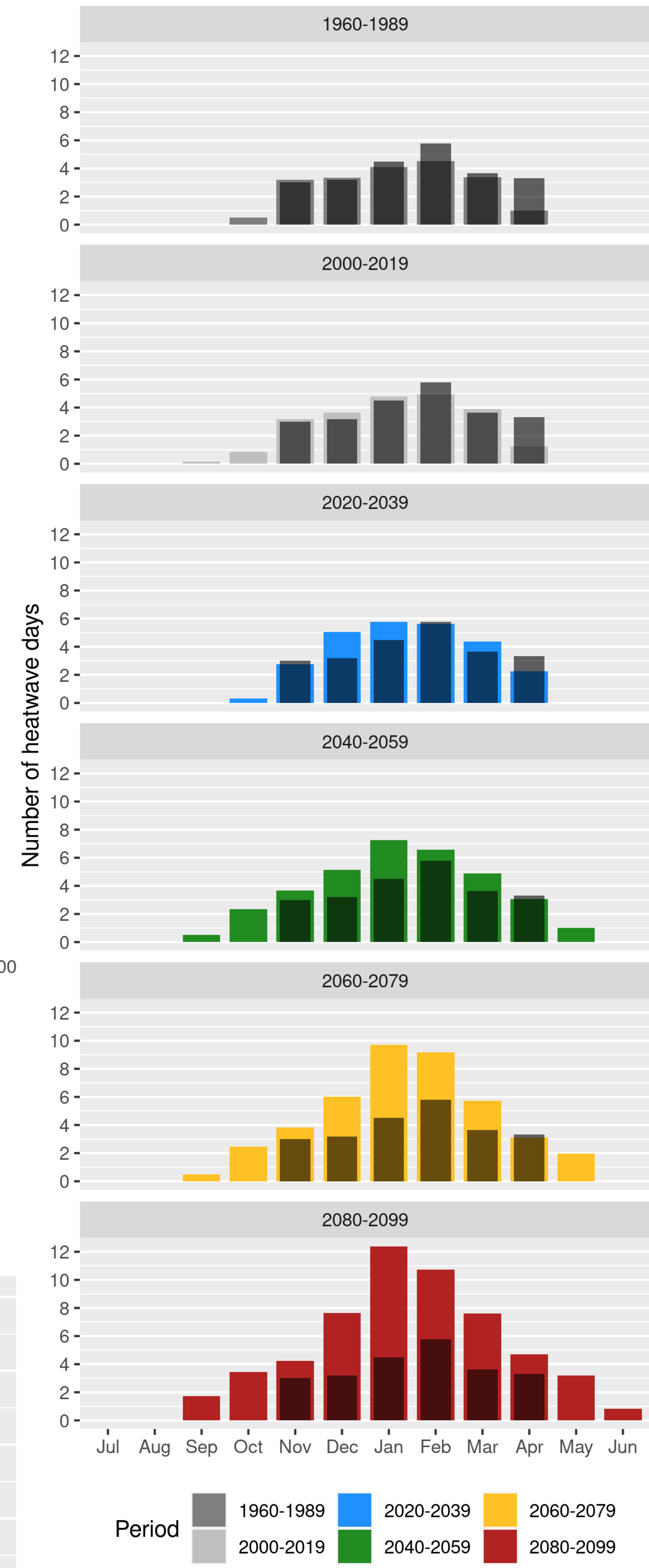


Figure 6: *Bar plots of typical number of heatwave days in each month* for 20-year time periods from 1961 to 2100. Each bar represents the 20-year *typical number of heatwave days in each month*, average across space and time. The observations for the baseline period (1961–1990) are shadowed on top of the future time periods to highlight any differences expected into the future. Higher (lower) bars indicate more (less) heatwave days.

Figure 1: Observed mean *annual number of heatwave days* across all years from 1997–2017.

Figure 2: The change in the mean *annual number of heatwave days* between the current (1997–2017) and historical (1961–1990) periods. Mean *annual number of heatwave days* has increased across the region over recent decades.

Figure 3: Projected mean *annual number of heatwave days* for 20-year time periods from 2001 to 2100. Mean *annual number of heatwave days* is expected to increase steadily into the future. Each grid cell is the mean of the 6 ensemble members.

# SOUTH EAST

## Heatwaves — Cumulative Intensity

### Figure 1: Observed mean cumulative intensity

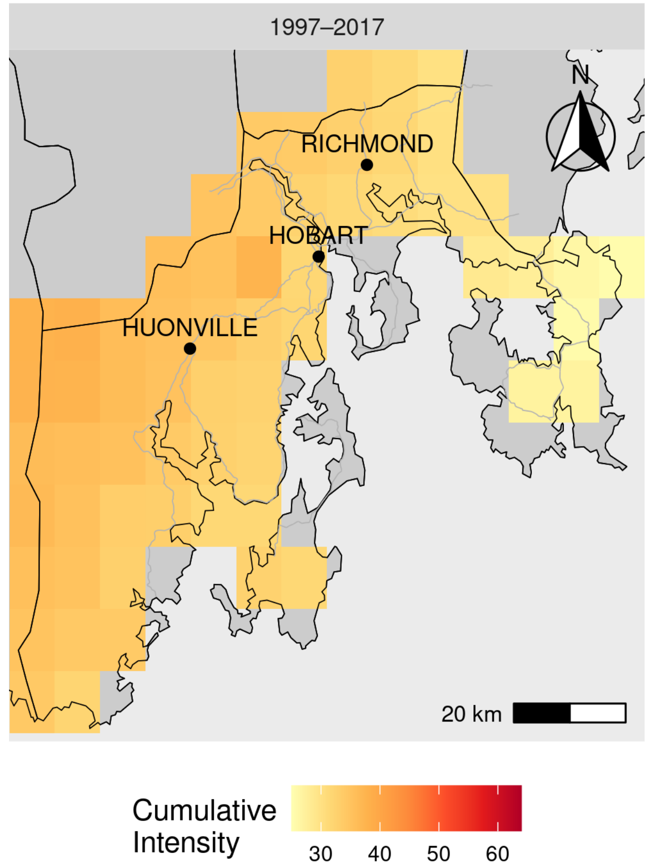


### Figure 2: Observed change in mean cumulative intensity

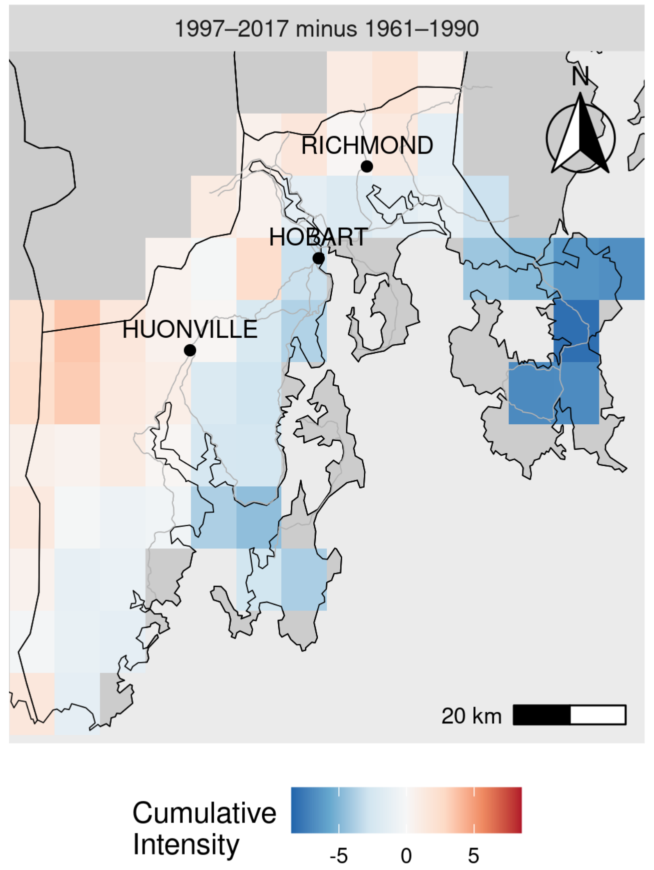


### Figure 3: Projected mean cumulative intensity

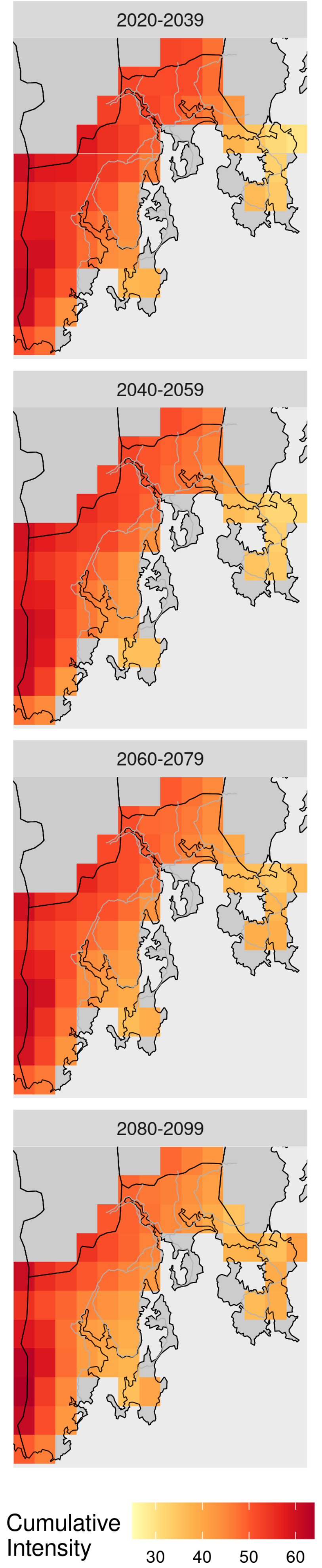


Figure 7: Observed mean *cumulative intensity during a heatwave* across all years from 1997–2017.

Figure 8: The change in mean *cumulative intensity during a heatwave* between the current (1997–2017) and historical (1961–1990) periods. Mean *cumulative intensity during a heatwave* has increased across the region over recent decades.

Figure 9: Projected mean *cumulative intensity during a heatwave* for 20-year time periods from 2001 to 2100. Mean *cumulative intensity during a heatwave* is expected to increase steadily into the future. Each grid cell is the mean of the 6 ensemble members.

### Figure 10: Projected cumulative intensity

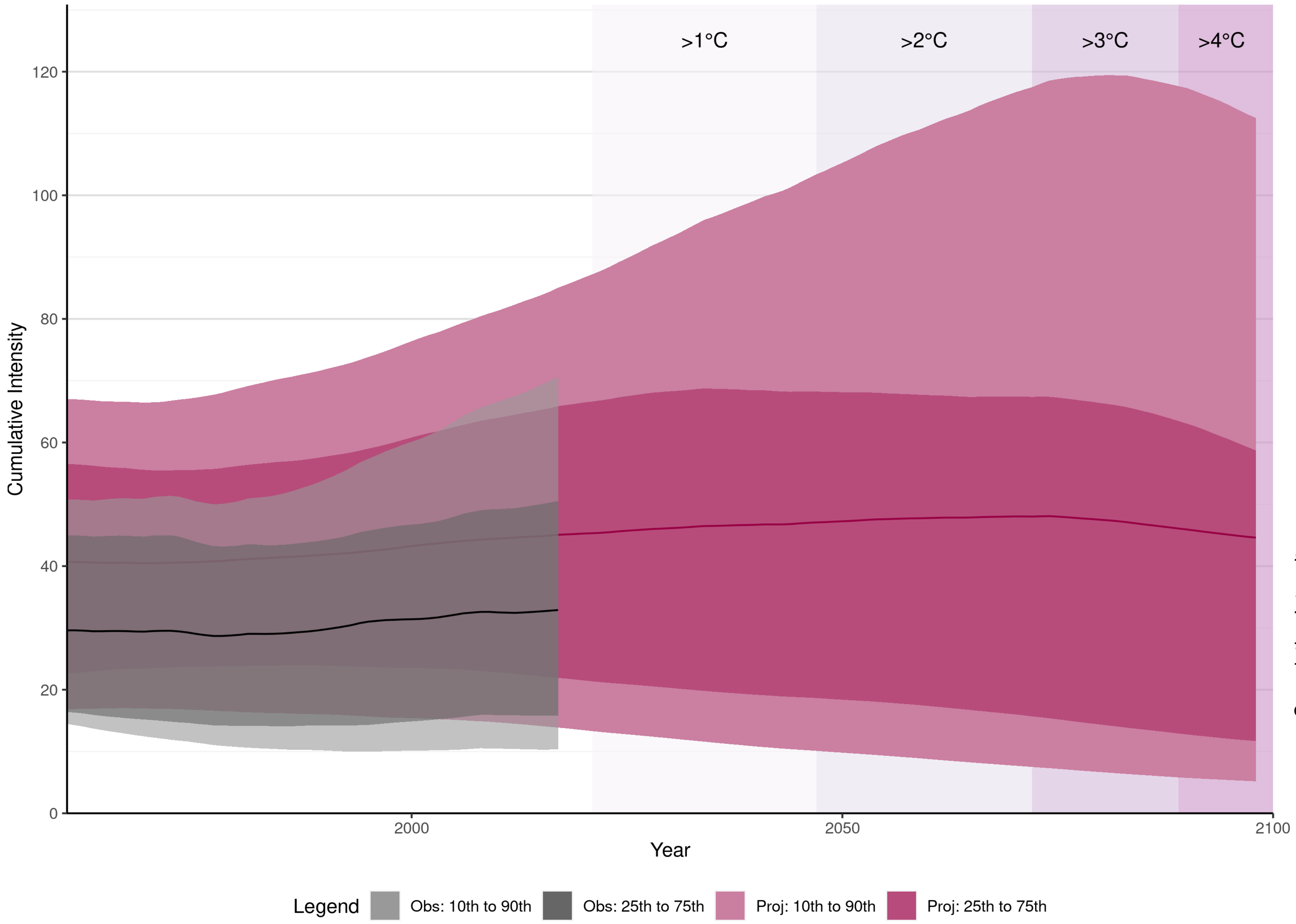


Figure 10: Projected change in *cumulative intensity during a heatwave* from 1990 to 2100. Historical values are the 30-year rolling means from AGCD (*grey*). Projected values (*peach*) are the ensemble mean of the 30-year rolling mean of each ensemble member. *Lighter ribbons* represent the 10th to 90th percentiles of *cumulative intensity during a heatwave*. *Darker ribbons* represent the 25th to 75th percentiles of *cumulative intensity during a heatwave*. *Solid lines* represent the mean of *cumulative intensity during a heatwave*.

### Figure 11: Distribution of cumulative intensity

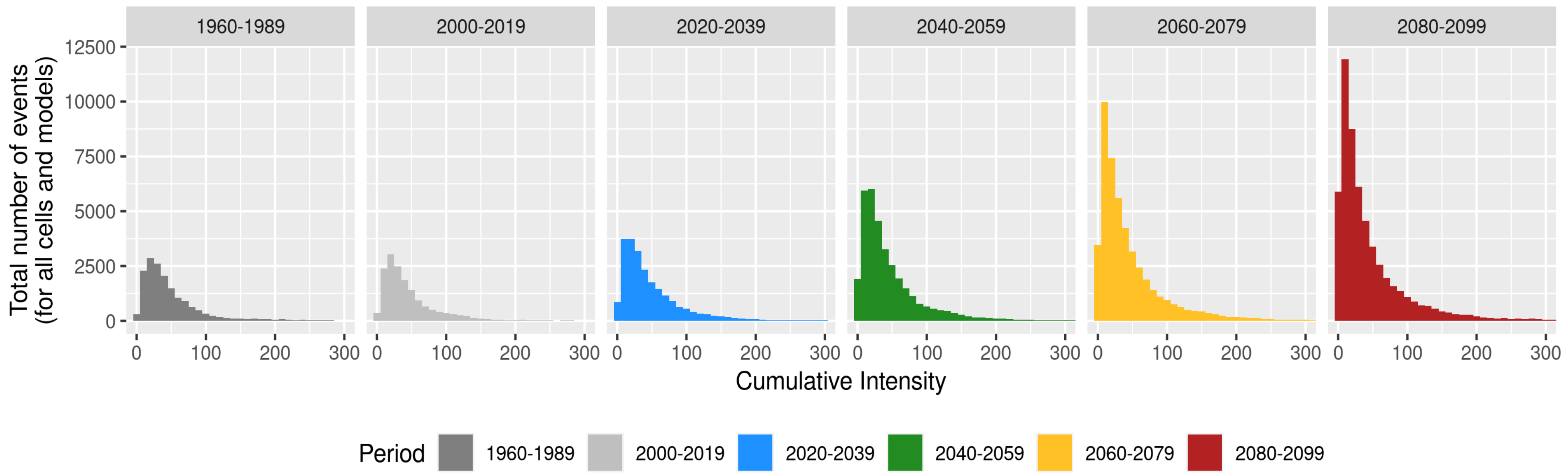


Figure 11: Comparison of the distribution of *cumulative intensity during a heatwave* for different time periods.

### Figure 12: Projected mean cumulative intensity

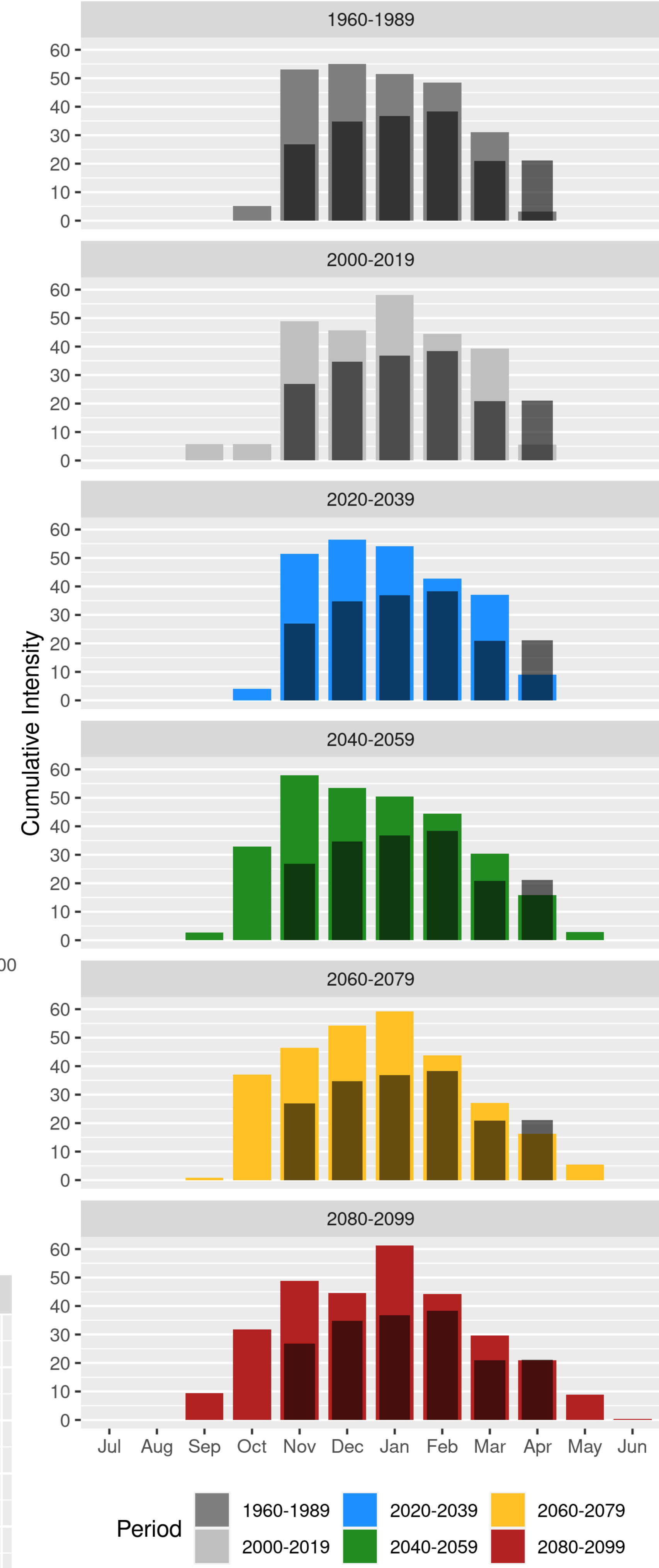


Figure 12: *Bar plots of cumulative intensity during heatwaves* in each month for 20-year time periods from 1961 to 2100. Each bar represents the 20-year mean of *cumulative intensity during a heatwave*, average across space and time. The observations for the baseline period (1961–1990) are shadowed on top of the future time periods to highlight any differences expected into the future. Higher (lower) bars indicate hotter (cooler) heatwave intensities.

# SOUTH EAST

## Heatwaves — Duration

Figure 1: Observed mean duration

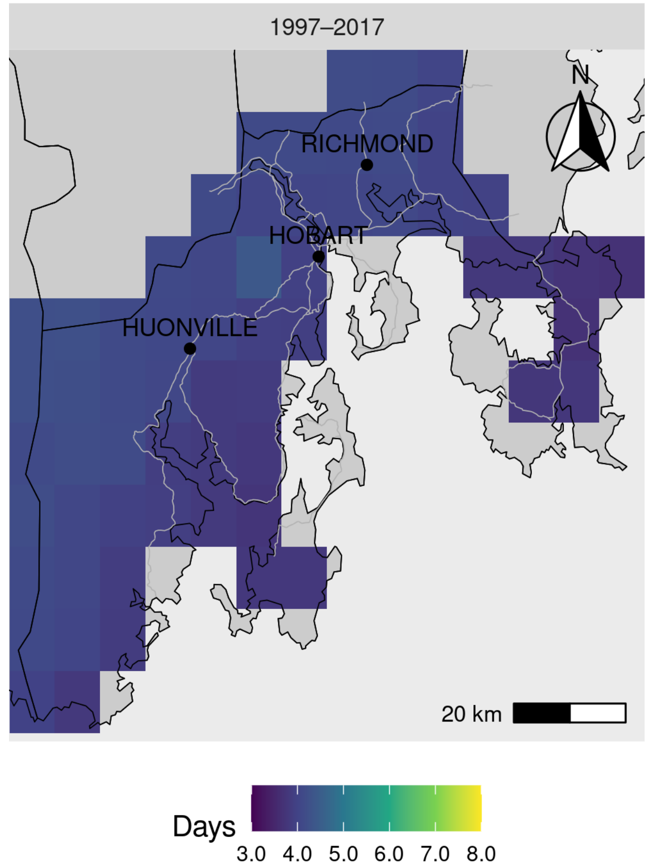


Figure 2: Observed change in mean duration

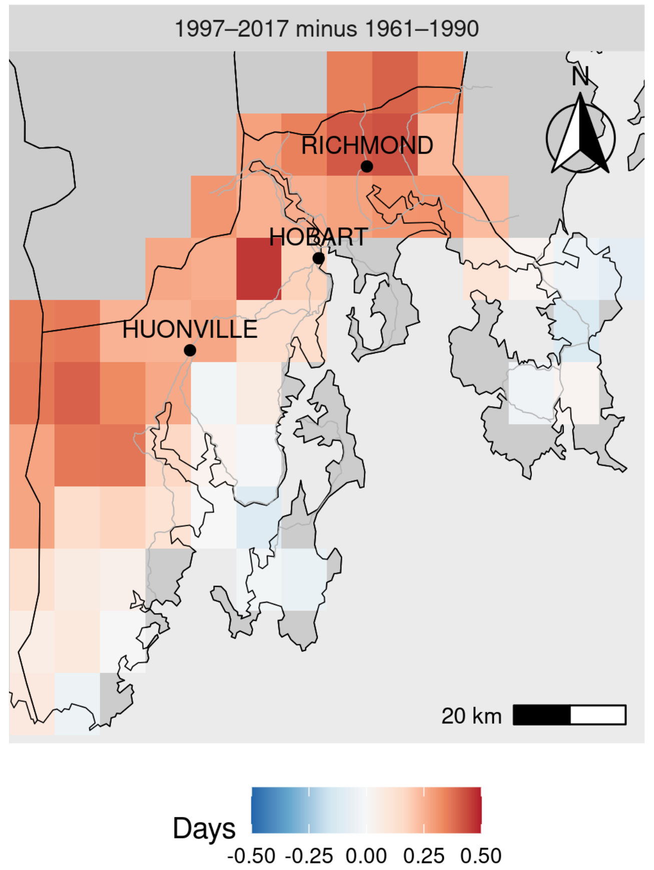


Figure 3: Projected mean duration

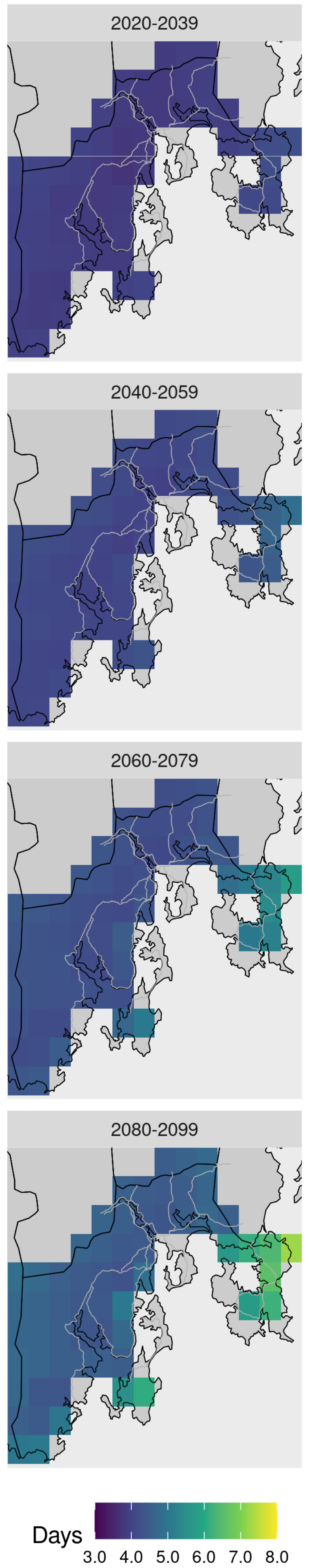


Figure 16: Projected heatwave duration

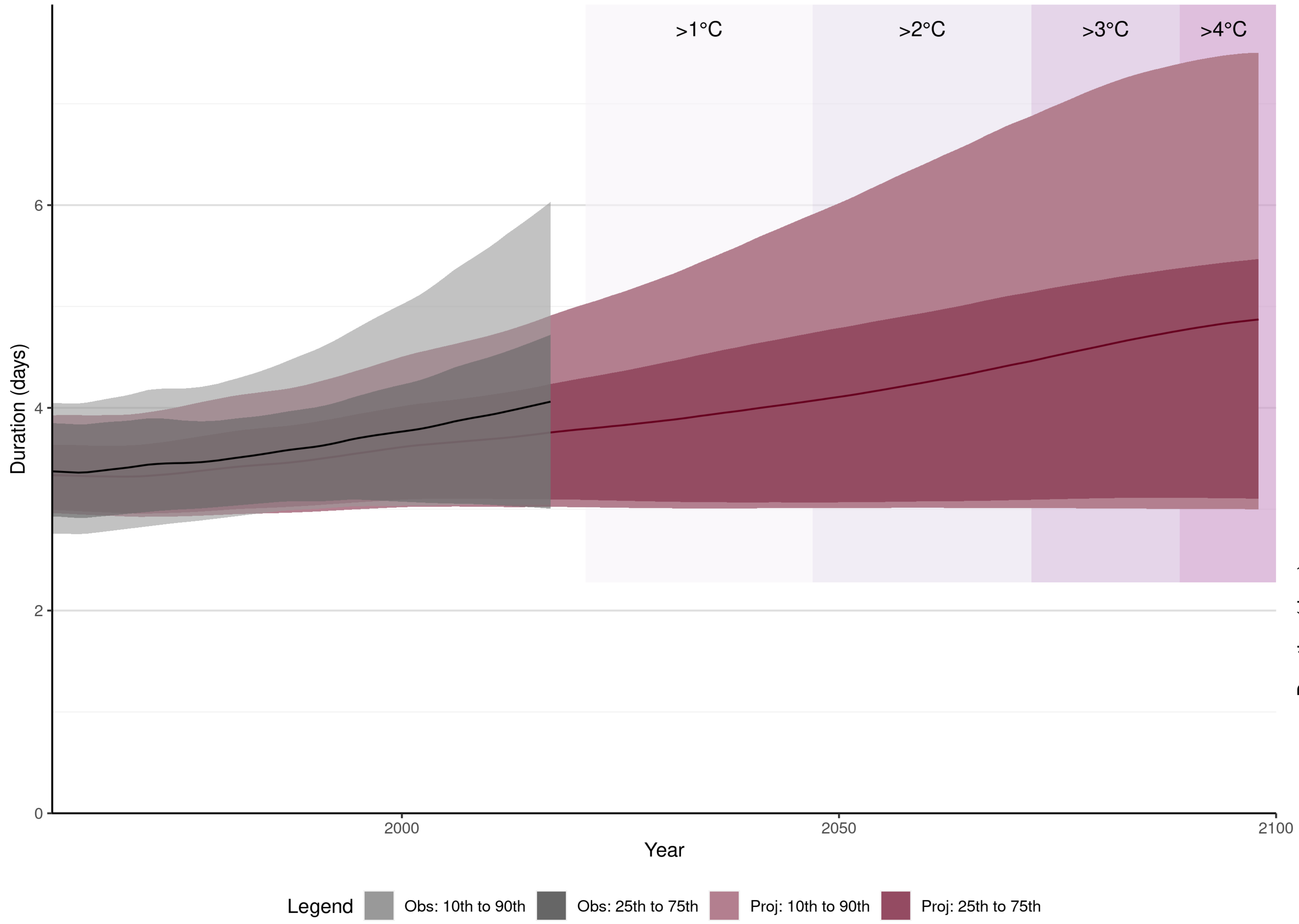


Figure 16: Projected change in *heatwave duration* from 1990 to 2100. Historical values (*grey*) are the 30-year rolling means of AGCD. Projected values (*orange*) are the ensemble mean of the 30-year rolling mean of each CCAM ensemble member. *Lighter ribbons* represent the 10th to 90th percentiles of *heatwave duration*. *Darker ribbons* represent the 25th to 75th percentiles of *heatwave duration*. *Solid lines* represent the mean of *heatwave duration*.

Figure 17: Projected count of heatwave duration

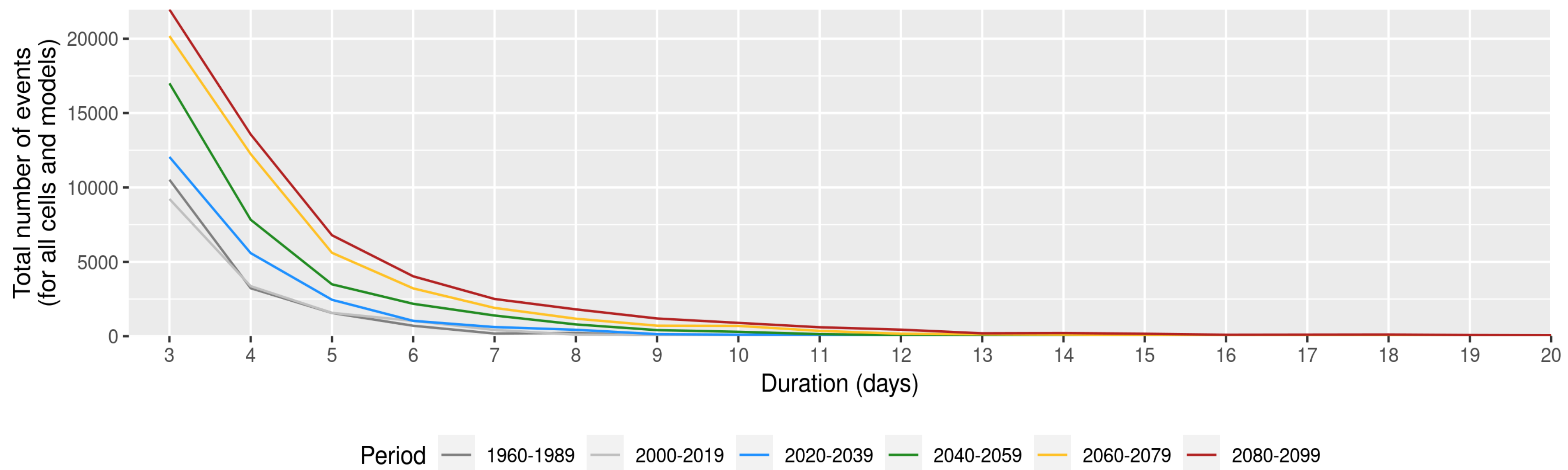


Figure 17: Comparison of the distribution of *heatwave durations* for different time periods.

Figure 18: Projected mean heatwave duration by

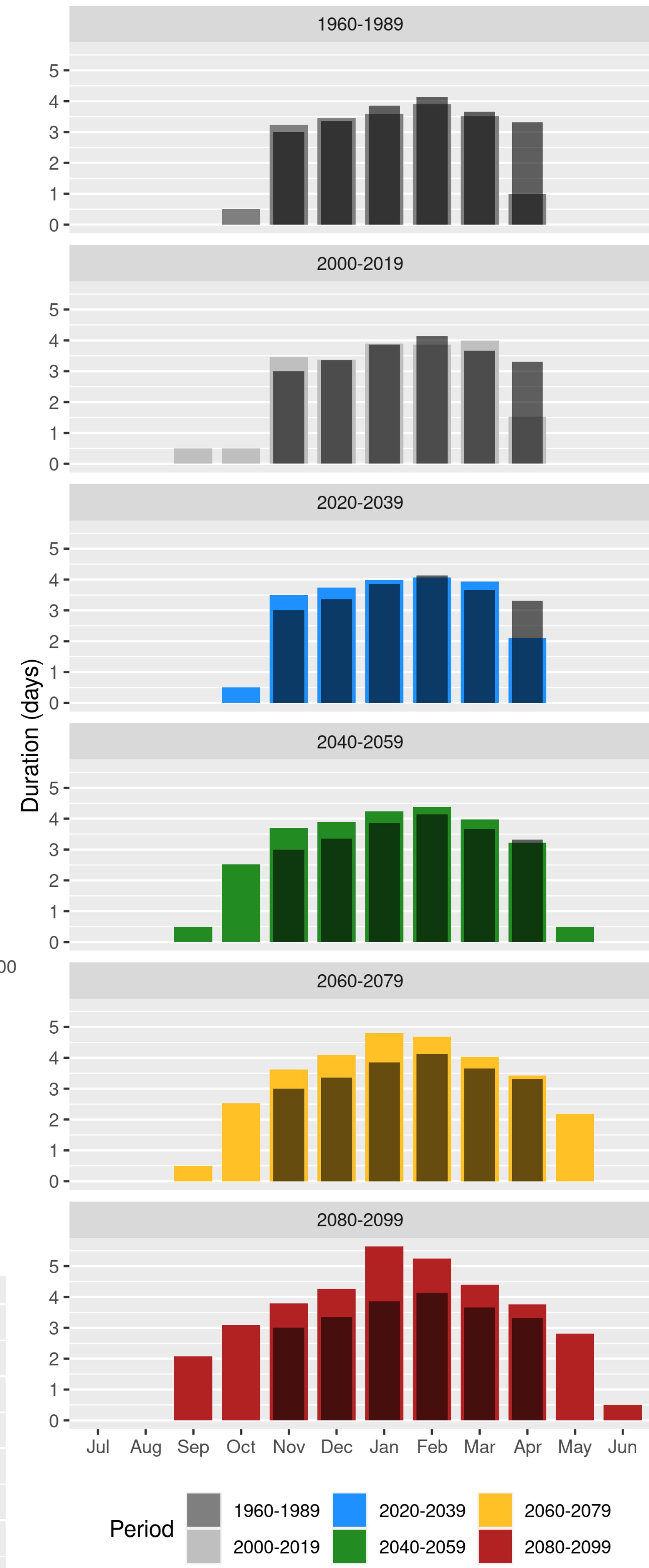


Figure 18: *Bar plots* of mean *heatwave durations* in each month for 20-year time periods from 1961 to 2100. Each bar represents the 20-year mean of *heatwave durations*, average across space and time. The observations for the baseline period (1961–1990) are shadowed on top of the future time periods to highlight any differences expected into the future. Higher (lower) bars indicate longer (shorter) *heatwave durations*.

Figure 13: Observed mean *heatwave durations* across all years from 1997–2017.

Figure 14: The change in mean *heatwave duration* between the current (1997–2017) and historical (1961–1990) periods. Mean *heatwave durations* have increased across the region over recent decades.

Figure 15: Projected mean *heatwave durations* for 20-year time periods from 2001 to 2100. Mean *heatwave duration* is expected to increase steadily into the future. Each grid cell is the mean of the 6 ensemble members.

# UPPER DERWENT VALLEY

## Heatwaves — Number of Heatwave Days

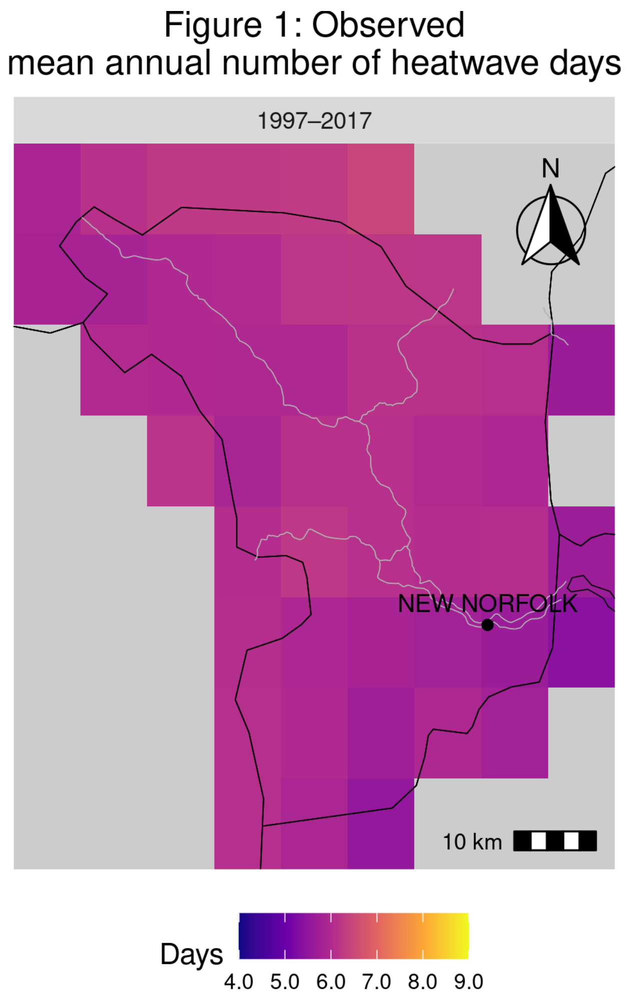


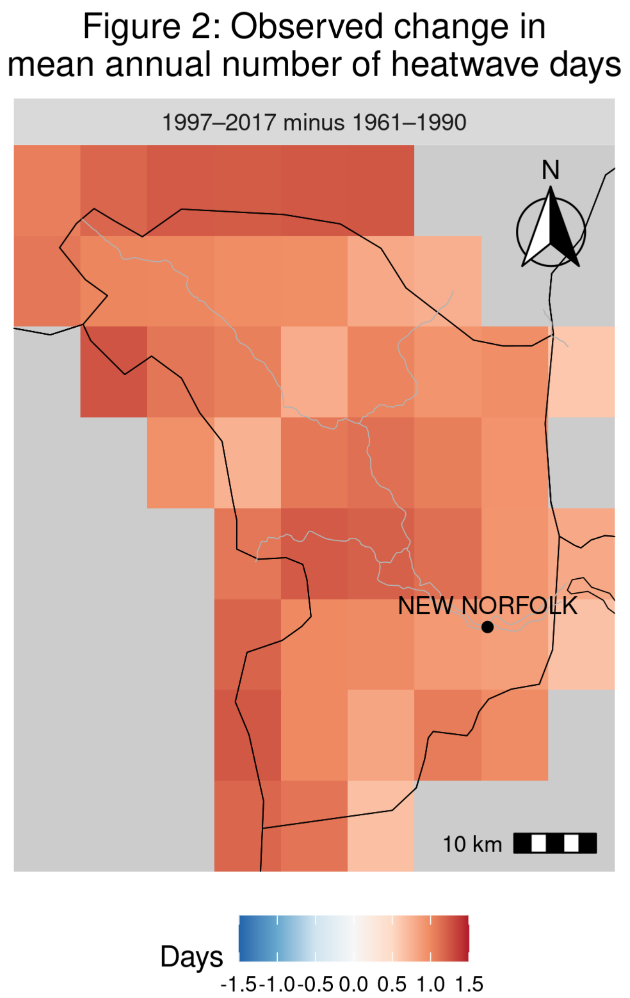


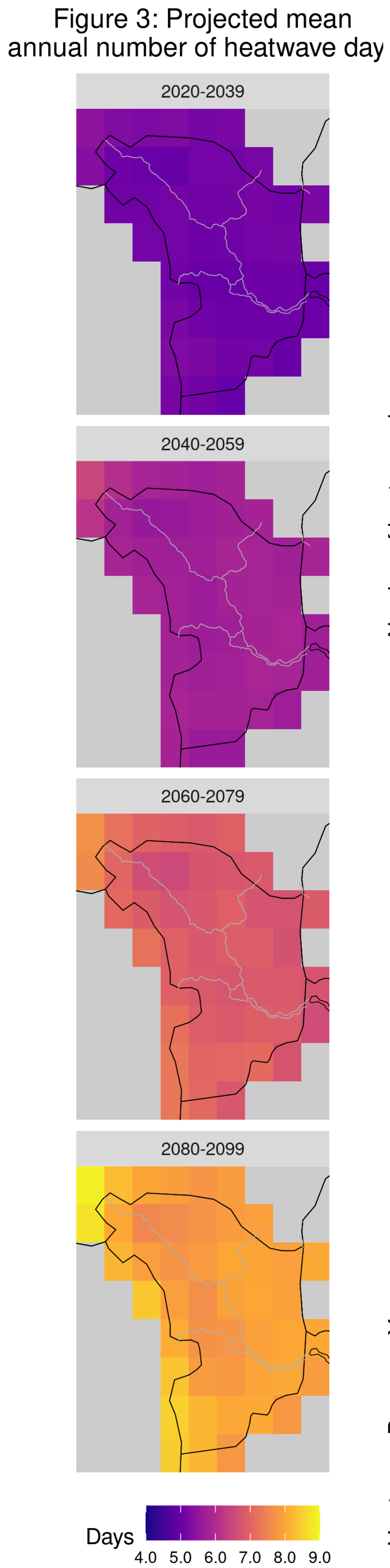


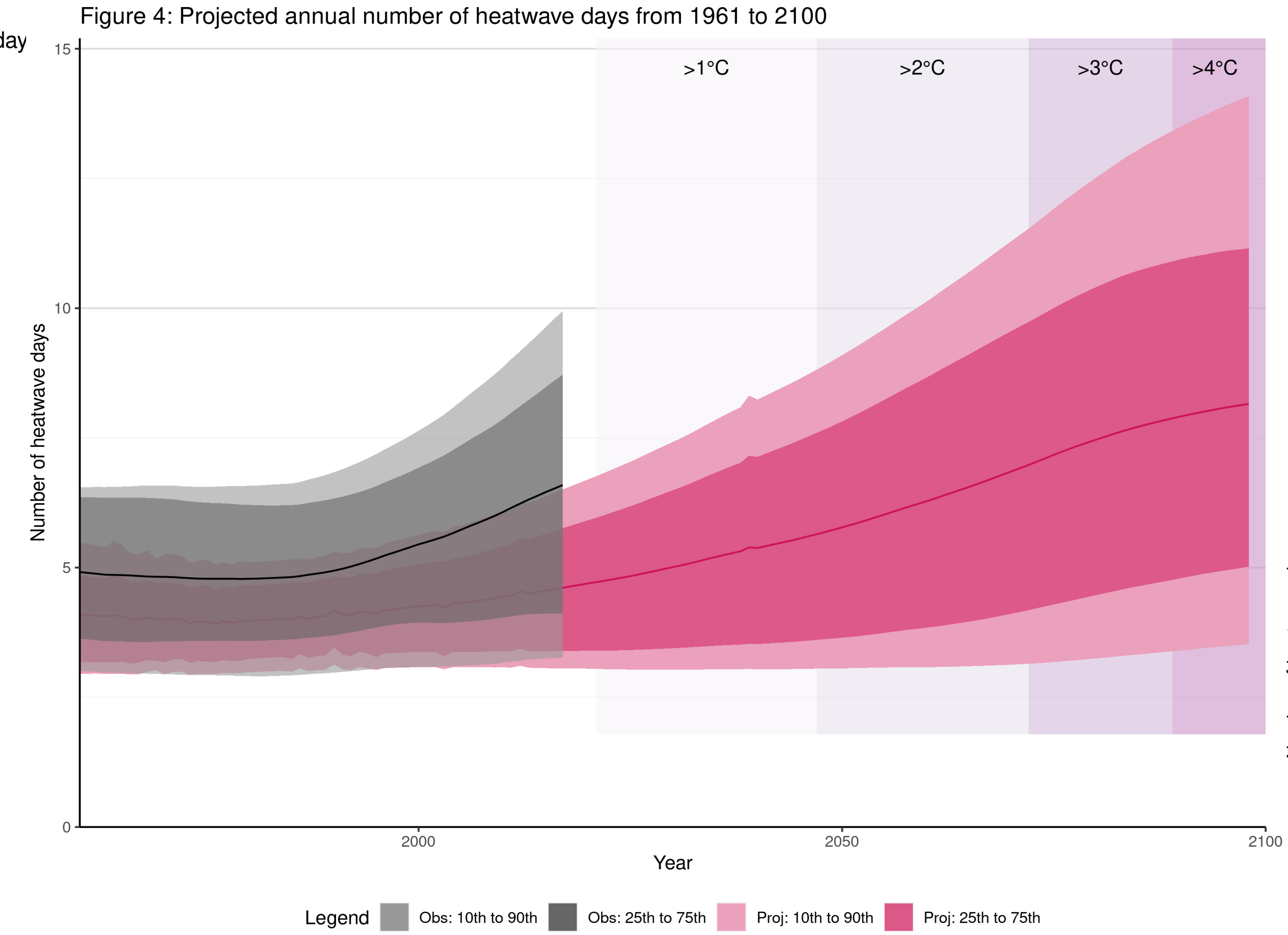


Figure 4: Projected change in mean *annual number of heatwave days* from 1990 to 2100. Historical values (*grey*) are the 30-year rolling means of AGCD. Projected values (*peach*) are the ensemble mean of the 30-year rolling mean of each CCAM ensemble member. *Lighter ribbons* represent the 10th to 90th percentiles of mean *annual number of heatwave days*. *Darker ribbons* represent the 25th to 75th percentiles of mean *annual number of heatwave days*. *Solid lines* represent the mean *annual number of heatwave days*.

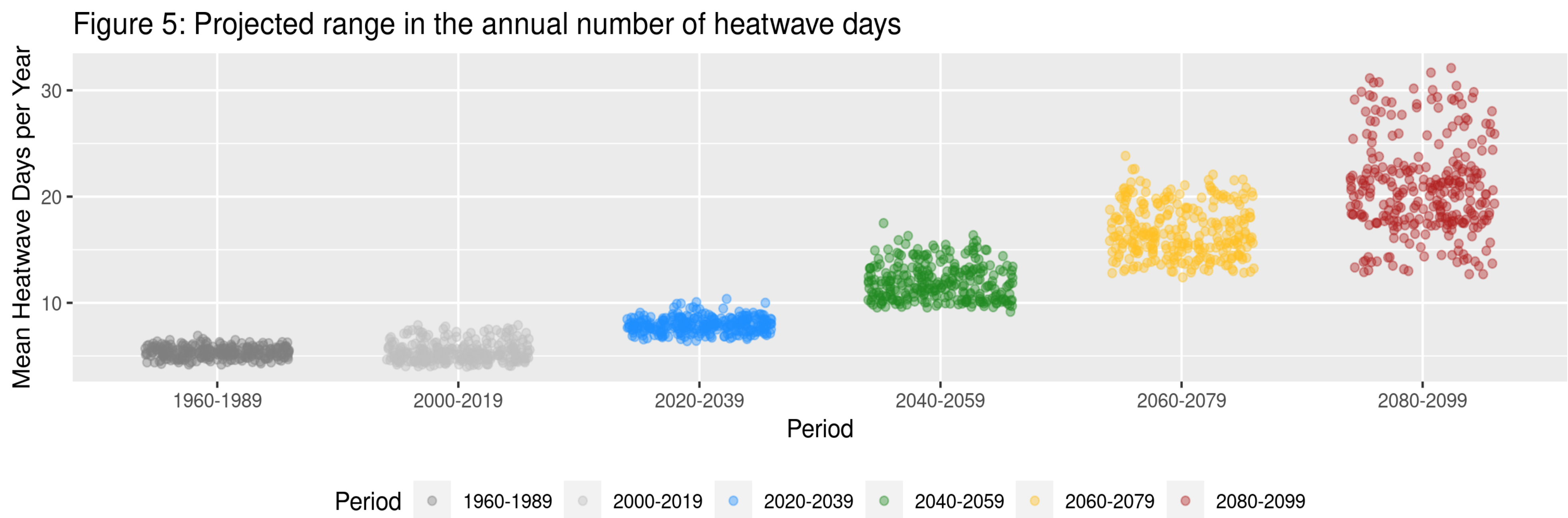


Figure 5: Comparison of the distribution of the *annual number of heatwave days* over the historical period for both model outputs (¡colour¿ and observations (*black*).

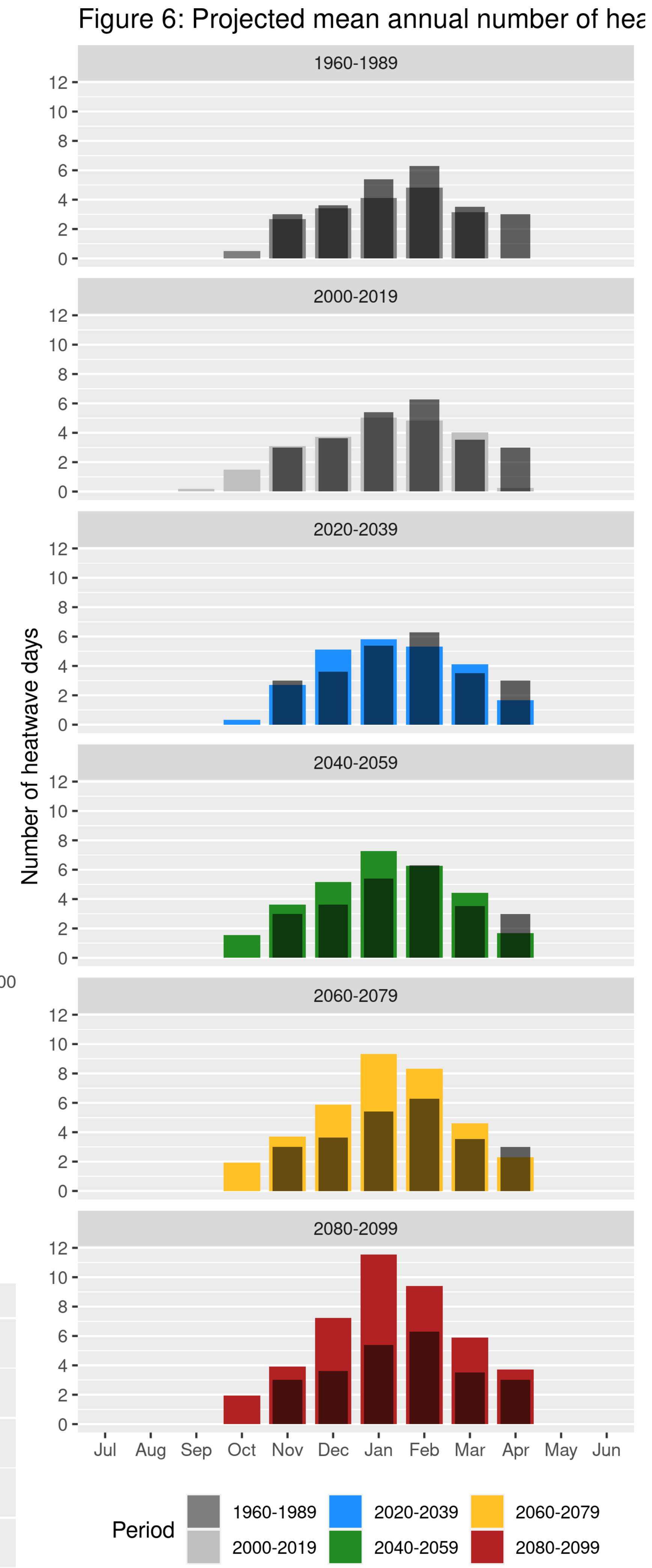


Figure 6: *Bar plots of typical number of heatwave days in each month* for 20-year time periods from 1961 to 2100. Each bar represents the 20-year *typical number of heatwave days in each month*, average across space and time. The observations for the baseline period (1961–1990) are shadowed on top of the future time periods to highlight any differences expected into the future. Higher (lower) bars indicate more (less) heatwave days.

Figure 1: Observed mean *annual number of heatwave days* across all years from 1997–2017.

Figure 2: The change in the mean *annual number of heatwave days* between the current (1997–2017) and historical (1961–1990) periods. Mean *annual number of heatwave days* has increased across the region over recent decades.

Figure 3: Projected mean *annual number of heatwave days* for 20-year time periods from 2001 to 2100. Mean *annual number of heatwave days* is expected to increase steadily into the future. Each grid cell is the mean of the 6 ensemble members.

# UPPER DERWENT VALLEY

## Heatwaves — Cumulative Intensity

Figure 1: Observed mean cumulative intensity

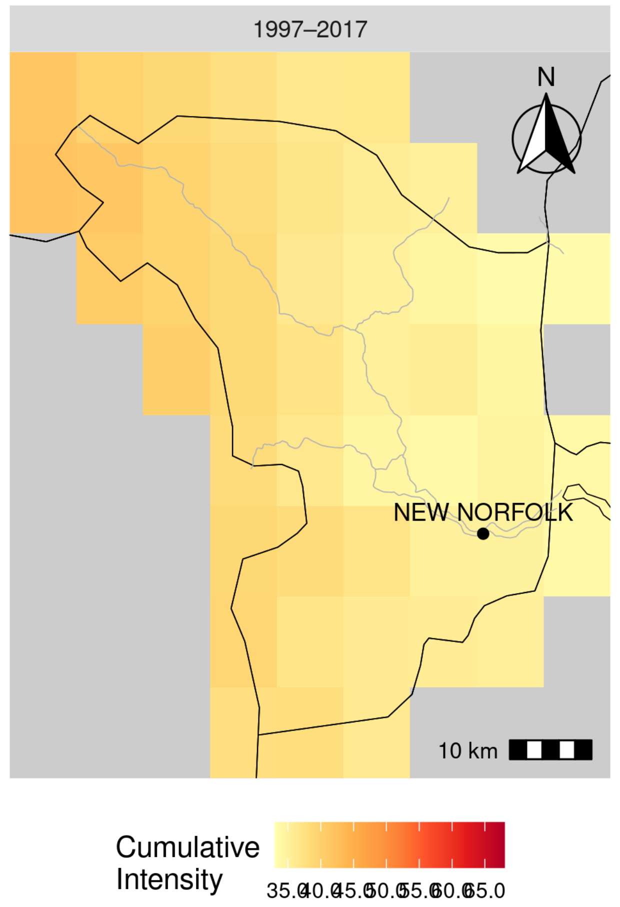


Figure 2: Observed change in mean cumulative intensity

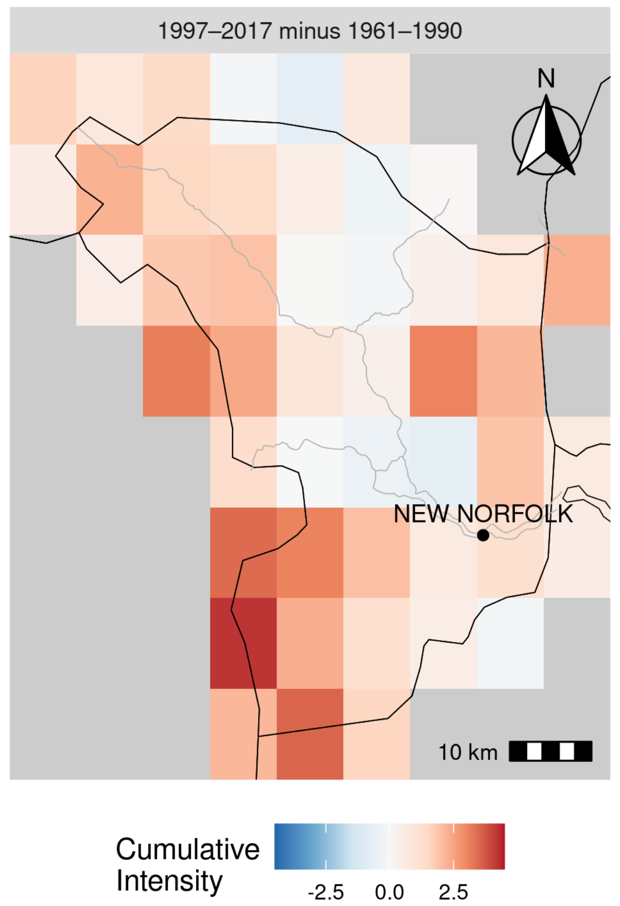


Figure 3: Projected mean cumulative intensity

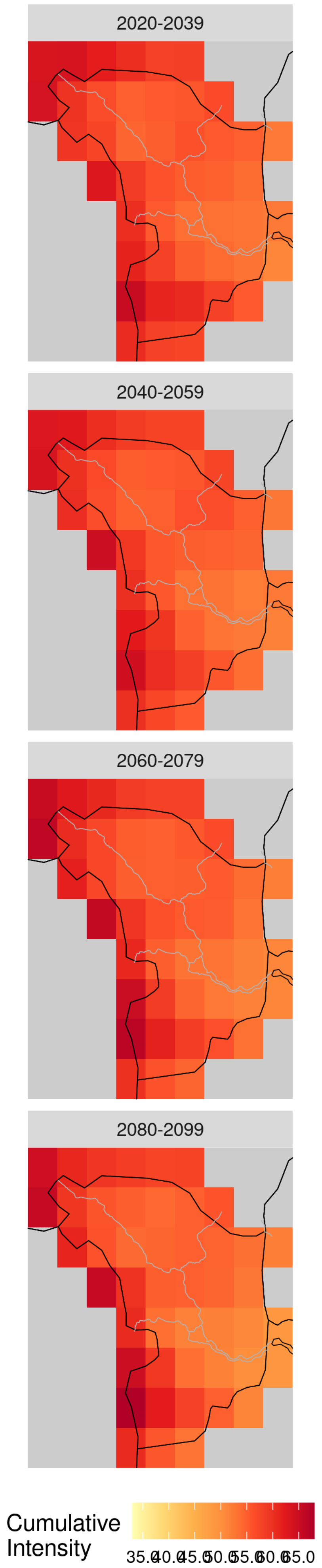


Figure 7: Observed mean *cumulative intensity during a heatwave* across all years from 1997–2017.

Figure 8: The change in mean *cumulative intensity during a heatwave* between the current (1997–2017) and historical (1961–1990) periods. Mean *cumulative intensity during a heatwave* has increased across the region over recent decades.

Figure 9: Projected mean *cumulative intensity during a heatwave* for 20-year time periods from 2001 to 2100. Mean *cumulative intensity during a heatwave* is expected to increase steadily into the future. Each grid cell is the mean of the 6 ensemble members.

Figure 10: Projected cumulative intensity

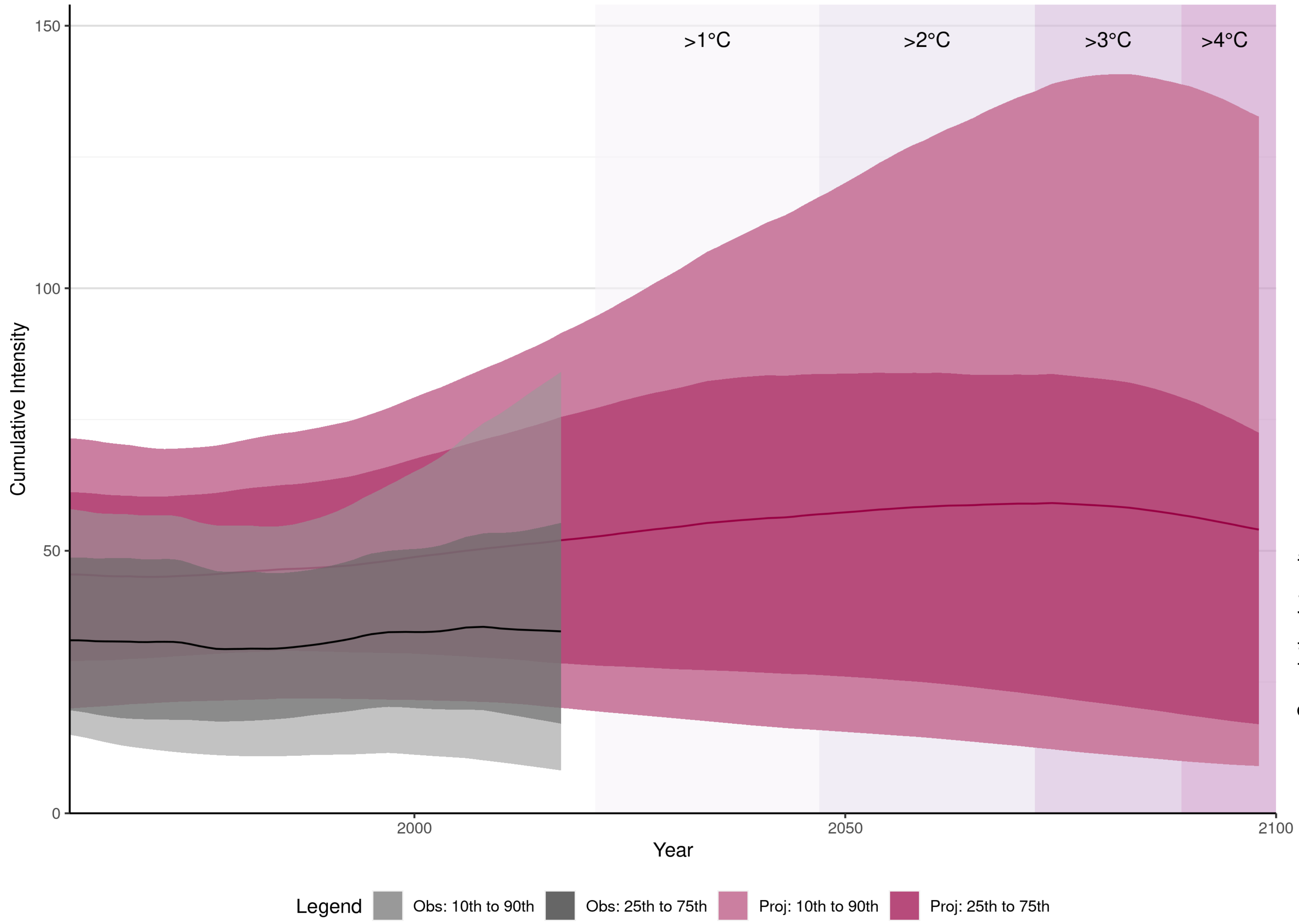


Figure 10: Projected change in *cumulative intensity during a heatwave* from 1990 to 2100. Historical values are the 30-year rolling means from AGCD (*grey*). Projected values (*peach*) are the ensemble mean of the 30-year rolling mean of each ensemble member. *Lighter ribbons* represent the 10th to 90th percentiles of *cumulative intensity during a heatwave*. *Darker ribbons* represent the 25th to 75th percentiles of *cumulative intensity during a heatwave*. *Solid lines* represent the mean of *cumulative intensity during a heatwave*.

Figure 11: Distribution of cumulative intensity

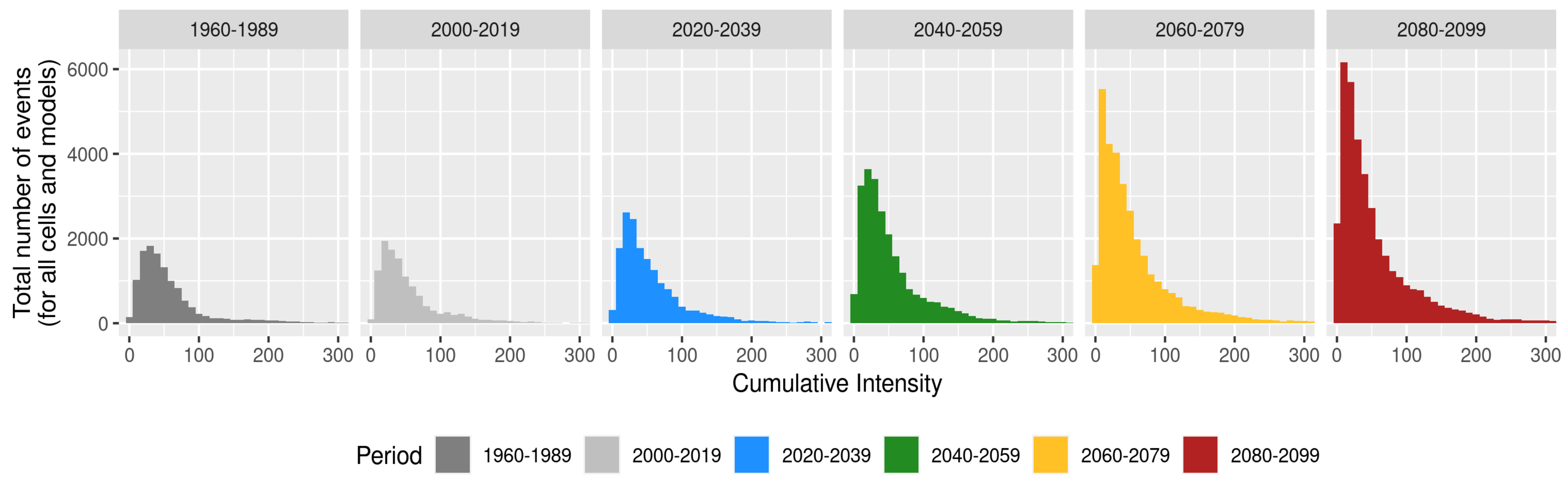


Figure 11: Comparison of the distribution of *cumulative intensity during a heatwave* for different time periods.

Figure 12: Projected mean cumulative intensity

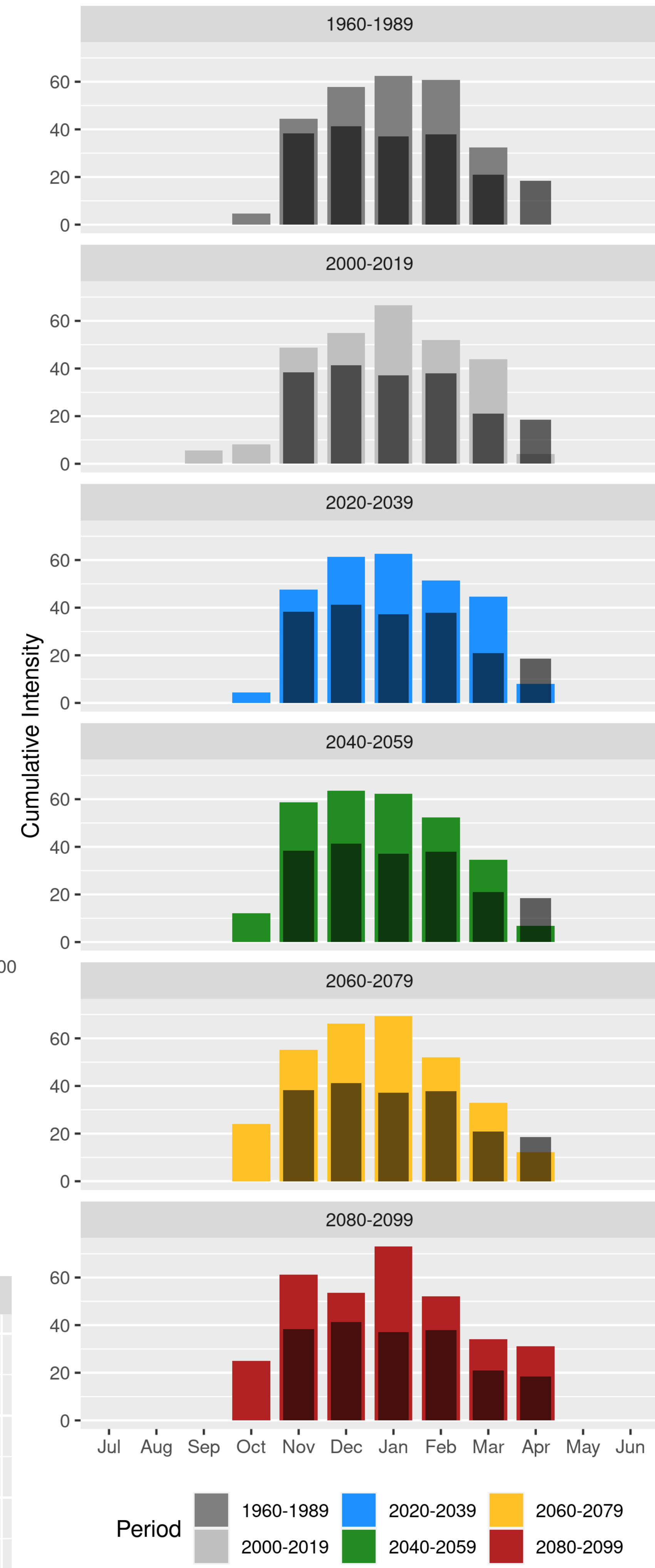


Figure 12: *Bar plots of cumulative intensity during heatwaves* in each month for 20-year time periods from 1961 to 2100. Each bar represents the 20-year mean of *cumulative intensity during a heatwave*, average across space and time. The observations for the baseline period (1961–1990) are shadowed on top of the future time periods to highlight any differences expected into the future. Higher (lower) bars indicate hotter (cooler) heatwave intensities.

# UPPER DERWENT VALLEY

## Heatwaves — Duration

Figure 1: Observed mean duration

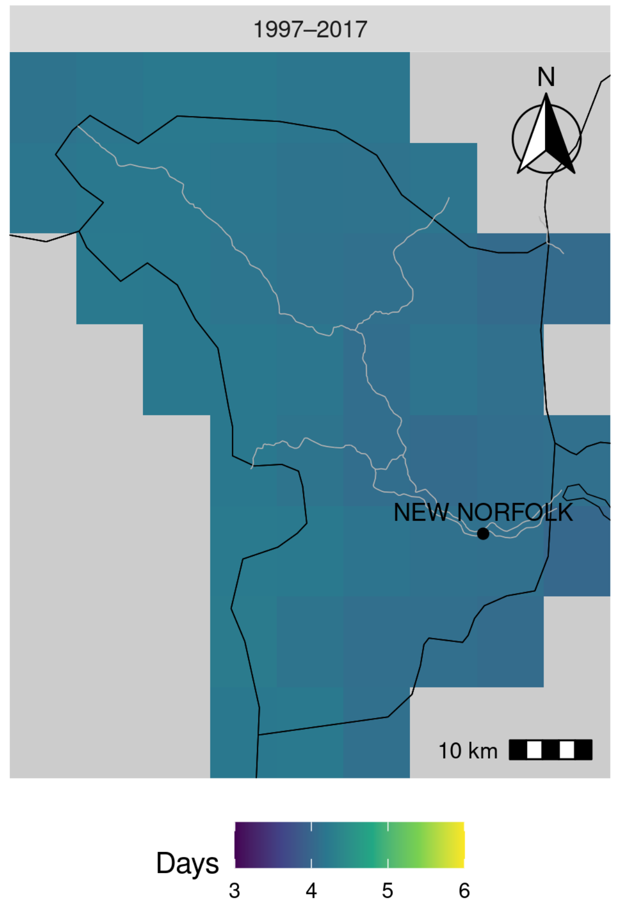


Figure 2: Observed change in mean duration

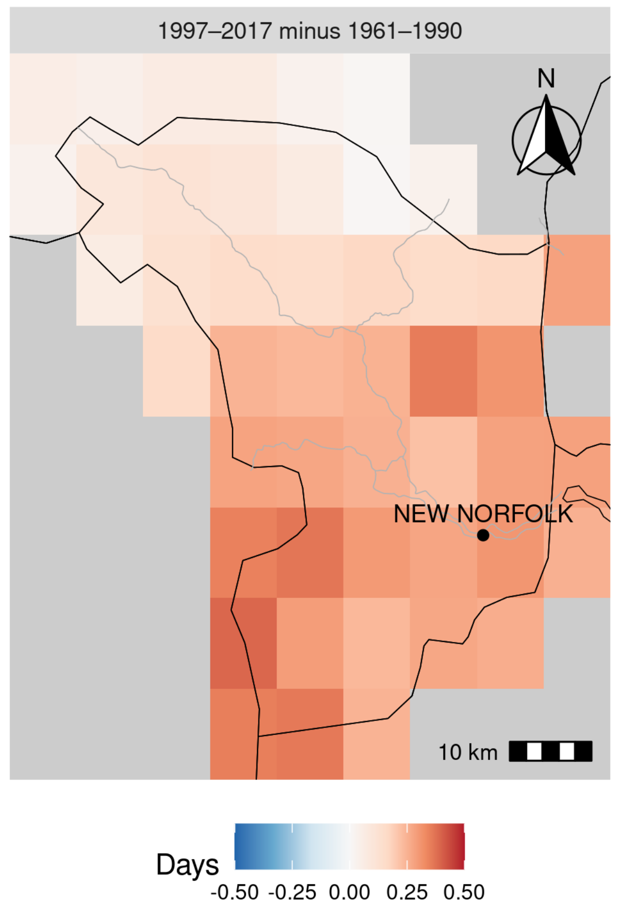


Figure 3: Projected mean duration

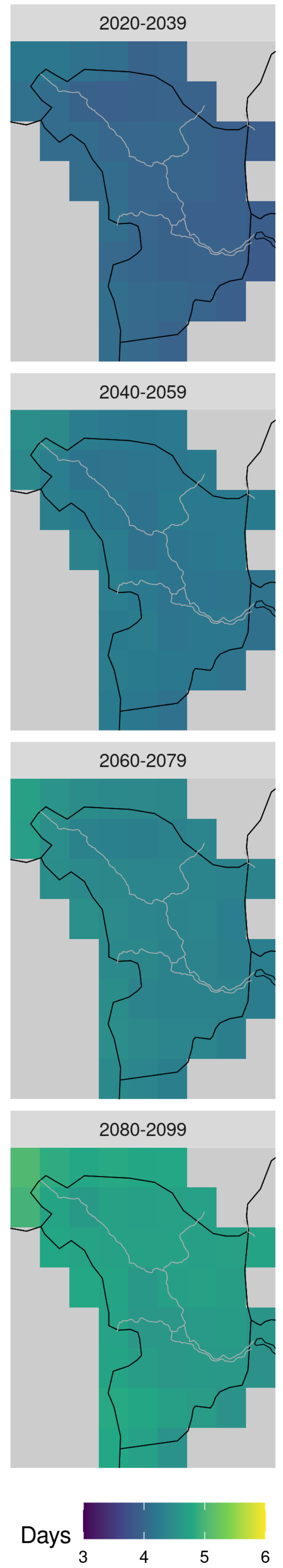


Figure 13: Observed mean *heatwave durations* across all years from 1997–2017.

Figure 14: The change in mean *heatwave duration* between the current (1997–2017) and historical (1961–1990) periods. Mean *heatwave durations* have increased across the region over recent decades.

Figure 15: Projected mean *heatwave durations* for 20-year time periods from 2001 to 2100. Mean *heatwave duration* is expected to increase steadily into the future. Each grid cell is the mean of the 6 ensemble members.

Figure 16: Projected heatwave duration

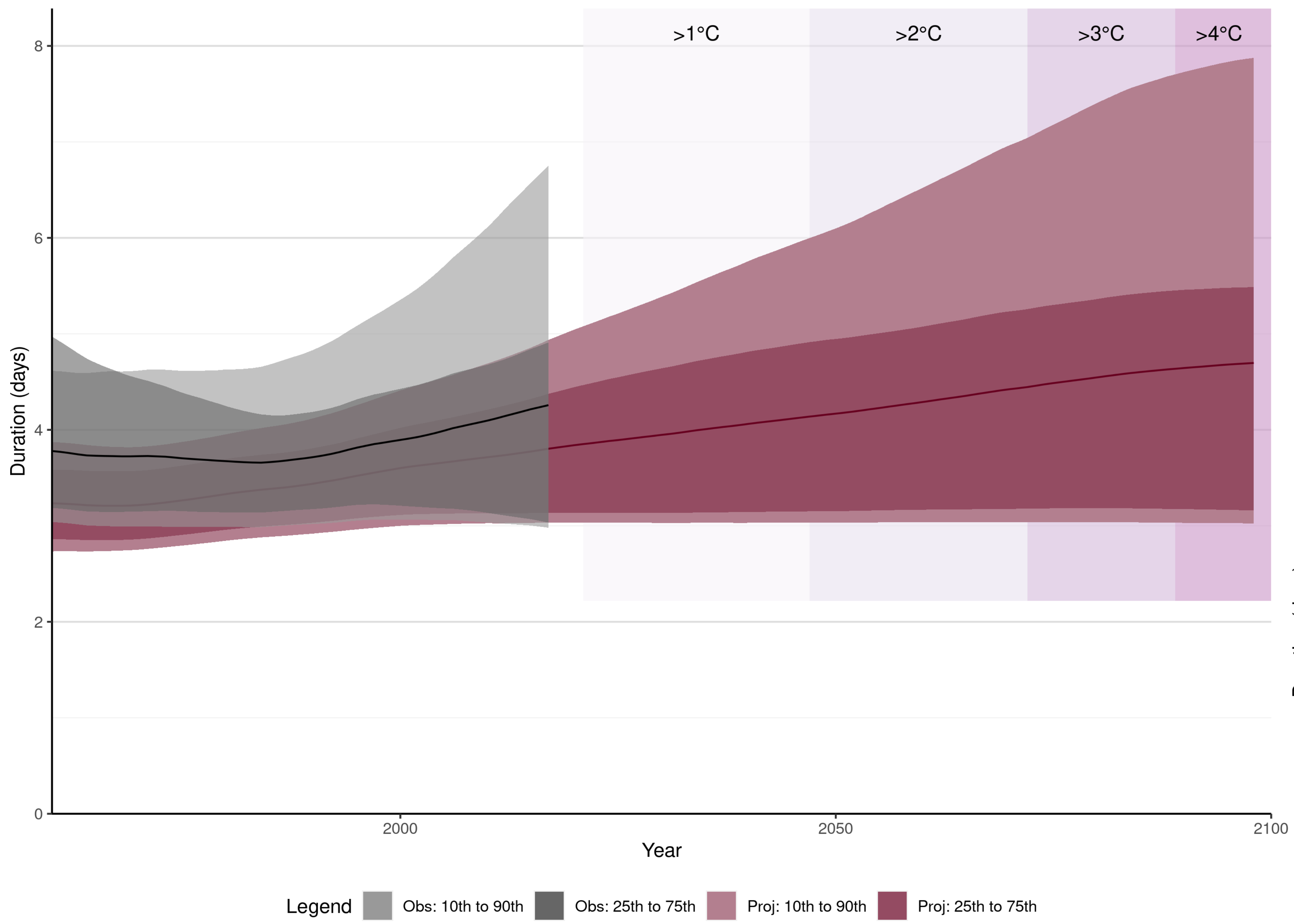


Figure 16: Projected change in *heatwave duration* from 1990 to 2100. Historical values (*grey*) are the 30-year rolling means of AGCD. Projected values (*orange*) are the ensemble mean of the 30-year rolling mean of each CCAM ensemble member. *Lighter ribbons* represent the 10th to 90th percentiles of *heatwave duration*. *Darker ribbons* represent the 25th to 75th percentiles of *heatwave duration*. *Solid lines* represent the mean of *heatwave duration*.

Figure 17: Projected count of heatwave duration

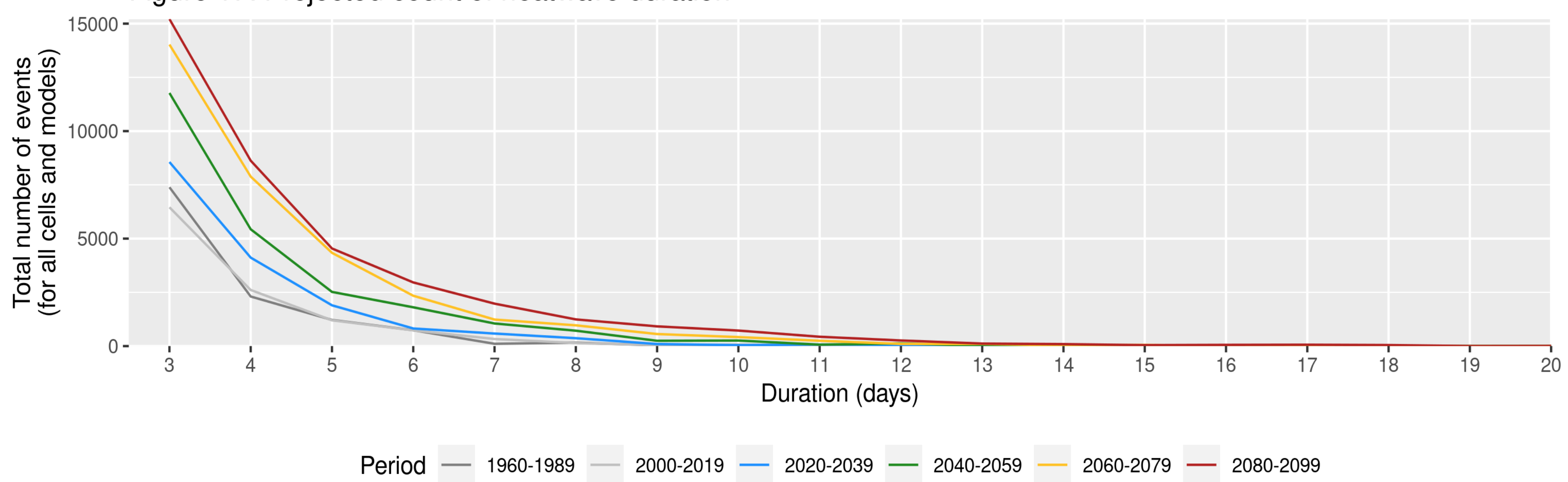


Figure 17: Comparison of the distribution of *heatwave durations* for different time periods.

Figure 18: Projected mean heatwave duration by

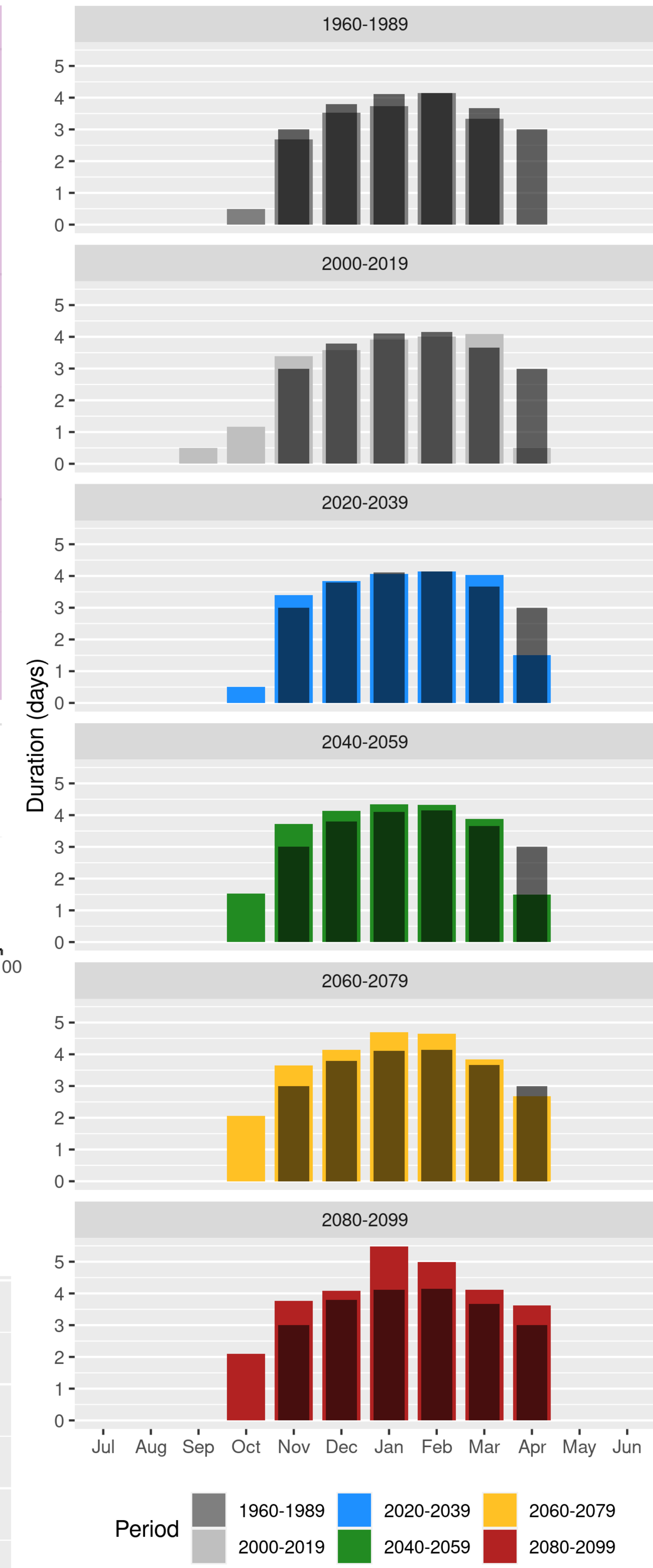


Figure 18: *Bar plots* of mean *heatwave durations* in each month for 20-year time periods from 1961 to 2100. Each bar represents the 20-year mean of *heatwave durations*, average across space and time. The observations for the baseline period (1961–1990) are shadowed on top of the future time periods to highlight any differences expected into the future. Higher (lower) bars indicate longer (shorter) *heatwave durations*.

Figure 1: Observed mean annual number of heatwave days

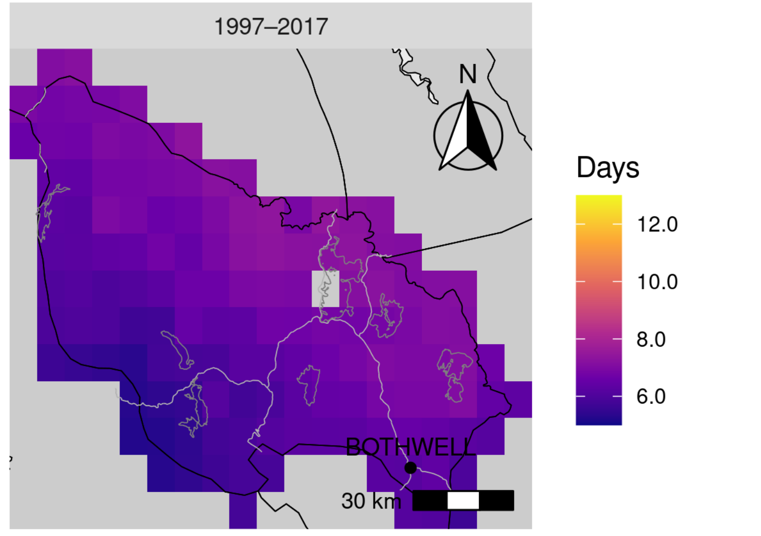


igure 2: Observed change in mean annual number of heatwave days

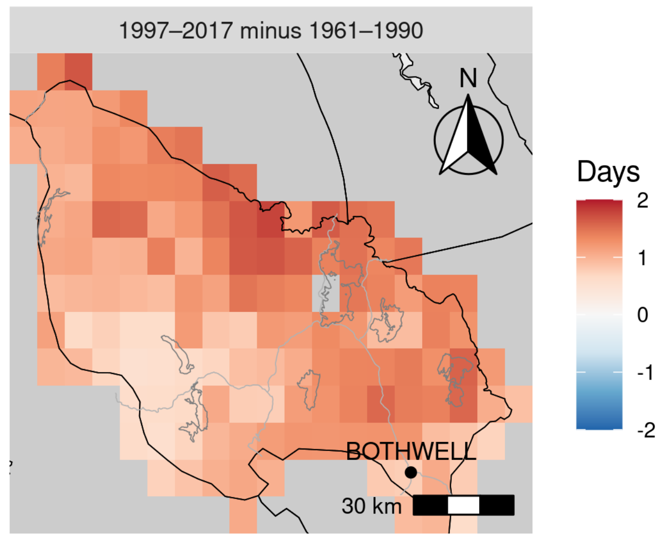


Figure 3: Projected mean annual number of heatwave days

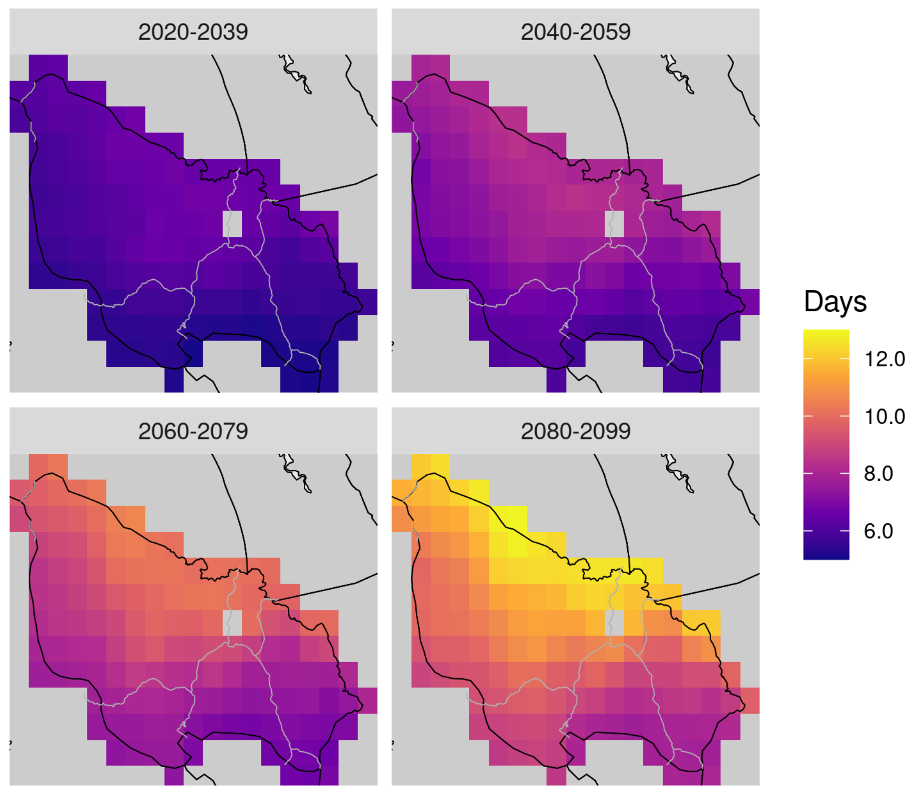


Figure 1: Observed mean *annual number of heatwave days* across all years from 1997–2017.

Figure 2: The change in the mean *annual number of heatwave days* between the current (1997–2017) and historical (1961–1990) periods. Mean *annual number of heatwave days* has increased across the region over recent decades.

Figure 3: Projected mean *annual number of heatwave days* for 20-year time periods from 2001 to 2100. Mean *annual number of heatwave days* is expected to increase steadily into the future. Each grid cell is the mean of the 6 ensemble members.

Figure 4: Projected annual number of heatwave days from 1961 to 2100

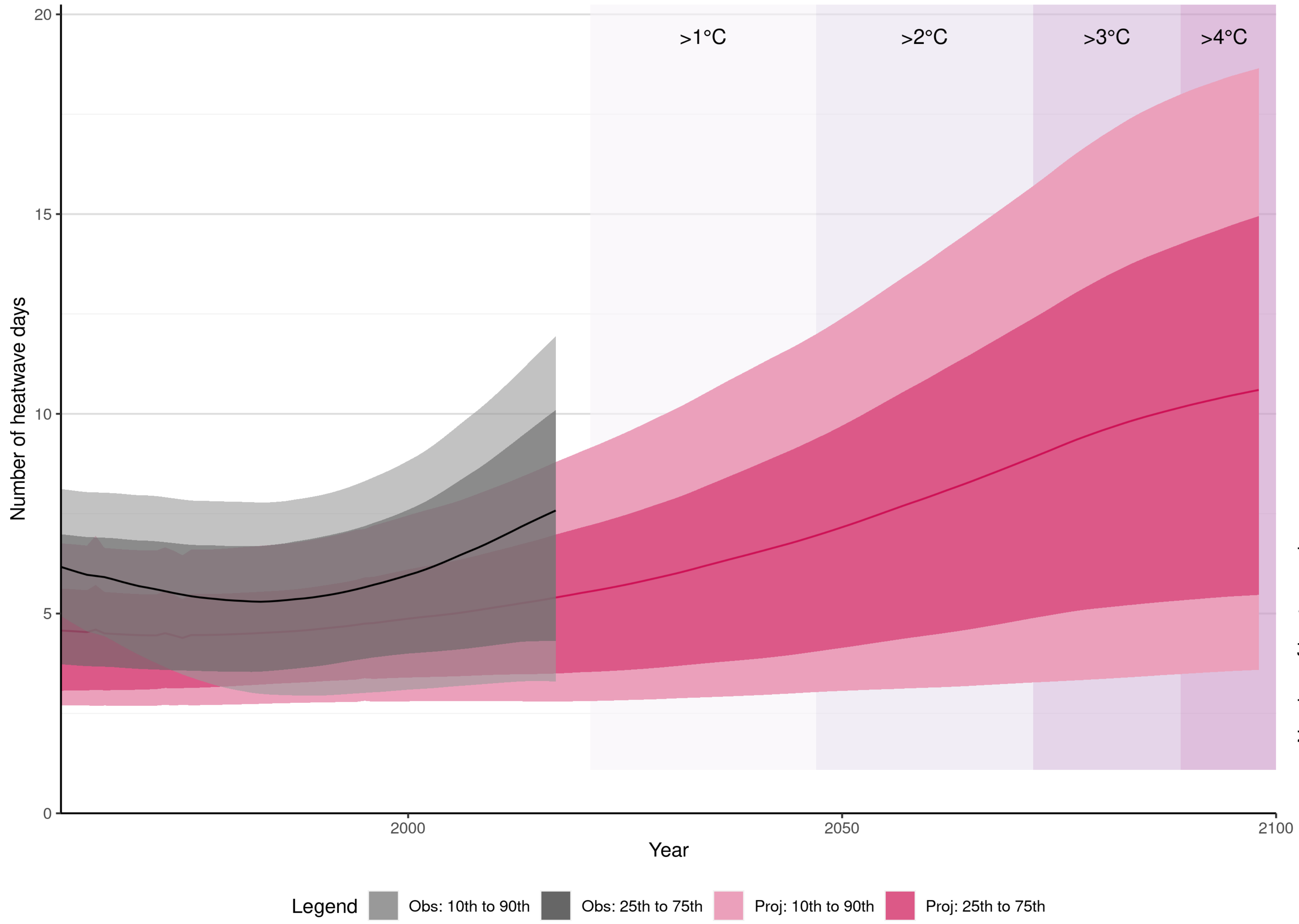


Figure 4: Projected change in mean *annual number of heatwave days* from 1990 to 2100. Historical values (*grey*) are the 30-year rolling means of AGCD. Projected values (*peach*) are the ensemble mean of the 30-year rolling mean of each CCAM ensemble member. *Lighter ribbons* represent the 10th to 90th percentiles of mean *annual number of heatwave days*. *Darker ribbons* represent the 25th to 75th percentiles of mean *annual number of heatwave days*. *Solid lines* represent the mean *annual number of heatwave days*.

Figure 5: Projected range in the annual number of heatwave days

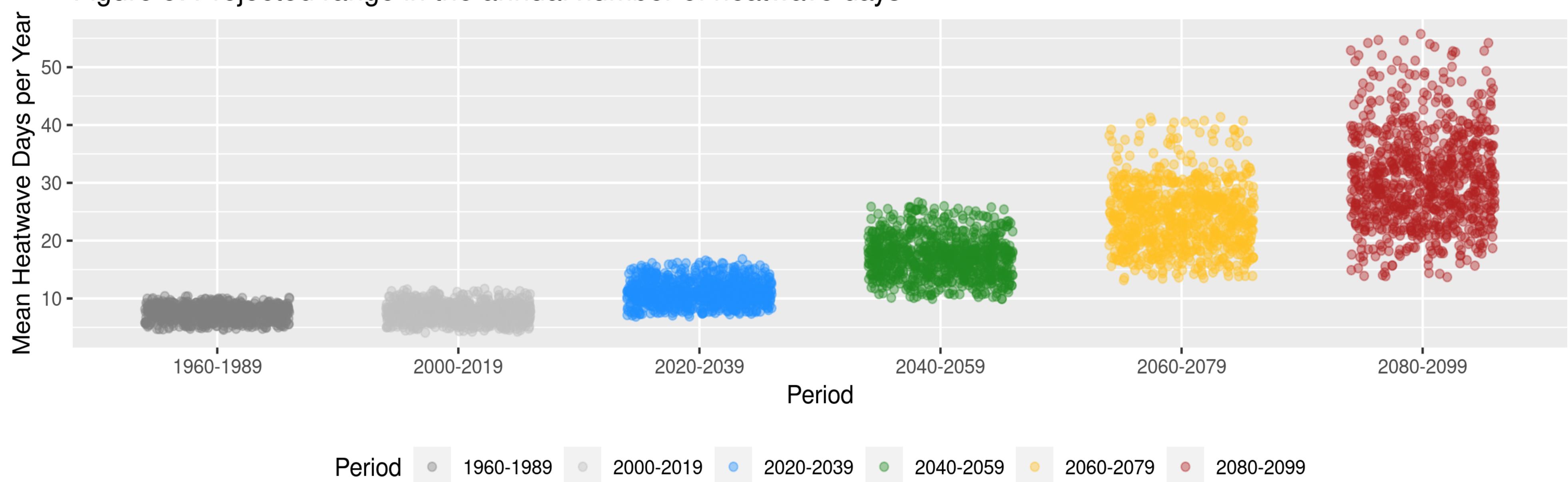


Figure 5: Comparison of the distribution of the *annual number of heatwave days* over the historical period for both model outputs (¡colour¿ and observations (*black*).

Figure 6: Projected mean annual number of hea

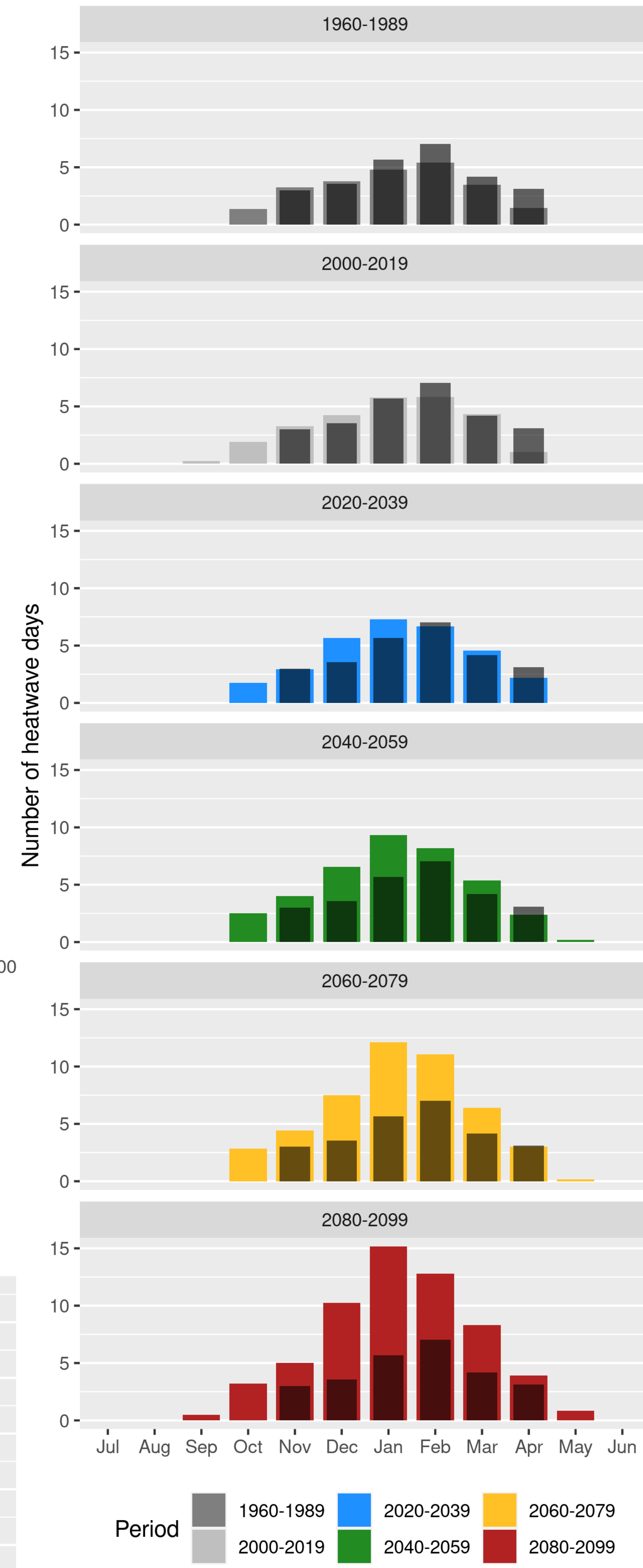


Figure 6: *Bar plots of typical number of heatwave days in each month* for 20-year time periods from 1961 to 2100. Each bar represents the 20-year *typical number of heatwave days in each month*, average across space and time. The observations for the baseline period (1961–1990) are shadowed on top of the future time periods to highlight any differences expected into the future. Higher (lower) bars indicate more (less) heatwave days.

## Figure 1: Observed mean cumulative intensity

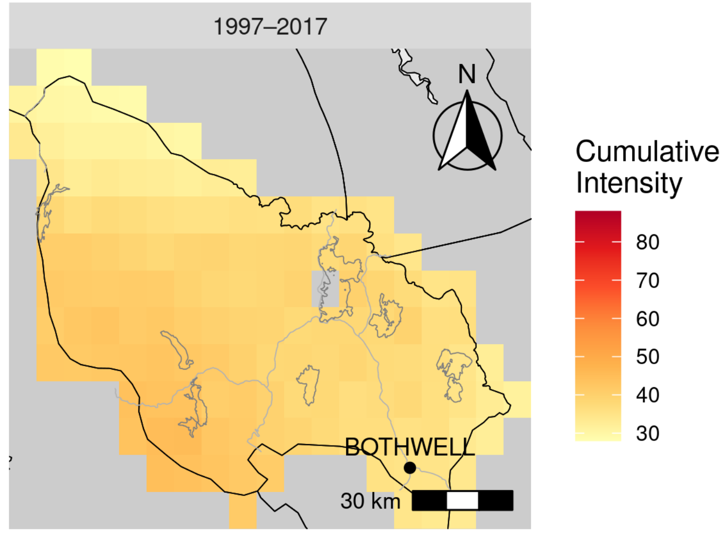


## Figure 2: Observed change in mean cumulative intensity

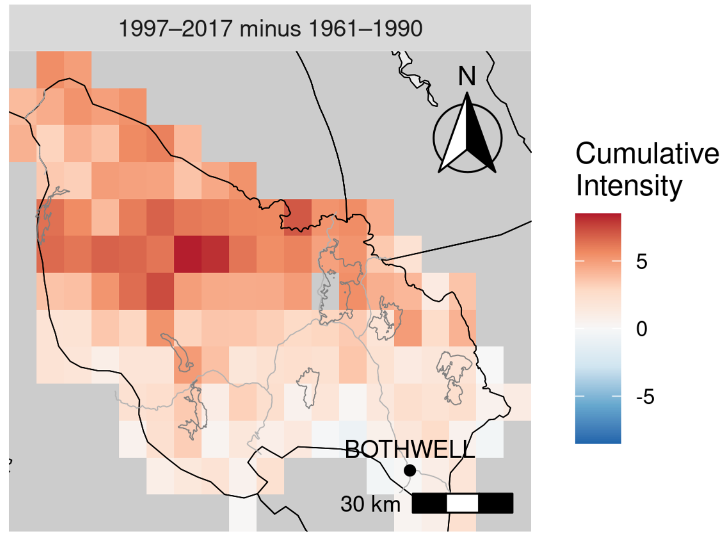


## Figure 3: Projected mean cumulative intensity

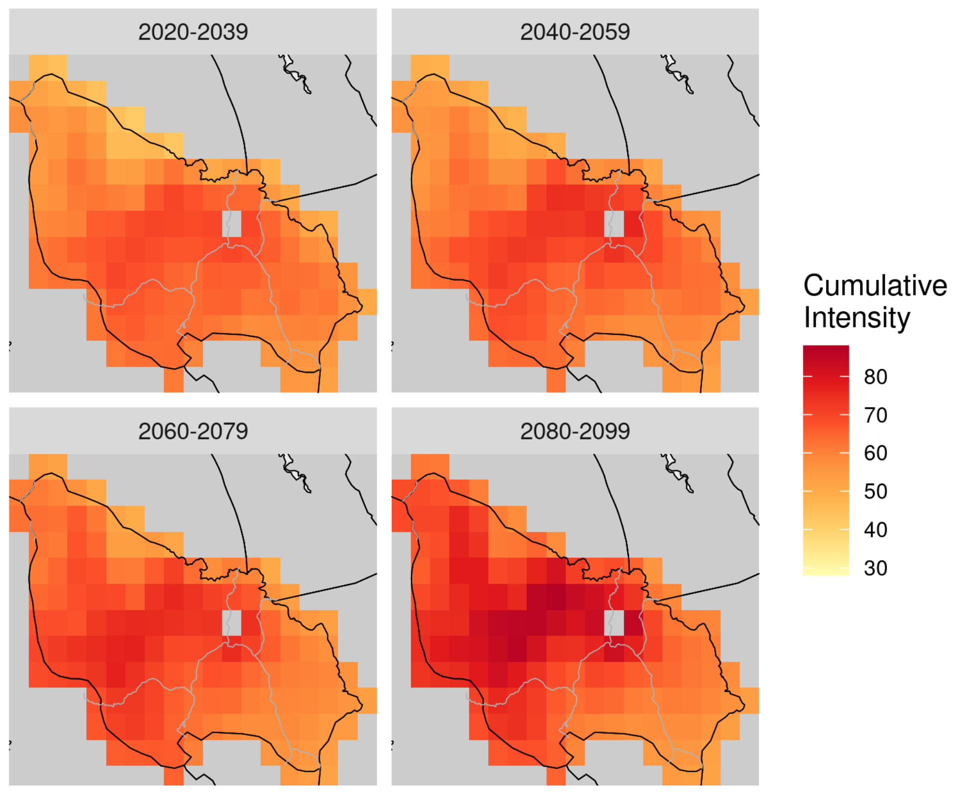


Figure 7: Observed mean *cumulative intensity during a heatwave* across all years from 1997–2017.

Figure 8: The change in mean *cumulative intensity during a heatwave* between the current (1997–2017) and historical (1961–1990) periods. Mean *cumulative intensity during a heatwave* has increased across the region over recent decades.

Figure 9: Projected mean *cumulative intensity during a heatwave* for 20-year time periods from 2001 to 2100. Mean *cumulative intensity during a heatwave* is expected to increase steadily into the future. Each grid cell is the mean of the 6 ensemble members.

## Figure 10: Projected cumulative intensity

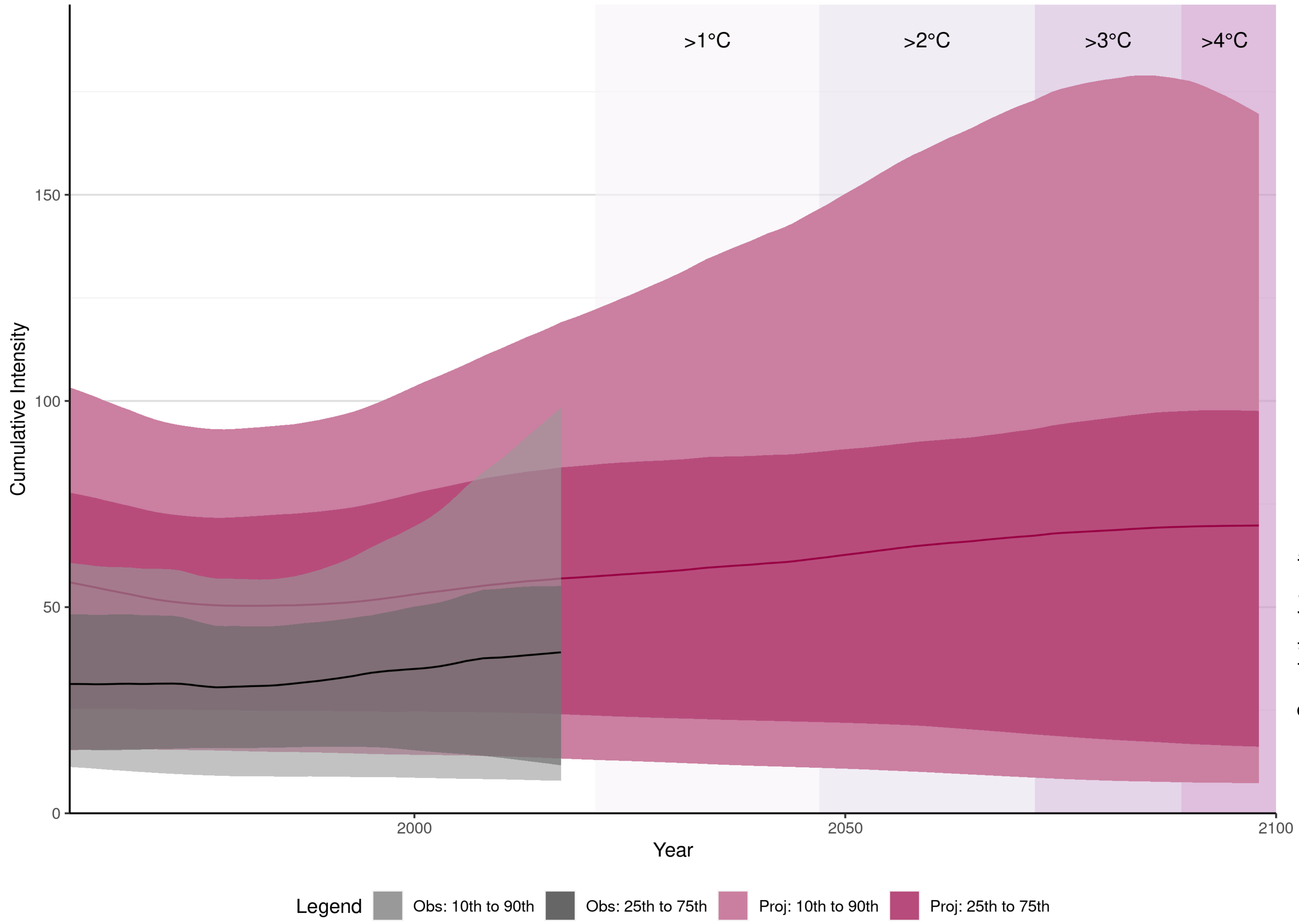


Figure 10: Projected change in *cumulative intensity during a heatwave* from 1990 to 2100. Historical values are the 30-year rolling means from AGCD (*grey*). Projected values (*peach*) are the ensemble mean of the 30-year rolling mean of each ensemble member. *Lighter ribbons* represent the 10th to 90th percentiles of *cumulative intensity during a heatwave*. *Darker ribbons* represent the 25th to 75th percentiles of *cumulative intensity during a heatwave*. *Solid lines* represent the mean of *cumulative intensity during a heatwave*.

## Figure 11: Distribution of cumulative intensity

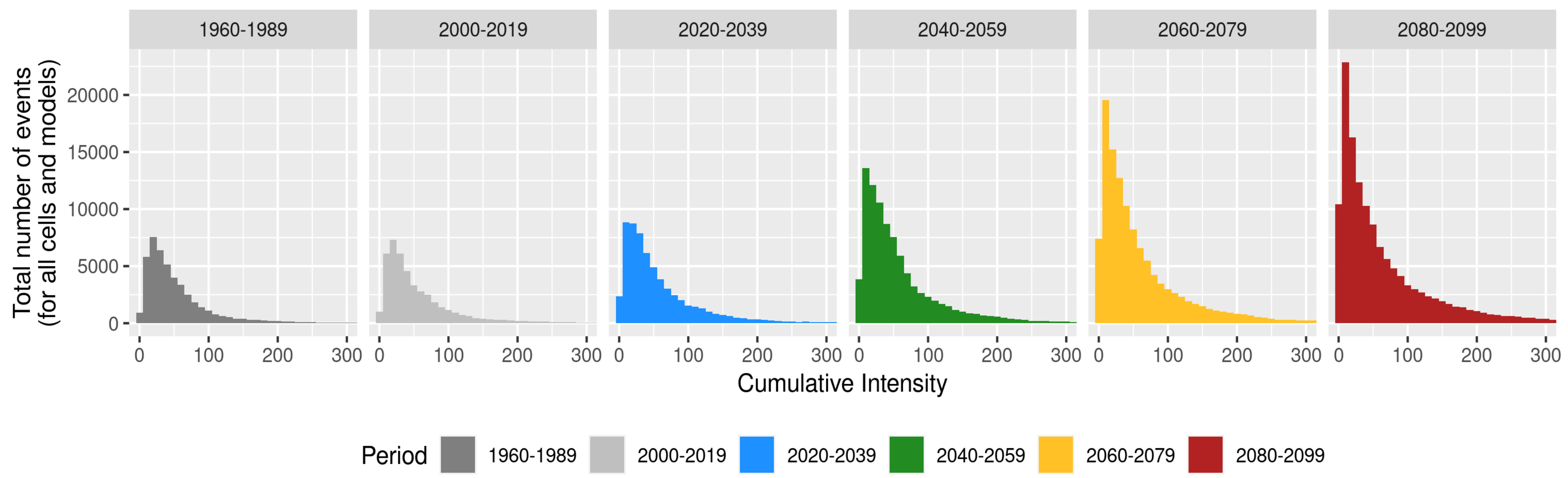


Figure 11: Comparison of the distribution of *cumulative intensity during a heatwave* for different time periods.

## Figure 12: Projected mean cumulative intensity

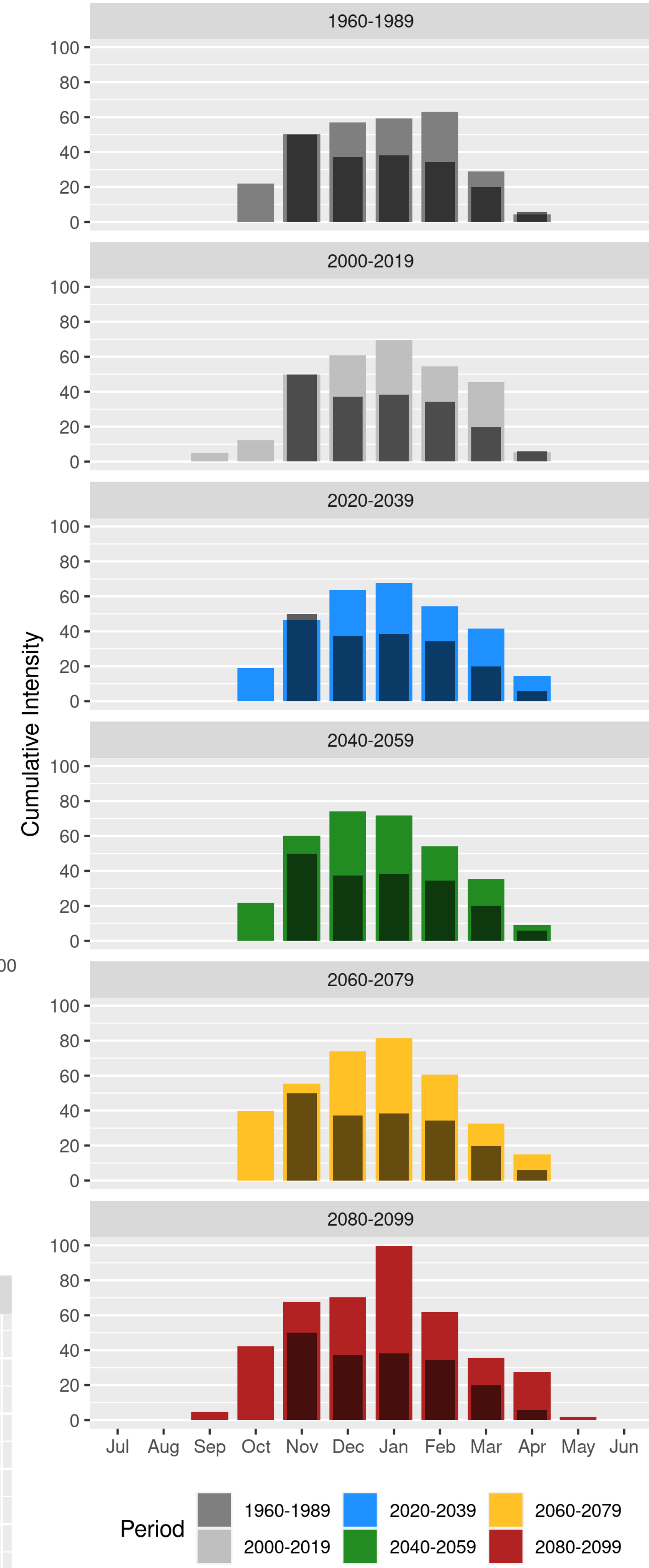


Figure 12: *Bar plots of cumulative intensity during heatwaves* in each month for 20-year time periods from 1961 to 2100. Each bar represents the 20-year mean of *cumulative intensity during a heatwave*, average across space and time. The observations for the baseline period (1961–1990) are shadowed on top of the future time periods to highlight any differences expected into the future. Higher (lower) bars indicate hotter (cooler) heatwave intensities.

Figure 1: Observed mean duration

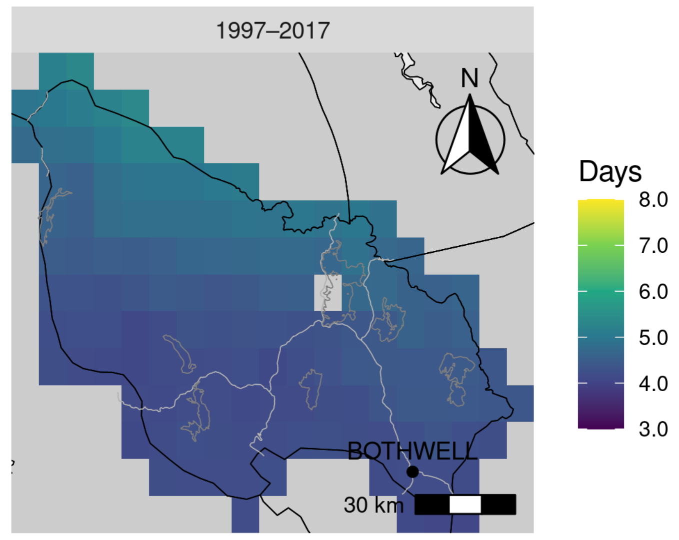


Figure 2: Observed change in mean duration

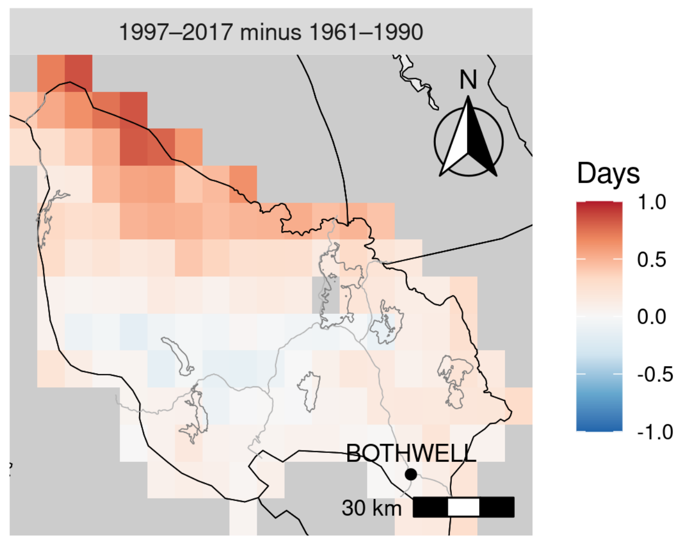


Figure 3: Projected mean duration

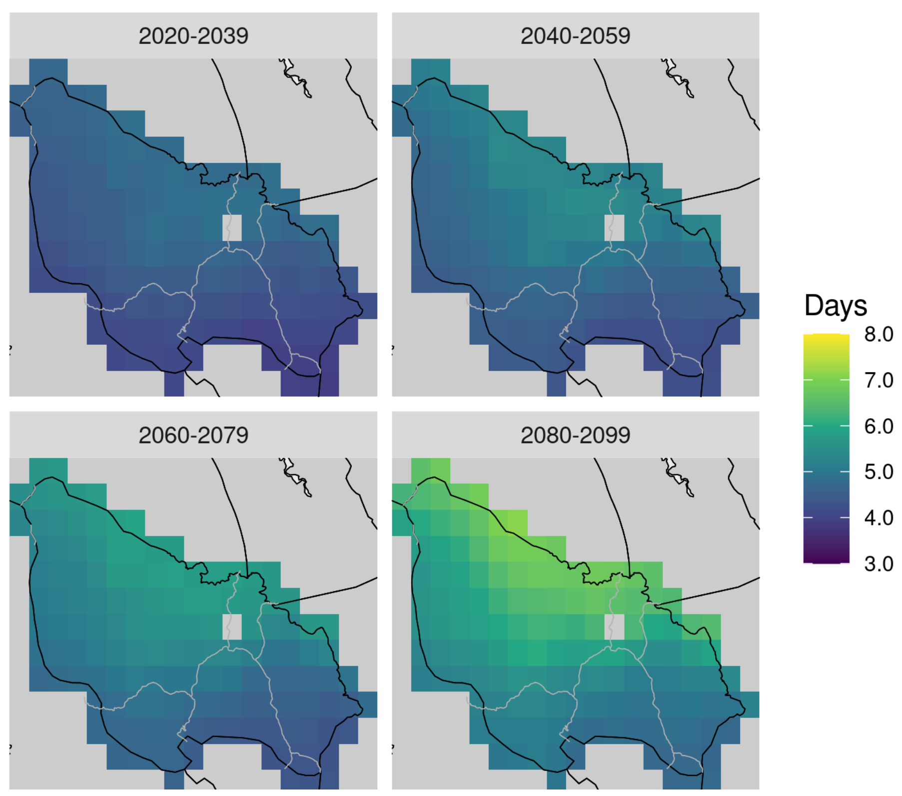


Figure 13: Observed mean *heatwave durations* across all years from 1997–2017.

Figure 14: The change in mean *heatwave duration* between the current (1997–2017) and historical (1961–1990) periods. Mean *heatwave durations* have increased across the region over recent decades.

Figure 15: Projected mean *heatwave durations* for 20-year time periods from 2001 to 2100. Mean *heatwave duration* is expected to increase steadily into the future. Each grid cell is the mean of the 6 ensemble members.

Figure 16: Projected heatwave duration

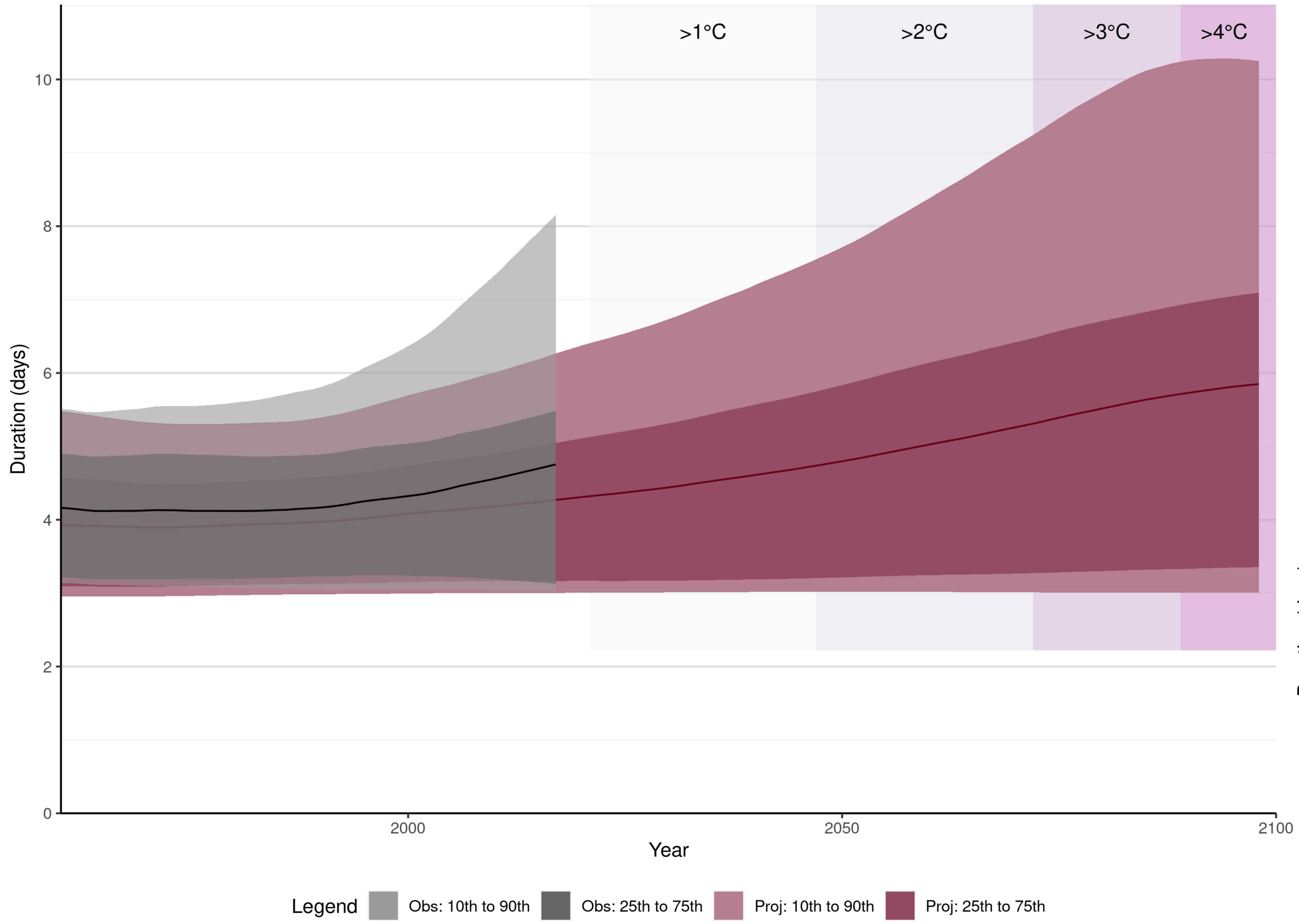


Figure 16: Projected change in *heatwave duration* from 1990 to 2100. Historical values (*grey*) are the 30-year rolling means of AGCD. Projected values (*orange*) are the ensemble mean of the 30-year rolling mean of each CCAM ensemble member. *Lighter ribbons* represent the 10th to 90th percentiles of *heatwave duration*. *Darker ribbons* represent the 25th to 75th percentiles of *heatwave duration*. *Solid lines* represent the mean of *heatwave duration*.

Figure 17: Projected count of heatwave duration

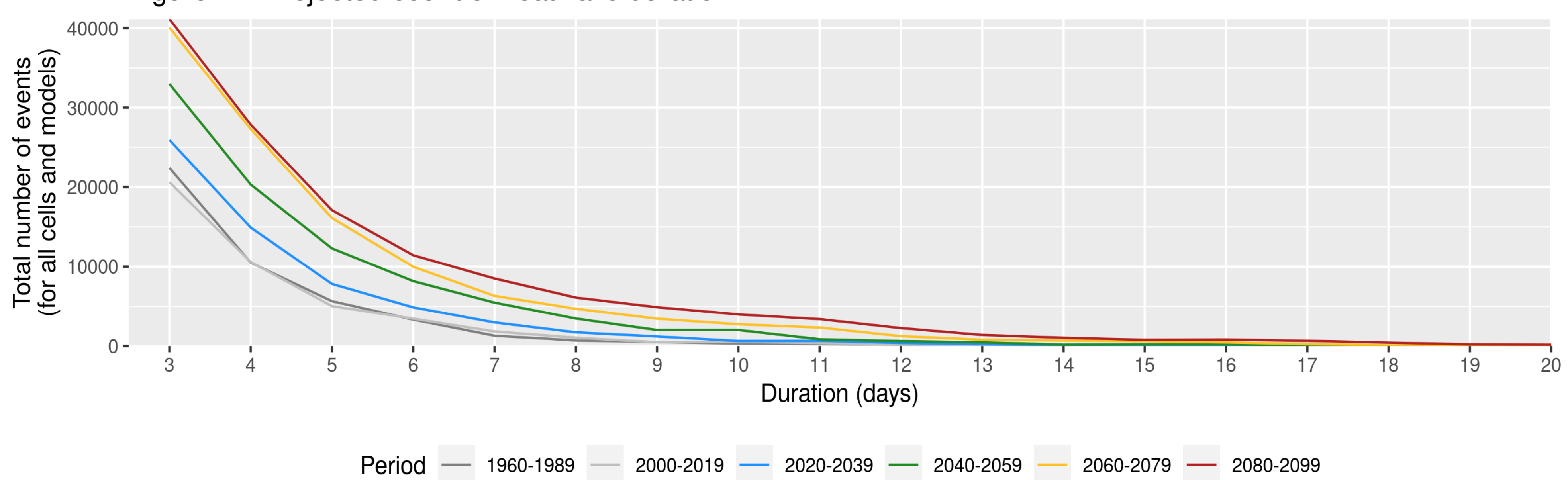


Figure 17: Comparison of the distribution of *heatwave durations* for different time periods.

Figure 18: Projected mean heatwave duration by

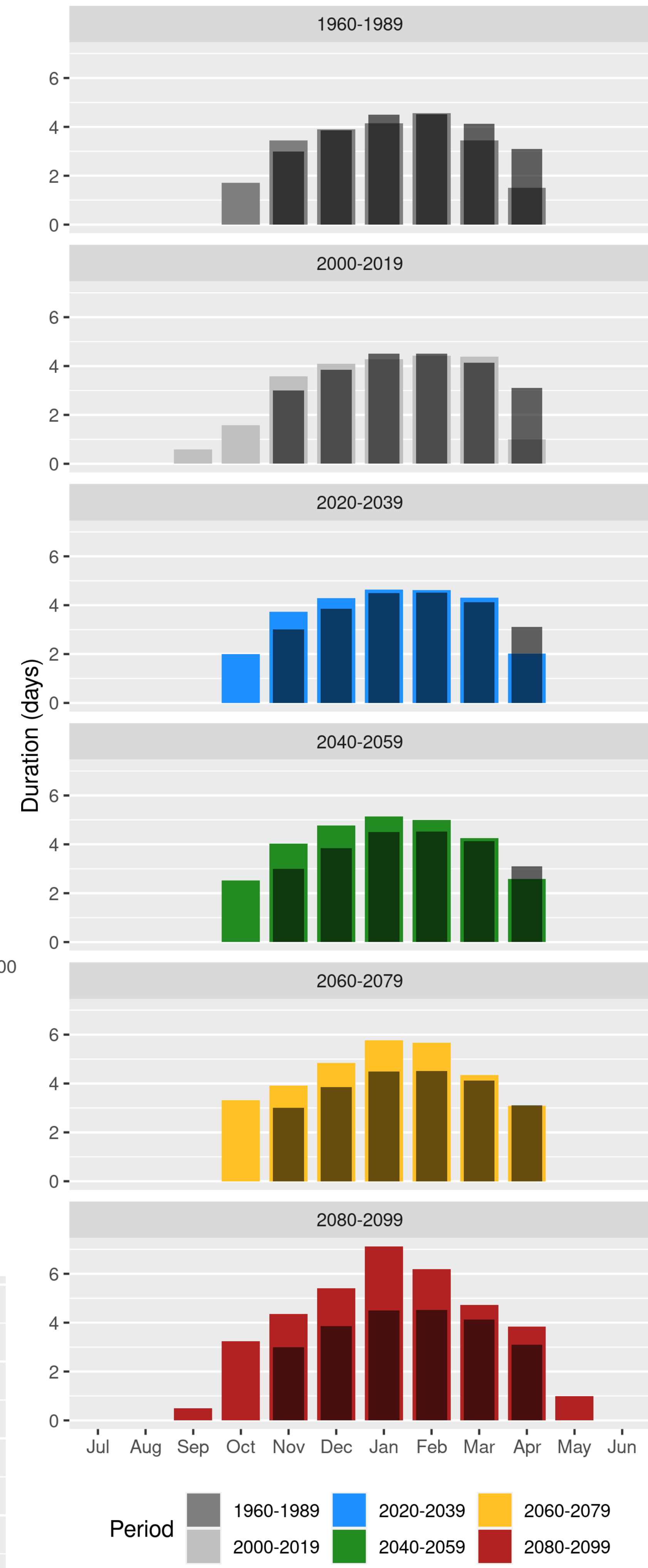


Figure 18: *Bar plots* of mean *heatwave durations* in each month for 20-year time periods from 1961 to 2100. Each bar represents the 20-year mean of *heatwave durations*, average across space and time. The observations for the baseline period (1961–1990) are shadowed on top of the future time periods to highlight any differences expected into the future. Higher (lower) bars indicate longer (shorter) *heatwave durations*.

Figure 1: Observed mean annual number of heatwave days

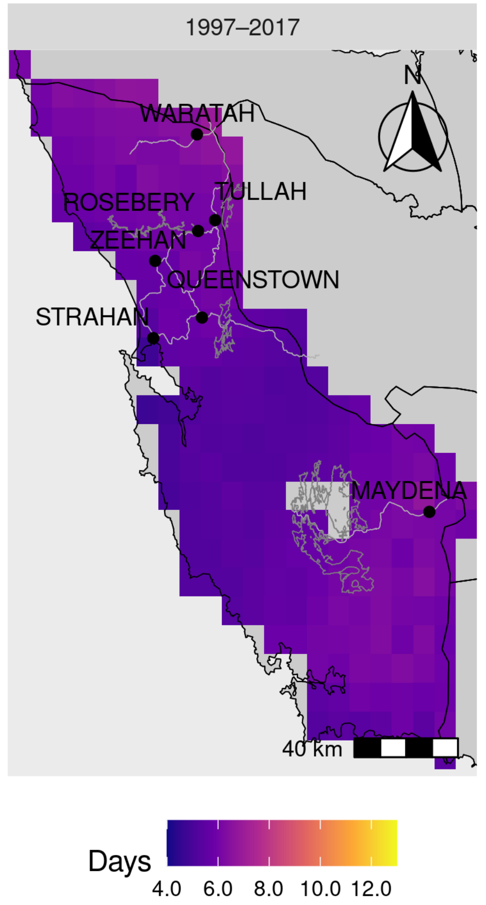


Figure 2: Observed change in mean annual number of heatwave days

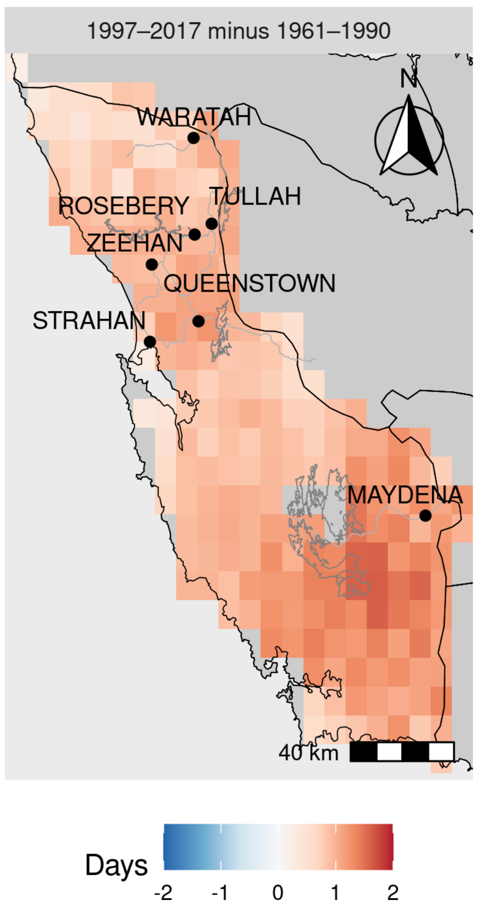


Figure 3: Projected mean annual number of heatwave day

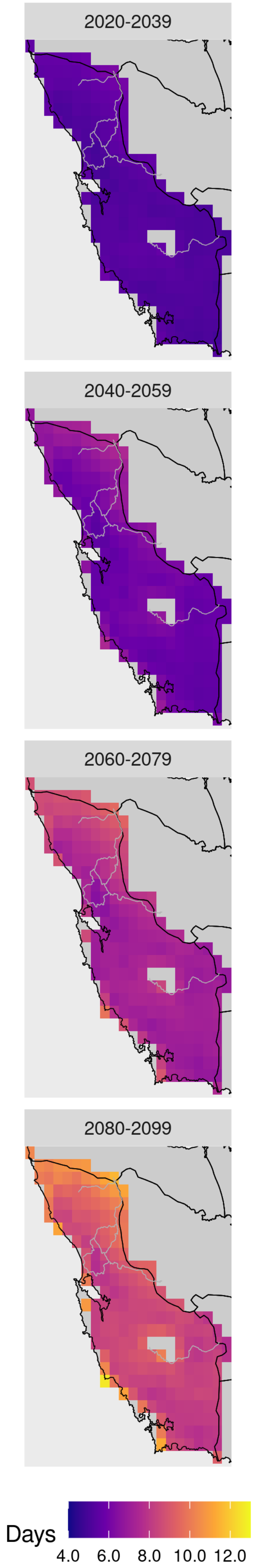


Figure 4: Projected annual number of heatwave days from 1961 to 2100

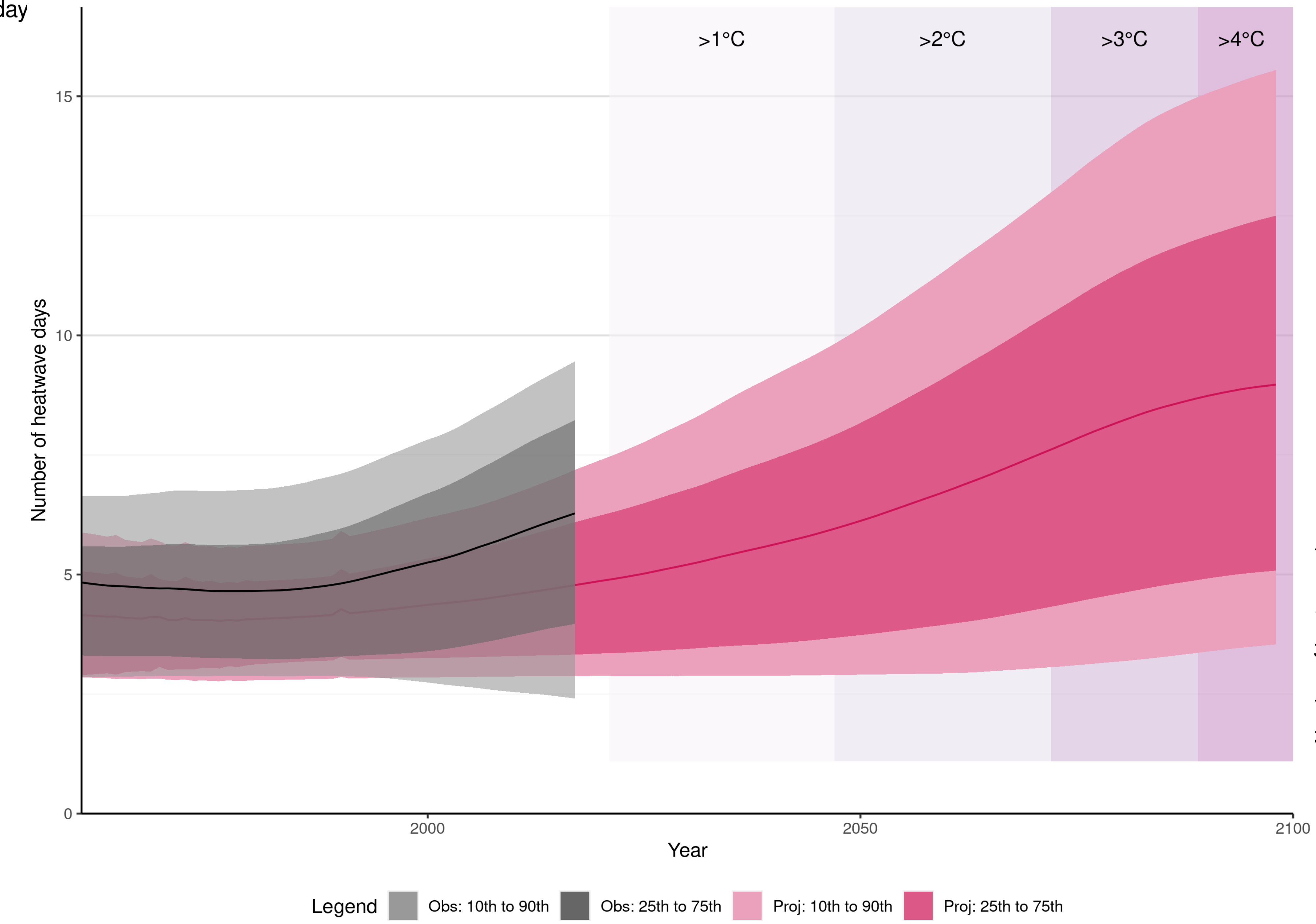


Figure 4: Projected change in mean *annual number of heatwave days* from 1990 to 2100. Historical values (*grey*) are the 30-year rolling means of AGCD. Projected values (*peach*) are the ensemble mean of the 30-year rolling mean of each CCAM ensemble member. *Lighter ribbons* represent the 10th to 90th percentiles of mean *annual number of heatwave days*. *Darker ribbons* represent the 25th to 75th percentiles of mean *annual number of heatwave days*. *Solid lines* represent the mean *annual number of heatwave days*.

Figure 5: Projected range in the annual number of heatwave days

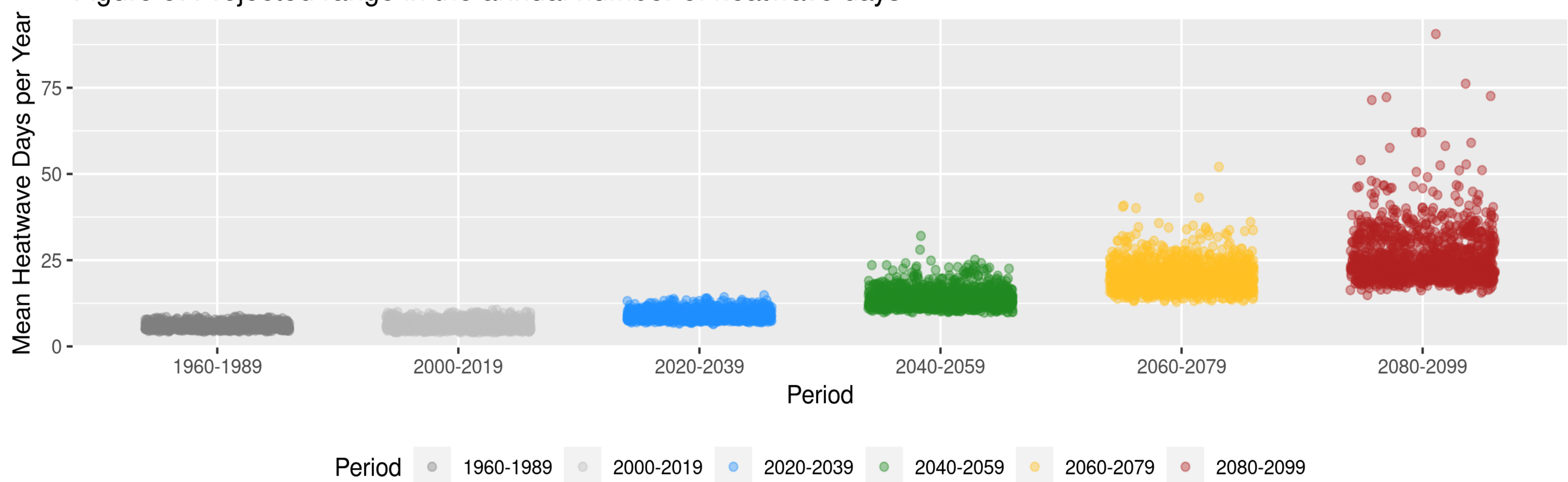


Figure 5: Comparison of the distribution of the *annual number of heatwave days* over the historical period for both model outputs (¡colour¿ and observations (*black*).

Figure 6: Projected mean annual number of hea

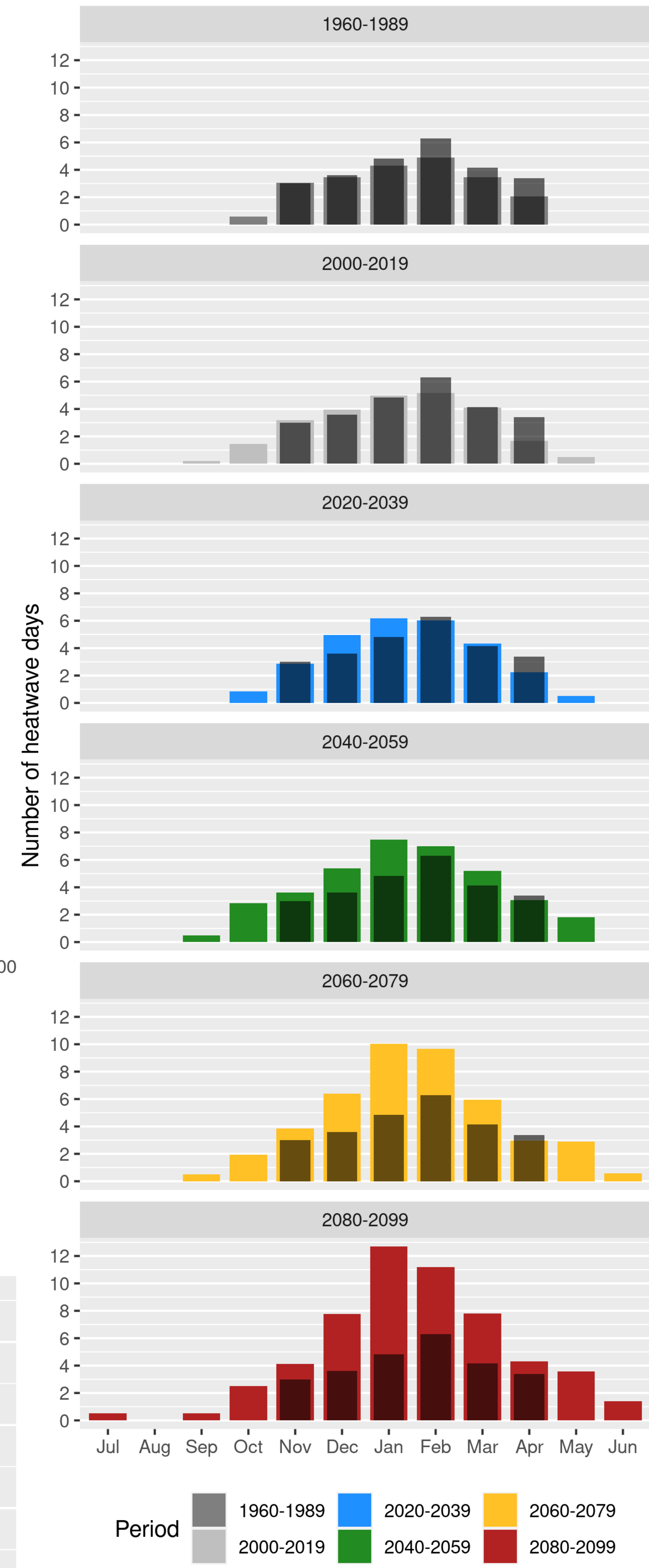


Figure 6: *Bar plots of typical number of heatwave days in each month* for 20-year time periods from 1961 to 2100. Each bar represents the 20-year *typical number of heatwave days in each month*, average across space and time. The observations for the baseline period (1961–1990) are shadowed on top of the future time periods to highlight any differences expected into the future. Higher (lower) bars indicate more (less) heatwave days.

Figure 1: Observed mean *annual number of heatwave days* across all years from 1997–2017.

Figure 2: The change in the mean *annual number of heatwave days* between the current (1997–2017) and historical (1961–1990) periods. Mean *annual number of heatwave days* has increased across the region over recent decades.

Figure 3: Projected mean *annual number of heatwave days* for 20-year time periods from 2001 to 2100. Mean *annual number of heatwave days* is expected to increase steadily into the future. Each grid cell is the mean of the 6 ensemble members.

Figure 1: Observed mean cumulative intensity

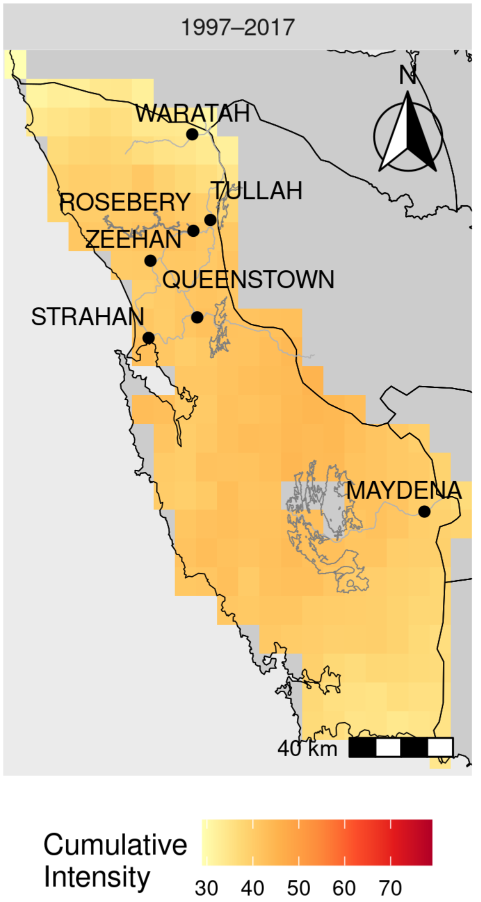


Figure 2: Observed change in mean cumulative intensity

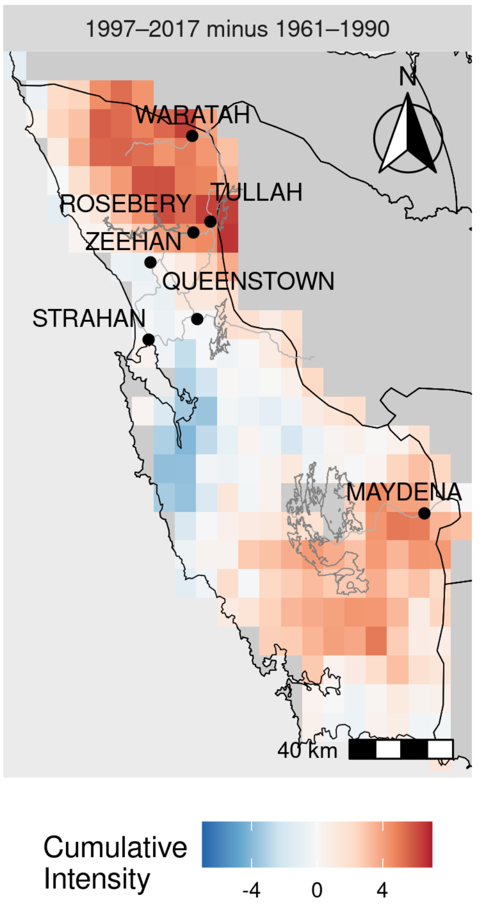


Figure 3: Projected mean cumulative intensity

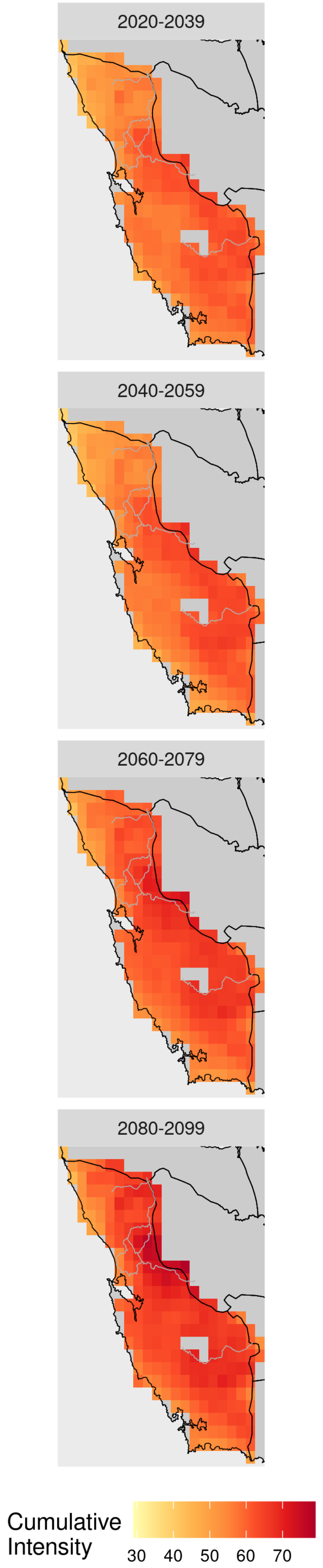


Figure 7: Observed mean *cumulative intensity during a heatwave* across all years from 1997–2017.

Figure 8: The change in mean *cumulative intensity during a heatwave* between the current (1997–2017) and historical (1961–1990) periods. Mean *cumulative intensity during a heatwave* has increased across the region over recent decades.

Figure 9: Projected mean *cumulative intensity during a heatwave* for 20-year time periods from 2001 to 2100. Mean *cumulative intensity during a heatwave* is expected to increase steadily into the future. Each grid cell is the mean of the 6 ensemble members.

Figure 10: Projected cumulative intensity

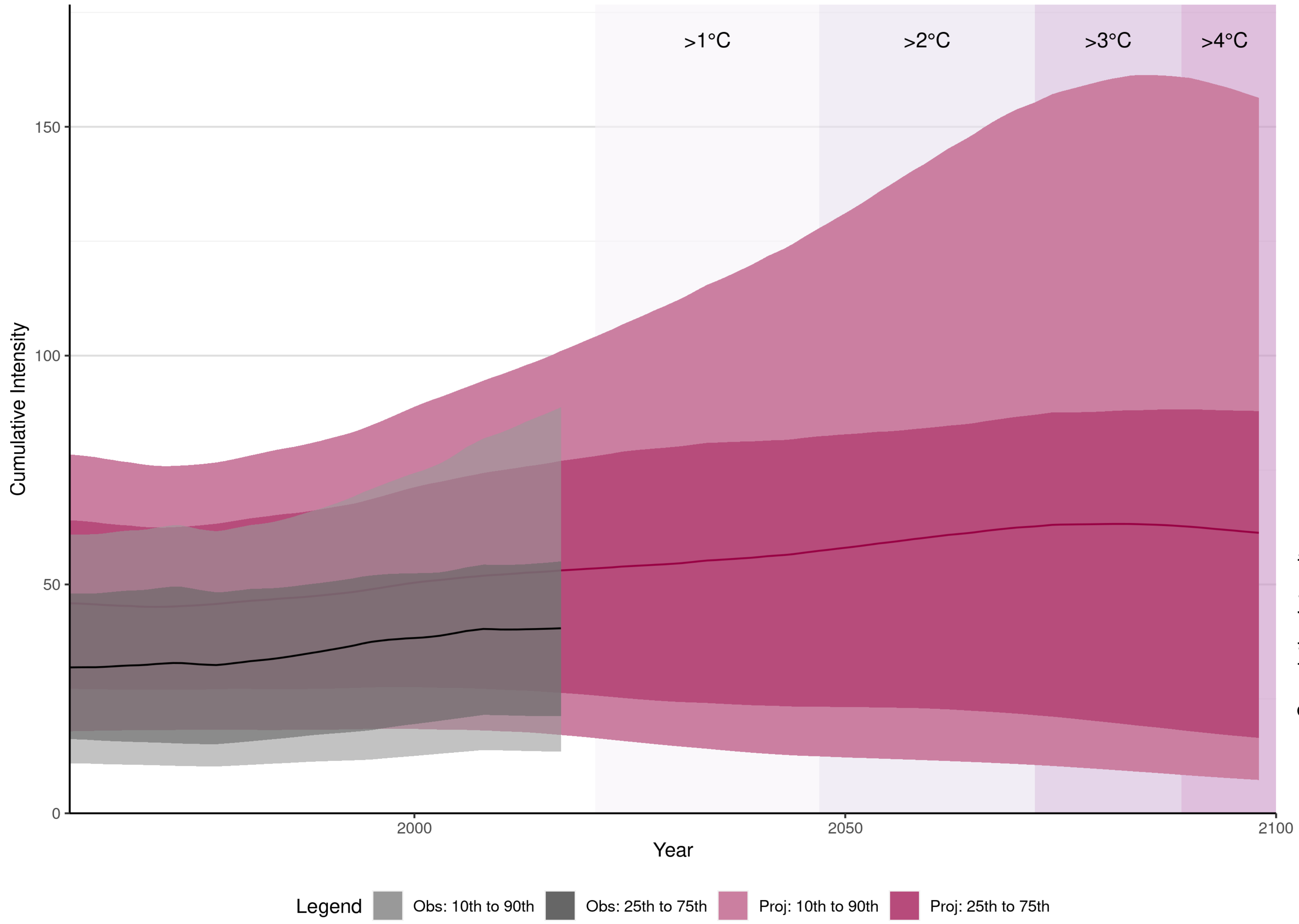


Figure 10: Projected change in *cumulative intensity during a heatwave* from 1990 to 2100. Historical values are the 30-year rolling means from AGCD (*grey*). Projected values (*peach*) are the ensemble mean of the 30-year rolling mean of each ensemble member. *Lighter ribbons* represent the 10th to 90th percentiles of *cumulative intensity during a heatwave*. *Darker ribbons* represent the 25th to 75th percentiles of *cumulative intensity during a heatwave*. *Solid lines* represent the mean of *cumulative intensity during a heatwave*.

Figure 11: Distribution of cumulative intensity

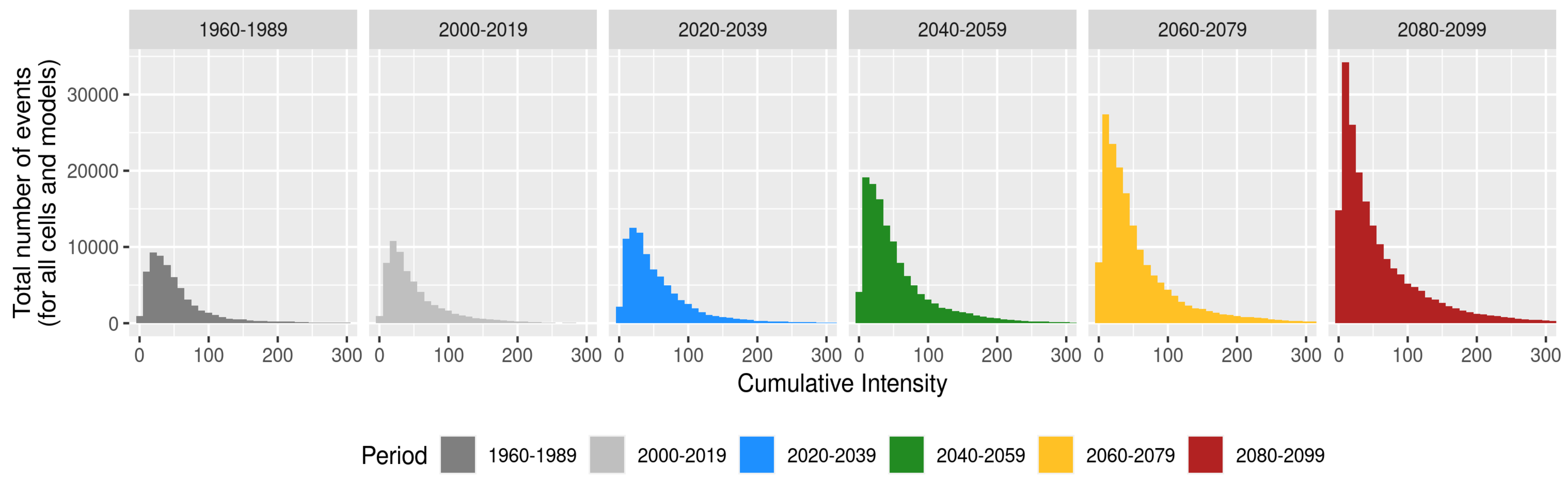


Figure 11: Comparison of the distribution of *cumulative intensity during a heatwave* for different time periods.

Figure 12: Projected mean cumulative intensity

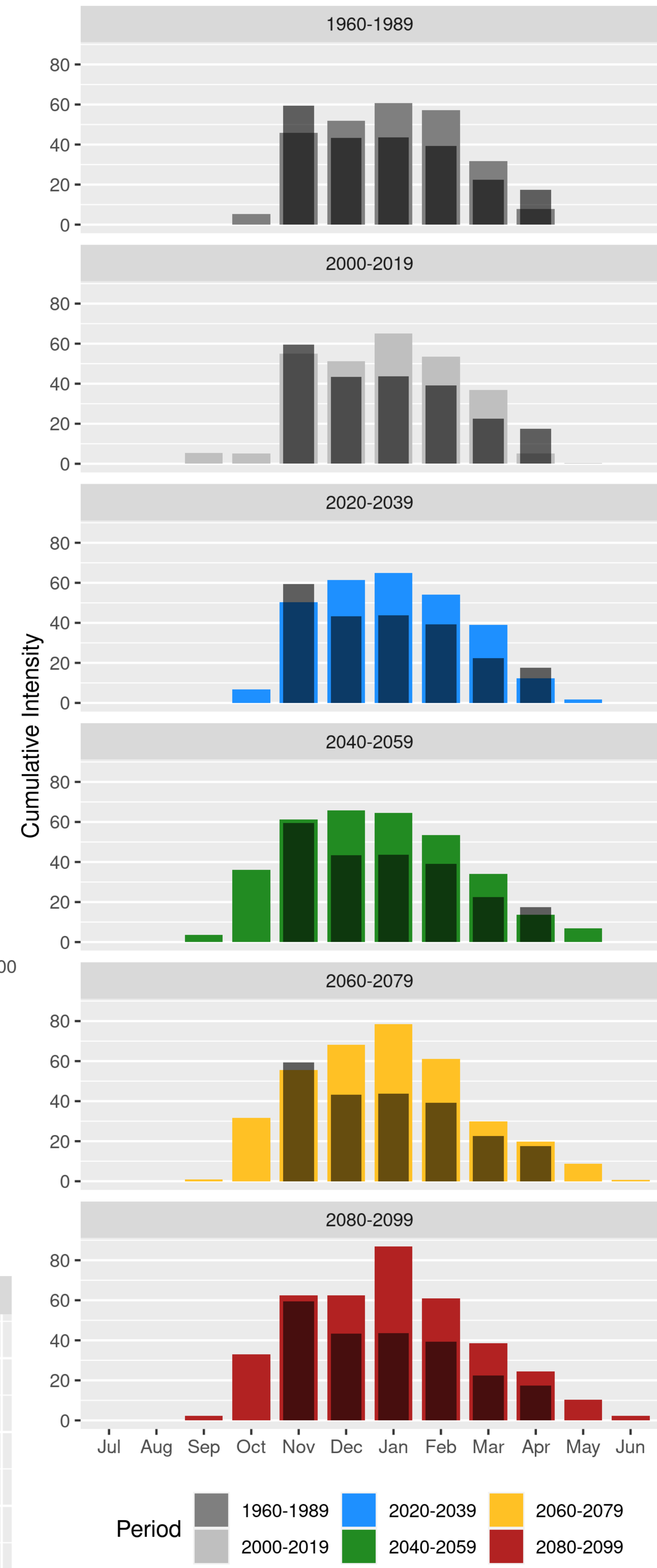


Figure 12: *Bar plots of cumulative intensity during heatwaves* in each month for 20-year time periods from 1961 to 2100. Each bar represents the 20-year mean of *cumulative intensity during a heatwave*, average across space and time. The observations for the baseline period (1961–1990) are shadowed on top of the future time periods to highlight any differences expected into the future. Higher (lower) bars indicate hotter (cooler) heatwave intensities.

Figure 1: Observed mean duration

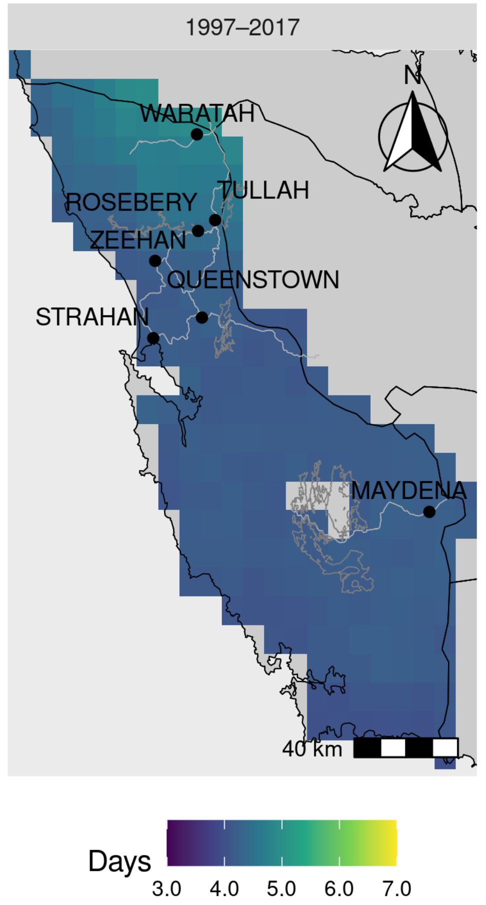


Figure 2: Observed change in mean duration

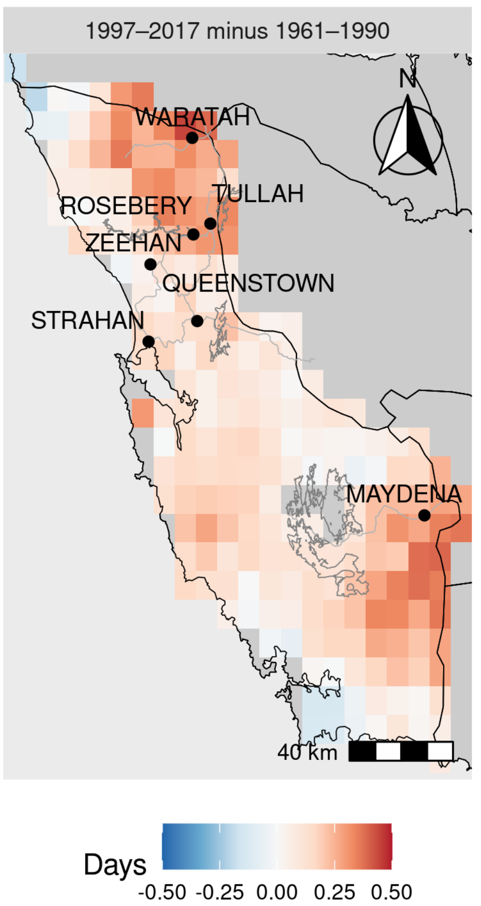


Figure 3: Projected mean duration

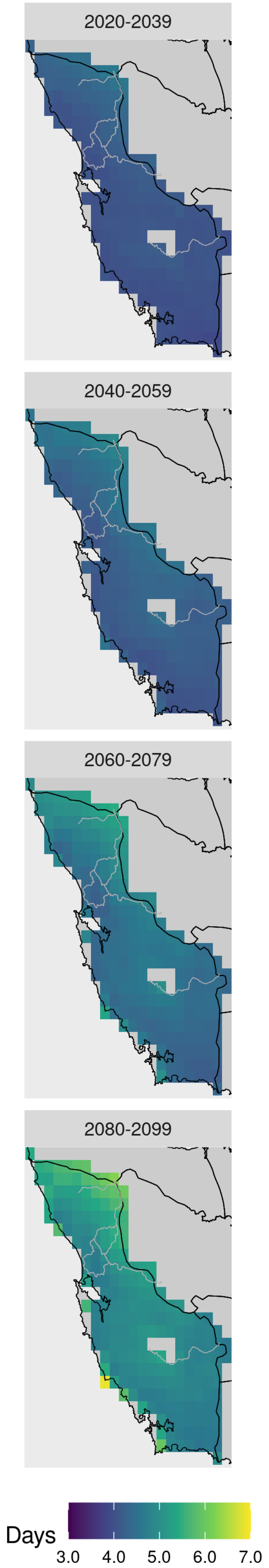


Figure 13: Observed mean *heatwave durations* across all years from 1997–2017.

Figure 14: The change in mean *heatwave duration* between the current (1997–2017) and historical (1961–1990) periods. Mean *heatwave durations* have increased across the region over recent decades.

Figure 15: Projected mean *heatwave durations* for 20-year time periods from 2001 to 2100. Mean *heatwave duration* is expected to increase steadily into the future. Each grid cell is the mean of the 6 ensemble members.

Figure 16: Projected heatwave duration

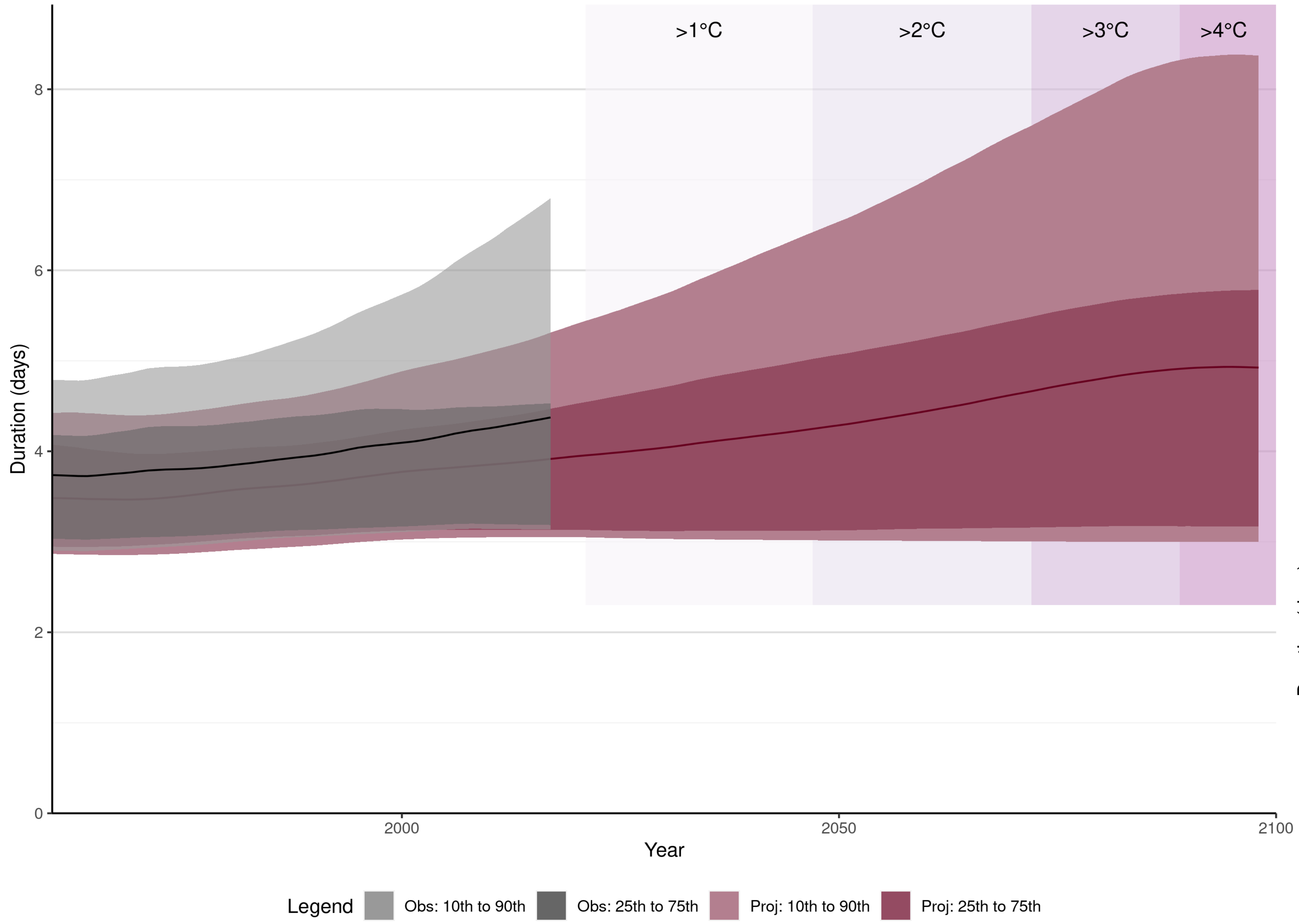


Figure 16: Projected change in *heatwave duration* from 1990 to 2100. Historical values (*grey*) are the 30-year rolling means of AGCD. Projected values (*orange*) are the ensemble mean of the 30-year rolling mean of each CCAM ensemble member. *Lighter ribbons* represent the 10th to 90th percentiles of *heatwave duration*. *Darker ribbons* represent the 25th to 75th percentiles of *heatwave duration*. *Solid lines* represent the mean of *heatwave duration*.

Figure 17: Projected count of heatwave duration

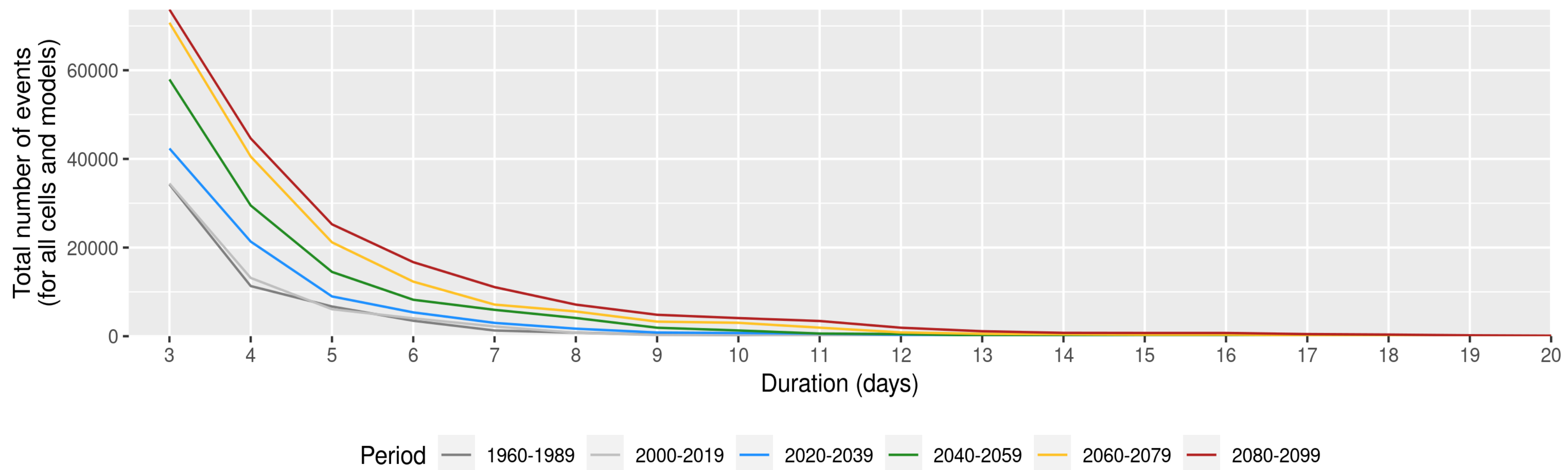


Figure 17: Comparison of the distribution of *heatwave durations* for different time periods.

Figure 18: Projected mean heatwave duration by

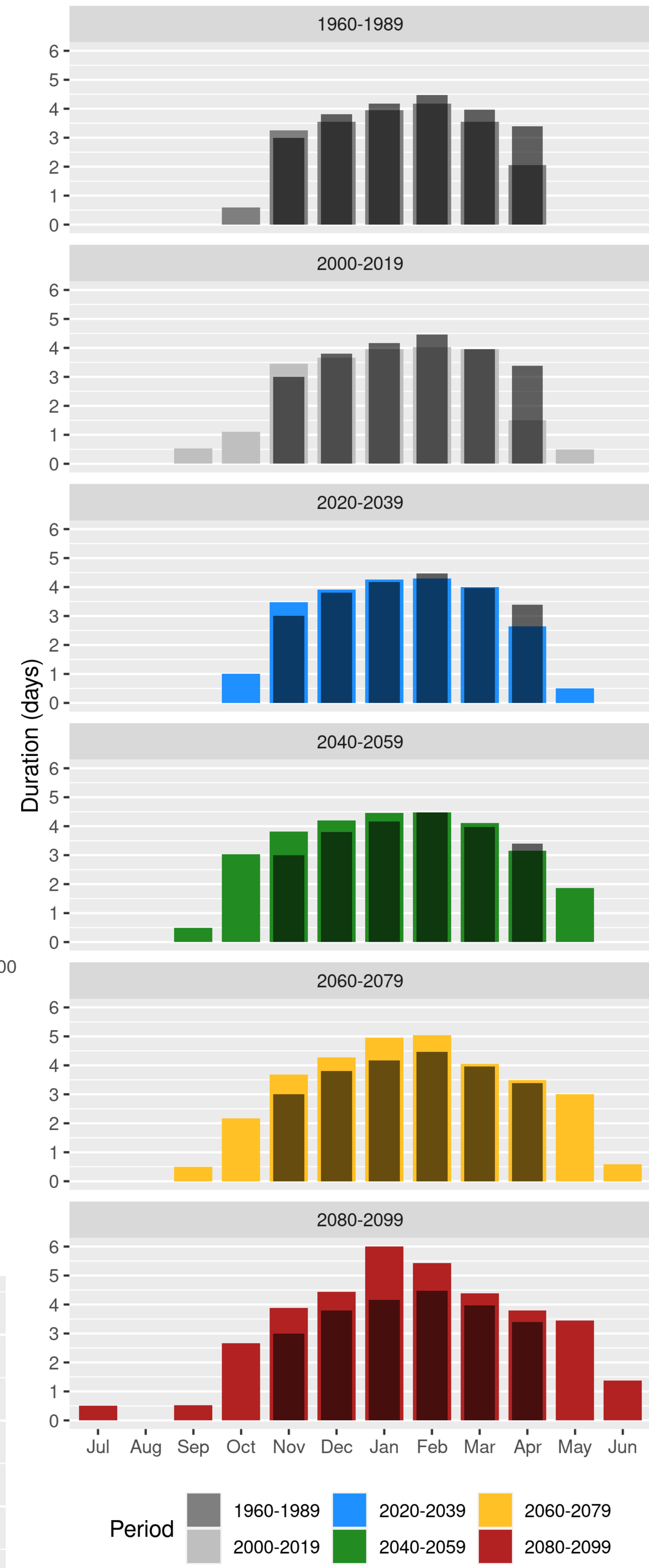


Figure 18: *Bar plots* of mean *heatwave durations* in each month for 20-year time periods from 1961 to 2100. Each bar represents the 20-year mean of *heatwave durations*, average across space and time. The observations for the baseline period (1961–1990) are shadowed on top of the future time periods to highlight any differences expected into the future. Higher (lower) bars indicate longer (shorter) *heatwave durations*.

# NORTH WEST COAST

## Heatwaves — Number of Heatwave Days

### Figure 1: Observed mean annual number of heatwave days

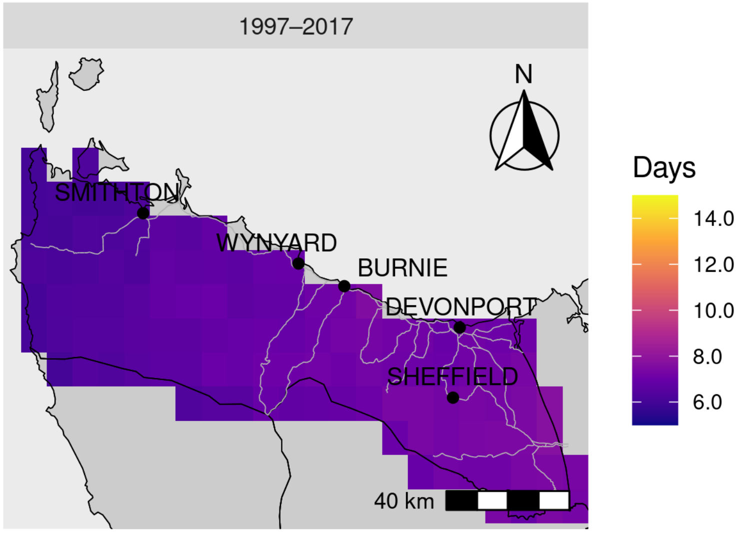


### Figure 2: Observed change in mean annual number of heatwave days

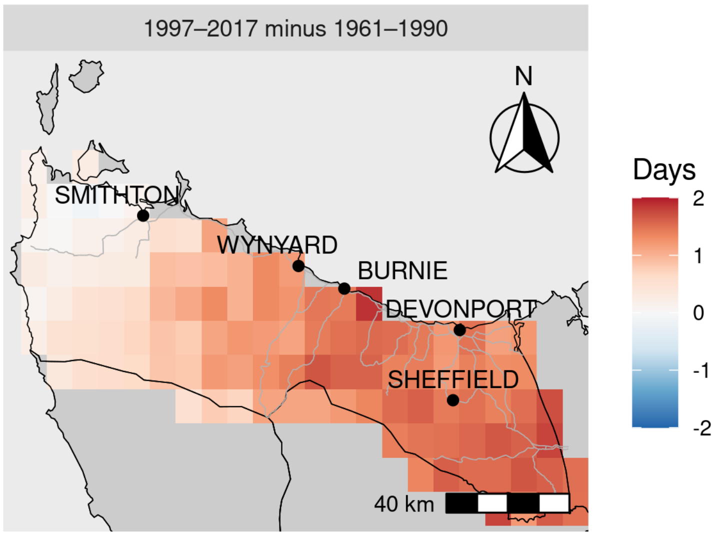


### Figure 3: Projected mean annual number of heatwave days

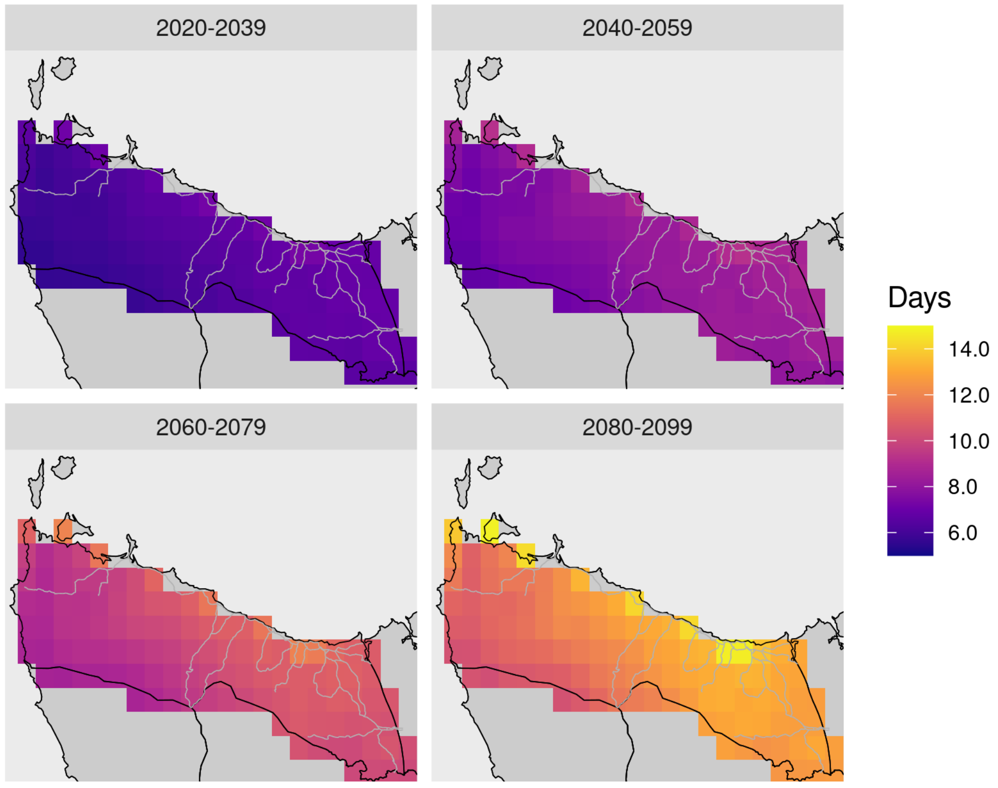


Figure 1: Observed mean *annual number of heatwave days* across all years from 1997–2017.

Figure 2: The change in the mean *annual number of heatwave days* between the current (1997–2017) and historical (1961–1990) periods. Mean *annual number of heatwave days* has increased across the region over recent decades.

Figure 3: Projected mean *annual number of heatwave days* for 20-year time periods from 2001 to 2100. Mean *annual number of heatwave days* is expected to increase steadily into the future. Each grid cell is the mean of the 6 ensemble members.

### Figure 4: Projected annual number of heatwave days from 1961 to 2100

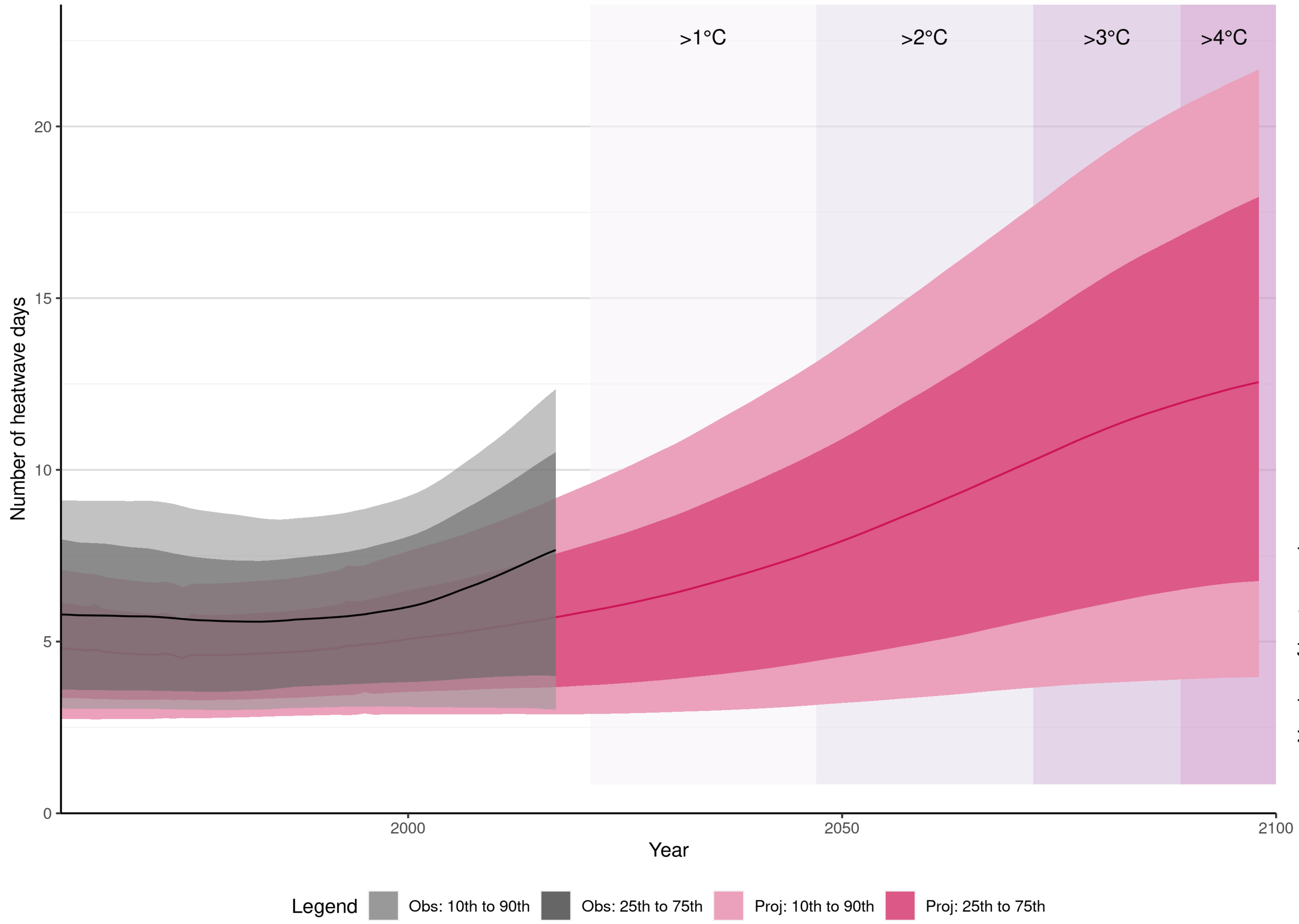


Figure 4: Projected change in mean *annual number of heatwave days* from 1990 to 2100. Historical values (*grey*) are the 30-year rolling means of AGCD. Projected values (*peach*) are the ensemble mean of the 30-year rolling mean of each CCAM ensemble member. *Lighter ribbons* represent the 10th to 90th percentiles of mean *annual number of heatwave days. Darker ribbons* represent the 25th to 75th percentiles of mean *annual number of heatwave days. Solid lines* represent the mean *annual number of heatwave days.*

### Figure 5: Projected range in the annual number of heatwave days

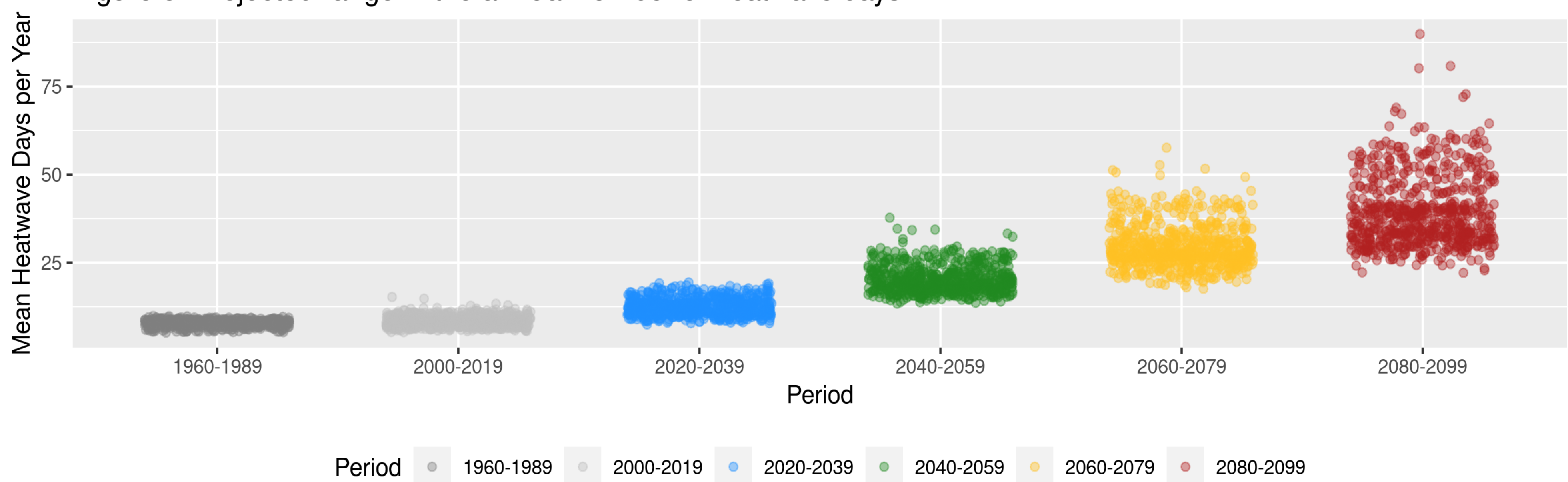


Figure 5: Comparison of the distribution of the *annual number of heatwave days* over the historical period for both model outputs (¡colour¿ and observations (*black*).

### Figure 6: Projected mean annual number of hea

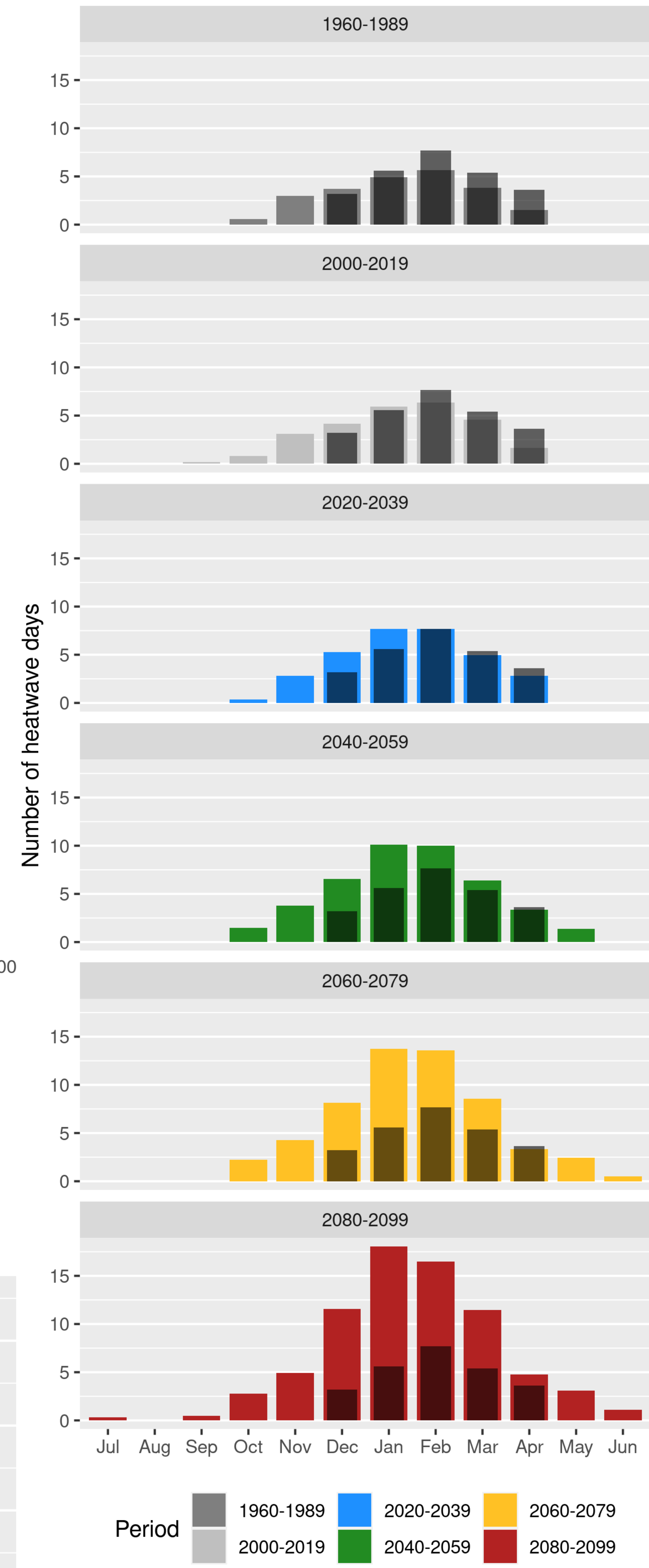


Figure 6: *Bar plots of typical number of heatwave days in each month* for 20-year time periods from 1961 to 2100. Each bar represents the 20-year *typical number of heatwave days in each month*, average across space and time. The observations for the baseline period (1961–1990) are shadowed on top of the future time periods to highlight any differences expected into the future. Higher (lower) bars indicate more (less) heatwave days.

# NORTH WEST COAST

## Heatwaves — Cumulative Intensity

### Figure 1: Observed mean cumulative intensity

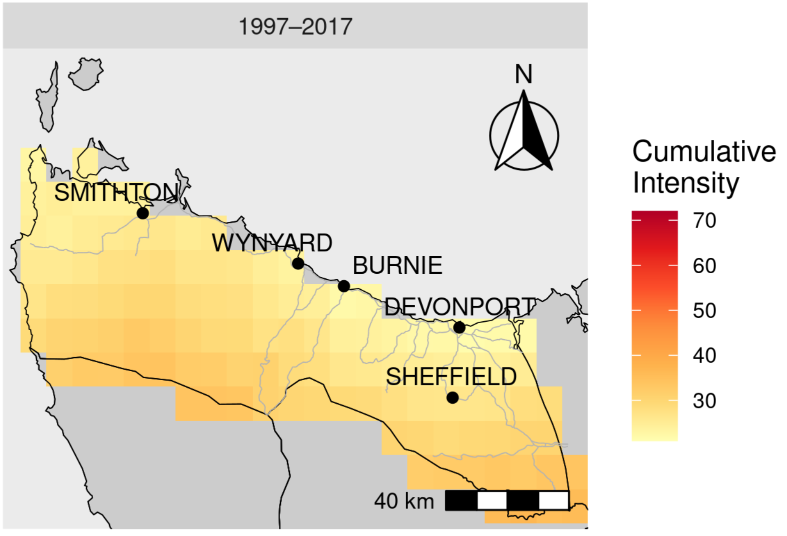


### Figure 2: Observed change in mean cumulative intensity

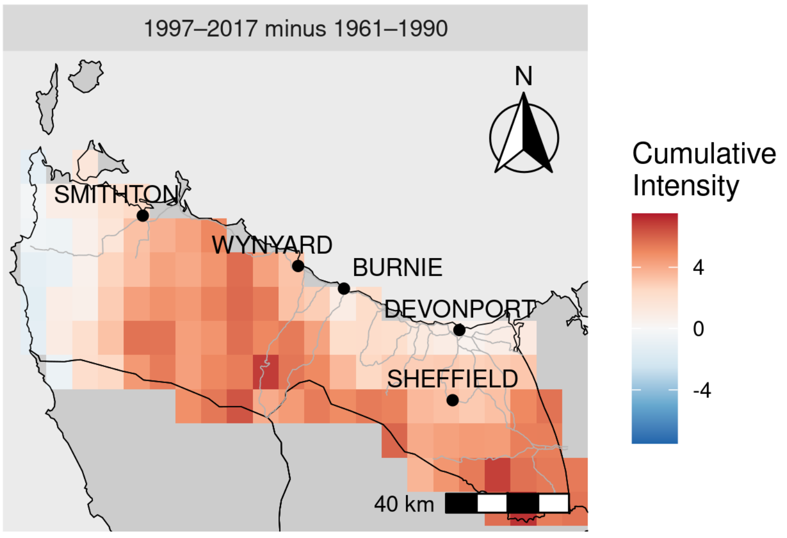


### Figure 3: Projected mean cumulative intensity

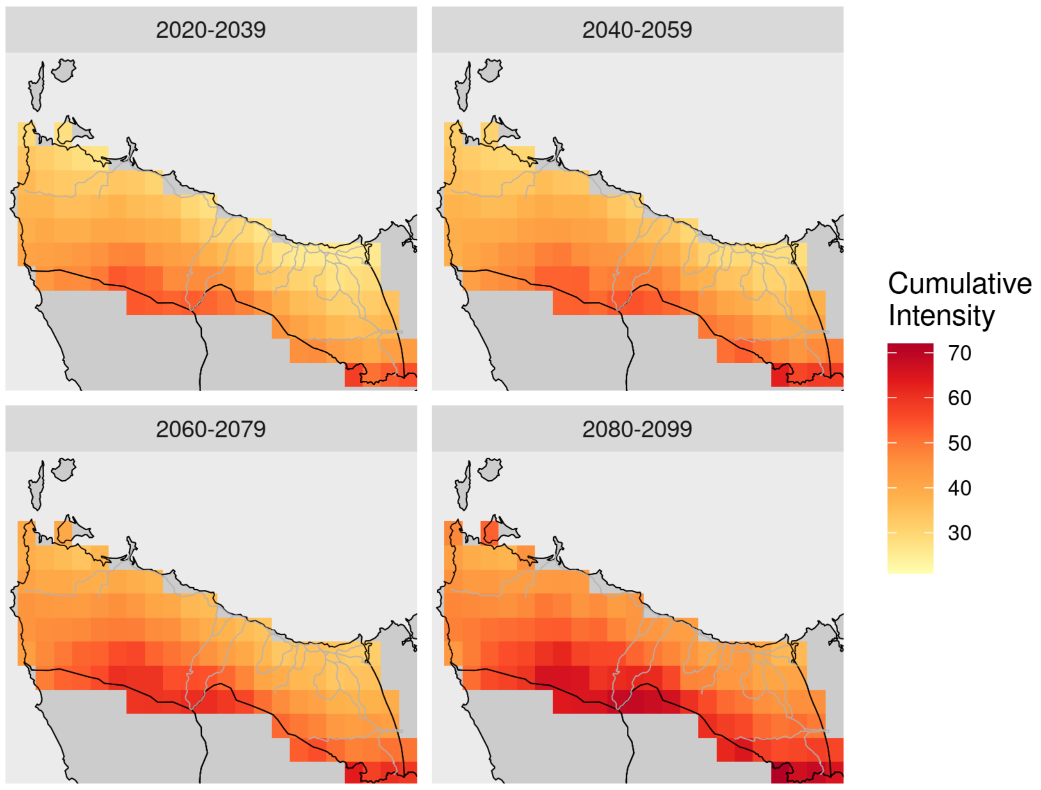


Figure 7: Observed mean *cumulative intensity during a heatwave* across all years from 1997–2017.

Figure 8: The change in mean *cumulative intensity during a heatwave* between the current (1997–2017) and historical (1961–1990) periods. Mean *cumulative intensity during a heatwave* has increased across the region over recent decades.

Figure 9: Projected mean *cumulative intensity during a heatwave* for 20-year time periods from 2001 to 2100. Mean *cumulative intensity during a heatwave* is expected to increase steadily into the future. Each grid cell is the mean of the 6 ensemble members.

### Figure 10: Projected cumulative intensity

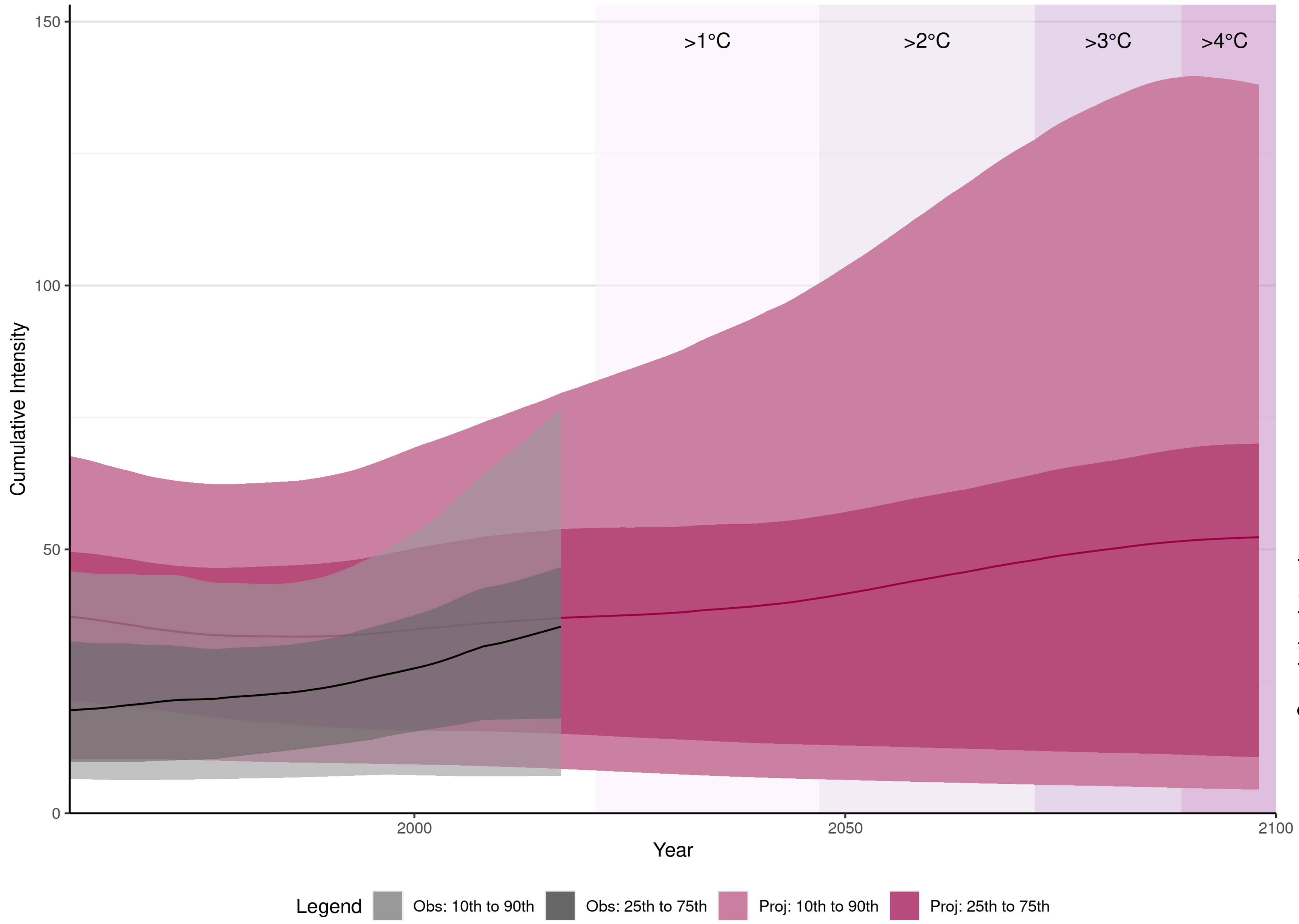


Figure 10: Projected change in *cumulative intensity during a heatwave* from 1990 to 2100. Historical values are the 30-year rolling means from AGCD (*grey*). Projected values (*peach*) are the ensemble mean of the 30-year rolling mean of each ensemble member. *Lighter ribbons* represent the 10th to 90th percentiles of *cumulative intensity during a heatwave*. *Darker ribbons* represent the 25th to 75th percentiles of *cumulative intensity during a heatwave*. *Solid lines* represent the mean of *cumulative intensity during a heatwave*.

### Figure 11: Distribution of cumulative intensity

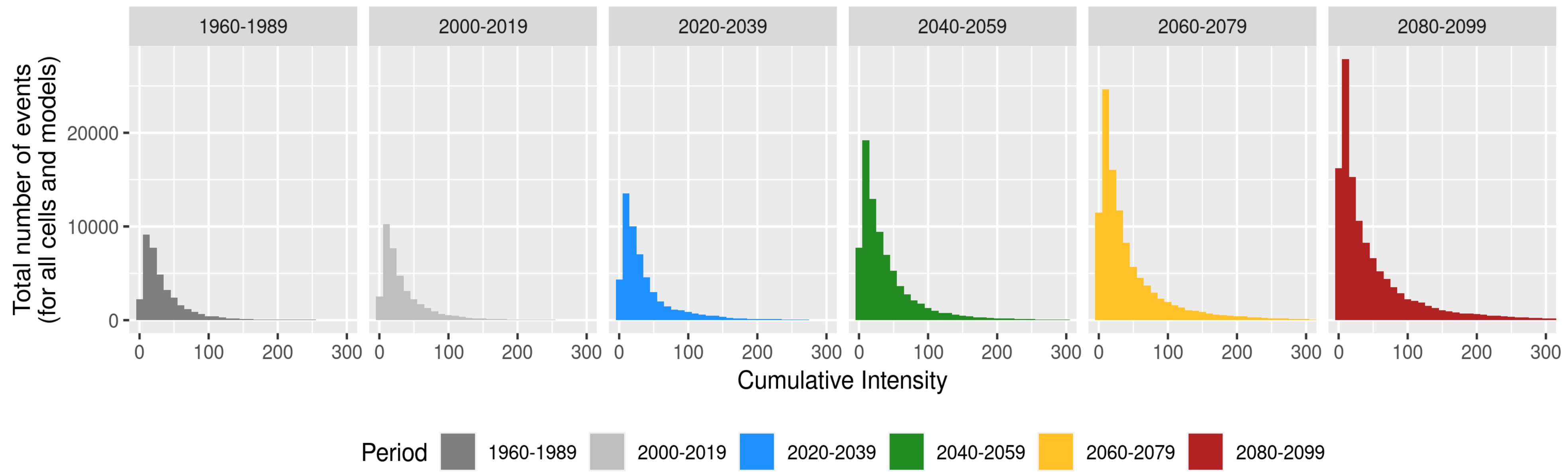


Figure 11: Comparison of the distribution of *cumulative intensity during a heatwave* for different time periods.

### Figure 12: Projected mean cumulative intensity

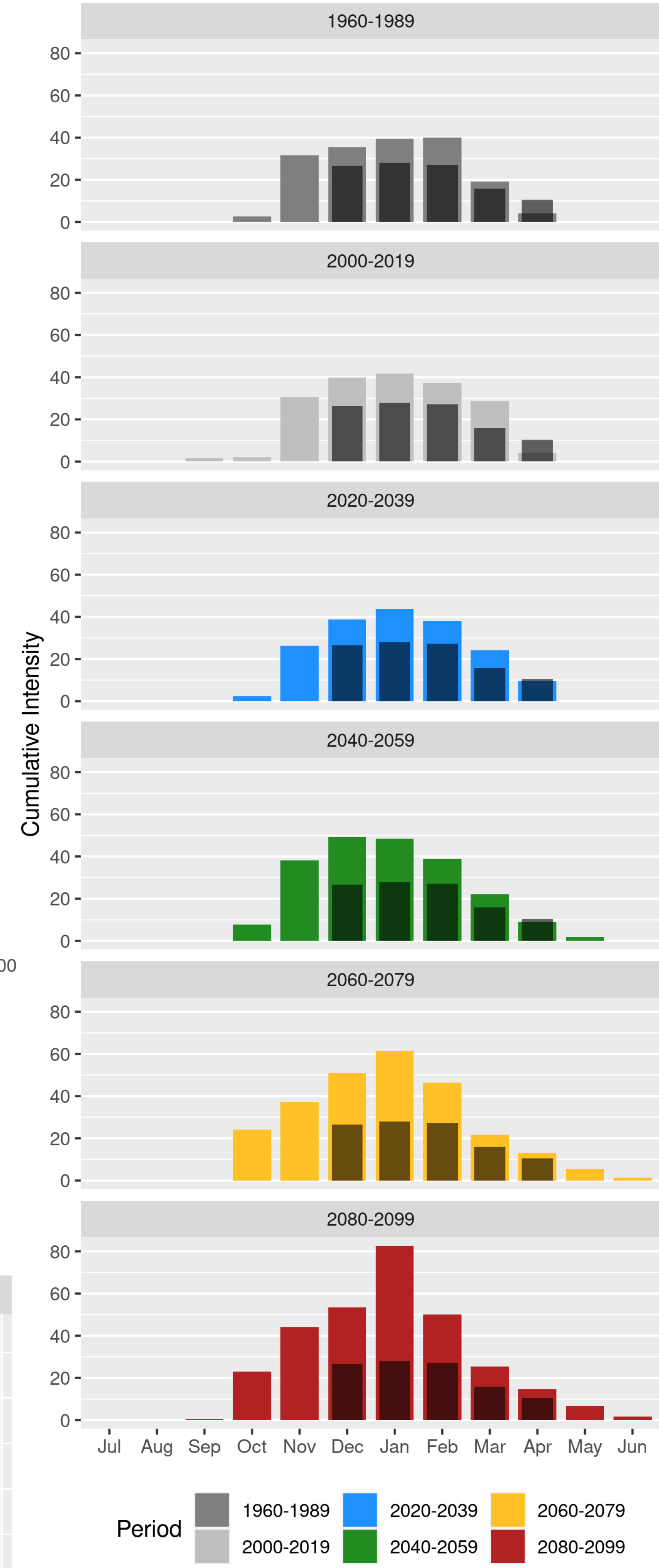


Figure 12: *Bar plots of cumulative intensity during heatwaves* in each month for 20-year time periods from 1961 to 2100. Each bar represents the 20-year mean of *cumulative intensity during a heatwave*, average across space and time. The observations for the baseline period (1961–1990) are shadowed on top of the future time periods to highlight any differences expected into the future. Higher (lower) bars indicate hotter (cooler) heatwave intensities.

Figure 1: Observed mean duration

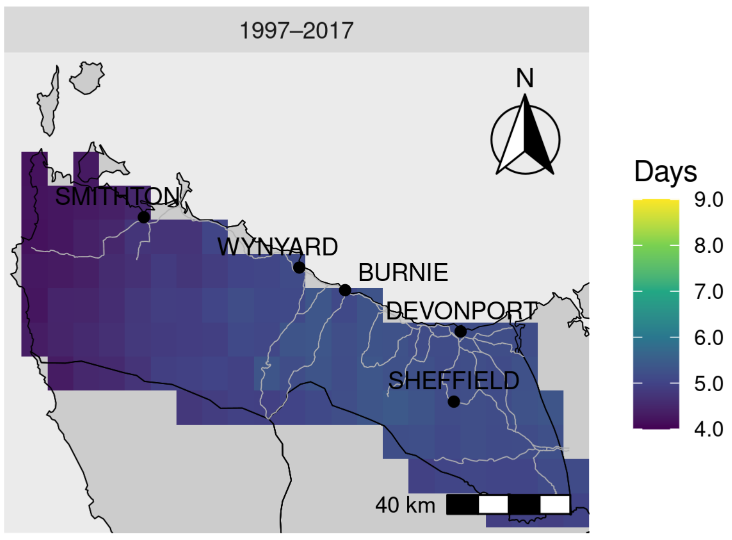


Figure 2: Observed change in mean duration

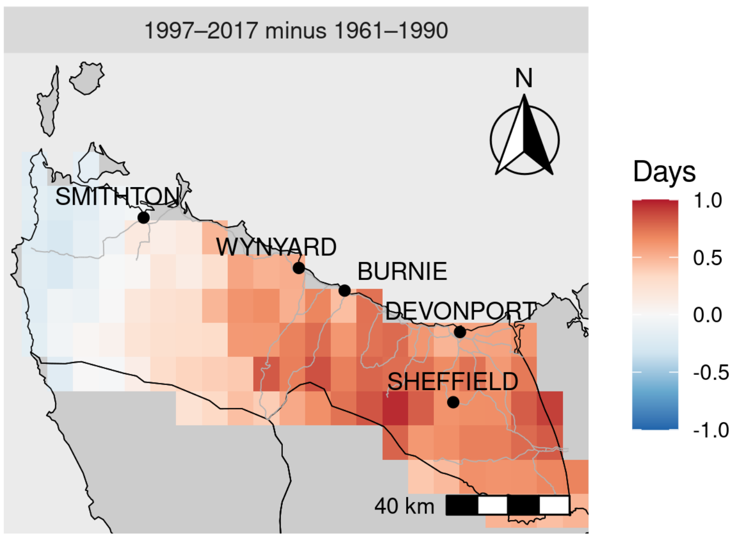


Figure 3: Projected mean duration

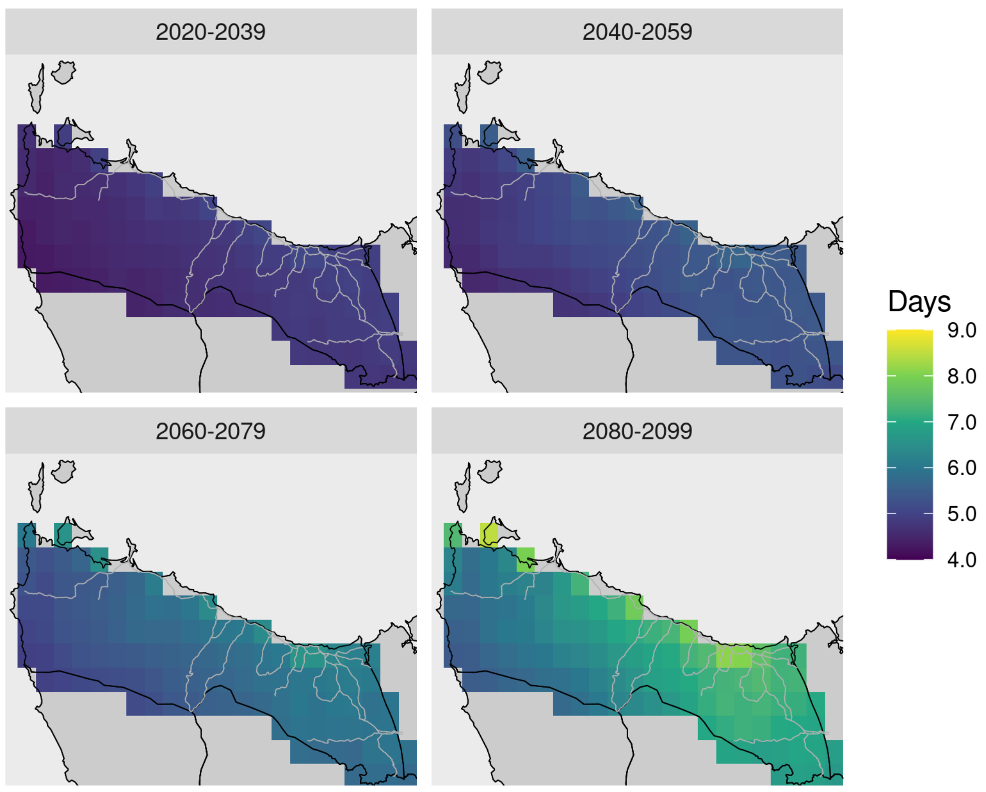


Figure 13: Observed mean *heatwave durations* across all years from 1997–2017.

Figure 14: The change in mean *heatwave duration* between the current (1997–2017) and historical (1961–1990) periods. Mean *heatwave durations* have increased across the region over recent decades.

Figure 15: Projected mean *heatwave durations* for 20-year time periods from 2001 to 2100. Mean *heatwave duration* is expected to increase steadily into the future. Each grid cell is the mean of the 6 ensemble members.

Figure 16: Projected heatwave duration

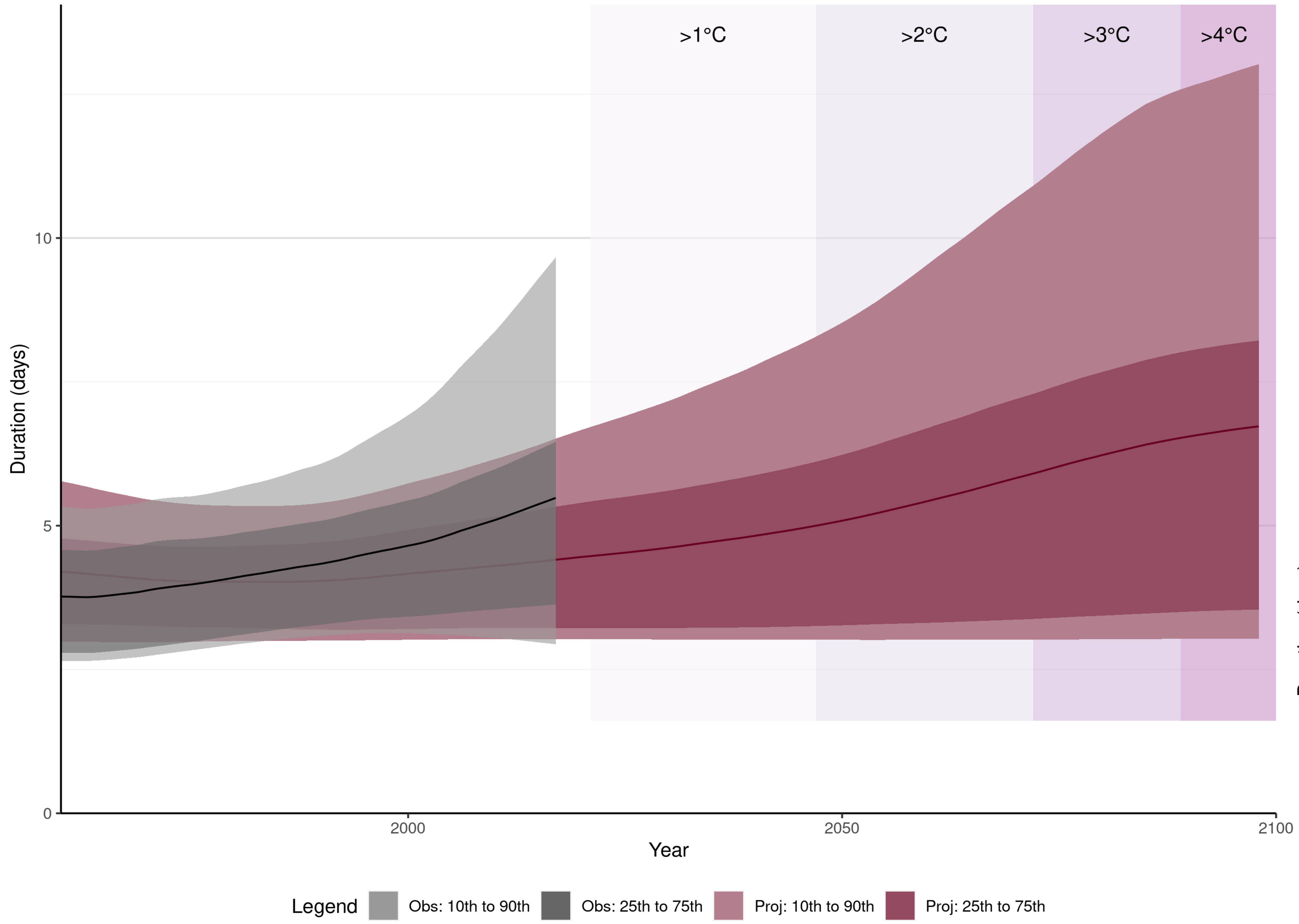


Figure 16: Projected change in *heatwave duration* from 1990 to 2100. Historical values (*grey*) are the 30-year rolling means of AGCD. Projected values (*orange*) are the ensemble mean of the 30-year rolling mean of each CCAM ensemble member. *Lighter ribbons* represent the 10th to 90th percentiles of *heatwave duration*. *Darker ribbons* represent the 25th to 75th percentiles of *heatwave duration*. *Solid lines* represent the mean of *heatwave duration*.

Figure 17: Projected count of heatwave duration

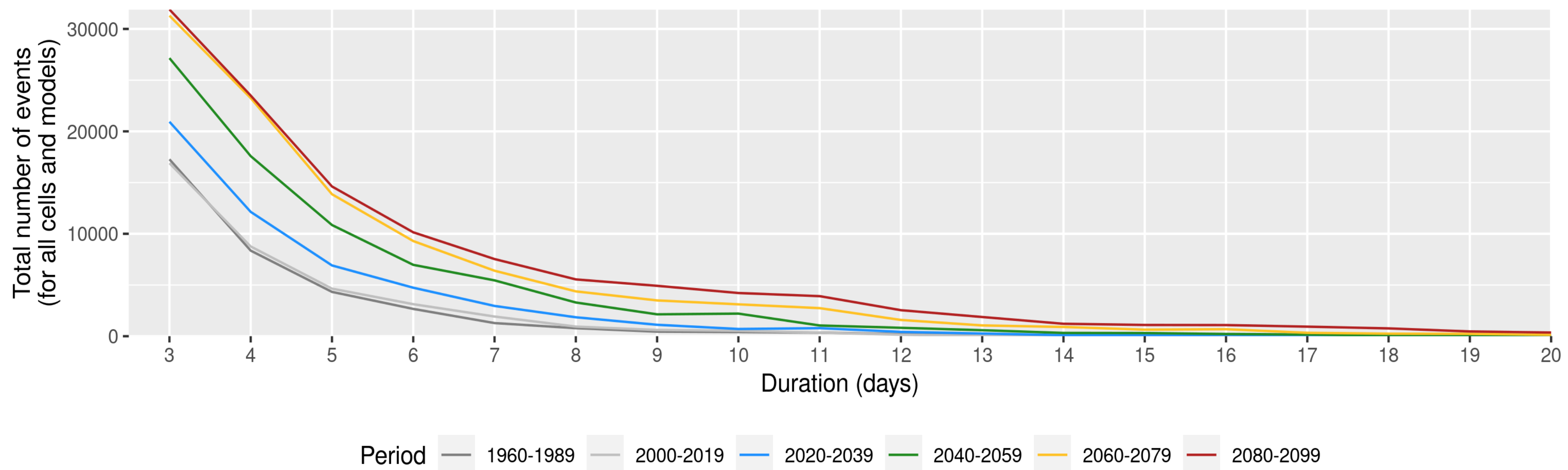


Figure 17: Comparison of the distribution of *heatwave durations* for different time periods.

Figure 18: Projected mean heatwave duration by

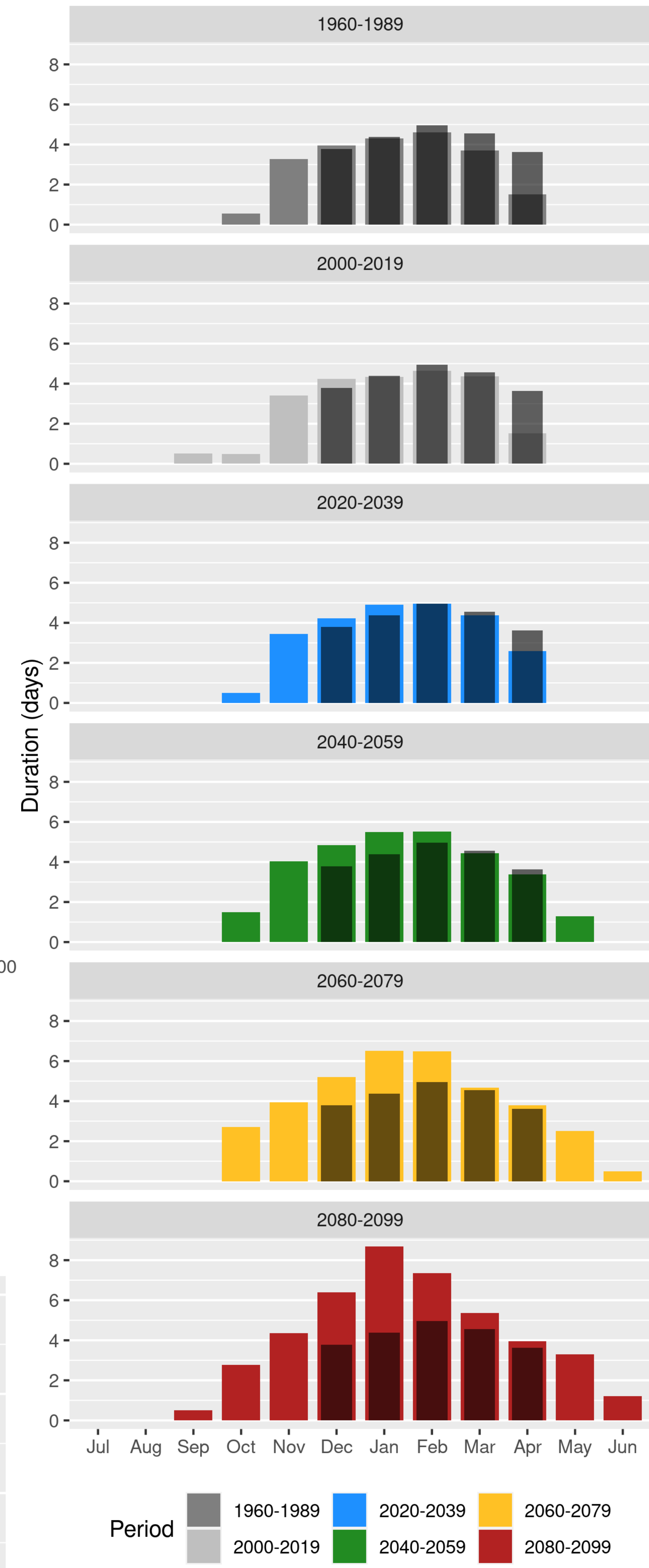


Figure 18: *Bar plots* of mean *heatwave durations* in each month for 20-year time periods from 1961 to 2100. Each bar represents the 20-year mean of *heatwave durations*, average across space and time. The observations for the baseline period (1961–1990) are shadowed on top of the future time periods to highlight any differences expected into the future. Higher (lower) bars indicate longer (shorter) *heatwave durations*.

# KING ISLAND

## Heatwaves — Number of Heatwave Days

Figure 1: Observed
mean annual number of heatwave days

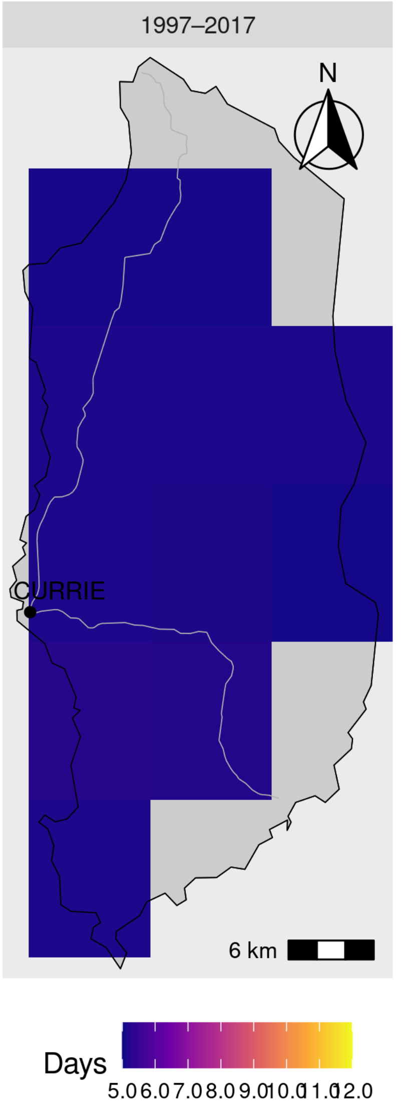


Figure 2: Observed change in
mean annual number of heatwave days

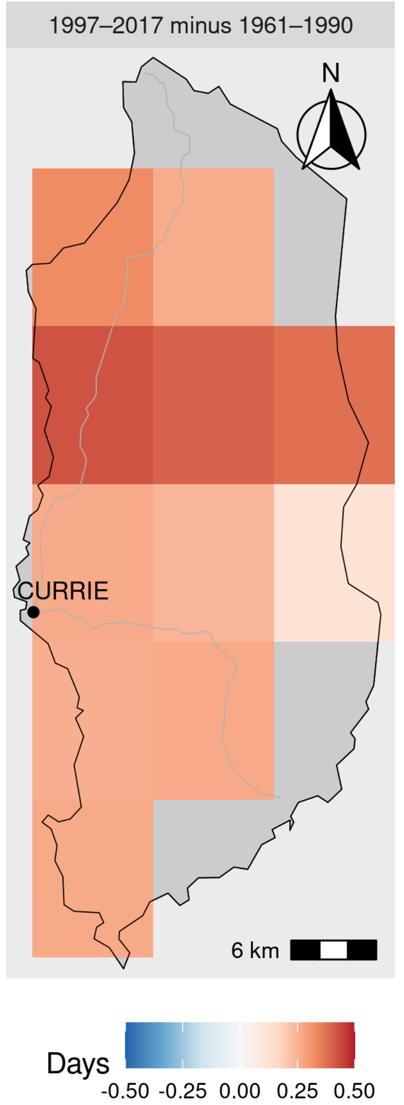


Figure 3: Projected mean annual number of heatwave days

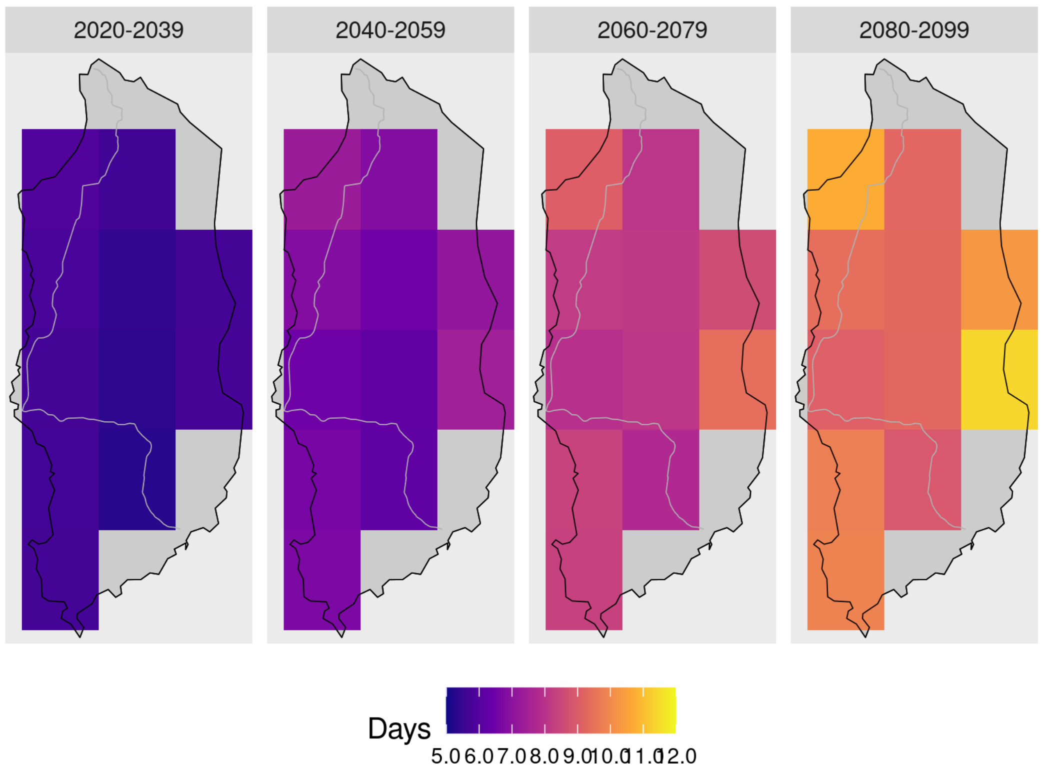


Figure 1: Observed mean *annual number of heatwave days* across all years from 1997–2017.

Figure 2: The change in the mean *annual number of heatwave days* between the current (1997–2017) and historical (1961–1990) periods. Mean *annual number of heatwave days* has increased across the region over recent decades.

Figure 3: Projected mean *annual number of heatwave days* for 20-year time periods from 2001 to 2100. Mean *annual number of heatwave days* is expected to increase steadily into the future. Each grid cell is the mean of the 6 ensemble members.

Figure 4: Projected annual number of heatwave days from 1961 to 2100

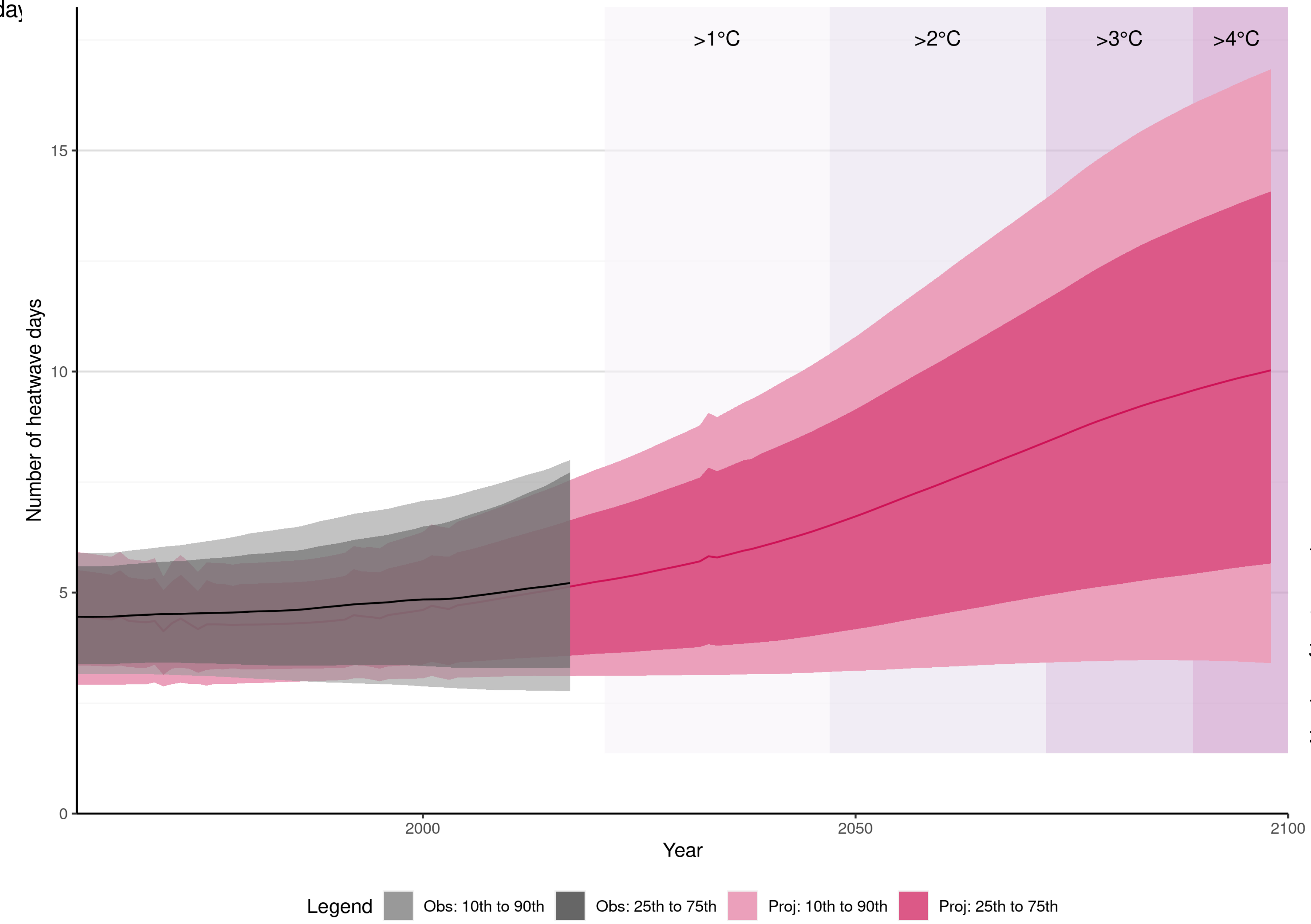


Figure 4: Projected change in mean *annual number of heatwave days* from 1990 to 2100. Historical values (*grey*) are the 30-year rolling means of AGCD. Projected values (*peach*) are the ensemble mean of the 30-year rolling mean of each CCAM ensemble member. *Lighter ribbons* represent the 10th to 90th percentiles of mean *annual number of heatwave days*. *Darker ribbons* represent the 25th to 75th percentiles of mean *annual number of heatwave days*. *Solid lines* represent the mean *annual number of heatwave days*.

Figure 5: Projected range in the annual number of heatwave days

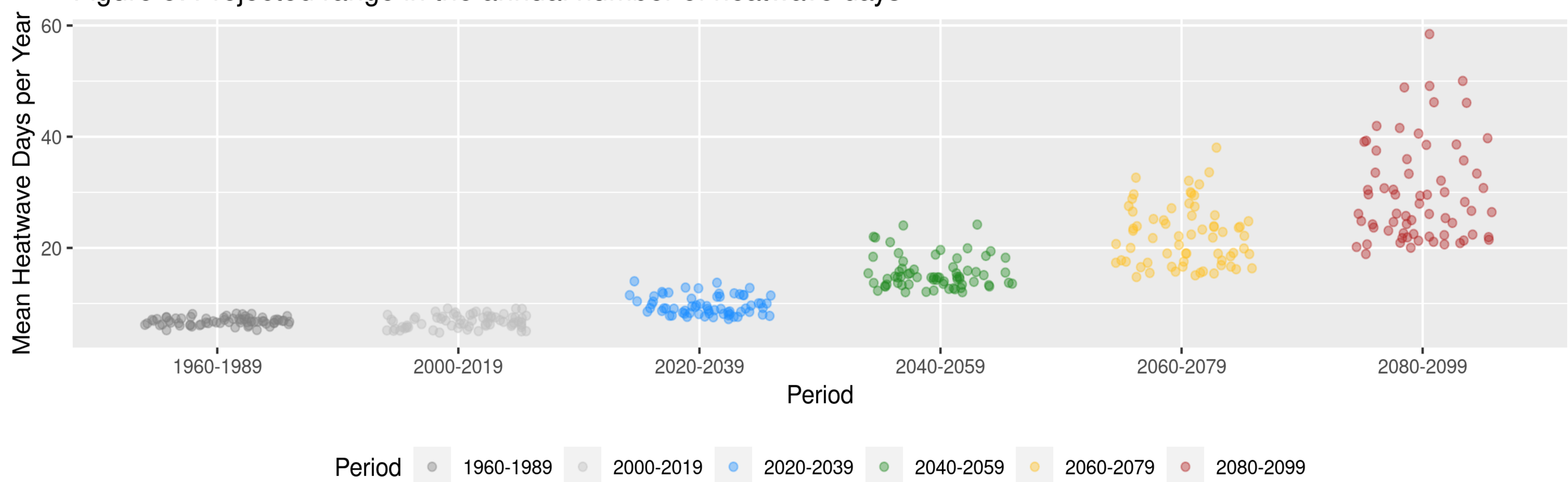


Figure 5: Comparison of the distribution of the *annual number of heatwave days* over the historical period for both model outputs (¡colour¿ and observations (*black*).

Figure 6: Projected mean annual number of hea

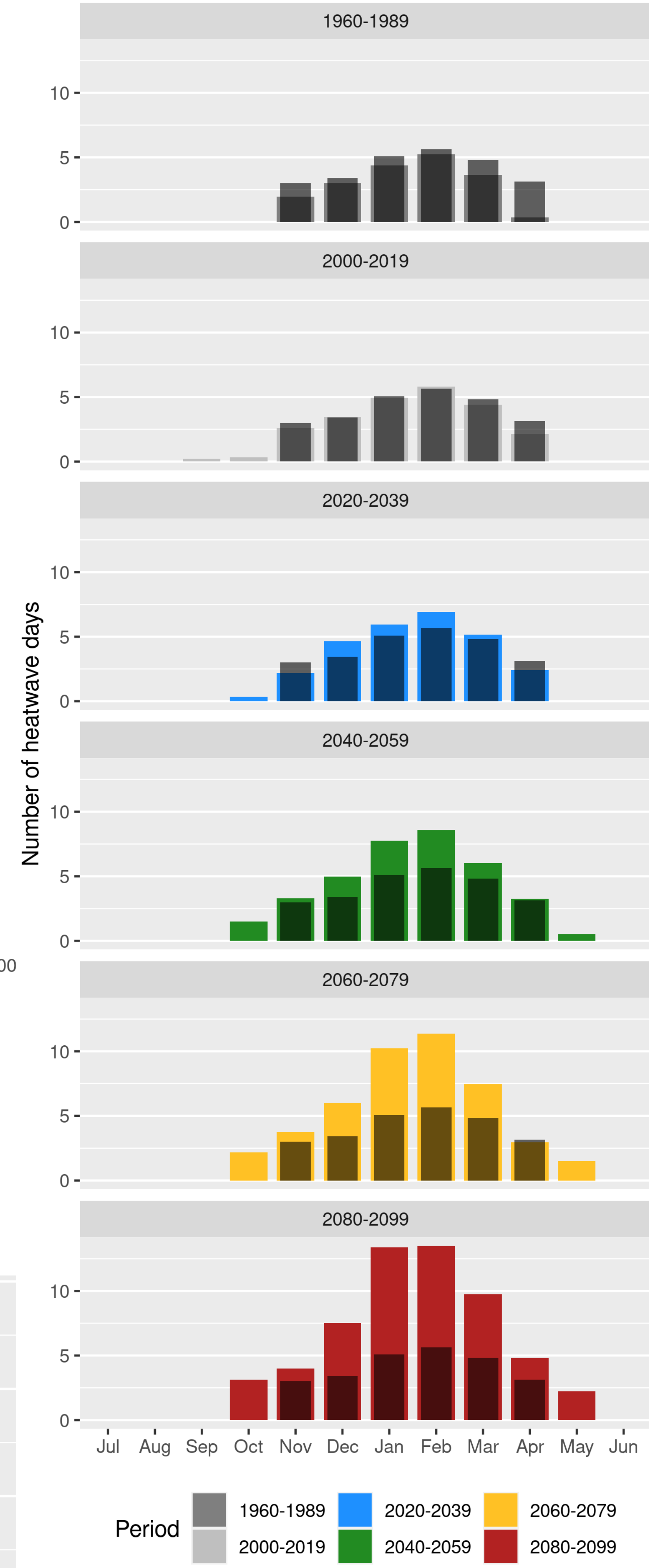


Figure 6: *Bar plots of typical number of heatwave days in each month* for 20-year time periods from 1961 to 2100. Each bar represents the 20-year *typical number of heatwave days in each month*, average across space and time. The observations for the baseline period (1961–1990) are shadowed on top of the future time periods to highlight any differences expected into the future. Higher (lower) bars indicate more (less) heatwave days.

# KING ISLAND

## Heatwaves — Cumulative Intensity

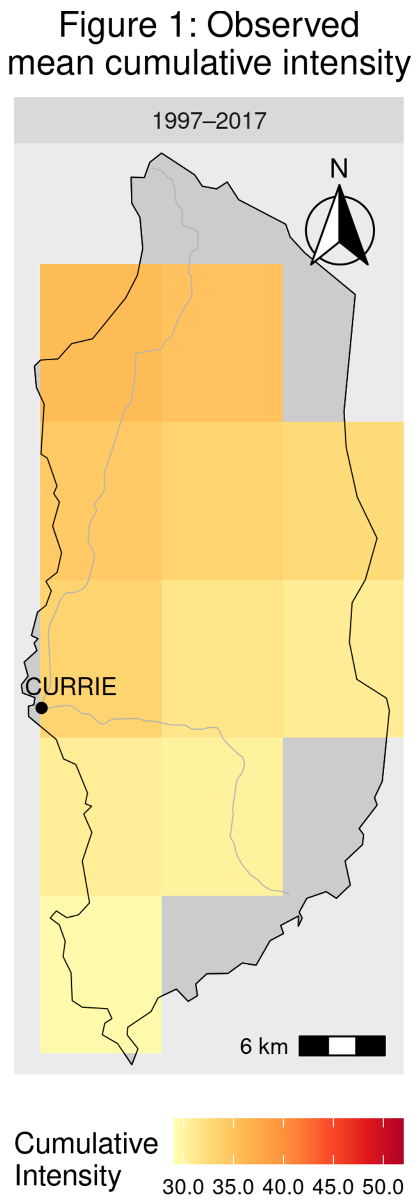


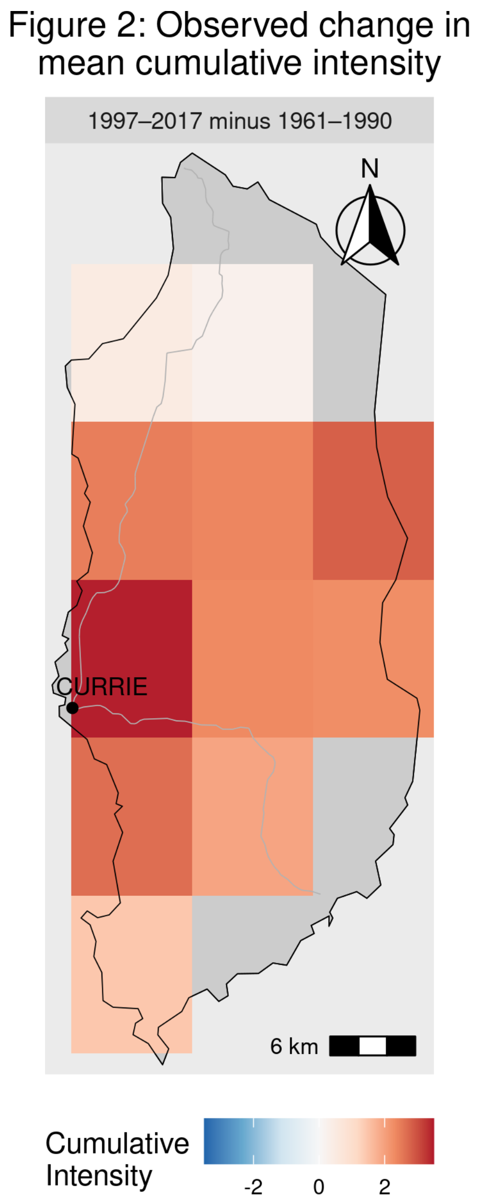


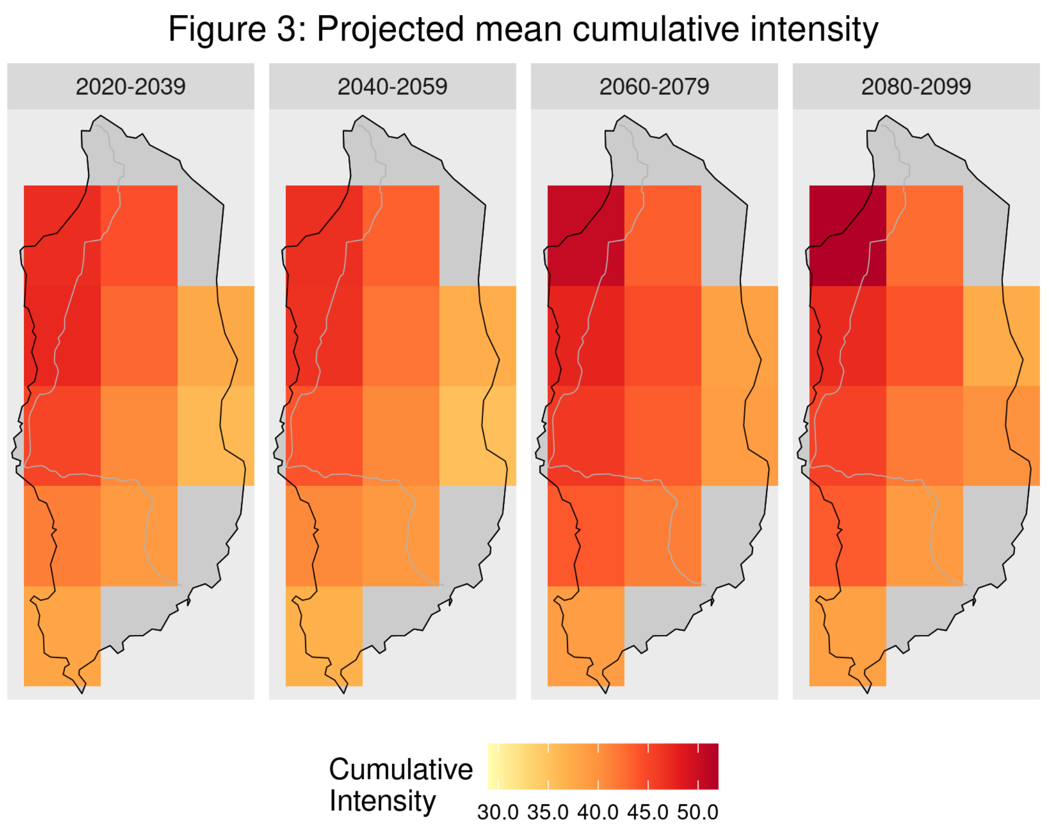


Figure 7: Observed mean *cumulative intensity during a heatwave* across all years from 1997–2017.

Figure 8: The change in mean *cumulative intensity during a heatwave* between the current (1997–2017) and historical (1961–1990) periods. Mean *cumulative intensity during a heatwave* has increased across the region over recent decades.

Figure 9: Projected mean *cumulative intensity during a heatwave* for 20-year time periods from 2001 to 2100. Mean *cumulative intensity during a heatwave* is expected to increase steadily into the future. Each grid cell is the mean of the 6 ensemble members.

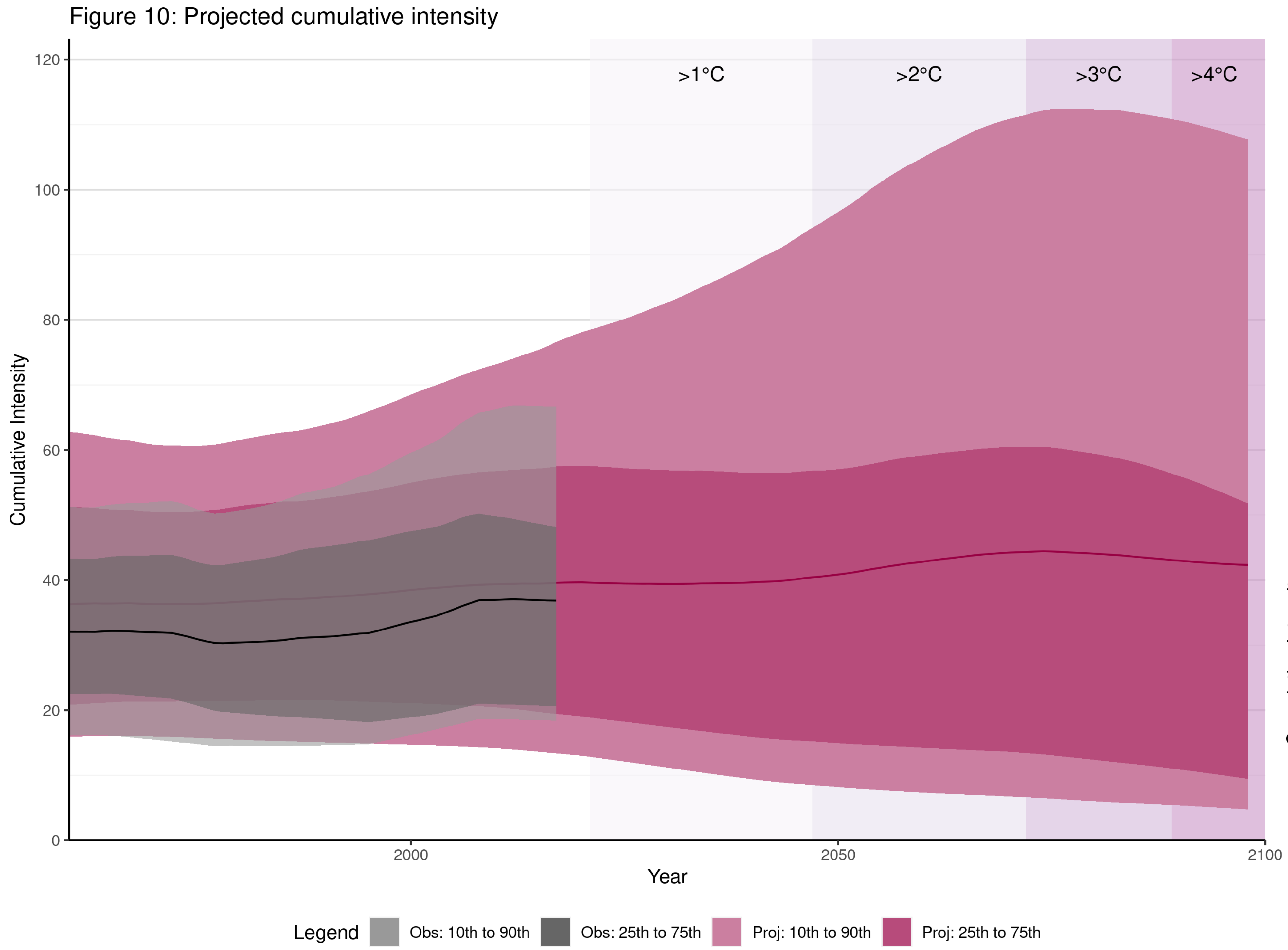


Figure 10: Projected change in *cumulative intensity during a heatwave* from 1990 to 2100. Historical values are the 30-year rolling means from AGCD (*grey*). Projected values (*peach*) are the ensemble mean of the 30-year rolling mean of each ensemble member. *Lighter ribbons* represent the 10th to 90th percentiles of *cumulative intensity during a heatwave*. *Darker ribbons* represent the 25th to 75th percentiles of *cumulative intensity during a heatwave*. *Solid lines* represent the mean of *cumulative intensity during a heatwave*.

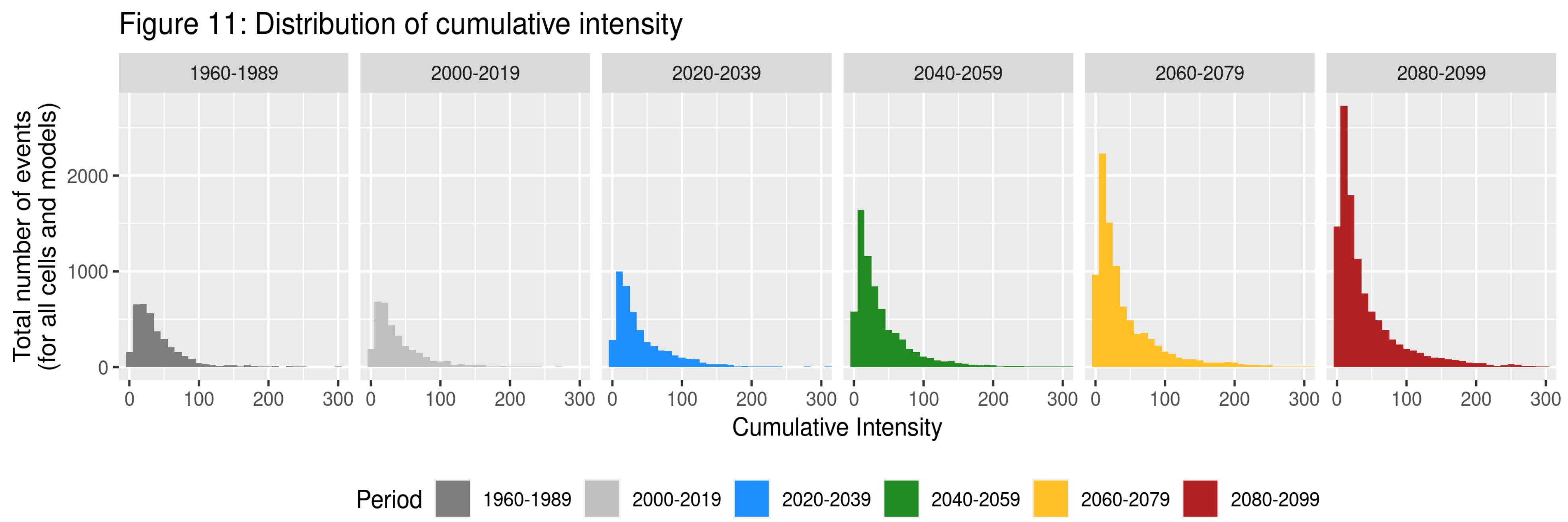


Figure 11: Comparison of the distribution of *cumulative intensity during a heatwave* for different time periods.

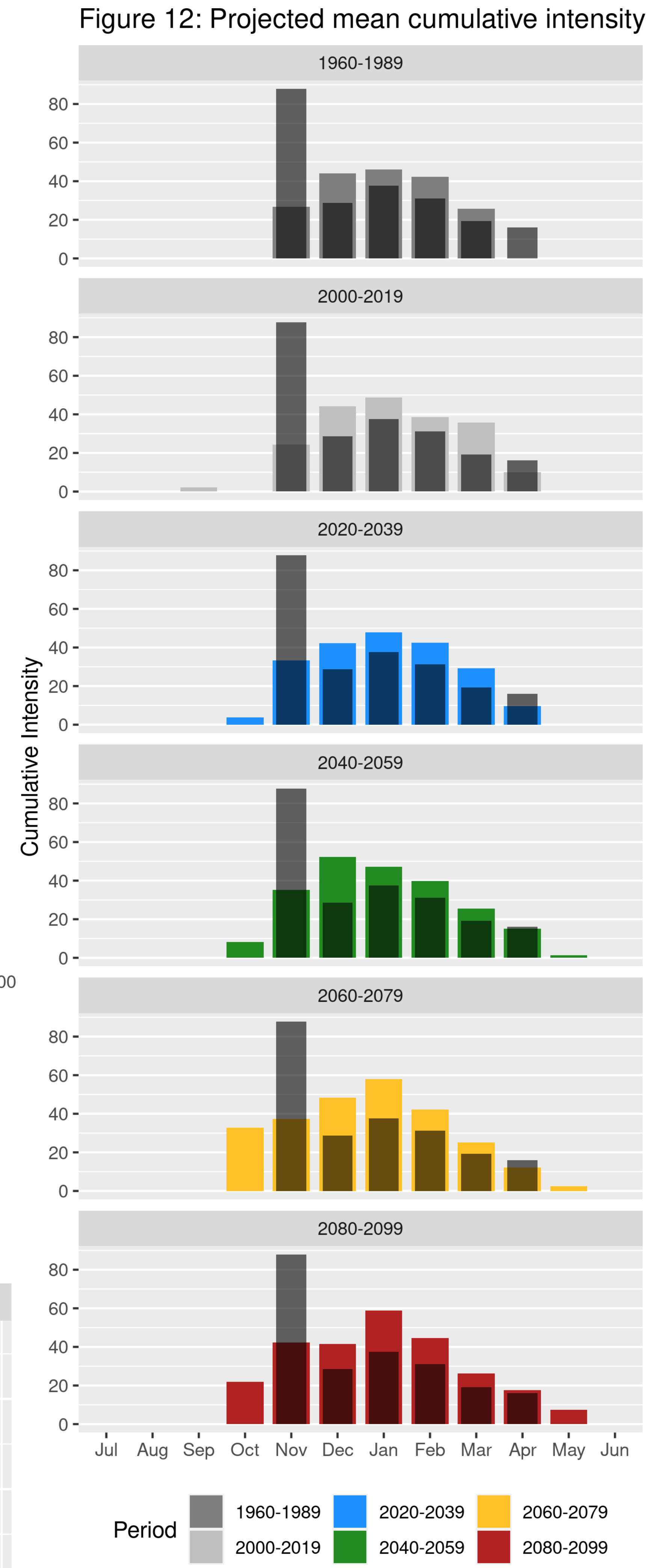


Figure 12: *Bar plots of cumulative intensity during heatwaves* in each month for 20-year time periods from 1961 to 2100. Each bar represents the 20-year mean of *cumulative intensity during a heatwave*, average across space and time. The observations for the baseline period (1961–1990) are shadowed on top of the future time periods to highlight any differences expected into the future. Higher (lower) bars indicate hotter (cooler) heatwave intensities.

# KING ISLAND

## Heatwaves — Duration

Figure 1: Observed mean duration

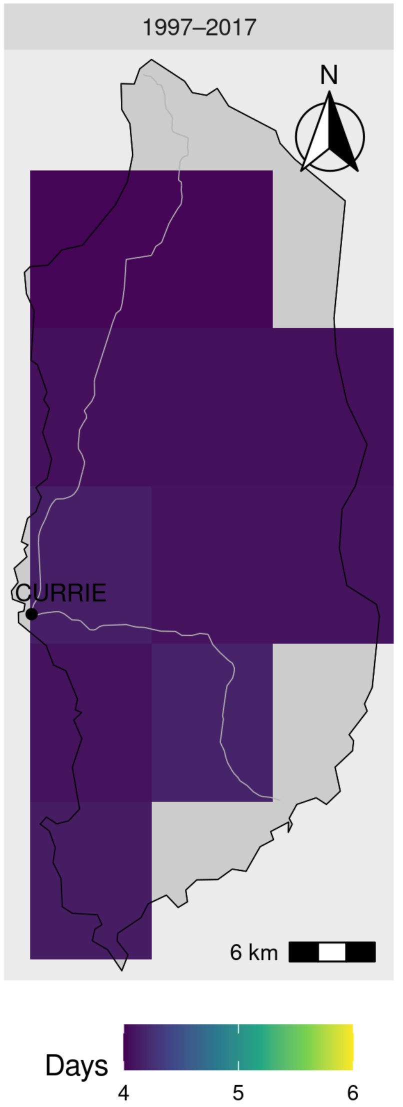


Figure 2: Observed change in mean duration

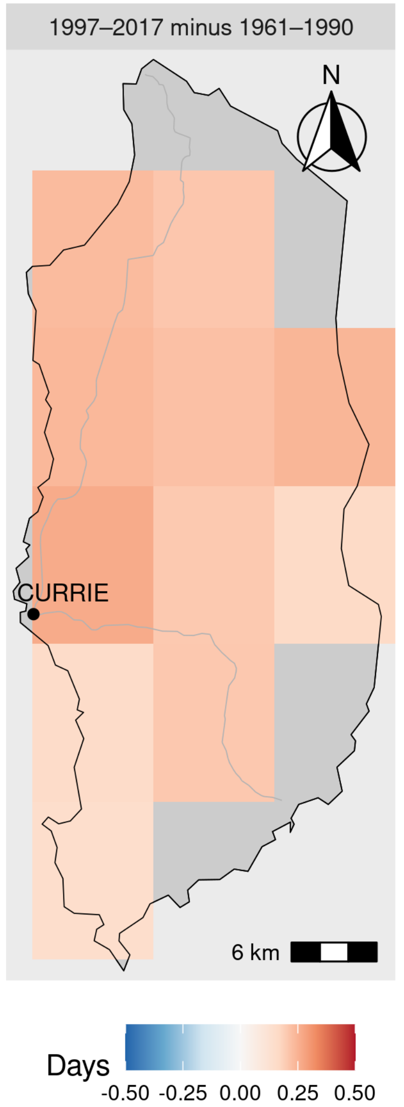


Figure 3: Projected mean duration

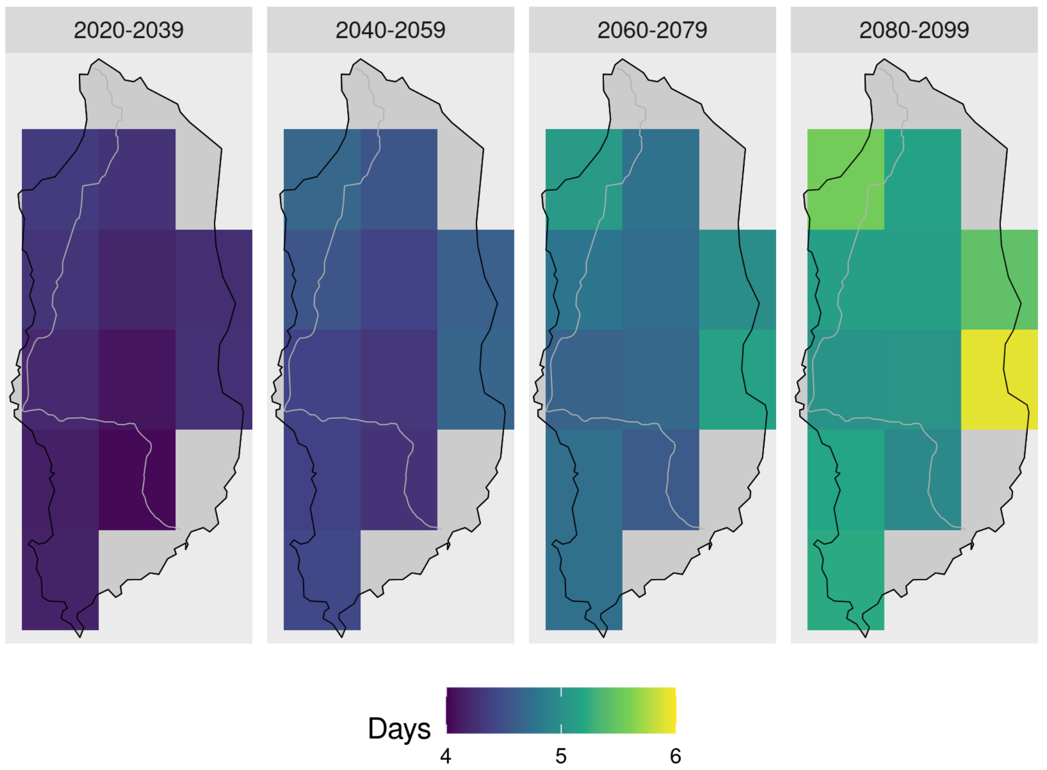


Figure 13: Observed mean *heatwave durations* across all years from 1997–2017.

Figure 14: The change in mean *heatwave duration* between the current (1997–2017) and historical (1961–1990) periods. Mean *heatwave durations* have increased across the region over recent decades.

Figure 15: Projected mean *heatwave durations* for 20-year time periods from 2001 to 2100. Mean *heatwave duration* is expected to increase steadily into the future. Each grid cell is the mean of the 6 ensemble members.

Figure 16: Projected heatwave duration

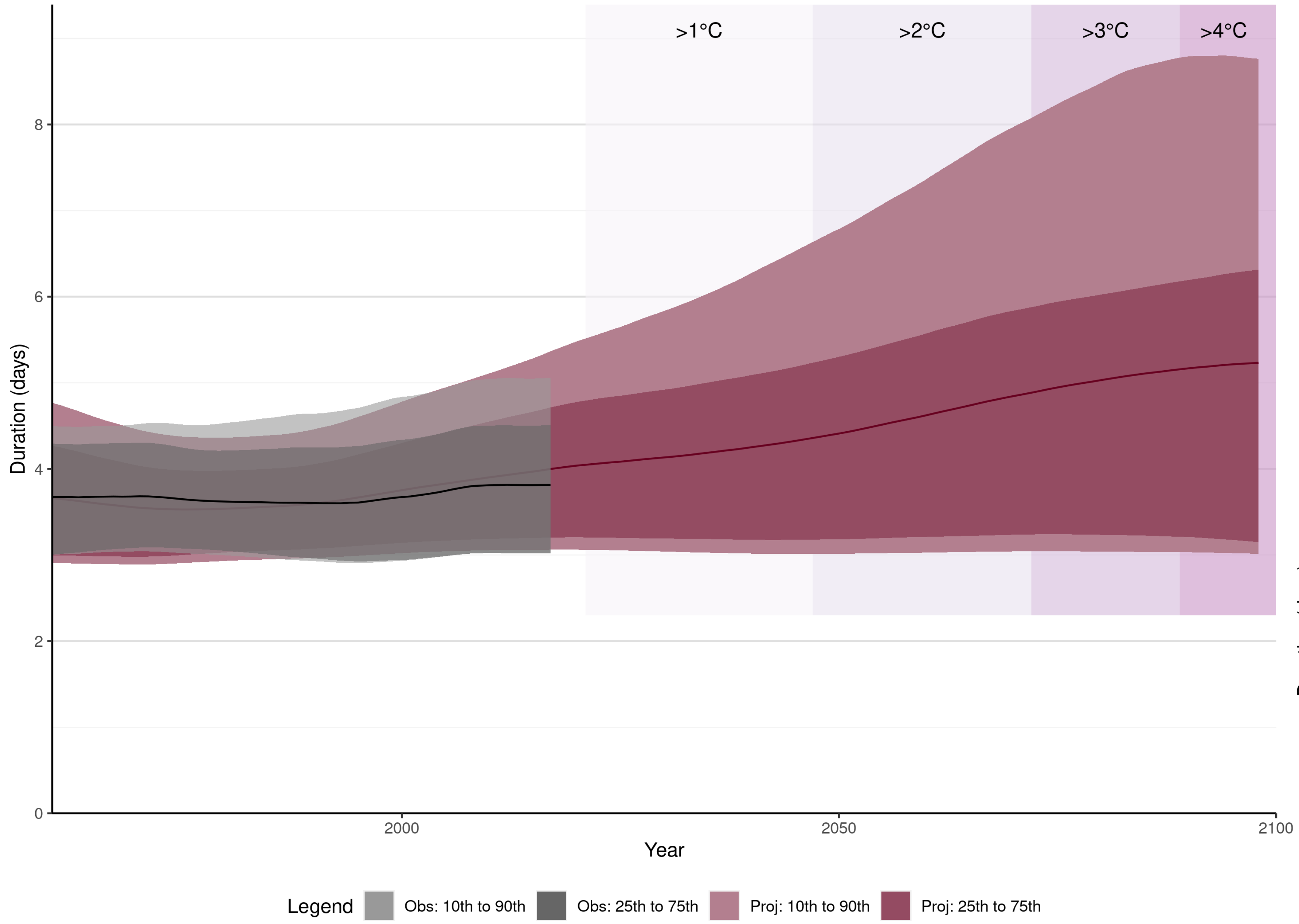


Figure 16: Projected change in *heatwave duration* from 1990 to 2100. Historical values (*grey*) are the 30-year rolling means of AGCD. Projected values (*orange*) are the ensemble mean of the 30-year rolling mean of each CCAM ensemble member. *Lighter ribbons* represent the 10th to 90th percentiles of *heatwave duration*. *Darker ribbons* represent the 25th to 75th percentiles of *heatwave duration*. *Solid lines* represent the mean of *heatwave duration*.

Figure 17: Projected count of heatwave duration

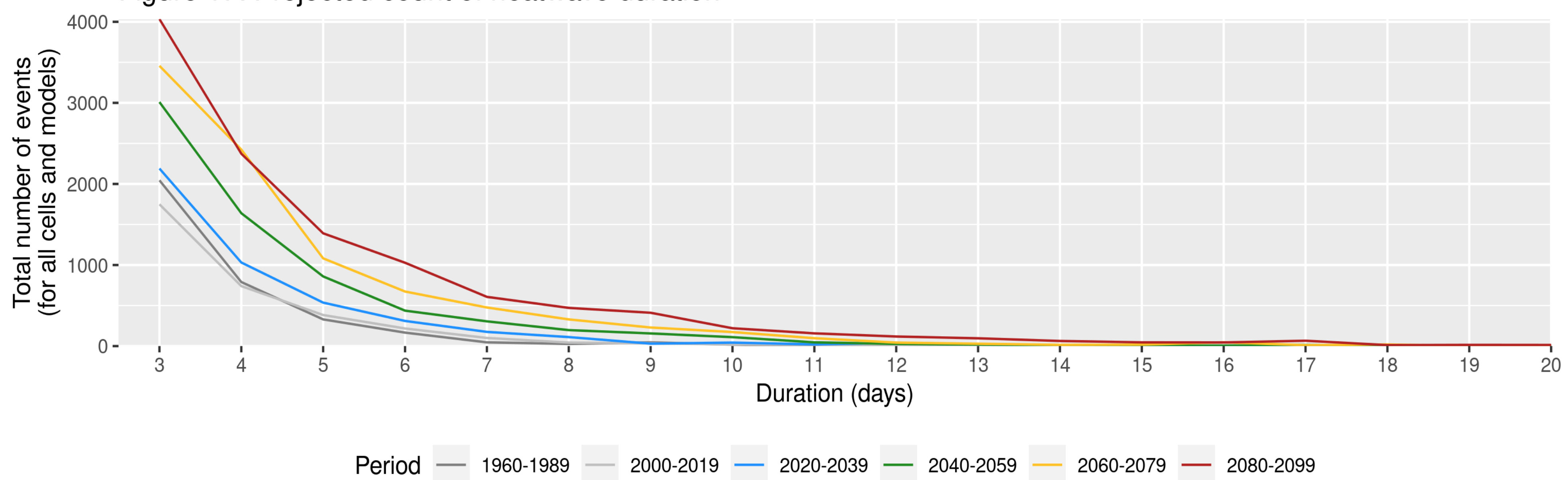


Figure 17: Comparison of the distribution of *heatwave durations* for different time periods.

Figure 18: Projected mean heatwave duration by

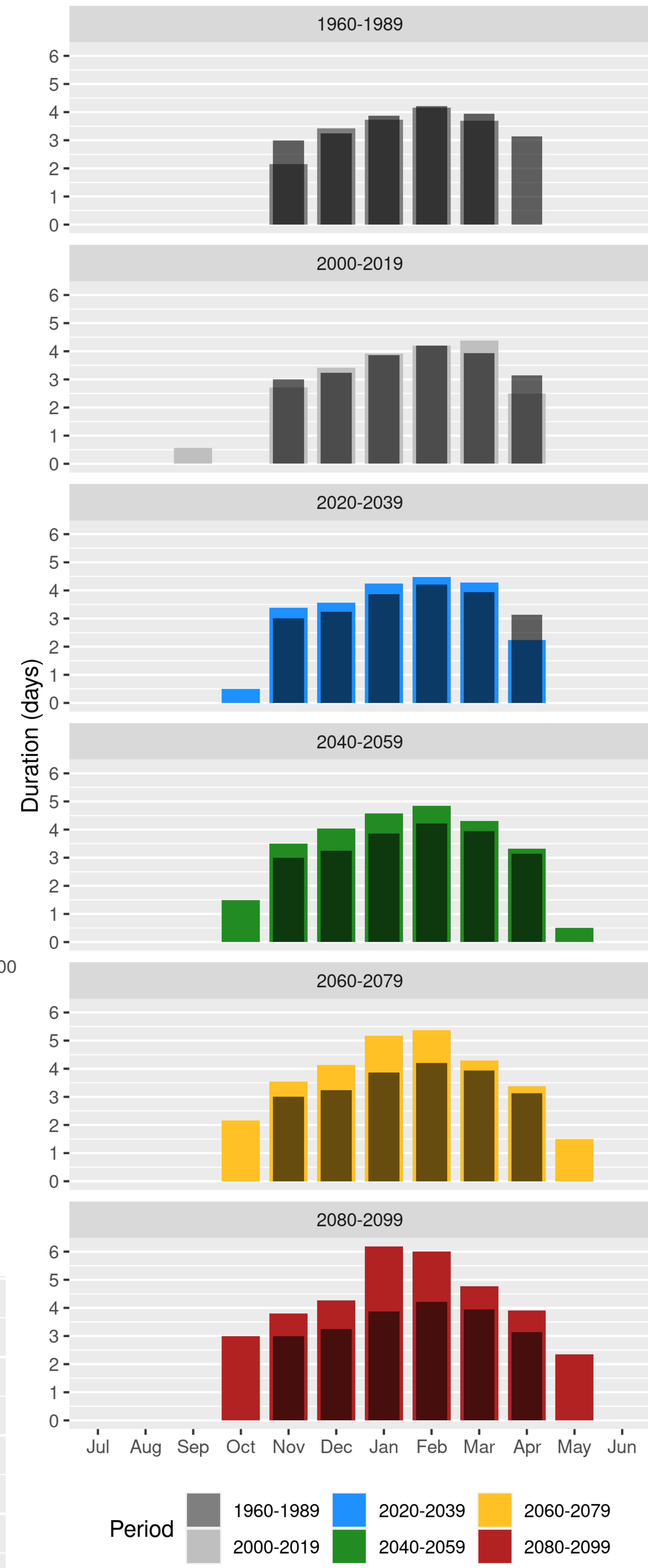


Figure 18: *Bar plots* of mean *heatwave durations* in each month for 20-year time periods from 1961 to 2100. Each bar represents the 20-year mean of *heatwave durations*, average across space and time. The observations for the baseline period (1961–1990) are shadowed on top of the future time periods to highlight any differences expected into the future. Higher (lower) bars indicate longer (shorter) *heatwave durations*.

Atlas of
Earth System Hazards
for Tasmania

–

# Part 2: Bushfire

Figure 1: Projected 90th, 95th and 99th percentile of daily max FFDI

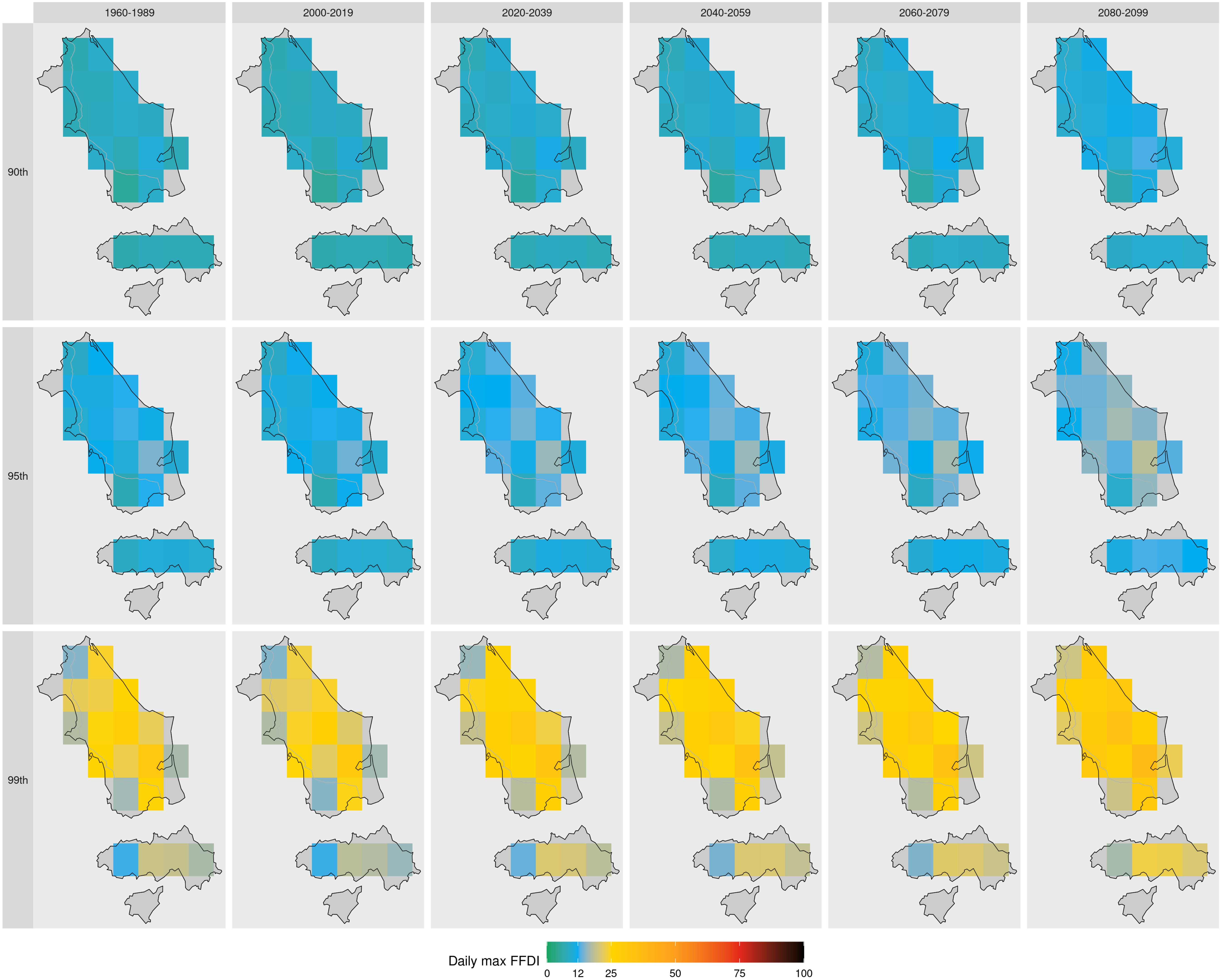


Figure 1: Projected 90th, 95th and 99th percentile values of *Forest Fire Danger Index* for the 30-year baseline period, and then 20-year time periods from 2001 to 2100. Each grid cell is the mean of the 6 ensemble members. The 99th percentile value reflects the 4th highest FFDI value year; the 95th percentile is the 18th highest FFDI value year; and the 90th percentile is the 36th highest FFDI value year. Extreme values of FFDI are expected to increase steadily into the future.

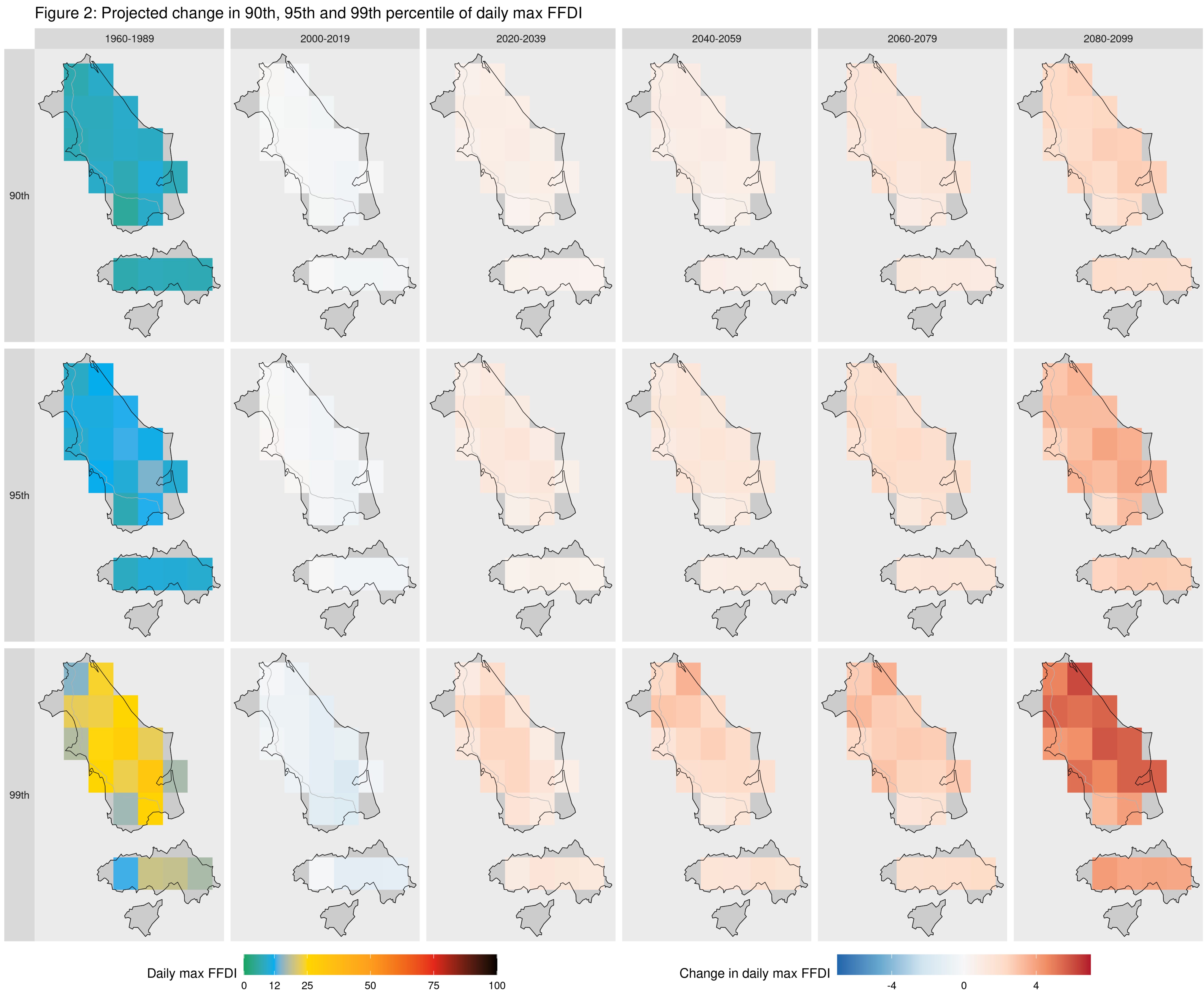


Figure 2: Projected change in the 90th, 95th and 99th percentile values of *Forest Fire Danger Index* for 20-year time periods from 2001 to 2100 compared to the 30-year baseline period 1961–1990. Each grid cell is the mean of the 6 ensemble members. The 99th percentile value reflects the 4th highest FFDI value year; the 95th percentile is the 18th highest FFDI value year; and the 90th percentile is the 36th highest FFDI value year. Extreme values of FFDI are expected to increase steadily into the future

Figure 3: Projected monthly FFDI with outliers removed

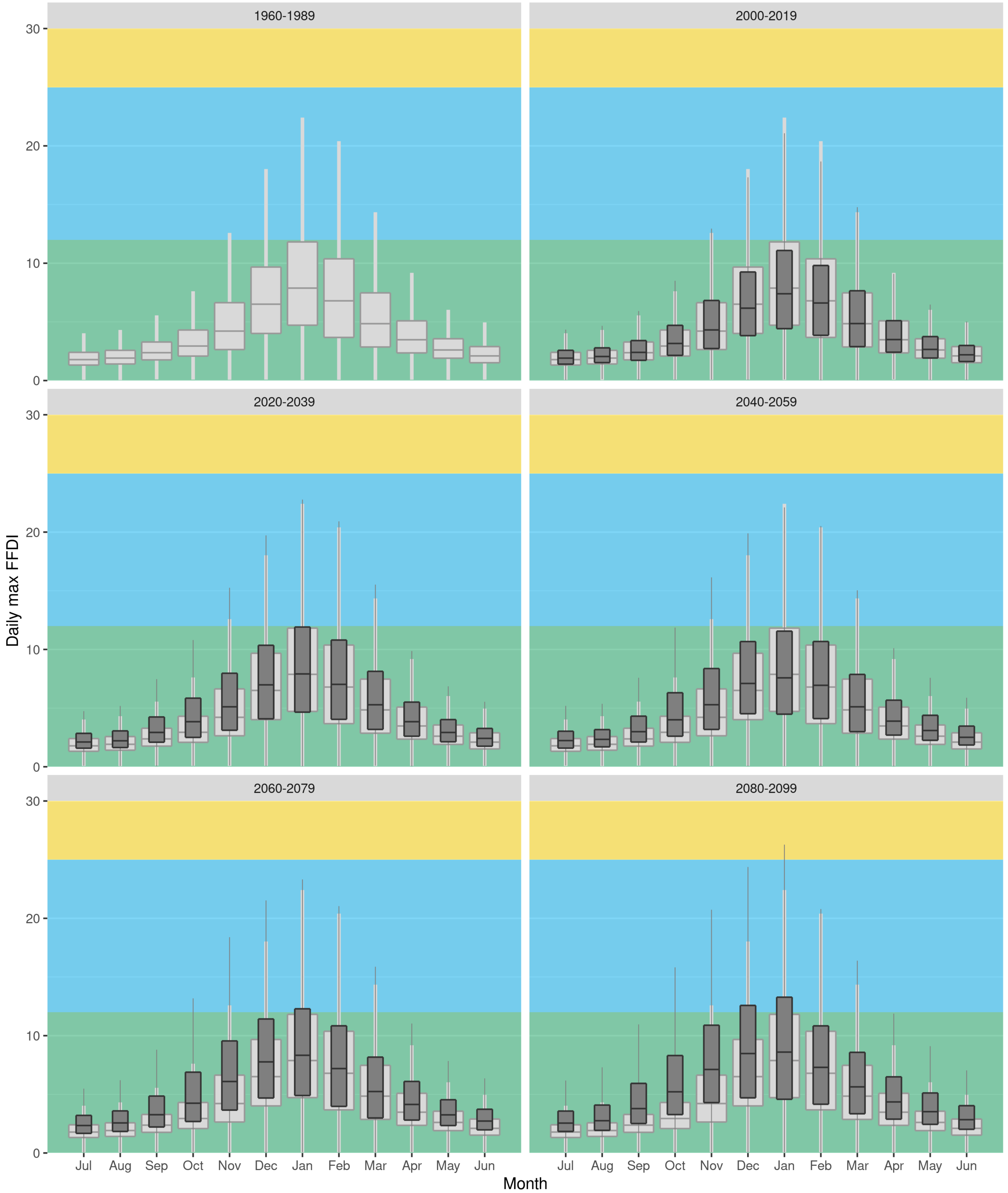


Figure 4: Projected monthly FFDI with outliers shown

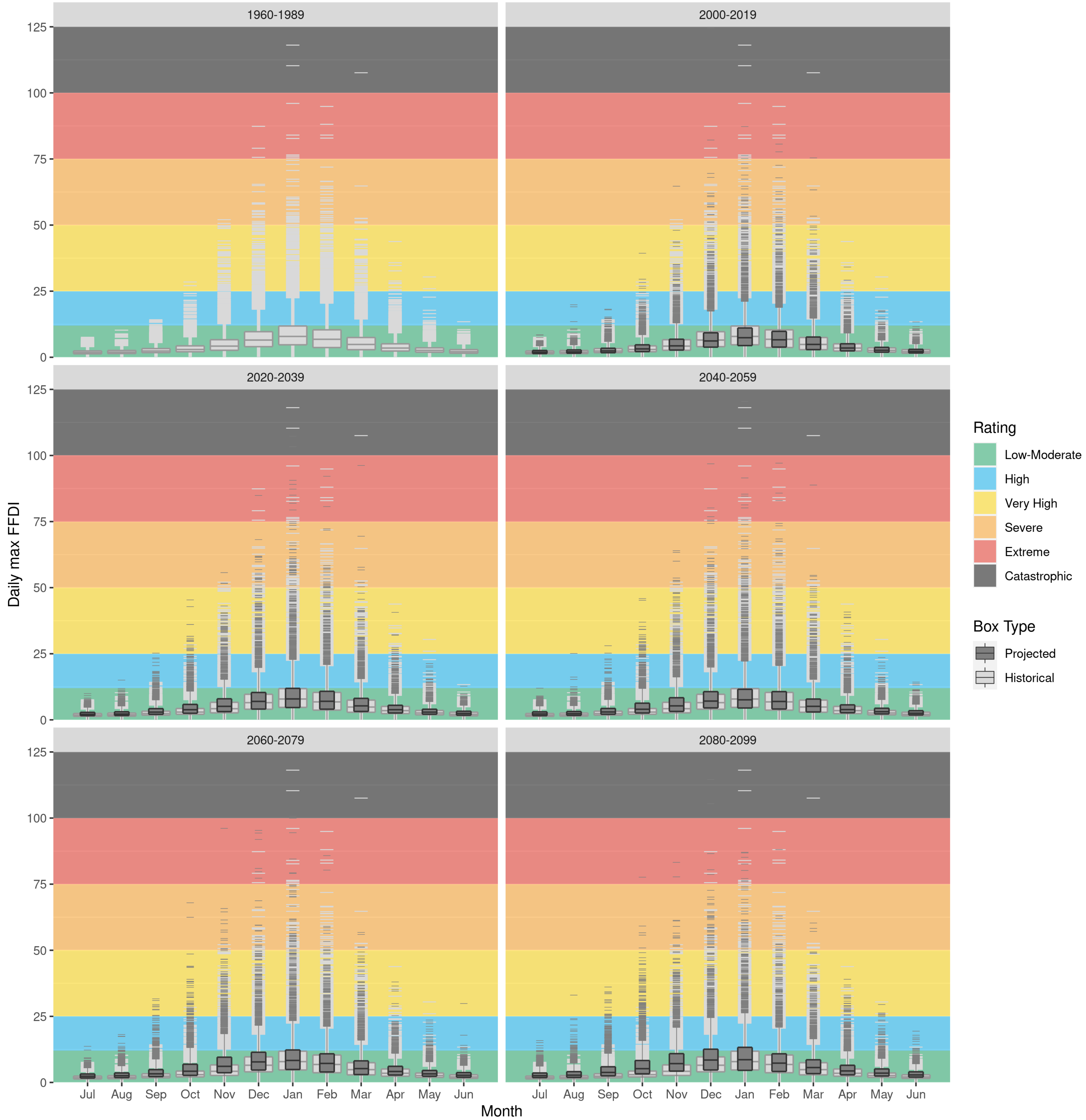


Figure 3: Boxplots of daily *Forest Fire Danger Index* for each month for the 30-year baseline period, and then 20-year periods from 2001 to 2100. Each boxplot represents a summary of daily data for each grid cell, for each of the 6 ensemble members within the time period; e.g. the top-left panel, the January boxplot represents the daily FFDI values for all January days in the period 1961–1990, for all grids cell in the region, for each of the 6 ensemble members. The baseline period (1961-1990) has been shadowed (*light grey*) underneath future time periods to highlight any differences expected into the future. Solid bars represent the median value. The box represents the 25th and 75th percentiles. The Whiskers represent the 1.5× the inter-quartile range. All months in all periods frequently have days of very low FFDI. Outliers have been excluded. If the boxplot shifts higher (lower) this indicates a change towards more (less) dangerous conditions.

Figure 4: Boxplots of daily *Forest Fire Danger Index* for each month for the 30-year baseline period, and then 20-year periods from 2001 to 2100. Each boxplot represents daily data for each grid cell, for each of the 6 ensemble members within the time period; e.g. ing the top-left panel, the January boxplot represents the daily FFDI values for all January days in the period 1961–1990, for all grids cell in the region, for each of the 6 ensemble members. The baseline period (1961-1990) has been shadowed (*light grey*) underneath future time periods to highlight any differences expected into the future. Solid bars represent the median value. The box represents the 25th and 75th percentiles. The Whiskers represent the 1.5× the inter-quartile range. All months in all periods frequently have days of very low FFDI. Outliers are values > 1.5× the interquartile range and are represented as a dash(-): *light grey* for historical; *dark grey* for other time periods. If the boxplot shifts higher (lower) this indicates a change towards more (less) dangerous conditions.

# FURNEAUX ISLANDS

## Bushfires — Timeseries

Figure 5: Projected number of days per year of bushfire danger ratings


Figure 6: Projected ratio of bushfire danger ratings

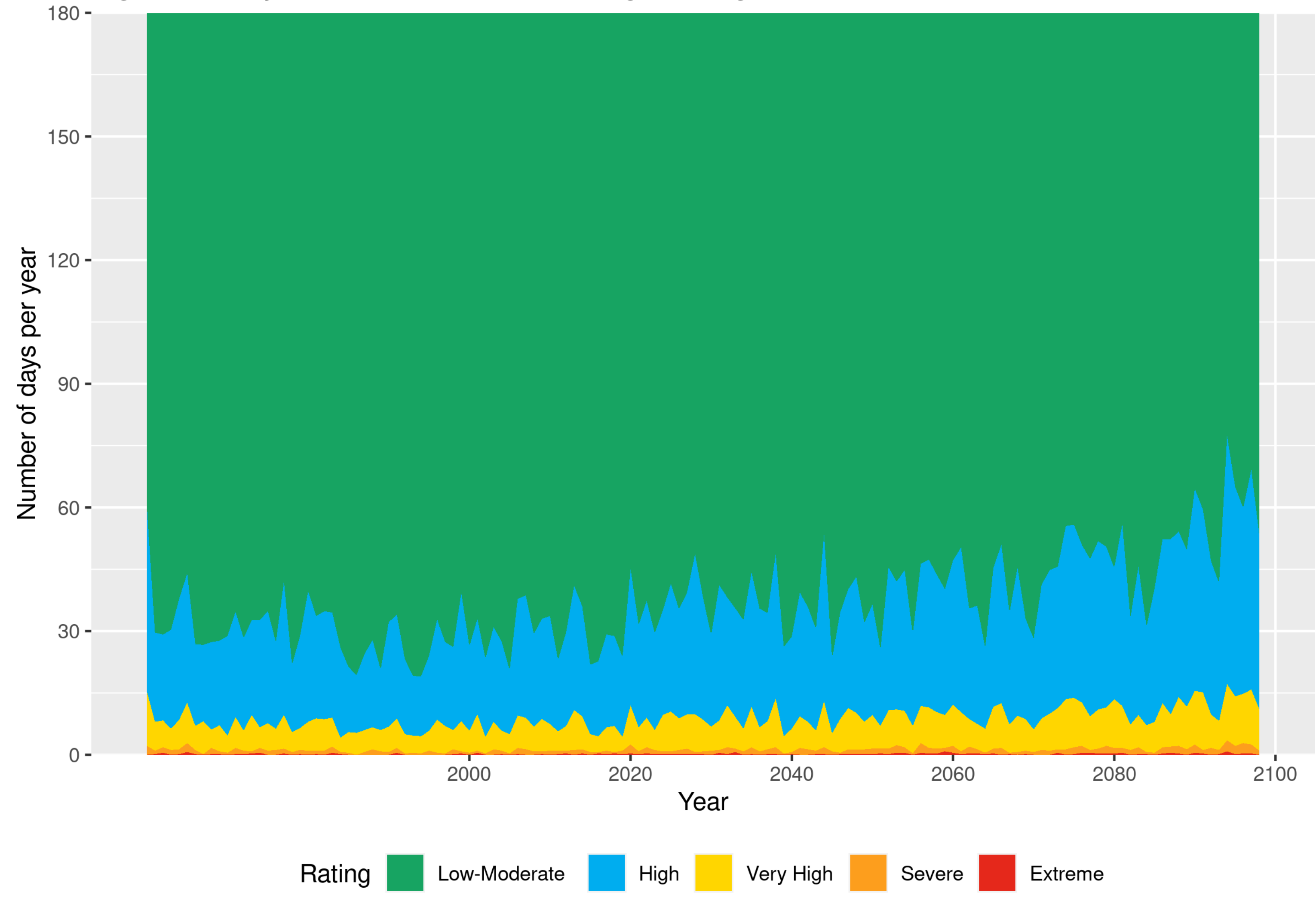


Figure 7: Projected returns curves for daily maximum FFDI

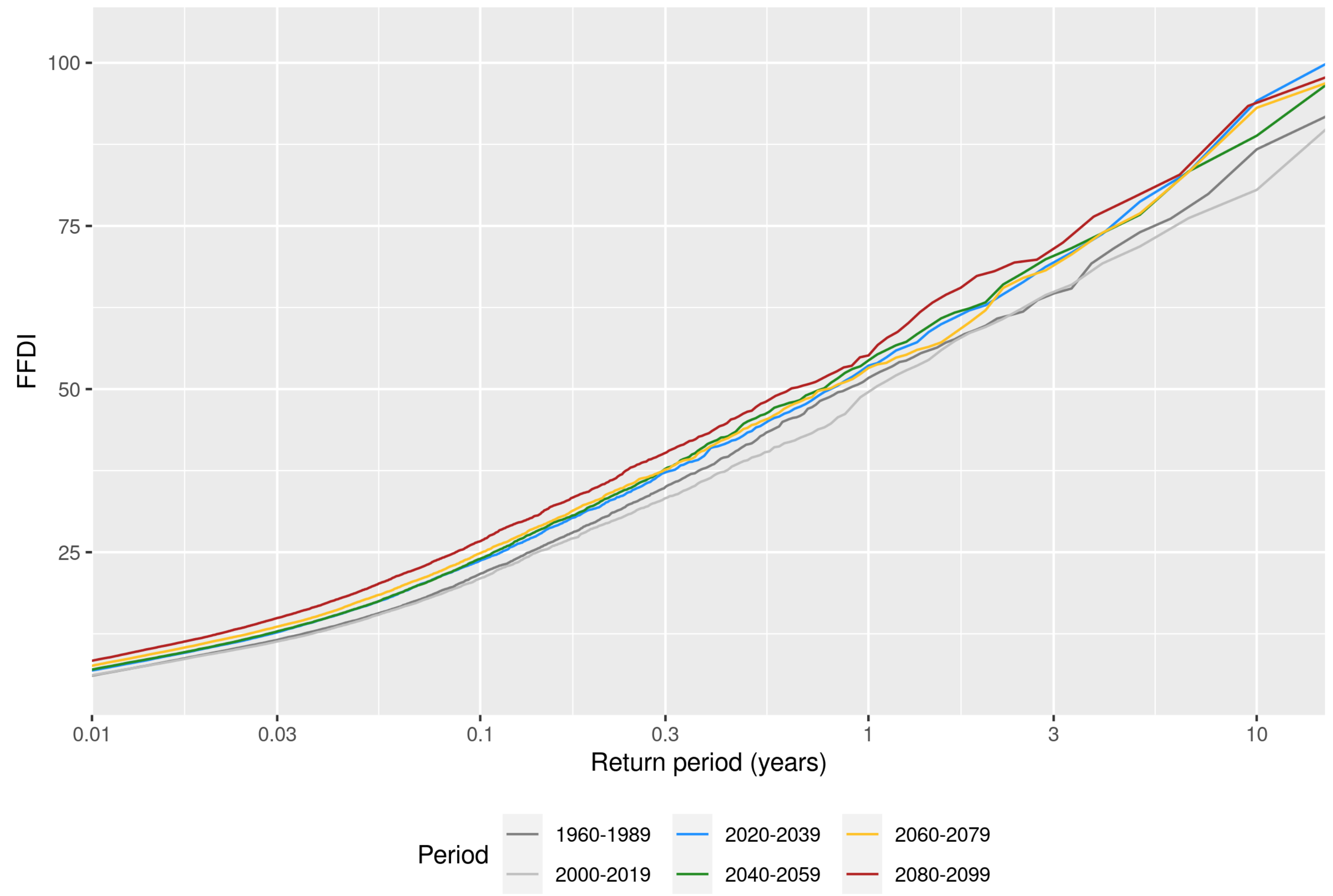


Figure 8: Driving variables of FFDI

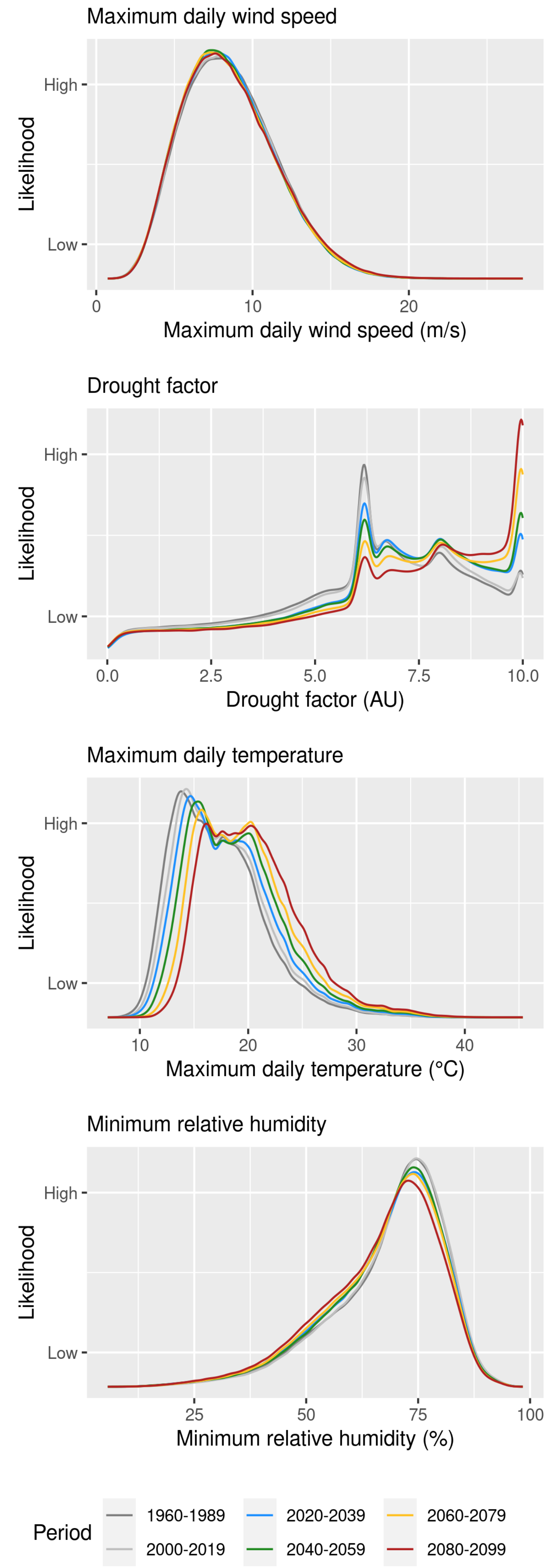


Figure 5: Time series of the ensemble-mean for the 30-year rolling mean of the number of days per year with fire danger ratings of *Low-Moderate*, *High*, *Very High*, *Severe*, *Extreme* from 1990 to 2100 (NB: *Catastrophic* had frequencies too low to reasonably present here). As every day has a fire danger rating, *Low-Moderate* rating frequencies decrease as they are replaced by higher categories.

Figure 6: Stacked area plot of the 30-year ensemble mean number of days of each forest fire danger index rating across each fire-season (October to April, 180 days) from 1990 to 2100. Decreased frequency of *Low-Moderate* days is due to increases in *High* or *Very High* categories.

Figure 7: Annual return periods for Forest Fire Danger Index values for the 30-year baseline period (1961-1990) and 20-year time periods from 2001 to 2100.

Figure 8: Distribution of values for each of the underlying drivers of Forest Fire Danger Index for each time period. a) Maximum daily wind speed (m/s); b) Drought Factor (AU); c) Maximum daily temperature; d) Daily minimum relative humidity (%). As wind speed is not projected to change significantly, the key drivers of change are temperature, humidity and drought factor. Drought factor has strong correlations with temperature change.

Figure 1: Projected 90th, 95th and 99th percentile of daily max FFDI

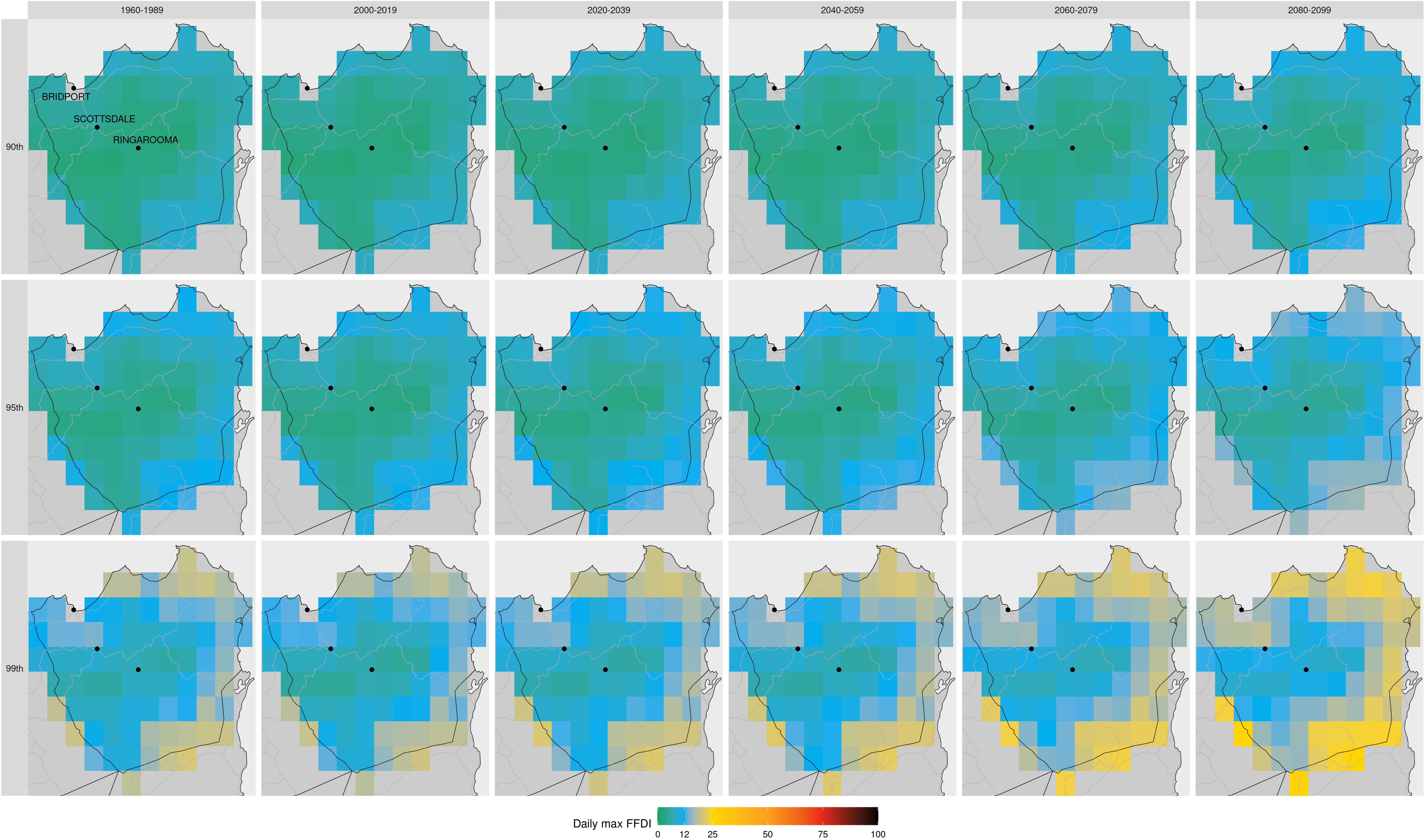


Figure 1: Projected 90th, 95th and 99th percentile values of *Forest Fire Danger Index* for the 30-year baseline period, and then 20-year time periods from 2001 to 2100. Each grid cell is the mean of the 6 ensemble members. The 99th percentile value reflects the 4th highest FFDI value year; the 95th percentile is the 18th highest FFDI value year; and the 90th percentile is the 36th highest FFDI value year. Extreme values of FFDI are expected to increase steadily into the future.

Figure 2: Projected change in 90th, 95th and 99th percentile of daily max FFDI

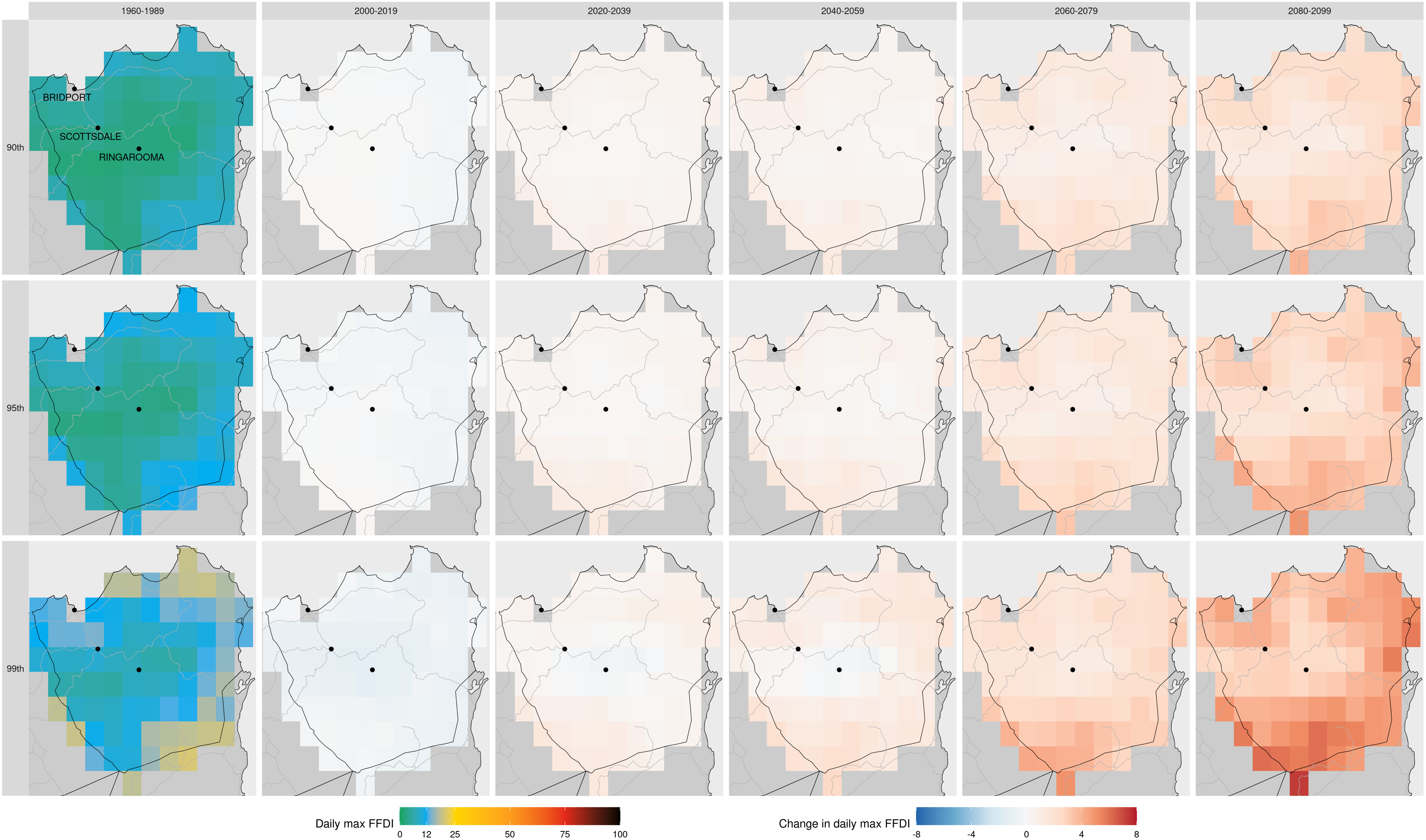


Figure 2: Projected change in the 90th, 95th and 99th percentile values of *Forest Fire Danger Index* for 20-year time periods from 2001 to 2100 compared to the 30-year baseline period 1961–1990. Each grid cell is the mean of the 6 ensemble members. The 99th percentile value reflects the 4th highest FFDI value year; the 95th percentile is the 18th highest FFDI value year; and the 90th percentile is the 36th highest FFDI value year. Extreme values of FFDI are expected to increase steadily into the future

Figure 3: Projected monthly FFDI with outliers removed

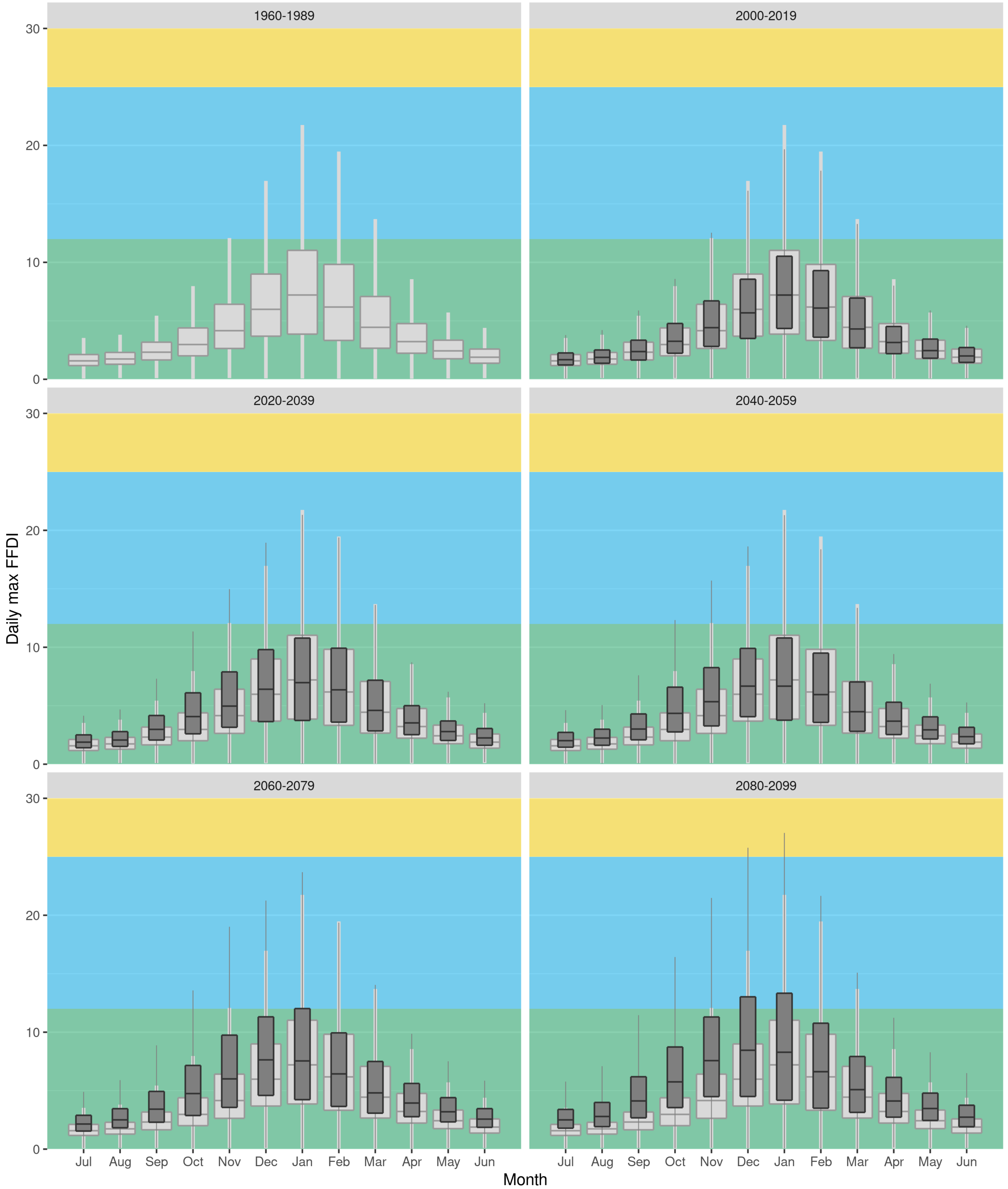


Figure 4: Projected monthly FFDI with outliers shown

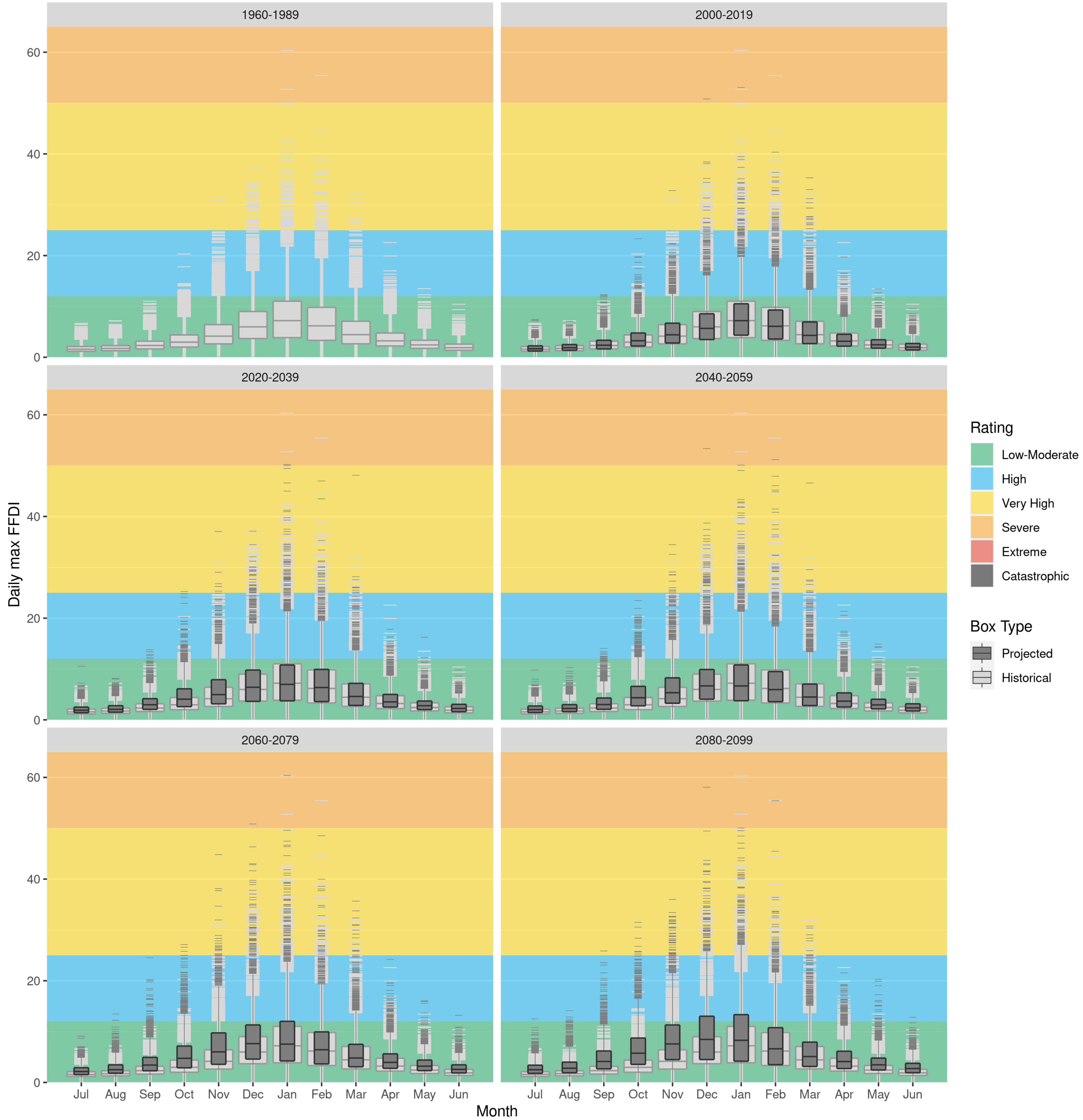


Figure 3: Boxplots of daily *Forest Fire Danger Index* for each month for the 30-year baseline period, and then 20-year periods from 2001 to 2100. Each boxplot represents a summary of daily data for each grid cell, for each of the 6 ensemble members within the time period; e.g. the top-left panel, the January boxplot represents the daily FFDI values for all January days in the period 1961–1990, for all grids cell in the region, for each of the 6 ensemble members. The baseline period (1961-1990) has been shadowed (*light grey*) underneath future time periods to highlight any differences expected into the future. Solid bars represent the median value. The box represents the 25th and 75th percentiles. The Whiskers represent the 1.5× the inter-quartile range. All months in all periods frequently have days of very low FFDI. Outliers have been excluded. If the boxplot shifts higher (lower) this indicates a change towards more (less) dangerous conditions.

Figure 4: Boxplots of daily *Forest Fire Danger Index* for each month for the 30-year baseline period, and then 20-year periods from 2001 to 2100. Each boxplot represents daily data for each grid cell, for each of the 6 ensemble members within the time period; e.g. ing the top-left panel, the January boxplot represents the daily FFDI values for all January days in the period 1961–1990, for all grids cell in the region, for each of the 6 ensemble members. The baseline period (1961-1990) has been shadowed (*light grey*) underneath future time periods to highlight any differences expected into the future. Solid bars represent the median value. The box represents the 25th and 75th percentiles. The Whiskers represent the 1.5× the inter-quartile range. All months in all periods frequently have days of very low FFDI. Outliers are values > 1.5× the interquartile range and are represented as a dash(-): *light grey* for historical; *dark grey* for other time periods. If the boxplot shifts higher (lower) this indicates a change towards more (less) dangerous conditions.

Figure 5: Projected number of days per year of bushfire danger ratings

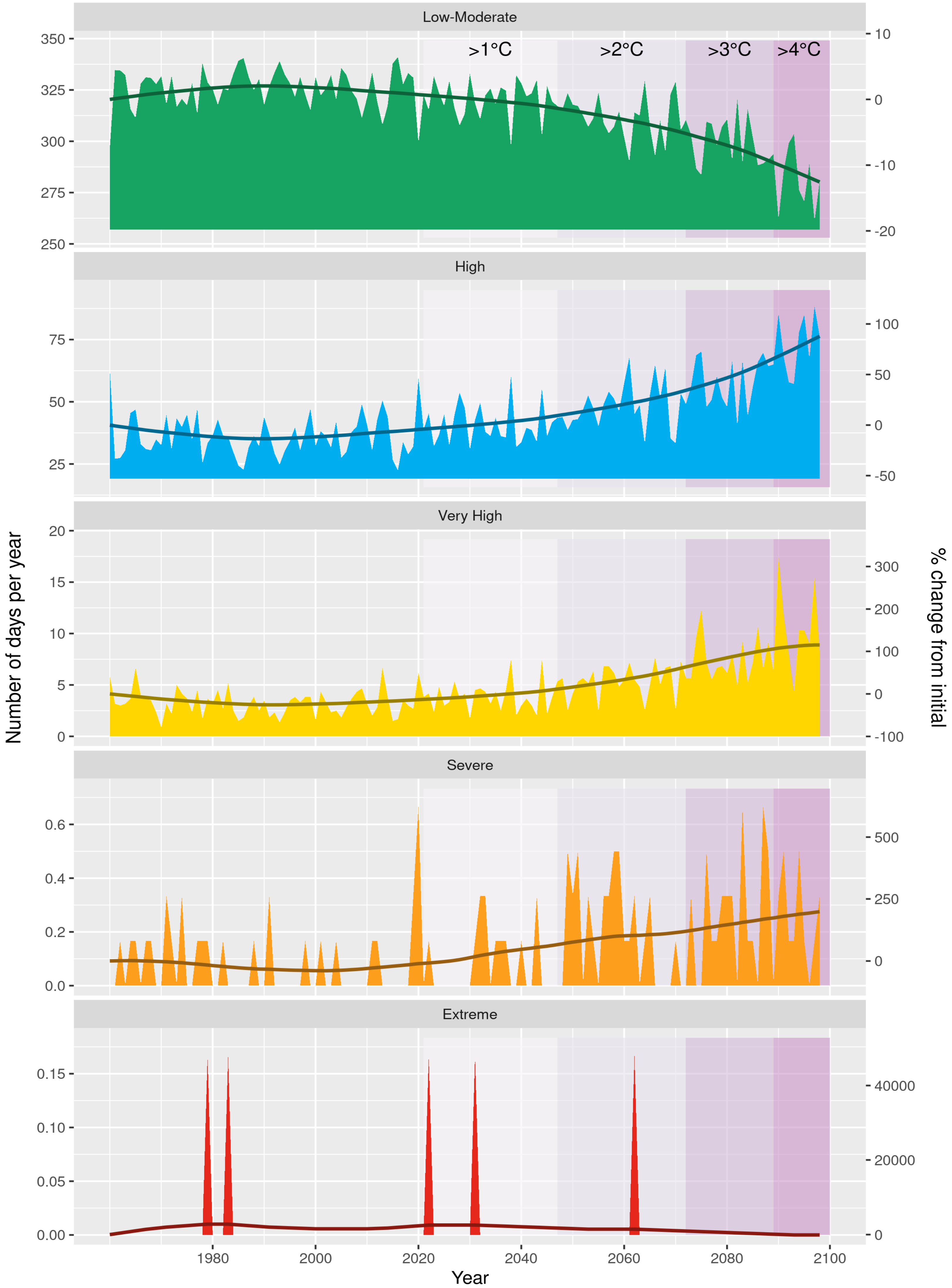


Figure 6: Projected ratio of bushfire danger ratings

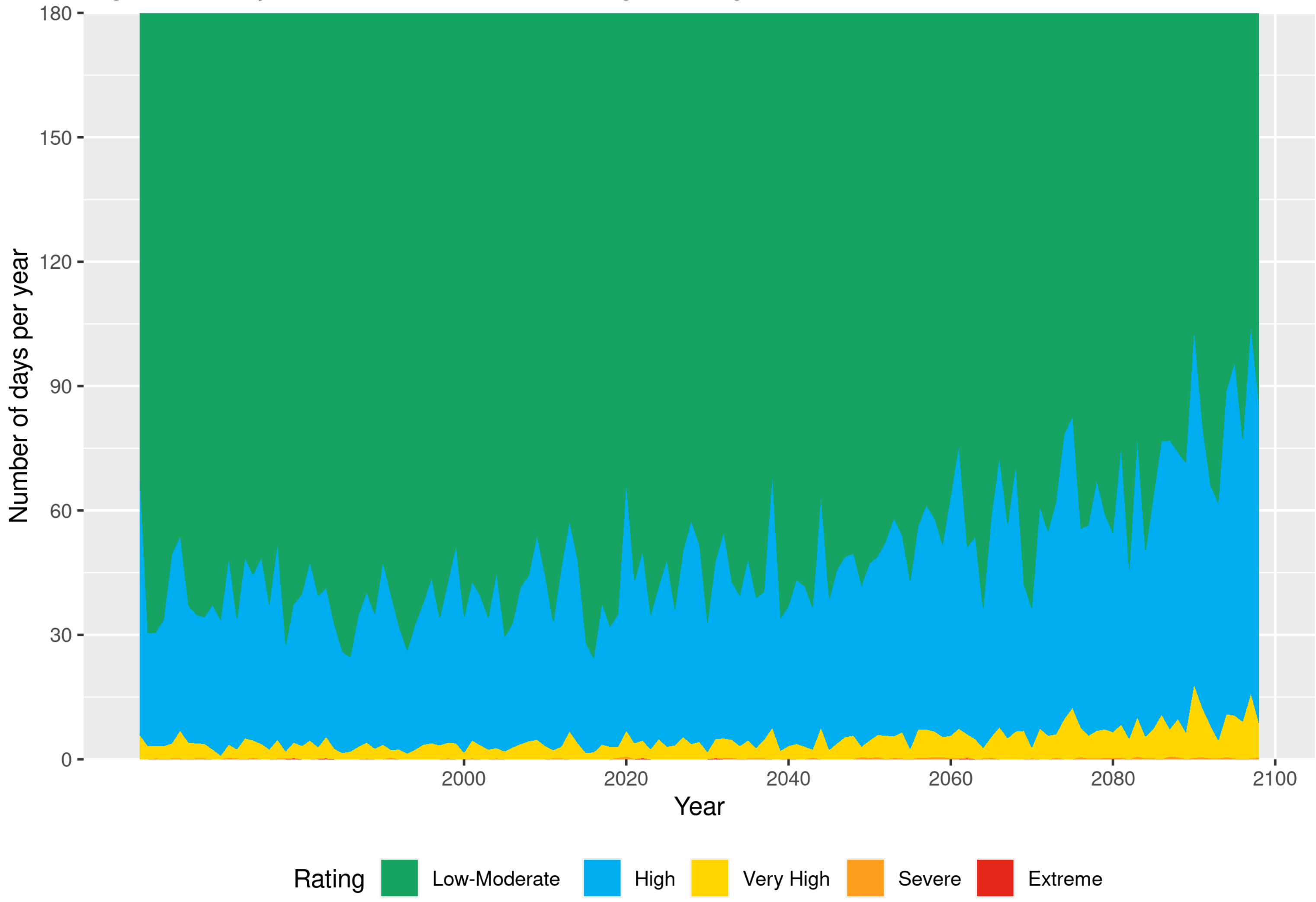


Figure 7: Projected returns curves for daily maximum FFDI

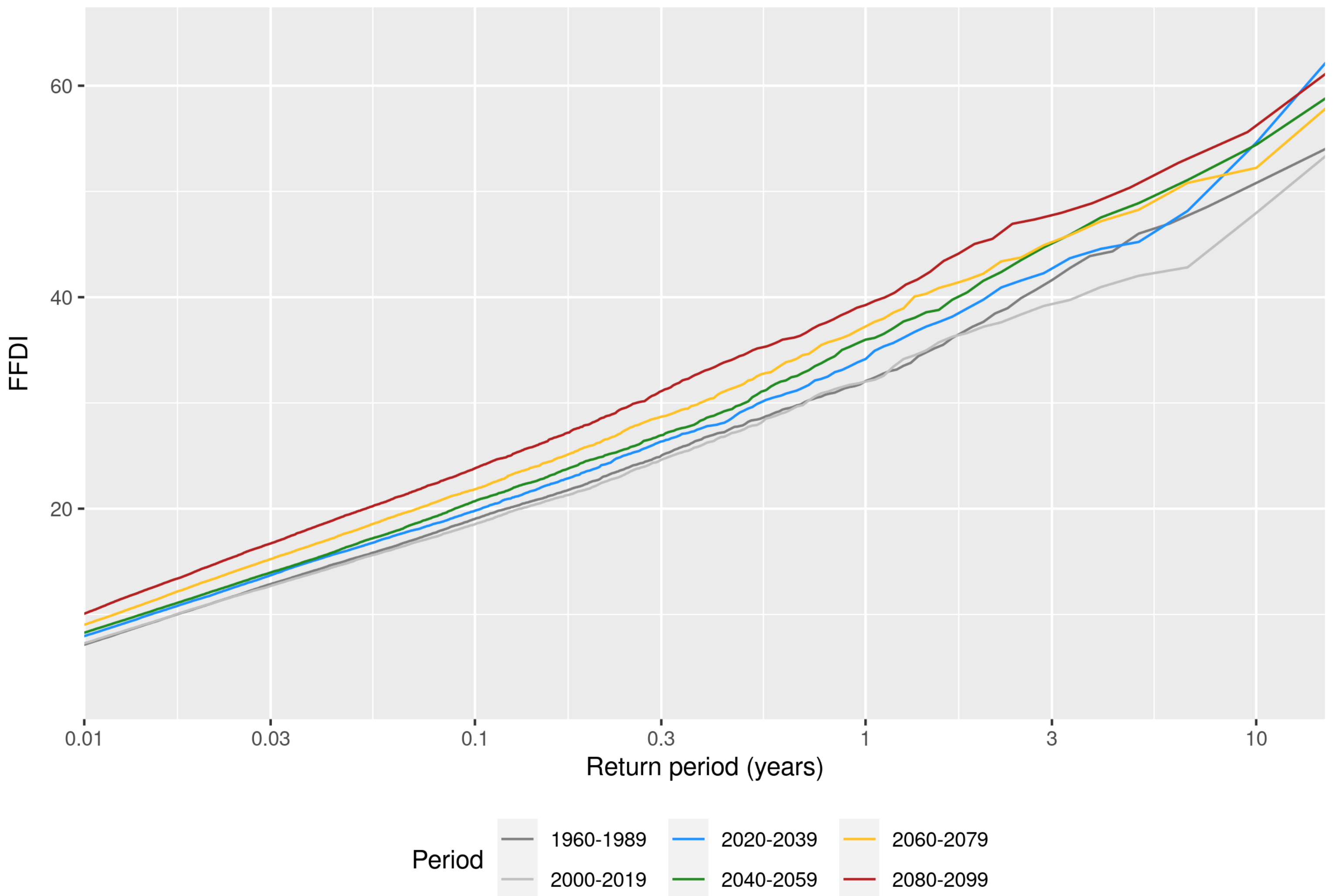


Figure 8: Driving variables of FFDI

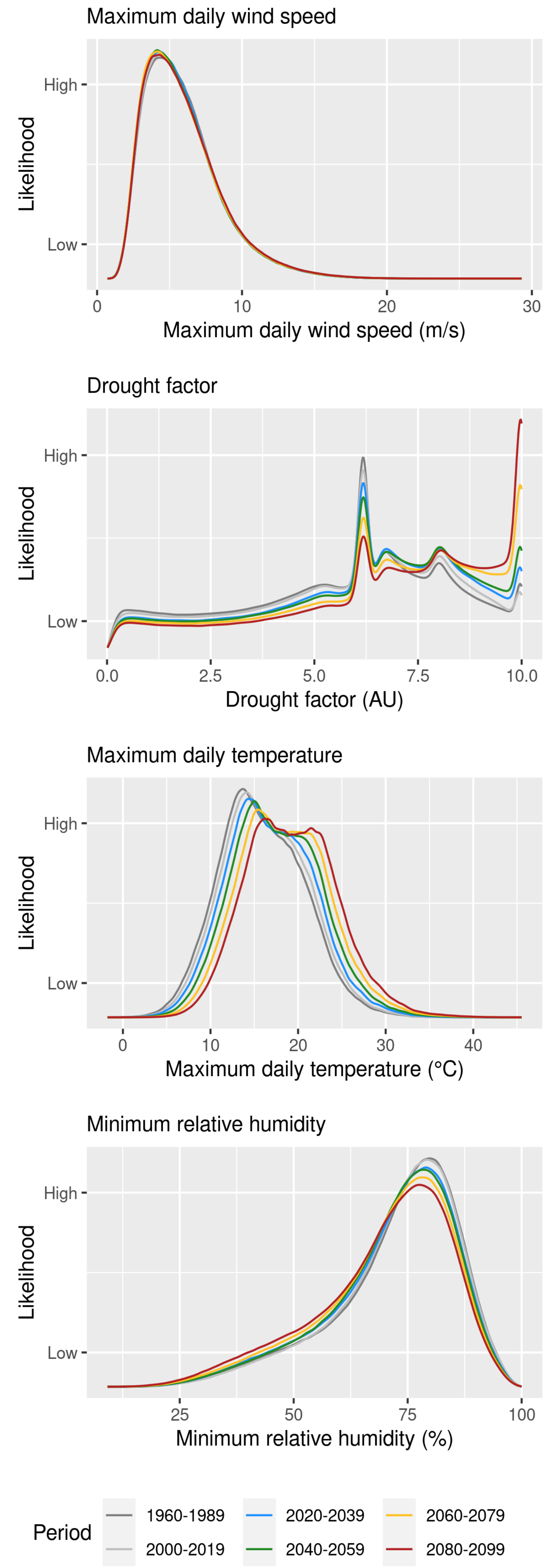


Figure 5: Time series of the ensemble-mean for the 30-year rolling mean of the number of days per year with fire danger ratings of *Low-Moderate*, *High*, *Very High*, *Severe*, *Extreme* from 1990 to 2100 (NB: *Catastrophic* had frequencies too low to reasonably present here). As every day has a fire danger rating, *Low-Moderate* rating frequencies decrease as they are replaced by higher categories.

Figure 6: Stacked area plot of the 30-year ensemble mean number of days of each forest fire danger index rating across each fire-season (October to April, 180 days) from 1990 to 2100. Decreased frequency of *Low-Moderate* days is due to increases in *High* or *Very High* categories.

Figure 7: Annual return periods for Forest Fire Danger Index values for the 30-year baseline period (1961-1990) and 20-year time periods from 2001 to 2100.

Figure 8: Distribution of values for each of the underlying drivers of Forest Fire Danger Index for each time period. a) Maximum daily wind speed (m/s); b) Drought Factor (AU); c) Maximum daily temperature; d) Daily minimum relative humidity (%). As wind speed is not projected to change significantly, the key drivers of change are temperature, humidity and drought factor. Drought factor has strong correlations with temperature change.

Figure 1: Projected 90th, 95th and 99th percentile of daily max FFDI

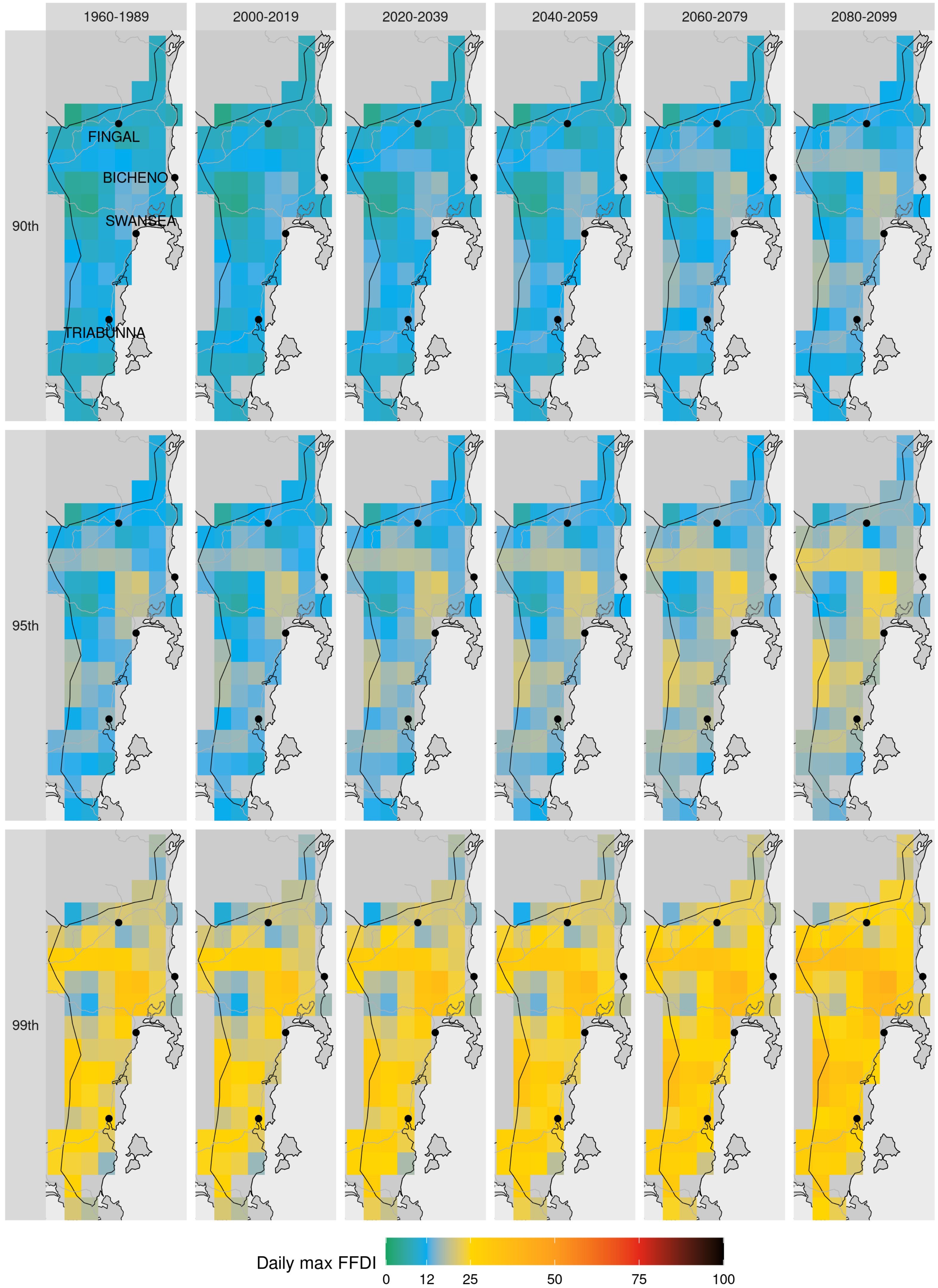


Figure 1: Projected 90th, 95th and 99th percentile values of *Forest Fire Danger Index* for the 30-year baseline period, and then 20-year time periods from 2001 to 2100. Each grid cell is the mean of the 6 ensemble members. The 99th percentile value reflects the 4th highest FFDI value year; the 95th percentile is the 18th highest FFDI value year; and the 90th percentile is the 36th highest FFDI value year. Extreme values of FFDI are expected to increase steadily into the future.

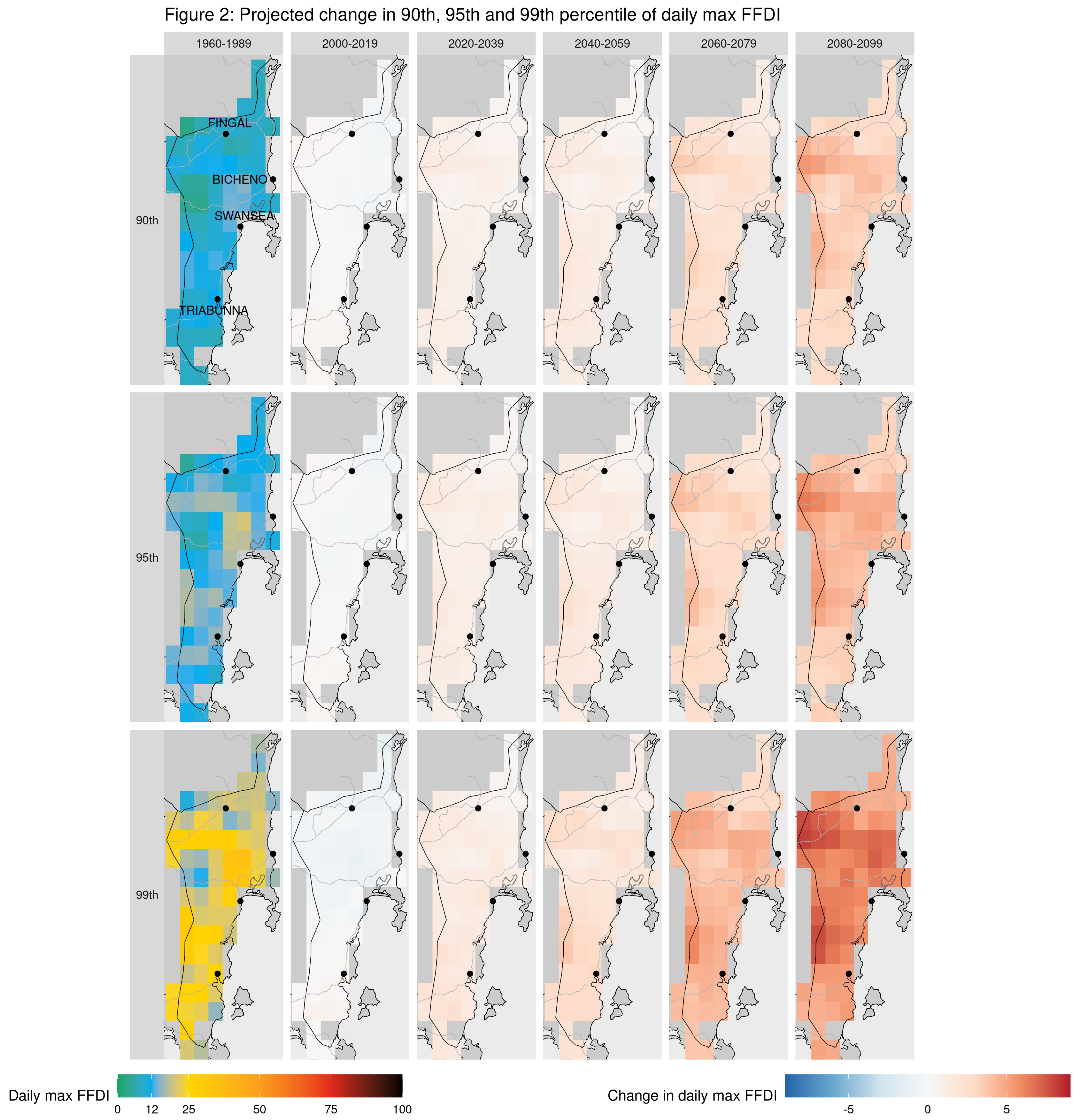


Figure 2: Projected change in the 90th, 95th and 99th percentile values of *Forest Fire Danger Index* for 20-year time periods from 2001 to 2100 compared to the 30-year baseline period 1961–1990. Each grid cell is the mean of the 6 ensemble members. The 99th percentile value reflects the 4th highest FFDI value year; the 95th percentile is the 18th highest FFDI value year; and the 90th percentile is the 36th highest FFDI value year. Extreme values of FFDI are expected to increase steadily into the future

Figure 3: Projected monthly FFDI with outliers removed

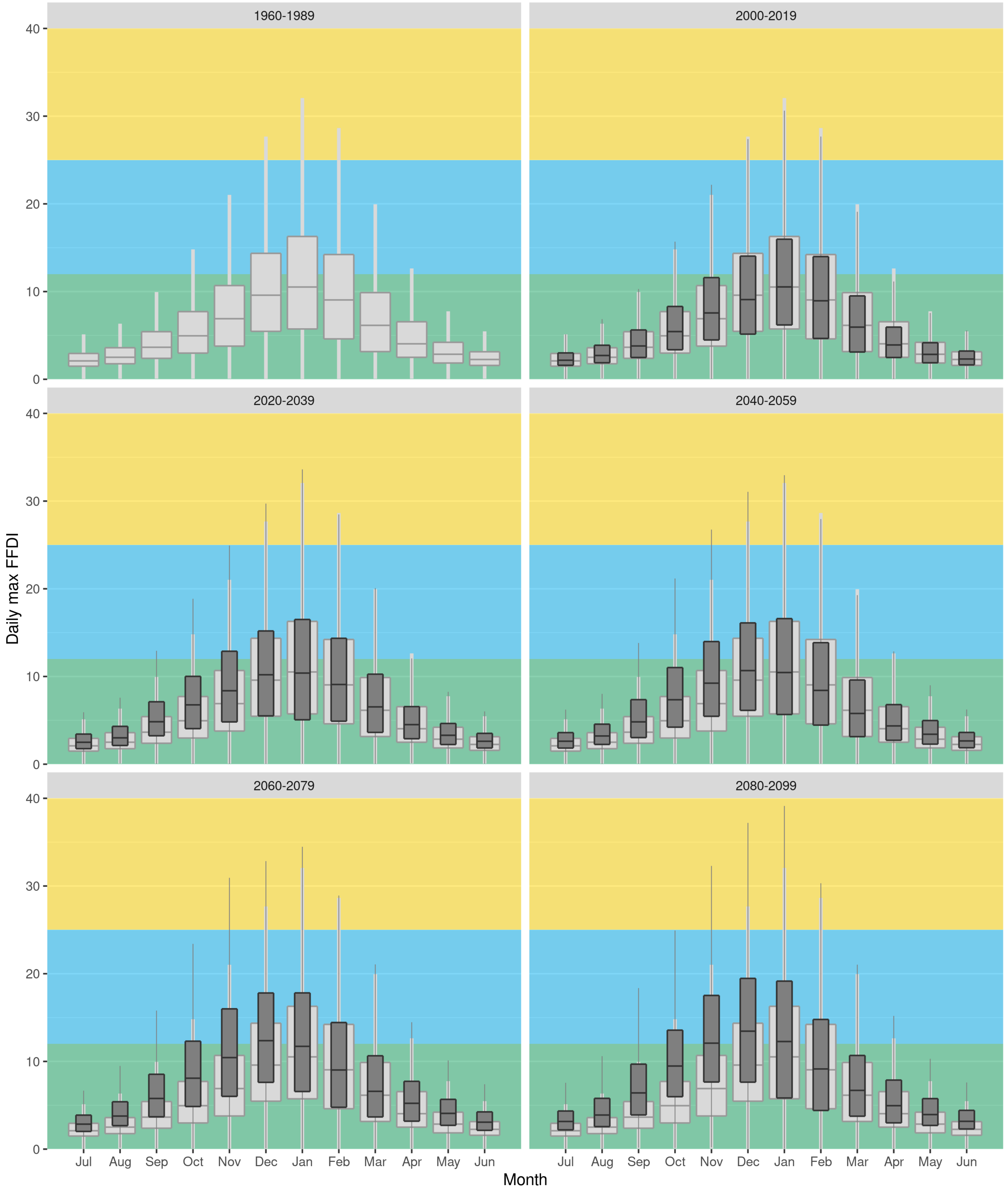


Figure 4: Projected monthly FFDI with outliers shown

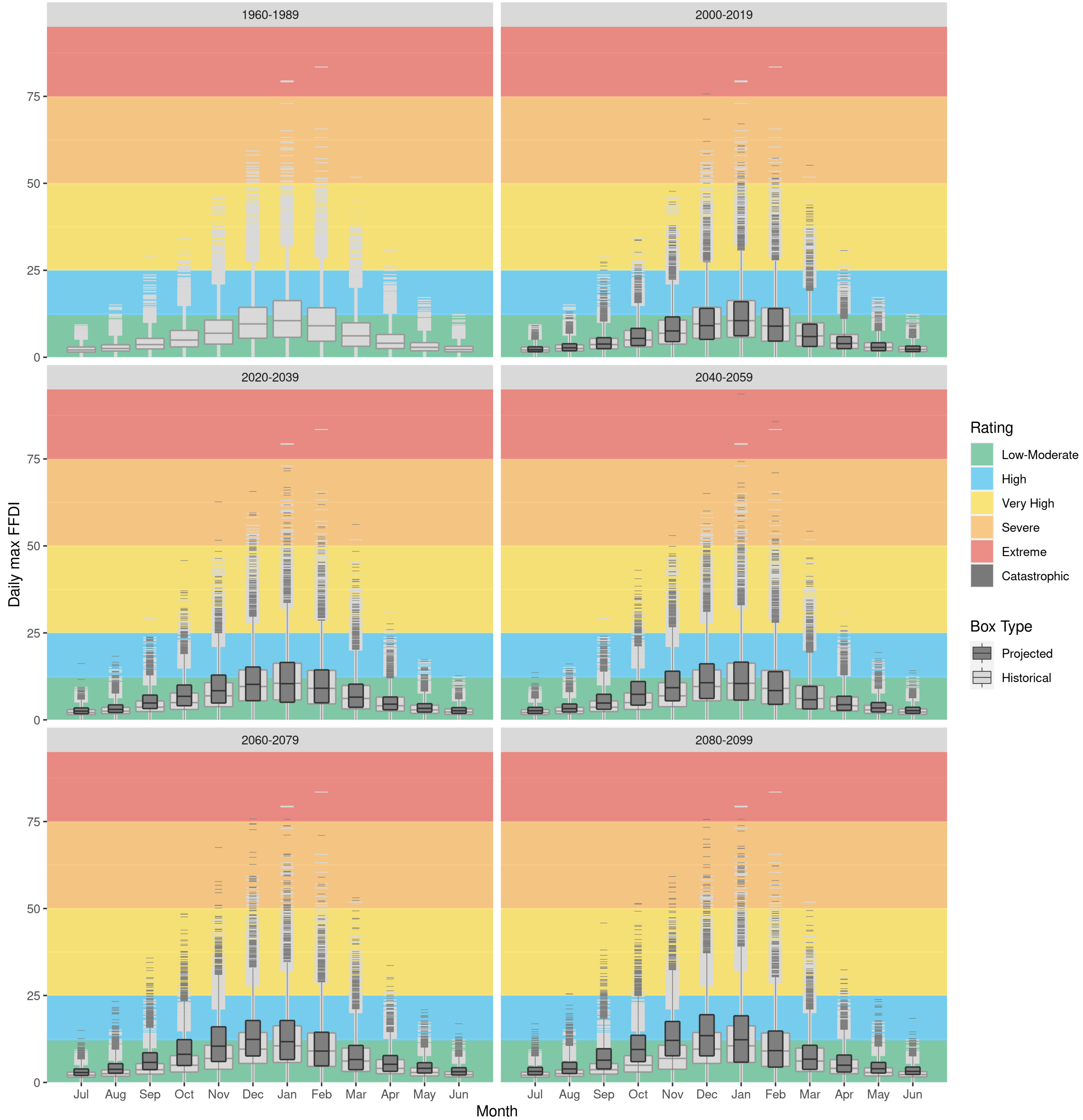


Figure 3: Boxplots of daily *Forest Fire Danger Index* for each month for the 30-year baseline period, and then 20-year periods from 2001 to 2100. Each boxplot represents a summary of daily data for each grid cell, for each of the 6 ensemble members within the time period; e.g. the top-left panel, the January boxplot represents the daily FFDI values for all January days in the period 1961–1990, for all grids cell in the region, for each of the 6 ensemble members. The baseline period (1961-1990) has been shadowed (*light grey*) underneath future time periods to highlight any differences expected into the future. Solid bars represent the median value. The box represents the 25th and 75th percentiles. The Whiskers represent the 1.5× the inter-quartile range. All months in all periods frequently have days of very low FFDI. Outliers have been excluded. If the boxplot shifts higher (lower) this indicates a change towards more (less) dangerous conditions.

Figure 4: Boxplots of daily *Forest Fire Danger Index* for each month for the 30-year baseline period, and then 20-year periods from 2001 to 2100. Each boxplot represents daily data for each grid cell, for each of the 6 ensemble members within the time period; e.g. ing the top-left panel, the January boxplot represents the daily FFDI values for all January days in the period 1961–1990, for all grids cell in the region, for each of the 6 ensemble members. The baseline period (1961-1990) has been shadowed (*light grey*) underneath future time periods to highlight any differences expected into the future. Solid bars represent the median value. The box represents the 25th and 75th percentiles. The Whiskers represent the 1.5× the inter-quartile range. All months in all periods frequently have days of very low FFDI. Outliers are values > 1.5× the interquartile range and are represented as a dash(-): *light grey* for historical; *dark grey* for other time periods. If the boxplot shifts higher (lower) this indicates a change towards more (less) dangerous conditions.

# EAST COAST

## Bushfires — Timeseries

Figure 5: Projected number of days per year of bushfire danger ratings

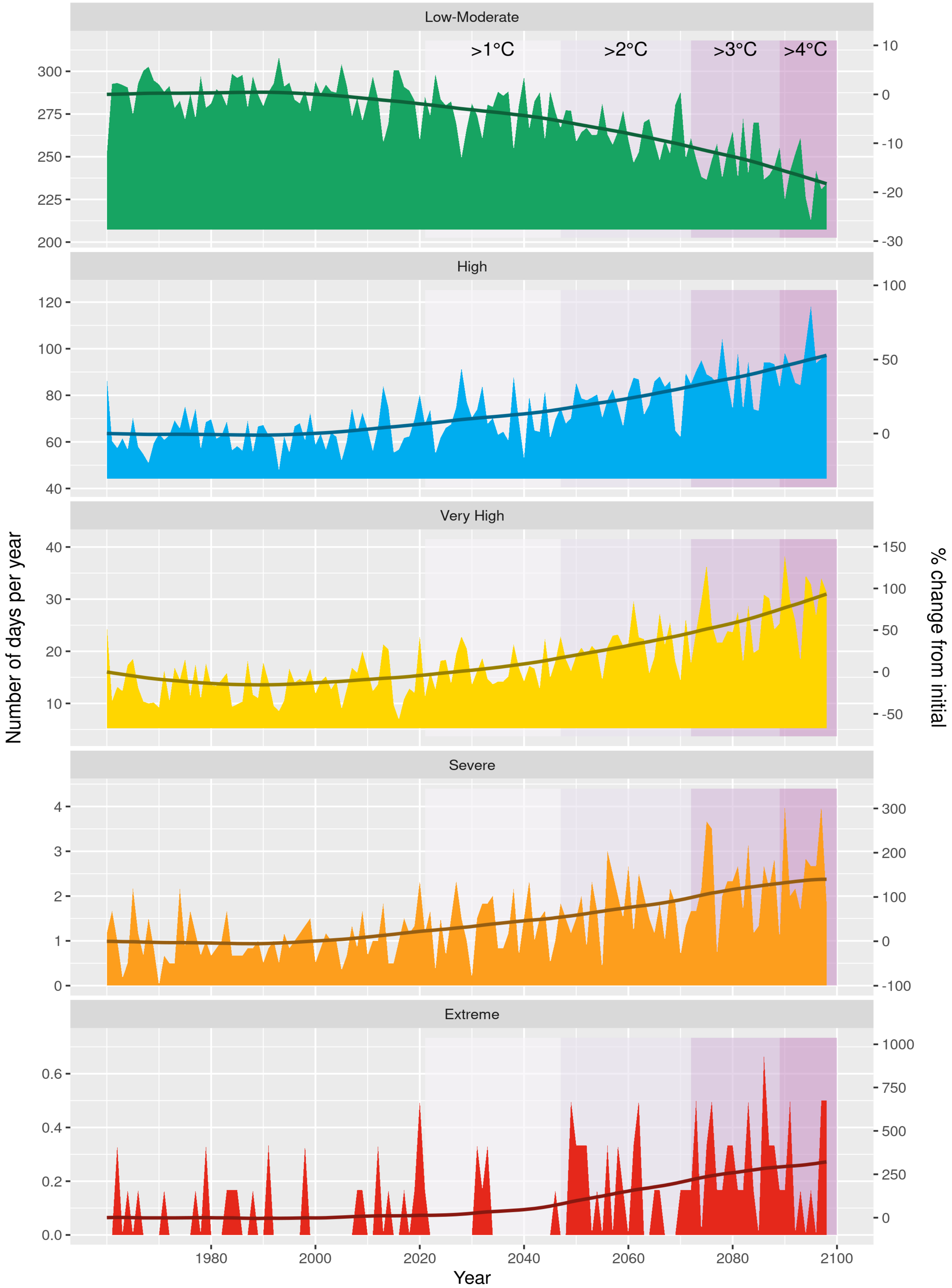


Figure 6: Projected ratio of bushfire danger ratings

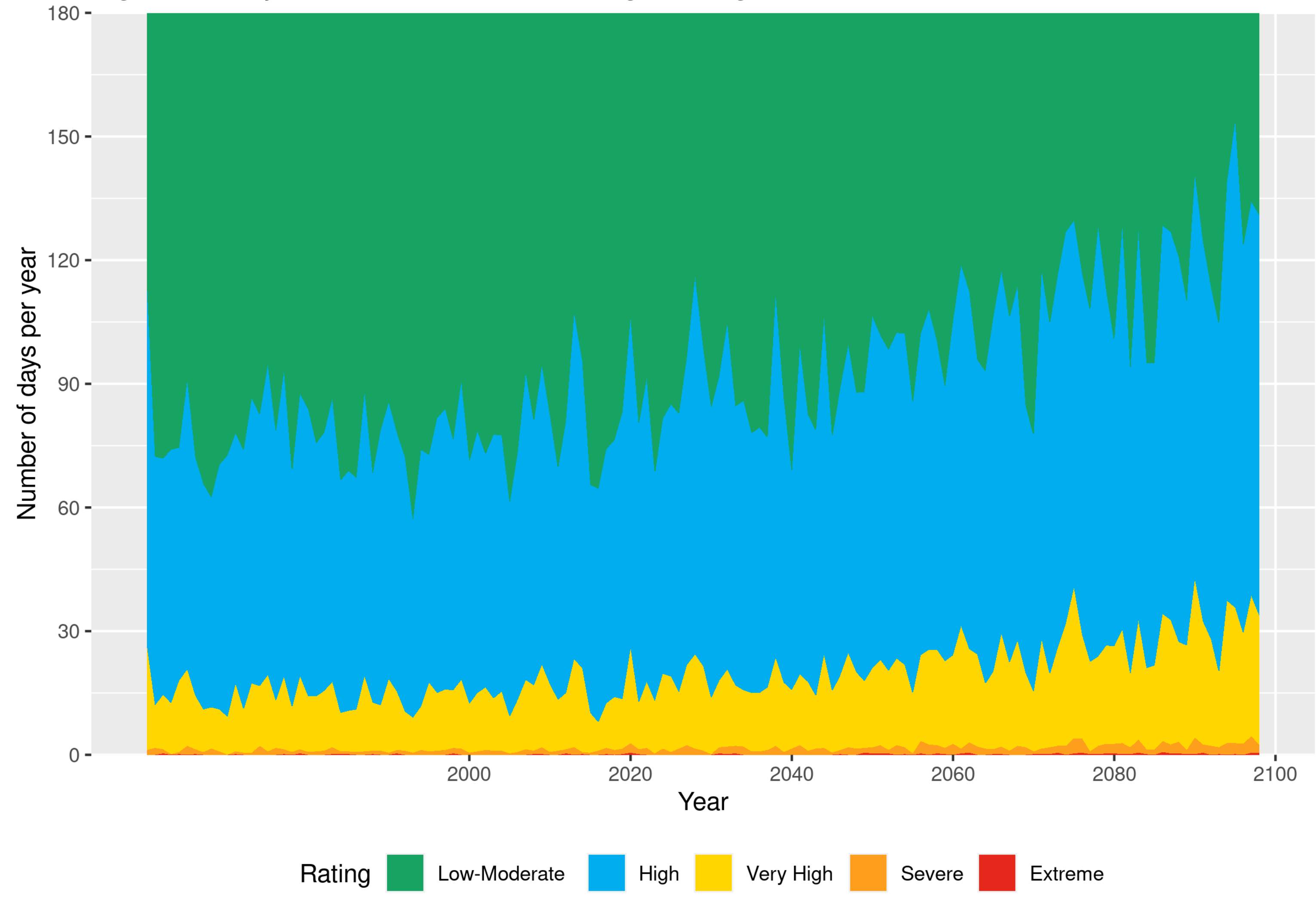


Figure 7: Projected returns curves for daily maximum FFDI

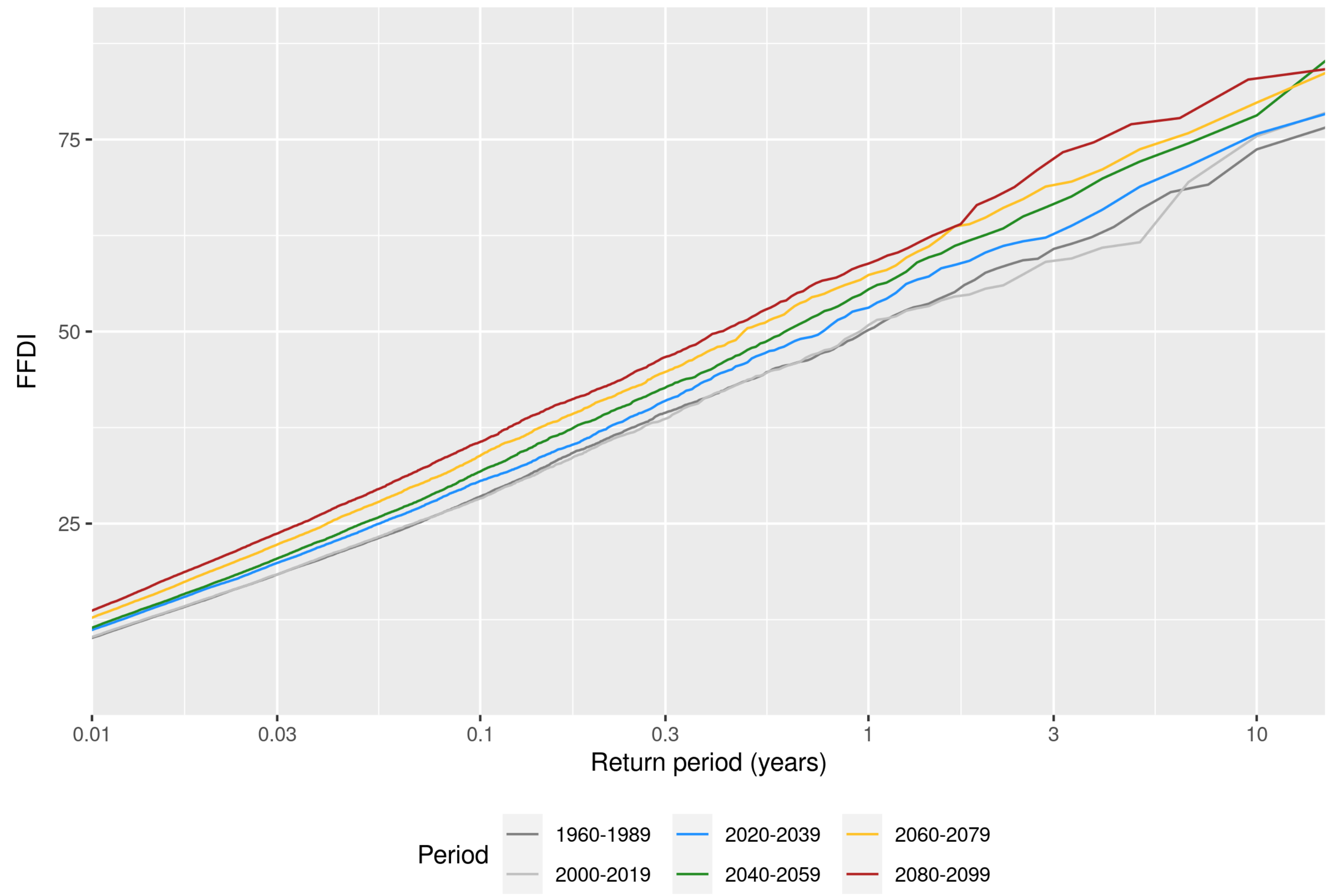


Figure 8: Driving variables of FFDI

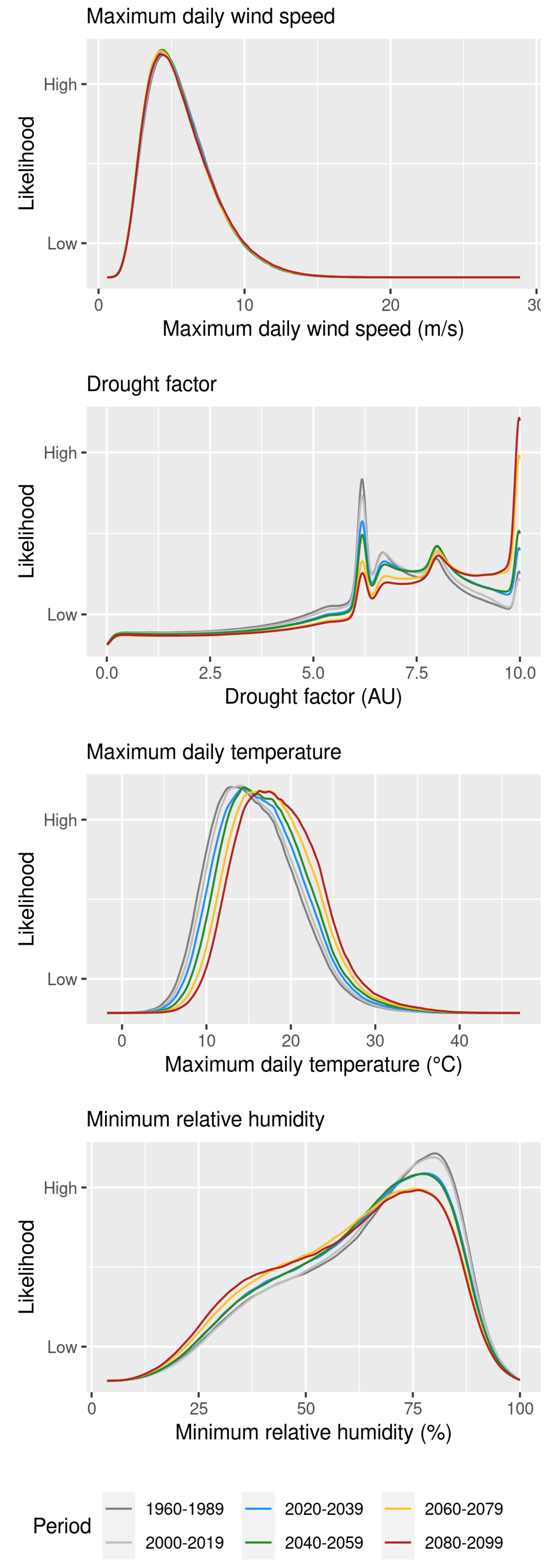


Figure 5: Time series of the ensemble-mean for the 30-year rolling mean of the number of days per year with fire danger ratings of *Low-Moderate*, *High*, *Very High*, *Severe*, *Extreme* from 1990 to 2100 (NB: *Catastrophic* had frequencies too low to reasonably present here). As every day has a fire danger rating, *Low-Moderate* rating frequencies decrease as they are replaced by higher categories.

Figure 6: Stacked area plot of the 30-year ensemble mean number of days of each forest fire danger index rating across each fire-season (October to April, 180 days) from 1990 to 2100. Decreased frequency of *Low-Moderate* days is due to increases in *High* or *Very High* categories.

Figure 7: Annual return periods for Forest Fire Danger Index values for the 30-year baseline period (1961-1990) and 20-year time periods from 2001 to 2100.

Figure 8: Distribution of values for each of the underlying drivers of Forest Fire Danger Index for each time period. a) Maximum daily wind speed (m/s); b) Drought Factor (AU); c) Maximum daily temperature; d) Daily minimum relative humidity (%). As wind speed is not projected to change significantly, the key drivers of change are temperature, humidity and drought factor. Drought factor has strong correlations with temperature change.

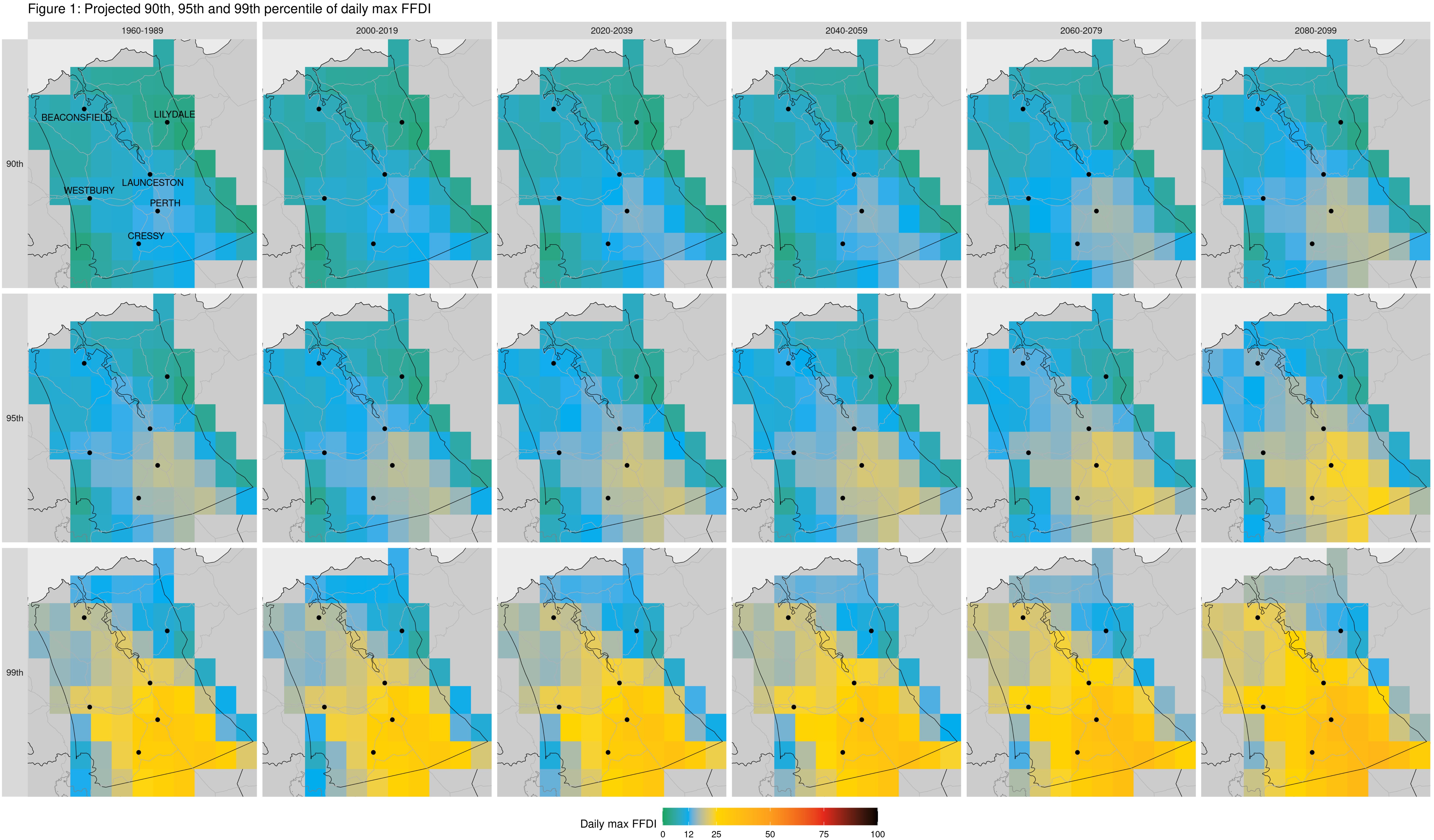


Figure 1: Projected 90th, 95th and 99th percentile values of *Forest Fire Danger Index* for the 30-year baseline period, and then 20-year time periods from 2001 to 2100. Each grid cell is the mean of the 6 ensemble members. The 99th percentile value reflects the 4th highest FFDI value year; the 95th percentile is the 18th highest FFDI value year; and the 90th percentile is the 36th highest FFDI value year. Extreme values of FFDI are expected to increase steadily into the future.

Figure 2: Projected change in 90th, 95th and 99th percentile of daily max FFDI

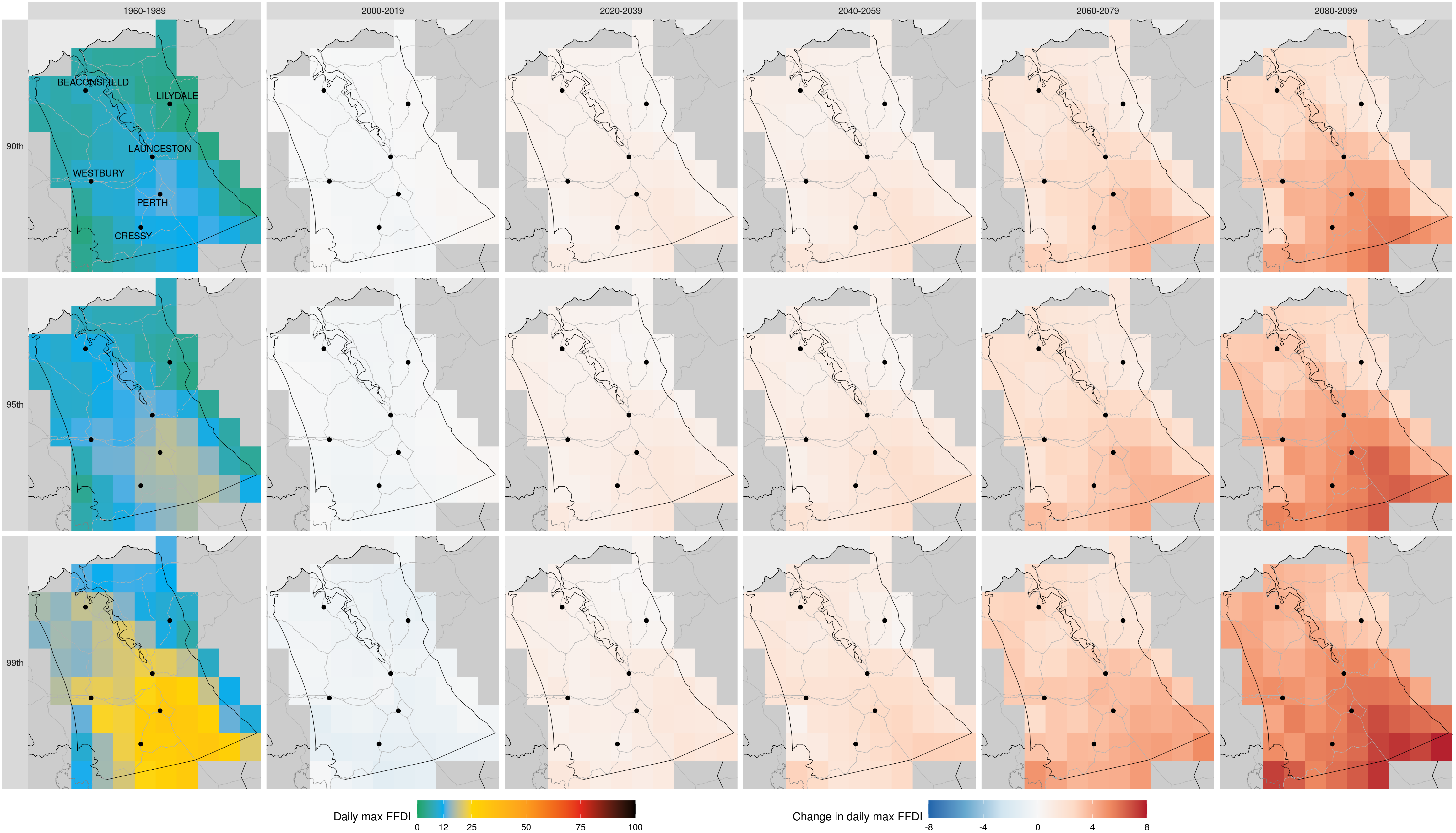


Figure 2: Projected change in the 90th, 95th and 99th percentile values of *Forest Fire Danger Index* for 20-year time periods from 2001 to 2100 compared to the 30-year baseline period 1961–1990. Each grid cell is the mean of the 6 ensemble members. The 99th percentile value reflects the 4th highest FFDI value year; the 95th percentile is the 18th highest FFDI value year; and the 90th percentile is the 36th highest FFDI value year. Extreme values of FFDI are expected to increase steadily into the future

Figure 3: Projected monthly FFDI with outliers removed

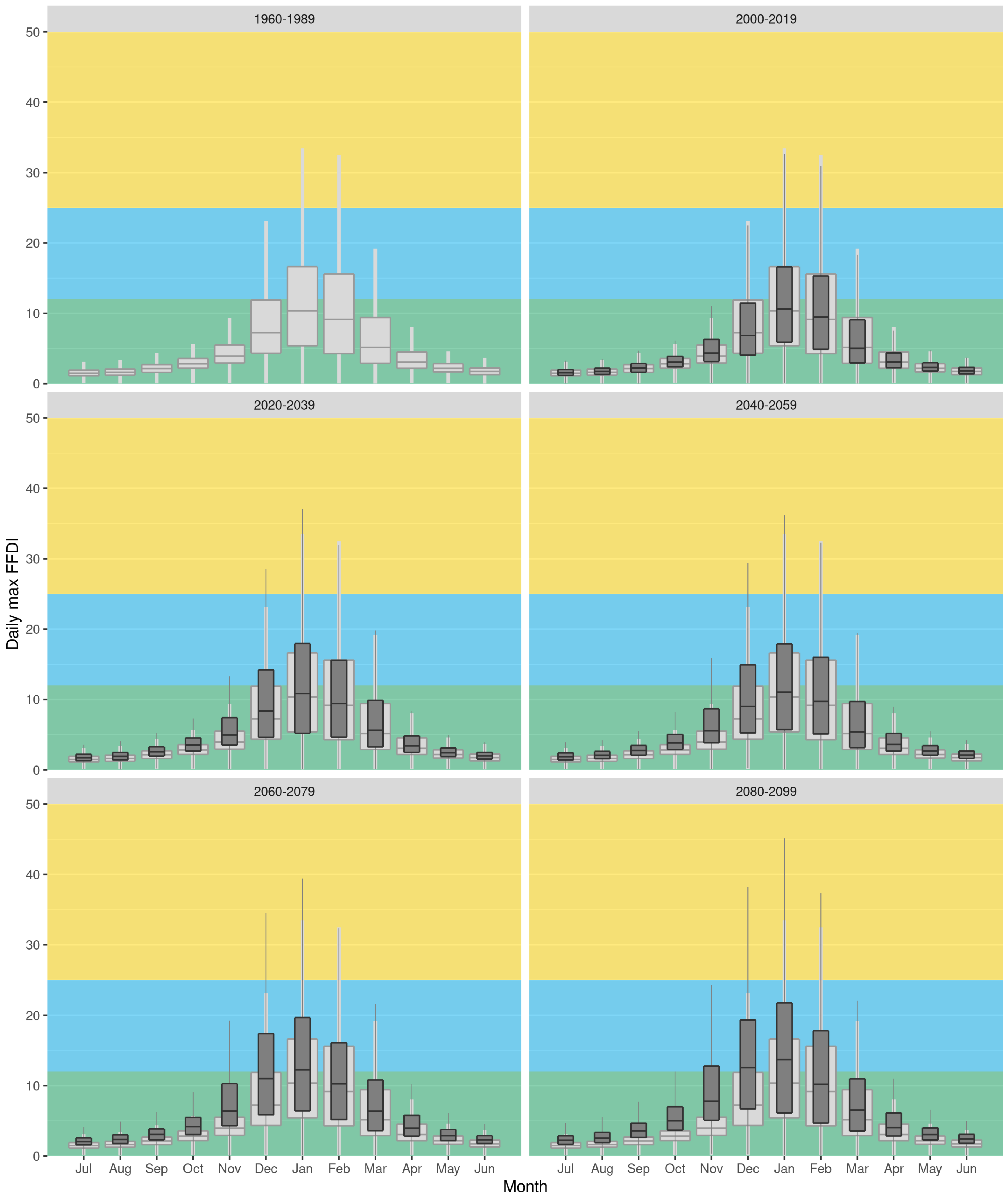


Figure 3: Boxplots of daily *Forest Fire Danger Index* for each month for the 30-year baseline period, and then 20-year periods from 2001 to 2100. Each boxplot represents a summary of daily data for each grid cell, for each of the 6 ensemble members within the time period; e.g. the top-left panel, the January boxplot represents the daily FFDI values for all January days in the period 1961–1990, for all grids cell in the region, for each of the 6 ensemble members. The baseline period (1961-1990) has been shadowed (*light grey*) underneath future time periods to highlight any differences expected into the future. Solid bars represent the median value. The box represents the 25th and 75th percentiles. The Whiskers represent the 1.5× the inter-quartile range. All months in all periods frequently have days of very low FFDI. Outliers have been excluded. If the boxplot shifts higher (lower) this indicates a change towards more (less) dangerous conditions.

Figure 4: Projected monthly FFDI with outliers shown

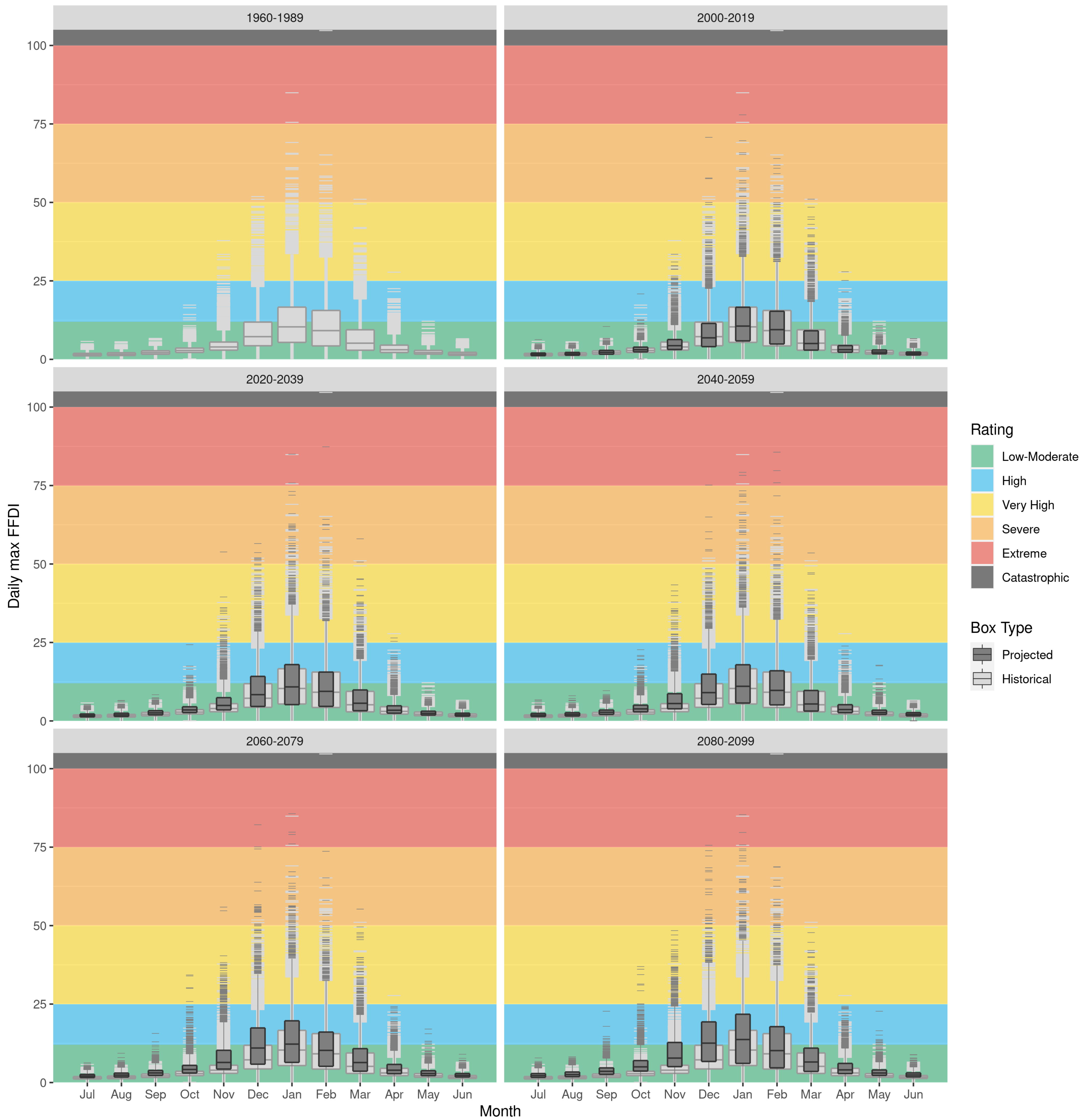


Figure 4: Boxplots of daily *Forest Fire Danger Index* for each month for the 30-year baseline period, and then 20-year periods from 2001 to 2100. Each boxplot represents daily data for each grid cell, for each of the 6 ensemble members within the time period; e.g. ing the top-left panel, the January boxplot represents the daily FFDI values for all January days in the period 1961–1990, for all grids cell in the region, for each of the 6 ensemble members. The baseline period (1961-1990) has been shadowed (*light grey*) underneath future time periods to highlight any differences expected into the future. Solid bars represent the median value. The box represents the 25th and 75th percentiles. The Whiskers represent the 1.5× the inter-quartile range. All months in all periods frequently have days of very low FFDI. Outliers are values > 1.5× the interquartile range and are represented as a dash(-): *light grey* for historical; *dark grey* for other time periods. If the boxplot shifts higher (lower) this indicates a change towards more (less) dangerous conditions.

# CENTRAL NORTH

## Bushfires — Timeseries

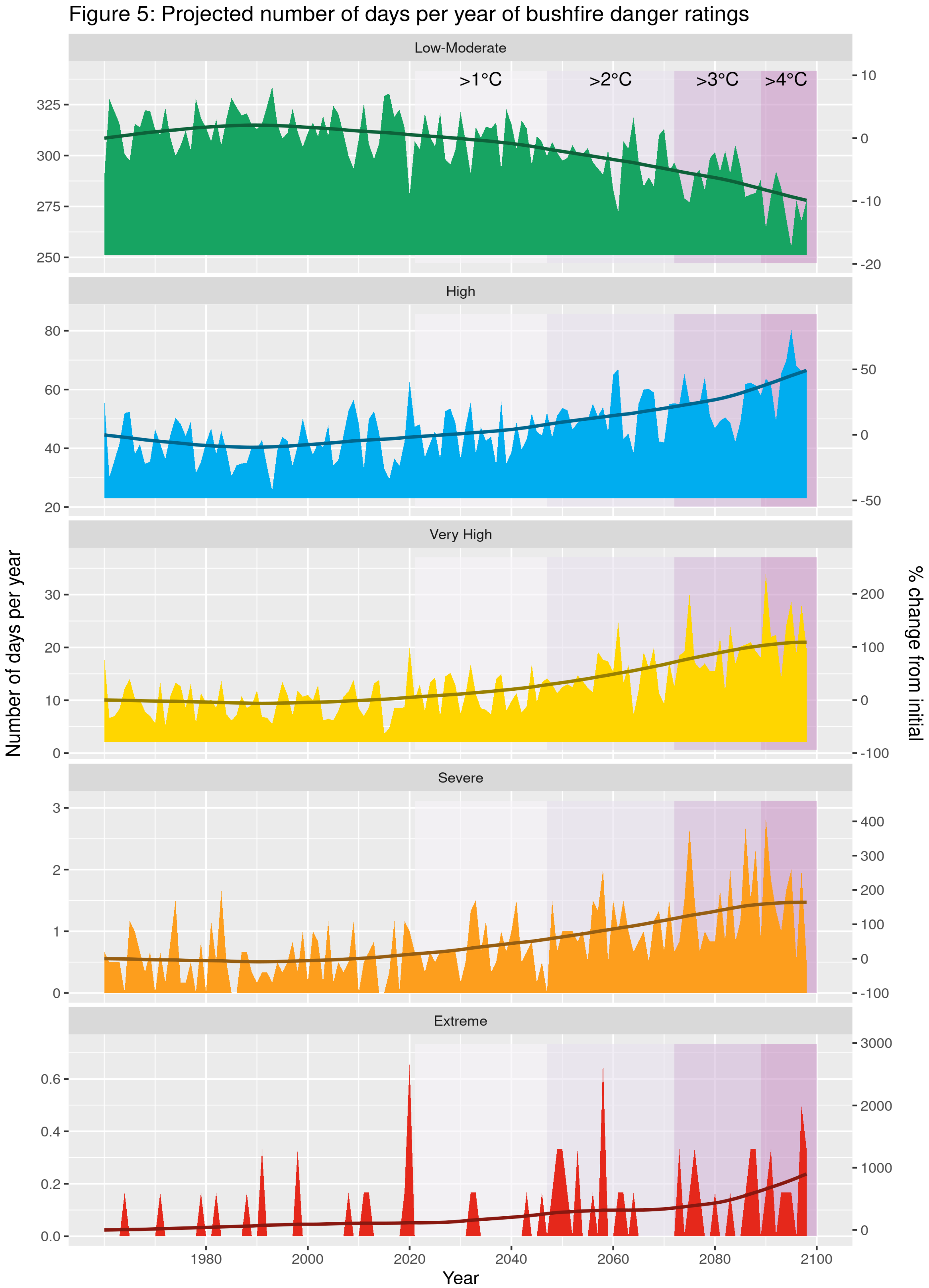


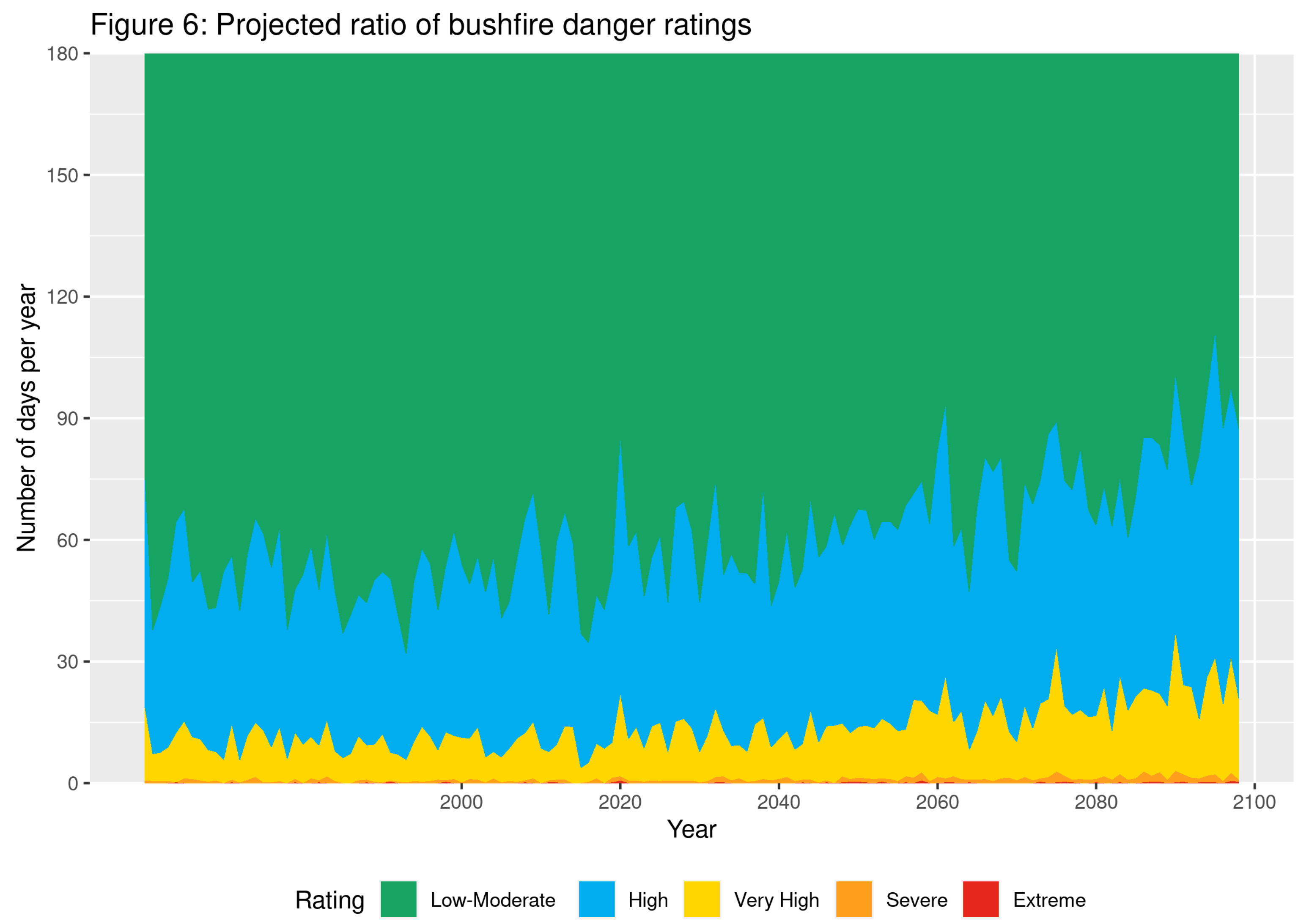


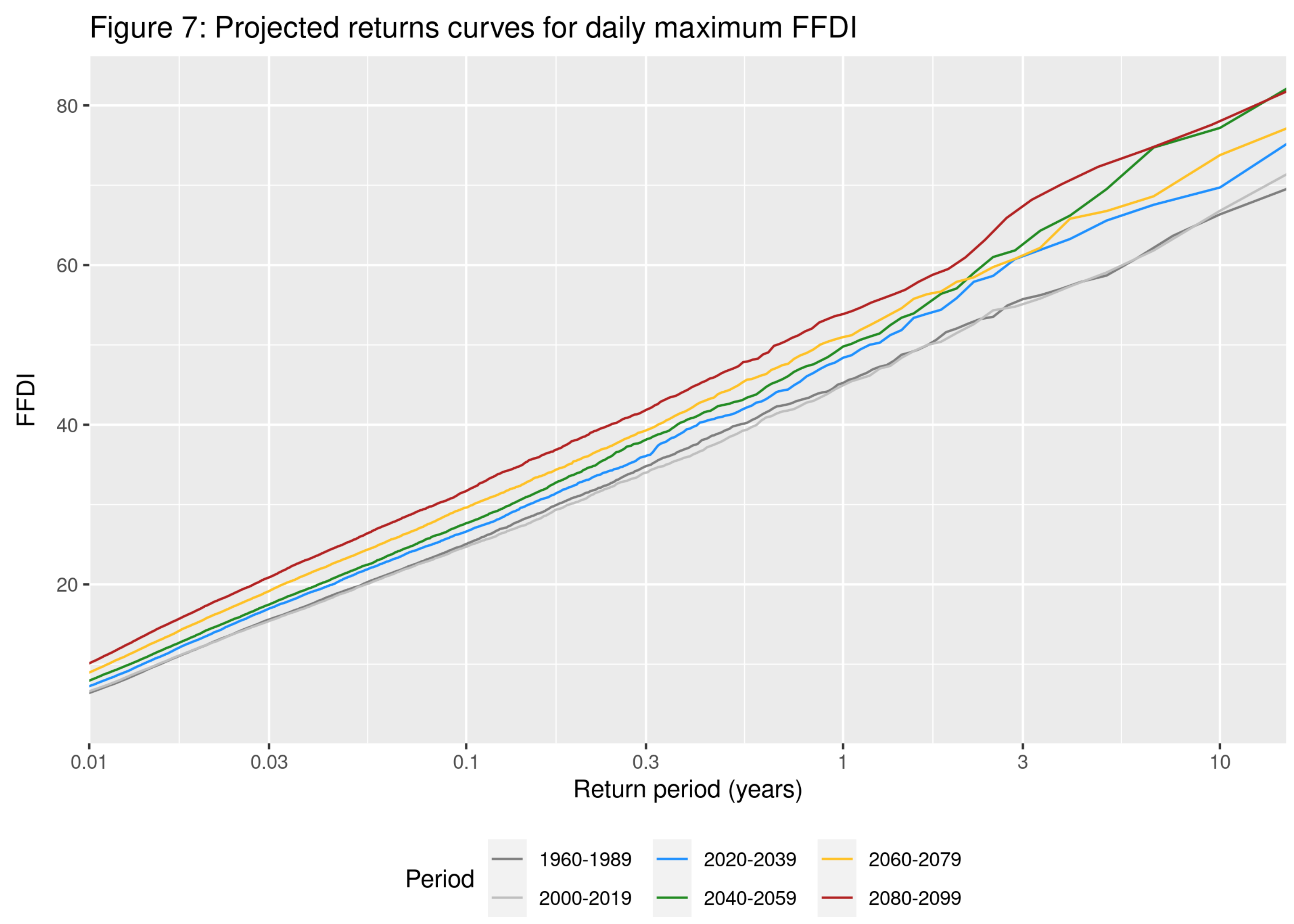


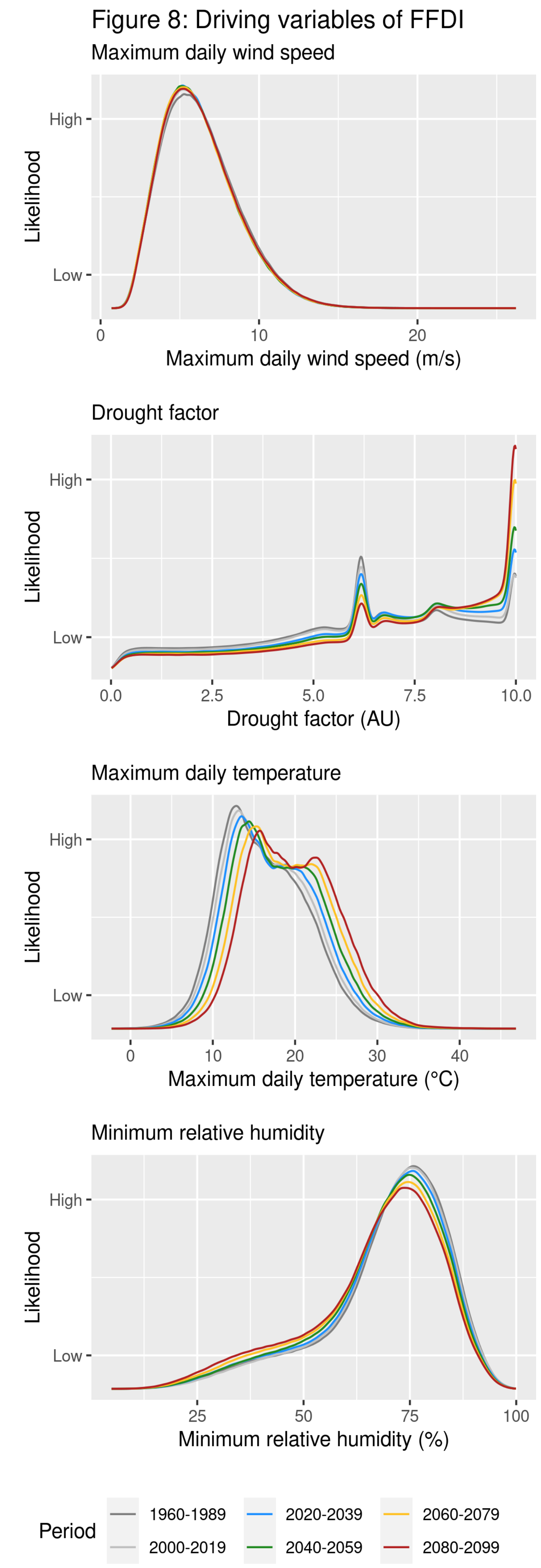


Figure 5: Time series of the ensemble-mean for the 30-year rolling mean of the number of days per year with fire danger ratings of *Low-Moderate*, *High*, *Very High*, *Severe*, *Extreme* from 1990 to 2100 (NB: *Catastrophic* had frequencies too low to reasonably present here). As every day has a fire danger rating, *Low-Moderate* rating frequencies decrease as they are replaced by higher categories.

Figure 6: Stacked area plot of the 30-year ensemble mean number of days of each forest fire danger index rating across each fire-season (October to April, 180 days) from 1990 to 2100. Decreased frequency of *Low-Moderate* days is due to increases in *High* or *Very High* categories.

Figure 7: Annual return periods for Forest Fire Danger Index values for the 30-year baseline period (1961-1990) and 20-year time periods from 2001 to 2100.

Figure 8: Distribution of values for each of the underlying drivers of Forest Fire Danger Index for each time period. a) Maximum daily wind speed (m/s); b) Drought Factor (AU); c) Maximum daily temperature; d) Daily minimum relative humidity (%). As wind speed is not projected to change significantly, the key drivers of change are temperature, humidity and drought factor. Drought factor has strong correlations with temperature change.

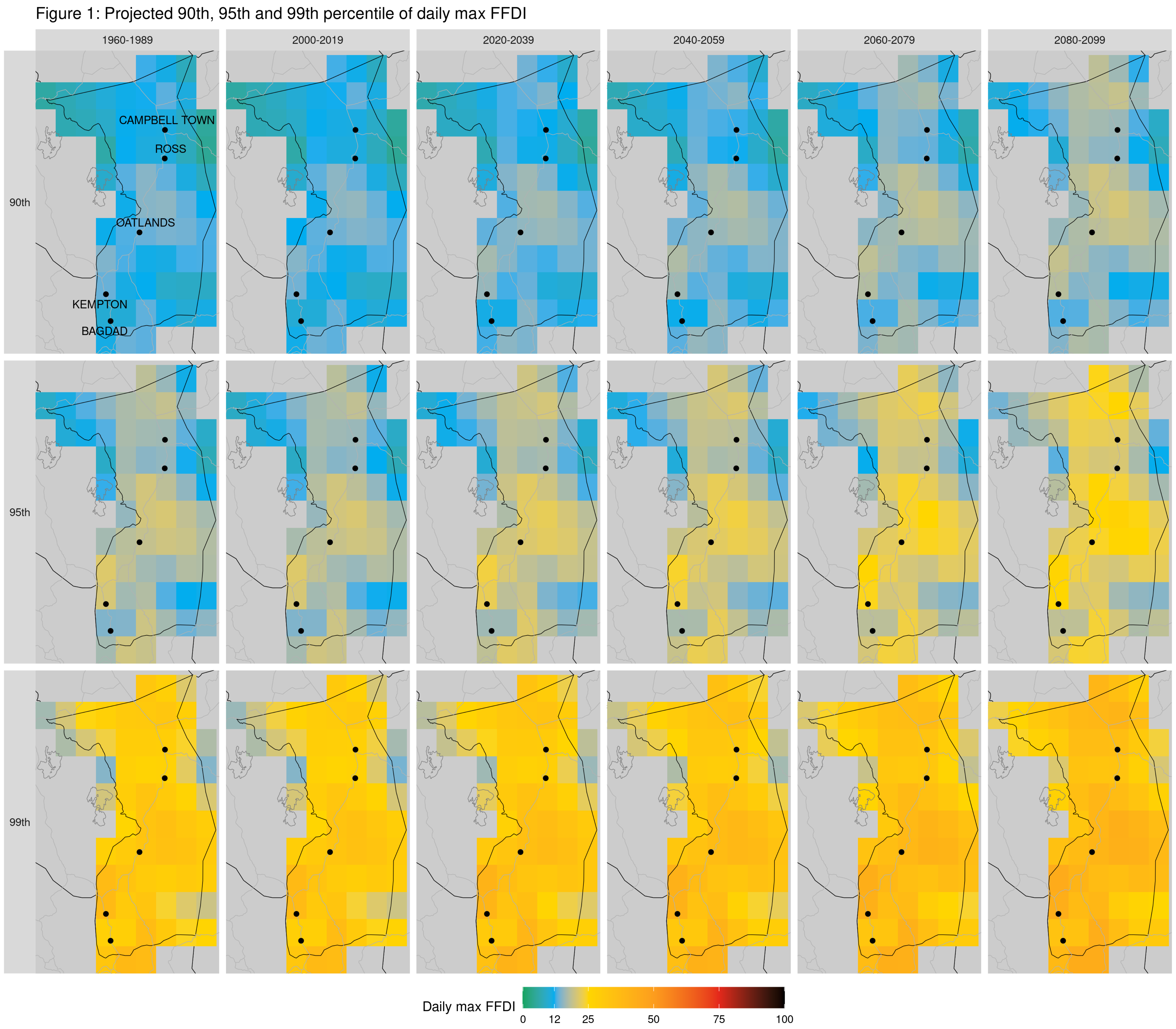


Figure 1: Projected 90th, 95th and 99th percentile values of *Forest Fire Danger Index* for the 30-year baseline period, and then 20-year time periods from 2001 to 2100. Each grid cell is the mean of the 6 ensemble members. The 99th percentile value reflects the 4th highest FFDI value year; the 95th percentile is the 18th highest FFDI value year; and the 90th percentile is the 36th highest FFDI value year. Extreme values of FFDI are expected to increase steadily into the future.

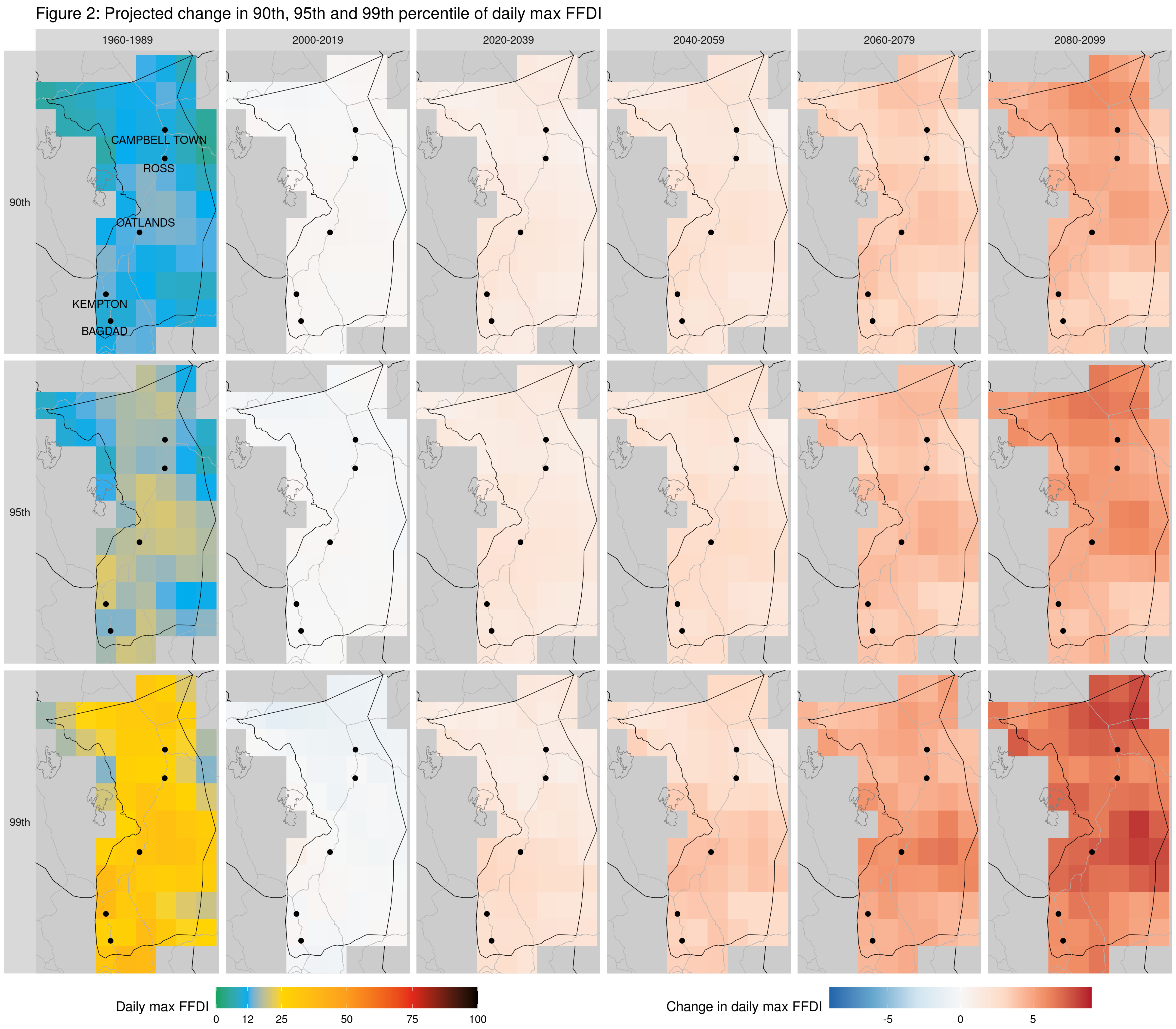


Figure 2: Projected change in the 90th, 95th and 99th percentile values of *Forest Fire Danger Index* for 20-year time periods from 2001 to 2100 compared to the 30-year baseline period 1961–1990. Each grid cell is the mean of the 6 ensemble members. The 99th percentile value reflects the 4th highest FFDI value year; the 95th percentile is the 18th highest FFDI value year; and the 90th percentile is the 36th highest FFDI value year. Extreme values of FFDI are expected to increase steadily into the future

Figure 3: Projected monthly FFDI with outliers removed

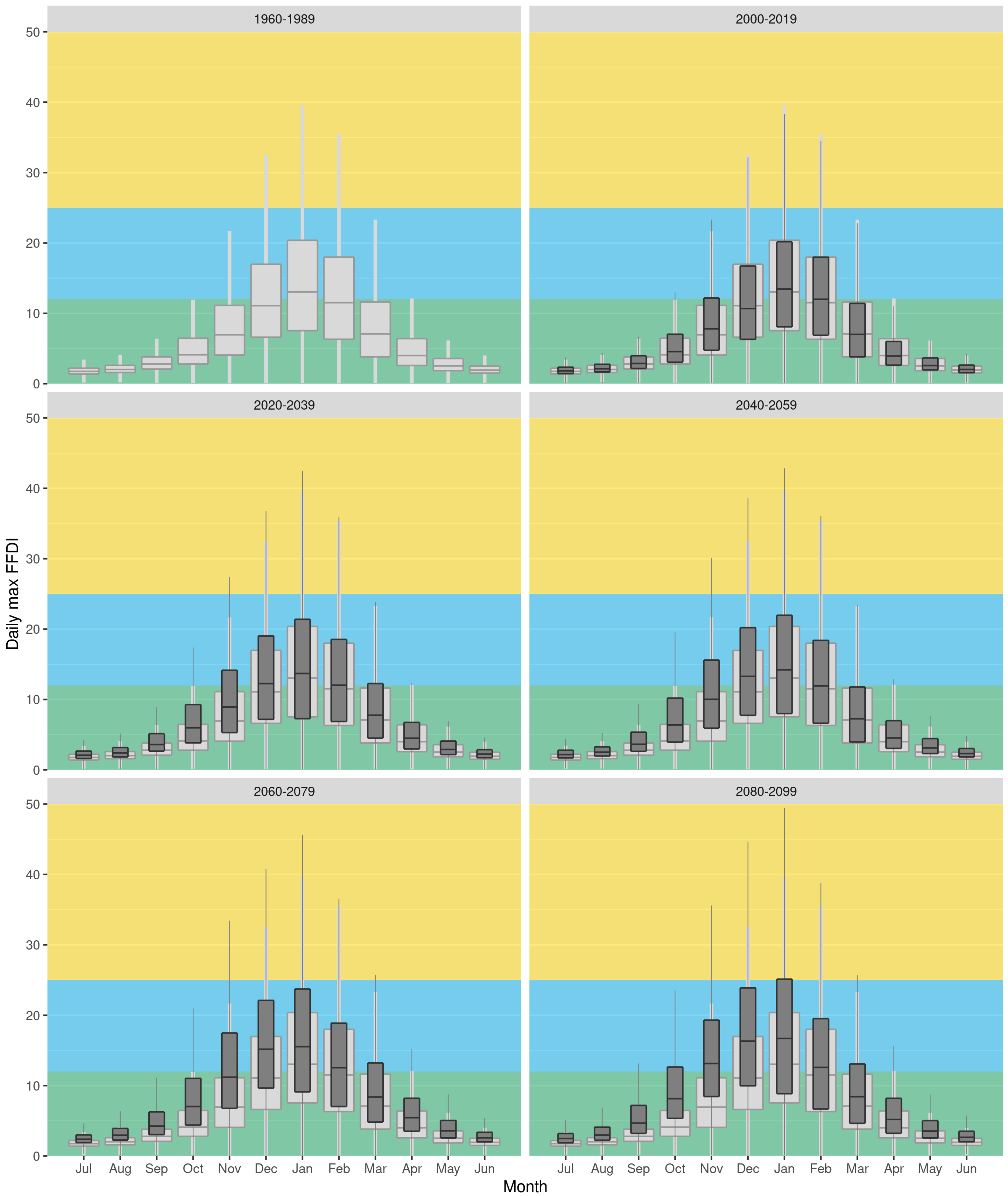


Figure 4: Projected monthly FFDI with outliers shown

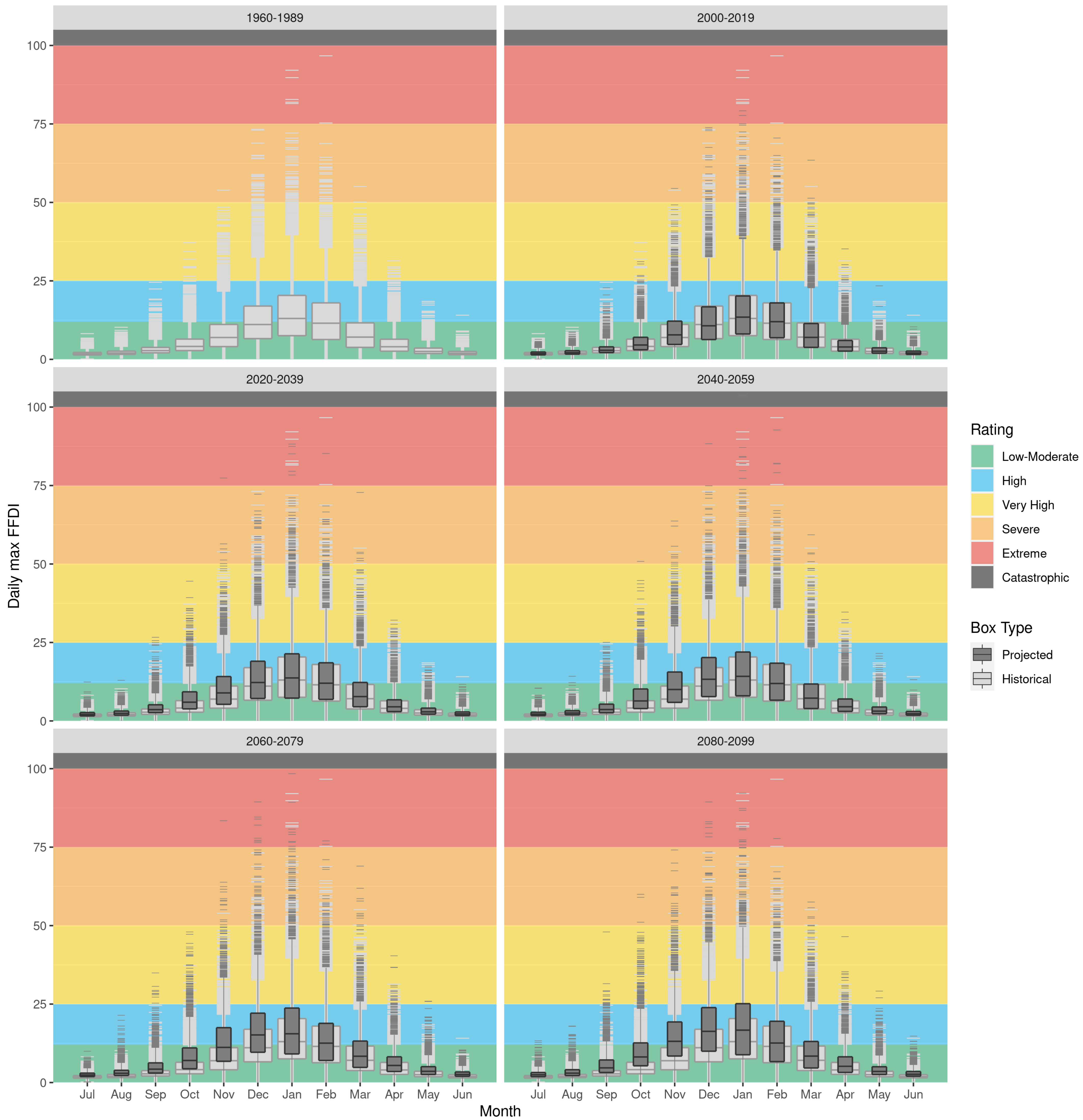


Figure 3: Boxplots of daily *Forest Fire Danger Index* for each month for the 30-year baseline period, and then 20-year periods from 2001 to 2100. Each boxplot represents a summary of daily data for each grid cell, for each of the 6 ensemble members within the time period; e.g. the top-left panel, the January boxplot represents the daily FFDI values for all January days in the period 1961–1990, for all grids cell in the region, for each of the 6 ensemble members. The baseline period (1961-1990) has been shadowed (*light grey*) underneath future time periods to highlight any differences expected into the future. Solid bars represent the median value. The box represents the 25th and 75th percentiles. The Whiskers represent the 1.5× the inter-quartile range. All months in all periods frequently have days of very low FFDI. Outliers have been excluded. If the boxplot shifts higher (lower) this indicates a change towards more (less) dangerous conditions.

Figure 4: Boxplots of daily *Forest Fire Danger Index* for each month for the 30-year baseline period, and then 20-year periods from 2001 to 2100. Each boxplot represents daily data for each grid cell, for each of the 6 ensemble members within the time period; e.g. ing the top-left panel, the January boxplot represents the daily FFDI values for all January days in the period 1961–1990, for all grids cell in the region, for each of the 6 ensemble members. The baseline period (1961-1990) has been shadowed (*light grey*) underneath future time periods to highlight any differences expected into the future. Solid bars represent the median value. The box represents the 25th and 75th percentiles. The Whiskers represent the 1.5× the inter-quartile range. All months in all periods frequently have days of very low FFDI. Outliers are values > 1.5× the interquartile range and are represented as a dash(-): *light grey* for historical; *dark grey* for other time periods. If the boxplot shifts higher (lower) this indicates a change towards more (less) dangerous conditions.

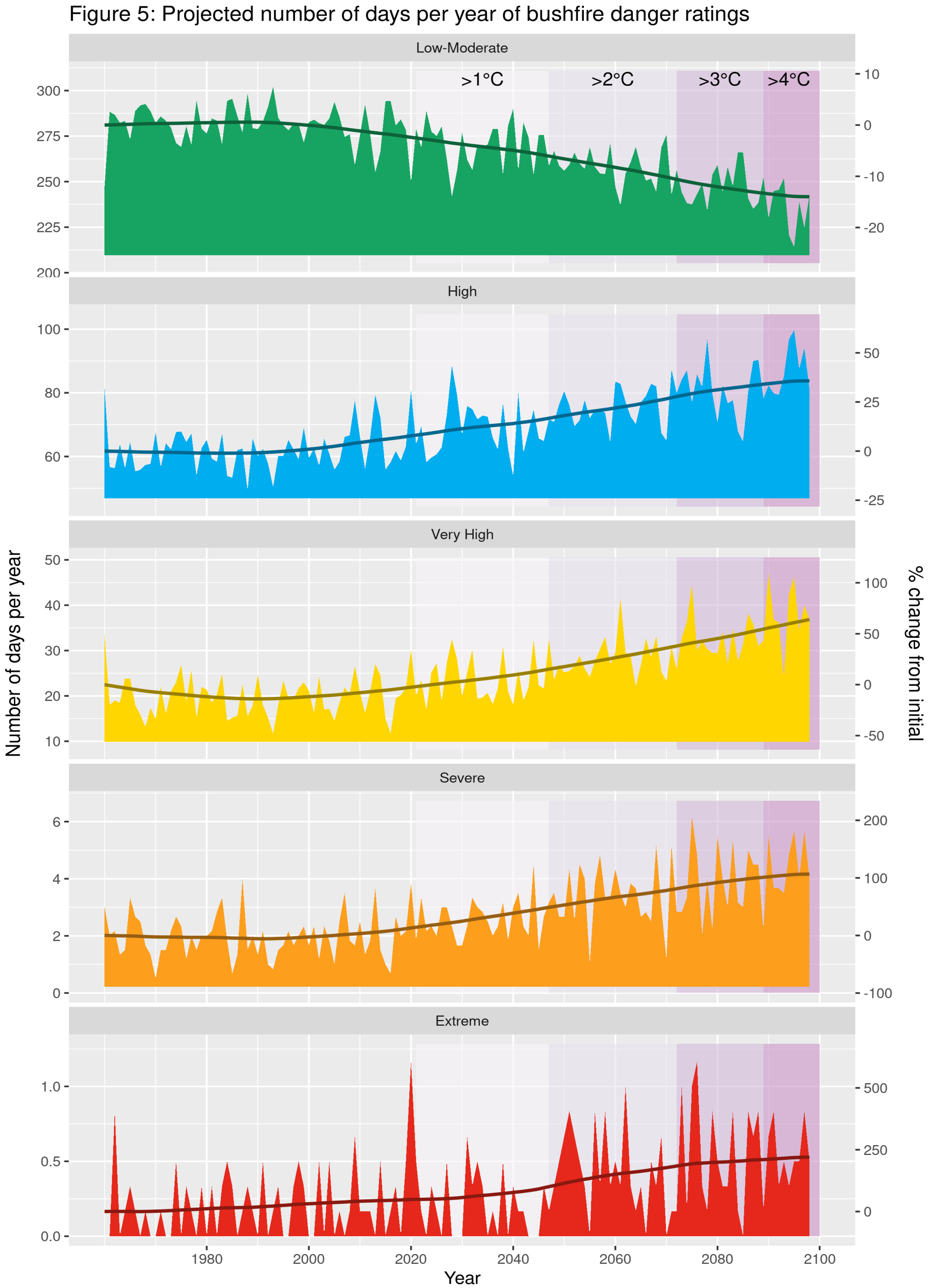


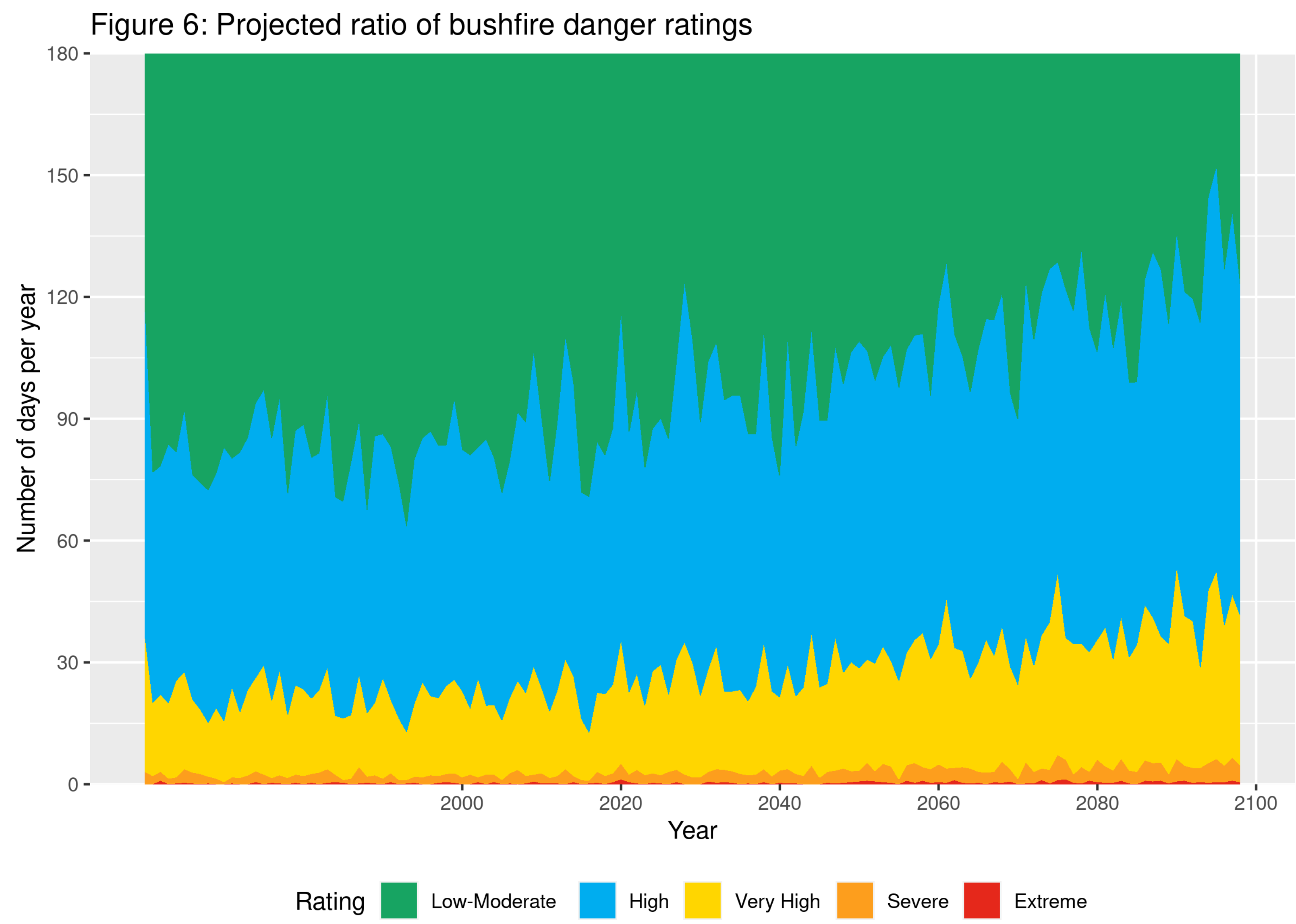


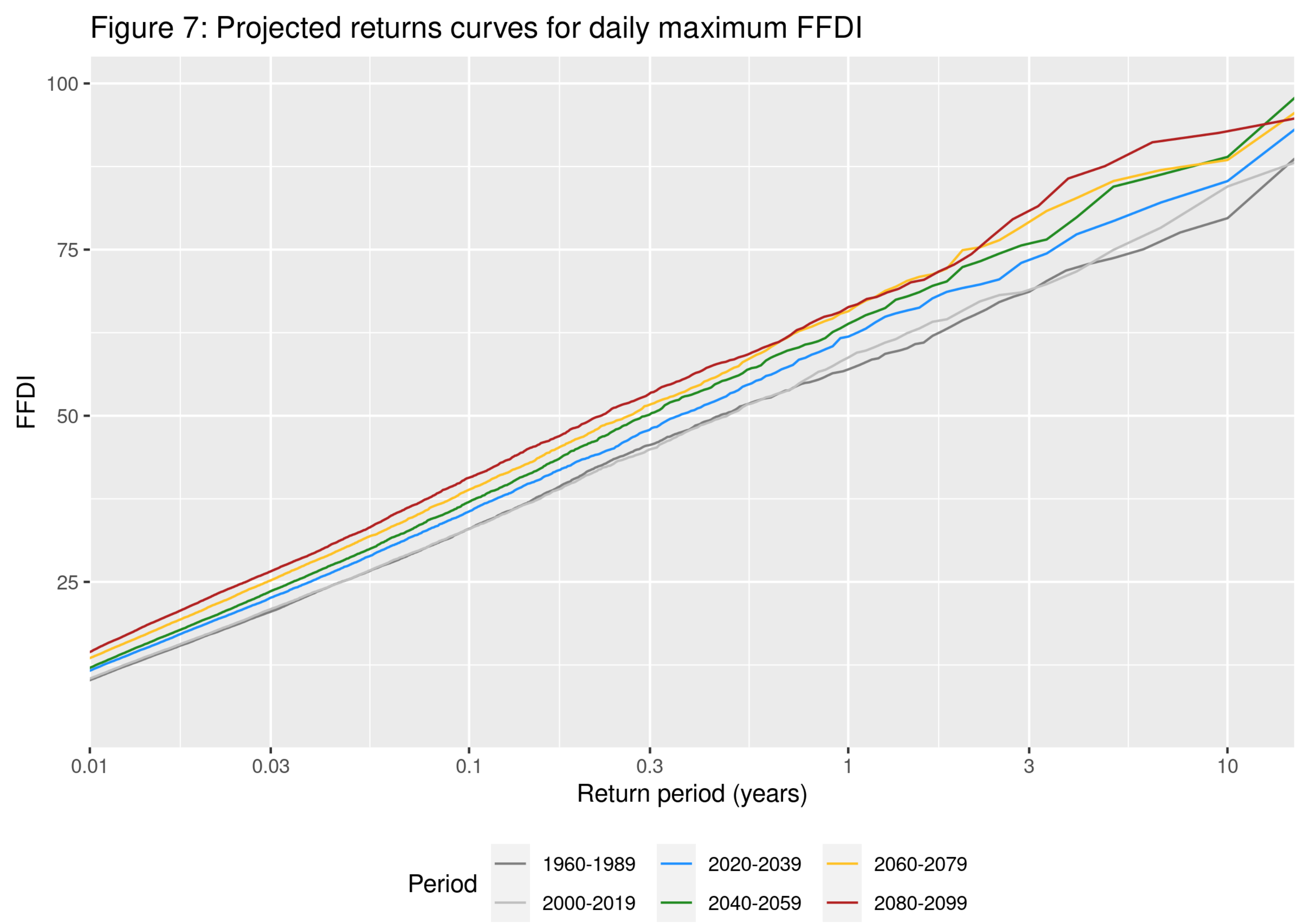


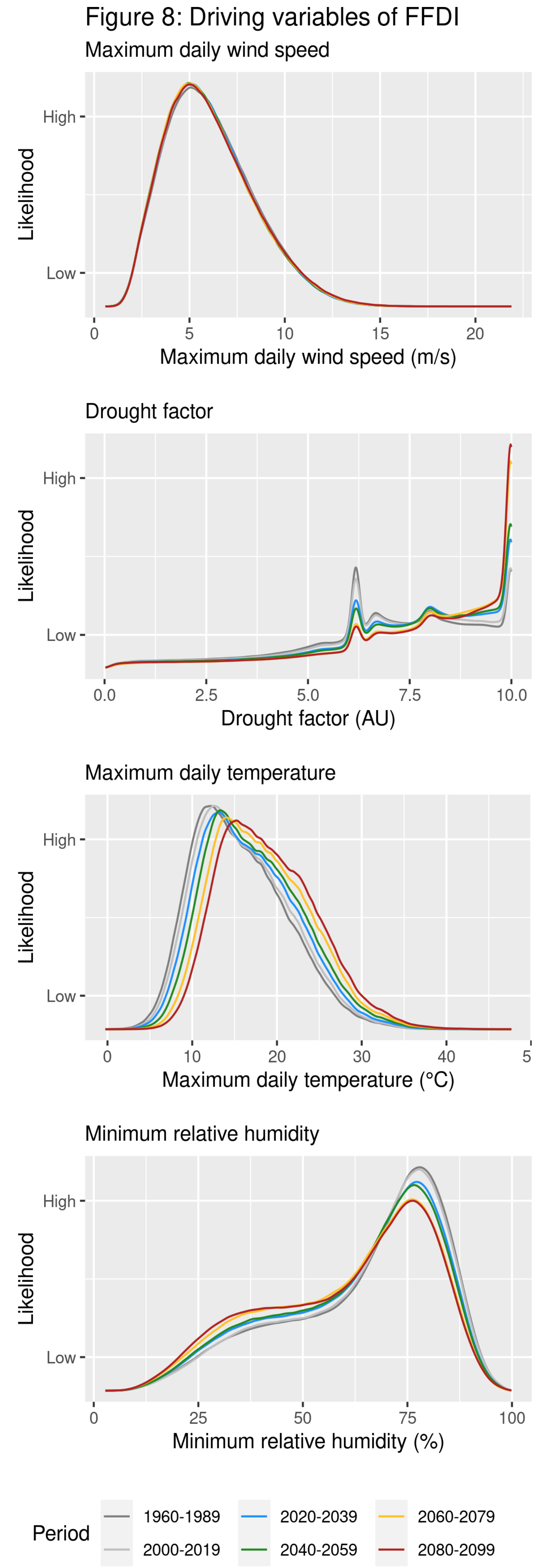


Figure 5: Time series of the ensemble-mean for the 30-year rolling mean of the number of days per year with fire danger ratings of *Low-Moderate*, *High*, *Very High*, *Severe*, *Extreme* from 1990 to 2100 (NB: *Catastrophic* had frequencies too low to reasonably present here). As every day has a fire danger rating, *Low-Moderate* rating frequencies decrease as they are replaced by higher categories.

Figure 6: Stacked area plot of the 30-year ensemble mean number of days of each forest fire danger index rating across each fire-season (October to April, 180 days) from 1990 to 2100. Decreased frequency of *Low-Moderate* days is due to increases in *High* or *Very High* categories.

Figure 7: Annual return periods for Forest Fire Danger Index values for the 30-year baseline period (1961-1990) and 20-year time periods from 2001 to 2100.

Figure 8: Distribution of values for each of the underlying drivers of Forest Fire Danger Index for each time period. a) Maximum daily wind speed (m/s); b) Drought Factor (AU); c) Maximum daily temperature; d) Daily minimum relative humidity (%). As wind speed is not projected to change significantly, the key drivers of change are temperature, humidity and drought factor. Drought factor has strong correlations with temperature change.

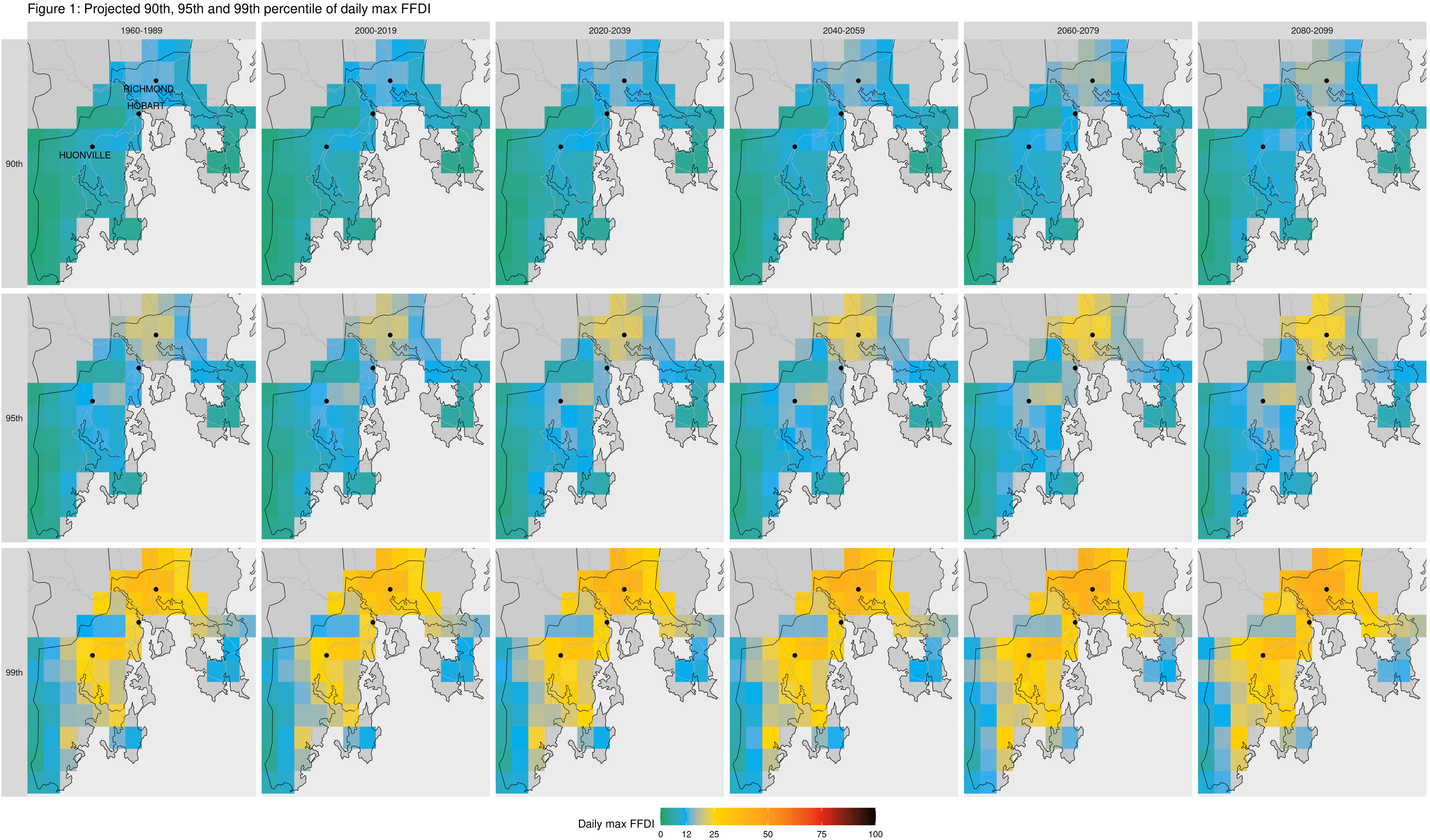


Figure 1: Projected 90th, 95th and 99th percentile values of *Forest Fire Danger Index* for the 30-year baseline period, and then 20-year time periods from 2001 to 2100. Each grid cell is the mean of the 6 ensemble members. The 99th percentile value reflects the 4th highest FFDI value year; the 95th percentile is the 18th highest FFDI value year; and the 90th percentile is the 36th highest FFDI value year. Extreme values of FFDI are expected to increase steadily into the future.

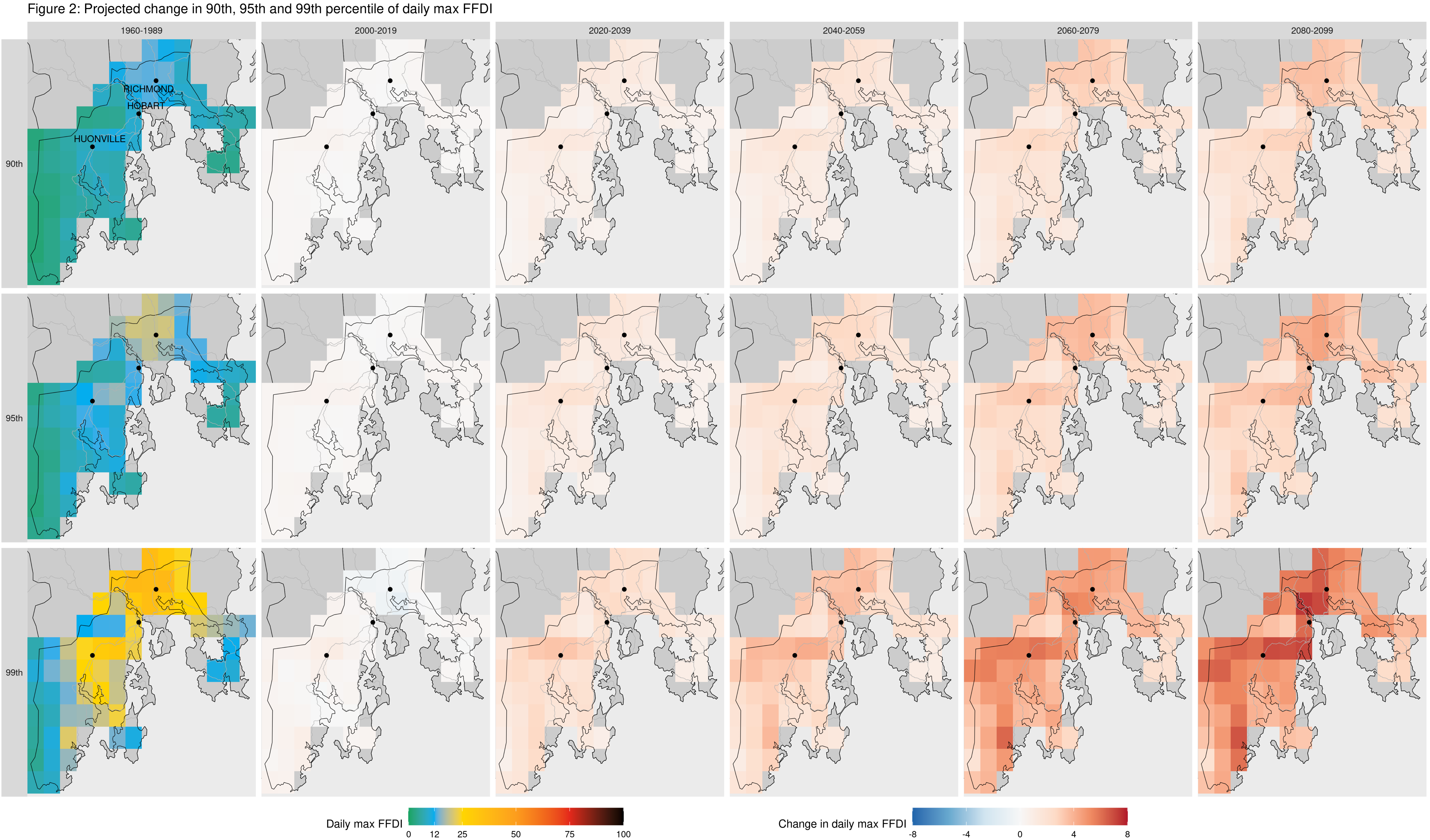


Figure 2: Projected change in the 90th, 95th and 99th percentile values of *Forest Fire Danger Index* for 20-year time periods from 2001 to 2100 compared to the 30-year baseline period 1961–1990. Each grid cell is the mean of the 6 ensemble members. The 99th percentile value reflects the 4th highest FFDI value year; the 95th percentile is the 18th highest FFDI value year; and the 90th percentile is the 36th highest FFDI value year. Extreme values of FFDI are expected to increase steadily into the future

Figure 3: Projected monthly FFDI with outliers removed

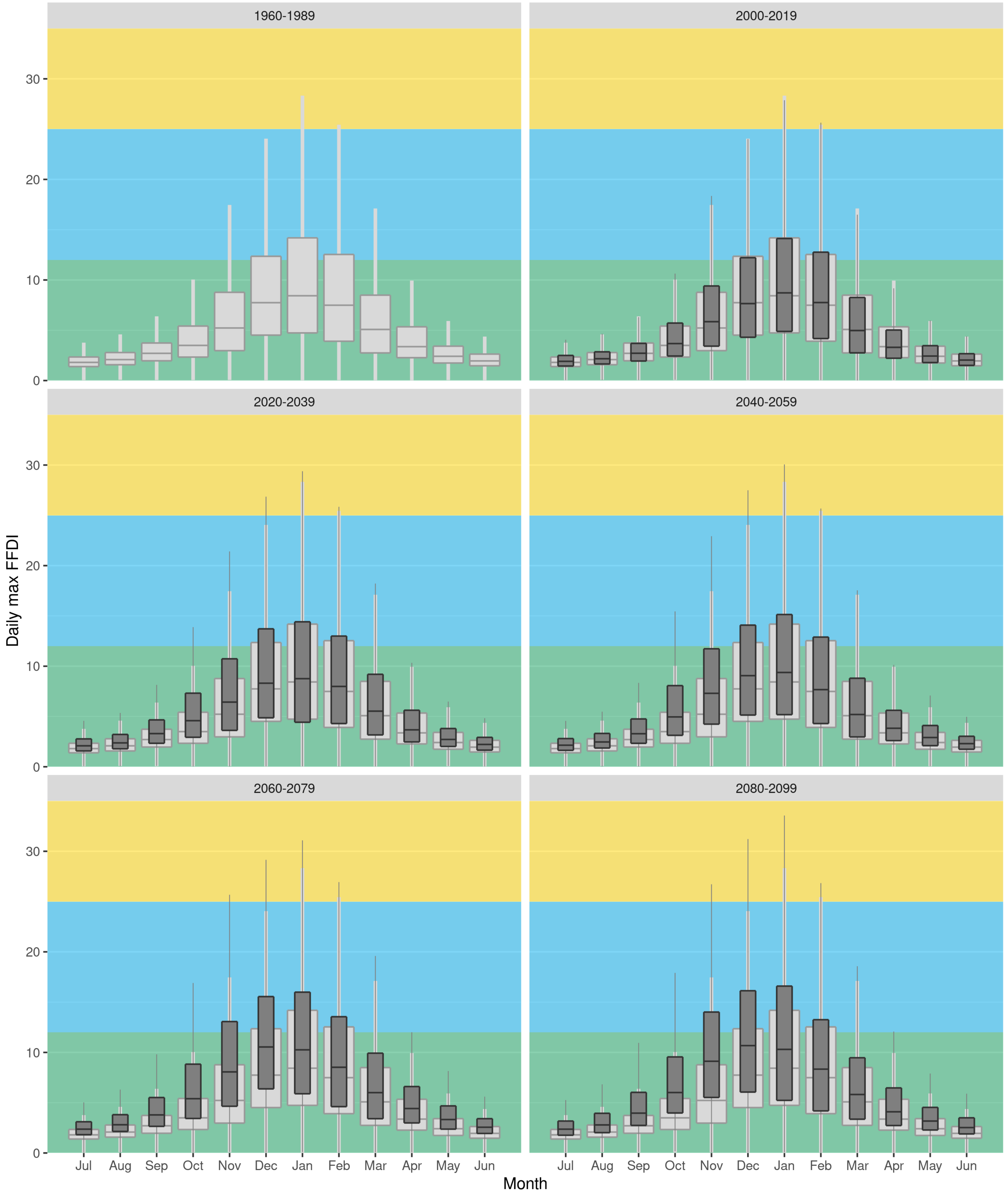


Figure 3: Boxplots of daily *Forest Fire Danger Index* for each month for the 30-year baseline period, and then 20-year periods from 2001 to 2100. Each boxplot represents a summary of daily data for each grid cell, for each of the 6 ensemble members within the time period; e.g. the top-left panel, the January boxplot represents the daily FFDI values for all January days in the period 1961–1990, for all grids cell in the region, for each of the 6 ensemble members. The baseline period (1961-1990) has been shadowed (*light grey*) underneath future time periods to highlight any differences expected into the future. Solid bars represent the median value. The box represents the 25th and 75th percentiles. The Whiskers represent the 1.5× the inter-quartile range. All months in all periods frequently have days of very low FFDI. Outliers have been excluded. If the boxplot shifts higher (lower) this indicates a change towards more (less) dangerous conditions.

Figure 4: Projected monthly FFDI with outliers shown

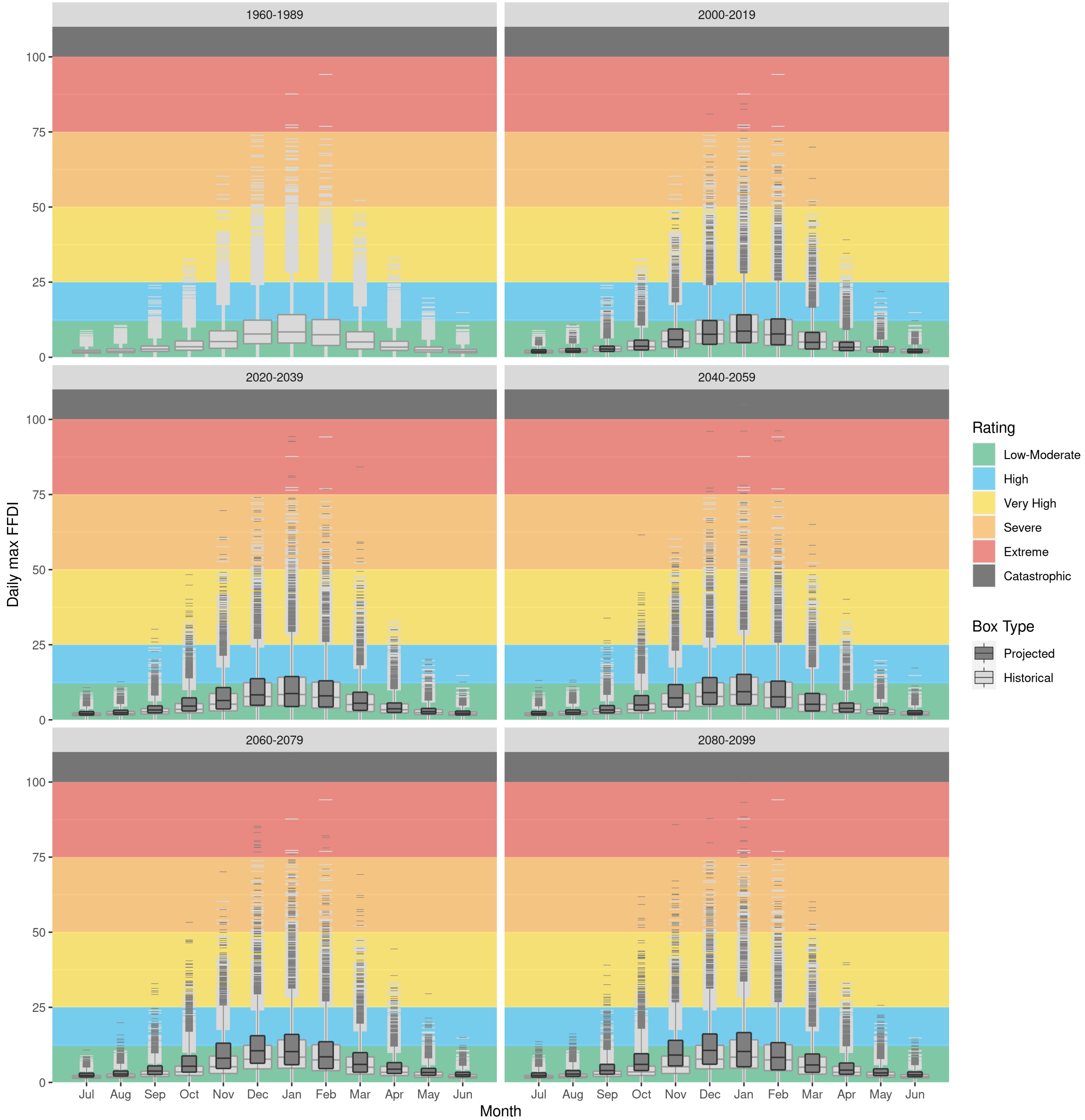


Figure 4: Boxplots of daily *Forest Fire Danger Index* for each month for the 30-year baseline period, and then 20-year periods from 2001 to 2100. Each boxplot represents daily data for each grid cell, for each of the 6 ensemble members within the time period; e.g. ing the top-left panel, the January boxplot represents the daily FFDI values for all January days in the period 1961–1990, for all grids cell in the region, for each of the 6 ensemble members. The baseline period (1961-1990) has been shadowed (*light grey*) underneath future time periods to highlight any differences expected into the future. Solid bars represent the median value. The box represents the 25th and 75th percentiles. The Whiskers represent the 1.5× the inter-quartile range. All months in all periods frequently have days of very low FFDI. Outliers are values > 1.5× the interquartile range and are represented as a dash(-): *light grey* for historical; *dark grey* for other time periods. If the boxplot shifts higher (lower) this indicates a change towards more (less) dangerous conditions.

Figure 5: Projected number of days per year of bushfire danger ratings

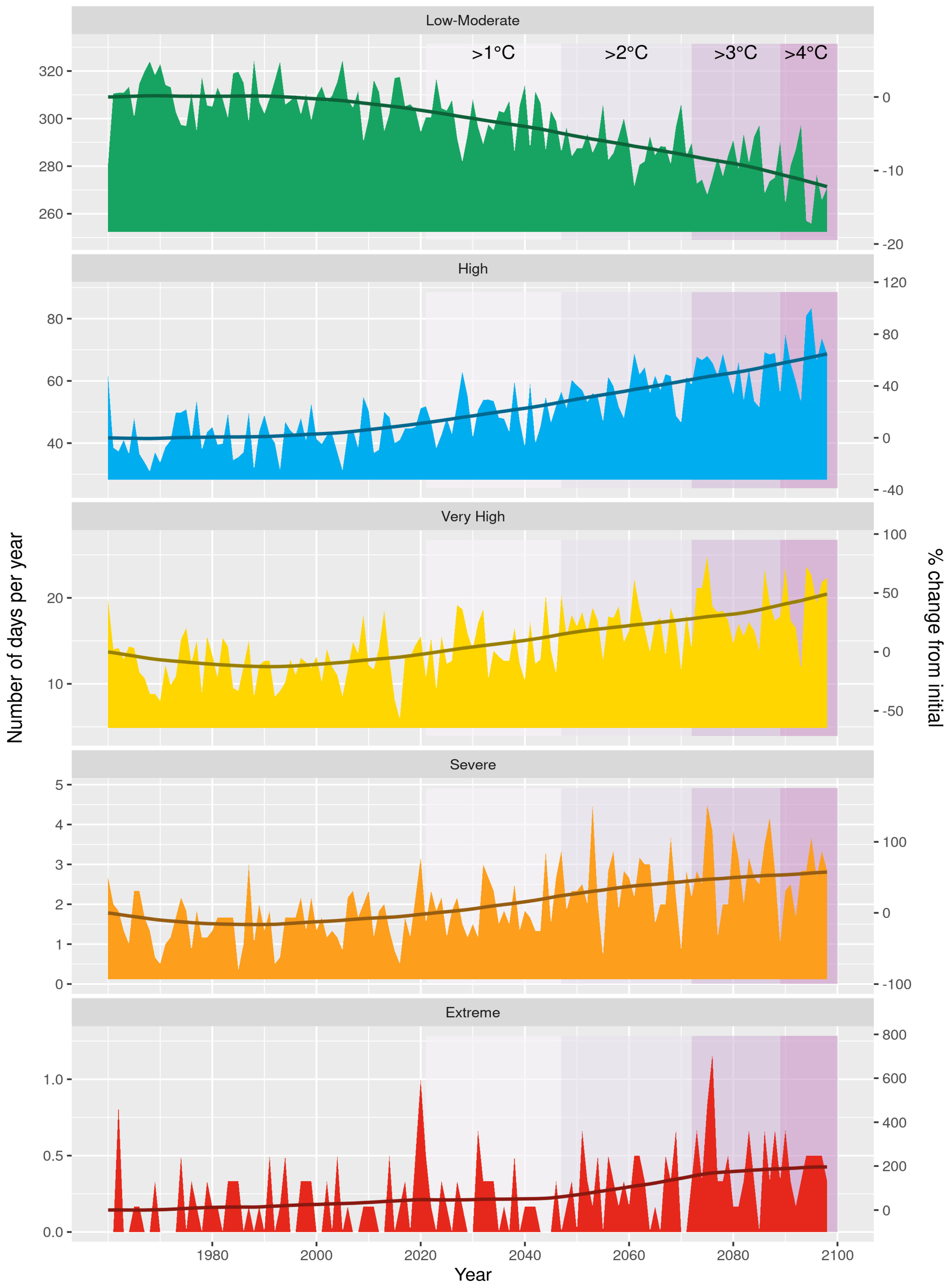


Figure 6: Projected ratio of bushfire danger ratings

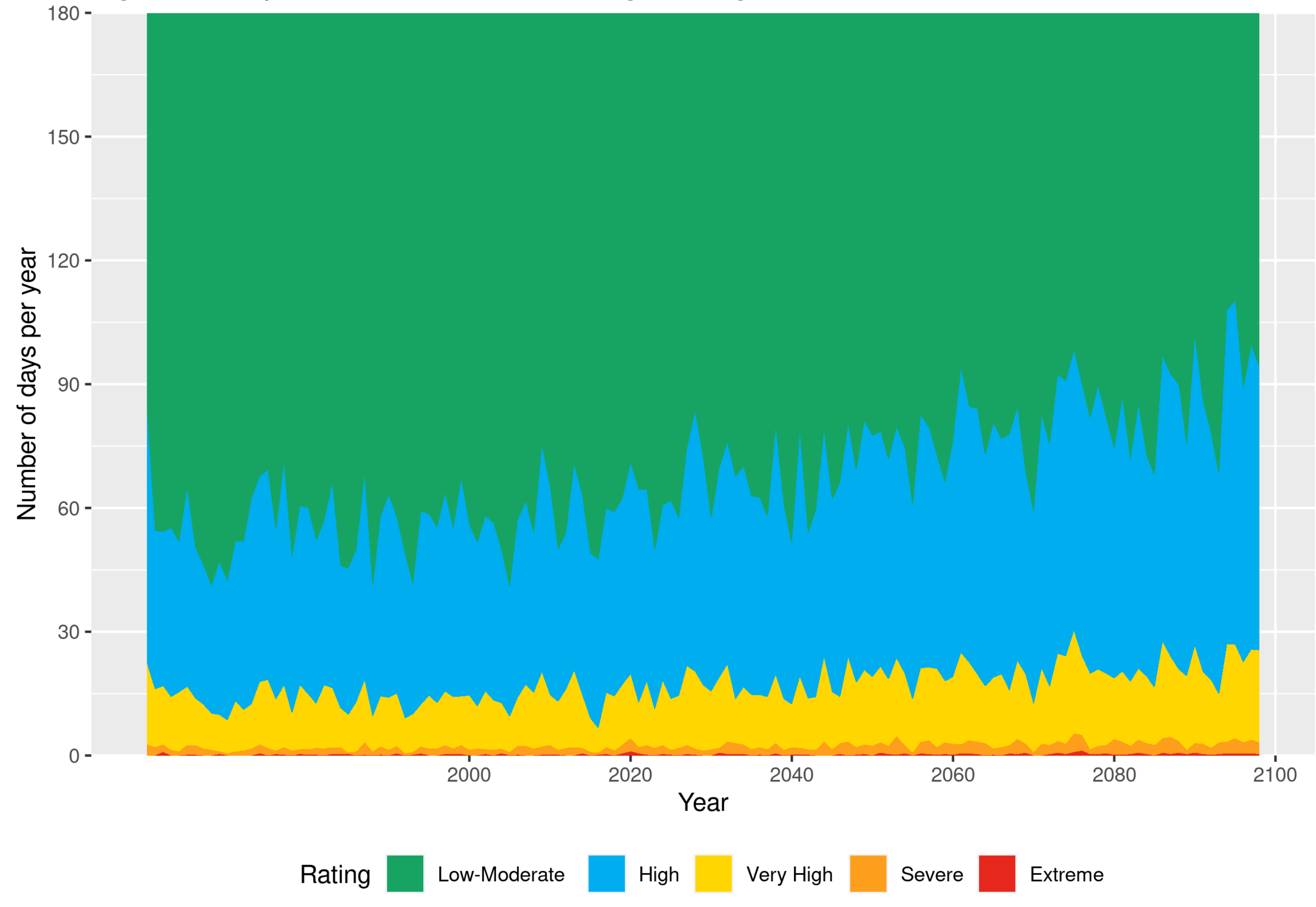


Figure 7: Projected returns curves for daily maximum FFDI

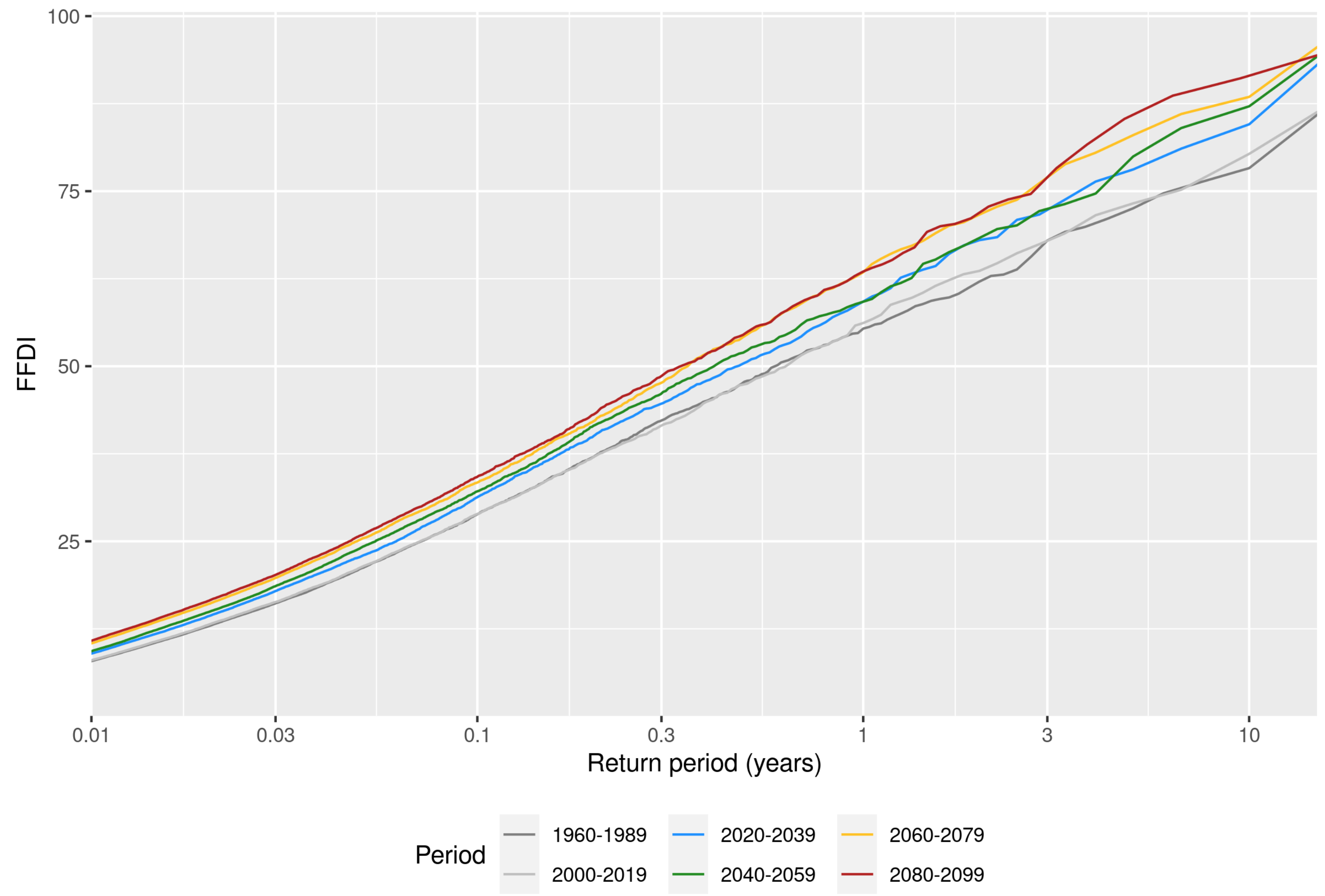


Figure 8: Driving variables of FFDI

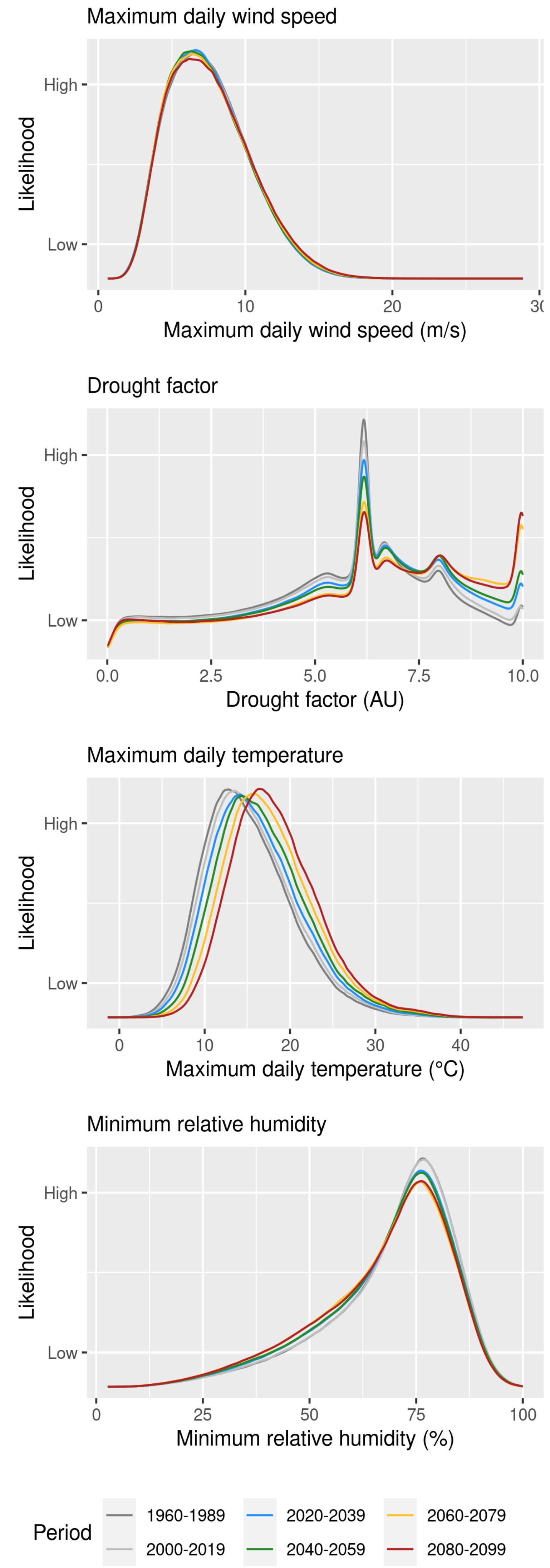


Figure 5: Time series of the ensemble-mean for the 30-year rolling mean of the number of days per year with fire danger ratings of *Low-Moderate*, *High*, *Very High*, *Severe*, *Extreme* from 1990 to 2100 (NB: *Catastrophic* had frequencies too low to reasonably present here). As every day has a fire danger rating, *Low-Moderate* rating frequencies decrease as they are replaced by higher categories.

Figure 6: Stacked area plot of the 30-year ensemble mean number of days of each forest fire danger index rating across each fire-season (October to April, 180 days) from 1990 to 2100. Decreased frequency of *Low-Moderate* days is due to increases in *High* or *Very High* categories.

Figure 7: Annual return periods for Forest Fire Danger Index values for the 30-year baseline period (1961-1990) and 20-year time periods from 2001 to 2100.

Figure 8: Distribution of values for each of the underlying drivers of Forest Fire Danger Index for each time period. a) Maximum daily wind speed (m/s); b) Drought Factor (AU); c) Maximum daily temperature; d) Daily minimum relative humidity (%). As wind speed is not projected to change significantly, the key drivers of change are temperature, humidity and drought factor. Drought factor has strong correlations with temperature change.

Figure 1: Projected 90th, 95th and 99th percentile of daily max FFDI

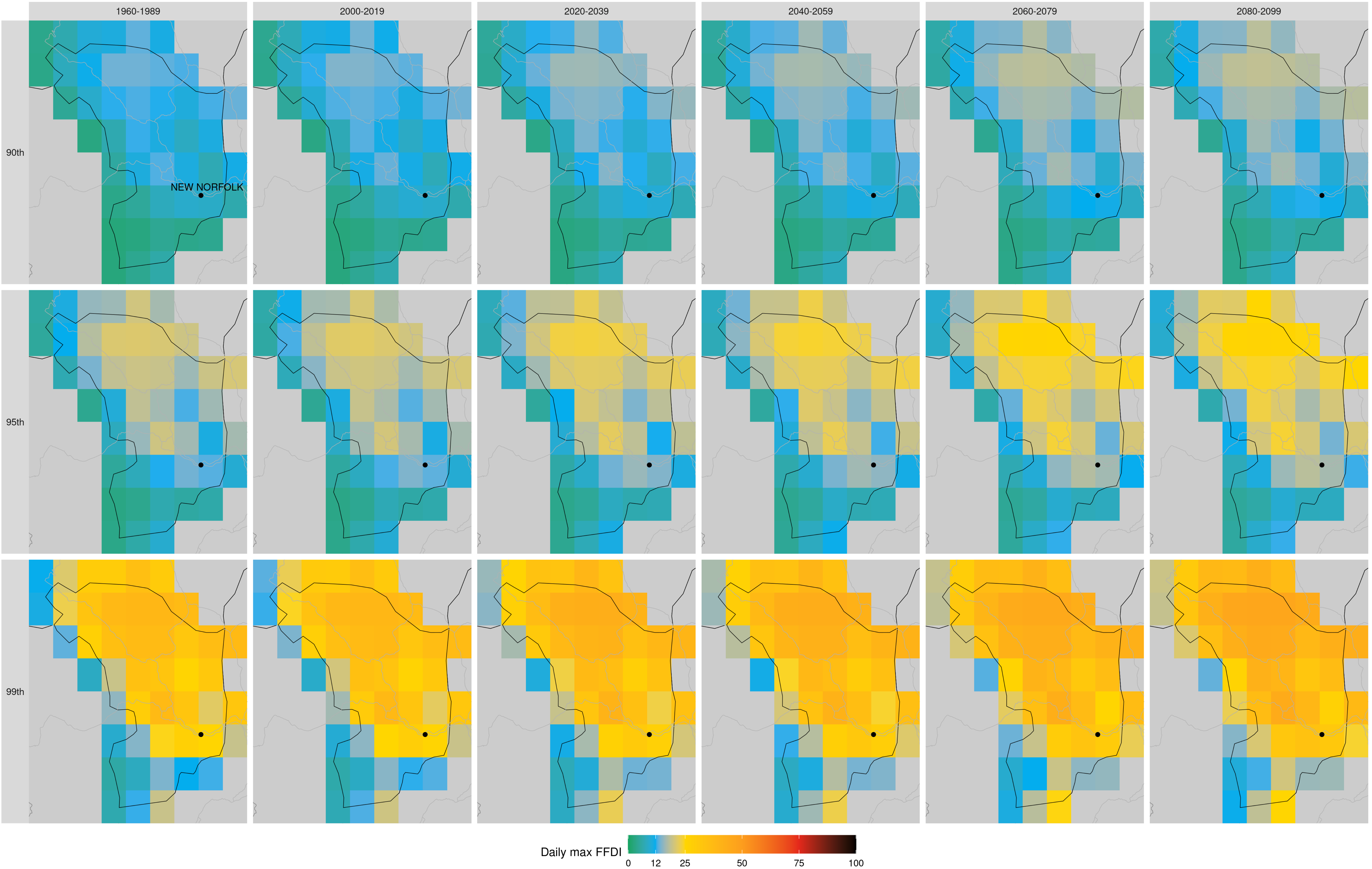


Figure 1: Projected 90th, 95th and 99th percentile values of *Forest Fire Danger Index* for the 30-year baseline period, and then 20-year time periods from 2001 to 2100. Each grid cell is the mean of the 6 ensemble members. The 99th percentile value reflects the 4th highest FFDI value year; the 95th percentile is the 18th highest FFDI value year; and the 90th percentile is the 36th highest FFDI value year. Extreme values of FFDI are expected to increase steadily into the future.

Figure 2: Projected change in 90th, 95th and 99th percentile of daily max FFDI

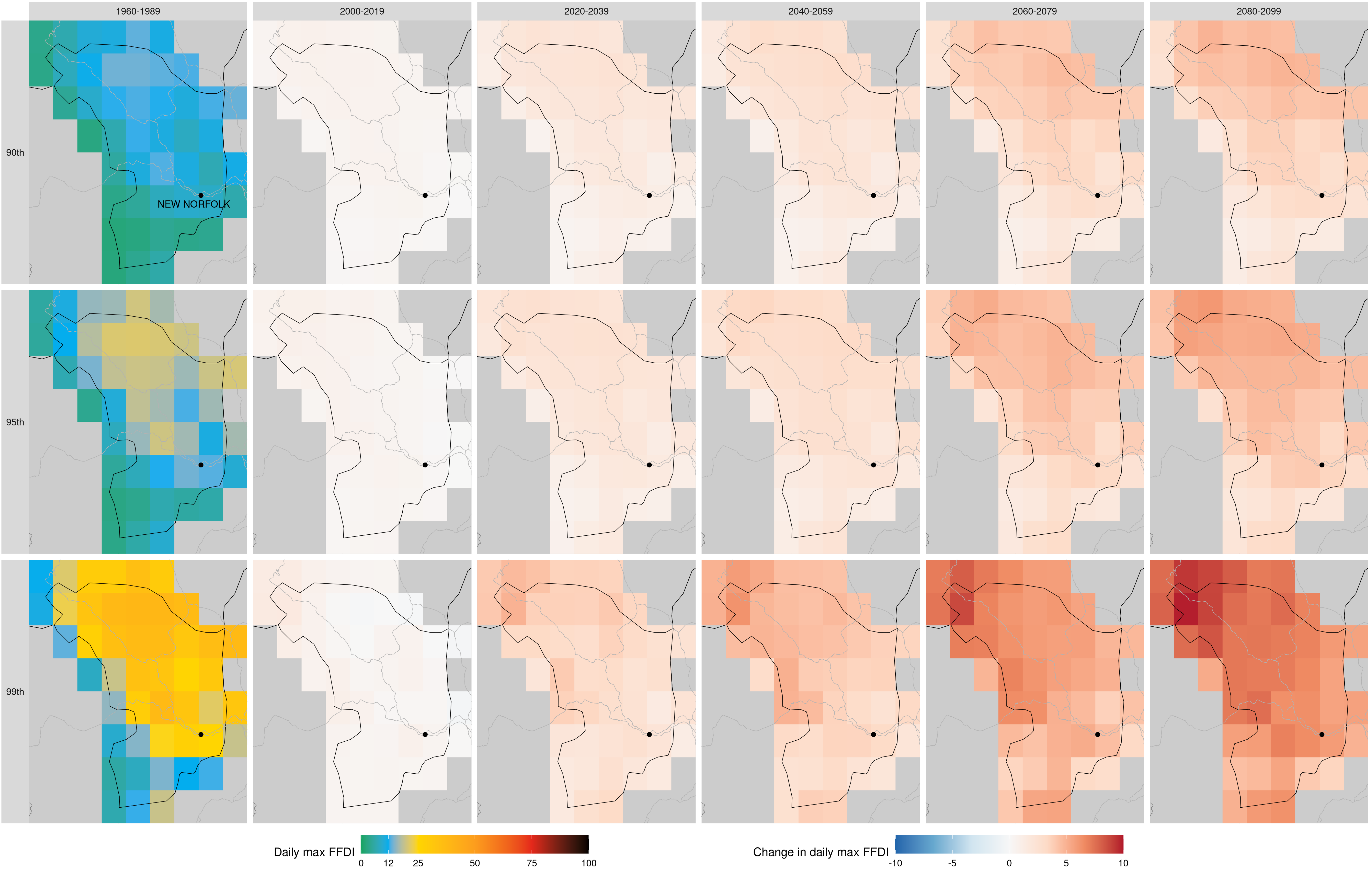


Figure 2: Projected change in the 90th, 95th and 99th percentile values of *Forest Fire Danger Index* for 20-year time periods from 2001 to 2100 compared to the 30-year baseline period 1961–1990. Each grid cell is the mean of the 6 ensemble members. The 99th percentile value reflects the 4th highest FFDI value year; the 95th percentile is the 18th highest FFDI value year; and the 90th percentile is the 36th highest FFDI value year. Extreme values of FFDI are expected to increase steadily into the future

Figure 3: Projected monthly FFDI with outliers removed

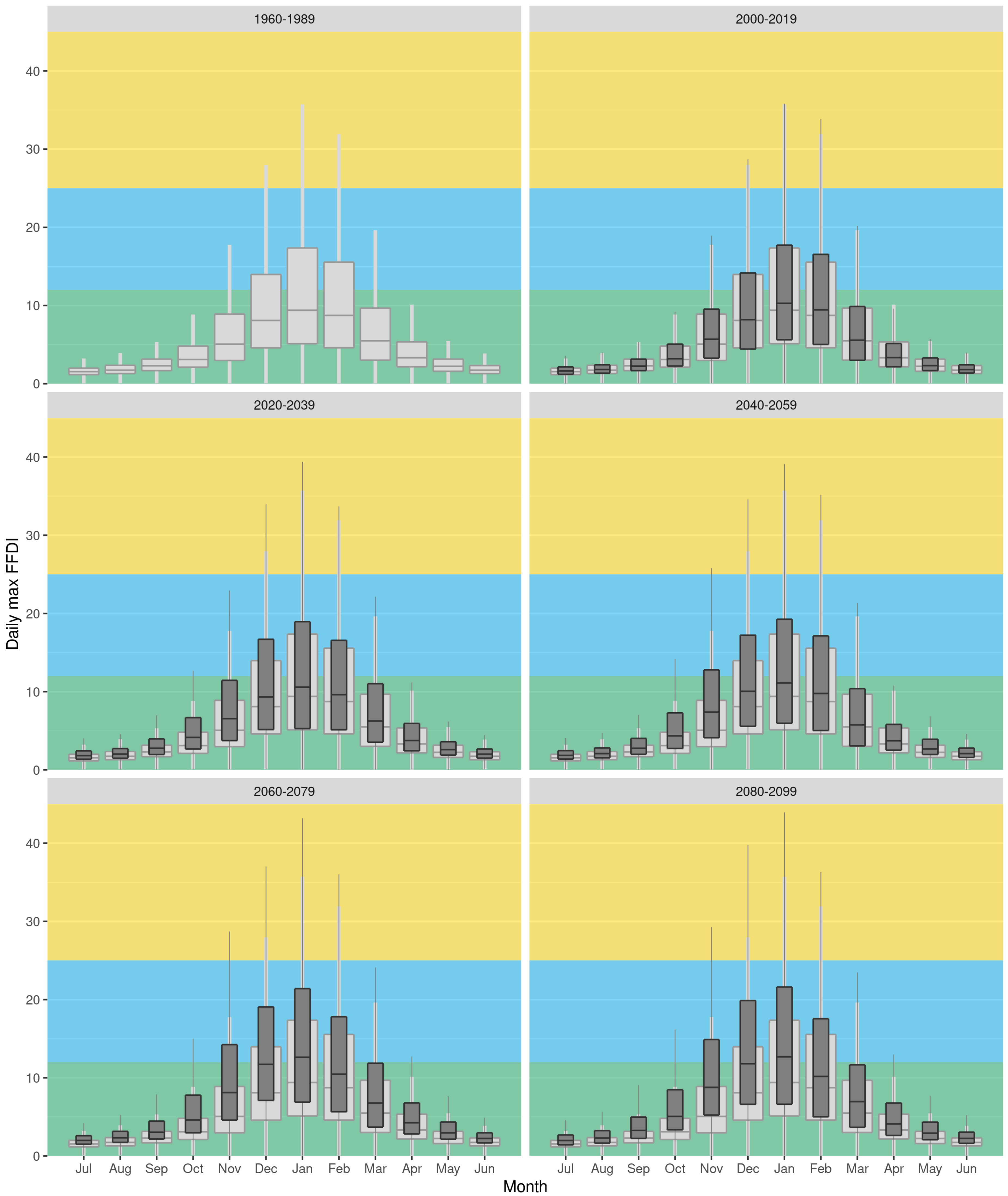


Figure 4: Projected monthly FFDI with outliers shown

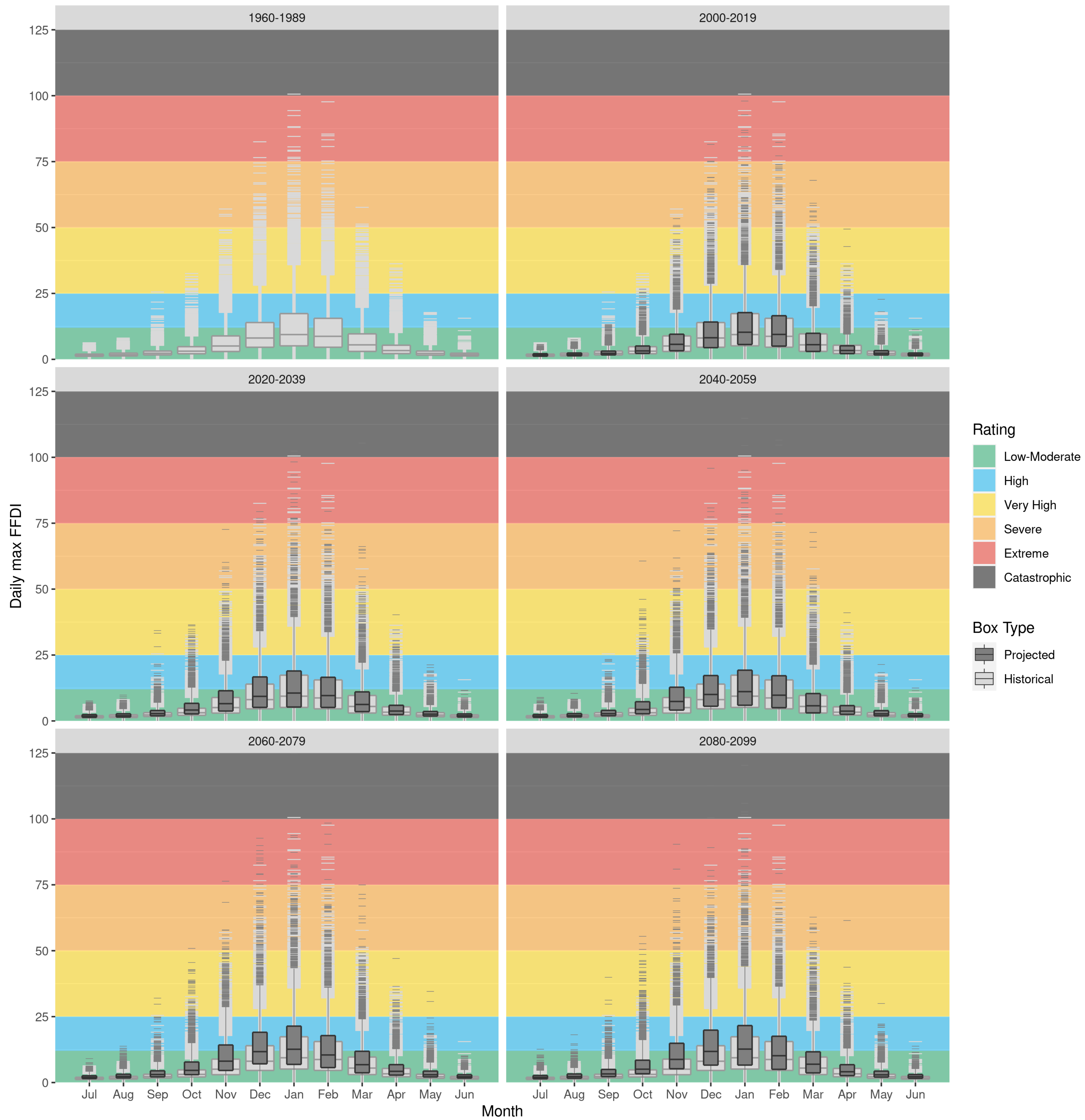


Figure 3: Boxplots of daily *Forest Fire Danger Index* for each month for the 30-year baseline period, and then 20-year periods from 2001 to 2100. Each boxplot represents a summary of daily data for each grid cell, for each of the 6 ensemble members within the time period; e.g. the top-left panel, the January boxplot represents the daily FFDI values for all January days in the period 1961–1990, for all grids cell in the region, for each of the 6 ensemble members. The baseline period (1961-1990) has been shadowed (*light grey*) underneath future time periods to highlight any differences expected into the future. Solid bars represent the median value. The box represents the 25th and 75th percentiles. The Whiskers represent the 1.5× the inter-quartile range. All months in all periods frequently have days of very low FFDI. Outliers have been excluded. If the boxplot shifts higher (lower) this indicates a change towards more (less) dangerous conditions.

Figure 4: Boxplots of daily *Forest Fire Danger Index* for each month for the 30-year baseline period, and then 20-year periods from 2001 to 2100. Each boxplot represents daily data for each grid cell, for each of the 6 ensemble members within the time period; e.g. ing the top-left panel, the January boxplot represents the daily FFDI values for all January days in the period 1961–1990, for all grids cell in the region, for each of the 6 ensemble members. The baseline period (1961-1990) has been shadowed (*light grey*) underneath future time periods to highlight any differences expected into the future. Solid bars represent the median value. The box represents the 25th and 75th percentiles. The Whiskers represent the 1.5× the inter-quartile range. All months in all periods frequently have days of very low FFDI. Outliers are values > 1.5× the interquartile range and are represented as a dash(-): *light grey* for historical; *dark grey* for other time periods. If the boxplot shifts higher (lower) this indicates a change towards more (less) dangerous conditions.

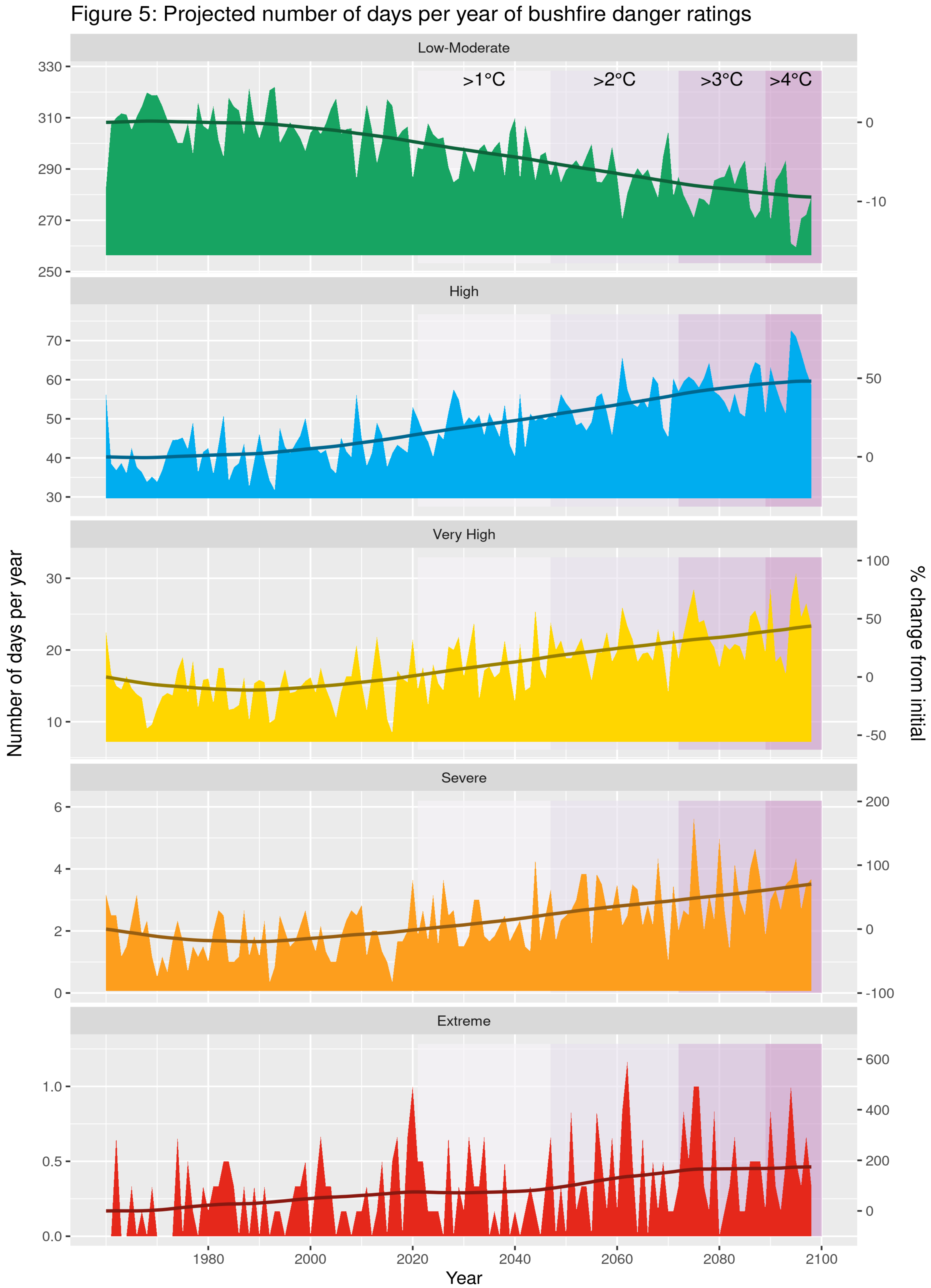


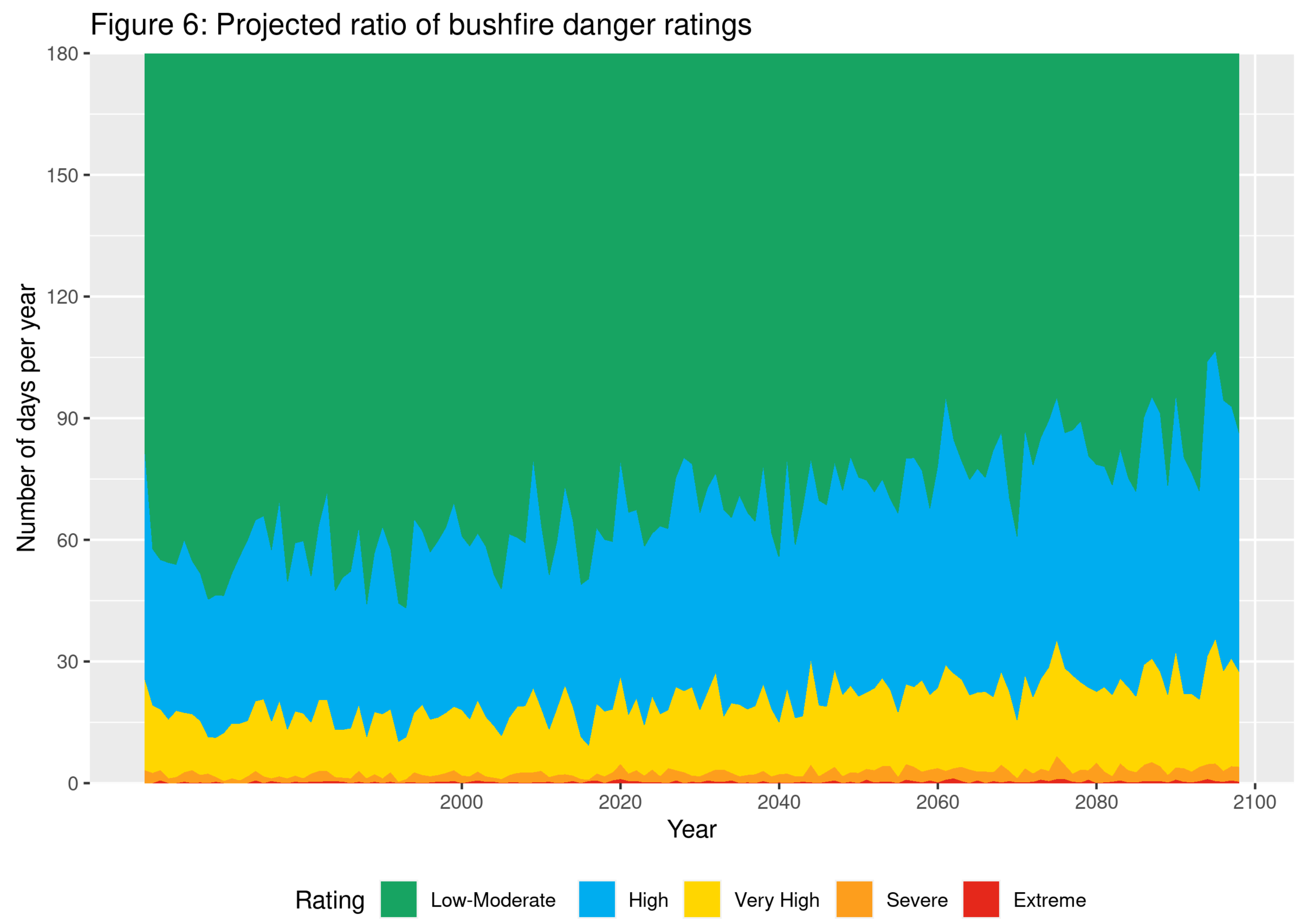


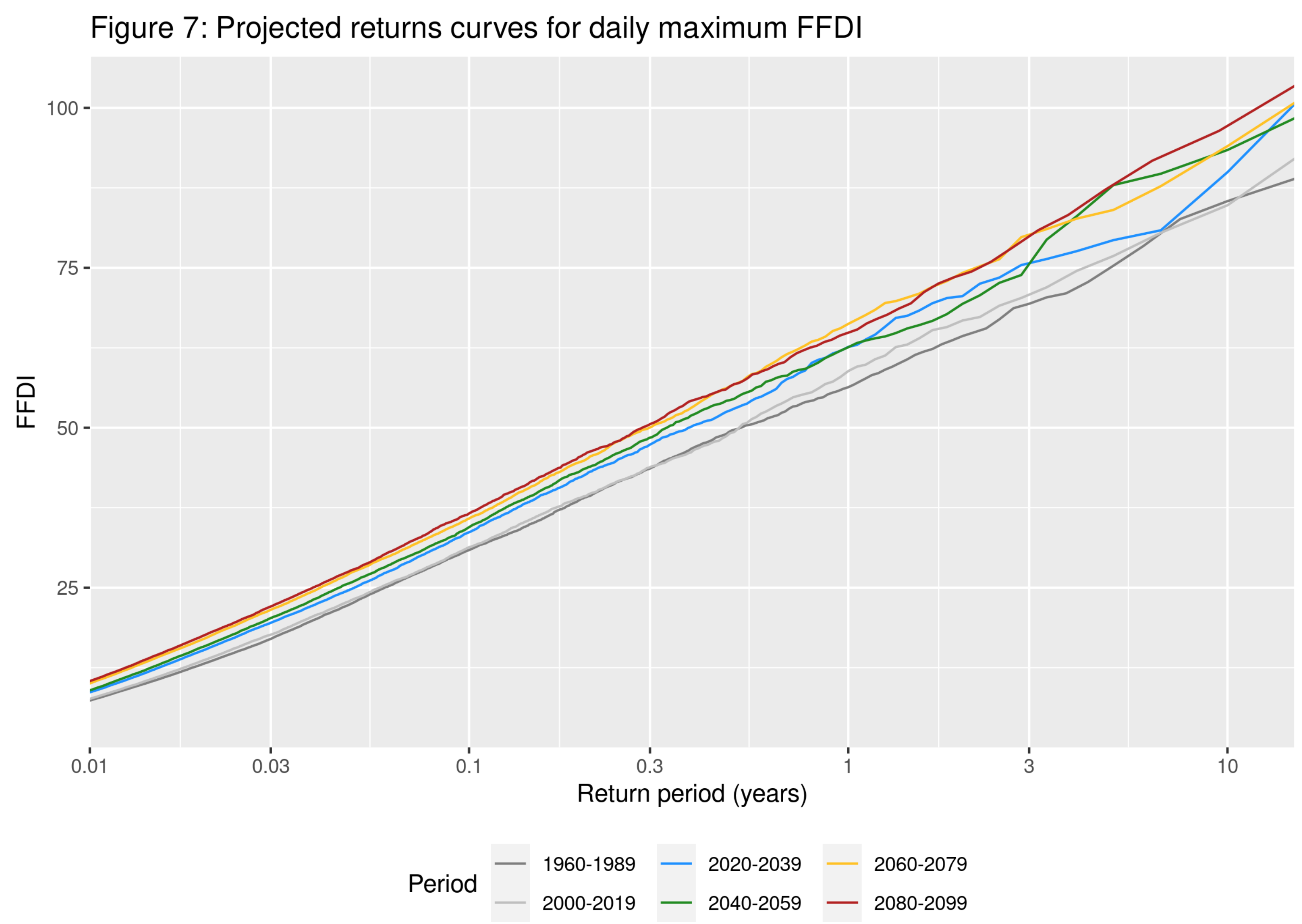


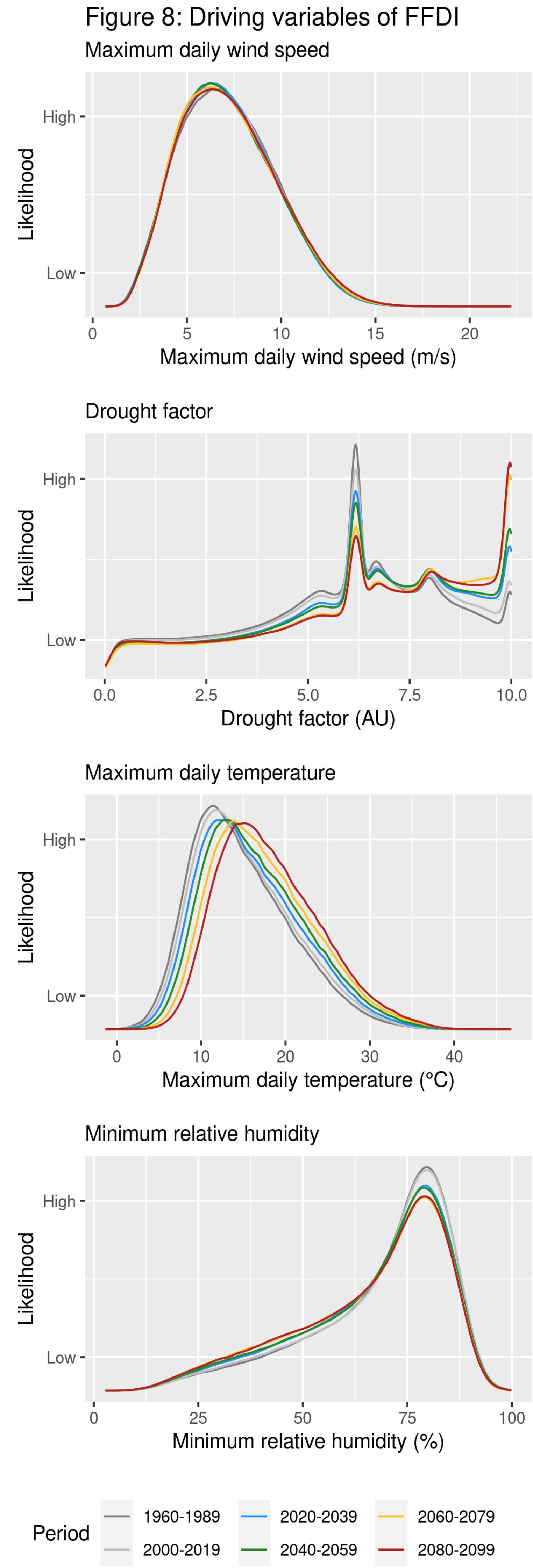


Figure 5: Time series of the ensemble-mean for the 30-year rolling mean of the number of days per year with fire danger ratings of *Low-Moderate*, *High*, *Very High*, *Severe*, *Extreme* from 1990 to 2100 (NB: *Catastrophic* had frequencies too low to reasonably present here). As every day has a fire danger rating, *Low-Moderate* rating frequencies decrease as they are replaced by higher categories.

Figure 6: Stacked area plot of the 30-year ensemble mean number of days of each forest fire danger index rating across each fire-season (October to April, 180 days) from 1990 to 2100. Decreased frequency of *Low-Moderate* days is due to increases in *High* or *Very High* categories.

Figure 7: Annual return periods for Forest Fire Danger Index values for the 30-year baseline period (1961-1990) and 20-year time periods from 2001 to 2100.

Figure 8: Distribution of values for each of the underlying drivers of Forest Fire Danger Index for each time period. a) Maximum daily wind speed (m/s); b) Drought Factor (AU); c) Maximum daily temperature; d) Daily minimum relative humidity (%). As wind speed is not projected to change significantly, the key drivers of change are temperature, humidity and drought factor. Drought factor has strong correlations with temperature change.

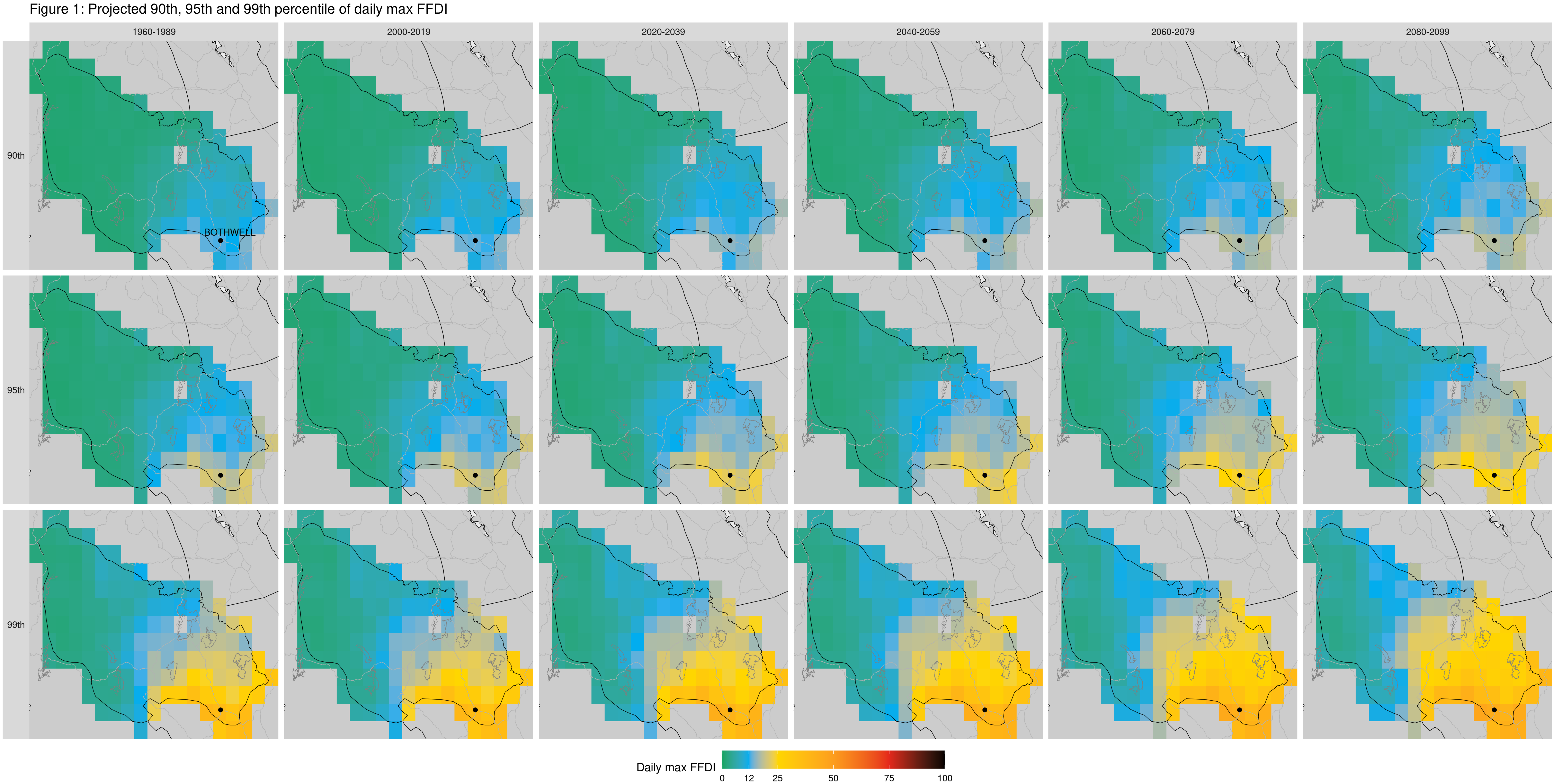


Figure 1: Projected 90th, 95th and 99th percentile values of *Forest Fire Danger Index* for the 30-year baseline period, and then 20-year time periods from 2001 to 2100. Each grid cell is the mean of the 6 ensemble members. The 99th percentile value reflects the 4th highest FFDI value year; the 95th percentile is the 18th highest FFDI value year; and the 90th percentile is the 36th highest FFDI value year. Extreme values of FFDI are expected to increase steadily into the future.

Figure 2: Projected change in 90th, 95th and 99th percentile of daily max FFDI

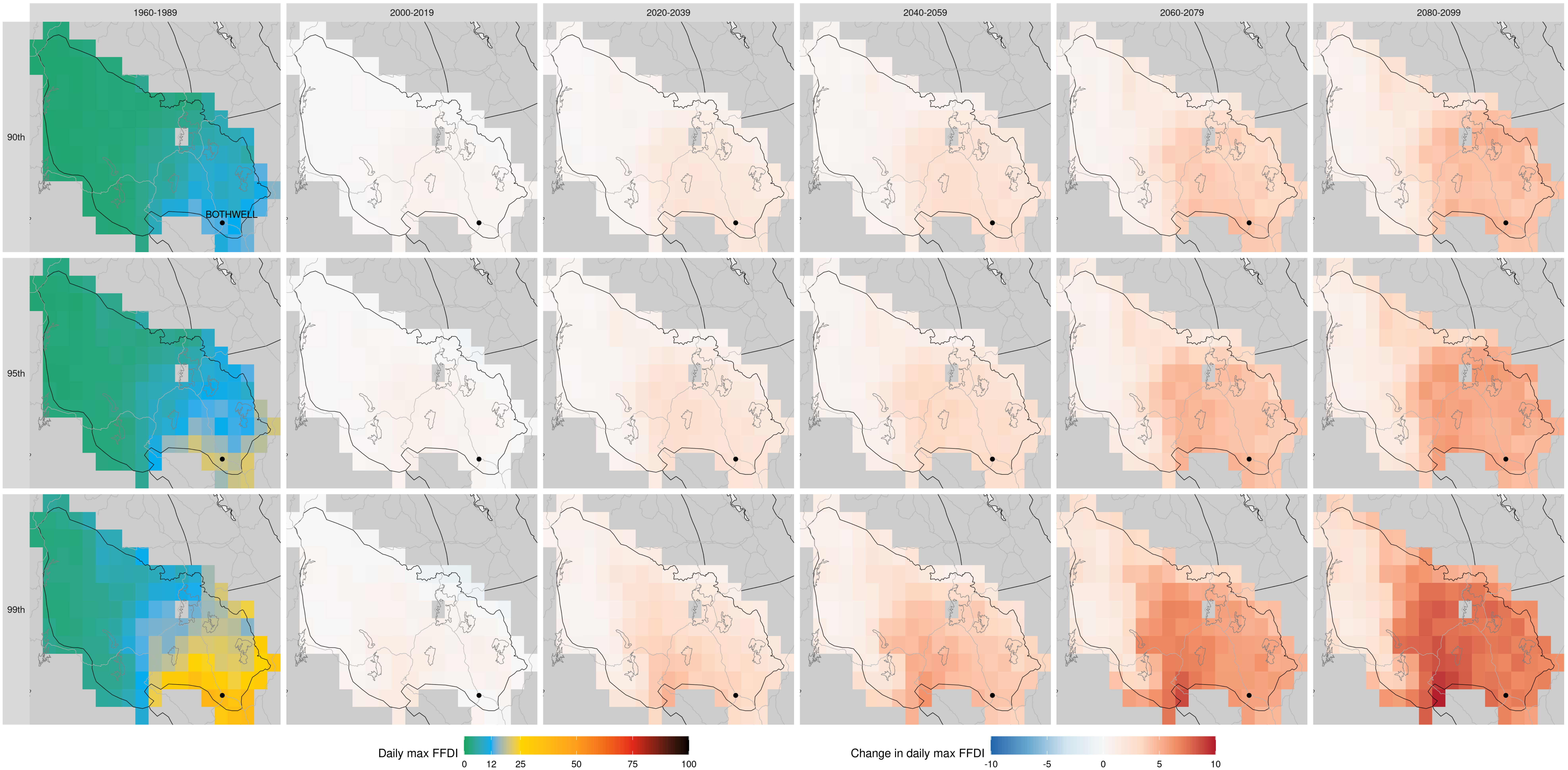


Figure 2: Projected change in the 90th, 95th and 99th percentile values of *Forest Fire Danger Index* for 20-year time periods from 2001 to 2100 compared to the 30-year baseline period 1961–1990. Each grid cell is the mean of the 6 ensemble members. The 99th percentile value reflects the 4th highest FFDI value year; the 95th percentile is the 18th highest FFDI value year; and the 90th percentile is the 36th highest FFDI value year. Extreme values of FFDI are expected to increase steadily into the future

Figure 3: Projected monthly FFDI with outliers removed

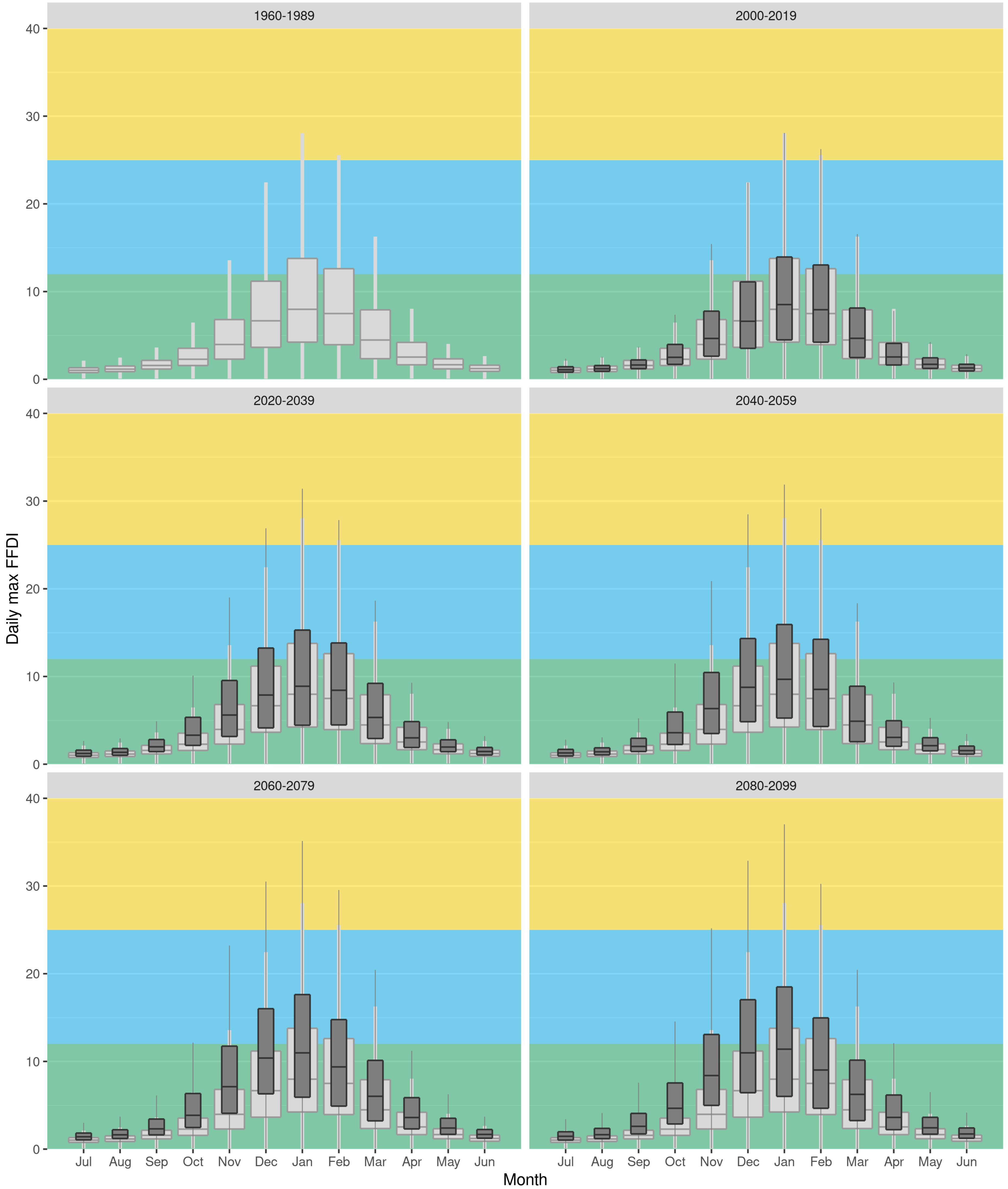


Figure 3: Boxplots of daily *Forest Fire Danger Index* for each month for the 30-year baseline period, and then 20-year periods from 2001 to 2100. Each boxplot represents a summary of daily data for each grid cell, for each of the 6 ensemble members within the time period; e.g. the top-left panel, the January boxplot represents the daily FFDI values for all January days in the period 1961–1990, for all grids cell in the region, for each of the 6 ensemble members. The baseline period (1961-1990) has been shadowed (*light grey*) underneath future time periods to highlight any differences expected into the future. Solid bars represent the median value. The box represents the 25th and 75th percentiles. The Whiskers represent the 1.5× the inter-quartile range. All months in all periods frequently have days of very low FFDI. Outliers have been excluded. If the boxplot shifts higher (lower) this indicates a change towards more (less) dangerous conditions.

Figure 4: Projected monthly FFDI with outliers shown

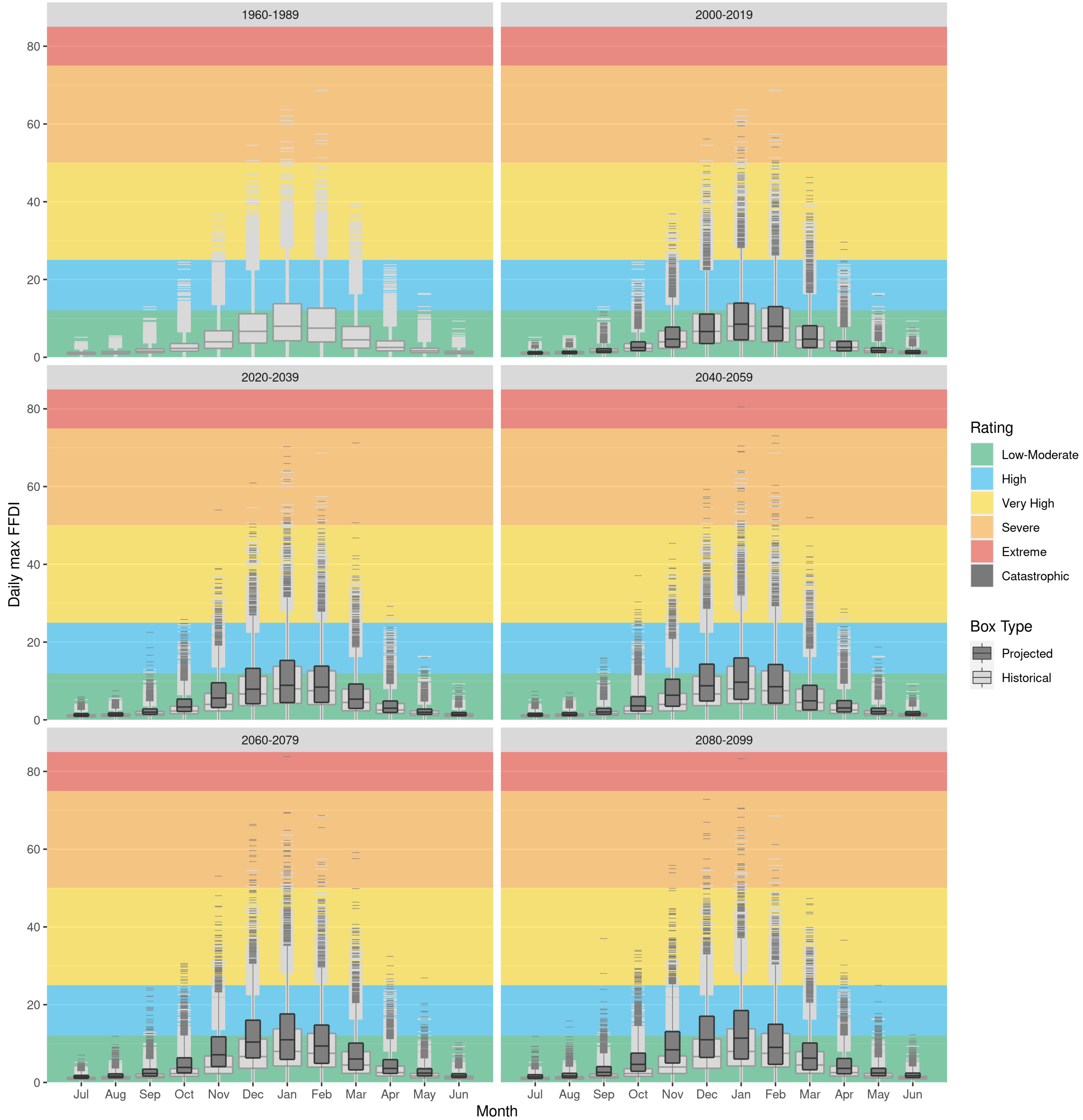


Figure 4: Boxplots of daily *Forest Fire Danger Index* for each month for the 30-year baseline period, and then 20-year periods from 2001 to 2100. Each boxplot represents daily data for each grid cell, for each of the 6 ensemble members within the time period; e.g. ing the top-left panel, the January boxplot represents the daily FFDI values for all January days in the period 1961–1990, for all grids cell in the region, for each of the 6 ensemble members. The baseline period (1961-1990) has been shadowed (*light grey*) underneath future time periods to highlight any differences expected into the future. Solid bars represent the median value. The box represents the 25th and 75th percentiles. The Whiskers represent the 1.5× the inter-quartile range. All months in all periods frequently have days of very low FFDI. Outliers are values > 1.5× the interquartile range and are represented as a dash(-): *light grey* for historical; *dark grey* for other time periods. If the boxplot shifts higher (lower) this indicates a change towards more (less) dangerous conditions.

# CENTRAL PLATEAU

## Bushfires — Timeseries

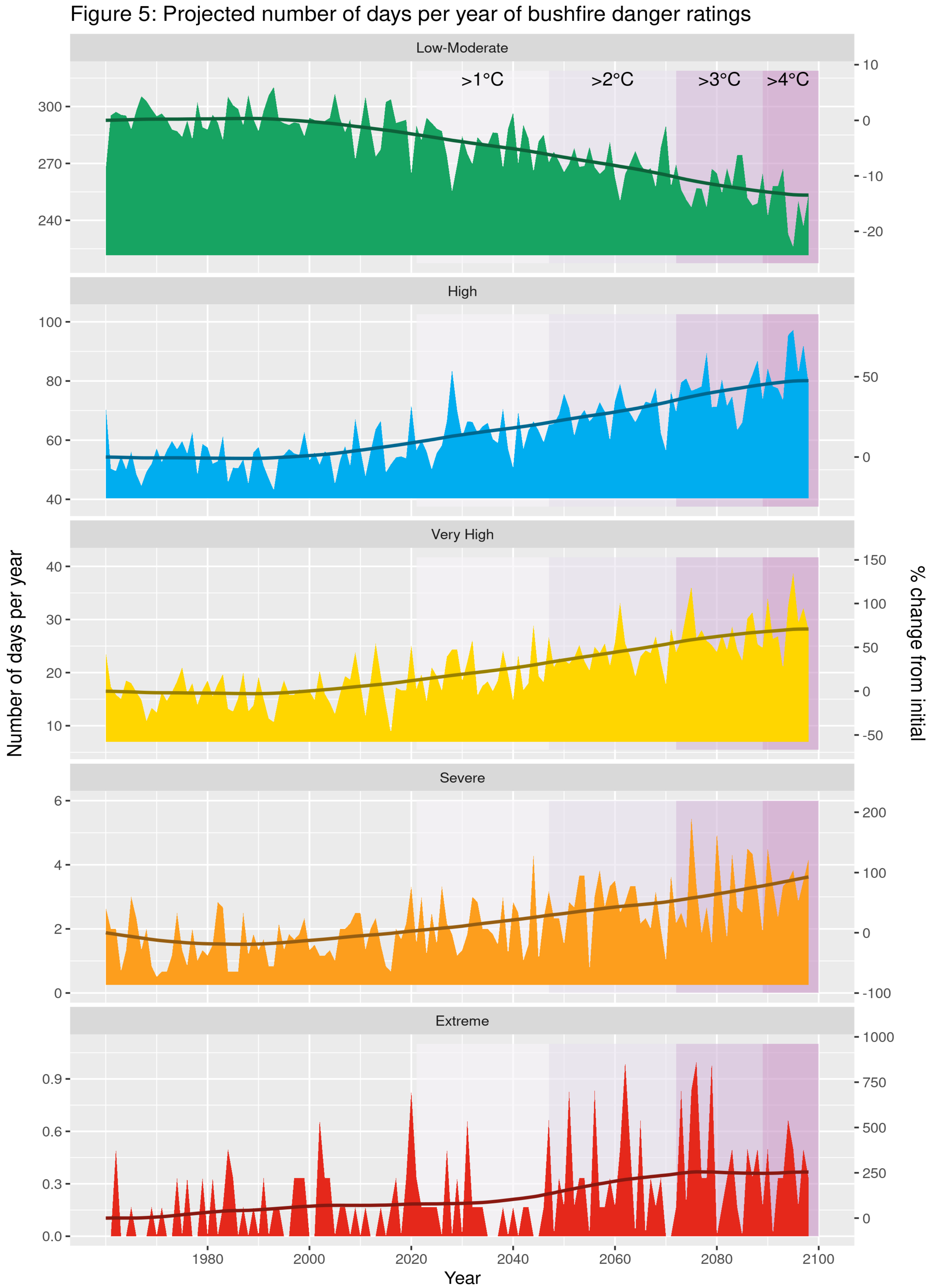


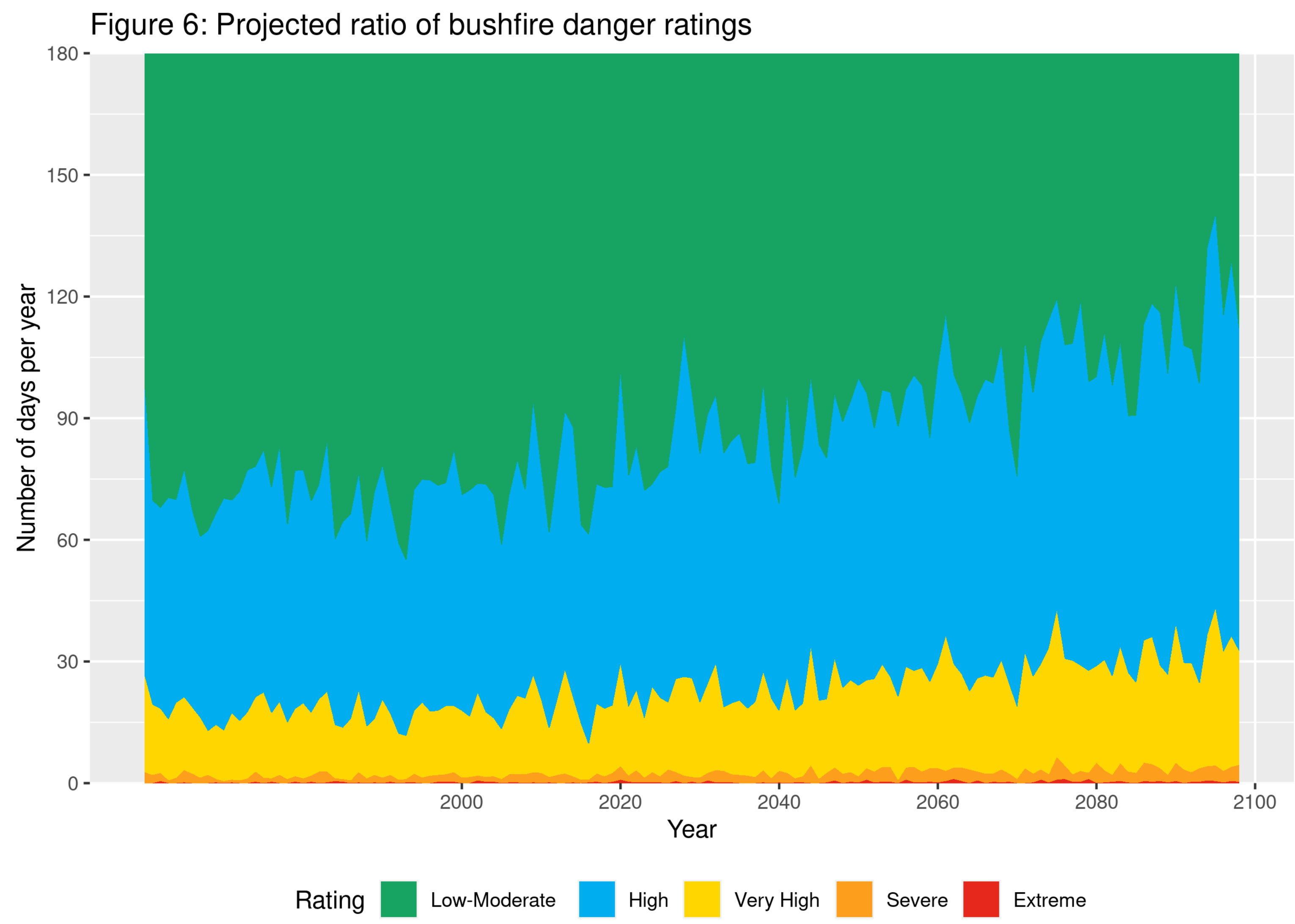


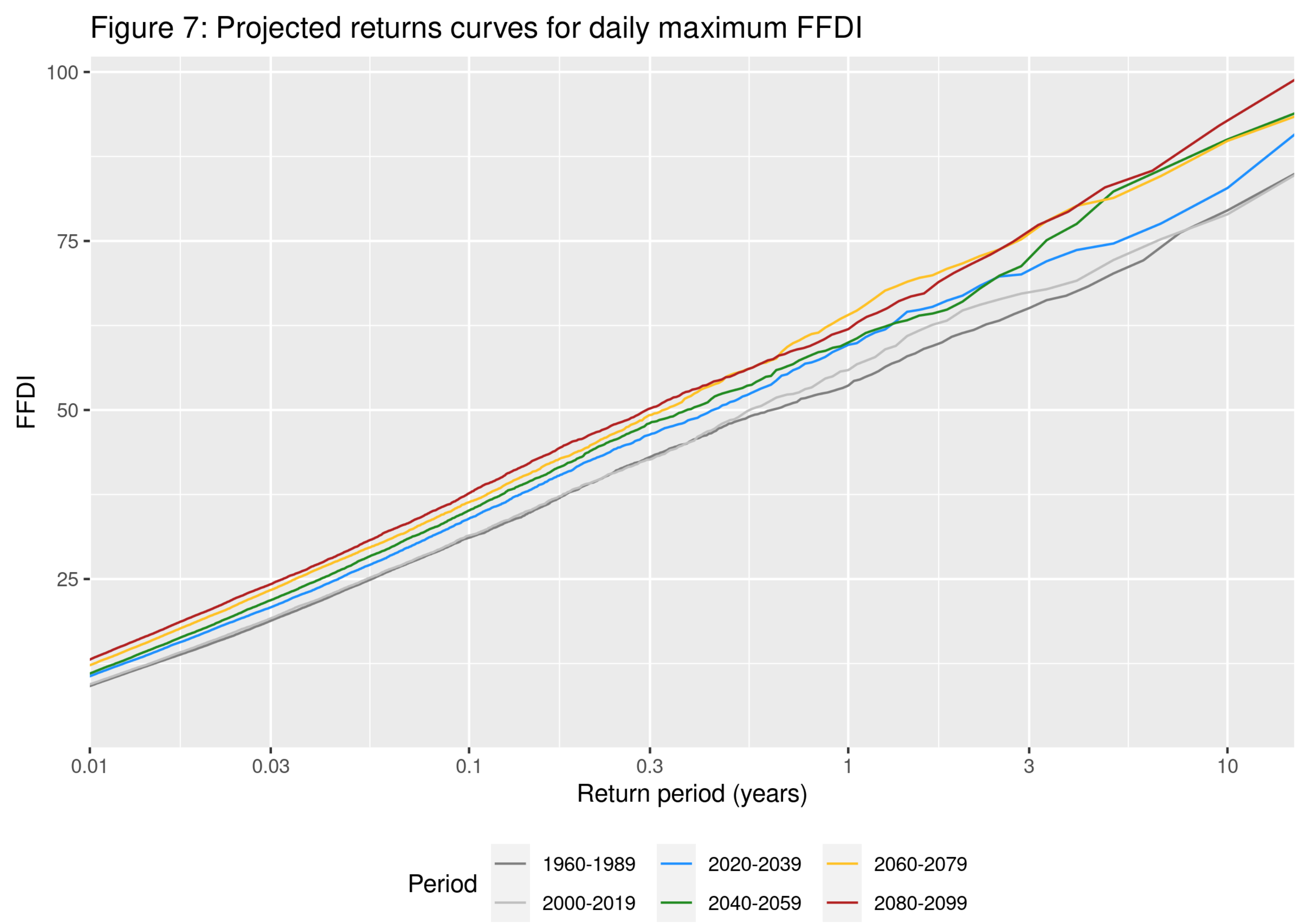


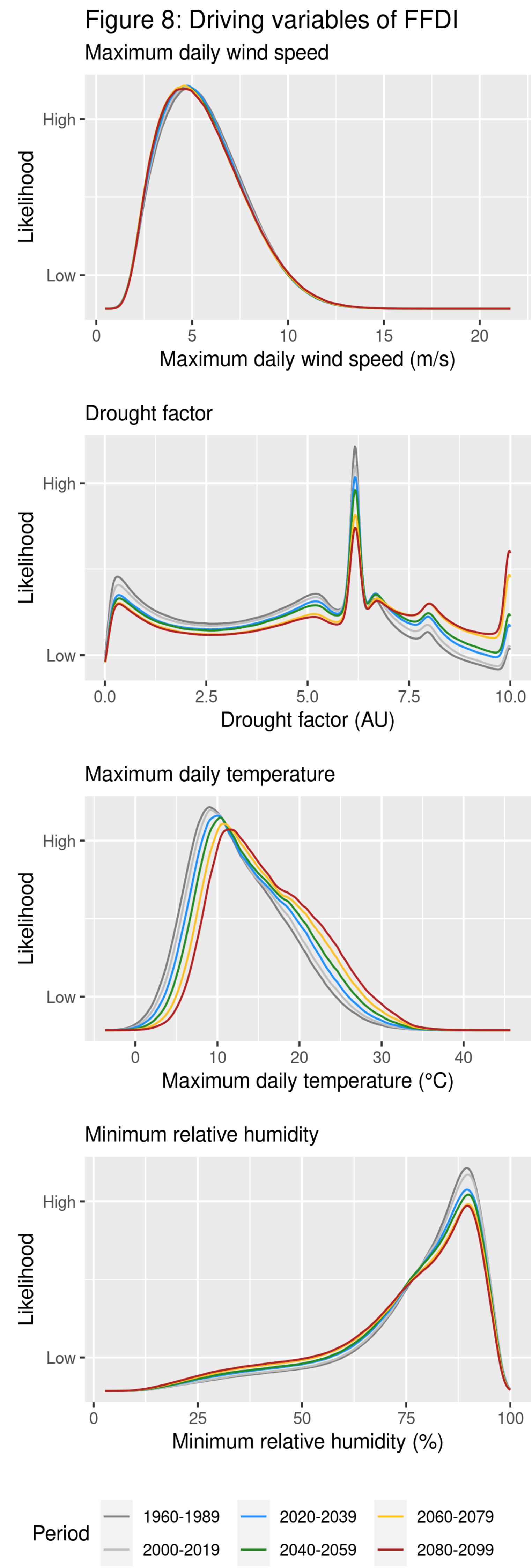


Figure 5: Time series of the ensemble-mean for the 30-year rolling mean of the number of days per year with fire danger ratings of *Low-Moderate*, *High*, *Very High*, *Severe*, *Extreme* from 1990 to 2100 (NB: *Catastrophic* had frequencies too low to reasonably present here). As every day has a fire danger rating, *Low-Moderate* rating frequencies decrease as they are replaced by higher categories.

Figure 6: Stacked area plot of the 30-year ensemble mean number of days of each forest fire danger index rating across each fire-season (October to April, 180 days) from 1990 to 2100. Decreased frequency of *Low-Moderate* days is due to increases in *High* or *Very High* categories.

Figure 7: Annual return periods for Forest Fire Danger Index values for the 30-year baseline period (1961-1990) and 20-year time periods from 2001 to 2100.

Figure 8: Distribution of values for each of the underlying drivers of Forest Fire Danger Index for each time period. a) Maximum daily wind speed (m/s); b) Drought Factor (AU); c) Maximum daily temperature; d) Daily minimum relative humidity (%). As wind speed is not projected to change significantly, the key drivers of change are temperature, humidity and drought factor. Drought factor has strong correlations with temperature change.

Figure 1: Projected 90th, 95th and 99th percentile of daily max FFDI

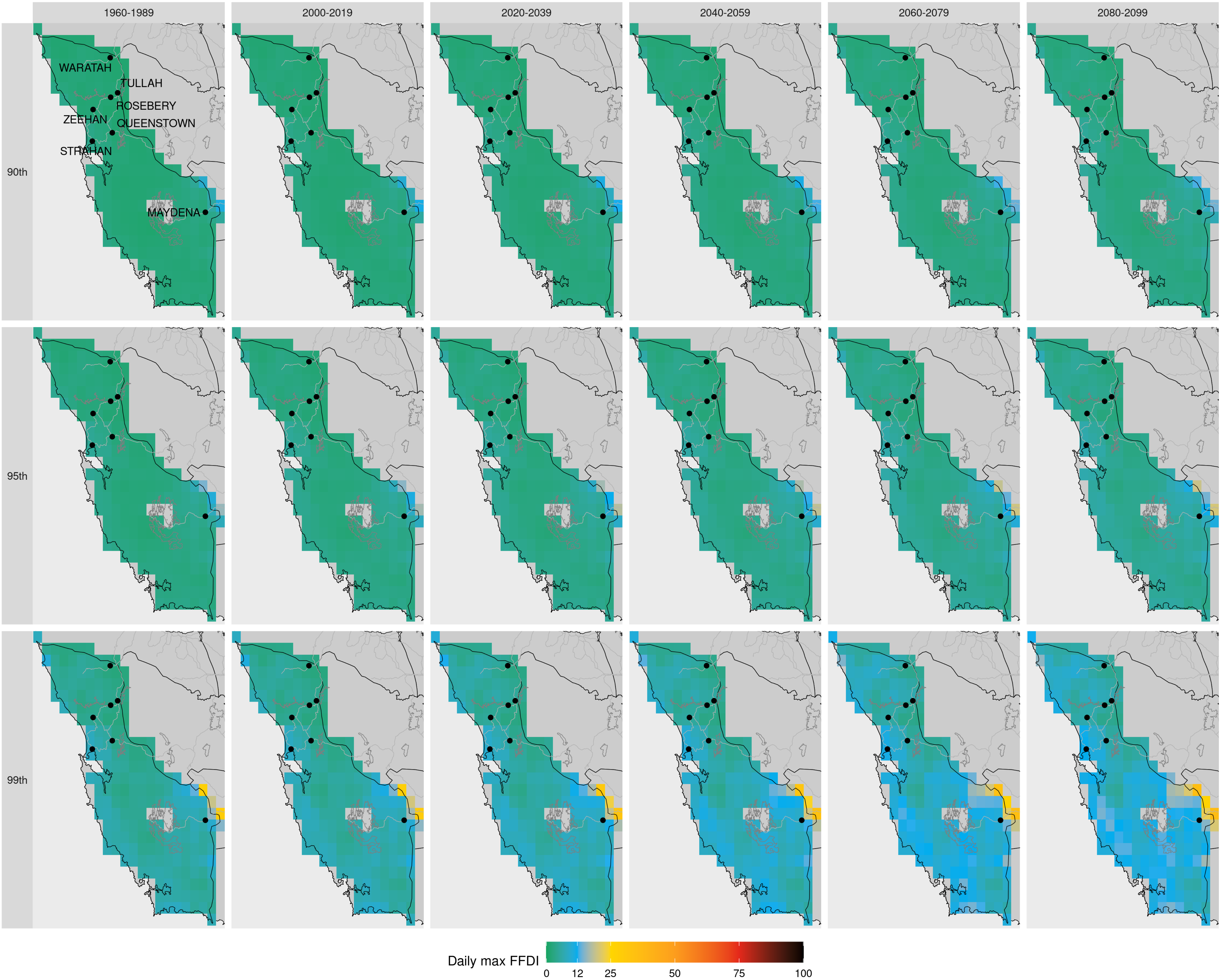


Figure 1: Projected 90th, 95th and 99th percentile values of *Forest Fire Danger Index* for the 30-year baseline period, and then 20-year time periods from 2001 to 2100. Each grid cell is the mean of the 6 ensemble members. The 99th percentile value reflects the 4th highest FFDI value year; the 95th percentile is the 18th highest FFDI value year; and the 90th percentile is the 36th highest FFDI value year. Extreme values of FFDI are expected to increase steadily into the future.

Figure 2: Projected change in 90th, 95th and 99th percentile of daily max FFDI

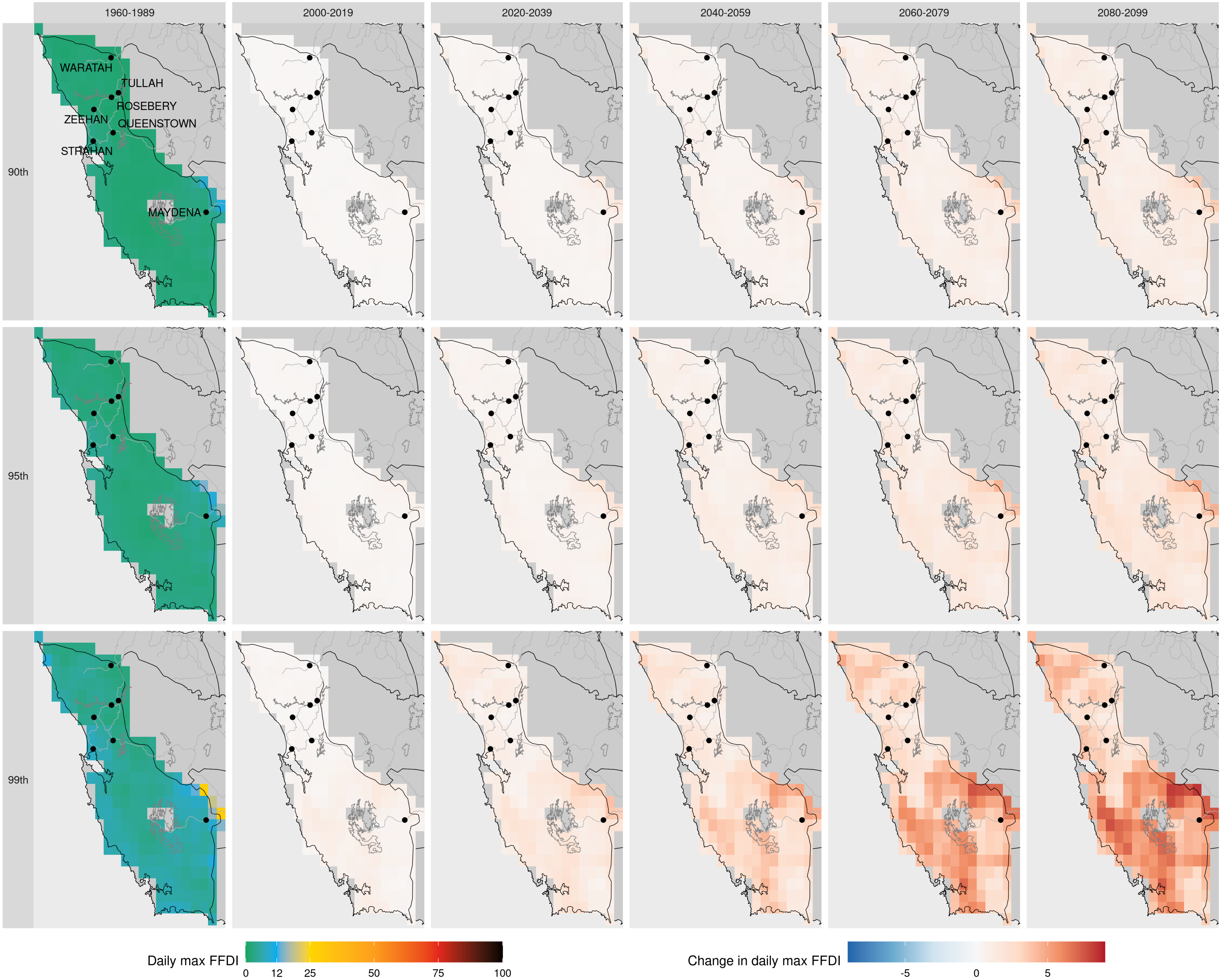


Figure 2: Projected change in the 90th, 95th and 99th percentile values of *Forest Fire Danger Index* for 20-year time periods from 2001 to 2100 compared to the 30-year baseline period 1961–1990. Each grid cell is the mean of the 6 ensemble members. The 99th percentile value reflects the 4th highest FFDI value year; the 95th percentile is the 18th highest FFDI value year; and the 90th percentile is the 36th highest FFDI value year. Extreme values of FFDI are expected to increase steadily into the future

Figure 3: Projected monthly FFDI with outliers removed

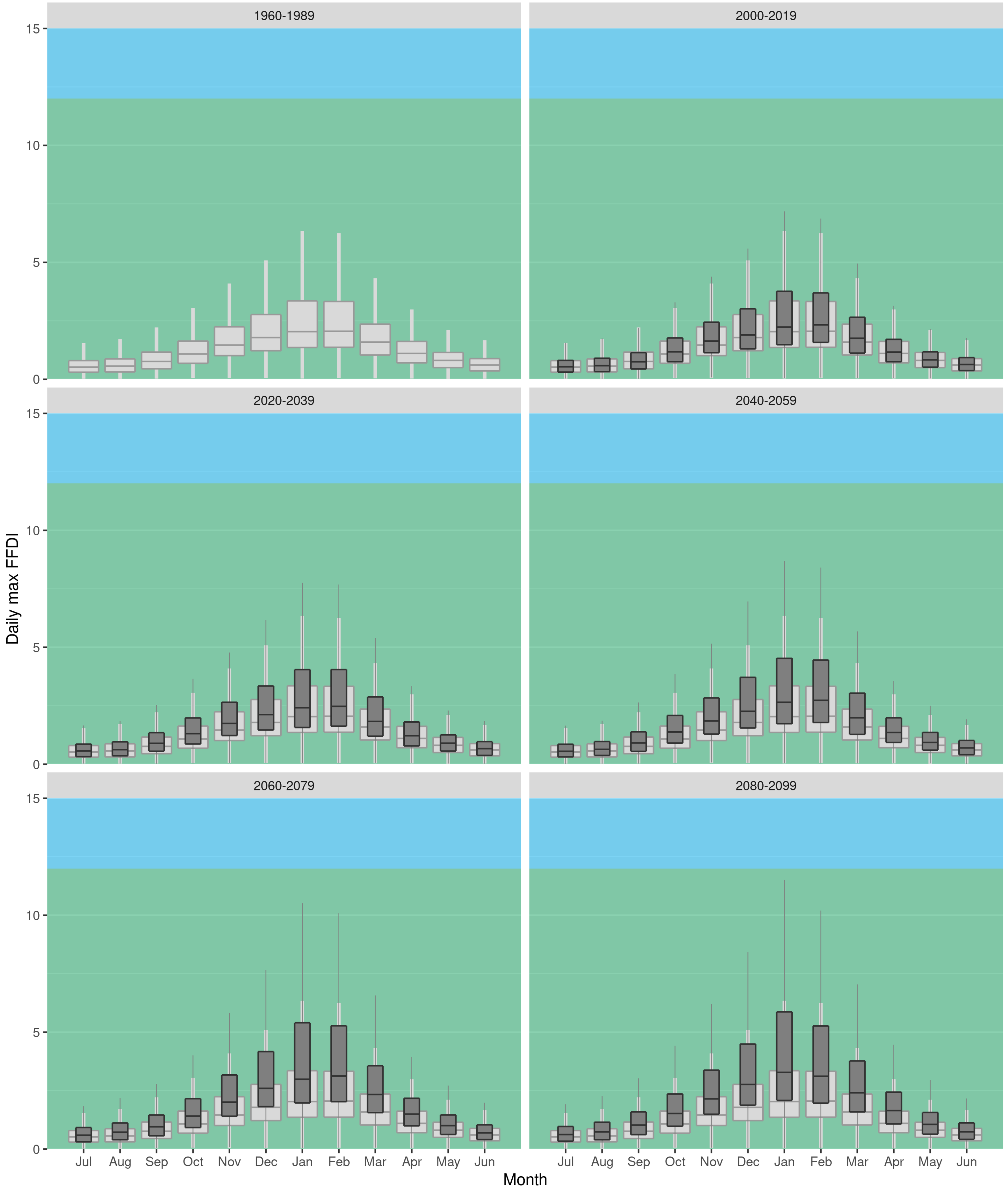


Figure 4: Projected monthly FFDI with outliers shown

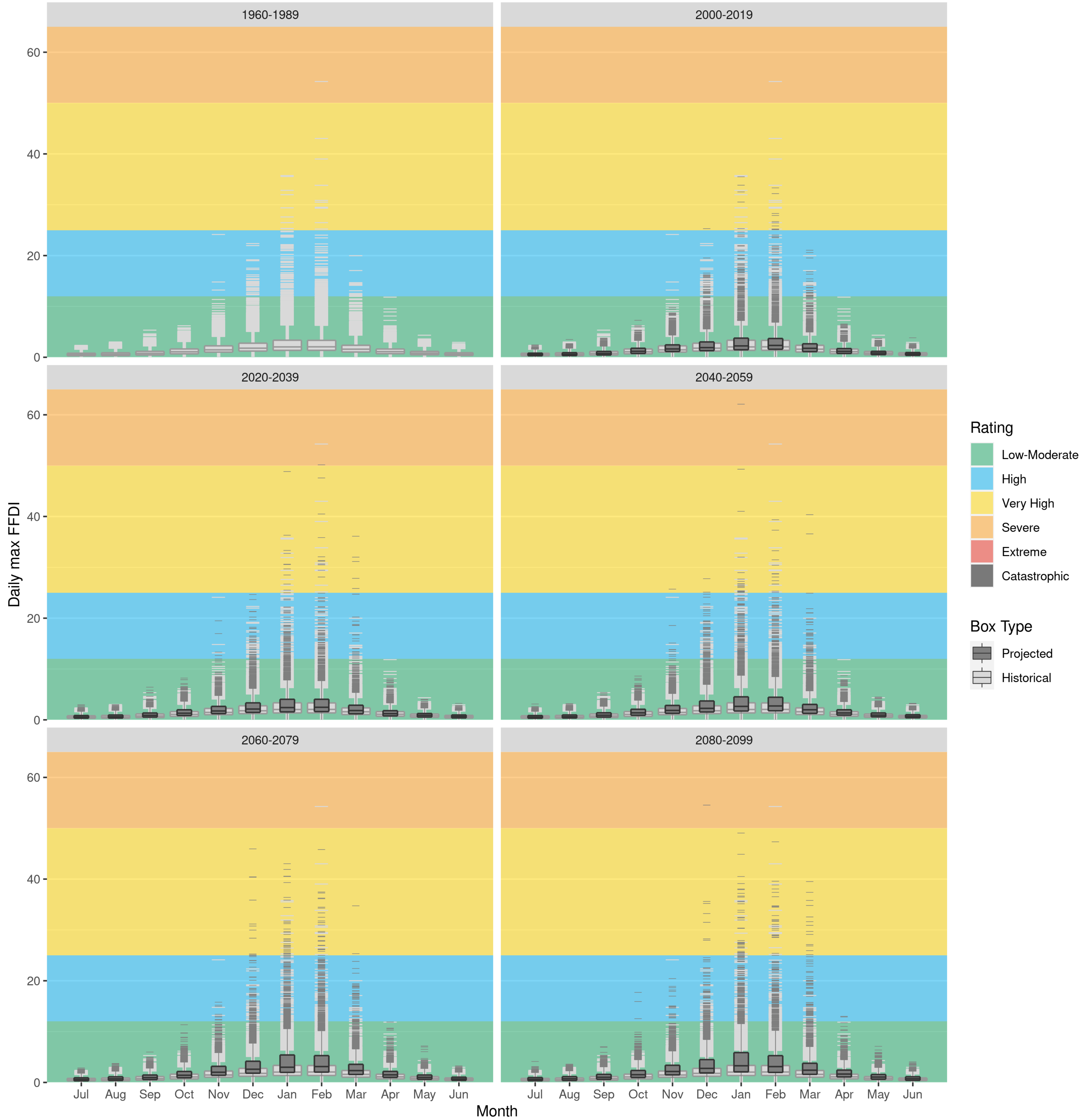


Figure 3: Boxplots of daily *Forest Fire Danger Index* for each month for the 30-year baseline period, and then 20-year periods from 2001 to 2100. Each boxplot represents a summary of daily data for each grid cell, for each of the 6 ensemble members within the time period; e.g. the top-left panel, the January boxplot represents the daily FFDI values for all January days in the period 1961–1990, for all grids cell in the region, for each of the 6 ensemble members. The baseline period (1961-1990) has been shadowed (*light grey*) underneath future time periods to highlight any differences expected into the future. Solid bars represent the median value. The box represents the 25th and 75th percentiles. The Whiskers represent the 1.5× the inter-quartile range. All months in all periods frequently have days of very low FFDI. Outliers have been excluded. If the boxplot shifts higher (lower) this indicates a change towards more (less) dangerous conditions.

Figure 4: Boxplots of daily *Forest Fire Danger Index* for each month for the 30-year baseline period, and then 20-year periods from 2001 to 2100. Each boxplot represents daily data for each grid cell, for each of the 6 ensemble members within the time period; e.g. ing the top-left panel, the January boxplot represents the daily FFDI values for all January days in the period 1961–1990, for all grids cell in the region, for each of the 6 ensemble members. The baseline period (1961-1990) has been shadowed (*light grey*) underneath future time periods to highlight any differences expected into the future. Solid bars represent the median value. The box represents the 25th and 75th percentiles. The Whiskers represent the 1.5× the inter-quartile range. All months in all periods frequently have days of very low FFDI. Outliers are values > 1.5× the interquartile range and are represented as a dash(-): *light grey* for historical; *dark grey* for other time periods. If the boxplot shifts higher (lower) this indicates a change towards more (less) dangerous conditions.

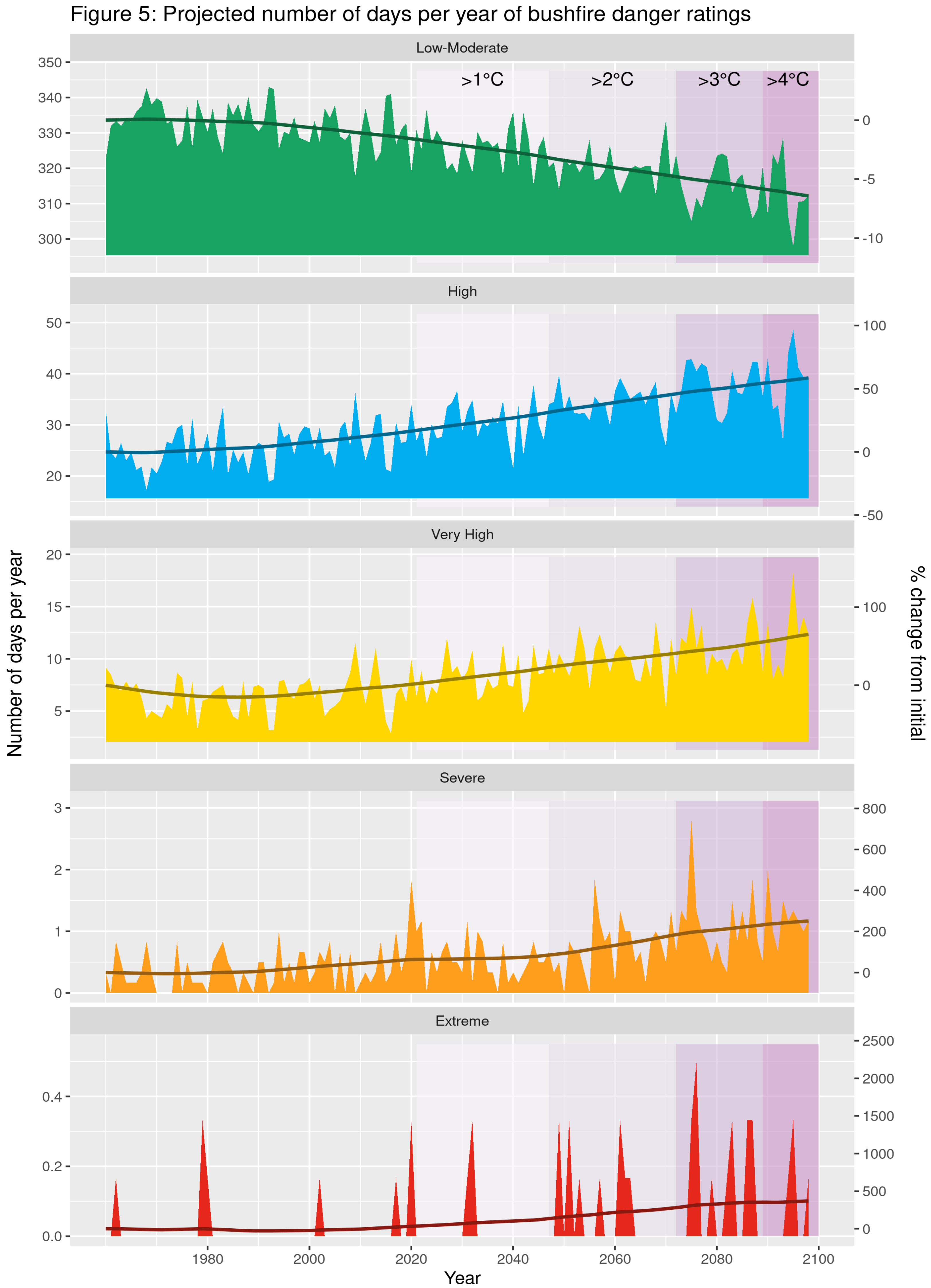


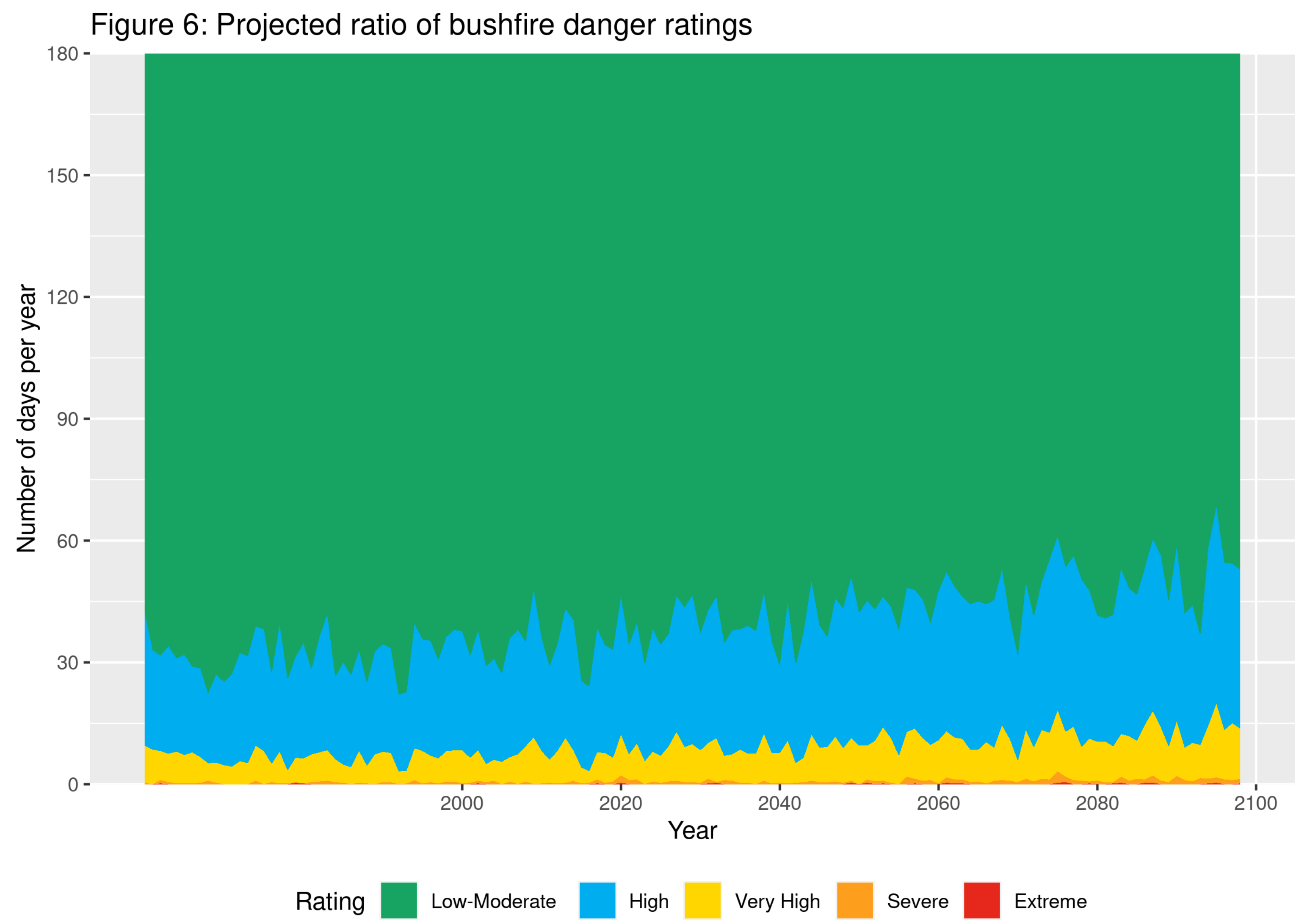


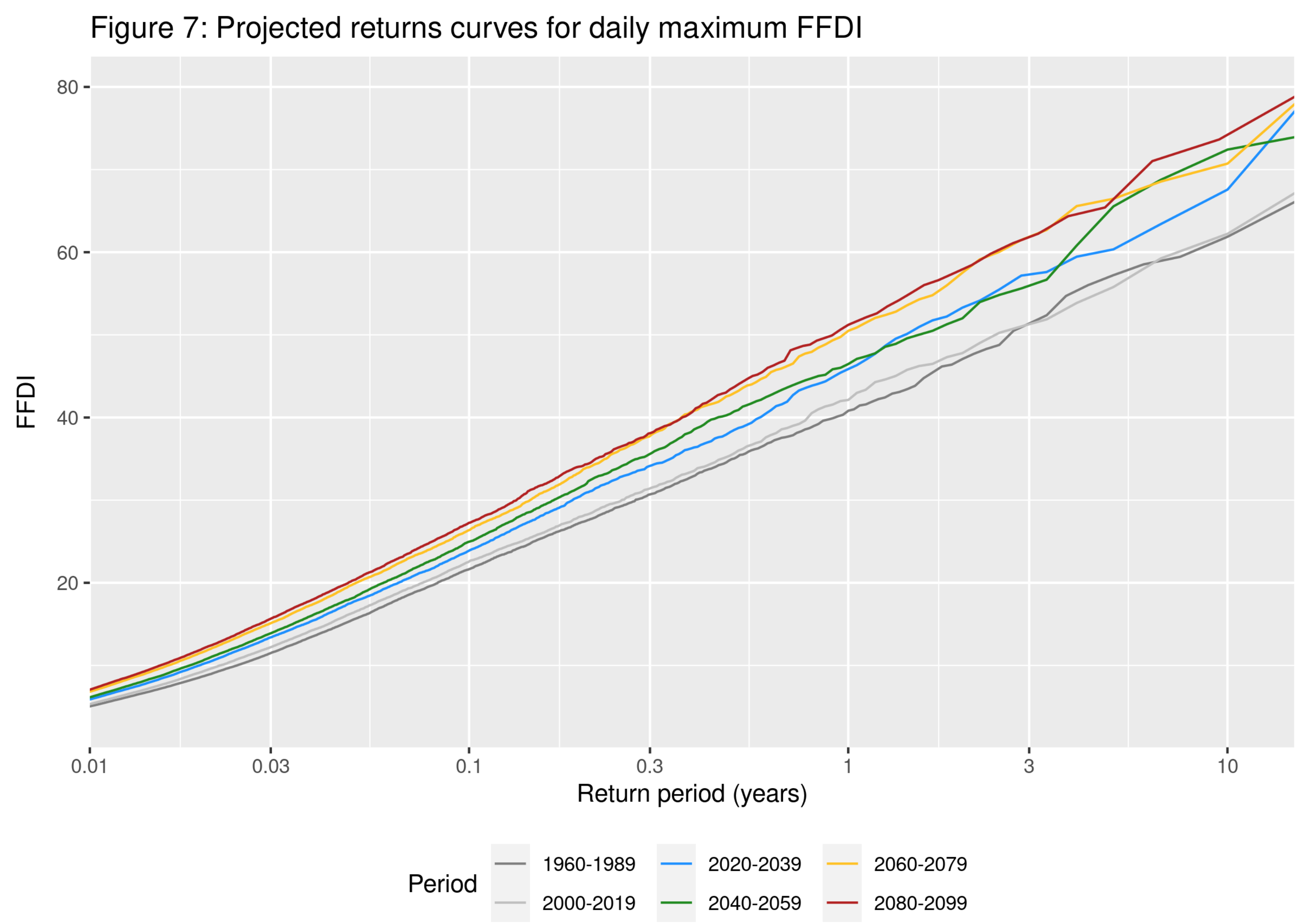


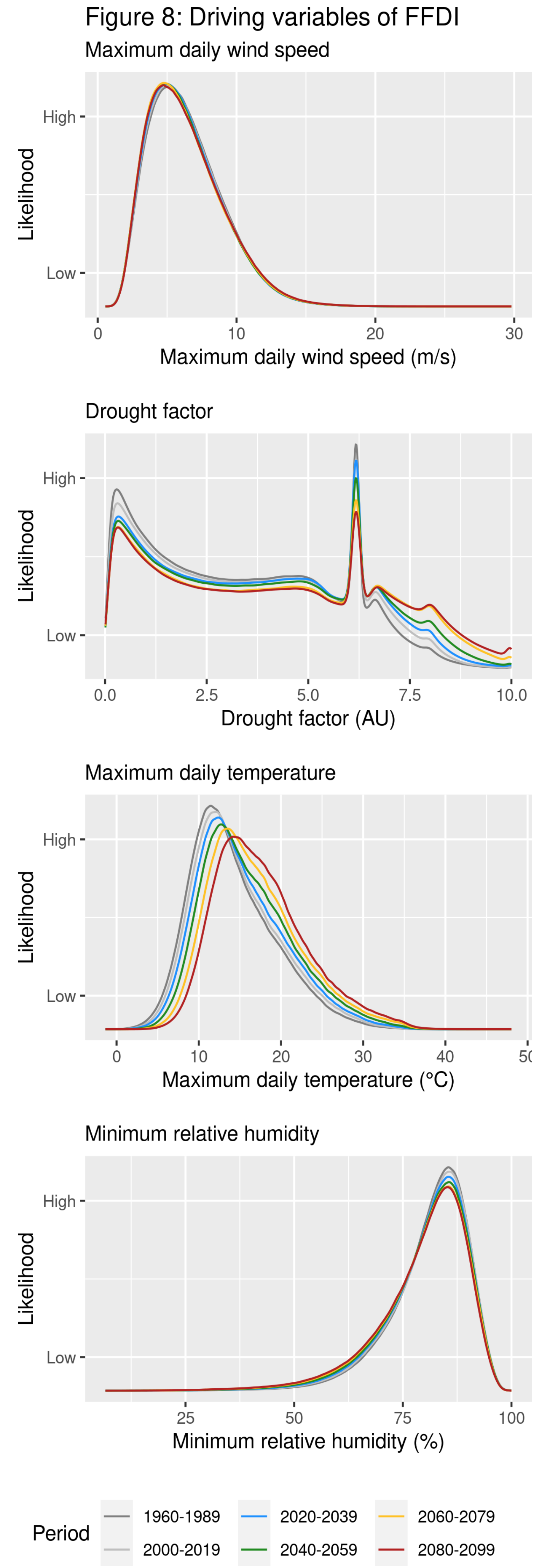


Figure 5: Time series of the ensemble-mean for the 30-year rolling mean of the number of days per year with fire danger ratings of *Low-Moderate, High, Very High, Severe, Extreme* from 1990 to 2100 (NB: *Catastrophic* had frequencies too low to reasonably present here). As every day has a fire danger rating, *Low-Moderate* rating frequencies decrease as they are replaced by higher categories.

Figure 6: Stacked area plot of the 30-year ensemble mean number of days of each forest fire danger index rating across each fire-season (October to April, 180 days) from 1990 to 2100. Decreased frequency of *Low-Moderate* days is due to increases in *High* or *Very High* categories.

Figure 7: Annual return periods for Forest Fire Danger Index values for the 30-year baseline period (1961-1990) and 20-year time periods from 2001 to 2100.

Figure 8: Distribution of values for each of the underlying drivers of Forest Fire Danger Index for each time period. a) Maximum daily wind speed (m/s); b) Drought Factor (AU); c) Maximum daily temperature; d) Daily minimum relative humidity (%). As wind speed is not projected to change significantly, the key drivers of change are temperature, humidity and drought factor. Drought factor has strong correlations with temperature change.

Figure 1: Projected 90th, 95th and 99th percentile of daily max FFDI

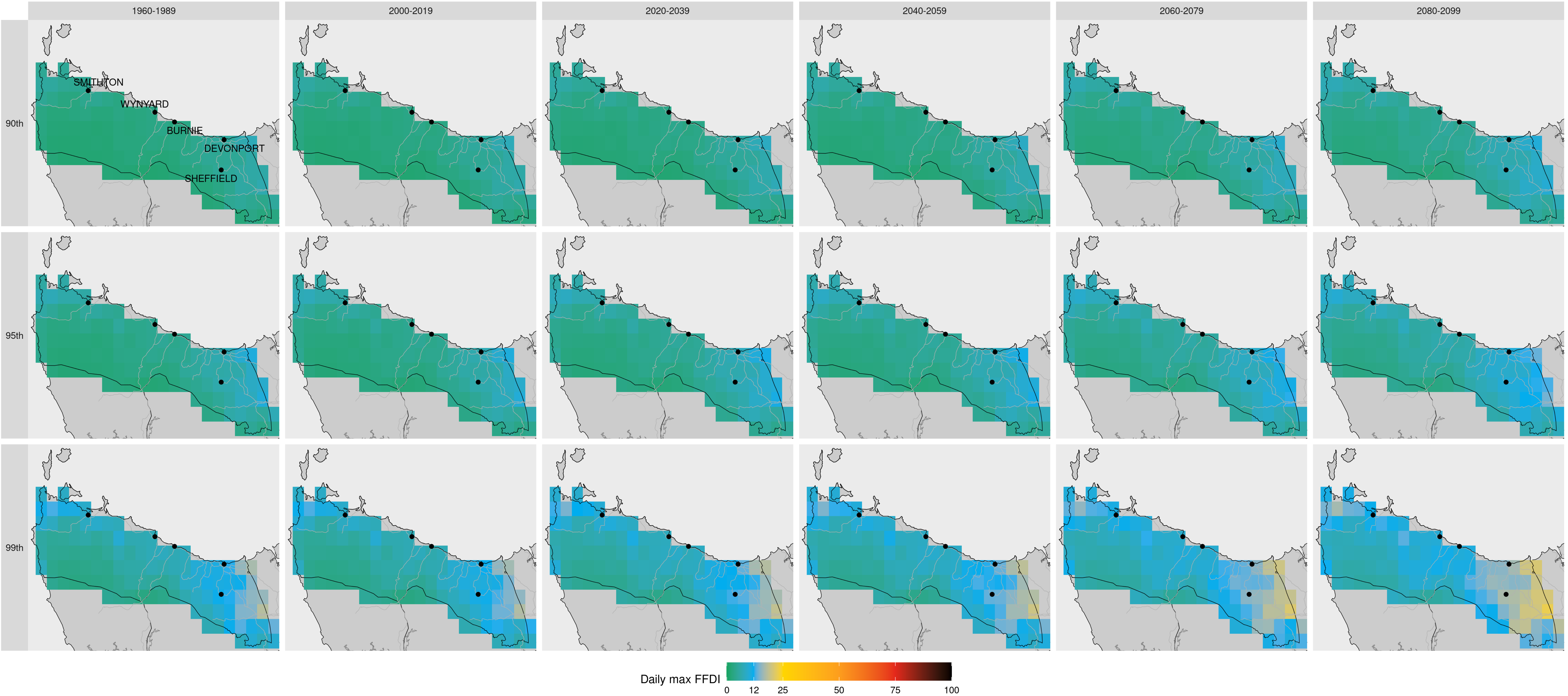


Figure 1: Projected 90th, 95th and 99th percentile values of *Forest Fire Danger Index* for the 30-year baseline period, and then 20-year time periods from 2001 to 2100. Each grid cell is the mean of the 6 ensemble members. The 99th percentile value reflects the 4th highest FFDI value year; the 95th percentile is the 18th highest FFDI value year; and the 90th percentile is the 36th highest FFDI value year. Extreme values of FFDI are expected to increase steadily into the future.

Figure 2: Projected change in 90th, 95th and 99th percentile of daily max FFDI

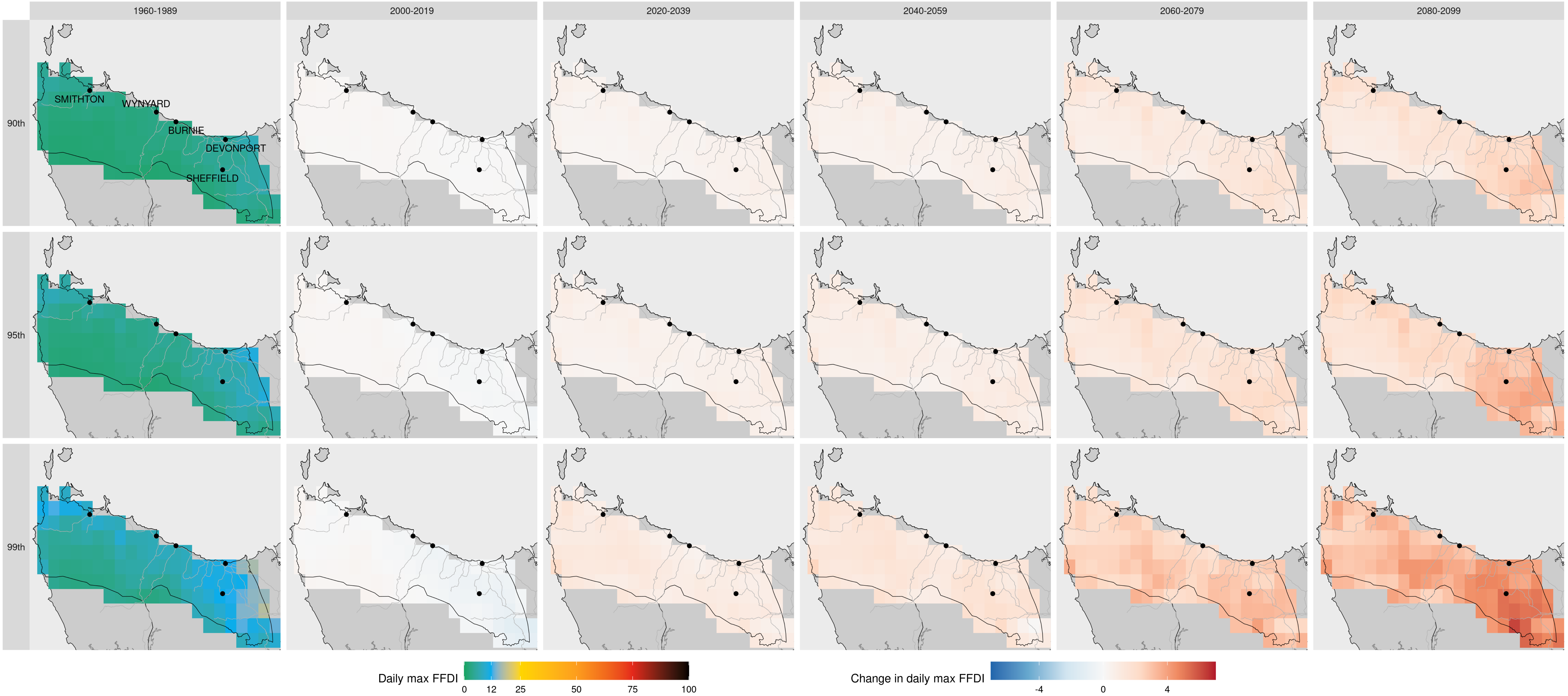


Figure 2: Projected change in the 90th, 95th and 99th percentile values of *Forest Fire Danger Index* for 20-year time periods from 2001 to 2100 compared to the 30-year baseline period 1961–1990. Each grid cell is the mean of the 6 ensemble members. The 99th percentile value reflects the 4th highest FFDI value year; the 95th percentile is the 18th highest FFDI value year; and the 90th percentile is the 36th highest FFDI value year. Extreme values of FFDI are expected to increase steadily into the future

Figure 3: Projected monthly FFDI with outliers removed

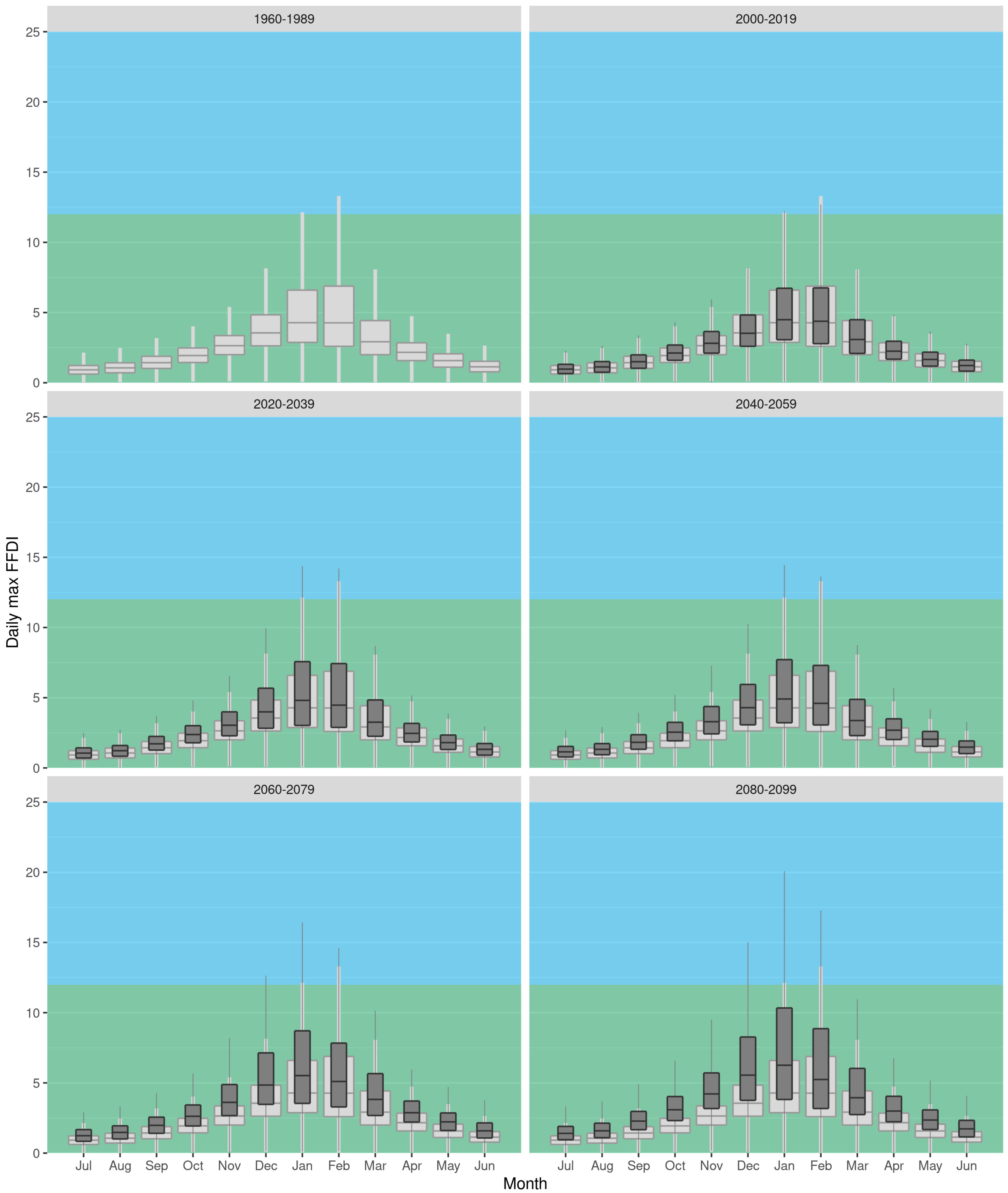


Figure 4: Projected monthly FFDI with outliers shown

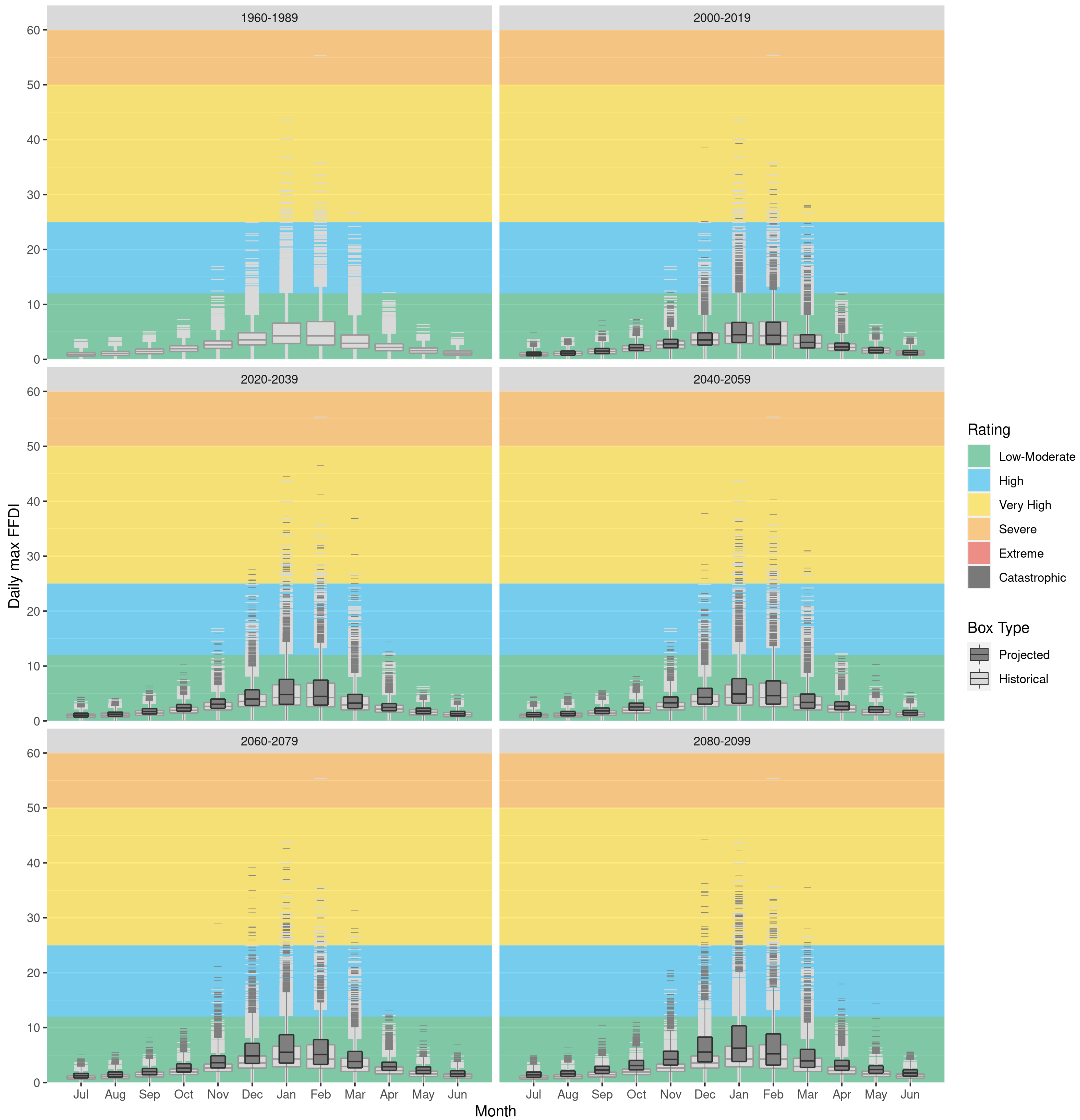


Figure 3: Boxplots of daily *Forest Fire Danger Index* for each month for the 30-year baseline period, and then 20-year periods from 2001 to 2100. Each boxplot represents a summary of daily data for each grid cell, for each of the 6 ensemble members within the time period; e.g. the top-left panel, the January boxplot represents the daily FFDI values for all January days in the period 1961–1990, for all grids cell in the region, for each of the 6 ensemble members. The baseline period (1961-1990) has been shadowed (*light grey*) underneath future time periods to highlight any differences expected into the future. Solid bars represent the median value. The box represents the 25th and 75th percentiles. The Whiskers represent the 1.5× the inter-quartile range. All months in all periods frequently have days of very low FFDI. Outliers have been excluded. If the boxplot shifts higher (lower) this indicates a change towards more (less) dangerous conditions.

Figure 4: Boxplots of daily *Forest Fire Danger Index* for each month for the 30-year baseline period, and then 20-year periods from 2001 to 2100. Each boxplot represents daily data for each grid cell, for each of the 6 ensemble members within the time period; e.g. ing the top-left panel, the January boxplot represents the daily FFDI values for all January days in the period 1961–1990, for all grids cell in the region, for each of the 6 ensemble members. The baseline period (1961-1990) has been shadowed (*light grey*) underneath future time periods to highlight any differences expected into the future. The box represents the 25th and 75th percentiles. The Whiskers represent the 1.5× the inter-quartile range. All months in all periods frequently have days of very low FFDI. Outliers are values > 1.5× the interquartile range and are represented as a dash(-): *light grey* for historical; *dark grey* for other time periods. If the boxplot shifts higher (lower) this indicates a change towards more (less) dangerous conditions.

Figure 5: Projected number of days per year of bushfire danger ratings

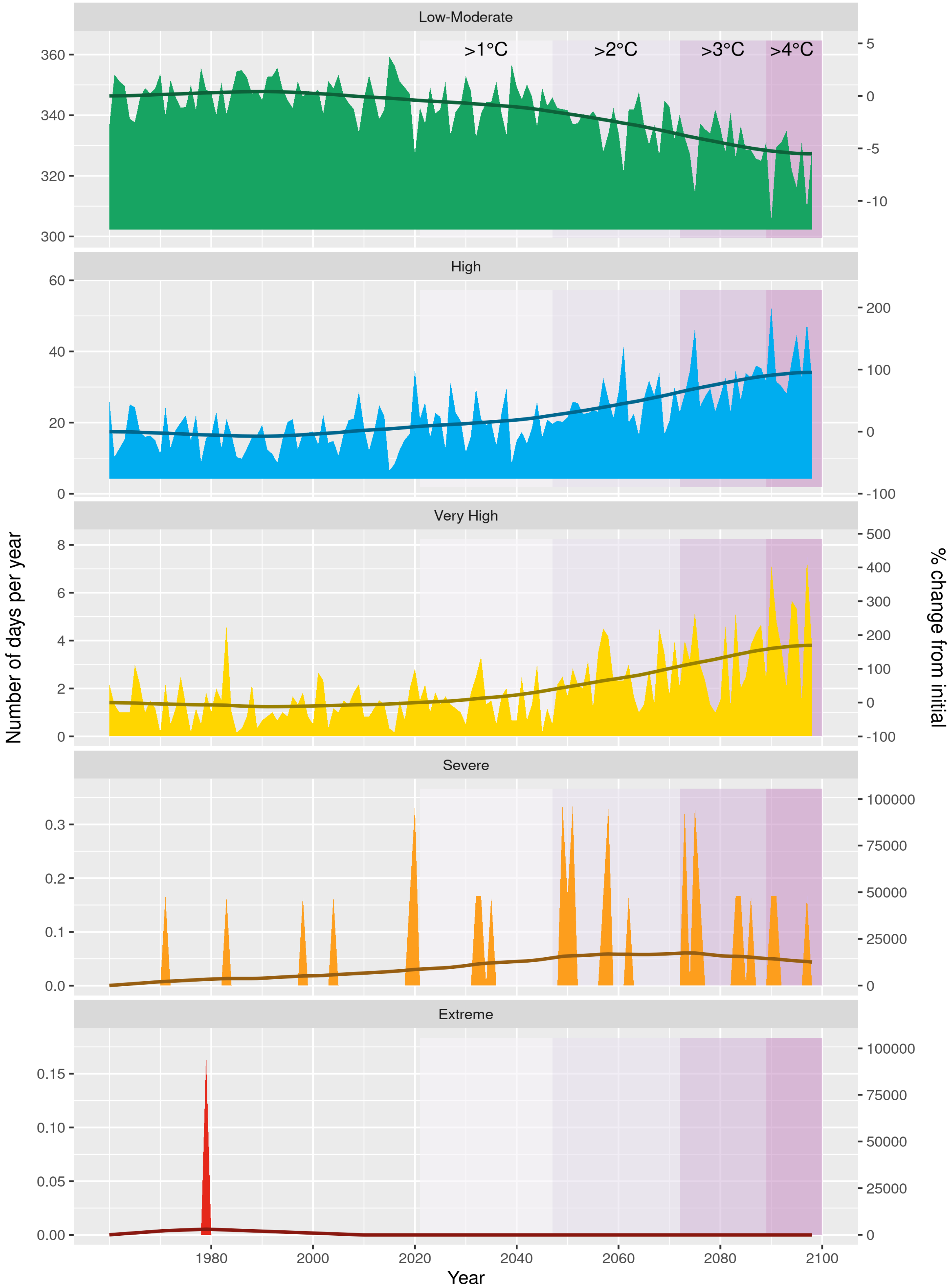


Figure 6: Projected ratio of bushfire danger ratings

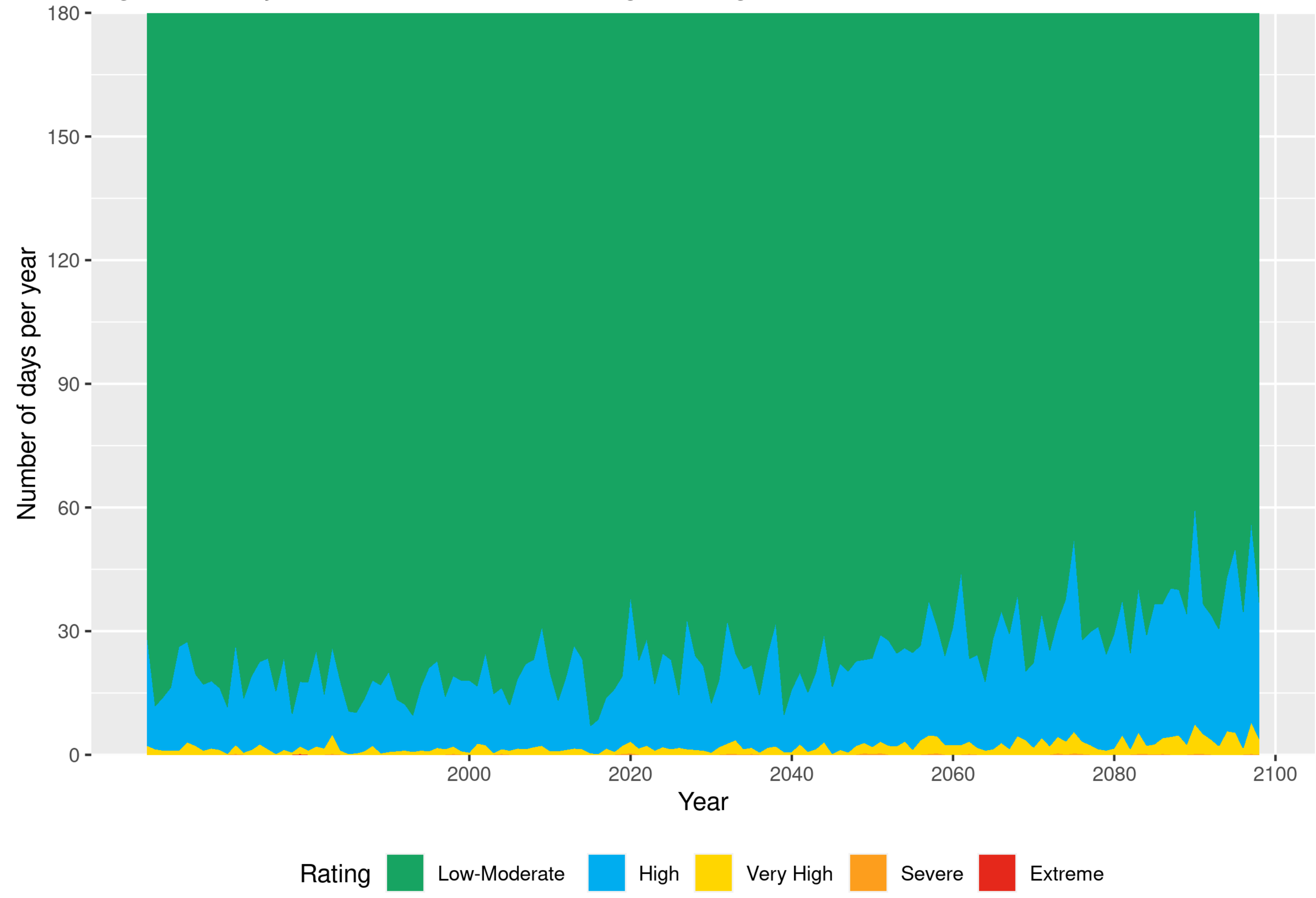


Figure 7: Projected returns curves for daily maximum FFDI

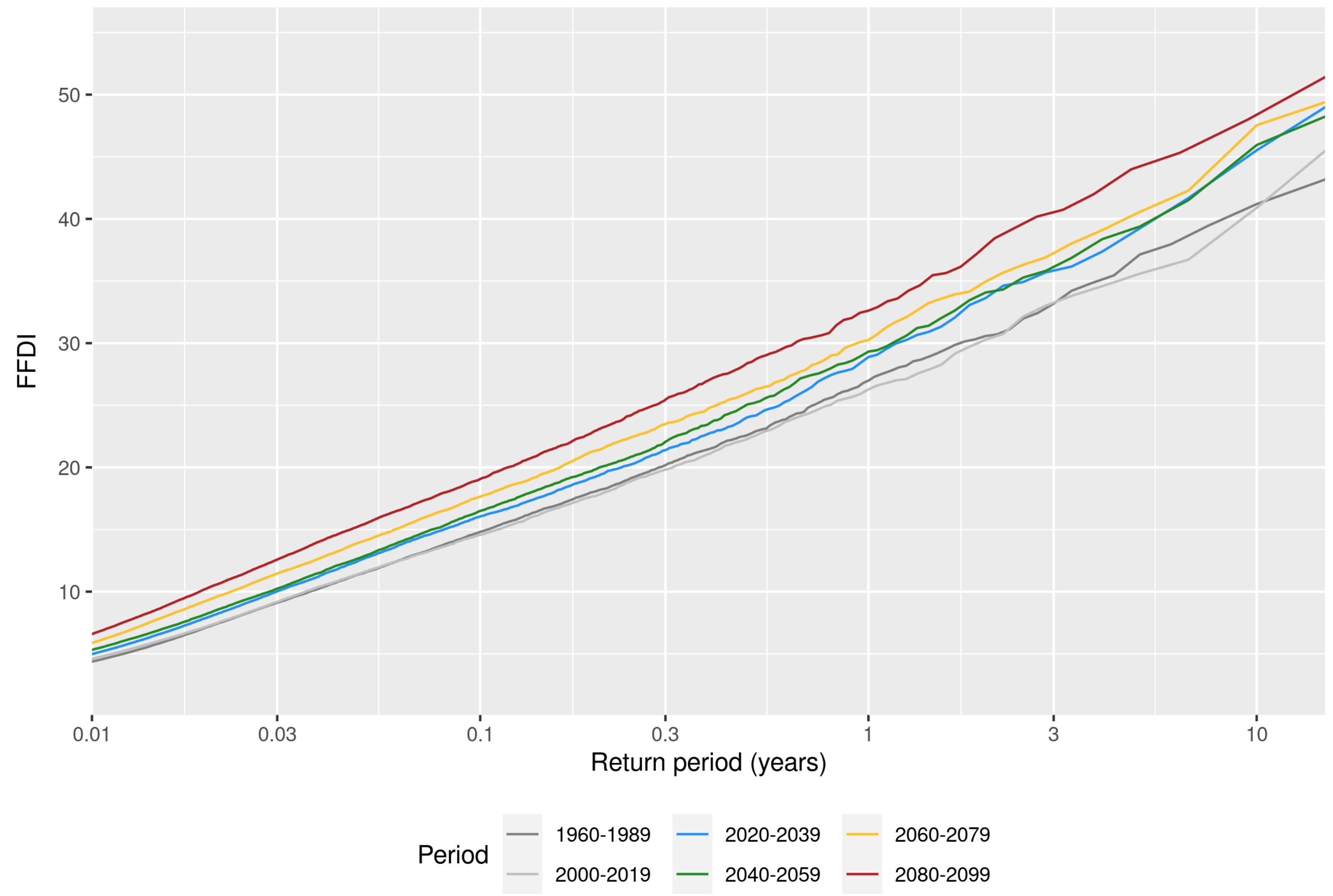


Figure 8: Driving variables of FFDI

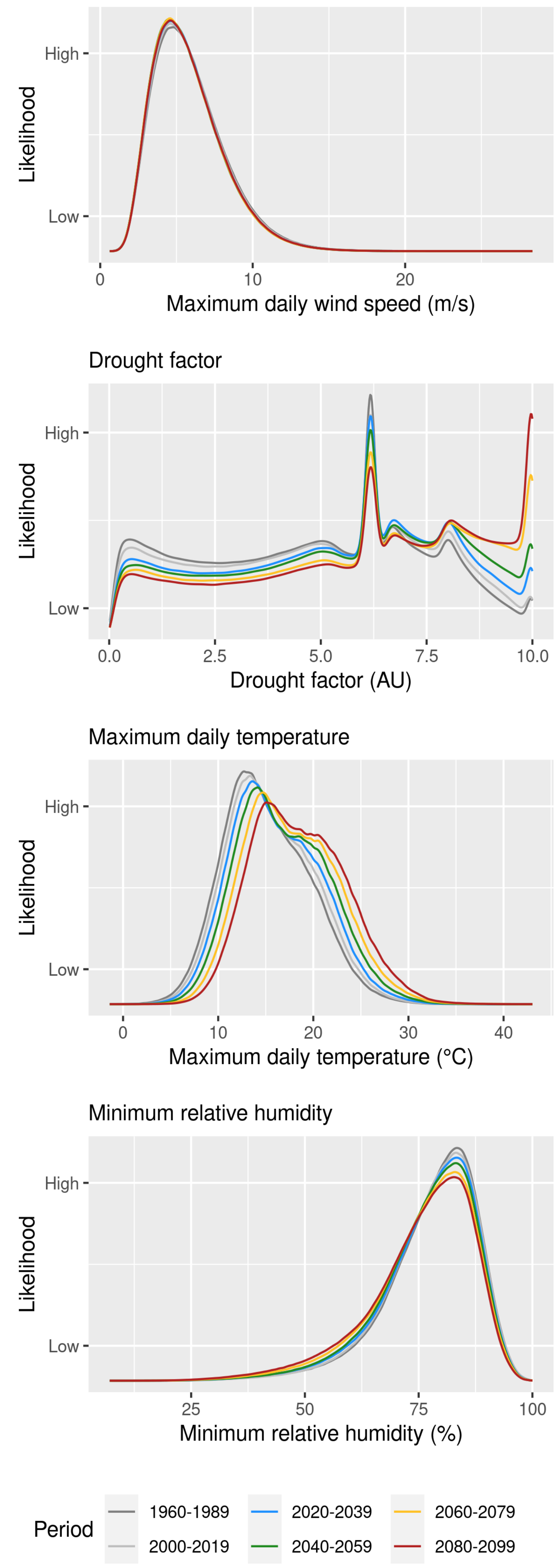


Figure 5: Time series of the ensemble-mean for the 30-year rolling mean of the number of days per year with fire danger ratings of *Low-Moderate*, *High*, *Very High*, *Severe*, *Extreme* from 1990 to 2100 (NB: *Catastrophic* had frequencies too low to reasonably present here). As every day has a fire danger rating, *Low-Moderate* rating frequencies decrease as they are replaced by higher categories.

Figure 6: Stacked area plot of the 30-year ensemble mean number of days of each forest fire danger index rating across each fire-season (October to April, 180 days) from 1990 to 2100. Decreased frequency of *Low-Moderate* days is due to increases in *High* or *Very High* categories.

Figure 7: Annual return periods for Forest Fire Danger Index values for the 30-year baseline period (1961-1990) and 20-year time periods from 2001 to 2100.

Figure 8: Distribution of values for each of the underlying drivers of Forest Fire Danger Index for each time period. a) Maximum daily wind speed (m/s); b) Drought Factor (AU); c) Maximum daily temperature; d) Daily minimum relative humidity (%). As wind speed is not projected to change significantly, the key drivers of change are temperature, humidity and drought factor. Drought factor has strong correlations with temperature change.

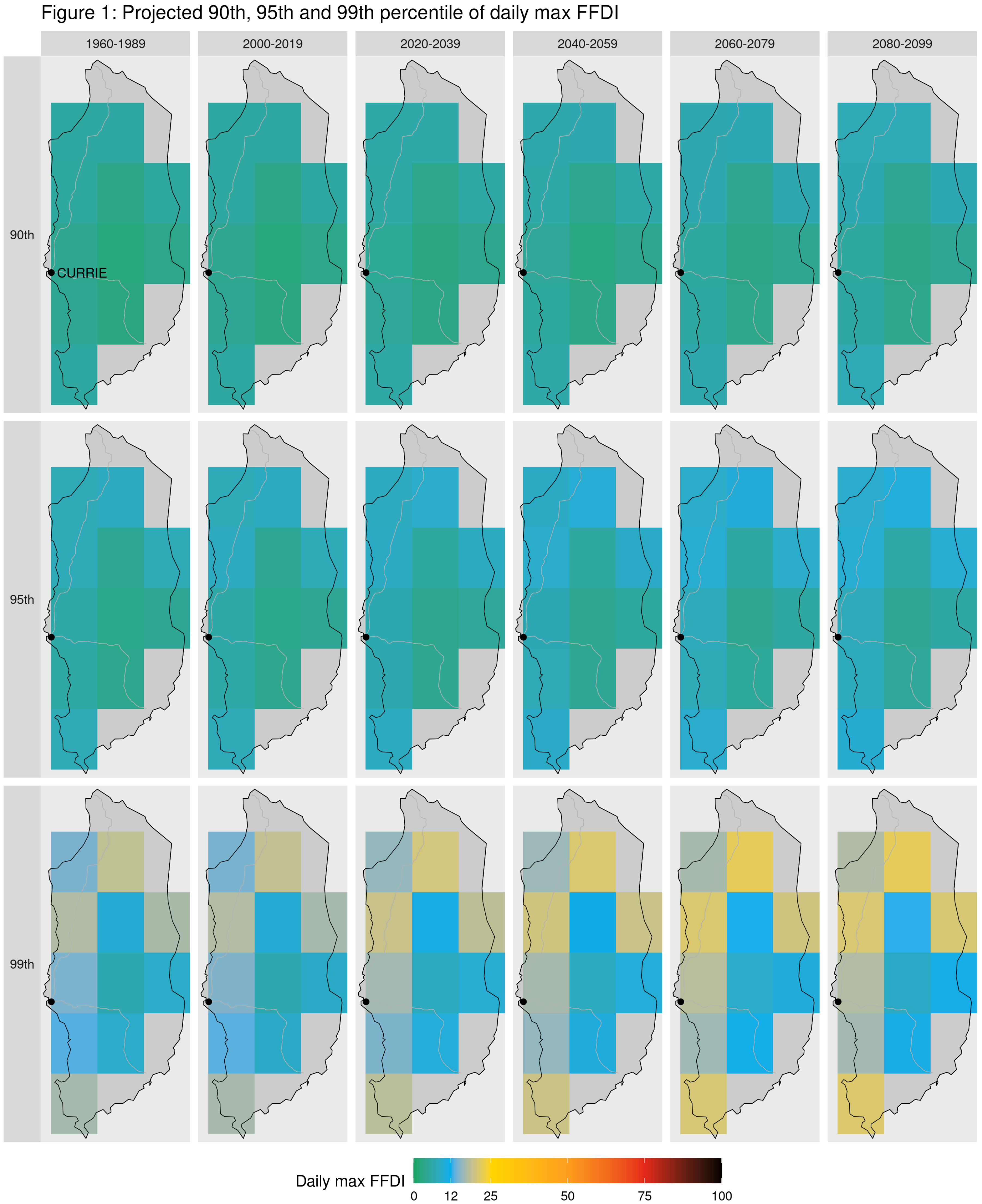


Figure 1: Projected 90th, 95th and 99th percentile values of *Forest Fire Danger Index* for the 30-year baseline period, and then 20-year time periods from 2001 to 2100. Each grid cell is the mean of the 6 ensemble members. The 99th percentile value reflects the 4th highest FFDI value year; the 95th percentile is the 18th highest FFDI value year; and the 90th percentile is the 36th highest FFDI value year. Extreme values of FFDI are expected to increase steadily into the future.

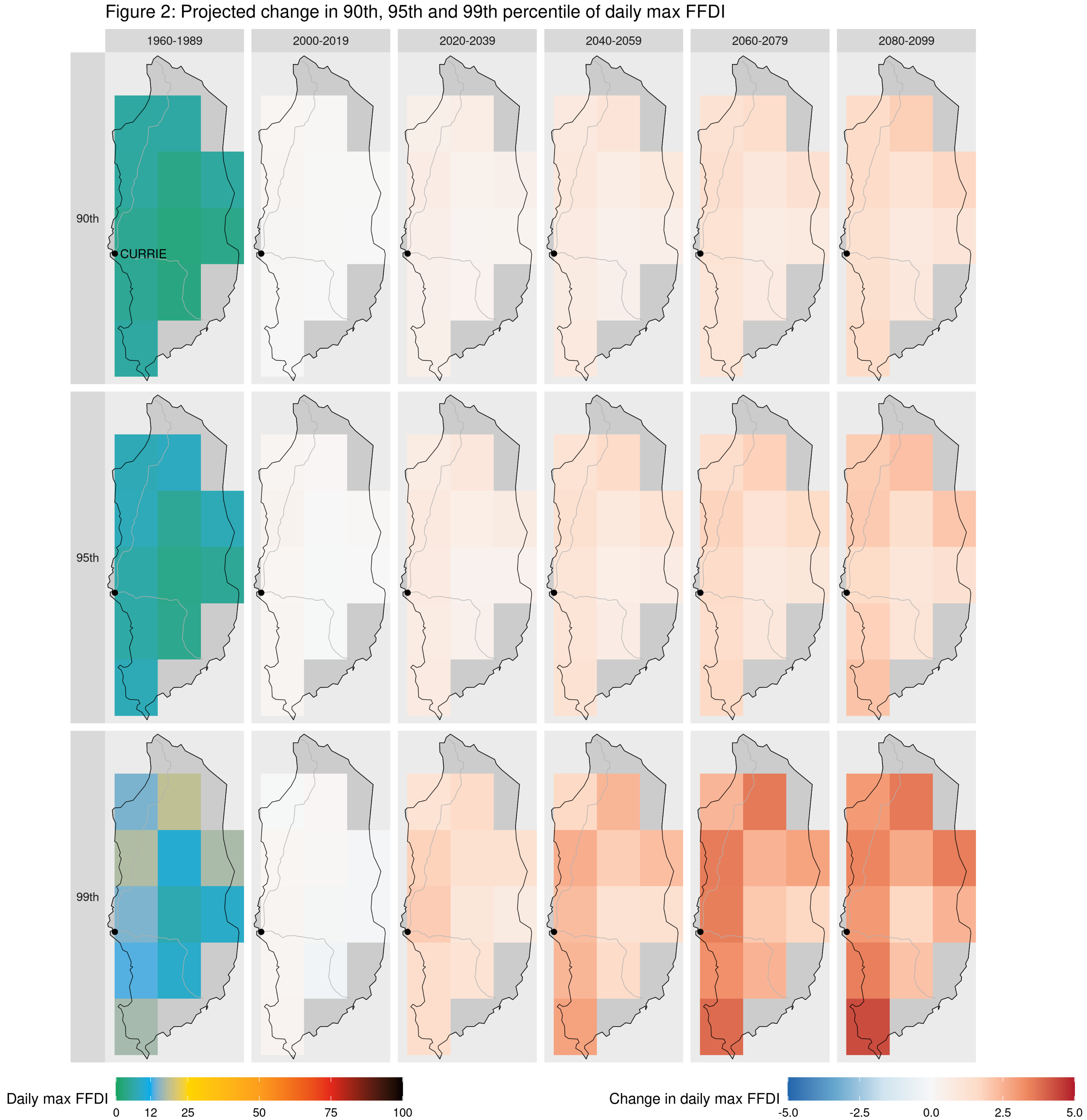


Figure 2: Projected change in the 90th, 95th and 99th percentile values of *Forest Fire Danger Index* for 20-year time periods from 2001 to 2100 compared to the 30-year baseline period 1961–1990. Each grid cell is the mean of the 6 ensemble members. The 99th percentile value reflects the 4th highest FFDI value year; the 95th percentile is the 18th highest FFDI value year; and the 90th percentile is the 36th highest FFDI value year. Extreme values of FFDI are expected to increase steadily into the future

Figure 3: Projected monthly FFDI with outliers removed

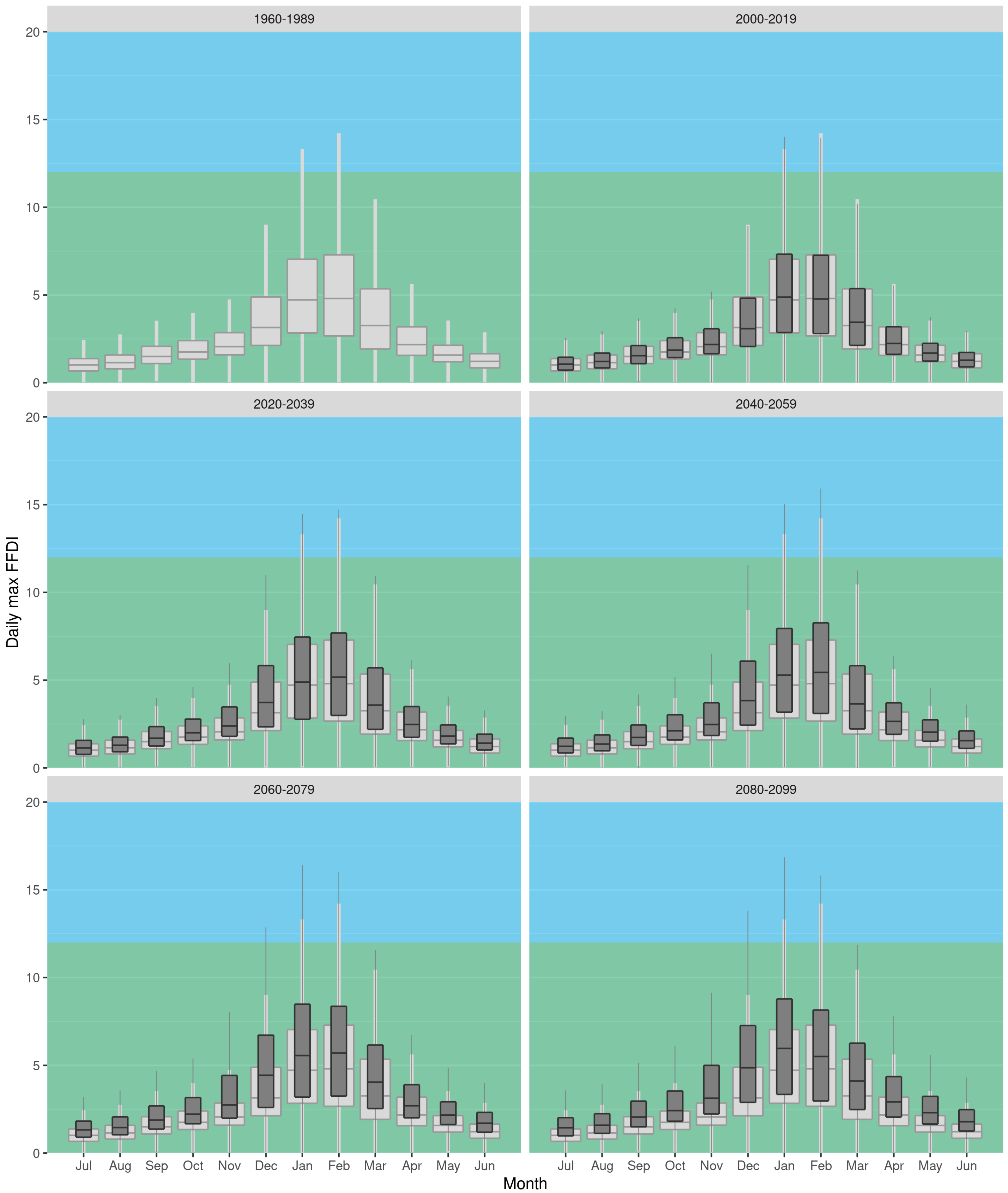


Figure 3: Boxplots of daily *Forest Fire Danger Index* for each month for the 30-year baseline period, and then 20-year periods from 2001 to 2100. Each boxplot represents a summary of daily data for each grid cell, for each of the 6 ensemble members within the time period; e.g. the top-left panel, the January boxplot represents the daily FFDI values for all January days in the period 1961–1990, for all grids cell in the region, for each of the 6 ensemble members. The baseline period (1961-1990) has been shadowed (*light grey*) underneath future time periods to highlight any differences expected into the future. Solid bars represent the median value. The box represents the 25th and 75th percentiles. The Whiskers represent the 1.5× the inter-quartile range. All months in all periods frequently have days of very low FFDI. Outliers have been excluded. If the boxplot shifts higher (lower) this indicates a change towards more (less) dangerous conditions.

Figure 4: Projected monthly FFDI with outliers shown

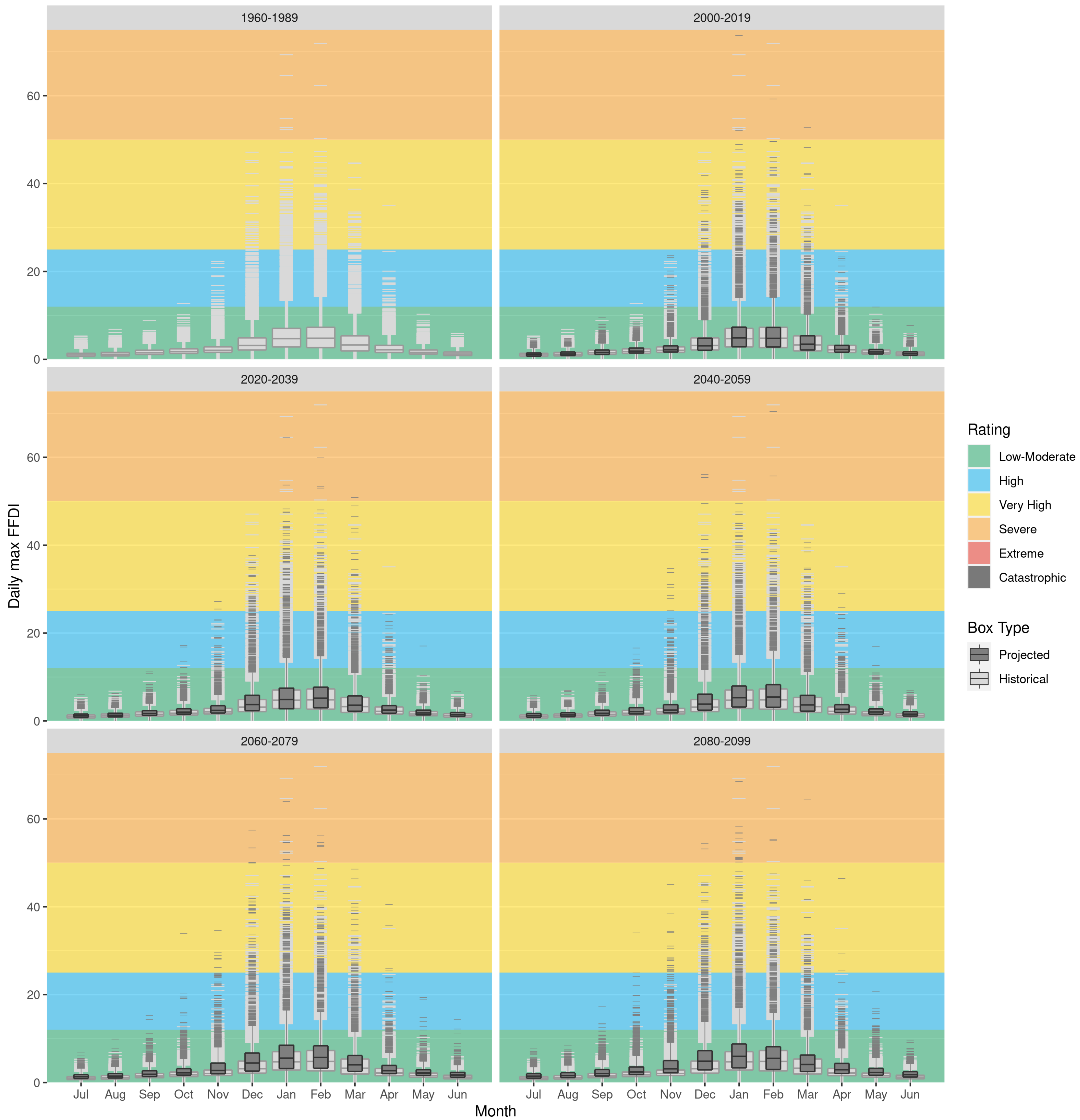


Figure 4: Boxplots of daily *Forest Fire Danger Index* for each month for the 30-year baseline period, and then 20-year periods from 2001 to 2100. Each boxplot represents daily data for each grid cell, for each of the 6 ensemble members within the time period; e.g. ing the top-left panel, the January boxplot represents the daily FFDI values for all January days in the period 1961–1990, for all grids cell in the region, for each of the 6 ensemble members. The baseline period (1961-1990) has been shadowed (*light grey*) underneath future time periods to highlight any differences expected into the future. Solid bars represent the median value. The box represents the 25th and 75th percentiles. The Whiskers represent the 1.5× the inter-quartile range. All months in all periods frequently have days of very low FFDI. Outliers are values > 1.5× the interquartile range and are represented as a dash(-): *light grey* for historical; *dark grey* for other time periods. If the boxplot shifts higher (lower) this indicates a change towards more (less) dangerous conditions.

# KING ISLAND

## Bushfires — Timeseries

Figure 5: Projected number of days per year of bushfire danger ratings

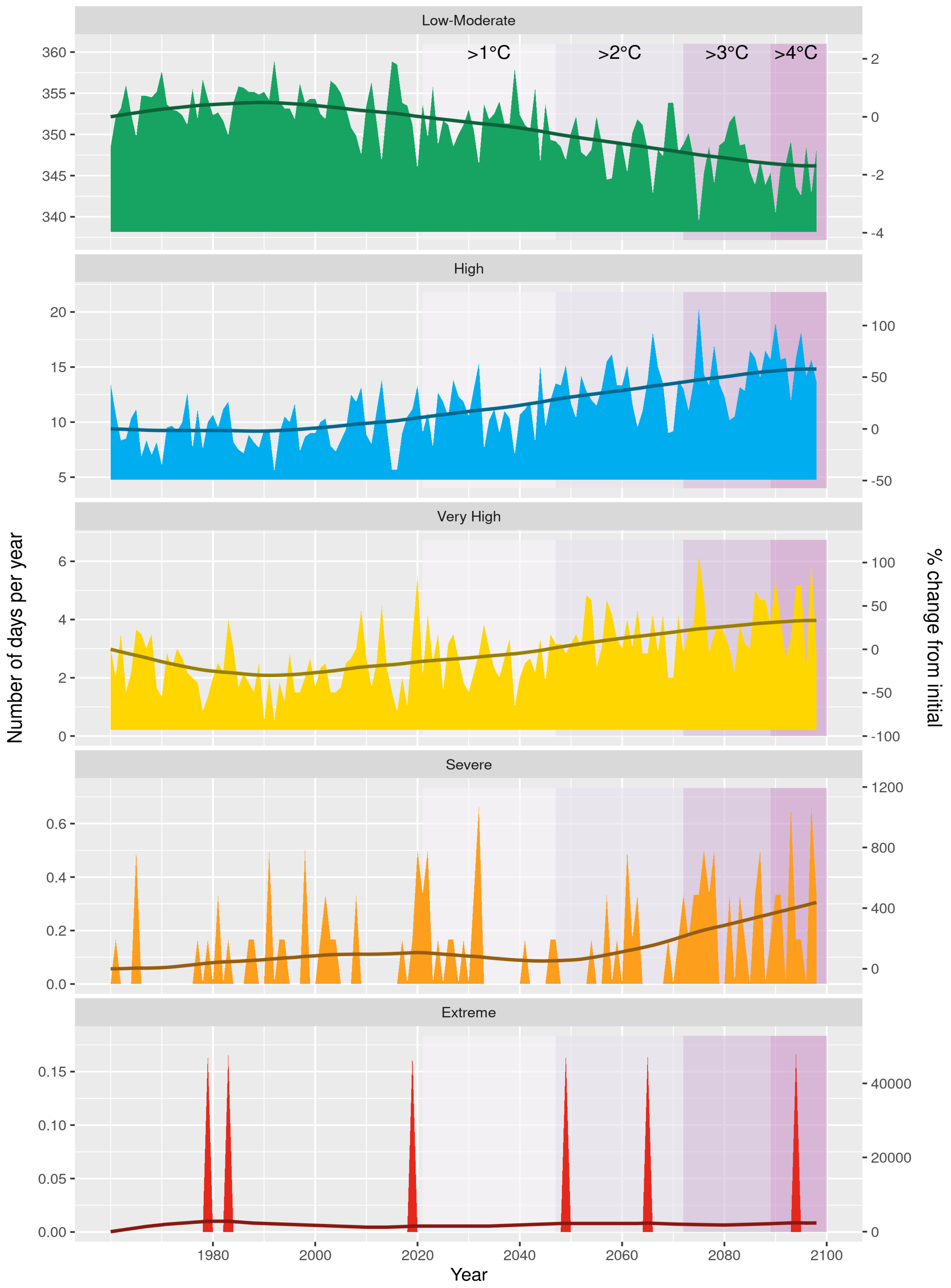


Figure 6: Projected ratio of bushfire danger ratings

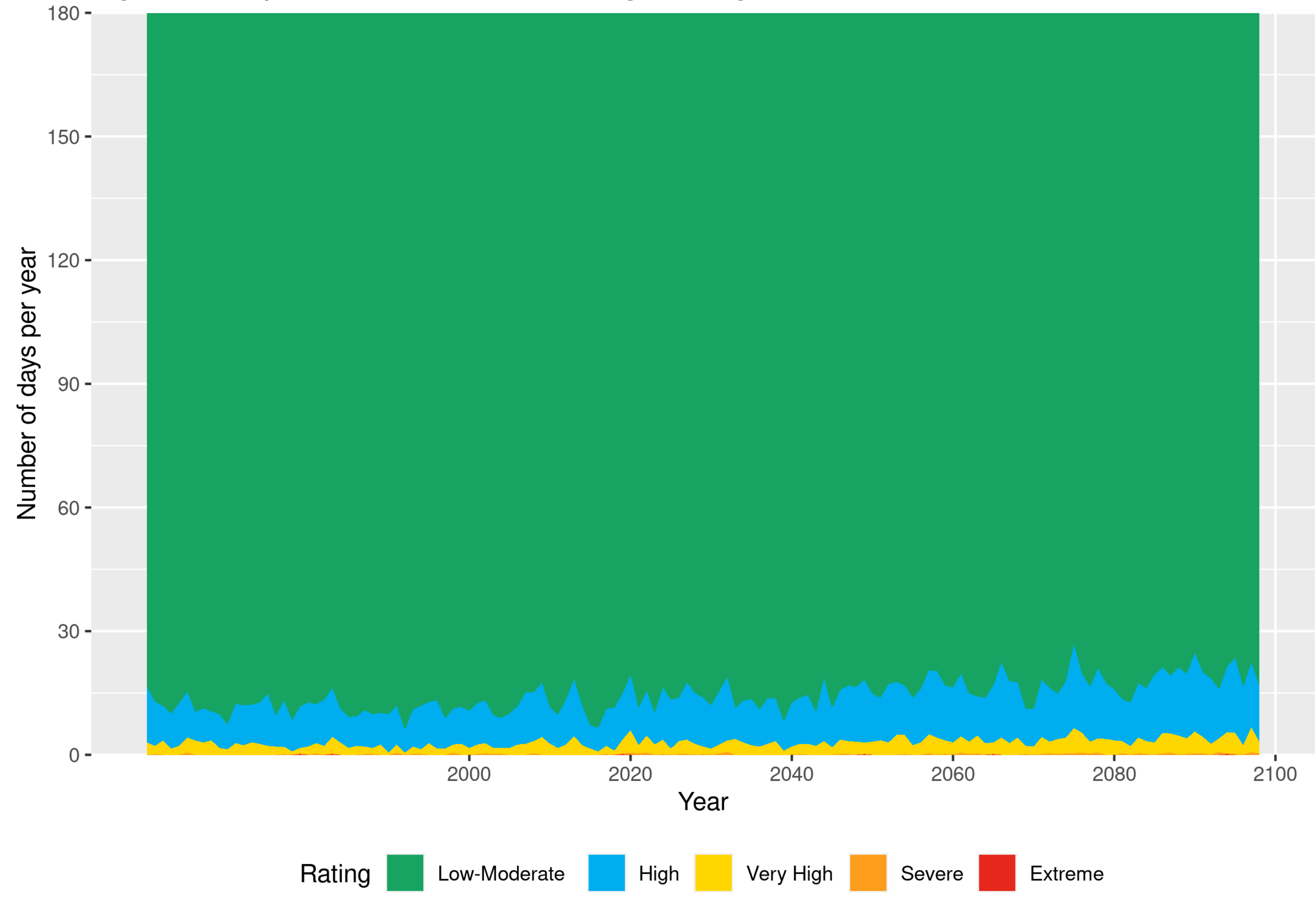


Figure 7: Projected returns curves for daily maximum FFDI

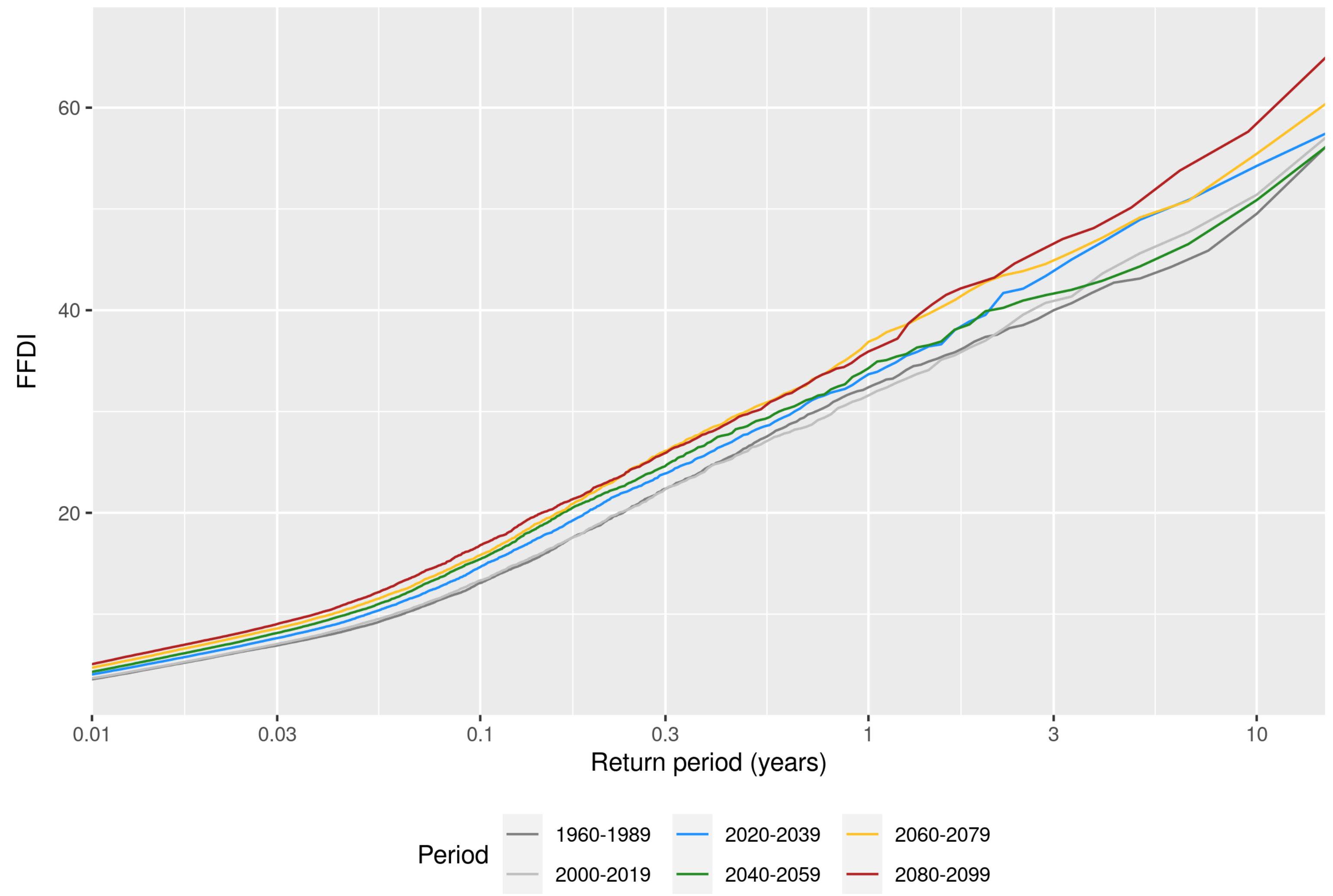


Figure 8: Driving variables of FFDI

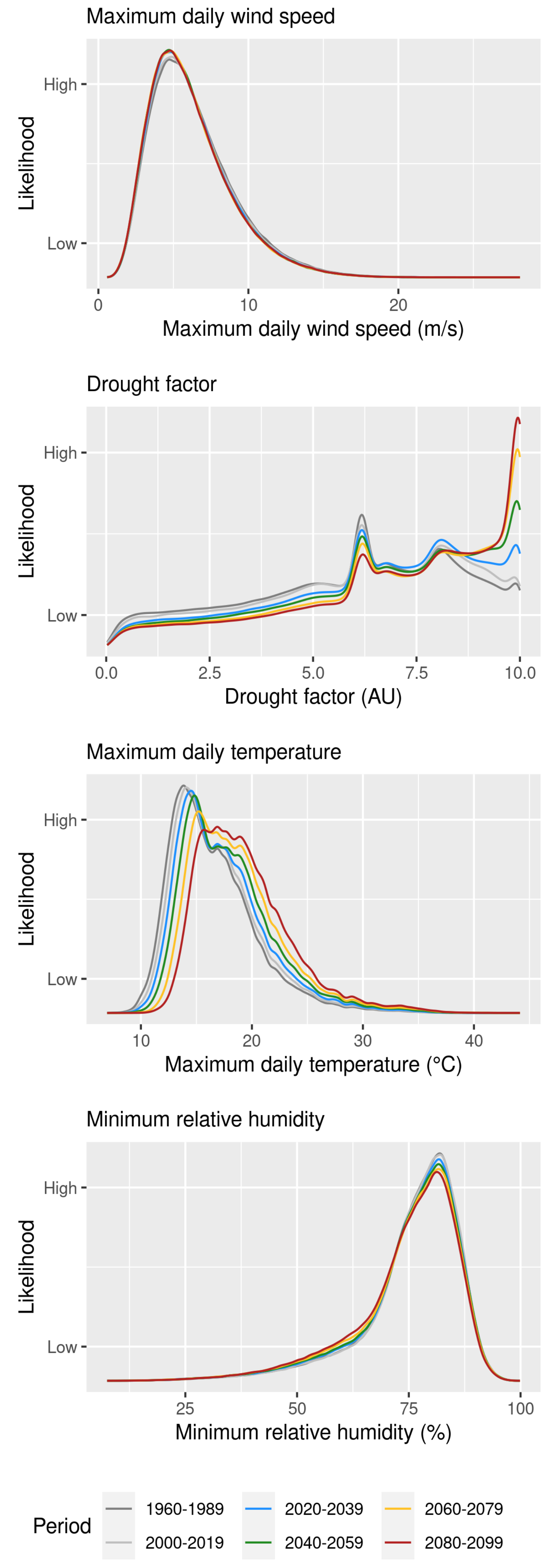


Figure 5: Time series of the ensemble-mean for the 30-year rolling mean of the number of days per year with fire danger ratings of *Low-Moderate*, *High*, *Very High*, *Severe*, *Extreme* from 1990 to 2100 (NB: *Catastrophic* had frequencies too low to reasonably present here). As every day has a fire danger rating, *Low-Moderate* rating frequencies decrease as they are replaced by higher categories.

Figure 6: Stacked area plot of the 30-year ensemble mean number of days of each forest fire danger index rating across each fire-season (October to April, 180 days) from 1990 to 2100. Decreased frequency of *Low-Moderate* days is due to increases in *High* or *Very High* categories.

Figure 7: Annual return periods for Forest Fire Danger Index values for the 30-year baseline period (1961-1990) and 20-year time periods from 2001 to 2100.

Figure 8: Distribution of values for each of the underlying drivers of Forest Fire Danger Index for each time period. a) Maximum daily wind speed (m/s); b) Drought Factor (AU); c) Maximum daily temperature; d) Daily minimum relative humidity (%). As wind speed is not projected to change significantly, the key drivers of change are temperature, humidity and drought factor. Drought factor has strong correlations with temperature change.

Atlas of
Earth System Hazards
for Tasmania

–

# Part 3: Background information, methods and interpretation

# General background information

## The difference between weather and climate

Weather describes what is happening in the atmosphere on a day-to-day basis or at a specific time, while climate describes the chance of experiencing particular kinds of weather at a specific location within a set period of time (typically >10 years).

The climate of a location is affected by latitude, topography, altitude and proximity to large water bodies and their associated currents and can only be assessed over long time periods in order to incorporate the natural variability that occurs over several years.

## Climate change

### Natural Greenhouse effect

Greenhouse gases such as carbon dioxide keep the earth warm by allowing radiation from the sun to enter the atmosphere, while trapping a greater portion of outgoing radiation within the climate system. This maintains an average global temperature at ~15°C. Without greenhouse gases, the average temperature on Earth would be ~-18°C, too cold to sustain life as we know it.

The amount of energy that the Earth receives from the sun changes over time naturally in response to variations in Earth's orientation and orbit relative to the sun and the internal radiation cycles occurring within the sun itself. Additionally, the distribution of tectonic plates influences the capacity of heat to be transported around the planet by the atmosphere and the oceans. For example, when the land areas are concentrated towards the poles (equator), there is more (less) snow and ice on Earth, which means more (less) energy is reflected straight back out to space, resulting in cooler (warmer) global average temperatures. The concentration of greenhouse gases also varies naturally over millions of years depending on volcanic activity, global vegetation types, interacting with biological inputs and outputs, controlled by long-term biogeochemical cycles. The complex interplay of these processes (and others) determines the Earth's climate at any point in geological time.

### Enhanced Greenhouse effect

Since the industrial revolution, humans have been increasing the concentration and composition of greenhouse gases in the atmosphere. These changes have occurred extremely rapidly, becoming the dominant influence on global climate, overshadowing the influence of any natural cycles (IPCC, 2014). Before the industrial revolution, $CO_2$ levels were 280 ppm. In 2013, $CO_2$ levels surpassed 400ppm for the first time in recorded history. This level is higher than it has been in at least 800,000 years.

The more greenhouse gases humans put into the atmosphere by burning fossil fuels (oil/coal), the more heat is trapped in the Earth's system and the warmer the globe becomes. This affects atmospheric and ocean circulation patterns, fundamentally changing the way the climate system behaves. This changes the characteristics of climate experienced at any one location, both in terms of average conditions and the magnitude and intensity of extreme events (e.g., droughts, floods, heatwaves, cyclones etc.).

## What are climate predictions/forecasts?

Climate forecasts aim to accurately and precisely predict the weather that will be experienced at a precise place and time in the future. In order to achieve this, climate forecasts use observations to configure the atmosphere within a climate model so it represents the configuration of the actual atmosphere as accurately as possible (at a particular time, usually *today* or *now*). The more accurately the atmosphere is configured, the more likely it is that a forecasting model can accurately predict the future. Forecasting has improved such that the accuracy and precision of a 5 day forecast in 2017 is more reliable than a 2 day forecast in the 1980s. These improvements have been driven by advances such as higher resolution observational data archives (due to satellite and surface ocean measurements), increased computer processing power and improved understanding and representation of atmospheric dynamics within climate models.

## What are weather reanalysis products?

Weather reanalysis products (such as the *ERA-Iterim* mentioned within the methods) are climate model outputs run over the historical period, explicitly designed to fill the gaps between observations (in both space and time) or provide estimates of atmospheric variables that are difficult to measure. A climate model is configured using observations and then is run forward in time until the next set of observations can be incorporated. Reanalysis data products provide data archives that are consistent (use the same assumptions and equations), have full spatial coverage across the target domain (no missing data), are continuous through time and estimate atmospheric variables that either were not measured or cannot be measured. Reanalysis products aim to provide a *better estimate of the observed atmosphere*. They can be more accurate than observations (due to site specific interferences such as shading, or protection from winds).

## What are climate projections?

Climate projections are outputs from computer models used to represent the Earth's mean climate state and variability. They are not intended to predict the weather on particular dates in the future and the initial conditions use to set up these model runs are not based on observations.

The advantage of climate models is they can be nudged in different ways to determine the influence of particular variables on the climate system, or even test the impact of different future scenarios on the climate system over long timescales into the future. This allows climate projections to establish the range of future climates that could plausibly occur. These model-derived descriptions of possible future climates are dependent on what humans do regarding the greenhouse gas (mainly $CO_2$) emissions, under a set of plausible scenarios.

Climate projections are generally described in 20 or 30 year periods, to incorporate natural variability in the climate system. This reduces the effect of annual to decadal events (e.g., droughts, cool/hot seasons or El Niño Southern Oscilation (ENSO) cycles) on the average.

### Global Climate Models (often referred to as GCMs)

Global Climate Models are used to simulate the Earth's climate and are important tools to understand how the global climate may change due to the warming influence of increased greenhouse gas concentrations. Global Climate Models simulate the different components of the Earth system, including the atmosphere, ocean, land-surface, sea-ice, aerosols and the carbon cycle.

The foundation of climate modelling is mathematical equations that describe the four-dimensional (horizontal, vertical and temporal) motion of air and its thermodynamic (heat and energetic) state. These equations, in conjunction with the idea that mass and energy must be conserved, are used to estimate the change in the state of the atmosphere within each grid cell within a model-grid. All grid cells pass information between each other to best represent the atmosphere from one time step to another, giving a numerical representation of the atmosphere and oceans.

As far as possible, climate models are based on physical theory, and processes are explicitly resolved using physical equations. However, there are some processes that cannot be described by these equations, either because they occur at a scale that is smaller than the size of the grid cells (e.g., atmospheric phenomena such as small clouds or thermal updrafts), or because they are experimentally derived. Such processes are incorporeated with simplified representations in the model.

The higher resolution (in both space and time) aglobal climate model is, the smaller the grid cells or timesteps, giving more information about the state of the atmosphere. This includes more detailed information about the land-surface characteristics and topography, which greatly affect the weather inside the model. Very high resolution models are very computationally intensive as all of the equations have to be calculated for each grid cell, while also having to be run for many timesteps (representing decades or even centuries). In comparison, weather forecasting models can be run at far higher resolution because they only need to represent the atmosphere for a few days. Global Climate Models are therefore generally run at coarse resolutions (~50km–250km horizontal resolution, 10–20 vertical layers in the atmosphere, and up to 30 layers in the oceans, at 6 hourly timesteps) to decrease computational requirements.

### Regional Climate Models (often referred to as RCMs)

The complexity of Global Climate Models results in them being configured for coarse resolutions (spatial resolution of 50 to 200km, temporal resolutions of 6 hourly timesteps), due to the limitations of current supercomputers. As a result, certain features in the regional climate are often poorly represented by Global Climate Models including mountain ranges, coastlines, urban areas and other atmospheric phenomena such as storms and rainfall processes. Downscaling methods are sometimes employed to address this limitation of the Global Climate Models, providing higher spatial and temporal resolution climate simulations for a region (typically improved resolutions of between 1 to 50km resolution, and temporal resolutions of 1 minute to 1 hourly timesteps). Two popular downscaling methods are statistical downscaling and dynamical downscaling. Statistical downscaling relies on historical statistical relationships between observations and large-scale behaviour of the atmosphere. Dynamical downscaling employs Regional Climate Models that are based on modelling techniques that are like those used by Global Climate Models, but with the computing resources focused over a region and with a focus on the atmosphere and land-surface components (i.e., a trade-off is made where there is less space covered/included, but higher resolution representation of the climate system). In both cases, the downscaling process has key inputs from (i.e., they are informed by) coarse resolution Global Climate Model projections, often referred to as a *host* or *parent* climate model.

### How well do climate models replicate the climate at different scales?

Scale is a key component of understanding the climate and fundamental to detecting climate change signals. Global Climate Models are run at low resolution, so do not perform well when compared with observations from specific locations, as the gridpoint is representing the average of a vast area rather than a single point, which is affected by local microclimatic characteristics. This means that the subgrid scale processes such as cumulus clouds, convection, updrafts and downdraft in storms are not well represented. These phenomena are linked to small-scale processes that cannot be simulated by the Global Climate Models due to limitations in computing power or limited scientific understanding of the physical processes. They do a good job at simulating global and continental scale climate and provide a general overview of how the climate is changing. Long term averages of parameters such as temperature and precipitation along with less dynamic parameters like ocean temperatures, boundary currents and ice cover, are well represented by the Global Climate Models. They are also adept at simulating aspects of regional climate variability, such as major monsoon systems and seasonal changes in temperature, often driven by these less dynamic parameters.

### Detecting climate change signals at different scales

Detecting climate change signals is all about signal-to-noise ratios. That is, being able to see the influence of a climate change trend (the signal) on top of the the natural variability (the noise) for the area of interest. The larger the area, the more the day-to-day variability is dampened down, so the more likely it is to reveal climate trends. Specific locations, especially in the extratropical parts of Australia on the boundary between the polar and tropical air masses, have high variability. A good example is somewhere like Melbourne. When looking at extreme heat days, 40°C days for example, and attempting to establish a climate change signal, it is difficult because the variability in temperature in Melbourne is very high. The summer range of daily maximum temperature is around 30°C, so a one degree climate change signal is going to have very little effect on how many 40°C days are experienced in Melbourne. When looking at Australia as a whole however, this day-to-day variability is lower because a hot day in Melbourne is often accompanied by a cool day in different parts of the continent, so the Australian average temperature is relatively stable. This means that if there's a heatwave, where Australia is for example three degrees warmer than the climatological mean, it's more likely that this event would have been impossible without climate change and that this event can be attributed to climate change. This is also true over shorter and longer timescales. The longer the timescale (e.g., annual vs decadal), the more variability (or noise) is averaged out and more of the signal is revealed.

### Uncertainty in climate projections

There are three main sources of uncertainty in climate models, which become more or less dominant as the model-runs go further into the future. These are internal climate variability, model uncertainty and future emission scenario. The importance of each of these sources of uncertainty varies across different variables, the size of the area of interest and the length of time period.

*Internal variability*

Internal variability is due to the year-to-year changes in the weather which are independent of climate change. This timescale is difficult for the climate models to simulate as they are driven by mesoscale processes (that are often at smaller scales than the grid resolution). This uncertainty remains present throughout the model-runs but has less weighting as time goes on due to the other sources growing. The smaller the area of interest, the more this internal variability dominates the total uncertainty, however it is still significant at the global scale. This is linked to phenomena such as ENSO and other drivers of natural variability.

*Model uncertainties*

Model uncertainties are either due to: different representations of the same process within different model configurations (i.e., differing equations to solve the same problem); different parameterisations due to differing model resolutions; or, poor understanding and simulation of processes within the model (i.e., the equations or parameterisation schemes are unable to represent the processes correctly). Many of these model uncertainties would be greatly improved with higher model resolution, however, there will always be model uncertainty because microscale processes are impossible to fully simulate. These uncertainties will always grow as a model run goes further into the future.

*Emission scenario uncertainty*

Uncertainty regarding emission scenarios are based on Representative Concentration Pathways (RCPs, discussed above). These are storylines of how humans act into the future and are represented by the resulting change in average global radiative forcing by 2100. The four RCPs are numbered according to the change in radiative forcing by 2100; +2.6, +4.5, +6.0 and +8.5 watts per square metre ($Wm^{-2}$). The spread in these emission scenarios add uncertainty to Global Climate Model projections which always increase through time. Until 2050, all scenarios result in similar climate change impacts, so do not add much uncertainty to the future outcome. However, past 2050, they begin to diverge rapidly, eventually becoming the dominant source of uncertainty when estimating the future climate.

*Importance of uncertainties with scales and parameters*

When investigating global mean temperature, at first the internal variability is the main source of spread, with the different models and emission scenarios having less of an impact early on in the projections. From 2000 to 2020 the model uncertainties begin to dominate the overall uncertainty, whereas the emission scenario, still has little influence (although for some variables, such as global mean precipitation, model uncertainty is by far the largest contributor throughout). Past 2050 it is the uncertainty surrounding the emissions scenario, the socio-economic pathway the global community chooses to take, that drives uncertainty around global (and in turn local) temperatures.

## How can uncertainty be dealt with when using projections?

Research into understanding why the uncertainties in the models exist and what can and can't be relied on is key to dealing with these uncertainties. The models produce plausible futures, rather than a single certain one, giving us an insight into what the future may look like. This means that we need to adapt to possible futures and be aware of the *worst case* scenarios. Using multi-model ensembles of simulations provides information covering all potential futures, allowing decision makers to apply a risk management approach with regards to imminent decisions being made today, while providing useful insights into what the longer term future may be to enhance the strategic decisions begin developed over the medium and longer terms.

## The Coupled Model Intercomparison Project (CMIP)

The Coupled Model Intercomparison Project (CMIP) is a collaborative effort designed to improve our knowledge of climate change. CMIP provides an archive of outputs from a collection of global climate models contributed from the international climate modelling community. The CMIP archive facilitates the study of climate models in a standardised way, enabling a diverse community of scientists to better understand how the climate is represented by simulations; implement changes that improve simulations of the Earth's climate; and interpret the impact that differing plausible futures may have on humanity. This multi-model approach allows the global community to identify the most plausible impacts that will be realised following different socio-political pathways into the future. The range of Global Climate Models included in CMIP5 represent the most diverse range of independent climate models and projections of how the global climate will change.

The CMIP collaboration is now within its $6^{\text{th}}$ phase (CMIP6), with coarse resolution (~100km$^2$) data operationaly available from 2020. This atlas is based on high-resolution (~10km$^2$) CMIP5 model output. The CMIP5 series of global climate simulations were designed to test how various climate drivers impact upon the Earth's climate. Instead of the SRES emissions scenarios (e.g., A2, B1), which were used in previous CMIP archives, CMIP5 presented a series of experiments called the Representative Concentration Pathways (RCPs). These were designed to test the impact of different concentrations of heat-trapping gases (e.g., atmospheric $CO_2$ concentrations) over a range of time periods (see section below on RCP's). To further appreciate the depth and breadth of CMIP5 experiments scope, as well as develop an understanding of the value and implications realised by this internationally coordinated research effort, we recommend referring to:

> IPCC, 2014: Climate Change 2014: Synthesis Report. Contribution of Working Groups I, II and III to the Fifth Assessment Report of the Intergovernmental Panel on Climate Change [Core Writing Team, R.K. Pachauri and L.A. Meyer (eds.)]. IPCC, Geneva, Switzerland, 151 pp. Available here:
>
> `https://ar5-syr.ipcc.ch/topic_summary.php`

## Emissions scenarios

One of the main sources of uncertainty around climate change is what choices humans make regarding the amount of greenhouse gases we release in the future. Different emissions scenarios are used to describe a range of socio-economic pathways the global community may follow, and the resulting influence on the Earth's climate. Some scenarios are based on the *business as usual* future where humans continue to be dependent on fossil fuels. Other scenarios are based on how well humans deal with the problem, with a range from making small, deliberate actions to reduce emissions, to actively removing greenhouse gases from the atmosphere. The resulting range reflects the uncertainty inherent in quantifying human activities and their influence on climate. Scenarios are essentially a set of storylines based on population projections, demographics, international trade, flow of information and technology, and other social, technological, and economic characteristics of plausible future worlds.

To ensure that the projections of Global Climate Models can be compared in a sensible way, various scenarios of future greenhouse gas emissions are applied consistently to all Global Climate Models. The scenarios used by the climate modelling community for the CMIP5 experiments that underpin the data in this report are known as Representative Concentration Pathways (RCPs). These are different to emission scenarios from previous experiments (i.e., CMIP3 and earlier) as they encompass all of the changes in the storyline leading to a range in average global radiative forcing (change in temperature due to change in atmospheric composition) by 2100.

The RCPs include RCP2.6, RCP4.5, RCP6.0 and RCP8.5. The size of the number indicates more energy (in the form of heat, in units of $Wm^{-2}$) being trapped in the Earth system so that RCP8.5 leads to a significantly warmer future climate than RCP2.6. The highest is RCP8.5 which is the *business as usual* scenario (though by no means the upper limit), whereas RCP2.6 is ambitious in that it achieves net negative carbon dioxide emissions before the end of the century by including a policy option. The other scenarios have different pathways and represent different future worlds, which result in different levels of overall warming.

- RCP2.6 — following a low emissions, intense mitigation scenario where the heat trapping capacity of the Earth is 2.6 $Wm^{-2}$. This is the emission scenario that is closest to a <2°C, warming consistent with the Paris Agreement target. As of 2019, this scenario is only achievable with dramatic and rapid changes to our economic and social systems and arrangements that must be implemented by ~2030;
- RCP4.5 — following a late start to a low emissions, intense mitigation scenario where the heat trapping capacity of the Earth is 4.5 $Wm^{-2}$. As of 2019, this scenario is only achievable with dramatic and rapid changes to our economic and social systems and arrangements that must be implemented by ~2040;
- RCP6.0 — following a moderate emissions, less effective mitigation scenario where the heat trapping capacity of the Earth is 6.0 $Wm^{-2}$. This is the scenario that current international commitments to emissions reductions (as of 2019) could achieve if targets are met;
- RCP8.5 — following a high emissions, limited mitigation scenario where the heat trapping capacity of the Earth is 8.5 $Wm^{-2}$. This is also referred to as the *worst case* or *business as usual* scenario, as this is the trajectory we are currently following.

# General methods

## Observations

Observed climate between 1997 and 2007 is summarised for each region, based on the Australian Gridded Climate Data products (AGCD). These are national gridded climate data at a resolution of 5km, based on interpolated weather station measurements. We use daily rainfall and daily maximum and minimum air temperature to calculate observed Growing Season Temperature and Rainfall, Aridity, Frost Risk Days and Excess Heat Factor. The AGCD were produced by the Australian Water Availability Project (AWAP), a collaborative effort of CSIRO and the Bureau of Meteorology (BoM).

## Global Climate Models used in the atlas

Six Global Climate Models from the CMIP5 archive were downscaled for the atlas, These were CSIRO-BOM-ACCESS1-0, CNRM-CERFACS-CNRM-CM5, NOAA-GFDL-GFDL-ESM2M, MOHC-HadGEM2-CC, MIROC-MIROC5 and NCC-NorESM1-M. These models are based on the recommended Global Climate Models for studying Australian climate change from the Climate Change in Australia web portal. The host Global Climate Models for downscaling were selected to show a range of possible climate futures such as changes in the amount of warming and reductions in rainfall (see Table 2). Note that because we are selectively downscaling Global Climate Models that show a range of possible futures, the downscaled simulations provide scenarios to explore the future climate, rather than an analysis of the most probable future climate, which lies within the range of downscaled climate.

The high-resolution downscaled climate simulations available at the time of publication were only for the RCP8.5 scenario. This scenario is useful as at the time of publication, it is the scenario most representative of trajectory the Earth is following based on social, economic and political actions and achievements as of 2019. Moving forward, if action to mitigate the impacts of climate change are successful, such that the Earth follows a scenario more similar to RCP6.0 (or at best RCP4.5), the RCP8.5 scenario provides a *worst case* scenario for risk managers to test future strategies against, while also being inclusive of the projected impacts of lower emissions scenarios.

## Description of the regional climate modelling approach

To develop high-resolution climate simulations for South East Australia, we used the Conformal Cubic Atmospheric Model (CCAM) developed at CSIRO (McGregor 2005 and McGregor and Dix 2008). Unlike most RCMs, CCAM is a global atmospheric model with a variable resolution grid that can be focused over an area of interest. In this way, CCAM can generate a higher resolution climate simulation, but is still coupled to the larger scale atmospheric circulation. Formally CCAM is a stretched grid global model, but we will refer to CCAM as an RCM in this atlas.

CCAM includes several sub-models that are useful for simulating the Australian climate, including:

- direct and indirect aerosol feedbacks (Boucher et al., 2013)
- gravity wave drag (Chouinard et al., 1986)
- convection (McGregor, 2003)
- cloud microphysics (Lin et al., 1983; Rotstayn et al., 1997)
- radiation (Schwarzkopf and Ramaswamy, 1999; Freidenreich and Ramaswamy, 1999)
- aerosols (Rotstayn and Lohmann, 2002; Rotstayn et al., 2011; Horowitz et al. 2017)
- boundary layer turbulent mixing (McGregor, 1993)
- the Australian developed Community Atmospheric Biosphere Land Exchange (CABLE) land-surface and carbon cycle model (Kowalczyk, 2013),
- the Urban Climate and Energy Model (UCLEM) for Australian cities (Lipson, et al., 2018)

CCAM has been used for several regional climate simulations in Australia and South East Asia, including the *CORDEX intercomparison experiment*, the *National Resource Management (NRM) national projections for Australia*, the *Climate Futures for Tasmania*, *Climate projections for the Australian Alps* and *High-resolution projections for Queensland*.

The downscaling process used by CCAM for the high-resolution climate simulations involves two stages. The first stage involves taking the projected changes in the Sea Surface Temperatures (SSTs) from the Global Climate Models, correcting the biases and variance on a month-by-month basis relative to the observed SSTs from 1980–2010 (Hoffman et al 2016).

The CCAM model is then used to rebuild the atmosphere at a uniformly global 50km resolution consistent with the corrected SSTs. This removes the first order errors that are present in the Global Climate Model output and helps to simulate a more realistic present day climate. The second stage is to then downscale the 50km CCAM simulations to 5km resolution (in this case it was centred over Victoria) using CCAM's stretched grid and scale-selective filters (Thatcher and McGregor 2009). Underlying model resolution is described in Figure 9. This approach ensures that the regional 5km resolution simulation is consistent with the large-scale behaviour of the global 50km resolution simulation, but also allows CCAM to add additional information such as extreme events. It is important to note that the SST bias correction process retains the amount of warming represented in the SSTs but can allow CCAM to modify the projections of the Global Climate Models in other respects (such as changes in mean sea level pressure or rainfall). When analysing the CCAM projections it can be useful to separate the regional-scale changes, the large-scale changes and the differences between the Global Climate Model projections so that the processes that explain the changes can be better understood.

The CFAP2019 ensemble were designed to balance competing needs of finer resolution, larger ensembles of downscaled host Global Climate Models and additional emission scenarios. By simulating the climate at these scales, we can expect to better resolve mountains, coastlines and urban areas. We can also expect to better simulate extreme rainfall events that may lead to flooding. The running of new simulations is computationally intensive, so new fine-scale projections were only done for south eastern Australia and Tasmania, where the greatest added value would be achieved over the mountains and coastlines.

The CCAM model was configured for 35 vertical levels ranging from 20m to 40km in height, with more vertical levels concentrated in the lower portion of the atmosphere. Near surface variables (e.g. 2m air temperature or 10m winds) are calculated in the usual way based on Monin-Obukhov Similarity Theory (MOST). Essentially the near surface data is estimated from interpolating between the first atmospheric level and the surface, with the weighting of the interpolate dependent on the stability of the atmosphere near the surface (i.e., is air rising due to the surface being warmer than the air above it, causing mixing of the air).

| Host Global Climate Model for downscaling | Relevance for downscaling regional climate |
|---|---|
| CSIRO-BOM-ACCESS1-0 | A hot, dry model that is representative of the consensus of Global Climate Model projections, especially for south-eastern Australia. Warming exceeds 2.5°C across most of Australia, and >3.5°C in central Australia. Drying is projected over most areas. This model shows a high skill score with regard to historical climate. |
| CNRM-CERFACS-CNRM-CM5 | A hot, wet model, consistent with the consensus of Global Climate Model projections in Southern Australia. It has a good representation of extreme El Niño in CMIP5 evaluations. |
| NOAA-GFDL-GFDL-ESM2M | A hot, very dry model, with warming in central regions exceeding 3.5°C. Drying is projected across most of the continent, with annual precipitation projected to decline more than 20% in many areas. |
| MOHC-HadGEM2-CC | A hot, dry model, with warming typically >2.5°C and >3.5°C in central regions. Annual precipitation is projected to increase in central Australia and decline elsewhere including the horticultural zone; Greatest reduction in wind. Maximum consensus for many regions. |
| MIROC-MIROC5 | A low warming, wet model for Australia, especially the south-eastern region. Warming does not exceed 3°C, and slight changes in annual precipitation are projected with declines in north-east Queensland and south-west Australia. |
| NCC-NorESM1-M | Low warming, wetter model, representative of the wettest scenarios within the CMIP5 archive. Warming over most of Australia exceeding 2°C. Little change in annual precipitation is projected, particularly in the south-east, although there is drying in south-west WA. |

Table 2: The six host Global Climate Models used for dynamical downscaling and the reason for their selection.

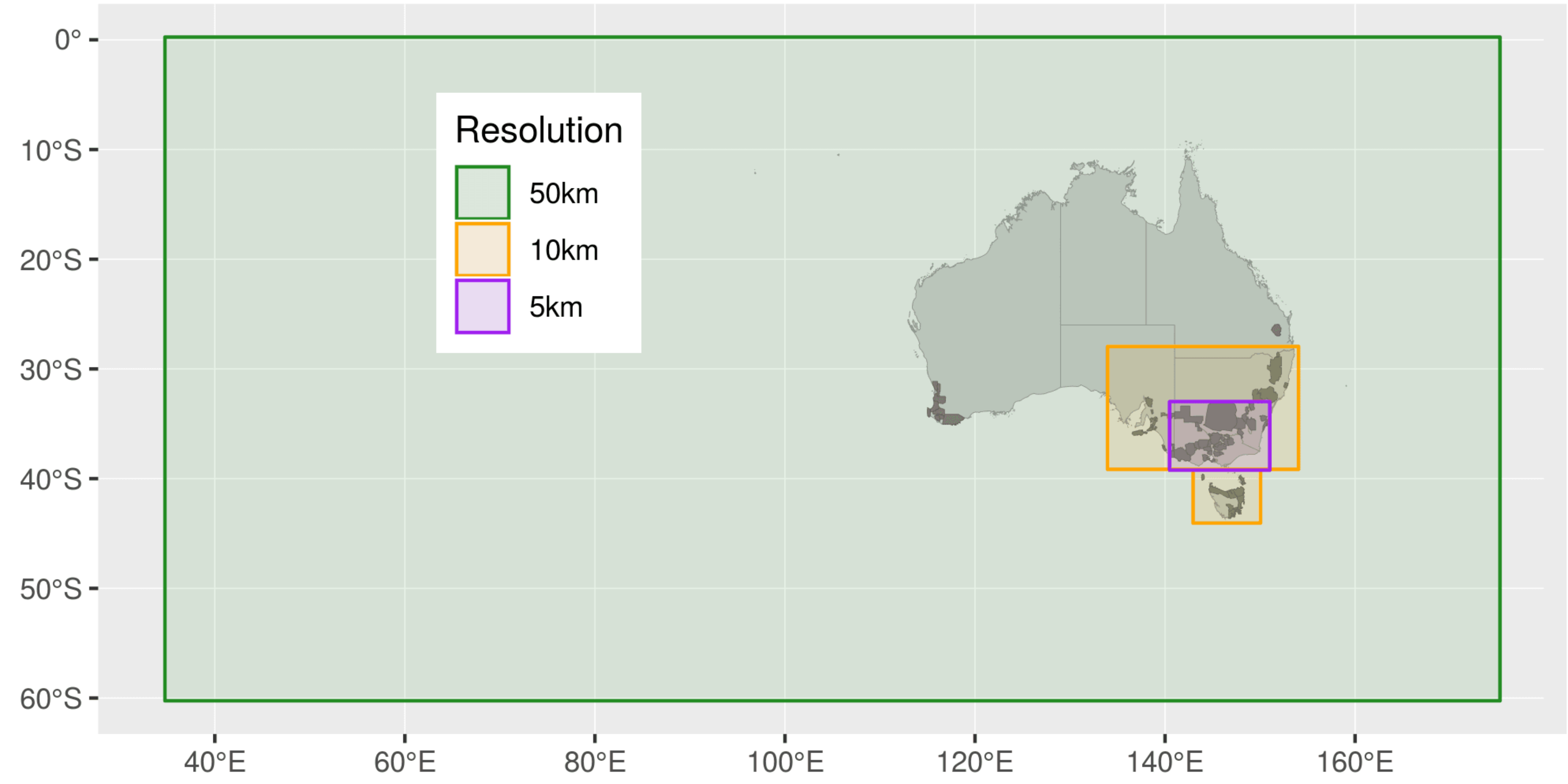


Figure 9: The domains of the CFAP2019 ensemble showing the different resolutions across Australia, ranging from 5km to 50km.

### Bias adjustment

Model biases introduce systematic errors which vary from place to place, as these errors are heavily dependent on the topography, altitude, latitude and distance from large water bodies. The biases are due to insufficient spatial resolution and the subsequent limited representation of meteorological processes (Rauscher et al. 2010). This is not a problem when investigating climate change as the interest is on the relative changes over time rather than the absolute values. However, when looking at climate impacts, the absolute values are needed, particularly when investigating temperature extremes. Therefore, in order to make the atlas more useful, there was a need to statistically bias adjusted the CCAM model outputs prior to climate impact assessment (Christensen et al., 2008).

Bias adjustment is a statistical method that adjusts the climate model output so that it matches the observations over the entire probability distribution. This adjustment is then applied to each quantile of the probability distribution into the future period, preserving any changes to the distribution projected by the climate models. The raw CFAP2019 ensemble outputs were bias-adjusted using the quantile statistical transformation, which has been widely used for adjusting modelled variables, especially temperature and rainfall (Gudmundsson et al., 2013). Temperature and rainfall were bias adjusted using the qmap package (Gudmundsson et al., 2013) within the R programming language. Specific parameter settings were: method = quant; qstep = 0.001 ; wet.day = FALSE for Temperature and TRUE for rainfall. Observation data inputs were from the Australian Gridded Climate Data product (Jones et al., 2009).

An example of the impact bias adjustment can have on the distribution of values is presented in Figure 10. The probability distribution of the model output has been adjusted such that it reflects the distribution of observed values.

### Time periods

Time periods were calculated based on Australian growing years, which are the period from July to June each annual cycle, winter to winter in the Southern Hemisphere. Growing years were labelled as the calendar year in which July fell. Time periods used within this atlas are defined as:

| Time period | Start and end month |
|---|---|
| 1961–1990 | July 1961 to June 1991 |
| 1997–2017 | July 1997 to June 2018 |
| 2001–2020 | July 2001 to June 2021 |
| 2021–2040 | July 2021 to June 2041 |
| 2041–2060 | July 2041 to June 2061 |
| 2061–2080 | July 2061 to June 2081 |
| 2081–2100 | July 2081 to June 2100[1] |

Table 3: Start and end months for each time period.

### Analysis Regions

Heatwave and Bushfire were assessed based on Bureau of Meterology Forecast Districts. Shapefiles were provided by the Bureau of Meteorology.

[1]this period is 19 years (instead of 20 years like the others) due to an absence of available data past December 2100

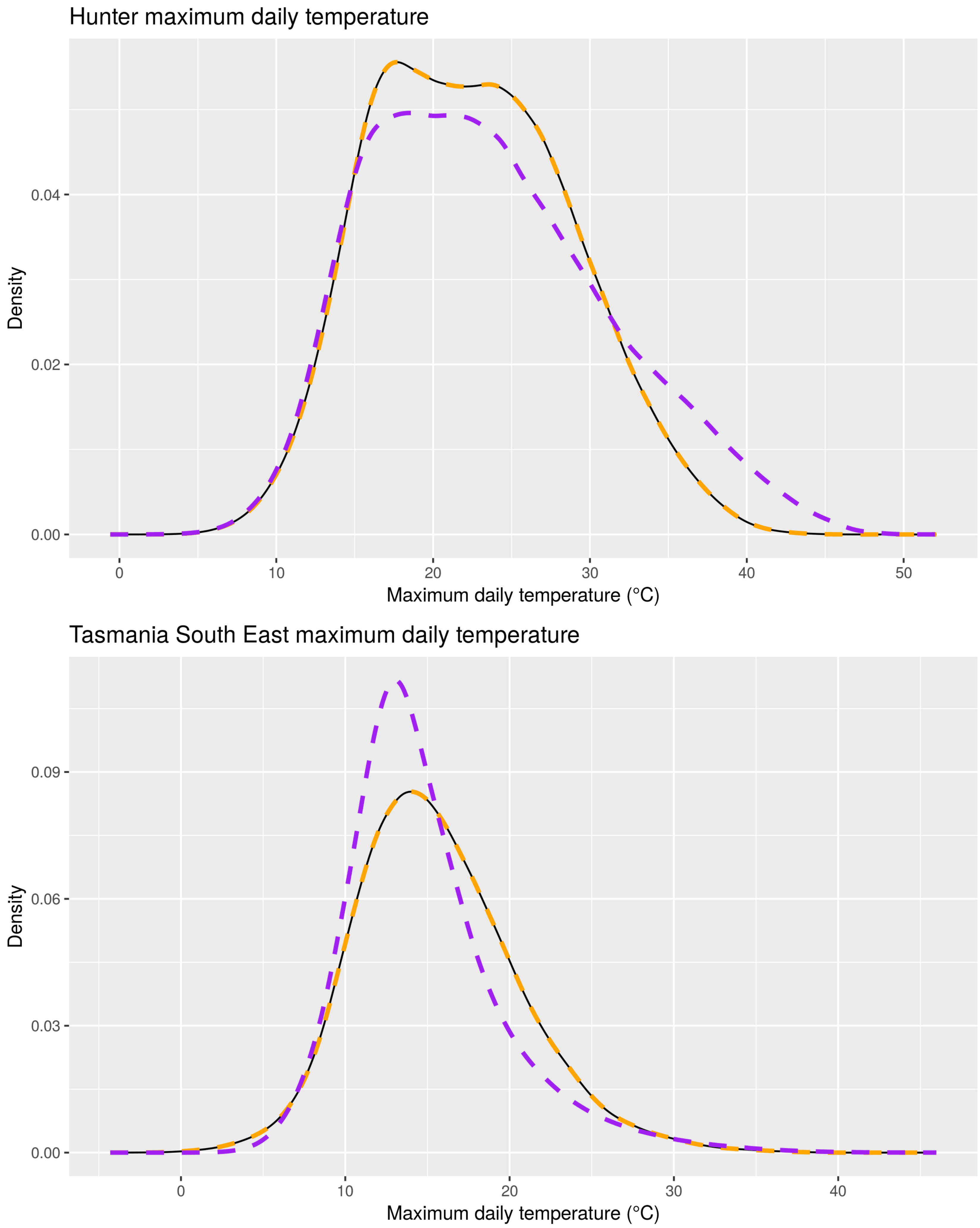


Figure 10: Probability distributions of maximum daily temperature at screen height (2m above the surface) for the period 1961-1990, for different data archives, displayed for the example regions nationally *Hunter* (the Hunter Valley wine region in NSW) and *Tasmania South East*. Observed data is sourced from AGCD. Only a single example ensemble member from CFAP2019 is displayed (CNRM-CERFACS-CNRM-CM5), similar impacts are observed when bias-adjusting the other ensemble members. The black solid thin lines are the observations *(NB: these are under the orange dashed lines)*. The purple dashed lines are the raw CFAP2019 output. The orange dashed lines are bias-adjusted CFAP2019 output. Note how the bias-adjusted CFAP2019 distributions (orange dashed lines) closely resemble the observed distributions (black thin solid line).

## Methods and interpretation of figures

This section has guidance on how to interpret each figure in this atlas. This is found in the *Interpretation* boxes. This is accompanied by an *Extended Caption* that describes the content of each figure type in long-form that could not be fit into the space available alongside the figures.

### Heatwaves

We have high confidence in how heatwaves will change into the future (depending on the emissions scenario). The physical drivers of how temperature and heat change within the climate system are well understood, are valid across large spatial scales and are therefore represented within climate models with high accuracy and precision. Thus weather and climate models have high skill in the predictions and projections they produce.

There is strong agreement across the CFAP2019 ensemble members regarding the rate and magnitude of warming projected into the future. As such, there is high confidence regarding projected variables related to temperature.

All metrics are calculated relative to the baseline period 1961–1990. This assumes zero adaptive capacity into the future. This assumption is true for many plants, animals and natural systems. Humans and social systems will have some adaptive capacity that will offset some of the drivers of heatwaves (such as improved air-conditioning systems), potentially decreasing the intensity, duration or frequency of heatwaves into the future.

Heatwaves were identified and characterised following Nairn and Fawcett (2015) and defined as the days when *Excess Heat Factor* (EHF) is positive for 3 consecutive days or more. Each heatwave was treated as a separate event.

The EHF index describes the severity of short term, acute heat impacts on humans during heat waves. It accounts for how hot a period of three days or more is in relation to an annual temperature threshold at a particular location, as well as how hot the period is with respect to the recent past (the previous 30 days). This reflects the fact that people acclimatise to a certain extent to their local climate but may not be prepared for a sudden rise in temperature above that of the recent past. Important temperature thresholds vary for each species. For this project, humans were considered the target species, so EHF is a relevant metric. The trends in heatwaves presented here will be useful as a guide for other species, but will not reflect the lethal heat-related thresholds relevant for all species in all landscapes.

#### Figure 1: Observed mean annual number of heatwave days

*Interpretation:*

Each grid cell represents the mean annual Number of Heatwave Days during the period 1997–2017, which is the period of recent memory. This map reflects the level of variability across the region as it is currently experienced. Grid cells are the resolution of the underlying data. Towns and roads are included to help identify specific sites within the region. Grid cells have an average elevation of the area they represent, so they best represent regions that have similar elevations (± 200m) across 5–10 km$^2$ scales. Typically, the highest peaks occur at smaller scales (~1 km$^2$) and thus are poorly represented. *(continued...)*

*(continued)*

This can influence the representation of some climatic features and should be considered when interpreting these figures.

*Underlying data source:* Australian Gridded Climate Data Product (Jones et al., 2009).

*Extended Caption:* Annual Number of Heatwave Days is calculated as the total number days for a given year that are classified as being a part of a heatwave. This metric quantifies the frequency of heatwave conditions occurring in a way that allows comparison across space and time. Grid cells selected were all land-cells within (or intersecting with the boundary of) the polygon that defines each Bureau of Meteorology Forecast District. Values were calculated for each grid cell. Mean annual Number of Heatwave Days is the average of the annual Number of Heatwave Days for all years within the *current period* (1997–2017).

#### Figure 2: Observed change in mean number of heatwave days

*Interpretation:*

Each grid cell represents how the mean annual Number of Heatwave Days during the current period (1997–2017) has changed when compared to mean annual Number of Heatwave Days during the historical period (1961–1990). Climate change is a large-scale feature, so the level of change observed is relatively similar when viewed at local scales. Towns and roads are included to help identify specific sites within the region. Grid cells have an average elevation of the area they represent, so they best represent regions that have similar elevations (± 200m) across 5–10 km$^2$ scales. Typically, the highest peaks occur at smaller scales(~1 km$^2$) and thus are poorly represented. This can influence the representation of some climatic features and should be considered when interpreting these figures.

*Underlying data source:* Australian Gridded Climate Data Product (Jones et al., 2009).

*Extended Caption:* Annual Number of Heatwave Days is calculated as the total number days for a given year that are classified as being a part of a heatwave. This metric quantifies the frequency of heatwave conditions occurring in a way that allows comparison across space and time. Mean annual Number of Heatwave Days is the average of the annual Number of Heatwave Days for all years within the *current period* (1997–2017), or the *baseline period* (1961–1990). The *baseline period* mean annual Number of Heatwave Days was then subtracted from the *current period* mean annual Number of Heatwave Days, resulting in the *observed change in mean annual Number of Heatwave Days*. Grid cells selected were all land-cells within (or intersecting with the boundary of) the polygon that defines each Bureau of Meteorology Forecast District. Values were calculated for each grid cell.

#### Figure 3: Projected mean number of heatwave days

*Interpretation:*

Each grid cell represents the mean annual Number of Heatwave Days during each 20-year period of 2021–2040, 2041–2060, 2061–2080, 2081–2100 (following the RCP8.5 scenario). These reflect the level of variability across the region, and the rate of change projected into the future. Grid cells are the resolution of the underlying data. Grid cells have an average elevation of the area they represent, so they best represent regions that have similar elevations (± 200m) across 5–10 km$^2$ scales. Typically, the highest peaks occur at smaller scales (~1 km$^2$) and thus are poorly represented. This can influence the representation of some climatic features and should be considered when interpreting these figures.

*Underlying data source:* Climate Futures Australasian Projections 2019 (CFAP2019).

*Extended Caption:* Annual Number of Heatwave Days is calculated as the total number days for a given year that are classified as being a part of a heatwave. This metric quantifies the frequency of heatwave conditions occurring in a way that allows comparison across space and time. Mean projected annual Number of Heatwave Days is the average of the annual Number of Heatwave Days across all ensemble members within the *CCAM ensemble*. Grid cells selected were all land-cells within (or intersecting with the boundary of) the polygon that defines each Bureau of Meteorology Forecast District. Values were calculated for each grid cell. Mean annual Number of Heatwave Days is the average of the annual Number of Heatwave Days for all years within each time period (2021–2040; 2041–2060; 2061–2080; 2081–2100). These were calculated for each ensemble member within the *CFAP2019*. The 6 ensemble member values (for each grid cell) are averaged generating the ensemble mean for each grid cell within the region.

#### Figure 4: Projected annual number of heatwave days from 1961 to 2100

*Interpretation:*

The light-grey ribbon represents the observed spread of the Number of Heatwave Days for all grid cells in the region from the 10$^{th}$ to 90$^{th}$ percentile, while the dark-grey ribbon represents the 25$^{th}$ to 75$^{th}$ percentiles and the dark-grey line the average. These are 30-year rolling means. The light-pink ribbon represents the modelled projected spread of the Number of Heatwave Days for all grid cells and ensemble members in the region from the 10$^{th}$ to 90$^{th}$ percentile, while the dark-pink ribbon represents the 25$^{th}$ to 75$^{th}$ percentiles and the red line the model average. It's clear that the spread of the Number of Heatwave Days looks set to increase into the future as well as the projected model average. However, when compared to observations, it suggest the projections under-estimate the rate at which this risk will increase into the future.

*Underlying data source:* Australian Gridded Climate Data Product (Jones et al., 2009); Climate Futures Australasian Projections 2019 (CFAP2019).

*Extended Caption:* Heatwave events are identified using the methods described in Nairn and Fawcett (2015). A *heatwave day* is a day identified as being a member of a heatwave event. The annual Number of Heatwave Days is calculated as the number of days identified as a *heatwave day* within a year. This metric describes the frequency of heatwaves. Years are assessed as July-June to align with the austral summer. Values were calculated for each grid cell. Points represent the annual Number of Heatwave Days for each year for each grid cell within year of each ensemble member. Grid cells selected were all land-cells within (or intersecting with the boundary of) the polygon that defines each Bureau of Meteorology Forecast District.

**Light-grey ribbons**: The light-grey ribbons represent the spread of the 10$^{th}$ to the 90$^{th}$ percentiles of annual Number of Heatwave Days from the observational record (AGCD), calculated as a 30-year rolling mean.

**Dark-grey ribbons**: The dark-grey ribbons represent the spread of the 25$^{th}$ to the 75$^{th}$ percentiles of annual Number of Heatwave Days from the observational record (AGCD), calculated as a 30-year rolling mean.

**Solid black line**: The solid black line represents the mean annual Number of Heatwave Days from the observational record (AGCD), calculated as a 30-year rolling mean.

**Light-pink ribbons**: The light-pink ribbons represent the spread of the 10$^{th}$ to the 90$^{th}$ percentiles of annual Number of Heatwave Days from the model projections record (CFAP2019). Each timestep is the ensemble-mean, calculated from the 30-year rolling mean of each ensemble member.

**Dark-pink ribbons**: The dark-pink ribbons represent the spread of the 25$^{th}$ to the 75$^{th}$ percentiles of annual Number of Heatwave Days from the model projections record (CFAP2019). Each timestep is the ensemble-mean, calculated from the 30-year rolling mean of each ensemble member.

**Solid pink line**: The solid pink line represents the mean annual Number of Heatwave Days from the model projections record (CFAP2019). Each timestep is the ensemble-mean, calculated from the 30-year rolling mean of each ensemble member.

**Coloured zones in background**: The coloured zones in the background indicate the time when *average global climate temperature* increases by 1 °C, 2 °C, 3 °C or 4 °C, following the Representative Concentration Pathway 8.5 scenario (RCP8.5, often referred to as the *business as usual* scenario). These estimates are the ensemble means as reported by the Intergovernmental Panel on Climate Change Fifth Assessment Report (IPCC-AR5), based on the World Climate Research Programme (WCRP) Coupled Model Intercomparison Project - phase 5 (CMIP5) global climate model archive (which has >100 ensemble members).

**Figure 5: Projected range in the annual number of heatwave days**

*Interpretation:*

Dots show the counts of the mean Number of Heatwave Days for all model ensemble members and each grid cell in the region for the 1961–1990 period and each 20-year period of 2001–2020, 2021–2040, 2041–2060, 2061–2080, 2081–2100 (following the RCP8.5 scenario). These reflect counts of the specific Number of Heatwave Days for each of the six time periods. Differences between the height of each dot highlights how many heatwave days occured across space for each year in the relevant time periods. The projected changes are assessed compared to the baseline period, 1961–1990, and assume zero adaptive capacity. This is true for many plants and animals and indicates that as the climate changes, entire months/seasons will be the equivalent to a heatwave for those species. However, this is less true for humans or human settlements, as some adaptation or acclimatisation is to be expected which would increase the population's resilience to heat, increasing the key temperature thresholds used to define when a heatwave is occurring.

*Underlying data source:* Australian Gridded Climate Data Product (Jones et al., 2009); Climate Futures Australasian Projections 2019 (CFAP2019).

*Extended Caption:* Heatwave events are identified using the methods described in Nairn and Fawcett (2015). A *heatwave day* is a day identified as being a member of a heatwave event. The annual Number of Heatwave Days is calculated as the number of days identified as a *heatwave day* within a year. This metric describes the frequency of heatwaves. Years are assessed as July-June to align with the austral summer. Values were calculated for each grid cell. Points represent the annual Number of Heatwave Days for each year for each grid cell within each ensemble member. Grid cells selected were all land-cells within (or intersecting with the boundary of) the polygon that defines each Bureau of Meteorology Forecast District.

Each panel presents the population of *annual Number of Heatwave Days* values within for each year, grid cell and ensemble member (no averaging) during each different 20-year period. Time periods were: 1961–1990; 2001–2020; 2021–2040; 2041–2060; 2061–2080; 2081–2100.

**Figure 6: Projected mean annual number of heatwave days per month**

*Interpretation:*

Each bar represents the counts for when the regional (averaged across time) and ensemble mean (the average of the six models) has a heatwave day during a particular month for the 1961–1990 period and each 20-year period of 2001–2020, 2021–2040, 2041–2060, 2061–2080, 2081–2100 (following the RCP8.5 scenario). The dark shading in each plot shows the observations for the base period (1961-1990) to highlight the changes in the Number of Heatwave Days. Differences between the months, or time periods is expressed as changes to the height of each bar.

*Underlying data source:* Australian Gridded Climate Data Product (Jones et al., 2009); Climate Futures Australasian Projections 2019 (CFAP2019).

*Extended Caption:* Heatwave events are identified using the methods described in Nairn and Fawcett (2015). A *heatwave day* is a day identified as being a member of a heatwave event. The annual Number of Heatwave Days per month is calculated as the number of days identified as a *heatwave day* within each month of a each year. The mean annual Number of Heatwave Days per month is the average of all monthly values across all years within the target time period. This metric describes the frequency of heatwaves, and how this varies across an annual season. Annual seasons (or years) were assessed as July-June to align with the austral summer. Values were calculated for each grid cell. Coloured bars represent the average Number of Heatwave Days values, averaged across all grid cells and all ensemble members within the *CCAM ensemble*. Grid cells selected were all land-cells within (or intersecting with the boundary of) the polygon that defines each Bureau of Meteorology Forecast District. Projected mean Number of Heatwave Days per month is presented from 1961 to 2100.

Each panel represents a bar plot of mean annual Number of Heatwave Days per month, averaged across all grid cells and all ensemble members during each different 20-year period. Time periods were: 1961–1990; 2001–2020; 2021–2040; 2041–2060; 2061–2080; 2081–2100.

**Shadowed bars**: The shadowed bars are the observed mean Number of Heatwave Days per month for the 1961–1990 baseline period. Diferences between the dark grey bars and the shadowed bars indicate how the models are different to the observations.

**Coloured bars**: The coloured bars are the projected ensemble-mean of the mean annual Number of Heatwave Days per month, generated by *CCAM*. Differences between the coloured bars and the shadowed bars indicate changes into the future relative to the observed baseline period.

**Figure 7: Observed mean cumulative intensity**

*Interpretation:*

Each grid cell represents the mean Cumulative Intensity during the period 1997–2017, (which is *the period of recent memory* at time of publishing). This map reflects the level of variability across the region as it is currently experienced. Grid cells are the resolution of the underlying data. Towns and roads are included to help identify specific sites within the region. Grid cells have an average elevation of the area they represent, so they best represent regions that have similar elevations (± 200m) across 5–10 km$^2$ scales. Typically, the highest peaks occur at smaller scales (~1 km$^2$) and thus are poorly represented. This can influence the representation of some climatic features and should be considered when interpreting these figures.

*Underlying data source:* Australian Gridded Climate Data Product (Jones et al., 2009).

*Extended Caption:* Cumulative Intensity during a heatwave is calculated as the sum of all EHF values for each of the days during a heatwave event. This metric quantifies the intensity of a heatwave in a way that allows comparison across space and time. Grid cells selected were all land-cells within (or intersecting with the boundary of) the polygon that defines each Bureau of Meteorology Forecast District. Values were calculated for each grid cell. Mean Cumulative Intensity is the average of all observed Cumulative Intensity values during heatwaves within the *current period* (1997–2017).

**Figure 8: Observed change in mean cumulative intensity**

*Interpretation:*

Each grid cell represents how mean Cumulative Intensity during the current period (1997–2017) has changed when compared to mean Cumulative Intensity during the historical period (1961–1990). Climate change is a large-scale feature, so the level of change observed is relatively similar when viewed at local scales. Towns and roads are included to help identify specific sites within the region. Grid cells have an average elevation of the area they represent, so they best represent regions that have similar elevations (± 200m) across 5–10 km$^2$ scales. Typically, the highest peaks occur at smaller scales(~ 1 km$^2$) and thus are poorly represented. This can influence the representation of some climatic features and should be considered when interpreting these figures.

*Underlying data source:* Australian Gridded Climate Data Product (Jones et al., 2009).

*Extended Caption:* Cumulative Intensity during a heatwave is calculated as the sum of all EHF values for each of the days during a heatwave event. This metric quantifies the intensity of a heatwave in a way that allows comparison across space and time. Mean observed Cumulative Intensity is the average of all Cumulative Intensity values for each heatwave over the *current period* (1997–2017), or the *baseline period* (1961–1990). The *baseline period* mean Cumulative Intensity was then subtracted from the *current period* mean Cumulative Intensity, resulting in the *observed change in mean Cumulative Intensity*. Grid cells selected were all land-cells within (or intersecting with the boundary of) the polygon that defines each Bureau of Meteorology Forecast District. Values were calculated for each grid cell.

**Figure 9: Projected mean cumulative intensity**

*Interpretation:*

Each grid cell represents the mean Cumulative Intensity during each 20-year period of 2021–2040, 2041–2060, 2061–2080, 2081–2100 (following the RCP8.5 scenario). These reflect the level of variability across the region, and the rate of change projected into the future. Grid cells are the resolution of the underlying data. Grid cells have an average elevation of the area they represent, so they best represent regions that have similar elevations (± 200m) across 5–10 km$^2$ scales. Typically, the highest peaks occur at smaller scales (~1 km$^2$) and thus are poorly represented. This can influence the representation of some climatic features and should be considered when interpreting these figures.

*Underlying data source:* Climate Futures Australasian Projections 2019 (CFAP2019).

*Extended Caption:* Cumulative Intensity during a heatwave is calculated as the sum of all EHF values for each of the days during a heatwave event. This metric quantifies the intensity of a heatwave in a way that allows comparison across space and time. Mean projected Cumulative Intensity is the ensemble mean of all Cumulative Intensity values for each heatwave across all ensemble members within the *CCAM ensemble*. Grid cells selected were all land-cells within (or intersecting with the boundary of) the polygon that defines each Bureau of Meteorology Forecast District. Values were calculated for each grid cell. Mean Cumulative Intensity is the average of all Cumulative Intensity values of all heatwaves within each time period (2021–2040; 2041–2060; 2061–2080; 2081–2100). These were calculated for each ensemble member within the *CFAP2019*. The 6 ensemble member values (for each grid cell) are averaged generating the ensemble mean for each grid cell within the region.

**Figure 10: Projected cumulative intensity**

*Interpretation:*

The light-grey ribbon represents the observed spread of Cumulative Intensity for all grid cells in the region from the $10^{th}$ to $90^{th}$ percentile, while the dark-grey ribbon represents the $25^{th}$ to $75^{th}$ percentiles and the dark-grey line the average. These are 30-year rolling means. The light-purple ribbon represents the projected spread of Cumulative Intensity for all grid cells and ensemble members in the region from the $10^{th}$ to $90^{th}$ percentile, while the dark-purple ribbon represents the $25^{th}$ to $75^{th}$ percentiles and the red line the model average. It is clear that the spread of Cumulative Intensity looks set to increase into the future as well as the projected average Cummulative Intensity during a heatwave. Compared to observations, it appears the projections under-estimate the rate of change into the future.

*Underlying data source:* Australian Gridded Climate Data Product (Jones et al., 2009); Climate Futures Australasian Projections 2019 (CFAP2019).

*Extended Caption:* Cumulative Intensity during a heatwave is calculated as the sum of all EHF values for each of the days during a heatwave event. This metric quantifies the intensity of a heatwave in a way that allows comparison across space and time. Mean projected Cumulative Intensity is the ensemble mean of all Cumulative Intensity values for each heatwave across all ensemble members within the *CCAM ensemble*. Grid cells selected were all land-cells within (or intersecting with the boundary of) the polygon that defines each Bureau of Meteorology Forecast District. Values were calculated for each grid cell. Projected Cumulative Intensity during a heatwave is presented from 1961 to 2100.

**Light-grey ribbons**: The light-grey ribbons represent the spread of the $10^{th}$ to the $90^{th}$ percentiles of Cumulative Intensity during a heatwave from the observational record (AGCD), calculated as a 30-year rolling mean.

**Dark-grey ribbons**: The dark-grey ribbons represent the spread of the $25^{th}$ to the $75^{th}$ percentiles of Cumulative Intensity during a heatwave from the observational record (AGCD), calculated as a 30-year rolling mean.

**Solid black line**: The solid black line represents the mean Cumulative Intensity during a heatwave from the observational record (AGCD), calculated as a 30-year rolling mean.

**Light-pink ribbons**: The light-pink ribbons represent the spread of the $10^{th}$ to the $90^{th}$ percentiles of Cumulative Intensity during a heatwave from the model projections record (CFAP2019). Each timestep is the ensemble-mean, calculated from the 30-year rolling mean of each ensemble member.

**Dark-pink ribbons**: The dark-pink ribbons represent the spread of the $25^{th}$ to the $75^{th}$ percentiles of Cumulative Intensity during a heatwave from the model projections record (CFAP2019). Each timestep is the ensemble-mean, calculated from the 30-year rolling mean of each ensemble member.

**Solid pink line**: The solid pink line represents the mean Cumulative Intensity during a heatwave from the model projections record

(CFAP2019). Each timestep is the ensemble-mean, calculated from the 30-year rolling mean of each ensemble member.

**Coloured zones in background**: The coloured zones in the background indicate the time when *average global climate temperature* increases by 1 °C, 2 °C, 3 °C or 4 °C, following the Representative Concentration Pathway 8.5 scenario (RCP8.5, often referred to as the *business as usual* scenario). These estimates are the ensemble means as reported by the Intergovernmental Panel on Climate Change Fifth Assessment Report (IPCC-AR5), based on the World Climate Research Programme (WCRP) Coupled Model Intercomparison Project - phase 5 (CMIP5) global climate model archive (which has >100 ensemble members).

**Figure 11: Distribution of cumulative intensity**

*Interpretation:*

Histograms showing the counts of the mean Cumulative Intensity for all model ensemble members and each grid cell in the region for the 1961–1990 period and each 20-year period of 2001–2020, 2021–2040, 2041–2060, 2061–2080, 2081–2100 (following the RCP8.5 scenario). These reflect counts of the number of times the value for all model ensemble members and each grid cell falls into the Cumulative Intensity of 1–10, 11–20, 21–30 etc. for each of the six time periods. Differences between the height of each bar highlights how many counts fall into that specific range of Cumulative Intensity.

*Underlying data source:* Australian Gridded Climate Data Product (Jones et al., 2009); Climate Futures Australasian Projections 2019 (CFAP2019).

*Extended Caption:* Cumulative Intensity during a heatwave is calculated as the sum of all EHF values for each of the days during a heatwave event. This metric quantifies the intensity of a heatwave in a way that allows comparison across space and time. The histograms represent all Cumulative Intensity values from all grid cells and all ensemble members within the *CCAM ensemble*. Grid cells selected were all land-cells within (or intersecting with the boundary of) the polygon that defines each Bureau of Meteorology Forecast District. Values were calculated for each grid cell. Projected Cumulative Intensity during a heatwave is presented from 1961 to 2100.

Each panel represents a histogram of Cumulative Intensity during a heatwave from all grid cells and all ensemble members during each different 20-year period. Time periods were: 1961–1990; 2001–2020; 2021–2040; 2041–2060; 2061–2080; 2081–2100.

**Figure 12: Projected mean cumulative intensity by month**

*Interpretation:*

Each bar represents the counts for when the regional (all times averaged) and ensemble mean (the average of the six models) of Cumulative Intensity falls into a particular month for the 1961-1990 period and each 20-year period of 2021–2040, 2041–2060, 2061–2080, 2081–2100 (following the RCP8.5 scenario). The dark shading in each plot shows the observations for the base period (1961-1990) to highlight the changes. Differences between the months, or time periods is expressed as changes to the height of each bar.

*Underlying data source:* Australian Gridded Climate Data Product (Jones et al., 2009); Climate Futures Australasian Projections 2019 (CFAP2019).

*Extended Caption:* Cumulative Intensity during a heatwave is calculated as the sum of all EHF values for each of the days during a heatwave event. This metric quantifies the intensity of a heatwave in a way that allows comparison across space and time. The bars represent the average Cumulative Intensity values across all grid cells and all ensemble members within the *CCAM ensemble*. Grid cells selected were all land-cells within (or intersecting with the boundary of) the polygon that defines each Bureau of Meteorology Forecast District. Values were calculated for each grid cell. Projected Cumulative Intensity during a heatwave is presented from 1961 to 2100.

Shadowed bars are the observed Cumulative Intensity during heatwaves for the 1961–1990 baseline period. Differences between the dark grey bars and the shadowed bars indicate how the models are different to the observations. Differences between the coloured bars and the shadowed bars indicate changes into the future relative to the observed baseline period.

Each panel represents a bar plot of mean Cumulative Intensity during a heatwave from all grid cells and all ensemble members during each different 20-year period. Time periods were: 1961–1990; 2001–2020; 2021–2040; 2041–2060; 2061–2080; 2081–2100.

**Figure 13: Observed mean heatwave duration**

*Interpretation:*

Each grid cell represents the mean Heatwave Duration during the period 1997–2017, (which is the period of recent memory). This map reflects the level of variability across the region as it is currently experienced. Grid cells are the resolution of the underlying data. Towns and roads are included to help identify specific sites within the region. Grid cells have an average elevation of the area they represent, so they best represent regions that have similar elevations (± 200m) across 5–10 km$^2$ scales. Typically, the highest peaks occur at smaller scales (~1 km$^2$) and thus are poorly represented. This can influence the representation of some climatic features and should be considered when interpreting these figures.

*Underlying data source:* Australian Gridded Climate Data Product (Jones et al., 2009).

*Extended Caption:* Heatwave duration is calculated as the the number of days in a row associated with a heatwave event. A heatwave event is three or more consecutive days with an EHF value greater than zero. This metric quantifies the length of a heatwave in a way that allows comparison across space and time. Grid cells selected were all land-cells within (or intersecting with the boundary of) the polygon that defines each Bureau of Meteorology Forecast District. Values were calculated for each grid cell. Mean Heatwave Duration is the average of all Heatwave Duration values within the *current period* (1997–2017).

**Figure 14: Observed change in mean heatwave duration**

*Interpretation:*

Each grid cell represents how mean Heatwave Duration during the current period (1997–2017) has changed when compared to mean Heatwave Duration during the historical period (1961–1990). Climate change is a large-scale feature, so the level of change observed is relatively similar when viewed at local scales. Towns and roads are included to help identify specific sites within the region. Grid cells have an average elevation of the area they represent, so they best represent regions that have similar elevations (± 200m) across 5–10 km$^2$ scales. Typically, the highest peaks occur at smaller scales(~1 km$^2$) and thus are poorly represented. This can influence the representation of some climatic features and should be considered when interpreting these figures.

*Underlying data source:* Australian Gridded Climate Data Product (Jones et al., 2009).

*Extended Caption:* Heatwave duration is calculated as the the number of days in a row associated with a heatwave event. A heatwave event is three or more consecutive days with an EHF value greater than zero. Mean Heatwave Duration is the average of all Heatwave Duration values within the *current period* (1997–2017), or the *baseline period* (1961–1990). The *baseline period* mean Heatwave Duration was then subtracted from the *current period* mean Heatwave Duration, resulting in the *observed change in mean Heatwave Duration*. Grid cells selected were all land-cells within (or intersecting with the boundary of) the polygon that defines each Bureau of Meteorology Forecast District. Values were calculated for each grid cell.

**Figure 15: Projected mean heatwave duration**

*Interpretation:*

Each grid cell represents the mean Heatwave Duration during each 20-year period of 2021–2040, 2041–2060, 2061–2080, 2081–2100 (following the RCP8.5 scenario). These reflect the level of variability across the region, and the rate of change projected into the future. Grid cells are the resolution of the underlying data. Grid cells have an average elevation of the area they represent, so they best represent regions that have similar elevations (± 200m) across 5–10 km$^2$ scales. Typically, the highest peaks occur at smaller scales (~1 km$^2$) and thus are poorly represented. This can influence the representation of some climatic features and should be considered when interpreting these figures.

*Underlying data source:* Climate Futures Australasian Projections 2019 (CFAP2019).

*Extended Caption:* Heatwave duration is calculated as the the number of days in a row associated with a heatwave event. A heatwave event is three or more consecutive days with an EHF value greater than zero. This metric quantifies the intensity of a heatwave in a way that allows comparison across space and time. Mean projected Heatwave Duration is the ensemble mean of all Heatwave Duration values for each heatwave across all ensemble members within the *CCAM ensemble*. Grid cells selected were all land-cells within (or intersecting with the boundary of) the polygon that defines each Bureau of Meteorology Forecast District. Values were calculated for each grid cell. Mean Heatwave Duration is the average of all Heatwave Duration values of all heatwaves within each time period (2021–2040; 2041–2060; 2061–2080; 2081–2100). These were calculated for each ensemble member within the *CFAP2019*. The 6 ensemble member values (for each grid cell) are averaged generating the ensemble mean for each grid cell within the region.

**Figure 16: Projected heatwave duration**

*Interpretation:*

The light-grey ribbon represents the observed spread of Heatwaves Duration for all grid cells in the region from the 10th to 90th percentile, while the dark-grey ribbon represents the 25th to 75th percentiles and the dark-grey line the average. These are 30-year rolling means. The light-maroon ribbon represents the modelled projected spread of Heatwaves Duration for all grid cells and ensemble members in the region from the 10th to 90th percentile, while the dark-maroon ribbon represents the 25th to 75th percentiles and the red line the model average. It's clear that the spread of Heatwaves Duration looks set to increase into the future as well as the projected model average. Compared to observations, the projections appear to under-estimate the rate of change into the future.

*Underlying data source:* Australian Gridded Climate Data Product (Jones et al., 2009); Climate Futures Australasian Projections 2019 (CFAP2019).

*Extended Caption:* Heatwave duration is calculated as the the number of days in a row associated with a heatwave event. A heatwave event is three or more consecutive days with an EHF value greater than zero. This metric quantifies the length of a heatwave in a way that allows comparison across space and time. Mean projected Heatwave Duration is the ensemble mean of all Heatwave Duration values for each heatwave across all ensemble members within the *CCAM ensemble*. Grid cells selected were all land-cells within (or intersecting with the boundary of) the polygon that defines each Bureau of Meteorology Forecast District. Values were calculated for each grid cell. Projected Heatwave Duration during a heatwave is presented from 1961 to 2100.

**Light-grey ribbons**: The light-grey ribbons represent the spread of the 10$^{th}$ to the 90$^{th}$ percentiles of Heatwave Duration during a heatwave from the observational record (AGCD), calculated as a 30-year rolling mean.

**Dark-grey ribbons**: The dark-grey ribbons represent the spread of the 25$^{th}$ to the 75$^{th}$ percentiles of Heatwave Duration during a heatwave from the observational record (AGCD), calculated as a 30-year rolling mean.

**Solid black line**: The solid black line represents the mean Heatwave Duration during a heatwave from the observational record (AGCD), calculated as a 30-year rolling mean.

**Light-marron ribbons**: The light-maroon ribbons represent the spread of the 10$^{th}$ to the 90$^{th}$ percentiles of Heatwave Duration during a heatwave from the model projections record (CFAP2019). Each timestep is the ensemble-mean, calculated from the 30-year rolling mean of each ensemble member.

**Dark-maroon ribbons**: The dark-maroon ribbons represent the spread of the 25$^{th}$ to the 75$^{th}$ percentiles of Heatwave Duration during a heatwave from the model projections record (CFAP2019). Each timestep is the ensemble-mean, calculated from the 30-year rolling mean of each ensemble member.

**Solid red line**: The solid red line represents the mean Heatwave

Duration during a heatwave from the model projections record (CFAP2019). Each timestep is the ensemble-mean, calculated from the 30-year rolling mean of each ensemble member.

**Coloured zones in background**: The coloured zones in the background indicate the time when *average global climate temperature* increases by 1 °C, 2 °C, 3 °C or 4 °C, following the Representative Concentration Pathway 8.5 scenario (RCP8.5, often referred to as the *business as usual* scenario). These estimates are the ensemble means as reported by the Intergovernmental Panel on Climate Change Fifth Assessment Report (IPCC-AR5), based on the World Climate Research Programme (WCRP) Coupled Model Intercomparison Project - phase 5 (CMIP5) global climate model archive (which has >100 ensemble members).

**Figure 17: Projected count of heatwave duration**

*Interpretation:*

> Lines showing the counts of the mean Heatwaves Duration in number of days for all model ensemble members and each grid cell in the region for the 1961–1990 period and each 20-year period of 2001–2020, 2021–2040, 2041–2060, 2061–2080, 2081–2100 (following the RCP8.5 scenario). These reflect counts of the number of times the Heatwaves Duration is each specific number of days (from three upwards), for each of the six time periods. Differences between the height of each line highlights how many counts fall into that specific number of days of heatwave.

*Underlying data source:* Australian Gridded Climate Data Product (Jones et al., 2009); Climate Futures Australasian Projections 2019 (CFAP2019).

*Extended Caption:* Heatwave duration is calculated as the the number of days in a row associated with a heatwave event. A heatwave event is three or more consecutive days with an EHF value greater than zero. The lines represent the total number of events with a particular Heatwave Duration for all heatwave events from all grid cells and all ensemble members within the *CCAM ensemble*. Grid cells selected were all land-cells within (or intersecting with the boundary of) the polygon that defines each Bureau of Meteorology Forecast District. Each line represents the total Heatwave Duration from all grid cells and all ensemble members during each different 20-year period. Time periods were: 1961–1990; 2001–2020; 2021–2040; 2041–2060; 2061–2080; 2081–2100.

**Figure 18: Projected mean heatwave duration by month**

*Interpretation:*

> Each bar represents the counts for when the regional (all times averaged) and ensemble mean (the average of the six models) of Heatwaves Duration falls into a particular month for the 1961–1990 period and each 20-year period of 2001–2020, 2021–2040, 2041–2060, 2061–2080, 2081–2100 (following the RCP8.5 scenario). The dark shading in each plot shows the observations for the base period (1961-1990) to highlight the changes. Differences between the months, or time periods is expressed as changes to the height of each bar.

*Underlying data source:* Australian Gridded Climate Data Product (Jones et al., 2009); Climate Futures Australasian Projections 2019 (CFAP2019).

*Extended Caption:* Heatwave duration is calculated as the the number of days in a row associated with a heatwave event. A heatwave event is three or more consecutive days with an EHF value greater than zero. This metric quantifies the intensity of a heatwave in a way that allows comparison across space and time.

The bars represent the mean Heatwave Duration for all heatwave events across all grid cells and all ensemble members within the *CCAM ensemble*. Grid cells selected were all land-cells within (or intersecting with the boundary of) the polygon that defines each Bureau of Meteorology Forecast District. Values were calculated for each grid cell. Projected Cumulative Intensity during a heatwave is presented from 1961 to 2100.

Shadowed bars are the observed mean Heatwave Duration during all heatwave events across for the 1961–1990 baseline period. Differences between the dark grey bars and the shadowed bars indicate how the models are different to the observations. Differences between the coloured bars and the shadowed bars indicate changes into the future relative to the observed baseline period.

Each panel represents a bar plot of mean Heatwave Duration during a heatwave from all grid cells and all ensemble members during each different 20-year period. Time periods were: 1961–1990; 2001–2020; 2021–2040; 2041–2060; 2061–2080; 2081–2100.

## Bushfire

Fire weather, associated with bushfire risk, can be estimated using a range of metrics, with the Forest Fire Danger Index (FFDI) being the most widely used and best understood across Tasmanian fire managment agencies and the public. Although this is not ideal (or appropriate) as an estimate of fire danger for all landscapes, it is a consistent metric that can be applied to quantify how atmospheric drivers of fire danger vary across space and time. FFDI is calculated based on four parameters: temperature, relative humidity, wind speed and drought factor (which incoprorates some landscape-type parameters, such as the rate of evaporation given aspect and elevation). FFDI can be calculated for any point in time. Daily maximum FFDI is the maximum value of FFDI for a given day. Daily maximum FFDI is the metric used in this report for understanding how fire danger has changed historically, and how it is projected to change into the future. In Tasmania (and across Australia), most days have low fire danger, with associated FFDI values also being low. Bushfires are relatively rare, with dangerous fire weather days even less common. Thus, average metrics are less informative than extreme values. Extreme values have been estimated in this report using the 90th, 95th and 99th percentile metrics (which account for the 37, 18 and 4 most dangerous fire weather days in a year, respectively).

FFDI values have been categorised into fire danger ratings as follows:

| Fire danger rating | FFDI value range |
|---|---|
| Low-Moderate | 0–12 |
| High | 12–25 |
| Very High | 25–50 |
| Severe | 50–75 |
| Extreme | 75–100 |
| Catastrophic | 100+ |

Table 4: FFDI value ranges for each fire danger rating

### Figure 1: Projected 90th, 95th and 99th percentile of daily max FFDI

*Interpretation:*

> Each grid cell represents the 90th, 95th and 99th percentile for the daily maximum FFDI rating day during the 1961-1990 period and each 20-year period of 2001-2020, 2021–2040, 2041–2060, 2061–2080, 2081–2100 (following the RCP8.5 scenario). These reflect the level of variability across the region, and the rate of change projected into the future for the three percentiles. Grid cells are the resolution of the underlying data. Grid cells have an average elevation of the area they represent, so they best represent regions that have similar elevations (±200m) across 5–10km2 scales. Typically, the highest peaks occur at smaller scales (~1km2 ) and thus are poorly represented. This can influence the representation of some climatic features and should be considered when interpreting these figures.

*Underlying data source:* Climate Futures Australasian Projections 2019 (CFAP2019).

*Extended Caption:* Daily maximum FFDI is the maximum value of FFDI for a given day. This metric quantifies the daily maximum FFDI a way that allows comparison across space and time. Grid cells selected were all land-cells within (or intersecting with the boundary of) the polygon that defines each region. Values were calculated for each grid cell. Each plot in the grid shows the given percentile value of projected daily max FFDI for all years within a given time period for each grid cell. Percentile values change with each row and are (from top to bottom) the 90th, 95th and 99th percentile of daily max FFDI. Time periods change with each column and are (from left to right) 1961–1990, 2021–2040; 2041–2060; 2061–2080; and 2081–2100. These were calculated for each ensemble member within the *CFAP2019*. The 6 ensemble member values (for each grid ell) are averaged generating the ensemble mean for each grid cell within the region.

### Figure 2: Projected change in 90th, 95th and 99th percentile of daily max FFDI

*Interpretation:*

> Each grid cell represents the change in the future period compared to the 90th, 95th and 99th percentile for the daily maximum FFDI rating day of the 1961-1990 period. Each panel represents a 20-year period of either 2001-2020, 2021–2040, 2041–2060, 2061–2080, 2081–2100 (following the RCP8.5 scenario). These reflect the level of variability across the region, and the rate of change projected into the future for the three percentiles. Grid cells are the resolution of the underlying data. Grid cells have an average elevation of the area they represent, so they best represent regions that have similar elevations (±200m) across 5–10km2 scales. Typically, the highest peaks occur at smaller scales (~1km2 ) and thus are poorly represented. This can influence the representation of some climatic features and should be considered when interpreting these figures.

*Underlying data source:* Climate Futures Australasian Projections 2019 (CFAP2019).

*Extended Caption:* Daily maximum FFDI is the maximum value of FFDI for a given day. This metric quantifies the daily maximum FFDI a way that allows comparison across space and time. Grid cells selected were all land-cells within (or intersecting with the boundary of) the polygon that defines each region. Values were calculated for each grid cell. The left-most column of plots in the grid shows the percentile value of projected daily max FFDI for all years within the 1961–1990 time period for each grid cell. Subsequent columns of plots in the grid show the change in the percentile value of projected daily max FFDI for all years within the given time period with respect to the 1961–1990 period. Percentile values change with each row and are (from top to bottom) the 90th, 95th and 99th percentile of daily max FFDI. Time periods change with each column and are (from left to right) 1961–1990, 2021–2040; 2041–2060; 2061–2080; and 2081–2100. These were calculated for each ensemble member within the *CFAP2019*. The 6 ensemble member values (for each grid cell) are averaged generating the ensemble mean for each grid cell within the region.

### Figure 3: Projected monthly FFDI with outliers removed

*Interpretation:*

> This is a representation of the range of FFDI values that occur during each month. Each box-and-whisker shows the medians (middle line) interquartile range (25th – 75th percentiles; thick bars) and 1.5 x interquartile range (12.5th – 87.5th percentiles; thin bars) of daily FFDI data for each grid cell, for each of the 6 ensemble members within each time period for each calendar month. The time period 1961–1990 is in light grey in each plot and each 20-year period of 2001–2020, 2021–2040, 2041–2060, 2061–2080, 2081–2100 are dark grey, following the RCP8.5 scenario. This allows for comparison between the base period (1961–1990) with every other projected time period. If the boxplot shifts higher (lower) this indicates a change towards more (less) dangerous conditions.

*Underlying data source:* Climate Futures Australasian Projections 2019 (CFAP2019).

*Extended Caption:* Daily maximum FFDI is the maximum value of FFDI for a given day. This metric quantifies the daily maximum FFDI a way that allows comparisons of monthly trends across time. Grid cells selected were all land-cells within (or intersecting with the boundary of) the polygon that defines each region. Values were calculated for each grid cell. Each plot shows the monthly distribution of daily max FFDI values for all days for all grid cells within each time period (1961–1990, 2001–2020, 2021–2040, 2041–2060, 2061–2080, 2081–2100). The values for all ensemble members within the *CFAP2019* are included in the distribution for each time period.

### Figure 4: Projected monthly FFDI with outliers shown

*Interpretation:*

> This is a representation of the range of FFDI values that occur during each month. Each box-and-whisker shows the medians (middle line) interquartile range (25th – 75th percentiles; thick bars) and 1.5 x interquartile range (12.5th – 87.5th percentiles; thin bars) of daily FFDI data for each grid cell, for each of the 6 ensemble members within each time period for each calendar month. Additionally, this plot shows the outliers above the 87.5th percentile out to the 100 percentile (the full range). The time period 1961-1990 is in light grey in each plot and each 20-year period of 2001–2020, 2021–2040, 2041–2060, 2061–2080, 2081–2100 are dark grey, following the RCP8.5 scenario. This allows for comparison between the base period (1961–1990) with every other projected time period. If the boxplot shifts higher (lower) this indicates a change towards more (less) dangerous conditions.

*Underlying data source:* Climate Futures Australasian Projections 2019 (CFAP2019).

*Extended Caption:* Daily maximum FFDI is the maximum value of FFDI for a given day. This metric quantifies the daily maximum FFDI a way that allows comparisons of monthly trends across time. Grid cells selected were all land-cells within (or intersecting with the boundary of) the polygon that defines each region. Values were calculated for each grid cell. Each plot shows the monthly distribution of daily max FFDI values for all days for all grid cells within each time period (1961–1990, 2001–2020, 2021–2040, 2041–2060, 2061–2080, 2081–2100). The values for all ensemble members within the *CFAP2019* are included in the distribution for each time period.

### Figure 5: Projected number of days per year of bushfire danger ratings

*Interpretation:*

> This metric quantifies the daily maximum FFDI a way that allows comparisons between the likelihood of each FFDI rating across time. The thicker the area for each year, the more days fit into the relevant fire danger rating. As every day has a fire danger rating, the maximum possible is 365 (or 366 in a leap year). Low-Moderate rating frequencies decrease through time and are replaced by corresponding increases in the frequency higher categories. Catastrophic had frequencies too low to reasonably present here. The percentage change from the first value of the smoothed line is highlighted on the 2nd y-axis. The y-axis does not necessarily start at zero, as this allows for better visualisation of the values for some ratings.

*Underlying data source:* Climate Futures Australasian Projections 2019 (CFAP2019).

*Extended Caption:* Daily maximum FFDI is the maximum value of FFDI for a given day. Each plot in the grid shows the projected number of days per year for a given fire danger rating. Fire danger ratings are based on the daily maximum FFDI and are categorised according to the table at the start of this section. These were calculated for each ensemble member within the *CFAP2019*. The 6 ensemble member values (for all grid cells) are averaged generating the ensemble mean across space for each region.

**Coloured areas**: Coloured sections are the projected values of the number of days per year for each fire danger rating, calculated from the ensemble mean of the 6 ensemble members for all grid cells in the region.

**Solid lines**: Solid lines are the smoothed line of best fit as described by Mann (2008) of the data in the *coloured areas.*

**Shaded background zones**: The shaded background zones indicate the time when *average global climate temperature* increases by 1°C, 2°C, 3°C or 4°C, following the Representative Concentration Pathway 8.5 scenario (RCP8.5, often referred to as the *business as usual* scenario). These estimates are the ensemble means as reported by the Intergovernmental Panel on Climate Change Fifth Assessment Report (IPCC-AR5), based on the World Climate Research Programme (WCRP) Coupled Model Intercomparison Project - phase 5 (CMIP5) global climate model archive (which has >100 ensemble members).

### Figure 6: Projected ratio of bushfire danger ratings

*Interpretation:*

> Representation of the relative frequency of different FFDI categories over time. Low-Moderate rankings are the most frequent. This is a time series of the ensemble– and region– mean (all six ensemble members and grid cells averaged) for the 30-year rolling mean of the number of days across each fire season (October to April, 180 days) per year with each fire danger rating. Data is presented over the period from 1990 to 2100. *(continued...)*

*(continued)*

Fire danger ratings presented are: Low-Moderate; High; Very High; Severe; and Extreme. This allows for the realtive influence of different fire ratings to be directly compared. The thicker the area for each year, the more days fit into the relevant fire danger rating (separated by colour rather than in separate graphs as in Figure 5). As every day has a fire danger rating, Low-Moderate rating frequencies decrease through time and are replaced by corresponding increases in the higher categories. Catastrophic had frequencies too low to reasonably present here. The y-axis scale terminates at 180 days to enhance the clarity of the fire danger levels other than Low-Moderate.

*Underlying data source:* Climate Futures Australasian Projections 2019 (CFAP2019).

*Extended Caption:* Daily maximum FFDI is the maximum value of FFDI for a given day. This metric quantifies the daily maximum FFDI a way that allows comparisons between the relative ratio of each FFDI rating across time. The plot shows the projected number of days per year for each fire danger rating based on the daily maximum FFDI represented as a portion of each year. Fire danger ratings are based on the daily maximum FFDI and are categorised according to the table at the start of this section. These were calculated for each ensemble member within the *CFAP2019*. The 6 ensemble member values (for all grid cells) are averaged generating the ensemble mean across space for each region.

**Figure 7: Projected returns curves for daily maximum FFDI**

*Interpretation:*

The projected return period is an estimate of the average time between scenarios occuring. Annual return periods for Forest Fire Danger Index values for the ensemble– and region– mean (all six ensemble members and grid cells averaged) for the 1961–1990 period and each 20–year period of 2001–2020, 2021–2040, 2041–2060, 2061–2080, 2081–2100 (following the RCP8.5 scenario). The higher the FFDI rating, the longer the time between events. The lower the line, the lower the FFDI for each given return period.

*Underlying data source:* Climate Futures Australasian Projections 2019 (CFAP2019).

*Extended Caption:* Daily maximum FFDI is the maximum value of FFDI for a given day. This metric quantifies the daily maximum FFDI in a way that allows comparisons between the projected return period of different scenarios of different daily maximum FFDI across time. The return period for a region is calculated by sorting and ranking the daily max FFDI values for all days in the time period and for all grid cells in the region, then calculating the exceedence probability for each FFDI value. This is the probability that another value occurring that exceeds this one, which is then converted to a measure of the number of years. These were calculated for each time period (1961–1990, 2001–2020, 2021–2040, 2041–2060, 2061–2080, 2081–2100) and for each ensemble member within the *CFAP2019*. The 6 ensemble member values (for all grid cells) are averaged generating the ensemble mean across space for each region.

**Figure 8: Driving variables of FFDI**

*Interpretation:*

As wind speed is not projected to change significantly, the key drivers of change are temperature (with the later time period lines shifted to the right), humidity (relative humidity decreasing with later time periods shifted to the left) and drought factor (more cases of higher drought factor). Drought factor and relative humidity have strong correlations with temperature change, with higher temperature meaning both lower relative humidity and increased evaporation which increases drought factor.

*Underlying data source:* Climate Futures Australasian Projections 2019 (CFAP2019).

*Extended Caption:* Each plot shows a probability distribution curve for each of the underlying driving drivers of FFDI. Included are the values for each grid cell for each day within each time period (1961–1990, 2001–2020, 2021–2040, 2041–2060, 2061–2080, 2081–2100). The drivers are: a) Maximum daily wind speed (m/s); b) Drought Factor (AU); c) Maximum daily temperature (°C); d) Daily minimum relative humidity (%). The y-axis scale is a qualitative measure of how likely each value on the x-axis is to occur relative to all values that are present. These were calculated for each ensemble member within the *CFAP2019*.

## References

Boucher, O., D. Randall, P. Artaxo, C. Bretherton, G. Feingold, P. Forster, V.-M. Kerminen, Y. Kondo, H. Liao, U. Lohmann, P. Rasch, S.K. Satheesh, S. Sherwood, B. Stevens and X.Y. Zhang, 2013: Clouds and Aerosols. In: Climate Change 2013: The Physical Science Basis. Contribution of Working Group I to the Fifth Assessment Report of the Intergovernmental Panel on Climate Change [Stocker, T.F., D. Qin, G.-K. Plattner, M. Tignor, S.K. Allen, J. Boschung, A. Nauels, Y. Xia, V. Bex and P.M. Midgley (eds.)]. Cambridge University Press, Cambridge, United Kingdom and New York, NY, USA.

Christensen, J. H., Boberg, F., Christensen, O. B., and Lucas-Picher, P.: On the need for bias correction of regional climate change projections of temperature and precipitation, Geophys. Res. Lett., 35, L20709, doi:10.1029/2008GL035694, 2008

Chouinard, C., M. B6land and N. McFarlane, 1986: A simple gravity wave drag parameterization for use in medium-range weather forecast models. Atmns. Ocean, 24, 9l-tto.

Freidenreich S.M. and Ramaswamy V. (1999) A new multiple-band solar radiative parameterization for general circulation models. Journal of Geophysical Research 104 D24 31389–31409.

Gudmundsson, L., Bremnes, J.B., Haugen, J.E. and Engen-Skaugen, T., 2013. Downscaling RCM precipitation to the station scale using statistical transformations—a comparison of methods. Hydrology and Earth System Sciences, 16(9), pp.3383–3390.

Hoffmann, P., Katzfey, J.J., McGregor, J.L. and Thatcher, M., 2016. Bias and variance correction of sea surface temperatures used for dynamical downscaling. Journal of Geophysical Research: Atmospheres, 121(21).

Horowitz HM, Garland RM, Thatcher M, Landman WA, Dedekind Z, van der Merwe J, Engelbrecht FA (2017) Evaluation of climate model aerosol seasonal and spatial variability over Africa using AERONET. Atmos. Chem. Phys. 17 13999–14023.

IPCC, 2014: Climate Change 2014: Synthesis Report. Contribution of Working Groups I, II and III to the Fifth Assessment Report of the Intergovernmental Panel on Climate Change [Core Writing Team, R.K. Pachauri and L.A. Meyer (eds.)]. IPCC, Geneva, Switzerland, 151 pp.

Jones, D.A., Wang, W. and Fawcett, R., 2009. High-quality spatial climate data-sets for Australia. Australian Meteorological and Oceanographic Journal, 58(4), p.233.

Kowalczyk E.A., Stevens L., Law R.M., Dix M., Wang Y.P., Harman, I.N., Haynes K., Srbinovsky J., Pak B. and Ziehn T. (2013) The land surface model component of ACCESS: description and impact on the simulated surface climatology. Australian Meteorological and Oceanographic Journal 63 65–82.

Lin Y-L, Farley RD and Orville HD (1983) Bulk parameterization of the snow field in a cloud model. Journal of climate and applied meteorology. 22 1065–1092.

Lipson, M, Thatcher, M, Hart, M and Pitman, A. (2018). A building energy demand and urban land surface model. Quarterly Journal of the Royal Meteorological Society. 144. 1–19.

Luke, R. H. and McArthur, A. G., 1986: Bushfires in Australia. Australian Government Publishing Service, Canberra.

McArthur, A. G., 1967: Fire Behaviour in Eucalypt Forests. Department of National Development Forestry and Timber Bureau, Canberra, Leaflet 107.

McGregor, J.L., H.B. Gordon, I.G. Watterson, M.R. Dix and L.D. Rotstayn, 1993: The CSIRO 9-level atmospheric general circulation model. CSIRO Division of Atmospheric Research technical paper No. 26. 89 pp.

McGregor JL (2003) A new convection scheme using a simple closure. Bureau of Meteorology Research Centre Research Report 93:33–36

McGregor 2005: C-CAM: Geometric aspects and dynamical formulation. CSIRO Oceans and Atmosphere Research Technical Paper, 70, 43 pp.

McGregor, J. L. and M. R. Dix, 2008: An updated description of the conformal-cubic atmospheric model. High Resolution Simulation of the Atmosphere and Ocean, Hamilton, K. and W. Ohfuchi, Eds., Springer, 51–76.

Mann, M. E. (2008), Smoothing of climate time series revisited, Geophys. Res. Lett., 35, L16708, doi:10.1029/2008GL034716.

Nairn, J.R. and Fawcett, R.J.B., The Excess Heat Factor: A Metric for Heatwave Intensity and Its Use in Classifying Heatwave Severity. International Journal of Environmental Research and Public Health, 2015, 12, 227–253; doi:10.3390/ijerph120100227

Rotstayn LD (1997) A physically based scheme for the treatment of stratiform cloud and precipitation in large-scale models. I: Description and evaluation of the microphysical processes. Q.J.R. Meteorol. Soc 123 pp 1227–1282

Rotstayn LD and Lohmann U (2002) Simulation of the tropospheric sulfur cycle in a global model with a physically based cloud scheme. Journal of Geophysical Research 107 D21 4592

Rotstayn LD, Collier MA, Mitchell RM, Qin Y, Campbell SK and Dravitzki SM (2011) Simulated enhancement of ENSO-related rainfall variability due to Australian dust. Atmos. Chem. Phys. 11, 6575–6592

Schwarzkopf MD and Ramaswamy V (1999) Radiative effects of CH4, N2O, halocarbons and the foreign-broadened H2O continuum: A GCM experiment. Journal of Geophysical Research 104 D8 9467–9448.

Thatcher, M. and Hurley, P. (2012) Simulating Australian urban climate in a mesoscale atmospheric numerical model. Boundary-Layer Meteorology, 142(1), 149–175.

Thatcher M and McGregor J (2009) Using a scale-selective filter for dynamical downscaling with the conformal cubic atmospheric model. Monthly Weather Review 137, 1742–1752.